On the ice-sediment-landform associations of surging glaciers on Svalbard

Harold Lovell

A thesis presented for the degree of
Doctor of Philosophy
in Geography
Queen Mary University of London
January 2014

Statement of Originality

I, Harold Lovell, confirm that the research included within this thesis is my own work or that where it has been carried out in collaboration with, or supported by others, that this is duly acknowledged below and my contribution indicated. Previously published material is also acknowledged below.

I attest that I have exercised reasonable care to ensure that the work is original, and does not to the best of my knowledge break any UK law, infringe any third party's copyright or other Intellectual Property Right, or contain any confidential material.

I accept that the College has the right to use plagiarism detection software to check the electronic version of the thesis.

I confirm that this thesis has not been previously submitted for the award of a degree by this or any other university.

Date:

Publications

This work has thus far contributed to the following publications:

Naegeli K., **Lovell H.**, Zemp M. and Benn D.I. (2014), Dendretic subglacial drainage systems in cold glaciers formed by cut-and-closure processes. *Geografiska Annaler: Series A, Physical Geography*

Fleming, E.J., **Lovell, H.**, Stevenson, C.T.E., Petronis, M.S., Benn, D.I., Hambrey, M.J., and Fairchild, I.J. (2013), Magnetic fabrics of basal ice in a surge-type glacier, *Journal of Geophysical Research*, **118**(4): 2263-2278.

Lukas, S., Benn, D.I., Boston, C.M., Brook, M., Coray, S., Evans, D.J., Graf, A., Kellerer-Pirklbauer, A., Kirkbride, M.P., Krabbendam, M., **Lovell, H.**, Machiedo, M., Mills, S.C., Nye, K., Reinardy, B.T., Ross, F.H., and Signer, M. (2013), Clast shape analysis and clast transport paths in glacial environments: A critical review of methods and the role of lithology, *Earth-Science Reviews*, **121**: 96-116.

Abstract

Glacier surges are amongst the most dynamic of glaciological phenomena, but their controlling mechanisms remain incompletely understood. Surging glaciers are characterised by cyclical flow instabilities and the rapid transfer of ice to the ablation area, typically resulting in significant mass loss. The High-Arctic archipelago of Svalbard is one of several regions in the northern hemisphere which contain a high-density of surge-type glaciers, variously estimated to be between 13-90% of the total glacier population across the islands. Developing a better understanding of which of these figures, if either, is most realistic is important in the context of glacier dynamics and related contributions of small glaciers and ice caps to sea level change in the immediate future. This study presents detailed assessments of the margins of several known surge-type glaciers in Svalbard in order to update and improve the existing framework by which they are identified, and to provide a foundation for future reassessments of the surge-type glacier population based on distinct ice-sediment-landform assemblages. A range of techniques is utilised, including geomorphological and structural glaciological mapping, sedimentological analysis, basal ice descriptions, and stable isotope analysis. This work provides further insight into diagnostic indicators of surge behaviour preserved in basal ice sequences; provides links between surge dynamics and basal ice sequences, the glaciological structure and the landform record; and investigates the structural and tectonic development of surge-type glaciers. Based on this, surge landsystems are proposed for: (1) small valley glaciers, (2) large land-terminating glaciers, and (3) large tidewater glaciers. It is suggested that these three landsystems, with some variability, broadly characterise the geomorphology of the vast majority of known Svalbard surge-type glaciers and, in conjunction with structural glaciological and basal ice investigations where relevant, may allow previously unknown surge-type glaciers to be identified in the field, from aerial photographs, and on sea floor imagery. This work adds to the existing repertoire of modern analogues and the breadth of surging glacier landsystems, and provides a holistic basis for assessing possible palaeo-surge behaviour within the Quaternary record.

Acknowledgements

Firstly, I would like to thank my supervisory team, both official and unofficial, without whom this work would have been unfeasible. **Sven Lukas** has been a great steering influence, allowing me to largely get on with things whilst also being ready with expert pieces of advice where necessary. His skills and on-the-job training in the field were essential to the project, particularly when a large amount of digging was required. Sven is also thanked for his field flapjack cooking and all-round entertaining, particularly in relation to marathon training whilst on fieldwork. He has also taught me a lot about the English language. **Doug Benn** has been crucial to this project in innumerable ways, chiefly by providing the all-important link to UNIS and consistent insightful observations when out in the field. I wish to thank Doug for introducing me to all things glaciological in Svalbard, and no small amount of Mack, whiskey and drunken singing. **Ed Fleming** has very much been my unofficial third supervisor, providing expert technical skills and good company on three consecutive spring field campaigns. I have no doubt this thesis would have been significantly poorer without Ed's influence. Finally, **Bryn Hubbard** provided fantastic advice to help me get my head around the basal ice aspects of the project.

The project was funded by the following sources: a NERC algorithm PhD studentship (NE/I528050/1), a Queen Mary Postgraduate Research Fund award, an Arctic Field Grant award, and a QRA conference award.

Umpteen people are thanked for their essential help with fieldwork: **Kathrin Naegeli**, **Philipp Schuppli**, **Heidi Sevestre**, **Endre Før Gjermundsen**, **Riccardo Scotti**, **Roberto Colucci**, **Stuart Thomson**, **Kier Stanley**, **Mauro Fischer**, **Nina Zoller**, **Andy Gray** and members of **AG-325** (2011 and 2012) in Svalbard; and **Chris Darvill** and **Will Christiansen** in Patagonia. **Martin Indreiten**, **Lars Frode Stangeland**, **Jukka Pekka Ikonen** and others from UNIS logistics provided important advice and equipment over six field campaigns. The **277** was essential for logistics whilst in London. **Ian Boomer** is thanked for running the stable isotope analyses on my ice samples.

The following indulged me with informal chats, usually over beers, that in some way influenced my work: **Clare Boston**, **Iestyn Barr**, **Chris Stokes**, **Mike Bentley**, **Dave Evans**, **Chris Clark**, **Matteo Spagnolo**, **Darrel Swift**, **Andy Hodson**, **Simon Carr**, **Jaap van der Meer**, **Richard Waller** and **Simon Cook**. **Jez Palfrey** and **Dave Croot** are thanked for setting me on the path to this in the first place. I would also like to thank the administrative and laboratory staff at QMUL and UNIS for their help, in particular **Helen McLurg**, **Simon Dobinson**, **Venke Ivarrud** and **Anne Bjørndal**.

Thanks to my football teams who gave me plenty of opportunity to play and watch football whilst in London: **Clissold Thistle FC**, **Capital Glovers**, **Bristol City FC** and **Yeovil Town FC**.

Penultimately, cheers to all those (as yet unmentioned) who joined me for beer, cafetière-loads of coffee and/or were generally excellent company at QMUL and at 96 Halton Mansions, including **G-Star Benardout** (104 office; chum), **Francis O'Shea**, **John Groves**, **Niall Lehane**, **James Holloway**, **room 104-ers, room 224-ers, Tom Brind, Molly Stevenson** and many more I've either forgotten or whose names I can't spell. Without getting embarrassingly emotional, this would probably have been a bit harder without you. I apologise to anyone I have neglected to mention, unless it was on purpose.

Finally, thanks to friends and family: you know who you are, and it's highly unlikely you'll read this anyway.

Contents

List of Figures

List of Tables

'They attributed the outburst flood to flamboyant behaviour by some young Tlingit men who had taunted the glacier, inciting it to surge'

Cruickshank (2001; p. 381)

Chapter One
Introduction

'Surging glaciers present some navigational, spiritual and intellectual challenges of a sentient 'land that listens''

Cruickshank (2001; p.388)

1. Introduction

1.1. Introduction and rationale

Glaciers are very sensitive to changes in climate and can experience dramatic fluctuations in response to variations in temperature and precipitation (Oerlemans and Fortuin, 1992; Oerlemans, 1994; Cruikshank, 2001; Koerner, 2005; Nuth *et al.*, 2010; Gardner *et al.*, 2011; James *et al.*, 2012; Nuth *et al.*, 2013). Of particular concern today are the Arctic regions (IPCC, 2007), which have experienced significant step-like increases in temperature since the 19th century and associated glacier decay (Hagen and Liestøl, 1990; Hansson-Bauer *et al.*, 1990; Dowdeswell *et al.*, 1995; Hanssen-Bauer and Førland, 1998; Lefauconnier *et al.*, 1999; Førland *et al.*, 2012). This decay, in the form of melting glaciers and ice caps, has made the largest contribution to eustatic sea level rise over the last century (e.g. Meier, 1984; Arendt *et al.*, 2002; Rignot *et al.*, 2003; Meier *et al.*, 2007; Jacob *et al.*, 2012) and, despite the increasing influence of the large ice sheets of West Antarctica, East Antarctica and Greenland (e.g. Thomas *et al.*, 2004; Shepherd and Wingham, 2007; Rignot *et al.*, 2011; Miles *et al.*, 2013), these are predicted to continue to make a significant contribution until at least 2100 (Raper and Braithwaite, 2006; Pfeffer *et al.*, 2008; Radić and Hock, 2011). As a result, a large body of research has focused on the present and future response of Arctic glaciers to climate forcing, typically by investigating mass balance variations, often linked to changes in glacier geometry (e.g. Nuth *et al.*, 2010, 2013; James *et al.*, 2012) and terminus position (e.g. Błaszczyk *et al.*, 2009; Carr *et al.*, 2013).

However, a proportion of these glaciers are known to exhibit highly unstable behaviour, called glacier surges, which are largely thought to be controlled by internal glaciological mechanisms rather than external forcing, and therefore their behaviour may not be a reliable indicator of glacier response to climatic perturbations (Meier and Post, 1969; Clarke, 1987). This highlights the importance of being able to differentiate between glaciers which surge and those which do not when attempting to decipher signals of climate change, in particular those recorded by Arctic glaciers (Grant *et al.*, 2009). Understanding how the unique behaviour of surge-type glaciers manifests itself in glaciological (Copland *et al.*, 2003) and geomorphological (Evans and Rea, 1999, 2005) evidence is, therefore, critical in order to determine their distribution. It is already known that surge-type glaciers are typically found in dense populations across the Arctic and sub-Arctic regions (Dowdeswell *et al.*, 1991; Murray *et al.*, 2003b); one such cluster is on the High-Arctic archipelago of Svalbard, which is ~60% glacierised but has experienced significant reductions in this coverage in response to 20th century increases in mean summer air temperatures (Kohler *et al.*, 2007; James *et al.*, 2012; Nuth *et al.*, 2013). This makes Svalbard a highly relevant study area for investigating the glaciological and geomorphological signatures of surging, and the behaviour of surge-type glaciers in the context of a warming climate and general trends of glacier retreat (Lefauconnier *et al.*, 1999).

1.2. Surging glaciers

Surging glaciers exhibit cyclical flow instabilities characterised by long periods of quiescence interspersed with short active phases of much faster ice flow (Meier and Post, 1969; Raymond *et al.*, 1987). During the active phase, ice velocities increase dramatically by 10 to 1000 times and mass is transferred rapidly downglacier to a receiving zone (Meier and Post, 1969; Clarke *et al.*, 1984; Clarke, 1987; Raymond *et al.*, 1987). This behaviour is traditionally thought to be controlled by changes within the glacier system itself rather than external factors such as climate, although it is increasingly becoming apparent that climate change can influence surge activity and cycles (Dowdeswell *et al.*, 1995; Eisen *et al.*, 2001; Harrison and Post, 2003; Flowers *et al.*, 2011; Striberger *et al.*, 2011). The global distribution of surge-type glaciers is remarkably non-random, and they are largely located in dense populations, or surge clusters, within the Northern Hemisphere. A detailed review of surging glaciers is presented in *Chapter 2*.

At a global scale, research into fast-flowing glaciers, including surges, is important in order to help constrain the causal mechanisms of modern and past ice sheet instabilities and their contribution to sea level rise, particularly in changing climatic conditions (Dowdeswell *et al.*, 1995; Clark *et al.*, 2002; Christoffersen *et al.*, 2005; Domack *et al.*, 2005). Identifying the location of both contemporary and former surges is, therefore, of utmost importance (Dowdeswell *et al.*, 1991, 1995; Grant *et al.*, 2009) and a number of glaciological (Copland *et al.*, 2003) and geomorphological (Evans and Rea, 1999, 2005; Ottesen and Dowdeswell, 2006) criteria have been outlined in order to help in this regard. In order to capture the full range of surge environments, it is necessary to extend these models with additional detailed observations from different surge clusters. One such cluster is Svalbard, where surge-type glaciers have typically been identified based on glaciological evidence for an active surge (e.g. intense crevassing, terminus advance; Dowdeswell and Benham, 2003; Sund *et al.*, 2009; Sund and Eiken, 2010) or geomorphological evidence at the margin (Croot, 1988; Christoffersen *et al.*, 2005; Ottesen and Dowdeswell, 2006). However, few studies have investigated the signature of surging exposed within basal ice sequences or the glaciological structure of a glacier, which has the potential to provide important information about former flow dynamics (e.g. Hambrey *et al.*, 2005; Hubbard *et al.*, 2009; Roberts *et al.*, 2009; Fleming *et al.*, 2013), and the links between these and landform-sediment assemblages. This thesis aims to address this imbalance by assessing the ice-sediment-landform associations exposed at the margins of surge-type glaciers on Svalbard, using the structure outlined below to achieve this aim.

1.3. Thesis outline

This thesis consists of ten chapters: this chapter has introduced the context of the study; *Chapter 2* examines the current level of understanding relating to surging glaciers, identifies some areas

which require further investigation and outlines the aims and objectives of the study; *Chapter 3* outlines the methods used in this study and briefly describes the geography of the Svalbard archipelago; *Chapters 4-8* present glaciological and geomorphological results from the five glaciers investigated in this study, Nathorstbreen, Tunabreen, Finsterwalderbreen, Scott Turnerbreen and Tellbreen; *Chapter 9* establishes the ice-sediment-landform signature produced by surges on Svalbard and discusses these results in a wider context; and *Chapter 10* summarises the main findings and highlights areas for further research.

Chapter Two
Surging Glaciers

'Other narratives attribute surges to glaciers that are dens for giant animals - giant copper-clawed owls or giant worms - easily provoked by human hubris'

Cruickshank (2001; p.388)

2. Surging Glaciers

2.1. Introduction

It has been estimated that surging glaciers constitute less than 1% of all glaciers worldwide (cf. Jiskoot *et al.*, 1998), yet their geographical distribution is remarkably non-random, with surge-type glaciers occurring in clusters in some regions whilst other glacierised areas are largely devoid of them (Post, 1969; Clarke *et al.*, 1986; Jiskoot *et al.*, 2000). Significant surge clusters have been recorded in Alaska (e.g. Post, 1969; Kamb *et al.*, 1985; Heinrichs *et al.*, 1996), Yukon (e.g. Clarke *et al.*, 1984), Arctic Canada (e.g. Copland *et al.*, 2003), Greenland (e.g. Murray *et al.*, 2002; Jiskoot *et al.*, 2003; Yde *et al.*, 2005), Iceland (e.g. Sharp, 1985a,b; Björnsson *et al.*, 2003; Benediktsson *et al.*, 2009, 2010), Svalbard (e.g. Liestøl, 1969; Schytt, 1969; Dowdeswell *et al.*, 1991; Hagen *et al.*, 1993; Murray *et al.*, 1997; Murray *et al.*, 2003b) and the Russian High Arctic (e.g. Dowdeswell and Williams, 1997; Grant *et al.*, 2009). Surges have also been reported in the Pamir, Tien Shan and Karakoram mountain ranges (e.g. Dolgoushin and Osipova, 1975; Krimmel and Meier, 1975; Aizen *et al.*, 2007; Hewitt, 2007; Quincey *et al.*, 2011). Table 2.1 summarises some of the key characteristics of a number of selected surges from these regions reported in the literature. These observations and more demonstrate that surges occur within both temperate (e.g. Alaska, Iceland) and polythermal (e.g. Arctic Canada, Svalbard) glaciers. In contrast, few if any surge-type glaciers have ever been reported in the European Alps, mainland Scandinavia, South America, New Zealand or the Rocky, Cascade and Coast mountains of North America (Hamilton and Dowdeswell, 1996).

This non-random global distribution implies that certain environmental factors control the location of surge-type glaciers (Post, 1969; Hamilton and Dowdeswell, 1996). However, despite a number of studies that have investigated the possible controlling parameters at a regional scale (Post, 1969; Clarke *et al.*, 1986; Clarke, 1991; Hamilton and Dowdeswell, 1996; Jiskoot *et al.*, 1998, 2000, 2003), the reasons for this distribution remain poorly understood. It has also been recognised that there are distinct differences in surge characteristics between clusters (Dowdeswell *et al.*, 1991; Murray *et al.*, 2003b). This is particularly apparent when polythermal glacier surges (e.g. Svalbard) are contrasted with examples from temperate regions (e.g. Alaska, Iceland; see Table 2.1). This contrast in surge activity between regions is one of the main reasons that, as yet, no "unifying theory" for the surge mechanism exists (Rea and Evans, 2011).

A brief overview of surging glaciers, and in particular their geomorphological imprints, will be provided in this chapter in order to establish a broad context for this study; for further in-depth reviews the reader is directed towards the work of Meier and Post (1969), Raymond *et al.* (1987), Jiskoot *et al.* (2000), Harrison and Post (2003) and Murray *et al*. (2003b). This chapter

Table 2.1 - Database of selected surging glaciers.

Glacier	Length (km)	Area (km²)	Surge Date(s)	Active Phase Duration	Quiescent Phase Duration (years)	Terminus Advance (km)	Active Phase Velocities (m d^{-1})	Surge Front Propagation (m d^{-1})	Quiescent Phase Velocities (m d^{-1})	References
Alaska										
Bering Glacier	180	5200	1957-60, 1965-67, 1993-95	2 years	20 to 30	>2	10 to 20	90	<1	Molnia (1993); Roush *et al*. (2003)
Black Rapids Glacier	43	246	1936-37	1 year	50 to 75				0.1 to 0.2	Heinrichs *et al.* (1996); Nolan (2003)
Muldrow Glacier	46	393	1956-57	2 years						Post (1960); Harrison (1964)
Peters Glacier	27	120	1890s, 1986-87	13 months	50 to 70?			50 to 110		Echelmeyer *et al*. (1987)
Variegated Glacier	20	29	1982-83	2 years	16 to 26	2 to 5	~50	23 to 80	0.1 to 1.0	Kamb *et al*. (2005); Raymond *et al*. (1987)
Canada										
Mittie Glacier*			2000s							
Trapridge Glacier	4		1941-49	<8 years		~1			<0.003	Clarke *et al*. (1984); Frappé and Clarke (2007)
Greenland										
Kuannersuit Glacier	26	91	1995-98	3 years		10.5	70			Gilbert *et al.* (2002); Yde *et al*. (2005); Knudsen *et al*. (2007)
Sortebræ*	65		1950, 1992-95	2 to 3 years	39 to 49	7 to 10	30	Possibly no front	0.02	Murray *et al.* (2002)
Iceland										
Breiðamerkurjökull			1912, 1919, 1954, 1969, 1978		6 to 38					
Brúarjökull	50	1500	1810, 1890, 1963-64	2 to 3 months	80 to 100	10	100 to 120			Thorarinsson (1969); Benediktsson *et al*. (2008)
Dyngjujökull					20 to 30	~1				Björnsson *et al*. (2003)
Skeiðararjökull	55	1370	1991	8 months	25 to 118	>1	9.4			Pállson *et al.* (1992); Björnsson (1998); Waller *et al*. (2008)
Tungnaárjökull	28	120	1880-90, 1915-20, 1945, 1994-95	10 months	~30	1.2	10			Thorarinsson (1964); Andrzejewski *et al*. (2002); Björnsson *et al*. (2003)
Pamir										
Medvezhiy Glacier	13	25	1937, 1951, 1963, 1973, 1988-89	2 to 3 months	12 to 15	1.6	100		0.01 to 0.02	Dolgoushin and Osipova (1975); Kotlyakov *et al.* (1997)
Svalbard										
Bakaninbreen*	17	61	1985-90s	5 to 10 years	>85	0	1 to 3	0.9 to 4.5	0.001	Murray *et al*. (1997, 1998);
Bodleybreen*	16	87	1970-80s	5 to 13 years		2.7	2.0 to 2.6		0.05 to 0.5	Dowdeswell and Collin (1990); Dowdeswell *et al*. (1991)
Bråsvellbreen*			1936-38	2 years		20				Hagen *et al.* (1993)
Finsterwalderbreen	11	45	1900s			1.5			0.002 to 0.03	Nuttall *et al*. (1997); Nuttall and Hodgkins (2005)
Freemanbreen*			1955-56							Hagen *et al.* (1993)
Fridtjovbreen	13	49	1860s, 1990s	4+ years	130	>2.5	2 to 3.3	No front	0.08 to 0.3	Murray *et al*. (2003a)
Fyrisbreen			1950s -66	~8 years			0.1			Liestøl (1969); Dowdeswell *et al*. (1991)
Hessbreen	5	5	1969-77	8 years	~70			No front	0.008 to 0.01	Hambrey and Dowdeswell (1997); Sund and Eiken (2004)
Hinlopenbreen*	68	1250	1968-72	4+ years		3	14 to 16			Liestøl (1973); Hagen (1988); Dowdeswell *et al*. (1991)
Hyllingebreen	3	4.5	1968-78	>10 years		1.5	0.2 to 0.5			Dowdeswell *et al.* (1991)
Kongsvegen*	26	102	before 1948			1.5 to 2.0	>1.0		0.008	Melvold and Hagen (1998)
Monacobreen*	42	408	1990s	6+ years		2	0.5 to 5.0	No front	0.005 to 0.008	Murray *et al*. (2003b)
Nathorstbreen*		390	~1870, 2008-	~5 years	~140	~18	>20			Liestøl (1977); Sund and Eiken (2010)
Negribreen*			1935-36	<1 year		12				Hagen *et al.* (1993)
Osbornebreen*	20	152	1980s	4+ years		2	1.2 to 6.0	No front		Dowdeswell *et al.* (1991); Rolstad *et al*. (1997); Murray *et al*. (2003b)
Scott Turnerbreen	4.5	3.3	1930s							Hagen et al. (1993); Hodgkins *et al.* (2004)
Sefströmbreen*	23	155	1880s			6.5	1.3		0.005	Boulton *et al*. (1996)
Skobreen	8	18	1990-05	>15 years	>100	at least 0.2 to 0.4		No front		Sund (2006)
Tunabreen*	35	203	1930, 1970, 2003-05		~40	1.5				Hodgkins and Dowdeswell (1994); Błaszczyk *et al*. (2009)
Usherbreen	13	29	1978-85	8 years		1.5	1.5 to 4.3			Hagen (1988); Dowdeswell *et al*. (1991)

*tidewater

Unless otherwise stated, surge attributes refer to the last recorded surge of each particular glacier

will outline the key characteristics of glacier surges and surge cycles, the currently proposed theoretical models for the surge mechanism, the increasing recognition that traditional surge definitions may be too restrictive, and the glaciological and geomorphological criteria used to identify both contemporary and former surges. Bearing in mind the study area of this project, examples will preferentially focus on surges in Svalbard, where estimates suggest between 13% (Jiskoot *et al.*, 1998) and 90% (Lefauconnier and Hagen, 1991) of all glaciers are of surge-type; reference to other regions will be included where relevant. The chapter ends by highlighting the specific research gaps that this project aims to address.

2.2. The surge cycle

The idealised surge cycle for any given surge-type glacier begins with a long quiescent phase starting immediately upon termination of the previous surge, followed by a shorter active or surge phase of high ice velocities (Meier and Post, 1969; Raymond *et al.*, 1987). Upon surge termination the glacier re-enters the quiescent phase, and the surge cycle begins again. The characteristics of the surge cycle (e.g. duration and number of phases, velocities, changes in glacier geometry) can vary significantly between regions and individual glaciers, as outlined below and in Table 2.1, which has led to the suggestion that there are at least two different types of glacier surges (Murray *et al.*, 2003b).

2.2.1. Quiescent phase

During the quiescent phase, surge-type glaciers accumulate mass in an upper reservoir zone (Fig. 2.1a), which in a non-surging glacier would be transported down to the ablation area, maintaining a steady-state longitudinal profile (Hagen, 1988). By contrast, surging glaciers in the quiescent phase have an ice flux which is too low to maintain the steady-state profile, and as a result the surface gradient gradually increases (Meier and Post, 1969; Hagen, 1988; Melvold and Hagen, 1998). As ice thickens in the reservoir zone, the lower section of the glacier stagnates and thins (Clarke *et al.*, 1984; Kamb *et al.*, 1985; Raymond and Harrison, 1988; Glazovskiy *et al.*, 1991), often accompanied by the retreat of the terminus from the previous surge maximum (Fig. 2.1a). Mass accumulation in the reservoir zone and loss in the receiving zone gradually return the longitudinal profile of the glacier to its pre-surge state (Raymond *et al.*, 1987). The evolution of the quiescent phase of Kongsvegen, Svalbard, was monitored from 1966-95 through surface geometry measurements, revealing a build-up of up to 32 m in the reservoir zone and a thinning of up to 75 m in the receiving zone (Melvold and Hagen, 1998). Similar changes have been observed on other surge-type glaciers, both in Svalbard (e.g. Nuttall *et al.*, 1997; Sund, 2006; Sund *et al.*, 2009; Nuth *et al.*, 2010) and in other regional clusters (e.g.

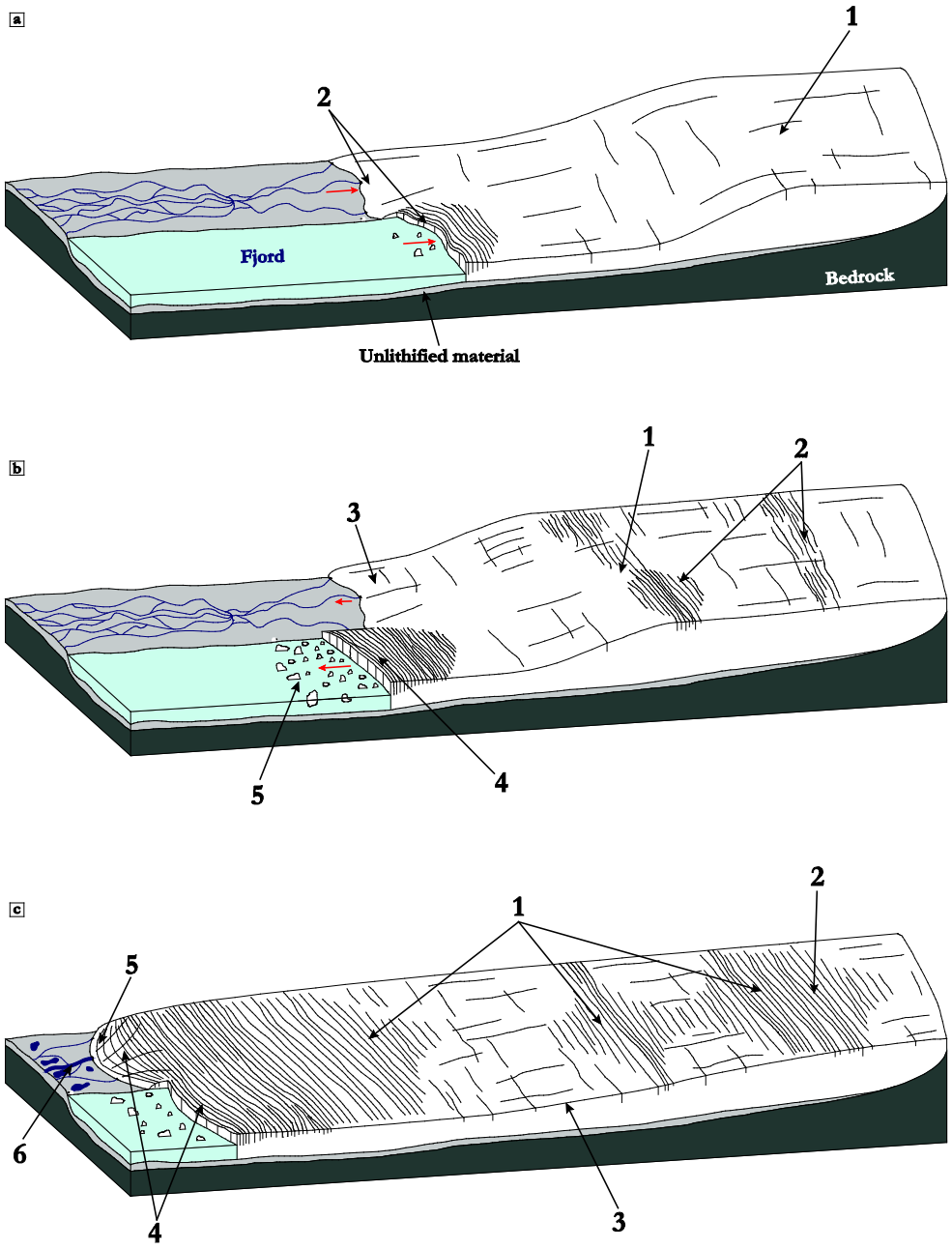

Figure 2.1 - Schematic illustration of the idealised surge cycle, showing both terrestrial and tidewater glacier margins. Red arrows indicate terminus advance/retreat. (a) Quiescent phase. (1) Thickening in the upper reservoir zone. (2) Thinning in receiving zone and retreat of glacier terminus. (b) Active phase. (1) Downglacier propagation of zone of increased mass as a kinematic wave, or surge front. Does not form in all cases, e.g. tidewater surges. (2) Crevassing in reservoir zone and associated with passage of the surge front. (3) Thickening in receiving zone. (4) Terminus advance and intense marginal crevassing in tidewater surges, which often initiate at the glacier front. Terminus advance in terrestrial glaciers occurs when/if surge front reaches the margin. (5) Increased calving associated with tidewater terminus advance. (c) Upon surge termination. (1) Intense surface crevassing throughout glacier. (2) Evidence of thinning and drawdown in reservoir zone. (3) Flattening of glacier profile. (4) Splayed lobate terminus following advance. (5) Steeper glacier profile in receiving zone. (6) Abrupt flood on termination (in some cases).

Dolgoushin and Osipova, 1975; Heinrichs *et al.*, 1996; Björnsson *et al.*, 2003; Nolan, 2003). Sund *et al.* (2009) proposed that the development of surges on Svalbard can be divided into three stages, based on geometric changes. They suggested that stage one was characterised by initial thinning in the upper section and stage two by subsequent thickening further downglacier, both during late quiescence; stage three represents the active phase of the surge.

Ice velocities are generally low during the quiescent phase (Table 2.1), but can display both a progressive increase leading up to the active phase (Dolgoushin and Osipova, 1975; Kamb *et al.*, 1985; Raymond *et al.*, 1987; Murray *et al.*, 2003a) and high levels of fluctuation throughout quiescence (Kamb *et al.*, 1985; Heinrichs *et al.*, 1996; Nolan, 2003; Sund and Eiken, 2004; Nuttall and Hodgkins, 2005). Quiescent phase velocities on Bakaninbreen, Svalbard, were estimated to be as low as 0.003 m d^{-1} (Murray *et al.*, 1998; Table 2.1), comparable to quiescent velocities recorded in the lower part of Trapridge Glacier, Alaska (Clarke *et al.*, 1984). The period leading up to the 1990s surge of Fridtjovbreen, Svalbard, included a progressive multi-year acceleration phase towards the end of quiescence (Murray *et al.*, 2003a). Similarly, monitoring of Variegated Glacier, Alaska, in an eight year period leading up to the 1982-83 surge revealed that ice velocities approximately doubled in the middle section and quadrupled in the upper section of the glacier (Kamb *et al.*, 1985).

The length of the quiescent phase varies between surge clusters and individual glaciers. The average surge cycle of most surge-type glaciers in Svalbard is thought to be somewhere between 40 and 500 years (Dowdeswell *et al.*, 1991; Murray *et al.*, 2003b). This lower number is derived from observations of Tunabreen, which surged in ca. 1930, 1970 and most recently in 2003-05 (Błaszczyk *et al.*, 2009; Forwick *et al.*, 2010; Mansell *et al.*, 2012). This is an unusually short return period by Svalbard standards, where only a handful of glaciers have been observed to surge more than once. By comparison, the length of the quiescent phase in temperate regions is typically about 20-30 years (Kamb *et al.*, 1985; Andrzejewski, 2002; Roush *et al.*, 2003; Striberger *et al.*, 2011). The last five surges of Medvezhiy Glacier in the Pamirs indicate a return period of 12-15 years (Dolgoushin and Osipova, 1975; Kotlyakov *et al.*, 1997), which is approximately the reported duration of the active phase of Skobreen, Svalbard (Sund, 2006). This highlights the variation in surge-cycle characteristics between clusters, and in particular between polythermal and temperate glacier surges.

2.2.2. Active phase

As with the quiescent phase, both the duration and character of the active phase vary significantly between regions and individual glaciers. In Svalbard, surges typically last for between three to ten years (e.g. Liestøl, 1969; Hagen, 1988; Dowdeswell *et al.*, 1991; Murray *et*

al., 1997; Sund and Eiken, 2004; Table 2.1). By contrast, active phase durations are typically between one to two years in Alaska (e.g. Kamb *et al.*, 1985; Echelmeyer *et al.*, 1987; Roush *et al.*, 2003) and less than a year in Iceland (e.g. Thorarinsson, 1969). Extreme end-members include the reported active phase of over 20 years of Trapridge Glacier (Frappé and Clarke, 2007), and Ryder Glacier, Greenland, which in 1995 experienced a seven week-long 'mini-surge' during which ice velocities increased threefold (from 100 to 500 m a^{-1}) before returning to normal conditions (Joughin *et al.*, 1996).

Ice velocities during surge active phases also vary significantly. In Svalbard, the surge front of Bakaninbreen propagated at rates of up to 4.7 m d^{-1} during the surge that began in 1985 (Murray *et al.*, 1998), and the measured maximum flow rate of Fridtjovbreen during its surge in the 1990s was ~2.5 m d^{-1}, compared to 0.08 m d^{-1} during quiescence (Murray *et al.*, 2003a). Similar surge velocities have also been reported from other glaciers in Svalbard (e.g Dowdeswell and Benham, 2003; Błaszczyk *et al.*, 2009; Mansell *et al.*, 2012). In addition, observations by Murray *et al.* (2003a,b) from Fridtjovbreen and Monacobreen in Svalbard suggest that the active phase can begin with a period of steady acceleration over several years, followed by a shorter period of rapid acceleration over a few months, before a prolonged, gradual deceleration phase (see *2.2.3.*). By contrast, peak active phase velocities in excess of 100 m d^{-1} have been reported from the temperate surges of Brúarjökull, Iceland (Thorarinsson, 1969) and Medvezhiy Glacier (Dolgoushin and Osipova, 1975), and during the 1982-83 Variegated Glacier surge, ice velocities as high as 65 m d^{-1} were recorded in the lower glacier compared to 0.2 m d^{-1} following surge termination (Kamb *et al.*, 1985). These studies highlight the contrast in peak surge velocities between temperate and polythermal regions, which can be up to an order of magnitude different (cf. Murray *et al.*, 2003b), although it should be noted that some polythermal surges experience similar peak velocities to temperate surges. For example, the 1992-95 surge of Sortebræ, Greenland, increased ice velocities by up to 60-1,500 times, from quiescent phase records of ~ 0.02 m d^{-1} up to 30 m d^{-1} (Murray *et al.*, 2002). In addition, an average velocity of over 20 m d^{-1} has been calculated for the ongoing surge of Nathorstbreen, Svalbard, based on the change in terminus position (Sund and Eiken, 2010). Finally, it has recently become apparent that some glaciers in Yukon Territory, Canada, surge at very low velocities over a long active phase (Frappé and Clarke, 2007; Flowers *et al.*, 2011). Trapridge Glacier reached peak velocities of just 0.1 m d^{-1} during an active phase lasting for over 20 years, four times higher than typical quiescent phase velocities (Frappé and Clarke, 2007).

The transfer of ice from the upper reservoir zone to the receiving zone and the associated geometric changes has been observed at a number of surges (Fig. 2.1). Detailed photogrammetric analysis of the surge of Bodleybreen, Svalbard, showed that between 1970

and 1971 there was a drop in surface elevations in the upper glacier whilst the lowest 3 km thickened by between 10-60 m (Dowdeswell and Collin, 1990). Also in Svalbard, Hagen (1988) estimated that about 20% of the total volume of Usherbreen was transported from the upper section to the lower section during the surge that terminated in 1985. Björnsson *et al*. (2003) estimated that 38% of the total area of the Vatnajökull ice cap in Iceland was affected by surges in the 1990s, resulting in the transport of approximately 25% of total ice flux to the ablation zone during that period.

In some cases, the transfer of mass during the active phase is associated with the development and propagation of a steep surge front (Figs 2.2a and 2.2b), which typically travels downglacier as a kinematic wave of increased ice thickness (McMeeking and Johnson, 1986). A surge front is a ramp or step that generally forms in the lower part of the enhanced velocity zone where faster ice flows into inactive ice (Kamb *et al.*, 1985; Raymond *et al.*, 1987; Björnsson *et al.*, 2003). In polythermal surges, the surge front is thought to mark the thermal boundary between warmer, surging ice and cold, inactive ice (Murray *et al.*, 1998). The passage of the surge front is associated with a wave of compression and extension travelling down-glacier (McMeeking and Johnson, 1986; Hodgkins and Dowdeswell, 1994; Murray *et al.*, 1997). This changing tectonic stress regime, in conjunction with high basal velocities, is largely responsible for the heavy crevassing displayed by the vast majority of surging glaciers during their active phase (Hodgkins and Dowdeswell, 1994; Lawson *et al.*, 1994; Rea and Evans, 2011; see *2.5.1.* for more details). The speed at which the surge front travels can be faster than the velocity of the ice; the propagation rate of the 60 m high Bakaninbreen surge front in 1986 (up to 4.7 m d^{-1}) was higher than the measured ice velocities at the same time (between 0.9-3.0 m d^{-1}; Murray *et al.*, 1998). Propagating surge fronts have been reported from a number of other surges in both temperate and polythermal glaciers and can result in the glacier advancing if they reach the terminus (Clarke *et al.*, 1984; Echelmeyer *et al.*, 1987; Hagen, 1988; Frappé and Clarke, 2007; see *2.5.1.* for more details). This is not always the case, however, as exemplified by Bakaninbreen, where the surge front was still 1.8 km from the terminus when the surge terminated in the 1990s and so did not result in an advance (Murray *et al.*, 1997). The observed lack of a surge front during the active phase of some polythermal surges has been attributed to low or non-existent flow restrictions at the margin, which could result if the bed of the glacier is at the pressure melting point throughout, or in tidewater glaciers (e.g. Monacobreen, Svalbard) that terminate in water of a sufficient depth to allow calving (Hodgkins and Dowdeswell, 1994; Murray *et al.*, 2003b).

2.2.3. Surge termination

The end of the active phase signals a return to quiescent phase conditions as the surge cycle begins again. Surge termination is characterised by a decrease in ice velocities, often to lower than pre-surge velocities (Kamb *et al.*, 1985). The manner of surge termination is markedly different between some surge clusters. The 1982-83 surge of Variegated Glacier terminated abruptly in a period of just a few hours, during which ice velocities dropped to about a quarter of their previous value (Kamb *et al.*, 1985). Abrupt terminations of the order of days have been reported from the temperate surges of Medvezhiy Glacier (Osipova and Tsvetkov, 1991) and West Fork Glacier, Alaska (Harrison *et al.*, 1994), and the polythermal tidewater surge of Sortebræ (Murray *et al.*, 2002). In some temperate surges, abrupt termination was associated with the release of turbid subglacial water in the form of outburst floods (Kamb *et al.*, 1985; Harrison *et al.*, 1994; Björnsson, 1998; Bennett *et al.*, 2000). In contrast, the terminations of observed surges in Svalbard (e.g. Bakaninbreen, Fridtjovbreen and Monacobreen) tend to be indistinct and characterised by a progressive deceleration phase over a number of years (Murray *et al.*, 1998; 2003b).

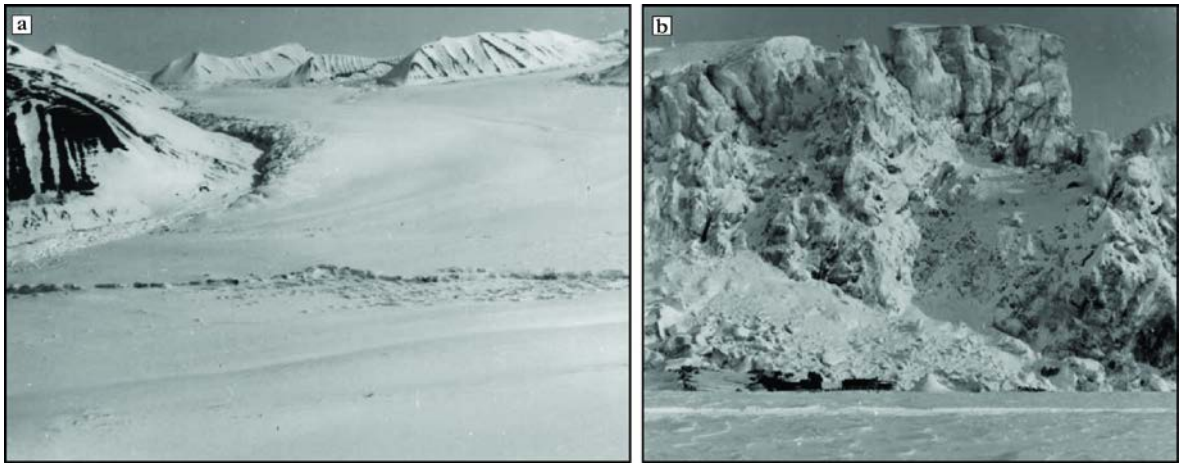

Figure 2.2 - Surge front of Bakaninbreen, Svalbard, in 1987. (a) Oblique aerial view of surge front looking upglacier. (b) Detail of surge front with snowscooter for scale. (Photographs by N. Riley; from Murray and Porter, 2001).

2.3. Surge mechanisms

The controls on the switch between low quiescent phase and higher active phase velocities displayed by all surges are incompletely understood (Woodward *et al.*, 2002; Clarke, 2005). This is undoubtedly in some part due to the variety in some surge characteristics between regions and individual glaciers, but also in spite of the fact that a number of other characteristics are common to all surges (Rea and Evans, 2011; see *2.2*). Previous suggestions for the triggering mechanism include earthquakes (Tarr and Martin, 1914), volcanic activity (Nielsen,

1937), englacial "ice-dams" (Nielsen, 1969), and landslides (Gardner and Hewitt, 1990). However, according to current understanding the switch appears to be due to a change in basal conditions, controlled by the reorganisation of the subglacial drainage system and influenced by glacier thermal regime and bed-type. Three theoretical models have been proposed, chiefly based on observations from active surges; a hard-bed hydrologic switch (cf. Kamb, 1987) and a soft-bed hydrologic switch (cf. Björnsson, 1998) for temperate glaciers, and a soft-bed thermal switch for polythermal glaciers (cf. Fowler *et al.*, 2001).

2.3.1. Hard-bed hydrologic switch (temperate)

Observations from the 1982-83 Variegated Glacier surge led to the development of a theoretical model for surging within temperate glaciers overlying hard bedrock (Kamb *et al.*, 1985; Kamb, 1987). This theory, often described as the linked-cavity mechanism, relies on the transition from an efficient quiescent phase drainage system dominated by tunnels cut into the base of the glacier (R-channels), to an inefficient, distributed linked-cavity system at the ice-bedrock interface (Figs 2.3a and 2.3b). This drainage configuration restricts the flow of water, elevating basal water pressures and causing rapid basal sliding which dominates the surface velocity (Kamb, 1987). The precise trigger which forces the breakdown in the efficient drainage system has never been specifically identified, but is assumed to be the result of thickening in an upper reservoir zone during quiescence leading to higher driving stresses and surface velocities, until a critical point is reached and the tunnel system collapses (Kamb, 1987; Rea and Evans, 2011). Lingle and Fatland (2003) suggested that the slow downward movement of a sufficiently large volume of englacially-stored water during winter could be responsible for overwhelming the basal drainage system. In reality, the linked-cavity mechanism may only be applicable to some temperate surges in Alaska, as many surge-type glaciers in other regions are underlain by unlithified sediments (Clarke *et al.*, 1984; Björnsson, 1998; Murray *et al.*, 2003b). Indeed, Rea and Evans (2011) have questioned whether the model is even fully applicable to Variegated Glacier, where soft sediments are thought to have been responsible for up to 50% of the pre-surge summer surface velocity in 1979 and 1980 (Harrison and Post, 2003).

2.3.2. Soft-bed hydrologic switch (temperate)

A second, not hugely dissimilar, theory has been proposed for temperate glaciers underlain by unlithified sediments, supported by observations from a number of Icelandic surges (Björnsson, 1998). During quiescence, effective pressure at the base of the glacier increases as the pore water pressure and permeability of basal sediments increase. Subglacial drainage is focused in "pipes" within the sediment, which preferentially remove fines (Clarke *et al.*, 1984; Fowler *et*

al., 2001). At some, again unspecified, threshold, the efficient pipe drainage system collapses and is replaced by an inefficient distributed system, elevating basal water pressures across the bed (Rea and Evans, 2011). This threshold may be reached as mass builds up in an upper reservoir zone leading to higher driving stresses and surface velocities, and/or by the slow downward movement of englacially-stored water (Lingle and Fatland, 2003). According to this model, a topographic ramp should form in the ice surface as the surge propagates downglacier, because the activation wave velocity equates to the surge front (Rea and Evans, 2011). This theory is probably most applicable to Icelandic surges, many of which are underlain by unlithified sediment and have inefficient drainage systems during at least part of the surge (Björnsson, 1998; Bennett *et al.*, 2000; Björnsson *et al.*, 2003; Rea and Evans, 2011).

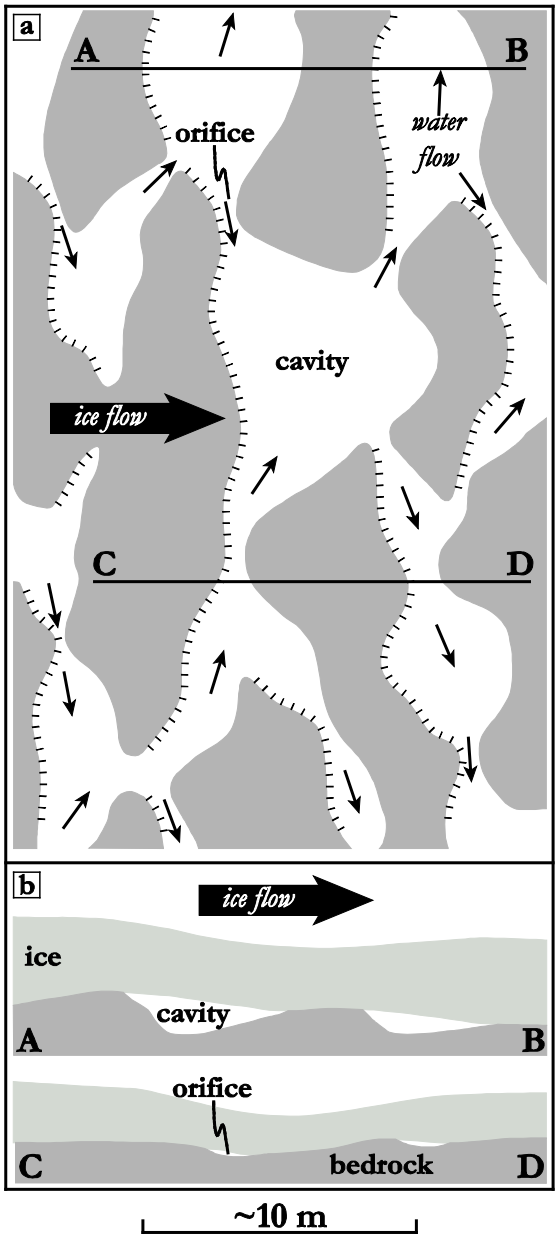

Figure 2.3 - Schematic illustration of the linked cavity basal drainage system portraying a small area of the glacier bed. Areas of ice contact with the bed are shaded in grey; areas of ice-bed separation are blank. (a) Map view of system. Ice separates from the bed along the hatched lines and reconnects with the bed along the plain lines. (b) Vertical cross sections along lines A-B and C-D shown in (a). The blank areas between ice and bedrock are water-filled volumes formed by ice-bed separation in the sliding process. The size of the orifices along C-D has been exaggerated for visibility in the diagram. (Adapted from Kamb, 1987).

2.3.3. Soft-bed thermal switch (polythermal)

In polythermal glacier surges, the switch from slow to fast ice velocities is thought to be controlled by a combination of the glacier thermal regime and the thickness and permeability of the unfrozen unlithified bed (cf. Clarke *et al.*, 1984; Fowler *et al.*, 2001). The Fowler *et al.* (2001) theory is primarily based on observations from Bakaninbreen (Murray *et al.*, 1997, 1998, 2000) and Trapridge Glacier (Clarke *et al.*, 1984), but is thought to be applicable to most, if not all, surging glaciers on Svalbard, the majority of which are polythermal and tend to overlie sedimentary bedrock (Hamilton and Dowdeswell, 1996; Jiskoot *et al.*, 1998, 2000; Murray *et al.*, 2003b). At the beginning of quiescence, the glacier is assumed to be either entirely cold-based or polythermal. Mass accumulates in the reservoir zone until the pressure melting point is reached over at least some of the bed, increasing basal water pressure. If the thickness and permeability of the unfrozen basal sediments are both low then drainage is impeded, leading to elevated pore water pressures and weakening the underlying till (Fowler *et al.*, 2001). Elevated pore water pressures leads to increased sediment deformation and frictional heating, providing a feedback mechanism which results in further melting and, in turn, increased pore water pressures. This positive feedback eventually leads to rapid basal motion and the initiation of the surge, which propagates both up- and downglacier as an activation wave at the thermal boundary between warm and cold ice (Murray *et al.*, 2000; Fowler *et al.*, 2001). If the surging ice velocity is greater than the activation wave velocity then a steep topographic surge front forms at the downglacier propagating thermal boundary (e.g. Clarke *et al.*, 1984; Murray *et al.*, 1997; Fowler *et al.*, 2001; Figs 2.1b and 2.2a). If the activation wave velocity is greater than or equal to the ice velocity, no surge front forms and the tectonic regime is extensional throughout the glacier (Rea and Evans, 2011). This is thought to be the case when there is no or very low resistance to ice flow at the margin, such as at tidewater glaciers that terminate in sufficiently deep water (Hodgkins and Dowdeswell, 1994; Murray *et al.*, 2003a,b). Surge termination may occur when the pressurised water escapes, possibly through pre-existing holes in the underlying permafrost (Smith *et al.*, 2002). The rate of surge termination is controlled by the rate of ice thinning, which may explain the prolonged terminations characteristic of some surges in Svalbard (Murray *et al.*, 2003b). Post-surge, the thinned glacier refreezes to the bed and the surge cycle begins again.

2.4. Surge-like behaviour

Meier and Post (1969) first noted that surging is a complex process covering a broad range of behaviours and characteristics and, as a result, it has becoming increasingly clear that traditional definitions are too restrictive. Perhaps the best example of this is the suggestion that surges

occur independently of external forcing, such as climate variations (Meier and Post, 1969; Post, 1969; Raymond *et al.*, 1987). Whilst it is widely accepted that the precise triggering mechanisms are internally generated (cf. Kamb, 1987; Fowler *et al.*, 2001; see *2.3.*), it is also evident that climatic changes exert a strong influence on surge timing, behaviour, characteristics and even the ability of some glaciers to surge (Dowdeswell *et al.*, 1995; Hodgkins *et al.*, 1999; Eisen *et al.*, 2001; Hansen, 2003; Eisen *et al.*, 2005; Frappé and Clarke, 2007; Hewitt, 2007; Flowers *et al.*, 2011; Striberger *et al.*, 2011). Climatic conditions clearly control the rate of net mass accumulation in the reservoir zone during quiescence. In Svalbard, the end of the Little Ice Age (LIA) was marked by an abrupt increase in mean annual air temperature after about 1920 (Hanssen-Bauer and Førland, 1998), which has led to reduced mass balance and a sustained period of retreat for most Svalbard glaciers (Nuth *et al.*, 2010). This period has also seen a marked reduction in the number of glaciers surging at one time, from 18 in the mid-1930s down to 5 in 1990, suggesting that there is a link between the change in climate and the intensity of surge activity (Dowdeswell *et al.*, 1995). The shift in mass balance also appears to have prevented glaciers which have surged in the past from accumulating sufficient mass to initiate future surge activity, thus removing them from the surge cycle (Hodgkins *et al.*, 1999; Hansen, 2003). An example of this is Scott Turnerbreen, which surged in the 1930s (Hagen *et al.*, 1993), but has received no net mass accumulation since and appears to be entirely cold-based throughout (Hodgkins *et al.*, 1999). This raises the possibility that a number of other currently small, cold-based glaciers in Svalbard may have exhibited much more dynamic behaviour, perhaps reminiscent of surging, under more favourable conditions during the LIA; such observations of increased glacier activity during the LIA have been reported from northwestern North America (Cruickshank, 2001).

Other examples of a climatic influence on surge activity include Variegated Glacier, where annual mass balance during the twentieth century has been demonstrated to exert a control on the length of the surge return period (Eisen *et al.*, 2001). It was also suggested that high summer temperatures contributed to the premature termination of its most recent surge in 1995 (Eisen *et al.*, 2005). Conversely, an unusually large grouping of tributary glacier surges in the Karakoram Himalaya has also been attributed to high temperatures (Hewitt, 2007). It has also been suggested that climate-driven mass balance changes may be responsible for ephemeral, perhaps episodic surge-like behaviour (Hoinkes, 1969; Lovell *et al.*, 2012). Further observations adding to the wide range of surging behaviour include the suggestion that some ice streams may also exhibit cyclical behaviour, although with different periodicities (Bougamont and Tulaczyk, 2003; Hulbe and Fahnestock, 2007). This is perhaps unsurprising, given that the internal mechanisms for rapid flow in both ice streams and surge-type glaciers may be similar,

and related to elevated basal water pressures and/or a soft, slippery bed (Alley *et al.*, 1986; Kamb, 1987; Engelhardt and Kamb, 1998; Fowler *et al.*, 2001). Together, these examples support the suggestion that surging may simply be an extreme end-member in a continuum of pulsating flow behaviour (cf. Raymond *et al.*, 1987).

2.5. Identifying surges: Glaciological characteristics

The identification of both contemporary and former surge-type glaciers is important for a number of reasons. In certain modern environments, studying surges can provide valuable information about glacier response to climate change (Dowdeswell *et al.*, 1995; Eisen *et al.*, 2001; Nuth *et al.*, 2010) and contributions to sea-level rise (Hagen *et al.*, 2003; Christoffersen *et al.*, 2005), as well as the absolute duration of the surge cycle (Dowdeswell *et al.*, 1991, 1995). As a result of their unique characteristics and dynamics, contemporary surge-type glaciers are instantly recognisable by their surface features (Meier and Post, 1969; Evans and Rea, 1999). This is particularly valuable as few glaciers have been continually observed throughout the surge cycle, largely due to the long duration of the quiescent phase and short duration of the active phase, lack of continuous monitoring, and their often remote and inaccessible locations (Grant *et al.*, 2009). Copland *et al.* (2003) synthesised the main glaciological criteria that can be used to identify surge-type glaciers (Table 2.2), and the key elements of these will be discussed in further detail below.

An increase in crevassing leading to a heavily-crevassed surface is often the first indication of the initiation of the active phase (Meier and Post, 1969; Hagen *et al.*, 1993; Copland *et al.*, 2003; Figs 2.4a and 2.4b). The formation of crevasses is controlled by the glacier tectonic regime (cf. Rea and Evans, 2011), which is dominated by zones of extensional and compressive flow during a surge (McMeeking and Johnson, 1986; Hodgkins and Dowdeswell, 1994). Extensional flow dominates where ice propagation velocities are high, and compressive flow occurs where surging ice meets inactive ice (McMeeking and Johnson, 1986; Hodgkins and Dowdeswell, 1994; Lawson *et al.*, 1994; Rea and Evans, 2011). Surges are not only characterised by an increase in crevasse formation, but also the spread of crevassing both up and down glacier, which is often associated with the passage of the surge front as non-surging ice is activated (Lawson *et al.*, 1994). In some tidewater surges in Svalbard, the pattern of crevassing appears to spread upglacier from the terminus, suggesting that the surges initiate at the front and ensuring an extensional regime throughout (Hodgkins and Dowdeswell, 1994; Murray *et al.*, 2003b). Rea and Evans (2011) provide a more in-depth analysis of the link between crevassing and surges.

Table 2.2 - Glaciological and geomorphological criteria for identifying surging glaciers.

Criteria	Description
Glaciological [1]	
(a) Looped moraines	Produced when medial moraines are deformed due to adjacent faster flowing surge-type glaciers and less active glaciers
(b) Deformed ice structures	In particular foliation, formed in a similar way to looped moraines
(c) Heavy crevassing	Indicative of the active phase of the surge cycle and develops due to increased longitudinal extension and compression
(d) Surface potholes	Typical of the quiescent phase; they form in crevasses that opened during the active phase or in depressions between transverse ridges
(e) High surface velocities	Occur during the active phase of the surge cycle
(f) Rapid glacier terminus advance	Indicative of the active phase of the surge cycle, particularly noticeable when surrounding glaciers have a relatively stable or retreating ice-margin position
(g) Shear margins on the glacier surface	Develop at the boundary between fast- and slow-flowing ice
(h) Strandlines of ice	Formed on the adjacent valley sides due to rapid thinning of the upper reservoir zone
(i) Splayed terminus	Terminus is splayed into lobes by longitudinal crevasses
(j) Steep surge front	Forms where surging ice meets inactive ice or at a thermal boundary
(k) Glacier naled accretions	Extrusive stratified ice accretion formed proglacially when successive discharge of water during the winter inundates frozen ground
Geomorphological [2]	
(a) Thrust/push moraines	Form as a result of marginal thrusting due to ice advance into proglacial sediments (e.g. glaciofluvial, glacier naled) and can result in belts of arcuate thrust ridges. In areas where sediment is limited, low-amplitude push moraines develop
(b) Overridden thrust moraines	Former thrust blocks are overridden by ice and form ice-moulded 'cupola' hills
(c) Concertina eskers	Develop during short-lived, high-discharge events which occur just prior to or immediately after surge termination
(d) Crevasse squeeze ridges	Form upon surge termination. As the glacier settles back to its bed, water-saturated sediments are squeezed up into basal crevasses that formed during the surge and are subsequently preserved in the foreland as a series of cross-cutting diamicton ridges
(e) Streamlined glacial lineations	Can indicate evidence for rapid ice advance over significant distances and often occur in association with crevasse squeeze ridges
(f) Hummocky moraine	Produced in belts at the margin of glaciers and consist of a chaotic landscape with kame and kettle topography, which evolves from the thrusting, squeezing and bulldozing of sediments and melt-out of buried ice (however, other origins are possible)
(g) Ice-cored outwash and glaciolacustrine sediments	Form in low-lying areas of the glacier snout and may be buried by large outwash fans and glaciolacustrine sediments. Subsequent modification by melt-out of underlying ice leads to a typically pitted, hummocky surface not dissimilar to (f)

[1] From Copland *et al.* (2003); Yde *et al.* (2005); Grant *et al.* (2009).
[2] From Evans and Rea (1999, 2005); Ottesen and Dowdeswell (2006); Evans *et al.* (2007); Ottesen *et al.* (2008).
Table adapted from Grant *et al.* (2009).

Many glacier surges are associated with a rapid advance of the terminus, usually when the surge front reaches the margin (e.g. Hagen, 1988; Björnsson *et al.*, 2003; Figs 2.4c and 2.4d). Some glaciers advanced ~10 km during surges (Liestøl, 1969; Thorarinsson, 1969; Murray *et al.*, 2002; Roberts *et al.*, 2009; Sund and Eiken, 2010), and the largest recorded advance of up to 20 km was during the 1936-38 surge of Bråsvellbreen, Svalbard (Schytt, 1969). Surges can produce splayed lobate margins (Fig. 2.4d) and advances of tidewater surge-type glaciers are often reported to be associated with a considerable increase in calving (Liestøl, 1969; Hodgkins and Dowdeswell, 1994; Murray *et al.*, 2002; Copland *et al.*, 2003; Sund and Eiken, 2010), although there are also observations of suppressed calving during surges (Mansell *et al.*, 2012).

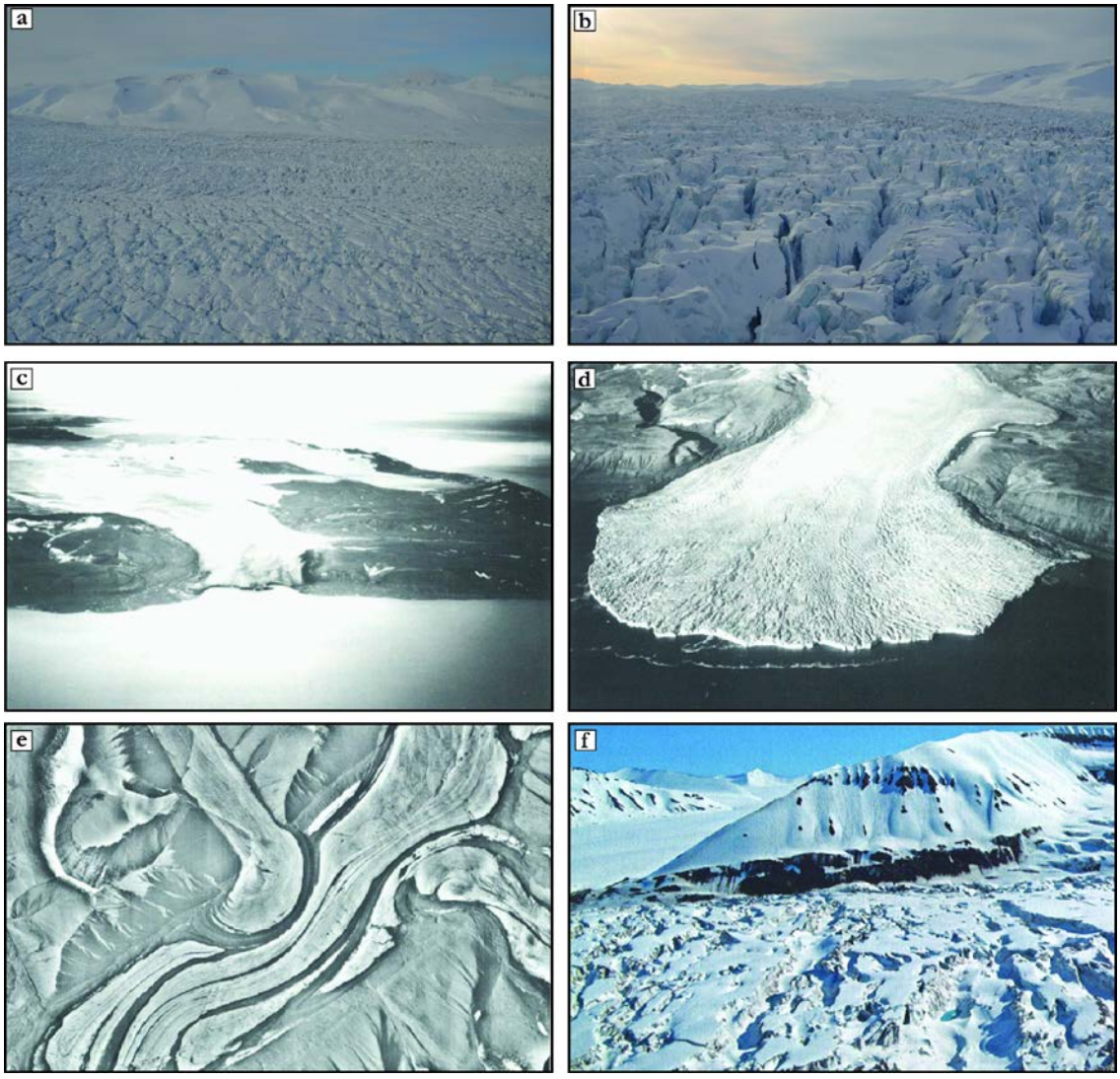

Figure 2.4 - Glaciological characteristics of surging glaciers on Svalbard. (a) and (b) Intense crevassing on the surface of Nathorstbreen mid-surge in April 2011. (c) Terminus of Freemanbreen on Barentsøya pre-surge in 1936; and (d) immediately after a surge in 1956. Note the advance of the terminus and development of a splayed lobate margin. (e) Looped moraines on Battyebreen many years after a surge. (f) The depleted reservoir area of Skobreen in 2006 following a surge. Note the dark band of abandoned pre-surge ice, indicating a drawdown of up to 50 m, and the intense crevassing. (Photographs (c), (d) and (e) from Hagen *et al.*, 1993; (f) by Doug Benn, from Benn and Evans, 2010).

Additional characteristics of surge-type glaciers outlined by Copland *et al.* (2003) include looped moraines (Fig. 2.4e) and deformed ice structures, which are formed as a fast flowing surging glacier flows past less active neighbours, distorting both the medial moraines between them and ice structures (e.g. foliation); the development of a surge front (see *2.2.2.* and Fig. 2.2a); shear margins delimiting the boundary between surging and non-surging ice; potholes which form in crevasses or between transverse ridges on the glacier surface during quiescence; and strandlines of ice abandoned on the valley side as the reservoir area thinned

rapidly (Fig. 2.4f). A further possible characteristic is the development of glacier naled (also known as aufeis or icing), which has been reported from surges in Greenland (Yde and Knudsen, 2005; Roberts *et al.*, 2009) and Svalbard (Liestøl, 1969). This was attributed to the unstable glacial drainage system, basal cavities and enhanced basal melt rates associated with surges, which mean that winter run-off is likely to increase during the active phase (Yde *et al.*, 2005).

It is clear that many of the characteristics outlined above and in Table 2.2 can also occur at non-surge-type glaciers and so care should be taken when using these criteria. Most features cannot be reliably used in isolation to identify a surging glacier, apart from looped moraines, but the presence of many of the features together is suggestive of surge behaviour (Copland *et al.*, 2003). For example, velocity increases and heavy crevassing can also occur during the tidewater glacier cycle (Meier and Post, 1987). Likewise, some criteria are more diagnostic of surge activity than others; glacier naled could only reliably be invoked as evidence for a surge-type glacier when in conjunction with more robust criteria. However, these characteristics do allow surging glaciers in remote locations to be identified from satellite images, aerial photographs and commercial flights (Dowdeswell and Benham, 2003), which is particularly important in Svalbard where glaciers are typically already heavily crevassed and fast-flowing by the time a surge is noticed (Murray *et al.*, 2003a).

2.6. Identifying surges: Geomorphological characteristics

Identifying evidence for surges in the palaeo-record can aid reconstructions of former ice sheet and glacier dynamics (Lovell *et al.*, 2012) and their links to the ocean-climate system (Clark *et al.*, 2002; Domack *et al.*, 2005). In addition, the beds of modern surge-type glaciers are largely inaccessible, and so the landforms and sediments associated with past surges provide a unique opportunity to investigate the subglacial processes that control the periodic switch between slow and rapid ice flow (Christoffersen *et al.*, 2005). For these reasons, the geomorphological and sedimentological record of glacier surges is an important area of research that has received a lot of attention over the years (e.g Sharp, 1985a,b; Knudsen, 1995; Bennett *et al.*, 1996, 1999; Boulton *et al.*, 1996, 1999; Hambrey *et al.*, 1996; Evans *et al.*, 1999; Woodward *et al.*, 2002, 2003a; Evans and Rea, 2005; Larsen *et al.*, 2006; Benediktsson *et al.*, 2008, 2009, 2010; Kristensen *et al.*, 2009a,b; Roberts *et al.*, 2009; Murray and Booth, 2010; Brynjólfsson *et al.*, 2012). The focus of much of this work has been to develop robust criteria for the landform and sediment assemblage, or landsystem (cf. Evans, 2005), produced by surges, which can be used to interpret evidence for possible former surging in the geological record (Evans and Rea, 1999, 2005) and to identify recent surges of modern glaciers (Grant *et al.*, 2009). This section will

briefly outline the characteristics of the Evans and Rea (1999, 2005) and Ottesen *et al.* (2008) surging glacier landsystems (Figs 2.5a and 2.5b; Table 2.2), which are based on a range of observations from the terrestrial and marine margins of surging glaciers in Alaska, Canada, Iceland and Svalbard. Additional landsystems have also been proposed for polythermal surge-type glaciers in Greenland (Roberts *et al.*, 2009; Fig. 2.5c) and small cirque surge-type glaciers in northwest Iceland (Brynjólfsson *et al.*, 2012; Fig. 2.5d), which share a number of characteristics with the Evans and Rea (1999, 2005) landsystem.

2.6.1. Thrust/push moraines

The rapid advance of a glacier terminus into proglacial sediments during a surge can produce moraines typically characterised by large-scale internal tectonic structures, often referred to as composite ridge systems or push moraine complexes (Sharp, 1985b; Croot, 1988; Evans and Rea, 1999; Bennett, 2001; Benediktsson *et al.*, 2008, 2009, 2010; Figs 2.5a, 2.6a and 2.6b). Thrust and push moraines are formed by proglacial deformation as the surge advances into pre-existing sediments, which can consist of subglacial, glaciofluvial, glaciolacustrine and glaciomarine material (Boulton *et al.*, 1996; Hart and Watts, 1997; Boulton *et al.*, 1999; Kristensen *et al.*, 2009a,b; Roberts *et al.*, 2009) and may be seasonally frozen, unfrozen or contain areas of permafrost (Evans and Rea, 1999). Croot (1988) made the observation that composite ridge systems were common at the margins of surge-type glaciers in Svalbard, and suggested they were a key indicator of surge behaviour. However, it has also been argued that surges are not necessary to form such sequences, with some studies invoking englacial thrusting within polythermal glaciers as an alternative mechanism for their formation (Hambrey and Huddart, 1995; Huddart and Hambrey, 1996; Bennett, 2001). Swath bathymetry from a number of Svalbard fjords has also revealed lobe-shaped debris flows on the distal side of terminal moraines associated with tidewater surges, in addition to small annual moraines produced by post-surge terminus retreat (Ottesen and Dowdeswell, 2006; Ottesen *et al.*, 2008; Fig. 2.5b), neither of which are observed in terrestrial surging glacier landsystems.

2.6.2. Concertina eskers

Eskers with a ‘concertina’ or ‘zig-zag’ appearance (Figs 2.5a and 2.6c) have been observed at the margins of surging glaciers in Iceland, and were suggested to be a result of active phase compression in the glacier snout shortening pre-surge sinuous eskers (Knudsen, 1995). However, Evans and Rea (1999) argued that any pre-surge eskers were likely to be destroyed by the compressional regime associated with the passage of the surge front, and instead suggested that concertina eskers form during an abrupt high-discharge drainage event associated with the

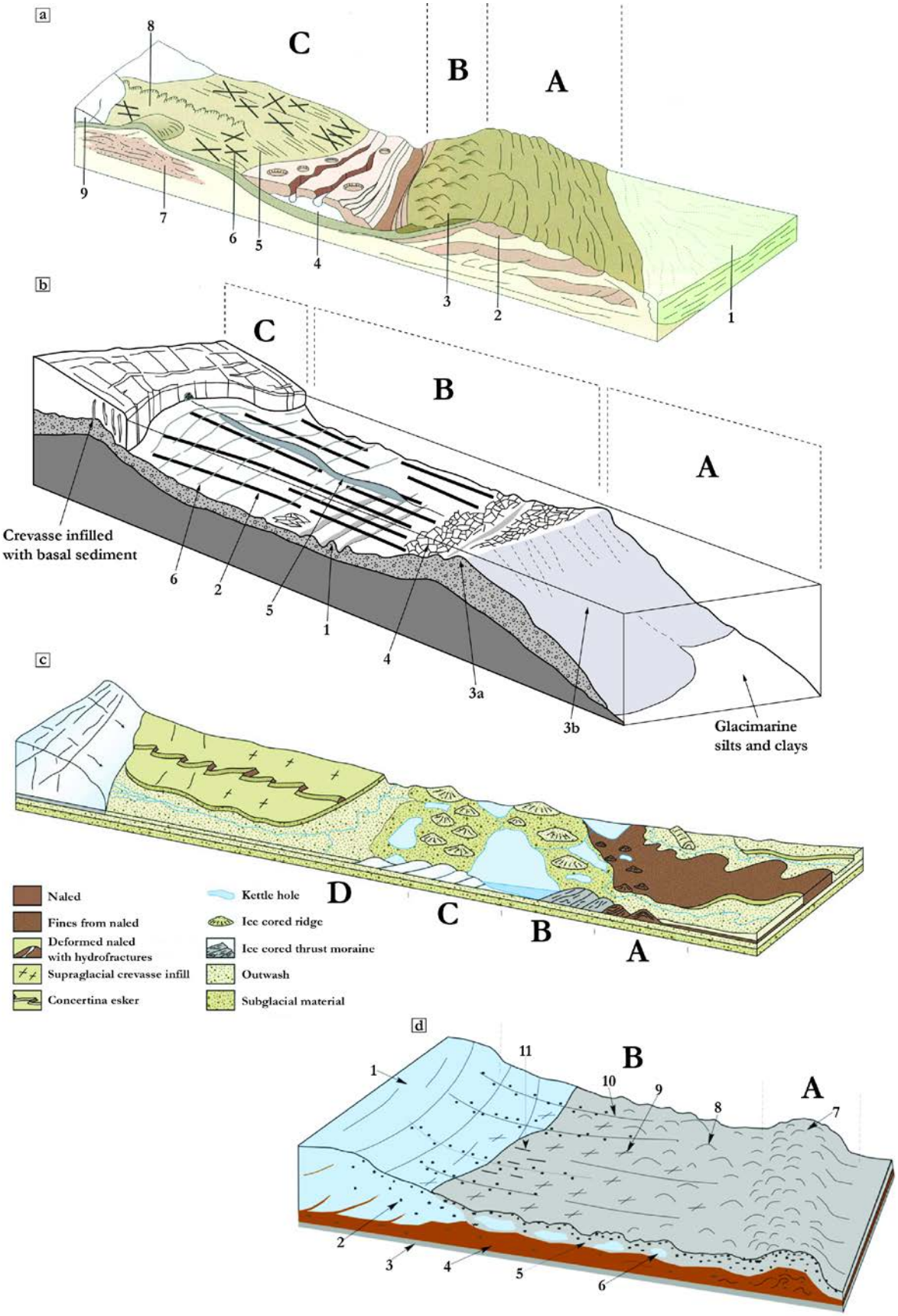
a
C
B
A
8
9
7
6
5
4
3
2
1
b
C
B
A
Crevasse infilled
with basal sediment
6
2
5
1
4
3a
3b
Glacimarine
silts and clays
c
D
C
B
A
Naled
Fines from naled
Deformed naled
with hydrofractures
Supraglacial crevasse infill
Concertina esker
Kettle hole
Ice cored ridge
Ice cored thrust moraine
Outwash
Subglacial material
d
B
A
1
11
10
9
8
7
2
3
4
5
6

Figure 2.5

Figure 2.5 (preceding page) - (a) Surging glacier landsystem (Evans and Rea, 1999, 2005). (A) Outer zone of proglacially thrust pre-surge sediment. (B) Zone of weakly developed supraglacial hummocky moraine. (C) Inner zone of flutings, crevasse squeeze ridges and concertina eskers. (1) Proglacial outwash fan. (2) Thrust/push moraine. (3) Hummocky moraine. (4) Stagnating surge snout covered by pitted and channelled outwash. (5) Flutings. (6) Crevasse squeeze ridge. (7) Overridden and fluted thrust moraine. (8) Concertina esker. (9) Glacier with crevasse squeeze ridges emerging at surface. (b) Svalbard tidewater surging glacier landsystem, based on swath bathymetric data from Borebukta, Rindersbukta and Van Keulenfjorden (adapted from Ottesen and Dowdeswell, 2006 and Ottesen *et al.*, 2008). Individual landform assemblages are numbered in order of formation. (A) Outer fjord. (B) Inner fjord. (C) Tidewater glacier. (1) Overridden recessional moraines. (2) Streamlined glacial lineations. (3a) Terminal moraine of glacier advance. (3b) Lobe-shaped debris flows. (4) Rhombohedral crevasse squeeze ridge network. (5) Esker. (6) Transverse annual retreat moraines. (c) Polythermal surge valley landsystem based on Kuannersuit Glacier, western Greenland (Roberts *et al.*, 2009). (d) Small surge-type cirque glacier landsystem based on examples in northwest Iceland (Brynjólfsson *et al.*, 2012). (A) Distal zone. (B) Proximal zone. (1) Glacier snout. (2) Rocks and sediment. (3) Basaltic bedrock. (4) Subglacial sediment. (5) Supraglacial and englacial sediment. (6) Dead ice. (7) Terminal moraine. (8) Hummocky moraine. (9) Crevasse-fill ridge. (10) Medial moraine. (11) Flute.

termination of the surge (cf. Kamb *et al.*, 1985). Few concertina eskers have been reported at the margins of contemporary surging glaciers outside of Iceland, or from the Quaternary glacial record, perhaps due to their poor preservation potential (Evans and Rea, 1999). It should be noted that sinuous eskers have been observed at the margins of both terrestrial and tidewater surging glaciers (e.g. Ottesen and Dowdeswell, 2006; Kjær *et al*., 2008; Ottesen *et al.*, 2008; Fig. 2.5b), but as they are also produced by non-surging glaciers this is not a diagnostic characteristic of surging activity.

2.6.3. Geometrical ridge networks

Geometrical ridge networks preserved on the deglaciated forelands of both terrestrial and tidewater surging glaciers (e.g. Sharp, 1985a,b; Solheim, 1985; Bennett *et al.*, 1996; Boulton *et al.*, 1996; Evans *et al.*, 1999; Woodward *et al.*, 2002; Ottesen and Dowdeswell, 2006; Kjær *et al.*, 2008; Ottesen *et al.*, 2008; Kristensen *et al.*, 2009a; Rea and Evans, 2011) are, in most cases, interpreted as crevasse squeeze ridges (Figs 2.5a, 2.5b and 2.6d). These landforms are thought to be the result of soft deformable sediment being squeezed up into a highly-fractured glacier base during or at the end of the active phase, forming sub-vertical or inclined englacial debris structures which are then preserved as the glacier snout stagnates during quiescence (Sharp, 1985a; Solheim, 1985; Evans and Rea, 1999; Ottesen and Dowdeswell, 2006; Rea and

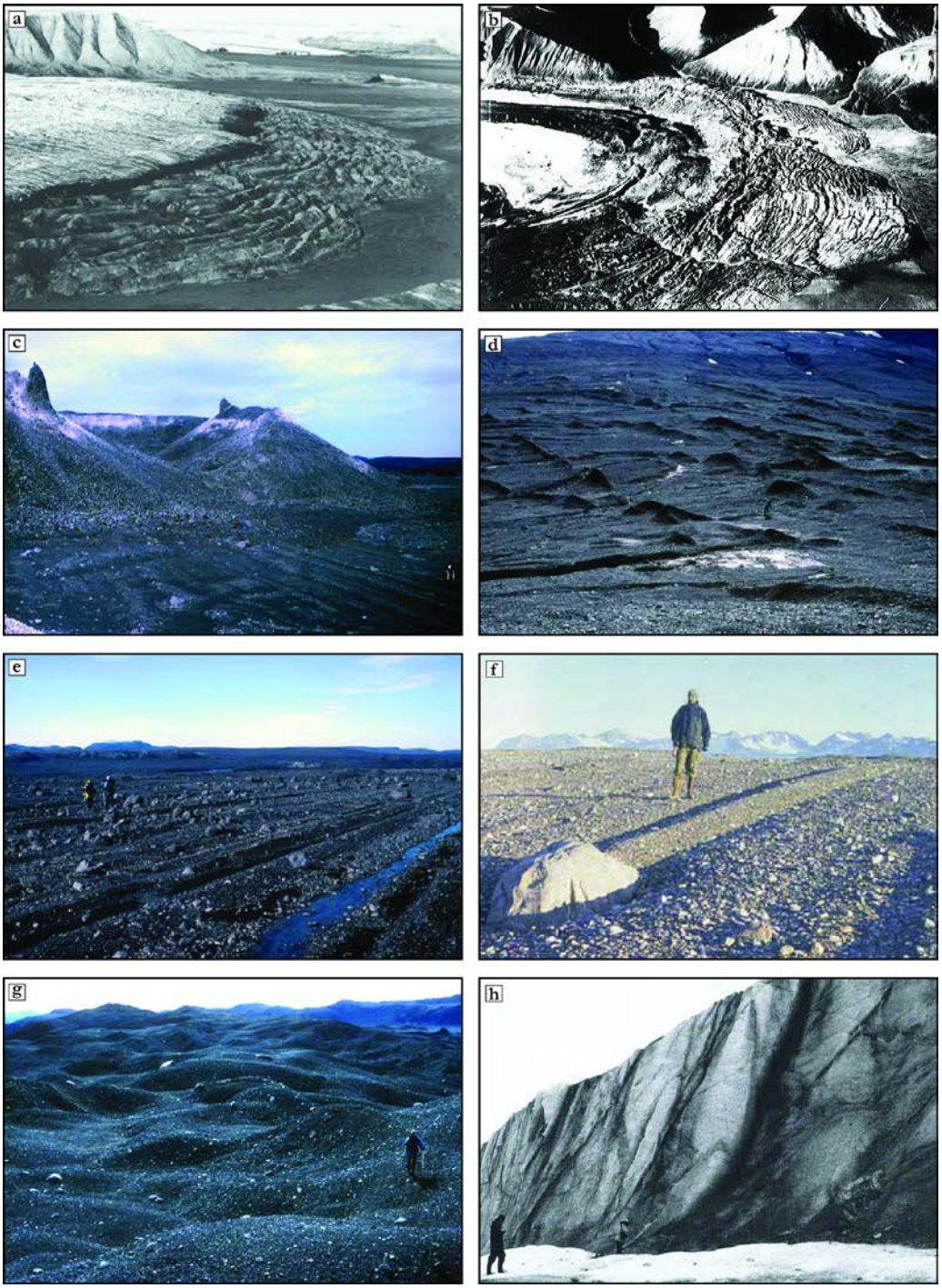

Figure 2.6 - Geomorphological characteristics of surging glaciers. (a) Push moraine system formed at the margin of Usherbreen, Svalbard, following a surge that began in 1978. (b) Norsk Polarinstitutt 1936 oblique aerial photograph of the Holmstrømbreen push moraine system in Svalbard. (c) Ice-cored concertina esker at the margin of Brúarjökull, Iceland. (d) Crevasse squeeze ridges at the margin of Eyjabakkajökull, Iceland. (e) Flutings on the foreland of Brúarjökull. (f) Fluting with initiating boulder at the margin of Elisebreen, Svalbard. (g) Chaotic hummocky moraine marking the former surge limit of Tungnaárjökull, Iceland. (h) Debris-rich structures within the ice cliff of Kongsvegen, Svalbard. (Photographs (a) from Hagen *et al.*, 1993; (b) from Boulton *et al.*, 1999; (c), (d), (e) and (g) by Dave Evans, from Benn and Evans, 2010; (f) from Christoffersen *et al.*, 2005); (h) from Glasser *et al.*, 1998b).

Evans, 2011). Their formation is reliant on crevasses being in contact with the bed, either as bottom-up or full-depth crevasses (Ensminger *et al.*, 2001; Rea and Evans, 2011). Crevasse squeeze ridges on the forelands of contemporary surging glaciers are generally composed of diamicton, of the order of 0.3-3 m high, and typically orientated transverse to ice flow or as part of a conjugate pair at some angle to ice flow; see Rea and Evans (2011) for a more in-depth assessment of their formation.

2.6.4. Streamlined glacial lineations

Flutes, drumlins and mega-scale glacial lineations occur on the forelands of known surging glaciers (e.g. Evans and Rea, 1999; Andrzejewski, 2002; Fuller and Murray, 2002; Christoffersen *et al.*, 2005; Ottesen and Dowdeswell, 2006; Kjær *et al.*, 2008; Ottesen *et al.*, 2008; Johnson *et al.*, 2010; Figs 2.5a, 2.5b, 2.6e and 2.6f). Highly-attenuated bedforms are generally accepted to be formed by rapid ice flow (Stokes and Clark, 2002; Evans *et al.*, 2008; King *et al.*, 2009), such as during the active phase of a surge. As flutings and drumlins are also found at the margins of many non-surging glaciers, it is their close association with crevasse squeeze ridges that is thought to be particularly diagnostic of surging (Sharp, 1985a,b; Evans and Rea, 1999).

2.6.5. Hummocky moraine

Areas of hummocky moraine (cf. Evans, 2009; Fig. 2.5a) have been observed at the margins of known surging glaciers in both Iceland (e.g. Sharp, 1985b; Evans and Rea, 1999; Benediktsson *et al.*, 2008; Fig. 2.6g) and Svalbard (e.g. Kristensen *et al.*, 2009a). According to Evans and Rea (1999, 2005), the formation of prominent belts of hummocky moraine relies upon the effective transport of subglacial debris to englacial and supraglacial positions, followed by ice stagnation. Crevasse infilling (e.g. Rea and Evans, 2011) and debris-bearing thrust faults (e.g. Glasser *et al.*, 1998b) have been suggested as mechanisms by which the elevation of large volumes of basal sediment occurs. Once in a supraglacial position, this debris cover may insulate the underlying stagnant ice for long periods, raising the possibility that subsequent surges will override, overthrust and incorporate the debris-rich ice of previous surges (Evans, 1989, 2009; Evans and Rea, 1999, 2005; Kjær *et al.*, 2008). Hummocky moraine can also be produced by non-surging glaciers (Evans, 2009) and so should not be used independently as a diagnostic criterion for palaeo-surge activity. Caution should also be applied when interpreting the origin of hummocky moraine in the palaeo-record based on comparisons to modern environments (Evans, 2009). An example of this is the proposed englacial thrusting/Svalbard polythermal glacier analogue for the British Younger Dryas record (Hambrey *et al.*, 1997; Bennett *et al.*, 1998), which fails to

account for the ice-cored nature of most Svalbard moraine belts and, as a result, the complex reworking processes associated with their degradation (Lukas, 2005; Benn and Lukas, 2006; Evans, 2009). In addition, the melting-out of ice-cored outwash and glaciolacustrine sediments can also form a similar pitted, hummocky landform assemblage, which is typically fan-shaped and located in topographic depressions (Evans and Rea, 1999, 2005).

2.6.6. Complex till stratigraphies

Rapid glacier advance into proglacial sediments during a surge can result in the formation of glaciotectonic structures and the thickening of sediments at the margin (e.g. Boulton *et al.*, 1996; Alley *et al.*, 1997; Evans and Rea, 1999). Complex till stratigraphies produced by proglacial and subglacial tectonic deformation, including evidence for folding, thrusting, reworking and sorting, have been reported from Sefströmbreen, Svalbard (Boulton *et al.*, 1996), Kongsvegen, Svalbard (Bennett *et al.*, 1999), Hagafellsjökull Vestari, Iceland (Fuller and Murray, 2002) and Eyjabakkajökull, Iceland (Evans and Rea, 2005; Benediktsson *et al.*, 2010). This evidence can often be found in the internal structure of larger landforms, such as push moraines (e.g. Boulton *et al.*, 1996).

2.6.7. Thrust faulting

Debris-bearing thrust faults have often been proposed as an important mechanism for elevating basal material to englacial and supraglacial positions during surges, particularly in polythermal glaciers (e.g. Bennett *et al.*, 1996, 1999; Hambrey *et al.*, 1996; Hambrey and Dowdeswell, 1997; Murray *et al.*, 1997, 1998; Porter *et al.*, 1997; Glasser *et al.*, 1998b; Hubbard *et al.*, 2004; Roberts *et al.*, 2009; Murray and Booth, 2010). These interpretations are largely based on analysis of the geometry and sedimentology of arcuate, dipping englacial debris-rich structures which typically crop-out on the surface near glacier margins and are often visible in tidewater ice cliffs (Figs 2.6h). Melting out of these thrust fault-derived structures has been suggested to form unique suites of marginal landforms, including hummocky moraine (Hambrey *et al.*, 1997; Bennett *et al.*, 1998) and geometrical ridge networks (Bennett, 1996, 1999; Glasser *et al.*, 1998b). Much of this work was based on observations and geophysical data from the margin of Kongsvegen (Bennett *et al.*, 1996, 1999; Glasser *et al.*, 1998b; Murray and Booth, 2010) and, although the link between the englacial structures and landform-sediment assemblages is unequivocal, their proposed origin as debris bearing thrust faults has been criticised (see Woodward *et al.*, 2002, 2003a,b; Glasser *et al.*, 2003a). This was primarily due to the lack of evidence for displacement, suggested to be a key criterion for identifying thrust faults (Hambrey *et al.*, 1999). Other studies have questioned the importance of widespread thrusting as a

mechanism for elevating large volumes of basal debris (Moore *et al.*, 2010; Rea and Evans, 2011). Although it is widely accepted that thrust faulting does occur in surging glaciers, both Moore *et al.* (2010) and Rea and Evans (2011) suggested that the only existing unequivocal observations are from the 1982-83 Variegated Glacier surge (Raymond *et al.*, 1987; Sharp *et al.*, 1988). In this case, thrusts faults formed as a result of high compressive strain formed as surging ice propagated into stagnant ice. A similar scenario can be envisaged at the thermal boundary that develops during polythermal surges, as warm ice surges into cold-based ice (e.g. Murray *et al.*, 1997, 1998; Fowler *et al.*, 2001; Smith *et al.*, 2002), but Moore *et al.* (2010) suggested that the interpretation of fault structures was usually more equivocal in these cases and, even in surging glaciers, compressive stain rates were rarely sufficient to cause widespread fracturing. Rea and Evans (2011) proposed that a clear separation between thrust faults and thrust-style displacement (TSD) may aid clarification of some of these issues, but that, even so, differential movement within TSD was unlikely to be sufficient to elevate basal debris to the surface of even a moderately thick glacier. Instead, it was suggested that, in most cases, englacial debris structures can be more easily explained as basal crevasse fills (see *2.6.3.*), which were initially vertical upon surge termination but were subsequently deformed during the quiescent phase (Evans and Rea, 1999, 2005; Rea and Evans, 2011), an interpretation favoured by Woodward *et al.* (2002, 2003a) for the Kongsvegen structures. Clearly this remains a key area of debate which also has important implications for interpretations of the palaeo-record (e.g. Hambrey *et al.*, 1997; Bennett *et al.*, 1998a; Lukas, 2005, 2007; Graham *et al.*, 2007; Evans, 2009; Rea and Evans, 2011; see *2.6.5.*).

2.6.8. Basal ice facies

A zone of debris-rich ice is typically found at the base of glaciers and ice sheets, known as basal ice (cf. Knight, 1997; Hubbard *et al.*, 2009). The properties and character of this debris-rich ice sequence can provide an insight into processes occurring at the glacier bed, particularly in relation to the entrainment and transport of sediment (cf. Lawson, 1979; Sugden *et al.*, 1987a; Alley *et al.*, 1997). Basal ice sequences therefore offer great potential for investigating the conditions at the bed of surge-type glaciers, which is of great importance as existing theories for surge mechanisms are thought to be in part related to changes in this zone (Kamb *et al.*, 1985; Fowler *et al.*, 2001). Despite this, very few studies have specifically focused on the formation and deformation of basal ice associated with surge-type glaciers (Sharp *et al.*, 1994; Bennett *et al.*, 2004; Roberts *et al.*, 2009; Larsen *et al.*, 2010). The basal ice sequence of a glacier is typically composed of three main facies, which are often further subdivided into subfacies and can vary significantly in character from site to site (Knight, 1997; Hubbard *et al.*, 2009). In very

simple terms, this sequence consists of a lowermost debris-rich layer (often termed solid/solid stratified facies); a stratified layer consisting of alternating bands/laminae of debris-rich and debris-poor ice (often termed banded/laminated facies); and an upper layer of debris-poor and bubble-poor ice (often termed clean, clotted or dispersed facies). This basal sequence is in turn overlain by debris-poor glacier ice, often termed englacial facies (Hubbard *et al.*, 2000). This stratigraphy is necessarily generalised and a huge degree of variety has been reported across all types of glaciers and from different regions, which is reviewed comprehensively in Knight (1997) and Hubbard *et al.* (2009).

The limited work on basal ice sequences at surge-type glaciers has highlighted the importance of tectonic deformation in their formation, typically resulting in the thickening of units through faulting and folding (Sharp *et al.*, 1994; Larsen *et al.*, 2010). Sharp *et al.* (1994) investigated the basal ice layer of Variegated Glacier following its surge in 1982-83, and identified three main subfacies: a widespread laminated subfacies consisting of alternating debris-rich and clean ice laminae, a clear subfacies consisting of largely bubble-free ice with scattered debris, and an underlying debris-rich solid subfacies characterised by structureless debris. It was suggested that the formation of this sequence could be linked to tectonic processes during the active phase of the surge, resulting in significant thrust-faulting and folding and an overall thickening of the layer, particularly noticeable within the laminated subfacies (Sharp *et al.*, 1994). Tectonic processes were also suggested to play a significant role in the formation of the clear subfacies, which was interpreted as metamorphosed englacial ice. Additional observations included the incorporation of ice blocks into the basal zone through apron overriding (cf. Evans, 1989) as the glacier advanced during the active phase (Sharp *et al.*, 1994). This type of entrainment was also reported from Kuannersuit Glacier by Roberts *et al.* (2009), where parts of the basal ice sequence were interpreted to relate to the incorporation of blocks of glacier naled and englacial ice during the surge. The debris-rich banded ice at Kuannersuit Glacier also displayed clear evidence for faulting and folding, resulting in significant thickening of the sequence and the elevation of basal material to the glacier surface (Roberts *et al.*, 2009; Larsen *et al.*, 2010). It was concluded that the formation of the debris-rich ice at Kuannersuit could be attributed to a combination of incremental (regelation) and *en masse* freeze on of basal debris, with the latter possibly being related to rapid conductive cooling post-surge (e.g. Alley *et al.*, 1997).

This limited number of studies illustrates that basal ice associated with surge-type glaciers can be related to processes that are active during surges, and therefore their investigation may provide an important insight into conditions at the glacier bed which are possibly unique to surges.

2.7. Summary

Surges are a cyclical glaciological phenomenon characterised by long quiescent periods of low ice velocities interspersed with much shorter active phases, during which ice velocities can increase by between 10-1000 times. The global distribution of surging glaciers is remarkably non-random, with distinct clusters in Alaska, Arctic Canada, Greenland, Iceland, Svalbard, Novaya Zemlya, and the Karakoram, Pamir and Tien Shan mountain ranges. The characteristics of the surge cycle vary between clusters, as demonstrated by polythermal surges in Svalbard which typically have longer quiescent and active phases and lower ice velocities than surging glaciers in temperate regions such as Alaska and Iceland. Surges are thought to be internally controlled, although climate can clearly have an influence on surge behaviour, which has led to the suggestion that some glaciers that are no longer able to surge may have been more active in the past. As yet, there is no unifying theory for the precise mechanism that controls surges, but three theoretical triggers have been proposed: the hard-bed hydrologic switch, the soft-bed hydrologic switch (both for temperate glaciers), and the soft-bed thermal switch (polythermal glaciers). A number of glaciological (Copland *et al.*, 2003) and geomorphological (Evans and Rea, 1999, 2005) criteria for identifying surging glaciers have been outlined. Observations from the margins of modern surging glaciers in Svalbard have revealed large volumes of englacial debris, which have provoked different hypotheses about the entrainment and elevation processes responsible. The preservation potential of these features, and the other ice-sediment-landform assemblages produced by surges, is of great importance in order to assess the validity of using observations from Svalbard as modern analogues for the Quaternary record.

2.8. Areas for further research

It is clear from the preceding sections in this chapter that a large amount still remains unknown about surging glaciers, including the precise nature of their triggering mechanisms, the reasons for their non-random geographical distribution, and the full suite of landform/sediment assemblages they produce. For obvious reasons, this project will not be able to address all of these points, but will focus on improving our understanding of the geomorphological and sedimentological imprint of surges. With this in mind, a number of existing research gaps which would benefit from further study can be identified.

Evans and Rea (1999) noted that additional work was necessary in order to refine and improve the surging glacier landsystem model (Fig. 2.5a). In particular, in order to capture the full range of landform-sediment assemblages produced during surges it is important to test the model with further observations from modern High-Arctic glaciers (Evans and Rea, 1999; Christoffersen *et al.*, 2005), as much of the existing landsystem is based on work at the margins

of temperate glaciers in Iceland (Sharp, 1985a,b; Evans and Rea, 1999). Recent work by Ottesen and Dowdeswell (2006) and Ottesen *et al.* (2008) has made important advances in this regard by detailing the submarine landform assemblages produced by a number of tidewater glacier surges on Svalbard (Fig. 2.5b). However, it is also important to assess the terrestrial imprint of surges in Svalbard (e.g. Boulton *et al.*, 1996, 1999; Christoffersen *et al.*, 2005) and its preservation potential, because this has important connotations for the use of Svalbard polythermal glaciers as modern analogues for glacier dynamics during the Quaternary (e.g. Bennett *et al*., 1998; Hambrey *et al.*, 1997; Evans, 2009). Additional observations from Svalbard surges are necessary in order to increase the repertoire of modern analogues and to assess the validity of such interpretations.

Furthermore, it is important to study recent or active surges because they provide an opportunity to observe 'fresh' ice-sediment-landform associations, unaltered by subsequent weathering and other processes, and can provide an insight into their development and any links to surge mechanisms and dynamics (e.g. Hambrey *et al.*, 1996). Very few studies have reported on the ice-sediment-landform assemblages of such glaciers in Svalbard, and those that have reported large volumes of englacial and supraglacial sediment (Hambrey *et al*., 1996; Murray *et al*., 1997; Glasser *et al*., 1998b). The entrainment mechanism of this sediment has been interpreted in different ways, primarily based on evidence from the historical surge of Kongsvegen (Bennett *et al.*, 1996, 1999; Glasser *et al.*, 1998a,b, 2003a; Woodward *et al.*, 2002, 2003a,b; Rea and Evans, 2011; see *2.6.5.* and *2.6.7.*). Therefore, in addition to testing the surging glacier landsystem, it is important to add observations of ice structures and sediments from recently-surged Svalbard glaciers in order to also test the generalised models for debris entrainment that have been hypothesised (Glasser *et al.*, 2003a). This should include the detailed analysis of the effect of surges on basal ice layers, as this has not been studied in Svalbard but could provide an important insight into both debris entrainment mechanisms and the tectonic regime that is active during a surge (e.g. Sharp *et al.*, 1994; Roberts *et al.*, 2009; Larsen *et al.*, 2010). This highlights the need for detailed assessment of the ice-sediment-landform associations produced by glacier surges in Svalbard, focusing on the links between debris-rich basal ice, englacial debris structures, and landforms. This in turn may divulge important information about basal conditions and links to the surge mechanism, surge dynamics, and landform preservation potential. Attempting to close these research gaps may also contribute in some way to the continuing search for a 'unifying surge theory' (cf. Rea and Evans, 2011).

2.9. Research aim

Based on the research gaps identified in *2.8.*, the aim of this thesis is to derive better understanding of the glaciological and geomorphological signatures produced during glacier surges on Svalbard, with a particular focus on how this is recorded in basal ice sequences, glaciological structure, and landform-sediment assemblages.

2.10. Research objectives

The research objectives are:

(1) To assess the characteristics and distribution of basal ice sequences, glaciological structures, and landform-sediment assemblages exposed at the margins of surge-type glaciers on Svalbard through a range of methods including mapping, facies description, sedimentological analysis and stable isotope analysis.

(2) To assess the links between the identified ice-sediment-landform associations and specific processes active during surges.

(3) On the basis of (1) and (2), to derive frameworks for the ice-sediment-landform signatures of surging which can be used to identify surges within glaciers on Svalbard which have not previously been recognised.

(4) To assess possible links between climate and changes to surge behaviour on Svalbard.

Chapter Three
Methods and Study Area

'Memories of 18th century clan migrations involving glacier travel remain vivid in indigenous oral traditions from this region, as do accounts from the 19th century about extremely cold summers and catastrophic consequences of surging glaciers'

Cruickshank (2001; p.378)

3. Methods and Study Area

3.1. Methods

Techniques at a variety of scales were utilised in order to address the research objectives highlighted at the end of *Chapter 2*. These include: the use of remote sensing data, published sources and field mapping to track glaciological changes and map glacial geomorphology; a range of techniques for sedimentological and cryofacies analysis; and the assessment of age constraints through a combination of dating techniques and historical sources. This chapter will briefly outline these methods, all of which are well-established techniques in glaciological and glacial geomorphological studies, starting with the large scale (e.g. remote sensing data sources, geomorphological mapping) through to the small scale (e.g. particle size analysis, stable isotope analysis). The different combinations used at each study site will also be described, as not all techniques were applied at every glacier.

3.1.1 Data sources

3.1.1.1. Published data

A number of different published sources, listed in Table A1 (see appendix), were used to reconstruct the surge history of Tunabreen from 1870 to present day. These include descriptions, photographs and maps from three journal articles in particular: Liestøl (1969), Hodgkins and Dowdeswell (1994), and Plassen *et al.* (2004). The latter source includes mapped terminus positions based on de Geer (1910) and Liestøl (1969). Two Norsk Polarinstitutt (NPI) 1:100,000 scale maps (C8 – Billefjorden, 2000 and 2008 versions) were also used. All maps were scanned and geo-rectified in the same manner as the satellite images. The surge history of Nathorstbreen was assessed using the 1898 map of Van Keulenfjorden from Hamberg (1905) and data presented by Sund *et al.* (2013).

3.1.1.2. Satellite imagery

Several satellite images were used to track glaciological changes during the surges of Nathorstbreen and Tunabreen, with a particular focus on terminus position changes and crevasse pattern developments. Details on the images used are listed in Table A1, including the data type, spatial resolution, date of capture, specific use in this project and source. The image types include Landsat MSS (Multispectral Scanner), TM (Thematic Mapper) and ETM+ (Enhanced Thematic Mapper Plus) scenes, and ASTER (Advanced Spaceborne Thermal Emission and Reflection Radiometer) scenes. All images were imported into ERDAS Imagine 9.3. and geo-rectified using the image geometric correction tool to a projection of Universal Transverse Mercator (UTM) Zone 33N (datum: WGS 84).

3.1.1.3. Aerial photographs

The mapping of surface glaciological structures and glacial geomorphology at all study sites was conducted from overlapping aerial photographs, provided by NPI and the Natural Environment Research Council (NERC) Earth Observation Data Centre (NEODC). Full details on the photographs used can be found in Table A1, including their scale, approximate spatial resolution and source. The photographs were all provided in digital format and were mosaiced using Adobe Photoshop CS5.1. The mosaiced photographs were then geo-rectified to Landsat ETM+ images. In some cases, hardcopies of overlapping photographs were also printed and examined as stereo-pairs using a stereoscope (Lillesand *et al.*, 2008; Boston, 2012).

3.1.2. Glaciological changes

Terminus positions of Nathorstbreen and Tunabreen were identified on all satellite images and published maps and were digitised as shapefiles (.shp) within ESRI ArcGIS 9.2. The differing spatial resolutions of imagery types and the accuracy and precision of geo-rectification are obvious potential sources of error, but for the purposes of this project (e.g. tracking large terminus changes during glacier surge cycles in order to place finer scale mapping and sedimentological work in context) are deemed acceptable. This approach has been used in a number of other studies to track terminus change during glacier surges (e.g. Dowdeswell and Benham, 2003; Benn *et al.*, 2009; Sund and Eiken, 2010). Crevasse pattern changes during the recent surge of Tunabreen were digitised as shapefiles from ASTER images.

3.1.3. Glacial geomorphological and structural glaciological mapping

The mapping of glacial geomorphology and glacier surface features was conducted digitally within ArcGIS. Features were identified based on criteria outlined in Table 3.1. and were digitised as shapefiles directly onto the geo-rectified aerial photographs. Manual mapping using photograph stereo-pairs and acetate overlays helped to accurately represent small areas of geometric ridges in the Tunabreen/Von Postbreen forelands. The acetate mapping was scanned and geo-rectified to the digital aerial photographs by matching prominent features, such as the shoreline, before being digitised. The symbology and mapping style loosely follows that of Evans *et al.* (2006b, 2007, 2009, 2010b, 2012), whereby individual features (e.g. meltwater channels, ridges) are represented as polygons or polylines superimposed on broader land surface types (e.g. outwash, hummocky sediment cover, glacier surface) mapped as polygons. The identification and mapping of structural glaciological features (e.g. longitudinal foliation, fracture traces, arcuate fracture traces) on the glacier surface followed established techniques (e.g. Hodgkins and Dowdeswell, 1994; Lawson *et al.*, 1994; Hambrey and Dowdeswell, 1997; Glasser *et al.*, 1998b; Roberson and Hubbard, 2010; Fleming *et al.*, 2013; Midgley *et al.*, 2013).

Field mapping during visits to all study sites was used to ground-truth and refine the maps. Identified features were described and drawn directly onto annotated aerial photograph

Table 3.1 - Descriptions and identification criteria for mapped glaciological and geomorphological features/landcover types. NHB = Nathorstbreen, TNB = Tunabreen, FWB = Finsterwalderbreen, STB = Scott Turnerbreen, TLB = Tellbreen.

Feature/ landcover type	Identification criteria	Possible identification errors	Study sites
Clean glacier ice	White to light blue surface, often appearing smooth, contains glaciological structures (see below).	Possible confusion with icing and snow cover.	TNB, FWB, STB, TLB
Stratification (S_0)	Irregular, flow-perpendicular linear stripes which appear as slight colour changes on the glacier surface.	Possible confusion with other linear surface structures (e.g. arcuate fracture traces, longitudinal foliation) towards glacier margins.	TNB, FWB, STB, TLB
Longitudinal foliation (S_1)	Thin (<0.1 m), linear flow-parallel stripes on the glacier surface.	Possible confusion with transverse surface structures (e.g. arcuate fracture traces) towards glacier margins.	TNB, FWB, STB, TLB
Arcuate fracture traces (S_2)	Thin (<0.1 m), curvilinear stripes on the glacier surface, generally orientated perpendicular to sub-perpendicular to ice flow, typically 100-200 m in length.	Possible confusion with other linear surface structures (e.g. fracture traces, longitudinal foliation) towards glacier margins.	TNB, FWB, STB, TLB
Fracture traces (S_3)	Thin (<0.1 m), linear stripes on the glacier surface, generally orientated perpendicular to sub-perpendicular to ice flow, typically <50 m in length.	Possible confusion with other linear surface structures (e.g. arcuate fracture traces, longitudinal foliation) towards glacier margins.	TNB, FWB, STB, TLB
Open fractures (S_4)	Linear features on the glacier surface with two identifiable edges separated by a clear gap (>0.5 m). Can contain snow or water.	At thinner end of scale there is possible confusion with closed fractures or longitudinal foliation. Possible, but unlikely confusion with meltwater channels.	TNB, FWB, STB, TLB
Debris-covered glacier	Rough, darker areas on generally flat glacier surface, particularly towards lateral and frontal margins. Often possible to identify individual boulders. Includes both medial moraines and more-widespread sediment cover. Varies from thin (<0.1 m) to thick (>1 m) cover.	Can sometimes be difficult to differentiate between general sediment cover and discrete ridges (see below) on aerial photographs. The delimitation of boundaries between debris-covered ice and ice-cored moraine/till cover can be challenging, and has been determined based on colour, textural and topographic contrasts. As a result, there is a possibility that one or the other has been underestimated/overestimated.	NHB, TNB, FWB, STB, TLB
Type A ridges	Dark, flow-parallel features on glacier surface. Typically 5-100 m long, <10 m wide and <2 m high. Often widen in a downglacier direction. Composed primarily of angular material. Typical debris thickness of <0.1 m over an ice core.	Lateral limits of the ridges can be difficult to determine due to sediment reworking, particularly within areas of widespread debris cover.	STB, TLB
Type B ridges	Arcuate, low (<0.5 m) features orientated perpendicular to ice flow. Typically 5-100 m long and <0.5 m wide. Composed of poorly-sorted diamicton, which has often been reworked as a highly-saturated slurry-like deposit surrounding the ridge core. This deposit is more-extensive in a downglacier direction and increases the apparent width of the ridges by up to 15 m.	Due to slurry-like deposit, it is possible that the width of the ridge core has been overestimated in some cases.	STB, TLB
Type C ridges	Linear features on glacier surface composed of sorted sands and gravels. Typically 5-50 m long, <5 m wide and <2 m high. Often have a sinuous planform, are orientated both perpendicular and sub-parallel to ice flow, and can be superimposed on Type A ridges.	Possible, but unlikely confusion with other surface features (e.g. type B ridges). Also similar to some ridges observed on glacier forelands (e.g. eskers, geometric ridge networks).	STB, TLB
Type D ridges	Small (<10 m2) cones of sorted sands and gravels, often appearing black against the glacier surface. Typically located on the surface immediately adjacent to active/inactive meltwater channels, predominantly in upper areas of the glacier.	Can be difficult to determine feature limits in areas of widespread debris cover.	STB, TLB
Meltwater channels (active)	Linear, often sinuous or meandering glacial meltwater features (1-15 m wide) located both on the glacier surface (typically containing blue water) and in ice-marginal areas (typically turbid water). Often form a highly-braided channel with interstream deposits. In some cases, water is not visible within supraglacial channels but they are still inferred to be active at depth due to the channel width and clarity	Possible to misidentify source of channel and therefore classify incorrectly (e.g. glacial vs. non-glacial, or stream). Possible that some inactive channels have been mapped as active, and *vice-versa*.	NHB, TNB, FWB, STB, TLB
Meltwater channels (inactive/unoccupied)	Linear, often sinuous or meandering erosional features located both on the glacier surface and in ice-marginal areas, typically <5 m wide, which contain no water. Often form braided networks on areas of outwash deposits, in close proximity to active channels.	Possible that some inactive channels have been mapped as active, and *vice-versa*.	NHB, TNB, FWB, STB, TLB
Streams	Linear, often sinuous or meandering features from a non-glacial source (e.g. valley sides, alluvium), typically containing non-turbid water. Often drain onto glacier surface or foreland and join meltwater channel network.	Possible to misidentify source of water and therefore classify incorrectly (e.g. stream vs. meltwater channel).	NHB, FWB, STB, TLB
Lakes and pools	Enclosed or semi-enclosed basins of water (up to 0.01 km2) forming a variety of shapes. Can contain both freshwater and meltwater.	Cloud shadows and dry depressions could be mis-identified as lakes.	NHB, TNB, FWB, STB, TLB
Outwash	Accumulations of fluvial sediment, typically dissected by active and inactive meltwater channels. Can be fan-shaped or form linear corridors surrounding active and inactive channels. Generally appears as a smooth, flat surface with identifiable clasts. Typically has a sharp boundary with surrounding terrain and can contain erosional scars and terracing (identified as breaks-of-slopes).	Possible, but unlikely confusion with sediment plains or debris flow deposits.	NHB, TNB, FWB, STB, TLB
Ridges/ composite ridge systems	Large (up to 500 m long, 100 m wide and 30 m high) semi-continuous discrete arcuate features with positive relief located in a proglacial position, typically conforming to the shape of the ice margin. Can occur as individual ridges or as multiple ridges in a complex. Individual ridge crests have been mapped where identified. Often closely associated with meltwater channels and outwash deposits.	Possible misidentification of ridge limits (e.g. lower break-of-slope). Some difficulties associated with identifying the transition from discrete latero-frontal ridges to lateral moraine (see below).	NHB, TNB, FWB, STB, TLB

Table 3.1 continued

Lateral moraine	Large (> 50 m high) ridges or slopes located above and on either side of glaciers, typically marking the boundary with the non-glacial valley side. Often grade into moraine ridges (see above) further downvalley, and are differentiated from these based on location (high above glacier surface in a lateral position), size and morphology (asymmetric cross-profile with considerably steeper and longer slope on ice-proximal side, compared to discrete ridge with a typically steeper and longer ice-distal slope). The ice-proximal slope often contains both active and older debris-flow scars.	Possible misidentification of boundaries with debris-covered glacier/hummocky till cover and transition to discrete latero-frontal moraine ridges.	TNB, FWB, STB, TLB
Isolated ridges and hummocks	Individual features with positive relief located on glacier forelands, typically < 50 m long, <10 m wide and < 10 m high, with no dominant alignment. Tension cracks are often present on the surface.	These are differentiated from moraine ridges on the basis of their isolated nature and smaller size, but there is the potential for misidentification.	NHB, TNB, FWB, STB, TLB
Geometrical ridges	Thin (<5 m wide) linear features with positive relief located on terrestrial and submarine glacier forelands, often on hummocky or flat sediment surfaces (see below). Can be up to 200 m long and 8-10 m high, but more typically are <5 m high. These ridges form closely-spaced, often interconnected, rhombohedral networks orientated in several directions, but predominantly perpendicular or sub-perpendicular to glacier flow. The ridges are typically sharp-crested, composed of diamicton, and contain little evidence of an ice-core.	Possible, but unlikely confusion with flutes, eskers and type C supraglacial ridges.	NHB, TNB, FWB, TLB
Flutes	Thin (<2-3 m wide) linear ridges located on glacier forelands which are orientated parallel to ice flow. Can be up to 50 m long.	Possible confusion with streamlined sediment cover, proglacial debris stripes and geometric ridge networks, particularly where a variety of orientations are displayed.	TNB, FWB,
Eskers	Sinuous ridges with positive relief up to 200 m long and 10 m wide located on glacier forelands. Typically orientated sub-parallel to ice flow.	Similar morphology to type C ridges on glacier surface raises possible, but unlikely, misidentification problems.	NHB, TNB, FWB, TLB
Proglacial debris stripes	Thin (<0.1 m), linear flow-parallel stripes on the glacier foreland, typically located on sediment plains. Often can be traced to longitudinal foliation on the glacier surface.	Possible confusion with flutes and streamlined sediment cover.	TNB, FWB, TLB
Streamlined sediment cover	Proglacial topography with a strongly parallel linear component evident, but where individual lineations cannot be defined.	Possible confusion with flutes and proglacial debris stripes.	NHB
Hummocky sediment cover	Often rough and irregular surface located on glacier forelands with undulating positive relief, composed predominantly of poorly-sorted diamicton. Individual large boulders and clasts can be identified from aerial photographs. Typically covered by small lakes and pools and debris flows (see below). Often dissected by active and inactive meltwater channels.	Potential errors associated with delimiting boundaries with moraine ridges, lateral moraine and debris-covered glacier.	NHB, TNB, FWB, STB, TLB
Sediment plain	Flat, often smooth, surface located on glacier forelands. Individual large boulders and clasts can be identified from aerial photographs. Geometric ridge networks and flutes are often situated on the surface. Occasionally dissected by active or inactive meltwater channels.	Possible, but unlikely confusion with outwash deposits.	TNB, FWB, TLB
Debris flows (active and inactive)	Smooth surfaces located on glacier forelands typically displaying a stepped or tiered arrangement. Predominantly, although not explicitly, contain erosional scarps (<2-3 m high) at their upper margins, often emanating from the proximal slope of moraine ridges or lateral moraine, or from older debris flow deposits. Freshest examples appear highly saturated and have well-defined scarps. Minor channels and small pools are common. Largest tiered examples are up to 0.01 km2. Predominantly composed of diamicton and sorted lacustrine sediments.	Possible, but unlikely confusion with outwash deposits and sediment plains (see above). Can be difficult to delimit individual features where fresh flows emanate from older debris flow deposits.	NHB, FWB, STB, TLB
Minor depressions	Small topographic hollows, often marking a former lake/pool.	Possible misidentification as lakes/pools.	NHB, TNB, FWB, STB, TLB
Icing	White surfaces located on glacier forelands, typically surrounding the main meltwater channels. Can cover an area of up to 0.5 km2. Pools and active channels are widespread across the surface. Thicknesses of up to 2m were observed in the field, and they are predominantly composed of clean, bubbly white ice.	Could be confused with snow cover.	TNB, FWB, TLB
Snow cover	White surfaces typically located on valley sides or in upper glacier areas. Can take the form of small patches or more widespread cover. Commonly aligned along topographic depressions (e.g. gullys) on valley sides.	Possible confusion with icings in valley floor location.	FWB, STB, TLB
Alluvium	Vegetated low-angle non-glacial surface, often dissected by streams, located at base of steep valley sides and (up to 5-10 m) above active meltwater channel/outwash deposits on valley floor.	Possible overestimation where talus cones are covered in vegetation.	FWB, STB, TLB
Talus	Cones or fans of loose scree material located on valley sides.	Possible underestimation where covered in vegetation towards valley centre.	TNB, STB, TLB
Exposed bedrock	Outcrops of bare surfaces with a rough an irregular upper texture. Usually only small (<300 m2) exposures within glacier forelands, more abundant on valley sides. Can take the form of multiple linear features orientated in the same direction, reflecting geological structures.	Possible, but unlikely confusion with linear unlithified features (e.g. flutes).	FWB, STB, TLB
Valley sides	Steep extraglacial surfaces dissected by streams and gullys. Contain both talus cones and areas of exposed bedrock (see above).	Possible, but very unlikely, problems associated with defining limits with talus cones, bedrock exposures, alluvium and lateral moraine.	NHB, TNB, FWB, STB, TLB

print-outs, which were used in conjunction with field sketches to help differentiate between features (e.g. types of supraglacial ridges) and guide the final mapping. The locations of all features mapped in the field were recorded with a handheld GPS in order to aid their identification on the geo-rectified aerial photographs.

3.1.4. Sedimentology and cryofacies analysis

3.1.4.1. Section logging and facies description

At all study sites, cleaned sedimentary sections were recorded in the field as accurate scaled vertical or two-dimensional logs (Evans and Benn, 2004b). High-resolution photograph mosaics of the full sections were used to log existing detailed structures with greater planimetric accuracy than is often possible in the field. Individual sedimentary units were identified in the field based on visual physical properties (e.g. grain size range, sedimentary structures) and were classified using an adapted version of the Eyles *et al.* (1983) lithofacies code (Evans and Benn, 2004b; Lukas, 2005).

Sections of cryofacies units at Tunabreen and Tellbreen were recorded as scaled two-dimensional logs, both in the field and from photograph mosaics. The physical characteristics of cryofacies units were described in terms of facies thickness, structure, debris content (distribution, grain size range, concentration) and estimated bubble content, as introduced by Lawson (1979) and Hubbard *et al.* (2009). The sedimentary characteristics of debris-rich cryofacies have been classified and analysed in the same manner as outlined above for sedimentary units (Evans and Benn, 2004b). This includes clast shape, clast fabric, debris concentration and particle size analyses, details of which are outlined below in *3.1.4.2.* Cryofacies exposed at the margins of glaciers take a variety of forms, ranging from massive debris-rich ice, which can be almost entirely frozen debris with very little ice content, to clean stratified ice characterised by alternating laminations of bubble-rich and clear ice. Four main cryofacies are typically observed, although these are by no means comprehensive and can exhibit a large range of variability. In stratigraphic order from the base of the glacier upwards, as described by a number of studies (e.g. Lawson, 1979; Knight, 1987, 1997; Sugden *et al.*, 1987a; Sharp *et al.*, 1994; Cook *et al.*, 2010; Larsen *et al.*, 2010), these are: massive, debris-rich ice (typically termed solid facies); alternating thin (millimetre to centimetre scale) laminae or bands of debris-rich ice and debris-poor, bubble-free ice (typically termed laminated or banded facies); debris-poor and often bubble-poor ice characterised by scattered grains and clots of fine sediment (typically termed dispersed or clotted facies); and debris-poor ice characterised by alternating bubble-poor and bubble-rich layers (typically termed englacial facies or simply ‘glacier ice’). Of these, solid, banded/laminated and dispersed/clotted facies are unique to the basal zone of glaciers, and are therefore commonly referred to as basal ice facies (e.g. Knight, 1997; Hubbard *et al.*, 2009). In an attempt to standardise the description and classification of basal ice facies, Hubbard *et al.* (2009) conducted a thorough review of existing case studies and

suggested a reclassification based on grouping descriptively-similar facies from across these different sites. The reclassified cryofacies names of Hubbard *et al.* (2009) have been used as a guideline for classifying the cryofacies observed in this study, although not the descriptive code system suggested by these authors. Descriptively-similar facies have also been interpreted to form through a variety of different processes at different sites (e.g. Cook *et al.*, 2011) and, therefore, in addition to detailed description of their physical characteristics, it is often also important to assess their isotopic compositions (see *3.1.4.3.*).

3.1.4.2. Analytical techniques

Clast shape

At all study sites except Finsterwalderbreen, samples of 50 clasts of a single lithology were extracted at random from each different sedimentary or cryofacies unit to be analysed for shape and roundness characteristics, following the methods outlined in Benn (2004b) and used in a number of different studies (Benn and Ballantyne, 1993, 1994; Lukas, 2005; Evans *et al.*, 2010a; Brook and Lukas, 2012; Lukas *et al.*, 2013). Clasts were sampled within the range 20-200 mm (a-axis length), and in some cases were melted out of debris-rich cryofacies units using a handheld blow-troch (Benn, 2004a). In addition to shape measurements and roundness classifications, clast asymmetry (e.g. 'bullet-shaped' clasts) and surface features (e.g. striations, grooves, gouges, facets) were recorded. Where possible, control samples were taken from deposits with a known history (Benn, 2004b). At Scott Turnerbreen, control samples were taken from talus slopes and at different points along the active meltwater channel. Fluvial control samples were also taken from the active meltwater channel in the Tunabreen-Von Postbreen foreland.

All clast shape data were plotted in TriPlot (Graham and Midgley, 2000). Clast shape data were displayed on ternary diagrams (ratios of c:a and b:a axes) and C_{40} indices were calculated for each sample, following Benn (2004a). Clast roundness data were plotted as frequency distributions and both RA- and RWR-indices were calculated and plotted for each sample (see Benn, 2004a and Lukas *et al.*, 2013).

Macrofabric and structural glaciology

Clast macrofabric data were collected from debris-rich ice and gravel units at Tunabreen and Tellbreen. Samples of 50 clasts with a:b axis ratios of >1.5:1 were selected, and the dip and dip-direction of the a-axes were measured for each clast with a compass-clinometer (cf. Benn, 2004b), following the example of a number of studies (Benn, 1995; Bennett *et al.*, 1999; Christoffersen *et al.*, 2005; Livingstone *et al.*, 2010a). A handheld blow-torch was used to extract clasts which were otherwise difficult to remove. The strike and dip of contacts between sedimentary and cryofacies units, debris bands, bedding, faults and fold axes (cf. Benn, 2004b) were also measured at several sites. At Tunabreen, additional fabric data were collected through

the measurement of the anisotropic magnetic susceptibility of suspended sediment within small (8 mm diameter) debris-rich ice cores (Fleming *et al.*, 2013).

A structural glaciological approach (Hubbard and Glasser, 2005) was applied to englacial and surface structures at Tunabreen, Scott Turnerbreen and Tellbreen. Planar structural elements (e.g. englacial debris-rich bands, fractures, ice stratification) were identified in the field and their strike and dip measured. These field data were then integrated with the structural mapping of the glacier surface, and the structures were classified and coded from S_0 upwards based on order of formation, in accordance with structural geology conventions (Glasser *et al.*, 1998; Hambrey *et al.*, 2005; Roberson and Hubbard, 2010). At Tunabreen and Tellbreen, the dip and dip-direction (linear structure) of sheared englacial debris laminae, or 'mineral stretching lineation' (Fleming *et al.*, 2013), were also recorded. All field-measured fabric data were corrected for magnetic declination from grid north (approximately 5°E) and plotted as equal-area stereographic projections using Stereo32 (Röller and Trepmann, 2008). Stereo32 was also used to calculate fabric statistics (S_1, S_2 and S_3 eigenvalues) following Benn (2004a) and Ó Cofaigh *et al.* (2013), among many others.

Debris concentration

The debris concentrations of cryofacies were measured by percentage volume, following the techniques outlined by Knight (1997) and used by Waller (1997). Decimetre-sized blocks were sampled from sections at Tunabreen and Tellbreen using an ice axe. Any ice clearly affected by surficial melting was removed first, although this was rarely found. The samples were bagged and taken back to the laboratory, where they were allowed to melt in a 1000 ml beaker. Once the samples were fully melted and the debris had settled out, the total volume and the volume of the debris were recorded, allowing the percentage debris concentration to be calculated. Similar to Waller (1997), a value of <1 % was recorded for samples with a very low debris concentration. Some previous studies used techniques which measured weight of sediment per unit volume of ice (Sugden *et al.*, 1987a; Hubbard, 1991; Hubbard and Sharp, 1995; Waller, 1997; Larsen *et al.*, 2010), which has been suggested to be a more accurate method (Waller, 1997). However, this technique is affected by complications arising from the different densities of different rock types (Knight, 1997), which can make interpretations difficult (Waller, 1997). As a result, for ease of both measurement and interpretation the debris concentration by volume method was favoured for this project, as also applied in a number of other basal ice studies (Waller *et al.*, 2000; Cook *et al.*, 2010, 2011; Larson *et al.*, 2010).

Particle size analysis

Samples for particle size analysis were taken from all study sites apart from Finsterwalderbreen. The sample size and collection method varied depending on facies type. Diamicts were collected as ~1 kg bulk samples from unfrozen sedimentary units. Cryofacies units were melted

as part of the debris content measurement process, filtered, and the sediment was then bagged. Smaller samples (~0.25 kg) were collected of finer sedimentary units, such as sands and marine muds. Fine-grained englacial debris laminae were sampled directly from where they had sublimated-out on the ice surface. Once transported to the laboratory, samples were either oven dried at 40°C (sedimentary and cryofacies diamicts) or freeze dried (muds). All samples were gently disaggregated using a rubber pestle and a plastic tray, then dry-sieved at half-phi intervals from -4.0 to 1.0 Φ (16 mm to 500 μm). Each size fraction was weighed and recorded. The sediment finer than 1.0 Φ was treated with hydrogen peroxide to remove organics, disaggregated with a dispersing agent, and analysed using a Beckman-Coulter Laser Sizer. All data were plotted as grain-size distributions using GRADISTAT (Blott and Pye, 2001). Distributions derived from laser sizing (percentage volume) were calculated as a percentage of the entire sample weight, and were plotted together with the distributions derived from sieving (percentage weight) after standardisation. The distinction between these methods has been made clear on the graphs. It is noted that combining data derived from two different methods, although widely practised (Nelson *et al.*, 2005; Cook *et al.*, 2011), may produce misleading or fragmented results which should be interpreted cautiously (Khatwa *et al.*, 1999; Hoey, 2004).

3.1.4.3. Stable isotope analysis

A number of studies have applied stable isotope analysis in glaciological research (Lawson, 1979; Jouzel and Souchez, 1982; Sugden *et al.*, 1987a; Knight, 1989; Hubbard and Sharp, 1995; Iverson and Souchez, 1996; Hubbard *et al.*, 2000; Glasser and Hambrey, 2002; Cook *et al.*, 2010; Larsen *et al.*, 2010; Larson *et al.*, 2010). Detailed analysis of the stable isotope composition of ice and water in glaciers can be used to infer the origin and history of cryofacies. One of the main applications of this technique has been to help differentiate ice of meteoric origin (e.g. snow, glacier ice) from that which has been re-frozen, often located in the basal zone of the glacier (Jouzel and Souchez, 1982; Sugden *et al.*, 1987a; Souchez *et al.*, 1988; Hubbard *et al.*, 2000). It has also been demonstrated that stable isotope composition can provide important information on the formation of re-frozen basal ice, which may be the result of different processes including regelation, freeze-on and the freezing of upwelling supercooled subglacial water, known as supercooling (Cook *et al.*, 2010, 2011; Larsen *et al.*, 2010; Larson *et al.*, 2010).

The basis of the stable isotope approach is that water contains different isotopes of hydrogen and oxygen in different proportions depending on its state (cf. Knight, 1997). Naturally occurring water or ice contains a combination of light and heavy oxygen isotopes (^{16}O and ^{18}O) and hydrogen isotopes (^{1}H and ^{2}H, or D – deuterium). The isotopic composition of a sample is measured as the ratio of heavy to light isotopes of oxygen and hydrogen, or $^{18}O/^{16}O$ and $D/^{1}H$, and their difference from a reference standard (cf. Knight, 1997). A delta system of notation is used:

$$\delta_x = \frac{\left(R_{x(Sample)} - R_{x(\text{Standard})}\right)}{R_{x(\text{Standard})}} \times 1000\ (per\ mil), \quad (1)$$

where R_x refers to the $^{18}O/^{16}O$ or $D/^{1}H$ ratio respectively, giving $\delta^{18}O$ or δD measured in parts per thousand (‰). The reference standard commonly used is Vienna Standard Mean Ocean Water (V-SMOW; e.g. Cook *et al.*, 2010).

During several natural processes, but most importantly freezing in this case, the separation of heavier from lighter isotopes (or fractionation) can occur. This happens when ice forms from an excess of water, resulting in an increase in $^{18}O/^{16}O$ or $D/^{1}H$ ratios compared to the original water source, and an associated decrease in the parent water which is left behind (Boulton and Spring, 1986; Souchez *et al.*, 1988; Knight, 1997). This means that the first ice to form is isotopically heavier than the source water, which in turn becomes depleted in heavy isotopes. Subsequent freezing therefore forms ice from a parent water which is isotopically lighter than the original water, producing isotopically lighter ice (compared to that which formed first) and further depleting the heavy isotope composition of the parent water (Knight, 1997). This progressive impoverishment in heavy isotopes means that in a closed system, where all of the parent water is frozen in successive stages, the last fraction of ice formed therefore has the lightest isotopic composition (Souchez *et al.*, 1988; Knight, 1997)). Because of this, the overall isotopic composition of ice formed through complete freezing of a water source in a closed system will be equal to the original composition of the parent water, and therefore the fractionation signal is not preserved within the ice (Knight, 1997).

The complete freezing of water in a closed system is only one of several possible scenarios for the formation of ice in a basal zone, however. If, for example, freezing of the parent water body is incomplete, perhaps due to some of the water escaping, then the processes of fractionation may be recorded in the isotopic composition of the ice (Knight, 1997). For example, Lawson (1979) found debris-rich basal ice to be isotopically heavier than its parent water, and this was interpreted to be the result of only partial refreezing of the available water. In addition, ice can form from parent waters in an open hydrological system, whereby the parent water source is continually replenished during the freezing process. The isotopic composition of the replenishing water may be similar to that of the original parent water, or may be sourced from a range of different waters with variable isotopic compositions (Souchez *et al.*, 1988; Hubbard and Sharp, 1995; Knight, 1997). This has an impact on the isotope values of the resultant ice; in the former example, the isotopic composition of the refrozen ice may be indistinguishable from meteoric (glacier) ice (Souchez and De Groote, 1985; Knight, 1987), whereas in the latter example, the isotope values may be offset from the expected parent water (Cook *et al.*, 2010).

If the fractionation of both hydrogen and oxygen isotopes within cryofacies are considered together, it may be possible to identify specific processes linked to specific isotopic signatures (Knight, 1997). In this approach, δD is plotted against $\delta^{18}O$ in a co-isotopic plot. The relationship between $\delta^{18}O$ and δD for meteoric water or glacier ice conforms to a linear relationship producing a line of gradient 8, known as the 'meteoric water line' (Fig. 3.1.). In contrast, ice formed by re-freezing of water can lie along a quite different line when plotted in this manner, known as a 'freezing slope', and so may be differentiated from meteoric ice on this basis. Similarly, this approach can be used to help discriminate between the different processes that form re-frozen basal ice (Cook *et al.*, 2010, 2011; Larsen *et al.*, 2010; Larson *et al.*, 2010). This is because ice formed by freezing of waters in a closed system (typically regelation and freeze-on) have a lower gradient freezing slope (typically 5.2) than those formed in an open system (e.g. glaciohydraulic supercooling) on a co-isotopic plot (Fig. 3.1; Cook *et al.*, 2010). In addition to the different regression line gradients, Cook *et al.* (2010) also suggested that ice formed by supercooling in an open system can be differentiated from that formed in a closed system (e.g. regelation) based on the absolute isotope values of the ice compared to the assumed parent water. Supercooled ice can be expected to be enriched in heavy isotopes in comparison to the parent water, by up to 3.5‰ for $\delta^{18}O$ and 18‰ for δD, whereas ice formed in a closed system (e.g. regelation) would not display such an offset towards a heavier isotopic composition (Cook *et al.*, 2010). The range in isotope values has also been used to elucidate the formation of different ice facies. For example, it was suggested by Souchez *et al.* (1988) that a large range in $\delta^{18}O$ (>4.5‰) and δD (>28‰) values can be due to multiple melting and refreezing events during freeze-on at the base of the glacier where there is a limited water source of a specific isotopic composition. During each melting-refreezing event, the ice which has been enriched due to fractionation during a previous freezing event becomes the parent water for the next event, thus incrementally increasing the isotopic values and creating a larger overall range. This demonstrates how isotope analysis can be used to help determine the formation processes of ice facies that may have very similar physical characteristics.

Examples of this can be found from different locations. Cook *et al.* (2010) interpreted frozen diamict (solid facies) at Svínafellsjökull in southeast Iceland to be of a supercooled origin based on isotopic data, which was suggested to be consistent with open system freezing (offset towards heavier isotopic composition in $\delta^{18}O$ and δD compared to source water, samples plot on same gradient as LMWL in a co-isotopic plot). By contrast, Larsen *et al.* (2010) suggested a characteristically similar facies at Kuannersuit Glacier, West Greenland, had formed due to freeze-on in a system that is progressively depleted in meltwater (samples plot on a lower gradient than the LMWL, or 'freezing slope'). Both Cook *et al.* (2010) and Larsen *et al.* (2010) identified similar banded facies ice, characterised by alternating layers of debris-rich and debris-poor ice, and there was agreement that these facies were likely to be the result of local regelation and freeze-on processes in a closed system (samples lie on a 'freezing slope' in a co-

isotopic plot). However, descriptively-similar banded facies ice has also been shown to be isotopically identical to its parent water, highlighting the importance that the isotopic composition of the initial water body has on that of the cryofacies that is formed from it (Souchez *et al.*, 1988; Hubbard and Sharp, 1993; Sharp *et al.*, 1994). In particular, the isotopic composition of parent water can vary according to its source area, the number of melting-refreezing events it has undergone prior to becoming the parent water for the measured cryofacies, and temporal differences relating to the initial precipitation, such as if it occurred during summer or autumn and winter; the latter can produce very light isotope values (Cook *et al.*, 2010). Finally, dispersed facies ice has been described by a number of studies at different sites, with a range of processes invoked for its formation (Cook *et al.*, 2011). For example, Lawson (1979) found that dispersed facies ice at Matunuska Glacier, Alaska, had a similar isotopic composition to meteoric (glacier) ice, and interpreted that it was the result of a combination of firnification processes and basal regelation. By contrast, Sharp *et al.* (1994) found that isotope values for clear ice (descriptively similar to dispersed facies) at Variegated Glacier, Alaska, were intermediate between those for meteoric ice and debris-rich basal ice, and concluded that it was the result of strain-induced metamorphism of meteoric ice in the basal zone.

In brief, these examples demonstrate the potential for using stable isotopes to differentiate between individual cryofacies, and to provide more information about possible formation processes. However, this also highlights the complexities surrounding the interpretation of stable isotope datasets, and the importance of utilising multiple lines of evidence (e.g. physical characteristics, stratigraphy) when interpreting basal ice facies. Comprehensive reviews of the stable isotope technique and its applications can be found in Souchez and Lorrain (1991), Knight (1997) and Cook *et al.* (2010).

Samples for stable isotope analysis were taken from cryofacies at Tunabreen and Tellbreen. The number of samples taken from each individual cryofacies at each site ranged from 2 to 24. The majority of these samples were extracted using a 19 cm long ice screw, from which the deepest 3-5 cm was kept. Several samples were taken from the entirely melted ice blocks used to calculate debris concentrations, once the water had been filtered to remove sediment. All samples were stored in 30 ml HDPE narrow-neck, screw-top bottles which were taped-up to reduce the likelihood of evaporation. Stable isotope analysis was undertaken at the University of Birmingham on a GV Instruments Isoprime continuous-flow mass spectrometer. Standardisation was carried by calibration against laboratory and IAEA reference standards. All analyses were duplicated and internal precision was 0.4‰ for hydrogen and 0.08‰ for oxygen with external precision estimates as approximately twice these values.

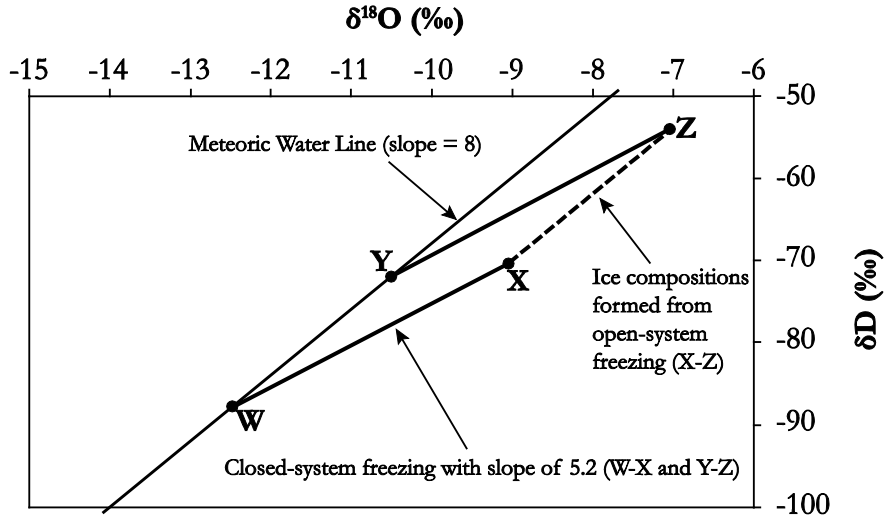

Figure 3.1. – Co-isotopic plot showing isotopic compositions of ice during open- and closed- system freezing. A meteoric water line with a slope of 8 is shown, as is the freezing behaviour of waters (similar in composition to Icelandic meltwater in this case) for comparison. Points X and Z represent the isotopic composition of ice forming from waters W and Y during open-system freezing. The parallelogram WXYZ delimits the isotopic composition of bulk ice samples formed by closed-system freezing of waters lying along the line WY. The lines WX and YZ (approximate slope of 5.2) show the locus of bulk isotopic compositions of ice formed by closed-system freezing of waters W and Y. Adapted from Cook *et al.* (2010).

3.1.5. Radiocarbon dating

Mollusc bivalve pairs and additional shell fragments of the *Hiatella arctica* and *Arctica islandica* species were sampled from the moraine complexes at Nathorstbreen and were radiocarbon dated at Queen's University, Belfast. The radiocarbon dates were calibrated using the Calib 7.0.0 software (Stuiver and Reimer, 2006) and the marine radiocarbon calibration (Reimer *et al.*, 2013) and are reported as radiocarbon years before present (cal. BP).

3.2. Study area

A brief introduction to the geographical setting of Svalbard is included here. Detailed study area descriptions for each of the studied glaciers are included at the beginning of *Chapters 4-8*.

3.2.1. Svalbard: climate, geology and glaciers

The High-Arctic archipelago of Svalbard consists of eight main islands which, in size order, are named Spitsbergen, Nordaustlandet, Edgeøya, Barentsøya, Kvitøya, Prins Karls Forland, Kong Karls Land and, located in the Barents Sea approximately 250 km to the south of the main group of islands, Bjørnøya (Fig. 3.2). The archipelago includes all islands, islets and skerries between 74-81º N and 10-35º E, amounting to a total surface area of ~62,000 km^2, of which Spitsbergen (~39,000 km^2) accounts for over half (Liestøl, 1993). The topography of Svalbard is generally mountainous, characterised by the iconic peaks, up to a highest elevation of ~1,700 m

a.s.l., which gave the main island of Spitsbergen its name. The archipelago, and Spitsbergen in particular, is dissected by large glacially-eroded fjords, which were occupied by fast-flowing ice streams within an extended ice sheet that covered Svalbard and the shelf edges of the Barents Sea at the last glacial maximum (Ottesen *et al.*, 2005; Ingólfsson, 2011). Of these, Wijdefjorden and Isfjorden are over 100 km long (Fig. 3.2). Strandflats are common in some coastal areas, characterised by low-lying bedrock plains and raised beach deposits (Ingólfsson, 2011). The geology of Svalbard is extremely diverse, ranging from Precambrian, Cambrian and Ordovician rocks in the basement (Dallmann *et al.*, 2002), including Neoproterozoic tillites (Fairchild and Hambrey, 1984); to sedimentary rocks deposited during the Tertiary which are prevalent in central and southern parts of Spitsbergen (Dallmann *et al.*, 2002).

Figure 3.2 – Location map of the Svalbard archipelago and glaciers featured in this study. NHB = Nathorstbreen; TNB = Tunabreen; FWB = Finsterwalderbreen; STB = Scott Turnerbreen; TLB = Tellbreen; GFB = Grønfjordbreen; HSB = Hessbreen.

Svalbard experiences remarkably high winter air temperatures (~-10 to -12º C) considering its high latitude, which also display a high degree of fluctuation (Førland *et al.*, 1997; Førland *et al.*, 2012). The average winter air temperatures recorded at Svalbard Lufthaven have increased by 3.5º C between the measurement periods of 1961-1990 and 1981-2010 (Førland *et al.*, 2012), in agreement with observations that Arctic land masses have experienced more warming than any other region on Earth in the last ~30 years (IPCC, 2007). Svalbard also experienced a significant step-like increase in warming in the early part of the 20th century (Hansson-Bauer *et al.*, 1990; Hanssen-Bauer, 2002), signalling the end of the Little Ice Age (LIA). Annual precipitation on Svalbard is low (~191-427 mm for the period 1981-2010) and records in general show a positive trend throughout the 20th century, with a 2% increase per decade observed at Svalbard Lufthaven (Førland *et al.*, 2012). The majority of the archipelago is located within the zone of continuous permafrost (Humlum *et al.*, 2003).

Approximately 60% of the land surface of Svalbard is glacierised, consisting of ~2,100 glaciers of all types, including ice caps, ice fields, and valley and cirque glaciers (Liestøl, 1993). Currently, ~68% of the glacierised area drains through 163 tidewater glaciers (Błaszczyk *et al.*, 2009; Nuth *et al.*, 2013), providing a direct link between land ice and the ocean. The glacierised area has experienced a significant reduction of 7% over the past ~30 years (Nuth *et al.*, 2013), largely due to the sustained retreat and thinning of most glaciers in response to consistently negative mass balances since the end of the LIA, when most glaciers are thought to have reached their most-extensive positions for the last 10,000 years, driven by temperature increases (Hagen and Liestøl, 1990; Dowdeswell *et al.*, 1995; Dowdeswell *et al.*, 1997; Mangerud and Landvik, 2007; James *et al.*, 2012).

3.3. Summary

A variety of methods and techniques were used in this project, ranging from the large scale (mapping from satellite images and aerial photographs) to small scale (particle size analysis; stable isotope analysis). Glaciological changes during the surges of Nathorstbreen and Tunabreen were tracked from Landsat and ASTER satellite images and published data, including NPI and historic maps. Mapping of geomorphology and glaciological structures was conducted from geo-rectified aerial photographs acquired from NPI and NERC, augmented by field mapping. The section logging and description of sedimentary and cryofacies units followed established methods outlined in Evans and Benn (2004a), Lawson (1979) and Hubbard *et al.* (2009). Analyses of sedimentary and cryofacies units included clast shape, macrofabrics, structural glaciology, debris concentration, particle size analysis and stable isotope analysis. Chronological control on the Nathorstbreen moraine system was provided by radiocarbon dating of mollusc samples.

The Svalbard archipelago is ~60% glacierised and consists of approximately 2,100 glaciers. The large majority of these are currently thinning and retreating due to a sustained

period of negative mass balance driven by significant warming since the end of the LIA, when most glaciers reached a maximum position during the Holocene.

Chapter Four
Nathorstbreen

77º 20.0' N, 16º 26.0' E

After Professor Alfred Gabriel Nathorst, 1850-1921, Swedish Arctic explorer, geologist, and palaeobotanist, professor at Riksmuseet, Stockholm, led expeditions to Spitsbergen in 1870, 1882 and 1898.

The place names of Svalbard, Norsk Polarinstitutt

4. Nathorstbreen

4.1. Introduction

This chapter describes the landform and sediment assemblage produced by surges of Nathorstbreen, a large tidewater glacier system located at the head of Van Keulenfjorden in southern Spitsbergen (Fig. 3.2). Fieldwork was conducted in July 2012 and focused on sedimentological and geomorphological investigations at the active margin of the glacier, which has been surging since 2008 (Sund and Eiken, 2010), and the terrestrial lateral moraine systems on either side of Van Keulenfjorden. The first part of this chapter will describe the study area (*4.2.*) and surge history (*4.3.*), including the currently ongoing surge. Sections *4.4.* and *4.5.* present geomorphological and sedimentological data from the active margin and the lateral moraine systems, and radiocarbon dates of mollusc shells are presented in *4.6.*; these are interpreted in section *4.7.*

4.2. Study area

Several tributaries feed the ~5 km-wide tidewater glacier front which terminates at the head of Van Keulenfjorden, a ~30 km-long fjord, of which Nathorstbreen is the central and longest flow-unit (~38 km in 2013) and drains from the accumulation area of Ljosfonn (Fig. 4.1). The major tributaries which are currently actively confluent with Nathorstbreen are Polakkbreen and Zawadzkibreen to the west and Dobrowolskibreen to the east (Fig. 4.1). Liestølbreen and Doktorbreen to the northeast have not been active during the ongoing surge (described below in *4.3.2*) but are currently adjacent to the splayed terminus and are likely to have formed part of the larger tidewater system at the end of the nineteenth century (Hamberg, 1905; described below in *4.3.1.*). Together, these glaciers cover an area of ~500 km^2 and form what has been referred to as the Nathorstbreen Glacier System (Sund and Eiken, 2010), but is simply termed Nathorstbreen in this study. Radio echo sounding data from the 1980s indicate that the main trunk of Nathorstbreen was over 300 m thick and polythermal at that time (Dowdeswell *et al.*, 1984). The neighbouring glaciers Penckbreen, Finsterwalderbreen (*Chapter 6*) and Hessbreen, located on the southern side of outer Van Keulenfjorden, have been suggested to also be of surge-type (Croot, 1988; Hambrey and Dowdeswell, 1997; Hart and Watts, 1997).

Inner Van Keulenfjorden is flanked by two large terrestrial lateral moraine systems, named the Nordre and Søre Nathorstmorenen, which terminate at the transition to the outer basin of the fjord (Fig. 4.1). These moraines, first mapped and described in detail by Hamberg (1905) and Gripp (1929), are the subject of this study, and sedimentological and geomorphological data from these are presented in *4.4.* The bedrock in the area is primarily composed of Cenozoic-age conglomerates, sandstones, shales and local coal of the Van Mijenfjorden Group (Dallmann *et al.*, 2002).

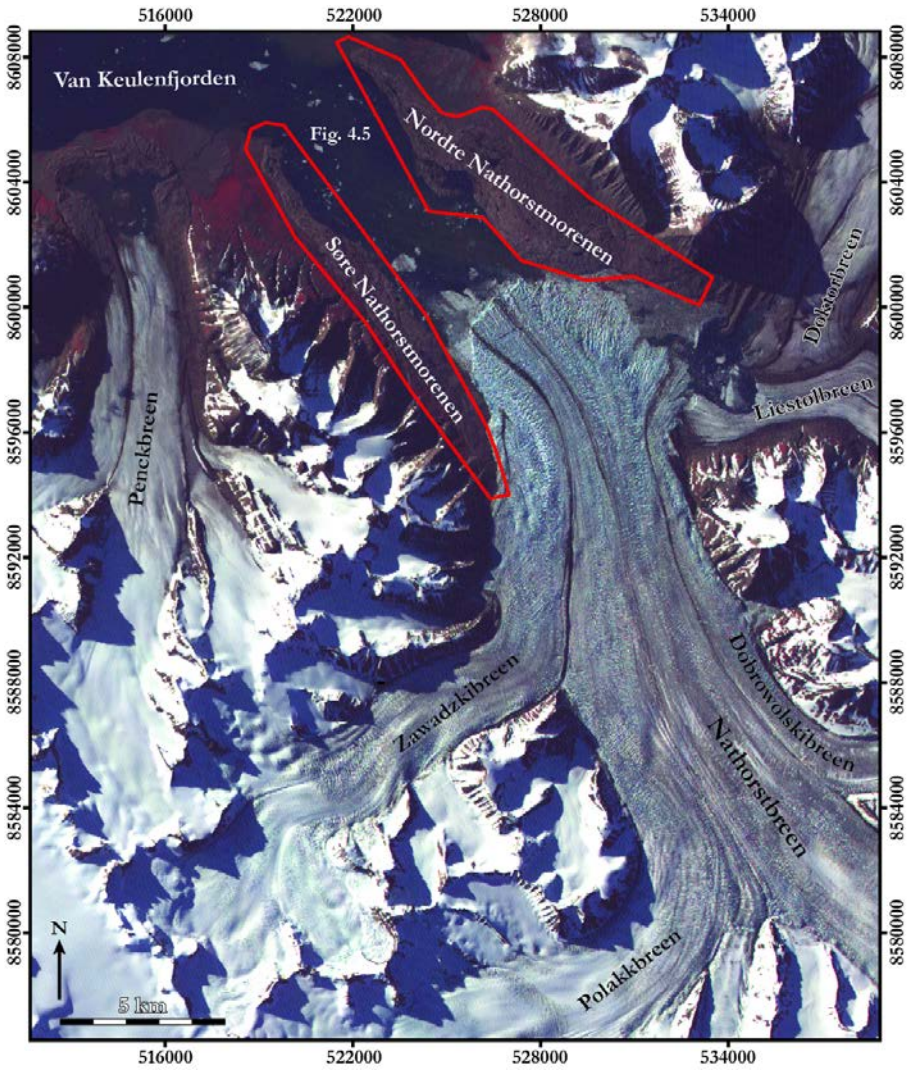

Figure 4.1 – Location map of Nathorstbreen, its tributaries and surrounding glaciers. Underlying image is ASTER scene from 2010 during the most-recent surge. Red polygons delimit the areas of the Nordre and Søre Nathorstmorenen mapped in Fig. 4.5. See Fig. 3.2 for location in Svalbard.

4.3. Surge history

4.3.1. Pre-1900 surges

Historical mapping and observations (Dunér and Nordenskiöld, 1865; Hamberg, 1905; Gripp, 1929) combined with marine geological investigations (Ottesen *et al.*, 2008; Kempf, 2011) provide strong evidence that Nathorstbreen has experienced previous surges. Photogrammetric mapping conducted in 1898 by Hamberg (1905) showed that Nathorstbreen (or 'Nathorst's Glacier') was confluent with Zawadzkibreen, Dobrowolskibreen, Doktorbreen and Liestølbreen and terminated ~3 km upfjord from the northern extents of the Nordre and Søre Nathorstmorenen and ~9 km downfjord from the location of the glacier at the head of Van Keulenfjorden in the 1865 map by Dunér and Nordenskiöld (1865; Figs 4.2a and 4.2b). From this, Ottesen *et al*. (2008) inferred that Nathorstbreen advanced approximately 12 km to the downfjord extent of the lateral moraines (Nordre and Søre Leirodden) sometime after 1865 and was in the early stages of retreat by 1898, as shown by its location ~3 km upfjord from the

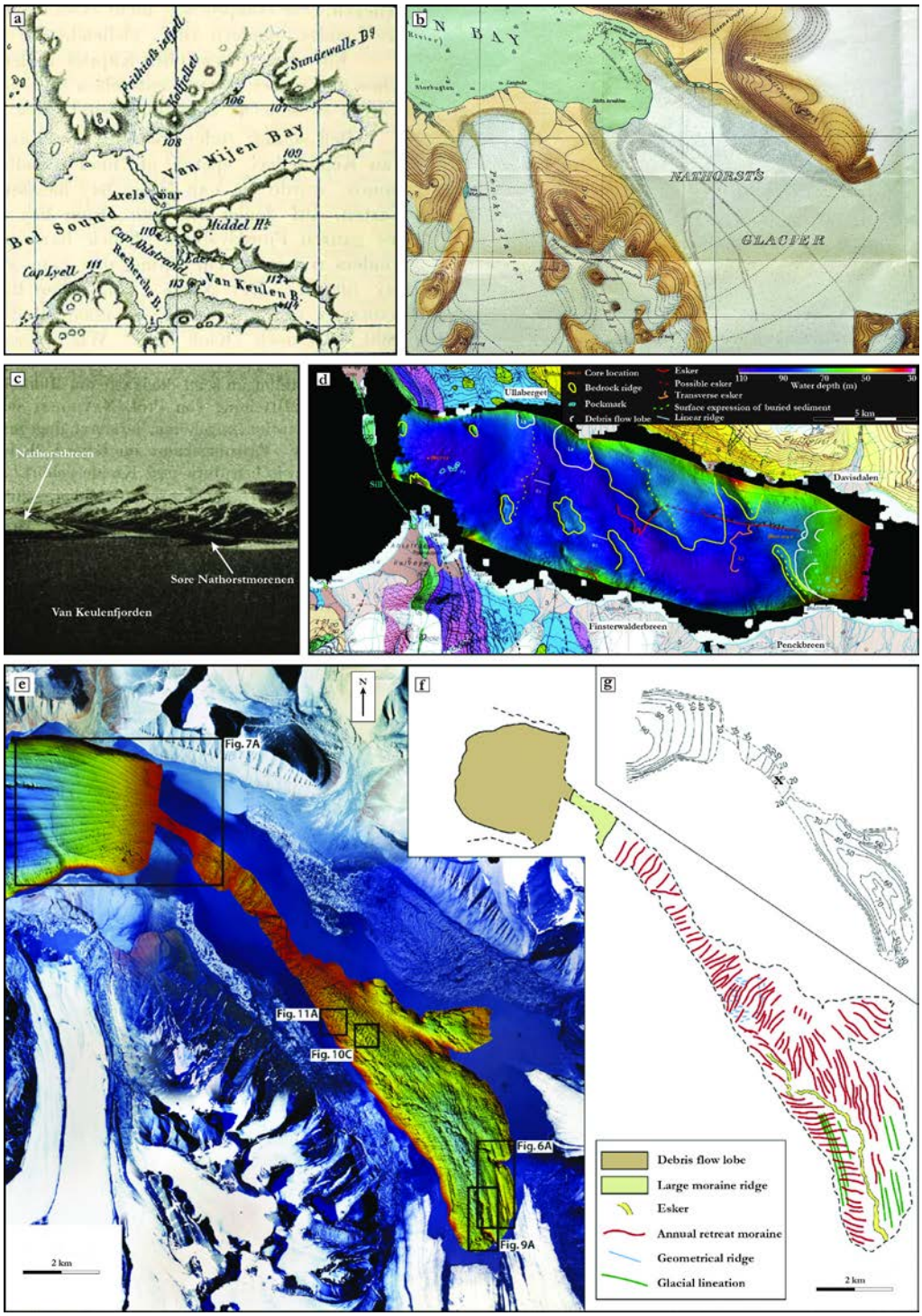

Figure 4.2 – Historical evidence of a previous surge of Nathorstbreen and submarine geomorphology in inner and outer Van Keulenfjorden. (a) Map of Bellsund, Van Mijenfjorden and Van Keulenfjorden region by Dunér and Nordenskiöld (1865). Reproduced from Hamberg (1905). (b) Map of Nathorstbreen and inner Van Keulenfjorden in 1898 by Hamberg (1905). (c) Photograph of southern margin of Nathorstbreen and Søre Nathorstmorenen in 1898 from Hamberg (1905). Note distinct looped moraines. (d) Swath bathymetry data and mapped landforms in outer Van Keulenfjorden. Reproduced from Kempf (2011). (e) Swath bathymetry of the fjord floor in inner Van Keulenfjorden and 1995 NPI aerial photographs of the adjacent land and glaciers. Reproduced from Ottesen *et al.* (2008). (f) Major submarine landforms in Van Keulenfjorden mapped by Ottesen *et al.* (2008). (g) Bathymetry of inner Van Keulenfjorden with contours at 10 m intervals. X marks approximate position where a water depth of <1 m was recorded in July 2012. Reproduced from Ottesen *et al.* (2008).

Nordre and Søre Leirodden and the presence of a calving bay (Figs 4.2b and 4.2c). This was suggested to record an advance of ~12 km in ~30 years followed by a subsequent retreat of ~3 km, indicating a surge which culminated in the 1870s or 1880s (Ottesen *et al.*, 2008). The presence of distinctive looped moraines on the surface of the southern side of the glacier terminus in 1898 (Figs 4.2b and 4.2c) provides further strong evidence that this late 1800s advance was a surge (cf. Meier and Post, 1969; Grant *et al.*, 2009).

Marine geological investigations within Van Keulenfjorden also support the interpretation of previous surges of Nathorstbreen. Ottesen *et al.* (2008) mapped submarine landforms from swath bathymetry data within inner Van Keulenfjorden (Figs 4.2e-g). This revealed several geomorphological indicators which are consistent with surging, including (i) a large terminal moraine located just beyond the northern extents of the Nordre and Søre Nathorstmorenen. This moraine marks the transition from the inner to outer basins of Van Keulenfjorden and has a glaciogenic debris flow lobe on its distal side; (ii) Annual retreat moraines, marking minor winter readvances during terminus retreat in the quiescent period (Boulton, 1986; Ottesen and Dowdeswell, 2006; Ottesen *et al.*, 2008); (iii) Geometrical ridges, interpreted as crevasse squeeze ridges (Ottesen *et al.*, 2008); (iv) Glacial lineations; and (v) eskers. Together, these features are suggested to represent a landsystem for tidewater glacier surges on Svalbard, and this is supported by observations from several other glaciers (Solheim, 1985; Solheim and Pfirman, 1985; Plassen *et al.*, 2004; Ottesen and Dowdeswell, 2006; Ottesen *et al.*, 2008; Flink, 2013; Flink *et al.*, submitted).

Ottesen *et al.* (2008) attributed this submarine landform assemblage to the surge in the late 1870s or 1880s identified from the early mapping. However, this has since been questioned by Kempf (2011) who collected swath bathymetry data, high-resolution seismics and sediment cores from outer Van Keulenfjorden (Fig. 4.2d). Kempf (2011) identified two stacked glaciogenic debris flows associated with the distal slope of the large terminal moraine mapped by Ottesen *et al.* (2008), which were both dated at ~2.7 cal. ka BP. This demonstrates that although Nathorstbreen clearly reached a similar position during the LIA, the large submarine terminal moraine may have been deposited by one or more earlier advances (Kempf, 2011). In combination, this provides compelling evidence that Nathorstbreen has surged several times to more-extensive positions than that reached so far by the currently ongoing surge.

4.3.2. Current surge

The combined terminus of Nathorstbreen, Dobrowolskibreen, Polakkbreen and Zawadzkibreen began to advance into Van Keulenfjorden during the winter of 2008/09 (Sund and Eiken, 2010). Dobrowolskibreen was the first of the tributaries that showed signs of surge activity prior to this advance (Sund *et al.*, 2009, 2013; Sund and Eiken, 2010), followed closely by Zawadzkibreen, which was observed to be surging in 2007 (Ottesen *et al.*, 2008). It appears that the entire system surged simultaneously shortly after this (personal communication from A. Luckman,

2013), and as a result distinctive looped moraines have not developed (Fig. 4.1). By September 2009, the terminus had advanced ~8 km, which represents the largest advance in a single year during the surge (Fig. 4.3). By 2010 the terminus began to splay towards Doktorbreen and Liestølbreen to the east, and in 2011 had advanced onto the Nordre Nathorstmorenen (Figs 4.3 and 4.4a). The glacier continued to advance down the central axis of Van Keulenfjorden and by July 2012, when the fieldwork in this study was conducted, had reached a position ~3.5 km upfjord from the 1898 limit reported by Hamberg (1905) (Fig. 4.3). By August 2013, the terminus had advanced a further ~1 km, including on to parts of the Nordre Nathorstmorenen mapped in this study. The terminus advanced ~1 km in both 2011-12 and 2012-13, indicating a reduction in the rate of advance during the most-recent years of the surge.

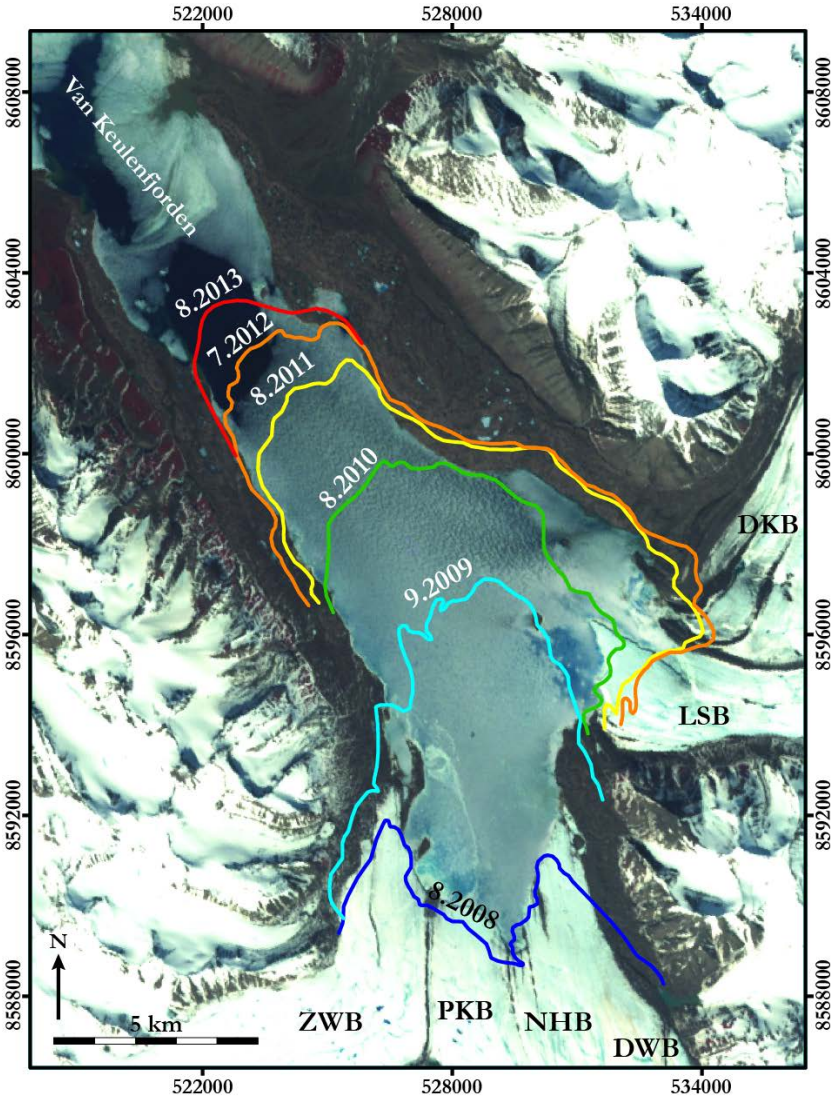

Figure 4.3 – Terminus change recording an advance of ~18 km during the most-recent surge of Nathorstbreen from 2008-2013. Terminus positions (month.year) are derived from georeferenced ASTER and Landsat ETM+ images and limits in Sund *et al.* (2013). Underlying image is a Landsat ETM+ scene from 2001. DKB = Doktorbreen; DWB = Dobrowolskibreen; LSB = Liestølbreen; NHB = Nathorstbreen; PKB = Polakkbreen; ZWB = Zawadzkibreen.

Over the entire five year period of 2008-13, Nathorstbreen has undergone a total advance of ~18 km (measured along the fjord axis; Fig. 4.3). Without factoring in mass loss through calving this equates to an average terminus advance rate of ~10 m d^{-1}, making the current surge of Nathorstbreen one of the largest surges ever recorded on Svalbard, comparable to the 1930s surges of Bråsvelbreen and Negribreen (Liestøl, 1969; Hagen *et al.*, 1993). Maximum ice velocities measured during this period were at least 25 m d^{-1} (Sund *et al.*, 2013). At the time of writing (November 2013), Nathorstbreen was still displaying enhanced velocities compared to other glaciers of a similar size on Svalbard, but much slower than during winter 2012/13, suggesting that the surge is coming to an end (personal communication from A. Luckman, 2013).

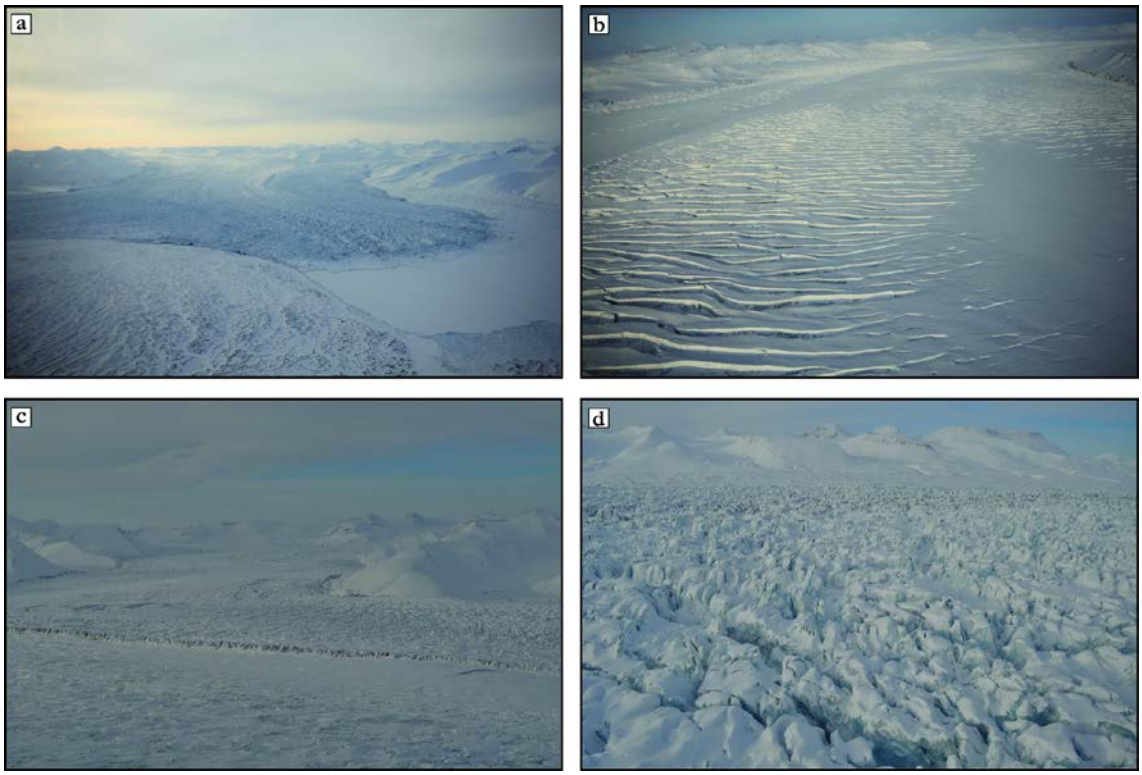

Figure 4.4 – Nathorstbreen in 2011 during the current surge. (a) Splayed terminus advancing on to Nordre Nathorstmorenen. Note buckled sea ice. (b) Large transverse crevassing on the main trunk of Nathorstbreen. View is downglacier. (c) Confluence between Polakkbreen (foreground) and Zawadzkibreen (background) flow-units. (d) Chaotic crevassing close to the tidewater margin.

4.4. Geomorphology, stratigraphy and sedimentology

The current surge has advanced onto the Nordre and Søre Nathorstmorenen, which extend for ~15 km along both sides of Van Keulenfjorden and cover a total area of ~40 km^2 (Fig. 4.5). The moraines are separated from the valley sides by large and heavily-braided lateral outwash corridors which are predominantly routed along the distal margins, but also cut across the moraine area in places, such as on the Søre Nathorstmorenen (Fig. 4.5). The moraine areas are characterised by ice-cored hummocky terrain with multiple pools, sharp-crested ridges forming

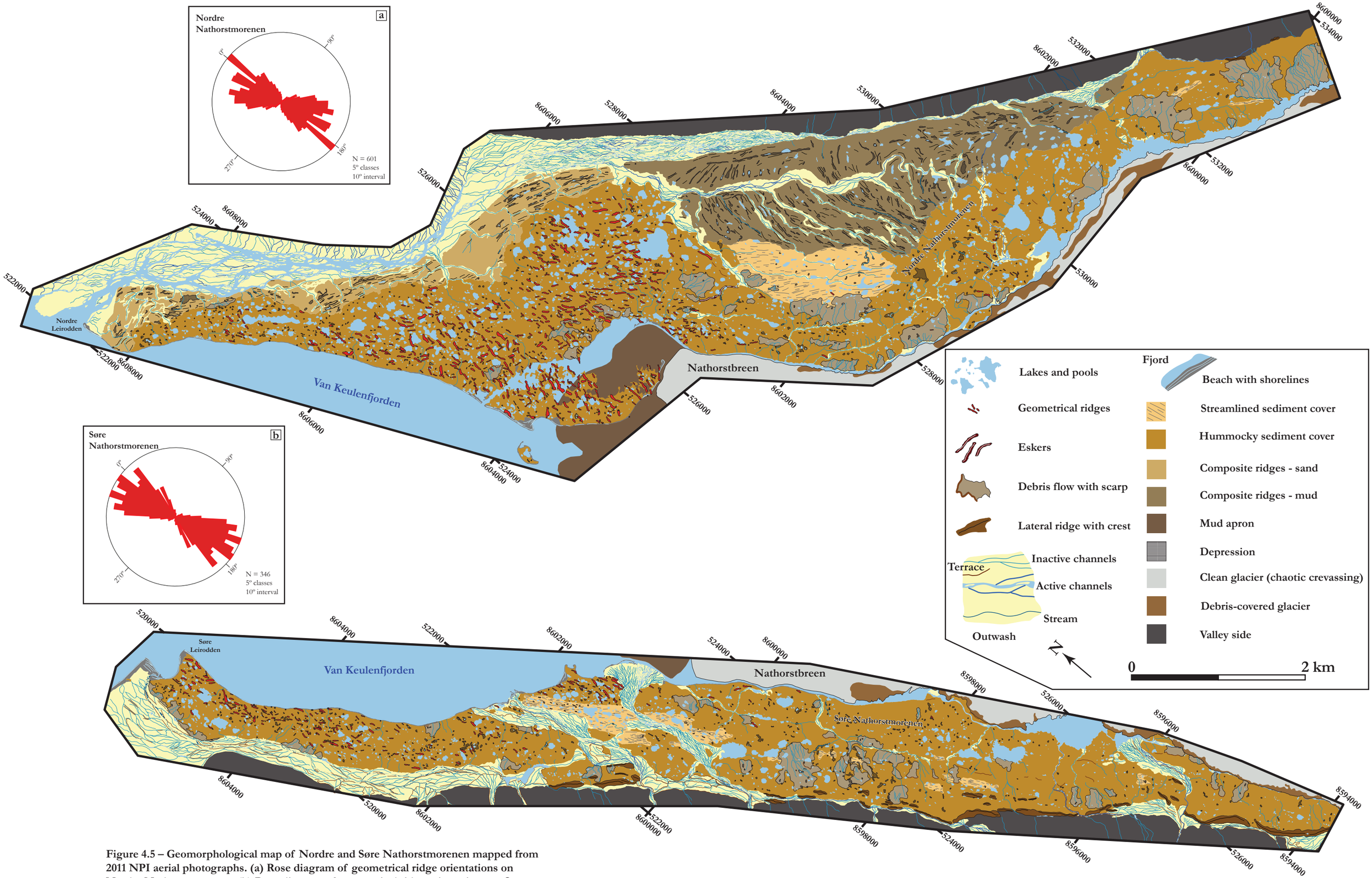

Figure 4.5 – Geomorphological map of Nordre and Søre Nathorstmorenen mapped from 2011 NPI aerial photographs. (a) Rose diagram of geometrical ridge orientations on Nordre Nathorstmorenen. (b) Rose diagram of geometrical ridge orientations on Søre Nathorstmorenen. A digital version of this map is included on the CD inside the back cover.

geometrical ridge networks, debris flows and, at the distal margins of the Nordre Nathorstmorenen, multiple-crested composite ridge systems (Fig. 4.5). The active ice margin is described in *4.4.1.,* and the geomorphology and sedimentology of the moraines, predominantly exposed within coastal sections, are described in *4.4.2.* and *4.4.3.*

4.4.1. Ice margin and mud apron

In July 2012, the terminus of Nathorstbreen reached a position ~50-100 m upfjord from the large curved, spit-like arm of the Nordre Nathorstmorenen (Figs 4.3 and 4.5). The glacier front was chaotically-crevassed and large areas of debris-rich ice were apparent, particularly close to the fjord level (Figs 4.6a-d). Despite having advanced onto the moraine areas, the ice could not be accessed due to the large (up to 15 m wide) and turbulent meltwater channels along the lengths of both the Nordre and Søre Nathorstmorenen (Figs 4.5 and 4.6a-d). These channels contain both larger, pooled areas, partly dammed by the moraine, and narrower, fast-flowing sections (Fig. 4.5). The marginal ice was heavily fractured, often formed pinnacles (Figs 4.6b and 4.6f) and in a number of locations contained refrozen breccias of smaller ice fragments and blocks. In several places, muddy debris could be observed within near-vertical crevasses, reaching heights of up to 10 m above the fjord/channel level (Fig. 4.6d). Glacier ice was observed to have advanced directly onto the moraine surface in a few places, largely leaving it apparently untouched; however, in some areas the moraine was observed to have been deformed, such as in Fig. 4.6c where a small part of the Søre Nathorstmorenen appears to have been ripped up and bulldozed in front of the glacier.

A large area of mud was apparent within the fjord at the ice margin in July 2012, typically in a frontal position and away from the lateral channels (Figs 4.5, 4.6e and 4.6f). This mud is hereafter referred to using the non-genetic term mud apron (Kristensen *et al.*, 2009a), and is characterised by a flat area of highly-saturated mud with surface pools (Figs 4.6f and 4.6h) which extends up to 500 m from the ice margin and was located within areas that had clearly been part of the fjord in previous years (e.g. Figs 4.1 and 4.3). The mud apron is more extensive towards the northern margin of the glacier, where it encroaches onto the Nordre Nathorstmorenen, than at the southern margin, where it typically forms only a narrow border ~10-20 m wide. The mud surrounds a number of icebergs, some of which are partly buried, and running water, flow structures and small (~1 m high and several metres long) transverse ridges are evident on the surface. Beyond the areas where it is visible subaerially, the mud apron extends as a low-gradient surface beneath the water. This was demonstrated by water depth measurements of <1 m up to 1 km downfjord from the margin, in an area which was ~20 m deep according to the pre-surge bathymetry (Fig. 4.2g). The extremely shallow water depth is also clear from the number of stranded icebergs in extremely turbid water, many of which contain evidence for elevated and tilted tidal notches (Fig 4.6g). The presence of the mud apron in effect means that the glacier was no longer calving into water in August 2012 and was only

Figure 4.6 – Details of the active margin. (a) View looking north towards the Nathorstbreen terminus from Søre Nathorstmorenen. (b) Southern margin of Nathorstbreen from Søre Nathorstmorenen. Note large lateral meltwater channel, chaotic crevassing and debris-rich ice. View is towards southeast. (c) Southern margin of Nathorstbreen encroaching on Søre Nathorstmorenen. Note deformation of moraine surface (arrowed) and supraglacial debris associated with a medial moraine. (d) Southern margin of Nathorstbreen and lateral meltwater channel. Note debris within fracture in the ice (arrowed). (e) View of mud apron at northern margin of Nathorstbreen from geometrical ridge on Nordre Nathorstmorenen. Note transverse ridges on apron surface. See Fig. 4.5 for mud apron location. (f) Mud apron at northern margin of Nathorstbreen encroaching on Nordre Nathorstmorenen and geometrical ridges. Note grounded ice bergs. Doug Benn circled for scale. (g) Large grounded iceberg in Van Keulenfjorden close to southern margin of Nathorstbreen. Note tidal notch at base. (h) Detail of mud apron at northern margin of Nathorstbreen.

dry-calving onto the mud. The only floating ice found in inner Van Keulenfjorden were tiny berglets transported by the lateral channels. Where it encroaches onto the large spit-like arm of the Nordre Nathorstmorenen, the mud apron was observed to have advanced by tens of centimetres from one day to the next relative to markers placed on the moraine, demonstrating that it is actively flowing. The grain size distribution of the mud apron sampled in this area (HL12NHBNNM15-20; Fig. 4.7) shows it is a clayey silt, with peaks in the medium and coarse-grained silt ranges (Fig. 4.8). In places, the mud apron surface has dried out and forms small blocks (Fig. 4.6h); this is particularly apparent within the transverse ridges which are elevated above the main surface by up to 1 m.

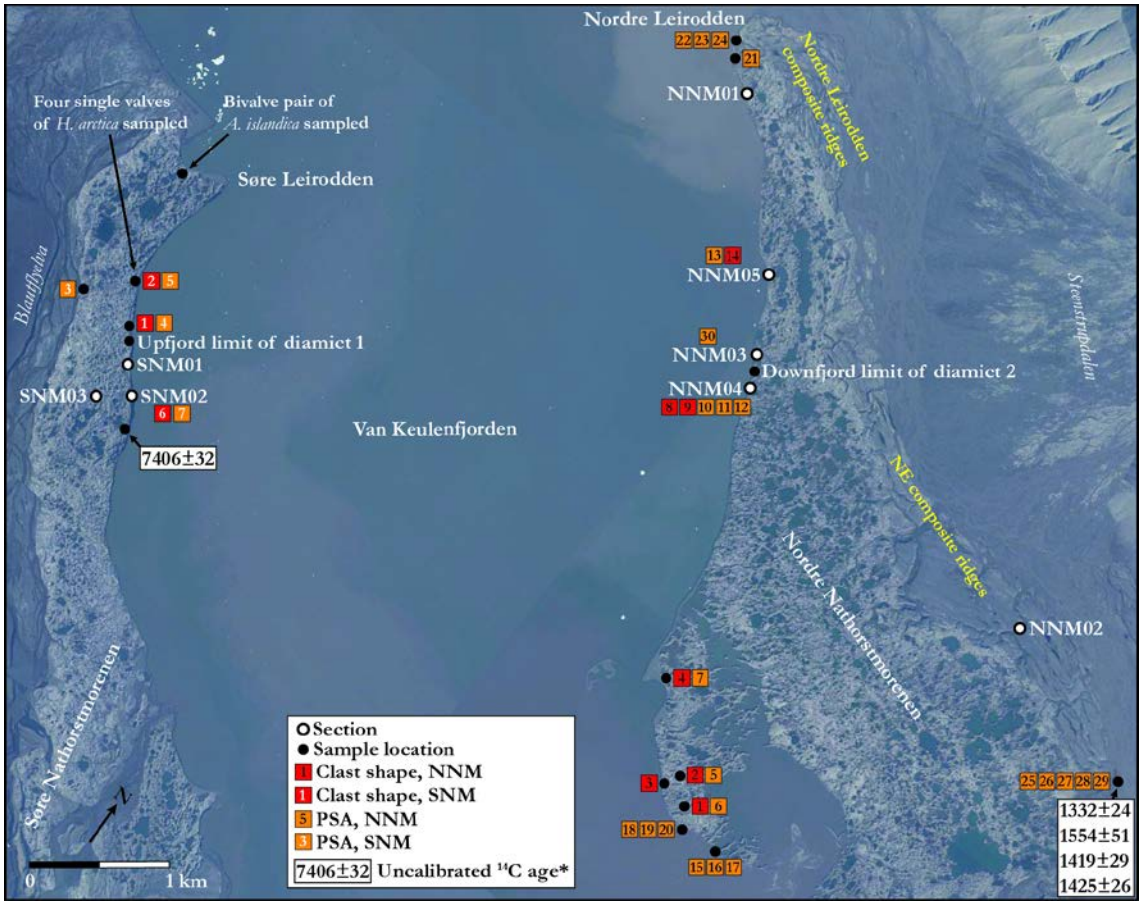

Figure 4.7 – Locations of section logs and sampling sites for particle size analysis (PSA), clast shape analysis and radiocarbon-dated shells (**Hiatella arctica***, bivalve pairs). NNM = Nordre Nathorstmorenen, SNM = Søre Nathorstmorenen.**

4.4.2. Nordre Nathorstmorenen

4.4.2.1. Lithofacies

Several sedimentary lithofacies were identified within the moraine, typically exposed in coastal sections. These include: (i) diamict 1, a shell-rich poorly-sorted diamict with a fine-grained matrix; (ii) diamict 2, which is characteristically similar to diamict 1 but contains far fewer shells; (iii) faulted, folded and sheared sands with clay inclusions; (iv) laminated clays and silts; (v) ripple-bedded sands; (vi) massive clay; and (vii) massive silt.

The two diamicts are found together at section NNM04 (Figs 4.7, 4.9d and 4.10aiii): (i) Diamict 1 is the lowermost of the two and is poorly-sorted, matrix-supported, typically contains a large amount of shells and shell fragments and is compacted and well-consolidated. The grain size distribution ranges from clay to occasional large boulders (~1 m diameter), with the finer (<2 mm) fraction displaying peaks in the medium silt and coarse silt/fine sand ranges (Fig. 4.8). Clast shape samples taken from sections NNM04 and NNM05 (Fig. 4.8; HL12NHBNNM08 and 14) contained predominantly sub-angular and sub-rounded clasts (Fig. 4.11), a number of which were striated. The diamict is typically structureless, but does contain thin clay stringers towards distal parts of the moraine and the sharp transition to composite ridges (e.g. section NNM01; Fig. 4.10ai). Diamict 1 could not be identified upfjord from section NNM04 within coastal exposures, indicating that, at least in a position adjacent to the fjord, its geographical distribution is restricted to the distal parts of the moraine complex.

(ii) Diamict 2 overlies, and forms a sharp contact with, diamict 1 at section NNM04 (Figs 4.7, 4.9 and 4.10aiii) and is also poorly-sorted and matrix-supported. The two are differentiated based on diamict 2 typically being friable, poorly-consolidated and having far fewer and much more fragmentary shells in comparison to diamict 1. Diamict 2 at section NNM04 also contains thin, sometimes contorted, lenses of sand, which are absent within the underlying diamict 1 (Fig. 4.10iii). These sorted lenses are largely absent close to the active margin and become more prevalent in a downfjord direction. The grain size distribution of diamict 2 ranges from clay to large boulders, with the finer fraction displaying peaks within the medium silt and coarse silt/fine sand ranges (Fig. 4.8). The similarity between the grain size distributions of diamicts 1 and 2 from both the Nordre and Søre Nathorstmorenen are shown on the composite plot in Fig. 4.8, with the main difference being the larger peaks within the coarse silt/fine sand ranges displayed by diamict 2. Clast shape samples from diamict 2 were taken from section NNM04 (HL12NHBNNM09) and within geometrical ridges located on the spit-like arm of the Nordre Nathorstmorenen (HL12NHBNNM01-04), and these contained predominantly sub-angular to sub rounded clasts (Fig. 4.11). Diamict 2 also has a restricted geographical distribution, and was not found downfjord from the position marked ‘Limit of diamict 2’ on Fig. 4.7, but is the dominant lithofacies closer to the active margin. Based on this, diamict 1 can be summarised as the lower diamict found in distal positions of the moraine, and diamict 2 as the upper diamict found primarily in the parts of the moraine which are proximal to the ice margin.

The other lithofacies identified within the Nordre Nathorstmorenen were typically observed within coastal exposures, which are outlined in further detail in *4.4.2.2.* These can be briefly characterised as: (iii) fine and coarse sand, laminated in places and containing very thin clay stringers, water escape features and evidence for minor faulting; (iv) wavy-laminated alternating clay-fine silt couplets (~1 cm thick), the uppermost ~1 m of which grades into

alternating silt to fine-sand couplets; (v) coarse sand with symmetrical ripple beds prograding in opposite directions; (vi) massive clay; and (vii) massive silt.

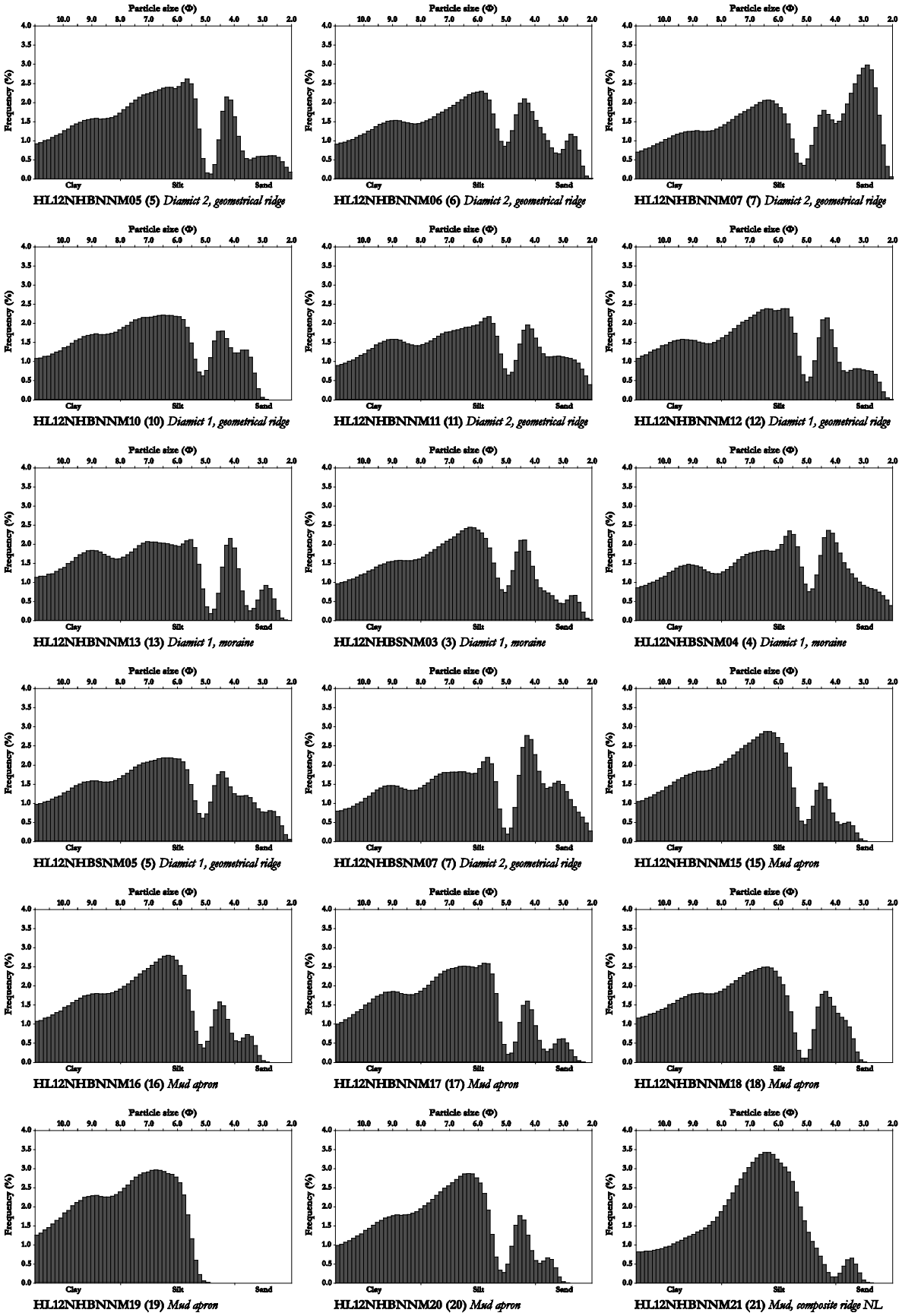

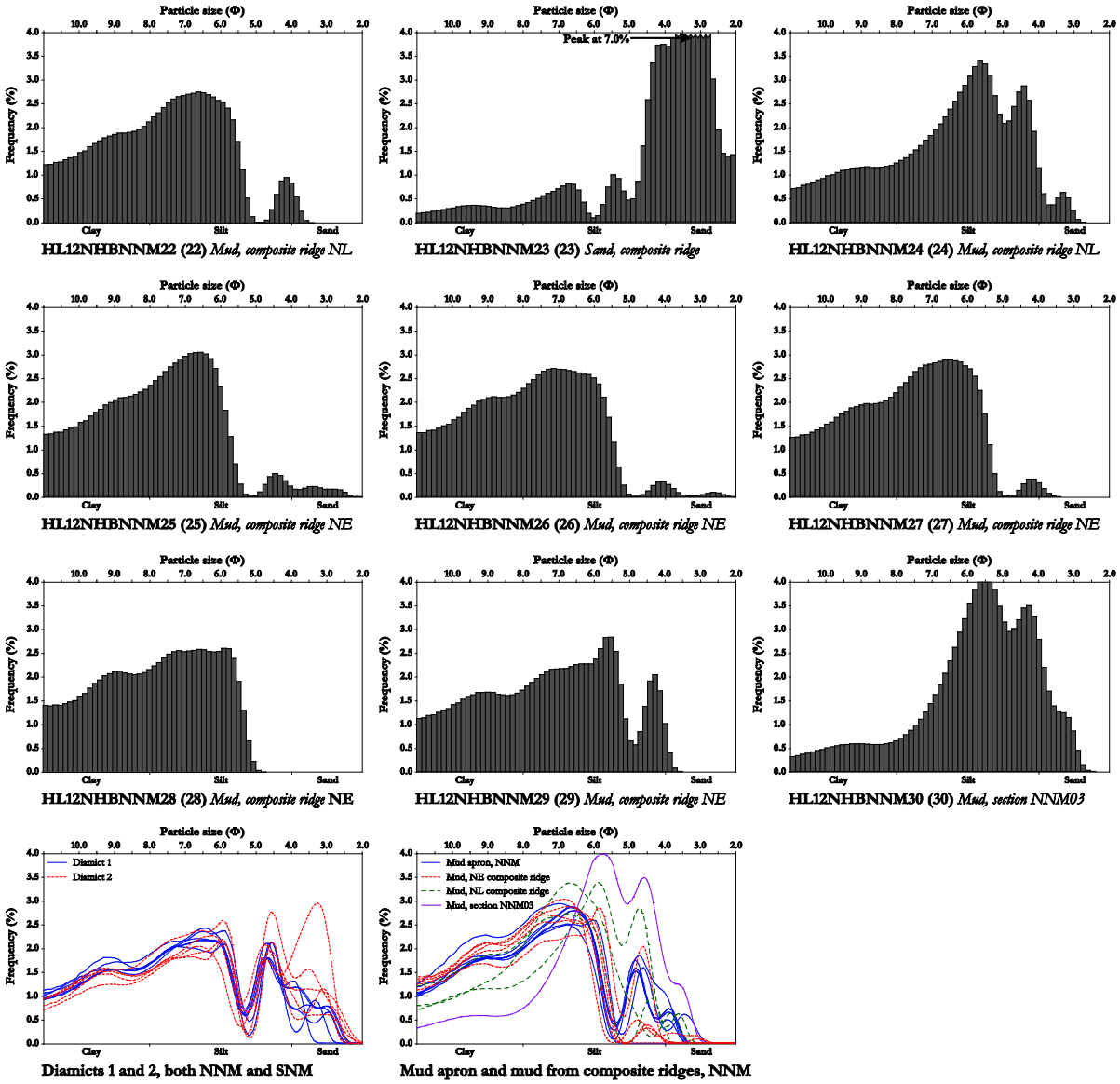

Figure 4.8 (and preceding page) – Grain size distributions of <2 mm fractions derived by laser sizing. Numbers after sample name refer to numbered sample locations on Fig. 4.7. NNM = Nordre Nathorstmorenen; SNM = Søre Nathorstmorenen; NL = Nordre Leirodden; NE = northeast.

4.4.2.2. Hummocky topography and geometrical ridge networks

The vast majority of the moraine complex is characterised by small hummocks, ridges and mounds interspersed with pools and depressions, recording an elevation range of ~6-8 m (Fig. 4.9a). The pools are widely distributed across the entire moraine complex; in general, the densest grouping and largest pools are located in a broad corridor towards the distal margins of the hummocky topography, whereas pools closer to the active margin tend to be smaller and more widely spaced (Fig. 4.5). Many of the depressions represent former pools which have drained, and surface precipitates of salt are common throughout the moraine complex (Figs 4.9a and 4.9c).

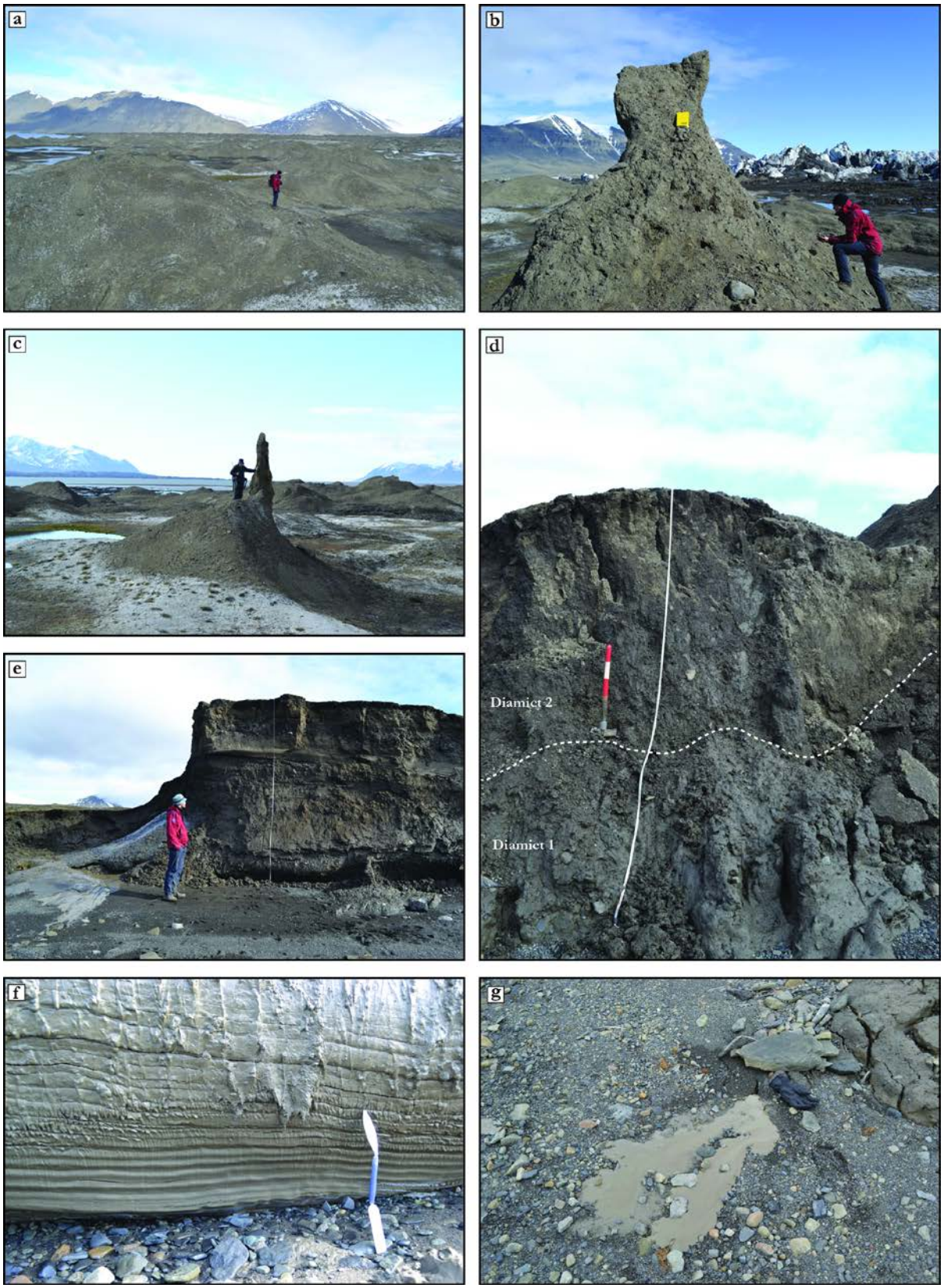

Figure 4.9 (continued on next page)

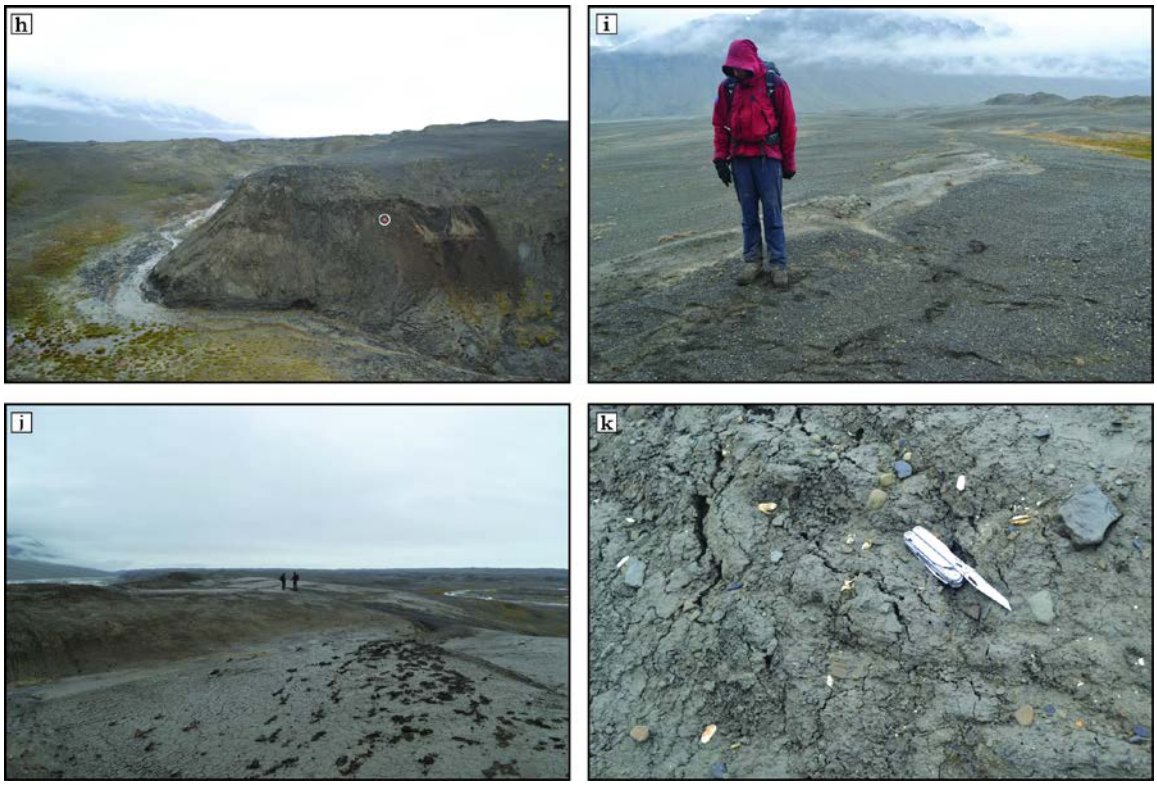

Figure 4.9 (this and previous page) – Details of Nordre Nathorstmorenen. (a) View towards north across moraine. (b) Sharp-crested geometrical ridge on the spit-like arm of the moraine close to the active margin. (c) 'Gripp's Finger', a pinnacle-like geometrical ridge. (d) Coastal exposure within geometrical ridge showing diamict 1 overlain by diamict 2, logged as NNM04 (Fig. 4.10). (e) Coastal exposure of laminated mud overlain by sand, logged as NNM03 (Fig. 4.10). Note buried ice at base. (f) Detail of laminated mud within section NNM03. (g) Highly-saturated mud oozing up through a crack in the beach. (h) Section NNM02 (Fig. 4.10) within NE composite ridges. Flare gun circled for scale. (i) Surface of sandy part of the NE composite ridges. Note muddy ridge, representing the surface expression of asymmetric folding within the ridges. (j) Surface of muddy part of the NE composite ridges, close to where PSA samples 25-29 and *Hiatella arctica* mollusc bivalve pairs were taken. (k) *In situ Hiatella arctica* mollusc bivalve pairs in life position sampled from the surface of the muddy part of the NE composite ridges.

In the central part of the moraine, extending from the active margin towards Nordre Leirodden, there is a dense grouping of predominantly sharp-crested ridges arranged in a crude network, which are mapped as geometrical ridges (Fig. 4.5); these were first identified by Gripp (1929), who described them as *Lehmmauern*, literally translated as 'loam walls' (van der Meer, 2004). These are typically between 2-8 m high, 1-3 m wide and extend for ~50-100 m. Ridge orientations are predominantly offset by 45º from or sub-parallel to the central axis of the fjord (Fig. 4.5a). The ridges display a variety of morphologies, ranging from rounded elongate hummocks to very thin vertical pinnacles or towers (Figs 4.9a-c). The sharpest-crested ridges and pinnacles are primarily located close to the active margin, particularly in the area around the spit-like arm of the moraine. The ridges become more rounded in a downfjord direction towards the Nordre Leirodden and laterally towards the distal margins of the moraine area, as noted by Gripp (1929), and as a result are harder to distinguish from the general hummocky terrain. The

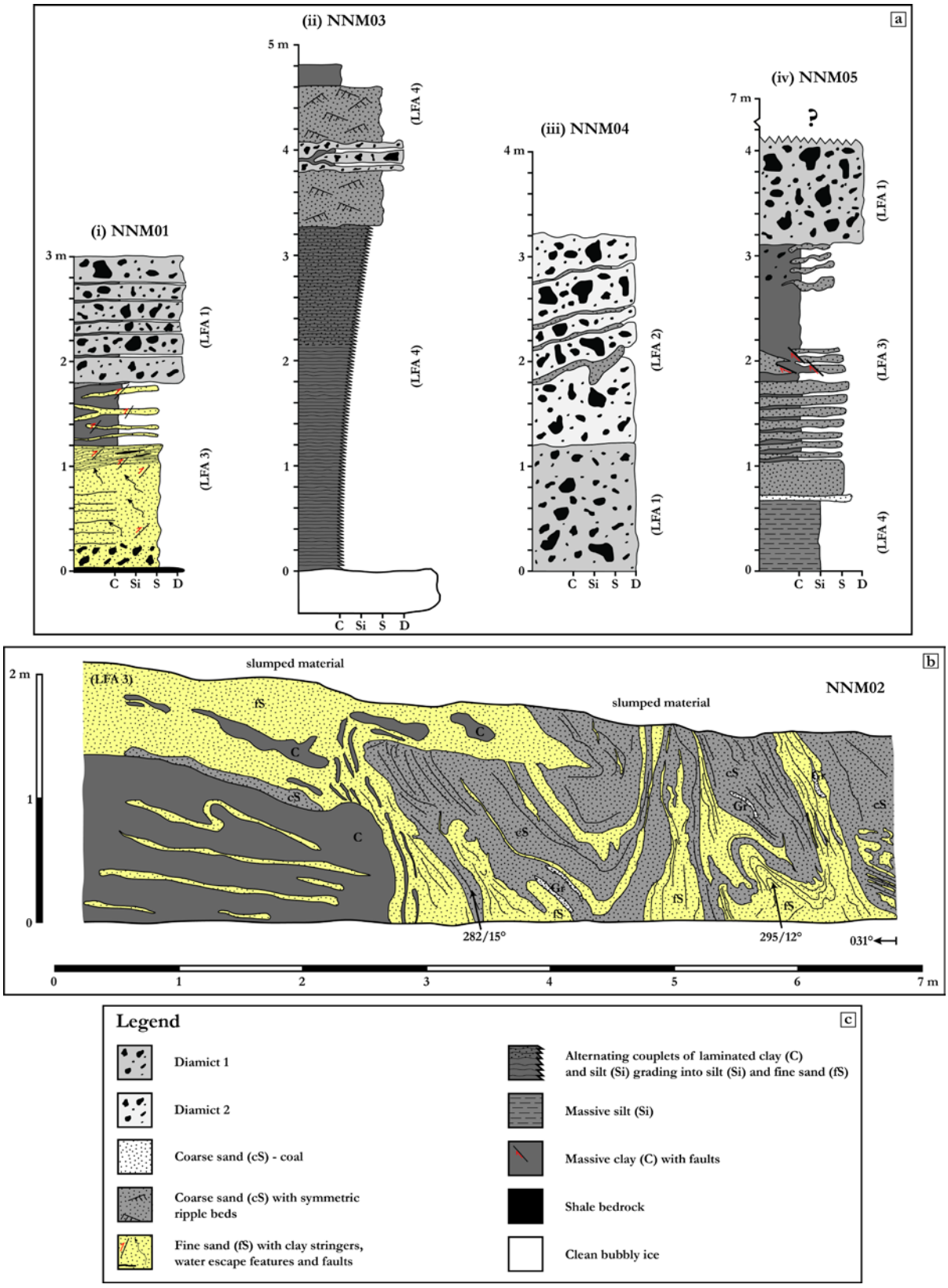

Figure 4.10 – Nordre Nathorstmorenen two-dimensional section logs. (a) Vertical logs of coastal exposures. (i) Section NNM01: exposure in moraine close to Nordre Leirodden composite ridge. (ii) Section NNM02. (iii) Section NNM04: exposure in geometrical ridge. (iv) Section NNM05. (b) Section NNM02: Exposure in sandy part of NE composite ridges. (c) Legend.

Immediately upfjord from the densest grouping of geometrical ridges, there is a 1 km^2 area of streamlined sediment cover aligned parallel to the fjord axis (Fig. 4.5). Individual lineations or flutes are hard to identify, but there is a clear linearity to the topography. Several smaller areas similar to this are located in the upglacier parts of the moraine, which is dominated by pools and debris flows, and only a few isolated geometrical ridges (Fig. 4.5).

Coastal sediment exposures

Section NNM01 is located within the hummocky topography, close to the boundary with the Nordre Leirodden composite ridges at the distal margin (Figs 4.7 and 4.10ai). The lowermost 120 cm of the section consist of fine sand with thin clay stringers and shells which overlies shale bedrock. The shale is broken up and extremely friable, and angular clasts have been ripped up from it and are present within the lowermost 20 cm of the fine sand. Thin, sinuous water escape features with flame-like structures are evident, trending upwards and towards the true left of the section. A number of small-scale minor reverse faults can also be identified; these are particularly noticeable in the upper ~20 cm, where the fine sand is laminated and contains small lenses of black shale coarse sand (Fig. 4.10ai). The fine sand is overlain by ~60 cm of massive sand interspersed with discontinuous thin, faulted fine sand lenses. This clay is overlain by ~120 cm of diamict 1 containing thin clay stringers. Immediately in front of the section, liquefied mud was observed to emanate from cracks in the beach; this is assumed to be the same as the features described as 'mud volcanoes' by Gripp (1929; van der Meer, 2004).

This sequence of sands and clays overlain by diamict 1 was identified in several places towards the northwestern extent of the moraine complex, such as at section NNM05, located ~1 km upfjord from NNM01 (Fig. 4.7). The section is in part of the moraine which reaches a height of ~7 m. The lowermost ~70 cm of the section is composed of massive silt, overlain by a thin (~5 cm) layer of coarse sand coal and ~130 cm of coarse sand with horizontally-interbedded 10 cm-thick clay layers (Fig. 4.10aiv). The uppermost 20 cm of this section are heavily faulted and broken up and transition into a 100 cm-thick layer of massive clay. The upper ~40 cm contains undeformed coarse sand lenses and scattered gravel and cobble-sized clasts. This is overlain by at least 1 m of structureless diamict 1, which probably extends to the height of the section but could not be investigated further (Fig. 4.10aiv).

Section NNM03 is located ~0.5 km upfjord from NNM05, and immediately upfjord from the observed limit of diamict 2 (Fig. 4.7). This exposure represents a distinct change from the rest of the coastal exposures and is characterised by a ~3 m-thick coarsening-upwards sequence of undisturbed wavy-laminated alternating clay-fine silt couplets (~1 cm thick), the uppermost ~1 m of which grades into alternating silt-fine sand couplets (Figs. 4.9e, 4.9f and 4.10aii). This sequence sits on top of bubbly, opaque ice at least 20-30 cm thick, and extends laterally for ~30 m. The laminated clays and silts are overlain by a ~50 cm-thick coarse sand

layer with symmetrical ripple beds prograding in opposite directions. This is overlain by a ~20 cm-thick diamict containing thin, wavy clay lenses and a concentration of clasts at the base, above which there is a further ~50 cm-thick layer of coarse sand with symmetrical ripple beds. The uppermost 20 cm of the section consists of massive clay (Fig. 4.10aii).

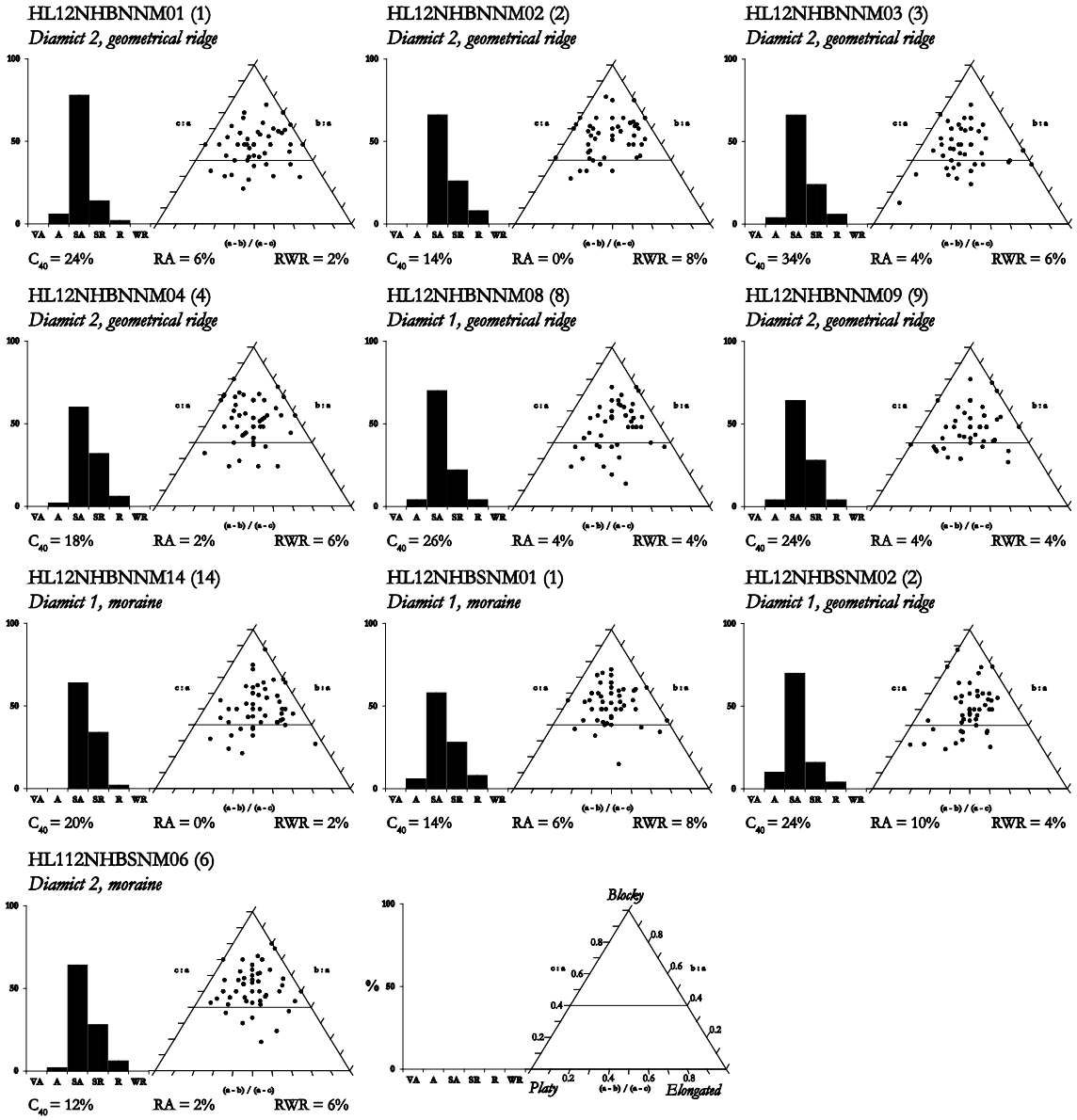

Figure 4.11 – Clast shape data plotted on histograms (roundness) and ternary diagrams (shape). Each sample is of 50 sandstone clasts. Numbers after sample name refer to numbered sample locations on Fig. 4.7.

The lithofacies distribution within the hummocky terrain of Nordre Nathorstmorenen, as exposed within coastal sections from an ice proximal to distal position, can be summarised as follows: sharp-crested geometrical ridges composed of initially structureless diamict 2, with increasing sorted inclusions (clay and sand stringers) in a downfjord direction; diamict 2 overlying diamict 1 within a geometrical ridge at section NNM04, after which diamict 2 can no longer be identified; an area consisting of an upward coarsening sequence of wavy laminated

alternating clay-silt grading to silt-fine sand couplets, overlain by ripple bedded sand; and an extended area of faulted sands and clays overlain by diamict 1.

4.4.2.3. Composite ridge systems

The composite ridges located at the distal margins of the hummocky terrain, and the boundary between the two, can be clearly differentiated in the field and from aerial photographs based on their smoother, undulating topography and sediment composition (Figs 4.5, 4.7 and 4.9h-j). The Nordre Leirodden composite ridges, which are briefly described by Gripp (1929; van der Meer, 2004), cover an area of 0.5 km^2 and are located at the northern margin of the moraine complex. These reach heights of up to 10 m and are dissected by several inactive outwash corridors. Identified low-amplitude ridge crests are aligned sub-perpendicular to the fjord axis close to Nordre Leirodden, and sub-parallel to the fjord axis in a lateral position (Fig. 4.5). These ridge crests are very subdued and reach typical heights of <50 cm, and as a result are often difficult to identify in the field (Figs 4.9i and 4.9j). This part of the composite ridge system is composed predominantly of sand and mud (Gripp, 1929), as exposed within coastal sections, with abundant evidence for sub-vertical mud stringers within the sand. Minor deformation is also evident, including small-scale thrust and reverse faults. Larger-scale anticline folding was also observed in several places where bedding dipped in opposite directions over distance of tens-of-metres. Mud samples taken from coastal sections within the Nordre Leirodden composite ridges (HL12NHBNNM21, 22 and 24) show a clayey silt with a peak in the medium silt range (Fig 4.8), and a number of shells (both fragments and complete) were found.

The Nordre Leirodden part of the composite ridges is joined to the NE composite ridges by a ~80 m-wide section which has been eroded into by the large lateral channel system (Fig. 4.5). The NE composite ridges can be subdivided into a ~1.5 km^2 area with a similar sediment composition, and connected, to the Nordre Leirodden composite ridges; and a ~5 km^2 area composed predominantly of mud, which is dissected by multiple outwash corridors and is separated from the sandy part of the ridges by the largest of these meltwater channels (Fig. 4.5). The sandy NE composite ridges contain multiple low-amplitude ridge crests displaying a more variable range of orientations than on the Nordre Leirodden composite ridges; many of these are broadly aligned sub-parallel to the central axis of the fjord (Fig. 4.5). The internal composition of the ridges was investigated in an exposure where an outwash corridor cuts through the ridges, logged as section NNM02 (Figs 4.7, 4.9h and 4.10b). This exposure, located ~5 m above the channel floor, is characterised by folded and contorted fine and coarse sand layers forming attenuated synclines, with evidence for water escape features in the form of flame structures (Fig. 4.10b). The true left-hand end of the section is composed of massive clay with fine sand stringers, overlain by fine sand with clay inclusions. Small lenses of fine gravel are also found within the folded sand, and shells are rare compared to the Nordre Leirodden composite ridges. Fold axis measurements from two of the folds show strikes and dips of 282/15º and 295/12º,

respectively (Fig. 4.10b). The surface expression of asymmetric folds are also apparent on the composite ridges in this area, taking the form of linear stripes or minor ridges which stand-out against the general sandy-gravelly composition (Fig. 4.9i). The linear stripes are best identified where the fold axes of clay layers have reached the surface of the ridges, and several fold axes orientations strike at ~290º, similar to that measured within section NNM02 (Fig. 4.10b). In several places, thin (~10-20 cm wide) gravel stripes cut-across the muddy ridges.

The undulating smooth topography continues within the muddy part of the NE composite ridges, which reach heights of 5-10 m above the outwash corridors, and the change in dominant sediment compositions compared to the sandy ridges is very clear (Figs 7.9h-k). The muddy part of the composite ridges are composed of massive clayey-silt displaying peaks in the medium to fine silt range (HL12NHBNM25-29; Figs 4.7 and 4.8). This part of the composite ridge system extends for ~6 km and reaches a maximum width of ~1.5 km. Ridge crests and linear depressions display a number of orientations, typically sub-perpendicular to the fjord axis (Fig. 4.5). The mud is shell-rich and contains both fragments and complete mollusc shells of predominantly *Hiatella arctica*, some of which are in life position (Fig. 4.9k).

4.4.3. Søre Nathorstmorenen

The majority of the Søre Nathorstmorenen complex is composed of ice-cored hummocky terrain (Figs 4.12a and 4.12b) with multiple pools and debris flows and, primarily in the downfjord ~6 km of the moraine, geometrical ridge networks (Figs 4.5, 4.12c and 4.12d). Unlike the Nordre Nathorstmorenen, no composite ridge systems could be identified at the distal margins of the moraine complex. However, single-crested ridges are located at the lateral margins of the moraine, particularly in the upglacier ~9 km section. The moraine is flanked by a braided lateral outwash corridor which, close to Søre Leirodden, merges with the large outwash fan extending from the eastern margin of Penckbreen (Fig. 4.1). Outwash corridors dissect the moraine complex in several places, most notably close to the active margin. Here, two heavily-braided outwash corridors extend across the moraine from a lateral position to the fjord over ~2 km, surrounding and isolating parts of the moraine in the process (Fig. 4.5). Buried ice is exposed in several places, particularly close to the active margin where the lateral channel has eroded the moraine (Fig. 4.12e), and elsewhere there is evidence for the degradation of buried ice cores in the form of large tension cracks within ridges, hummocks and the general moraine surface (Fig. 4.12f); these were also observed by Gripp (1929; van der Meer, 2004).

4.4.3.1. Lithofacies

The sedimentary lithofacies identified at the Søre Nathorstmorenen are broadly similar to those observed within the Nordre Nathorstmorenen, and include: (i) diamict 1; (ii) diamict 2; (iii) deformed sands with thin clay stringers and layers; (iv) laminated sands with symmetrical ripple beds; (v) massive clay; and (vi) massive fine sand with contorted coarse sand lenses.

(i) Diamict 1 is the dominant lithofacies on the downfjord ~1.5 km of the Søre Nathorstmorenen, extending from the position marked 'Upfjord limit of diamict 1' on Fig. 4.7. Particle size analysis and clast shape data for diamict 1 are very similar to the samples from the Nordre Nathorstmorenen, consisting of a poorly-sorted muddy matrix with peaks in the medium and coarse silt ranges (Fig. 4.8) and containing predominantly sub-angular and sub-rounded clasts (Fig. 4.11). Large (up to 1 m diameter) edge-rounded and striated boulders were found on the beach in front of coastal exposures.

(ii) Diamict 2 is notably less shell-rich than diamict 1, similar to at the Nordre Nathorstmorenen, and the shells are typically very fragmented. This is the dominant diamict observed in coastal sections extending downfjord from close to the active margin to the position where only diamict 1 is observed (Fig. 4.7). The transition from predominantly diamict 2 to predominantly diamict 1 is indistinct and, unlike at the Nordre Nathorstmorenen, the two diamicts were not observed together in section. Particle size analysis and clast shape data for diamict 2 are very similar to the samples from the Nordre Nathorstmorenen, consisting of a poorly-sorted muddy matrix with peaks in the medium silt, coarse silt and medium sand ranges (Fig. 4.8) and containing predominantly sub-angular and sub-rounded clasts (Fig. 4.11). Similar to diamict 1, large (up to 1 m diameter) edge-rounded and striated boulders were found on the beach in front of coastal exposures. Close to the active margin, diamict 2 is observed to be massive with very few inclusions of sorted material. Lenses of sorted and sometimes contorted sand and occasional clay stringers are observed to become increasingly more common in a downfjord direction (Fig. 4.12h), such as at section SNM01 where the underlying diamict 2 contains several thin sand layers (Figs 4.7 and 4.13ai).

The other lithofacies identified within the Søre Nathorstmorenen were typically observed within coastal exposures, which are outlined in further detail in *4.4.3.2.*, and these can be broadly summarised as: (iii) intensely sheared and folded sand with clay lenses; (iv) wavy laminated sand containing symmetrical ripple beds which prograde in opposite directions; (v) massive clay layers; and (vi) massive fine sand with a number of small lenses of coarser sand, some of which are contorted.

4.4.3.2. Hummocky topography and geometrical ridges

The general topography of the Søre Nathorstmorenen is similar to that of the Nordre Nathorstmorenen and is characterised by hummocks and ridges interspersed with pools, small depressions and debris flows of all sizes; the latter sometimes contain multi-tiered flow lobes and are typically associated with small, inactive channels (Figs 4.5, 4.12a and 4.12b). The pools are widely distributed across the moraine, with dense groupings located at Søre Leirodden and at the fjord edge between the two large outwash corridors that dissect the moraine (Fig. 4.5). The moraine area contains an elevation range of ~10-15 m from the fjord to the tops of the highest ridges at the lateral margins.

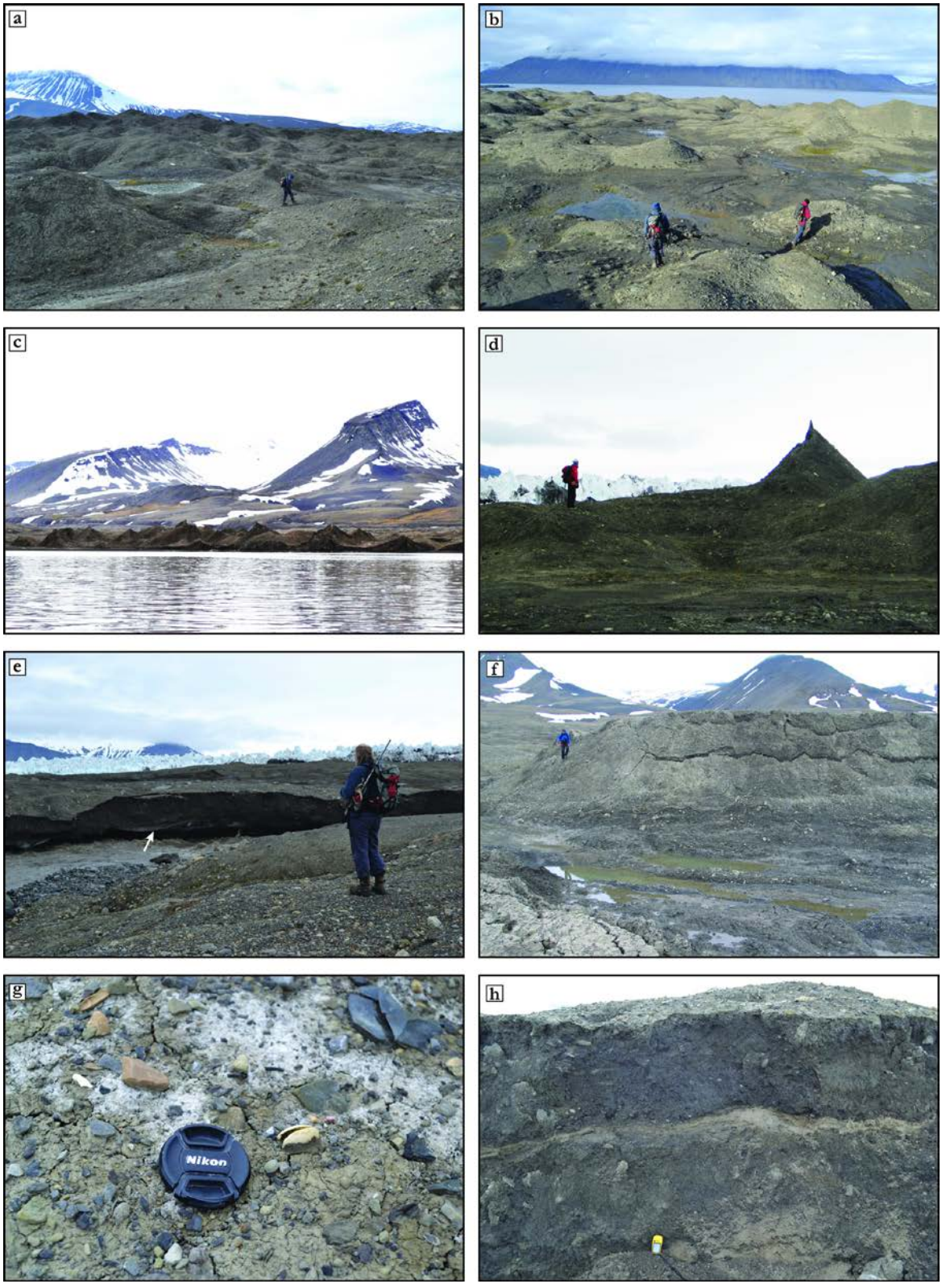

Figure 4.12

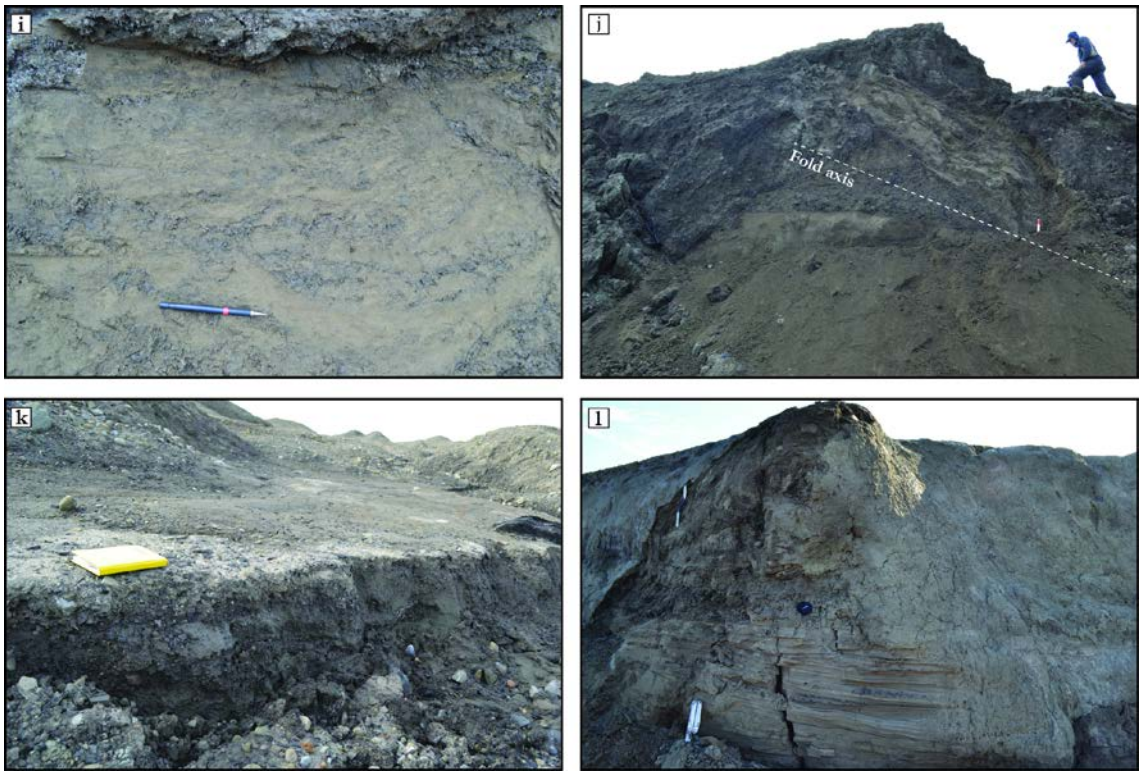

Figure 4.12 (this and preceding page) – Details of Søre Nathorstmorenen. (a) and (b) General topography of ridges, hummocks and pools. (c) View of geometrical ridges close to active margin. (d) Sharp-crested geometrical ridge close to active margin. Photograph by Schwen Lukas. (e) Buried ice (arrowed) in moraine exposed by lateral meltwater channel. (f) Tension cracks in moraine. Photograph by Sven Lukas. (g) *In situ* bivalve pair within diamict 1 at Søre Leirodden sampled for radiocarbon dating. (h) Sorted sand layers within diamict 2. (i) Sheared sand and clay lenses, logged as section SNM01 (Fig. 4.13ai). (j) Overturned fold of sand and clay lenses around a core of diamict 2, logged as section SNM02 (Fig. 4.13c). (k) Sorted sand with gravel layers in a debris flow overlying diamict 1 at the margin of the moraine. (l) Laminated sands with symmetric rippled beds overlain by deformed sands exposed in the interior part of the moraine and logged as SNM03 (Fig. 4.13aii).

Geometrical ridge networks are common in the ~6 km-long part of the moraine extending downfjord from the active margin to Søre Leirodden, and are typically located within a ~200-300 m-wide corridor adjacent to the fjord. (Fig. 4.5). Close to the active margin, these are very sharp-crested and sometimes form near-vertical pinnacles and towers up to ~8 m high, such as the dense network located at the fjord edge between the large dissecting outwash corridors (Figs 4.5, 4.12c and 4.12d), and become more rounded towards Søre Leirodden. The ridges display similar orientations to those on the Nordre Nathorstmorenen, typically aligned between sub-parallel-to and offset at 45º from the fjord axis (Fig. 4.5b). The spaces between individual ridges are generally occupied by pools or depressions (Figs 4.5, 4.12d and 4.12f). The geometrical ridges exposed in coastal sections typically contained structureless diamict 2, or within the downfjord ~1.5 km part of the moraine.

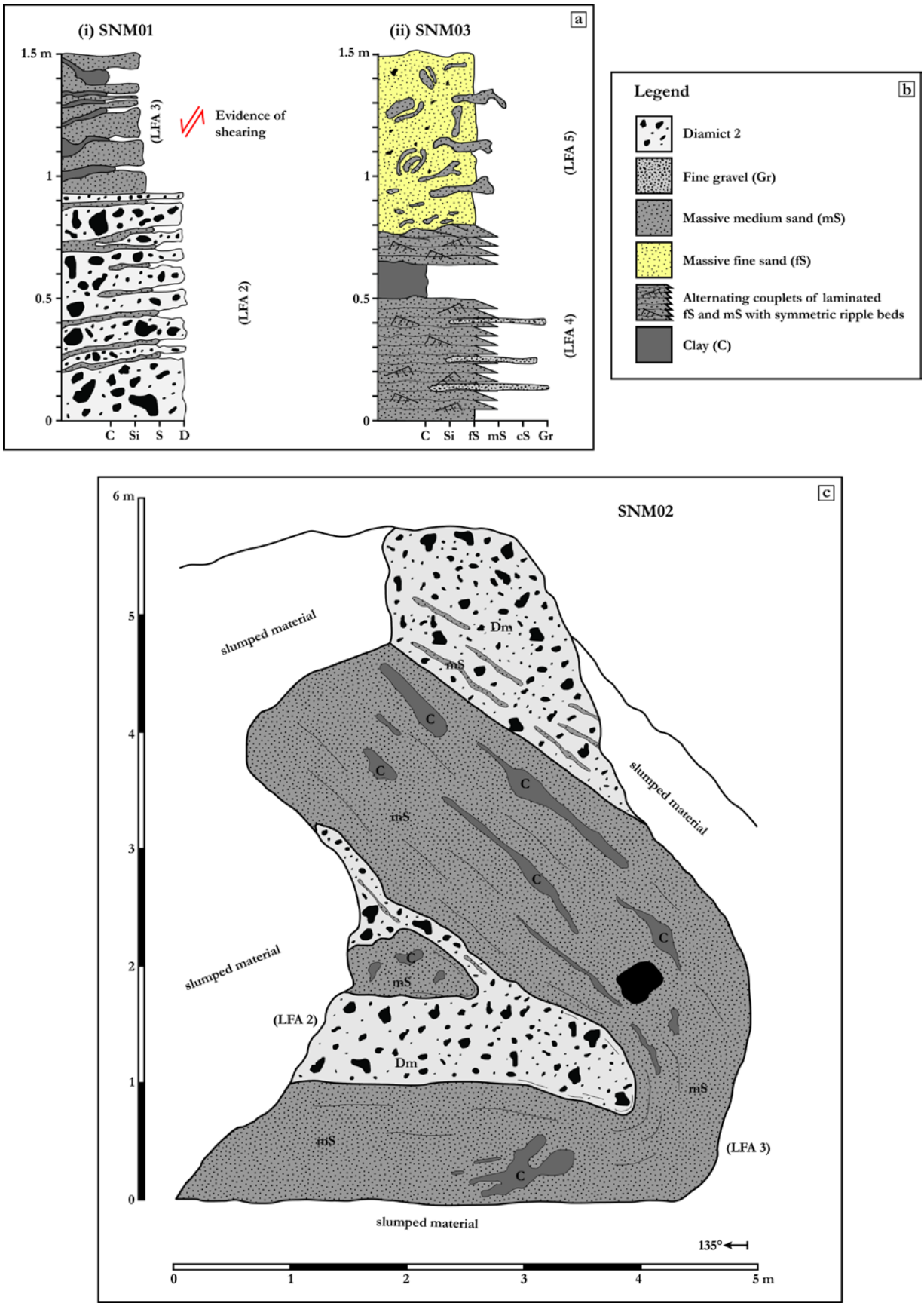

Figure 4.13 - Søre Nathorstmorenen two-dimensional section logs. (a) Vertical logs. (i) Section SNM01: coastal exposure within moraine. (ii) Section SNM03. (b) Legend. (c) Section SNM02: coastal exposure within moraine.

Close to the active margin there is a prominent 2.5 km-long, <0.5 km-wide corridor of streamlined sediment cover, the main area of which is bookended between the two large dissecting outwash corridors, and adjacent to the densest network of sharp-crested geometrical ridges (Fig. 4.5). Fragmentary patches of streamlined sediment cover in a similar alignment can be traced upglacier for a further ~3 km, and the streamlining within all these areas is aligned broadly sub-parallel to the central axis of the fjord.

Sediment exposures

Lithofacies (iii) to (vi) were observed within exposures located close to the downfjord limit of diamict 2 and the transition to diamict 1 being the dominant lithofacies. The areas of deformed sand and clay layers have often been intensely sheared together and display multiple small-scale faults (Fig. 4.12i), as shown in section SNM01 (Fig. 4.13ai). Here, a ~10 m-long exposure in the moraine has been recorded as a composite vertical log, and reveals ~1 m of diamict 2 containing several thin sand layers, overlain by ~0.5 m of sheared sand with clay lenses (Figs 4.12i and 4.13ai). Approximately 200 m upfjord from SNM01, an exposure within a 6 m-high part of the moraine shows a ~1 m-wide layer of sands and thin clay lenses which forms a downfjord-verging overturned fold around a core of diamict 2 (section SNM02; Figs 4.12j and 4.13c). The clay lenses within the sand and the thin sand layers within diamict 2 are all aligned parallel to the axial surface of the fold. Deformed sands with sheared clay lenses were also observed to be overlain by up to 1-2 m of diamict 2 with thin sand layers in this area. In contrast, evidence for sorted material in the distal parts of the moraine dominated by diamict 1 were confined to exposures within depressions or debris flows within the moraine area; here, diamict 1 was overlain by tens-of-centimetres of massive sand, often containing gravel-rich layers (Fig. 4.12k).

Similar to the Nordre Nathorstmorenen, exposures of undeformed sorted sediment were also found, although not within coastal sections. A ~5-10 m-long exposure within a ridge located ~200 m inland from section SNM02, which consisted of laminated sands overlain by deformed sands, was recorded as a composite log (SNM03; Figs 4.12l and 4.13aii). The lowermost 50 cm of the exposure consists of wavy laminated alternating couplets of fine and medium sand containing symmetrical ripples prograding in opposite directions, interspersed with thin (<3 cm) horizontally-bedded lenses of fine gravel (Figs 4.12l and 4.13aii). This is overlain by ~15 cm of structureless clay and a further ~10 cm of laminated and rippled sands. The uppermost extent of the laminated sands forms an erosional contact with an overlying ~170 cm of fine sand containing contorted coarser sand lenses and scattered gravel-sized clasts (Fig. 4.13aii). There is evidence for small rip-ups of medium sand sourced from the underlying laminated sands within the lowermost ~10-20 cm of the overlying sand unit, and the thin lenses of coarser sand within the otherwise fine sand matrix display a variety of shapes and alignments.

The lithofacies distribution within the Søre Nathorstmorenen follows a similar pattern to that within the Nordre Nathorstmorenen, and from an ice proximal to distal position can be summarised as follows: sharp-crested geometrical ridges composed of initially structureless diamict 2, with increasing sorted inclusions (clay and sand stringers) in a downfjord direction, grading into more-rounded ridges; deformed and sheared sands and clays both overlain and underlain by diamict 2, and in some places forming large-scale overturned folds; a downfjord limit to the distribution of diamict 2, close to areas of undeformed and laminated sands overlain by deformed sands in an interior position of the moraine; and an extended area of largely structureless diamict 1 and rounded geometrical ridges extending to the Søre Leirodden.

4.5. Lithofacies associations

Five lithofacies associations (LFAs) are defined across the Nordre and Søre Nathorstmorenen based on the observations predominantly from coastal exposures extending from the active margin to the Nordre and Søre Leirodden.

4.5.1. Lithofacies association 1

LFA 1 consists of diamict 1, the character and distribution of which are described above in *4.4.2.1.* and *4.4.3.1.*

4.5.2. Lithofacies association 2

LFA 2 consists of diamict 2, the character and distribution of which are described above in *4.4.2.1.* and *4.4.3.1.*

4.5.3. Lithofacies association 3

LFA 3 (folded, faulted and sheared muds, sands and fine gravel) is exposed in sections NNM01, NNM02, NNM05, SNM01 and SNM02 (Figs 4.10 and 4.13). It is characterised by sand of all grain sizes and intercalated clay stringers, layers and lenses which have been subject to minor faulting (e.g. NNM01; NNM05), shearing (e.g. SNM01) and/or intense folding (e.g. NNM02; SNM02). At NNM01, it is also characterised by faulted fine sand layers within a clay matrix. Water escape features and flame structures are identified within LFA 3 in sections NNM01 and NNM02. This LFA may also include the muddy parts of the composite ridge system (Fig. 4.5), but these were not investigated in section. This LFA is primarily found (i) underlying LFA 1 towards the distal parts of the Nordre Nathorstmorenen; (ii) in close association with LFA 2 at its downfjord limit within both moraine complexes; and (iii) within the composite ridge systems at the distal margins of the Nordre Nathorstmorenen (Fig. 4.7).

4.5.4. Lithofacies association 4

LFA 4 (undeformed massive or wavy laminated and rippled muds and sands; occasional fine gravel layers) is exposed in sections NNM03, NNM05 and SNM03 (Figs 4.10 and 4.13). It is characterised by wavy laminated alternating couplets of clay-fine silt grading into coarse silt-fine sand (NNM03; Figs. 4.9e and 4.9f) or couplets of fine sand-medium sand; sand with symmetrical ripple beds prograding in opposite directions (SNM03; Fig. 4.12l); and massive clay, silt and sand (NNM03, NNM05 and SNM03). This LFA is primarily found at the transition between the zones of LFA 1 and 2 (e.g. where they are the predominant lithofacies associations) in both moraine complexes (Fig 4.7).

4.5.5. Lithofacies association 5

LFA 5 (massive fine sand with contorted coarser sand lenses and scattered gravel-sized clasts) is only observed within section SNM03, where it overlies and has an erosional contact with LFA 4. This LFA is characterised by massive fine sand with occasional gravel-sized clasts and lenses and layers of medium sand, some of which are contorted (Fig. 4.13aii).

4.6. Dates from the Nordre and Søre Nathorstmorenen

Four paired bivalves of *H. arctica* in living position (e.g. Fig. 4.9k) from the surface of the muddy part of the NE composite ridge system at the margins of Nordre Nathorstmorenen returned ages of between 854-1297 cal. a^{-1} BP (Table 4.1; Fig. 4.7). At the Søre Nathorstmorenen, a single valve fragment of *H. arctica* sampled from LFA 2 (diamict 2) within a coastal exposure in the moraine had an age of 5840-5994 cal. a^{-1} BP (Table 4.1; Fig. 4.7). Single valves of *H. arctica* exposed in coastal sections and a bivalve pair of *Arctica islandica* in life position on the surface of the moraine near Søre Leirodden, both within LFA1 (diamict 1), were also sampled (Fig. 4.7) and are currently being dated.

Table 4.1 – Radiocarbon dating results from the Nordre and Søre Nathorstmorenen. *Calibrated with the Calib 7.0.0 calibration software and the Marine13 radiocarbon calibration (Reimer *et al.*, 2013).

Sample name	Location (UTM - 33X)	Position	Species	^{14}C a^{-1} BP	cal. a^{-1} BP*
NNM1	E 527370 N 8605300	Surface	*H. arctica* (pair)	1332±24	854-997
NNM2	E 527370 N 8605300	Surface	*H. arctica* (pair)	1554±51	1042-1297
NNM3	E 527370 N 8605300	Surface	*H. arctica* (pair)	1419±29	967-1107
NNM4	E 527370 N 8605300	Surface	*H. arctica* (pair)	1425±26	974-1107
SNM1	E 520520 N 8603480	Section	*H. arctica* (single)	7406±32	5840-5994

4.7. Interpretation

The landform and sediment assemblage described in *4.5.* is interpreted here in relation to the history of surging in Van Keulenfjorden, starting with the observed lithofacies and lithofacies associations (*4.6.1.*).

4.7.1. Lithofacies associations

4.7.1.1. LFA 1 (Diamict 1 - lower)

Based on its poorly-sorted texture, fine-grained matrix and presence of multiple shells and shell fragments and predominantly sub-angular to sub-rounded and striated clasts, LFA 1 is interpreted as subglacial debris derived from glaciomarine sediments (Boulton *et al.*, 1996; Kristensen *et al.*, 2009a). This is stratigraphically the lowermost of the two diamicts observed and, as exposed in coastal sections, is geographically confined to the distal (downfjord) ~2-3 km of the moraine systems. LFA 1 is interpreted to have been transported during a surge advance that reached the Nordre and Søre Leirodden, and deposited by melt-out as the glacier stagnated during quiescence. LFA 1 overlies LFA 3 sediments in several places at Nordre Nathorstbreen, implying that ice overrode and deformed sands and clays; the lenses of clay within the diamict at section NNM01 (Fig. 4.10ai) are interpreted as evidence of the reworking of underlying material into the subglacial debris during overriding (Kristensen *et al.*, 2009a).

4.7.1.2. LFA 2 (Diamict 2 - upper)

Based on the similarity in the sedimentary characteristics of the two lithofacies associations (poorly-sorted, fine-grained matrix, and sub-angular to sub-rounded and striated clasts), LFA 2 is interpreted as subglacial debris with a similar glaciomarine origin as LFA 1. Two main observations suggest that LFA 2 is related to a separate, more-recent glacier advance within Van Keulenfjorden than that which deposited LFA 1: (i) at section NNM04, LFA 2 directly overlies LFA 1 and there is a sharp contact between the two, which is interpreted as evidence for ice overriding LFA 1 post-depositionally, and subsequently depositing LFA 2 on top; and (ii) LFA 2 is not found in the distal parts of the moraine complexes but is the dominant lithofacies close to the active margin and within the sharpest-crested of the geometrical ridges, which is consistent with its deposition during a secondary, less extensive glacier advance than that which reached the Nordre and Søre Leirodden and deposited LFA 1. The sorted and sometimes contorted lenses of sand within LFA 2 are interpreted as the reworking of sediments within LFA 3 into the diamict.

The shell-poor nature of LFA 2 compared to LFA 1 could be the result of the effective entrainment and transportation, and therefore exhaustion, of shells during the earlier, more-extensive advance. In addition, the fragmentary nature of the shells that are found within LFA 2 is consistent with the re-working of shells which have already been entrained, transported and

deposited by ice. This is supported by the age of 5840-5994 cal. a^{-1} BP for the shell fragment within LFA 2 on the Søre Nathorstmorenen, which is far older than existing dates for glacier advances in Van Keulenfjorden which reached a position ~6 km further downfjord from the sampling site (Kempf, 2011), and therefore is likely to represent reworking of much older material, possibly over multiple glacier advance cycles.

4.7.1.3. LFA 3 (deformed sands and muds association)

The massive and, in places, laminated sands and shell-rich muds which contain evidence for faulting, folding and shearing are interpreted as shallow marine sediments which have been subject to glaciotectonic deformation in proglacial (e.g. NNM02 within the composite ridges) and ice-marginal/subglacial (e.g. NNM01, NNM05, SNM01 and SNM02) settings (Kristensen *et al.*, 2009a). At several locations on the Nordre Nathorstmorenen, LFA 3 sediments are overlain by LFA 1 (NNM01 and NNM05), which is interpreted as evidence for the overriding and deformation of shallow marine sediments by ice which advanced to the Nordre and Søre Leirodden; the water escape features and reverse faulting within LFA 3 at section NNM01 are consistent with dewatering and compaction caused by overlying ice, and could be described as a glaciotectonite (Benn and Evans, 1996). LFA 3 is also found in close association with LFA 2 at the transition in dominance between the two diamicts (e.g. SNM01 and SNM 02), where it has been subject to shear and large-scale folding. This is also interpreted as evidence for the deformation of shallow marine sediments in an ice-marginal position and, as it is in a location ~2 km upfjord from the distal extent of the moraine at Søre Leirodden, indicates that there is a second former ice contact position within the moraine complex; this in turn provides support for a second, less-extensive glacier advance which deposited LFA 2.

The exposure of highly folded LFA 3 within the composite ridge systems on the Nordre Nathorstmorenen, combined with an absence of diamict and a notable change in morphology compared to the hummocky topography of the rest of the moraine complex, is compelling evidence that the composite ridge systems are proglacial push moraines formed at the margin of a glacier advance. The style of folding and strike of fold axes within NNM02 (Fig. 4.10b) and exposed on the surface (Fig. 4.9i), in conjunction with the alignment of ridge crests on this part of the composite ridge (Fig. 4.5), are consistent with ice push from the south towards the lateral margins. The origin of the composite ridge systems are discussed further in *4.6.2.*

4.7.1.4. LFA 4 (undeformed sands and muds association)

This association is interpreted as undeformed shallow marine sediments which have been elevated into a subaerial position. The upwards-coarsening wavy laminated clays to sand exposed at NNM03 (Fig. 4.10aii) are interpreted as cyclopels grading into cyclopsams, which are suggested to represent sediments which have been subject to tidal influences (Stewart, 1991; Evans and Benn, 2004b) and are, therefore, consistent with a marine origin. This sequence is

overlain by sand with symmetrical ripple beds prograding in opposite directions, which is also consistent with tidally-influenced shallow marine sediments and indicates that NNM03 records a shallowing-upwards sequence. Cyclopsams and symmetrical ripple beds are also identified in SNM03 (4.13aii) at a position ~200 m inland from the fjord. Together, these sections indicate that shallow marine sediments have been elevated to a subaerial position and transported hundreds of metres without any evidence for deformation. An explanation for this is that the sediments were frozen at the time they were transported, presumably in a proglacial position in front of advancing ice. Both of these sections are also located immediately distal to the downfjord limits of LFA 2, providing further support for a second former ice contact position within the hummocky topography of the moraine complex (in addition to that at the distal margins).

4.7.1.5. LFA 5 (massive and contorted sand association)

This association was only observed within SNM03 and is interpreted as a mass flow deposit based on the homogenous nature of the fine sand matrix, the scattered gravel-sized clasts and the contorted coarse sand inclusions. This material was probably sourced from a similar shallow marine sequence as that which underlies it (Fig. 4.13aii). This interpretation is favoured ahead of a glaciotectonic origin due to the undeformed nature of the underlying laminated sands (LFA 4); it is difficult to conceive how the lower LFA 4 would remain untouched if the upper LFA 5 had been deformed by ice, but a mass flow could cover the lower sediments without affecting them.

4.7.2. The landform-sediment assemblage

4.7.2.1. Mud apron

The position, morphology and sedimentary characteristics of the mud apron at the active margin of Nathorstbreen are consistent with a continuously-failing mobile push moraine formed through the bulldozing of fjord-floor sediments in front of the advancing glacier (Fig. 4.14). The following observations support this interpretation: (i) the sediment composition of the mud apron, consisting of highly-saturated clayey silt (Fig. 4.8) with very few larger clasts, is consistent with material deposited in a marine setting (Prior *et al.*, 1984; Boulton *et al.*, 1996; Kristensen *et al.*, 2009a); (ii) the position of the mud apron within the fjord at locations where the pre-surge bathymetry indicated a water depth of ~20 m (Fig. 4.2g) is best explained by the tectonic thickening of fjord floor sediments in response to glacial push. The observed low gradient of both the subaerial and submarine parts of the mud apron, the latter demonstrated by the large grounded and elevated icebergs and measured water depths of <1 m in the centre of the fjord up to 1 km downfjord from the margin, are consistent with the oversteepening and subsequent failure as a debris flow of fjord floor sediments with low shear strength (Kristensen *et al.*, 2009a); (iii) the transverse ridges within the mud apron (Fig. 4.6e), which are typically

aligned parallel to the ice margin, are interpreted as minor compressional ridges formed as a result of glacial push (Boulton *et al.*, 1996; Kristensen *et al.*, 2009a); and (iv) the presence of flow structures on the surface of the mud apron and the observations of apron advance of tens-of-centimetres in a day indicate that it is actively flowing, supporting the interpretation of a continuously-failing push moraine that is in the process of being constructed.

These observations indicate that the mud apron is the result of both proglacial glaciotectonic deformation, bulldozing and folding the soft fjord floor sediments into a wedge that is at least 20 m thick at the ice margin; and gravitational processes, facilitating the continuous failure of the oversteepened front of the sediment wedge and forming a low gradient debris flow lobe extending downfjord (Fig. 4.14; Kristensen *et al.*, 2009a). The location of the 2012 margin and the mud apron is at the shallowest part of the fjord, and this has probably had a significant influence on its formation and, in particular, its emergence in a subaerial position. This is likely to be related to the fact that, based on the pre-surge bathymetry (Fig. 4.2g), Nathorstbreen was advancing against a reverse slope for ~10 km from the deepest part of Van Keulenfjorden from 2009 to its 2012 position. The glacier front would have effectively pushed the soft fjord floor sediment upslope as it advanced, incrementally increasing the vertical thickness of the sediment wedge over a distance of ~10 km through stacking and folding. By the time the glacier front reached the top of the reverse slope, e.g. at the shallowest part of the fjord in 2012, the sediment wedge was thick enough to breach the fjord surface. The advance against a reverse slope also explains why the mud apron is able to attain a significant vertical thickness despite being composed of sediment with a very low shear strength and high porewater pressure, which might be expected to fail continuously (Kristensen *et al.*, 2009a); the gravitational forces acting on the distal slope of the sediment wedge would be less influential than glaciotectonic deformation as it advanced upslope, therefore allowing the sediments to thicken vertically. Once the glacier reached the top of the reverse slope in 2012 and the fjord bed begins to slope away, gravitational processes exert a bigger influence on the sediment wedge, which fails and forms the low gradient debris flow lobe extending from the distal slope of the wedge (Fig. 4.14).

It is worth noting that Hamberg (1905; p. 11), when trying to reach Steenstrupdalen (Fig. 4.7) in 1898, reported that '*…der innere Teil des Fjords war wegen des bedeutenden Schlammabsatzes von Nathorst's Glacier so seicht, dass das Boot unablässlich auf den Grund lief*', which loosely translates as the inner part of Van Keulenfjorden being too shallow for boats due to the large amount of mud deposited by Nathorstbreen. In addition, the Hamberg (1905; Fig. 4.2b) map contains annotations near Nordre Leirodden describing '*Sehr seichtes und trübes Wasser*' (very shallow and turbid water) and '*Gestrandete Eisberge*' (stranded icebergs). These observations are consistent with a mud apron within the fjord associated with the 1898 position of Nathorstbreen.

4.7.2.2. Hummocky moraine

The hummocky topography which characterises the majority of the Nordre and Søre Nathorstmorenen contains large areas of irregular hummocks and ridges interspersed with zones of regular ridges, mapped as geometrical ridge networks and interpreted below in *4.7.2.3.* The sediment composition of the moraine primarily consists of LFAs 1 and 2 (diamicts 1 and 2), which have restricted geographical distributions; LFA 1 is stratigraphically the lowermost of the two and is located towards the distal margins of the moraine complexes, and LFA 2 is the dominant lithofacies close to the active margin (Fig. 4.15). These are interpreted as subglacial debris of a glaciomarine origin which has been transported by advances of Nathorstbreen to the distal margins of the moraine complexes. Buried ice is observed within the moraine complexes in several locations, indicating that large parts remain ice-cored. The melting of ice cores and degradation of the moraine through thermo-erosion processes (Etzelmüller *et al.*, 1996, 2000; Etzelmüller and Hagen, 2005) is evident across the Nordre and Søre Nathorstmorenen in the form of tension cracks (Fig. 4.12f) and numerous debris flows, which indicate internal instabilities and sediment remobilisation (Bennett *et al.*, 2000b; Lukas *et al.*, 2005). The numerous pools within the moraine complexes are interpreted as kettle lakes formed by the complete or partial melting of buried ice bodies; these are often more densely-grouped towards the distal margins of the moraines (Fig. 4.5). Together, the general topography and sediment composition of the moraine complexes are consistent with the subaerial stagnation and degradation of the former bed of Nathorstbreen through thermo-erosion processes, leading to topographic inversion (Etzelmüller *et al.*, 1996).

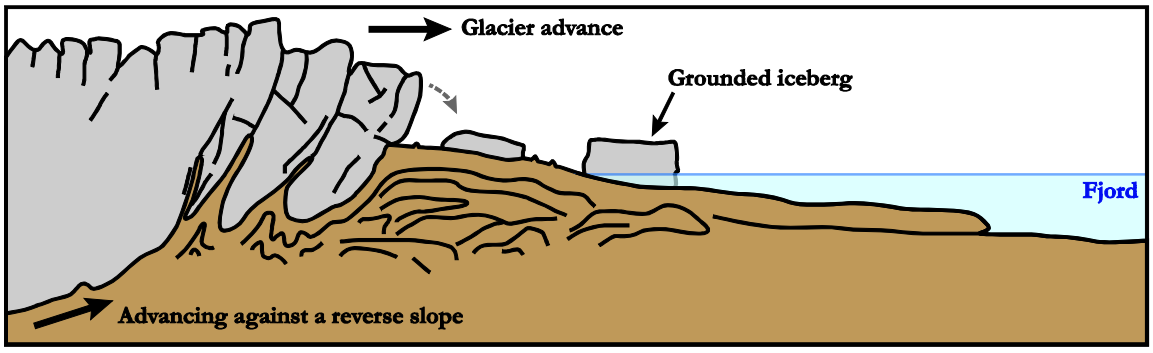

Figure 4.14 – Formation of the mud apron at the active margin. Adapted from Kristensen *et al.* (2009a).

Aside from the geometrical ridge networks (*4.7.2.3.*), evidence for organisation and linearity within the moraine complexes is limited to the corridors of streamlined sediment cover (Fig. 4.5). The alignment of the streamlining parallel or sub-parallel to the central axis of the fjord is consistent with these areas representing fluted surfaces formed at the bed as the glacier advanced downfjord. The preservation of this linearity may reflect less buried ice and, therefore,

limited re-working due to thermo-erosion activity, although numerous pools are still associated with these areas.

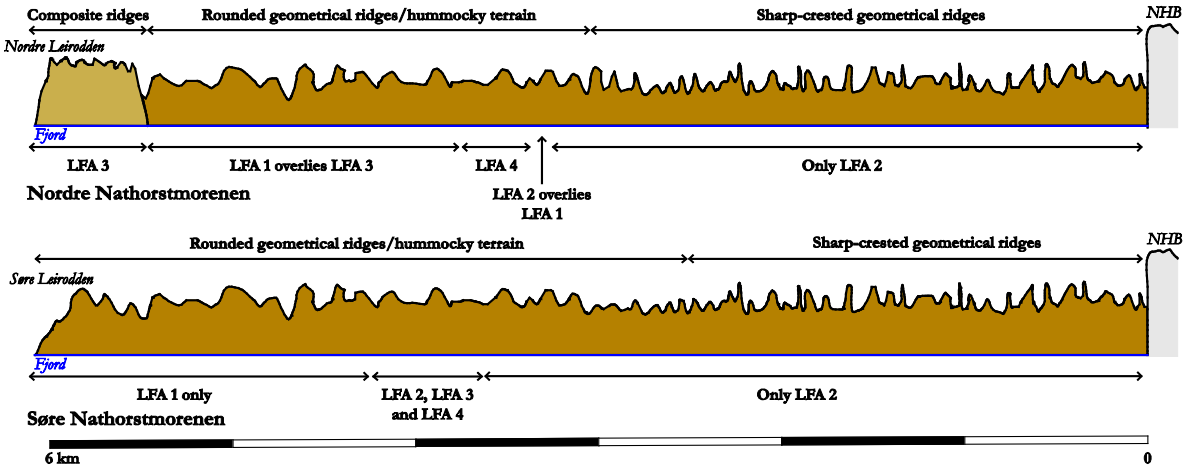

Figure 4.15 – Composite diagram of moraine structure showing geographical distribution of lithofacies associations.

The distribution of lithofacies and lithofacies associations observed in sediment exposures provides a strong indication that at least two separate glacier advances are recorded within the moraine system. This is based on the identified downfjord transition from predominantly LFA 2, typically within sharp-crested geometrical ridges, to areas of deformed shallow marine sediments (LFA 3) closely associated with LFA 2 and tidally-influenced shallow marine sediments elevated to a subaerial position without being deformed (LFA 4). Both LFA 3 and LFA 4 in these positions are interpreted to have been transported and emplaced proglacially, based on: (i) their location at the downglacier transition from the (proximal) zones of LFA 2 to the (distal) zones of LFA 1 (Fig. 4.15), which are inferred to have been deposited by two separate glacier advances. LFA 3 and LFA 4 are, therefore, located at the distal margin of the inner advance which deposited LFA 2; (ii) the style of deformation within LFA 3 is consistent with proglacial glaciotectonic deformation, e.g. SNM02 where LFA 2 and LFA 3 form an overturned fold (Fig. 4.13c). This demonstrates that some of the ridges and hummocks within the moraine system are the result of proglacial deformation, rather than all being degraded geometrical ridges; (iii) the presence of undeformed shallow marine sediments with preserved laminations and ripple structures within LFA 4 in not only subaerial positions (Fig. 4.10aii), but also hundreds-of-metres inland, is hard to explain in any other way apart from transport and emplacement by an advancing ice margin. The undeformed nature of LFA 4 suggests that the shallow marine sequences are likely to have been frozen during this process.

The transition from diamict 2 to deformed or undeformed shallow marine sediments (LFA 2 to LFA3/4) occurs at approximately the same position within both Nordre and Søre Nathorstmorenen (Figs 4.7 and 4.14), indicating that this represents the former ice contact face of the inner advance. This also coincides with the downfjord limit of the area of sharp-crested

geometrical ridges (Fig. 4.15; *4.7.2.3.*). The ice contact face of the outer advance, which deposited LFA 1, is located at the distal limits of the hummocky moraine (Søre Nathorstmorenen), or the transition from hummocky moraine to composite ridges (Nordre Nathorstmorenen). This also delimits the lateral margins of the outer advance. The lateral margins of the inner advance are harder to determine, as there are no obvious geomorphological features to mark it (e.g. large lateral channels or composite ridge system) and sediment exposures were not investigated in the internal parts of the moraine complex. However, one observation may provide an indication of the approximate position of the lateral margins: on the Nordre Nathorstmorenen, there is an identifiable corridor immediately adjacent to the fjord/active margin which contains far fewer pools than the outermost part of the moraine (Fig. 4.5). This corridor widens from ~0.2 km at NNM04 to ~1.5 km adjacent to the active margin (Fig. 4.16). This is tentatively interpreted as the area associated with the inner advance based on the logic that the outermost, pool-rich zone is older and has therefore had a longer time to de-ice, resulting in more pools. A similar observation can be made in parts of the Søre Nathorstmorenen, but the lateral transition between pool-rich and pool-poor parts of the moraine is not as distinct.

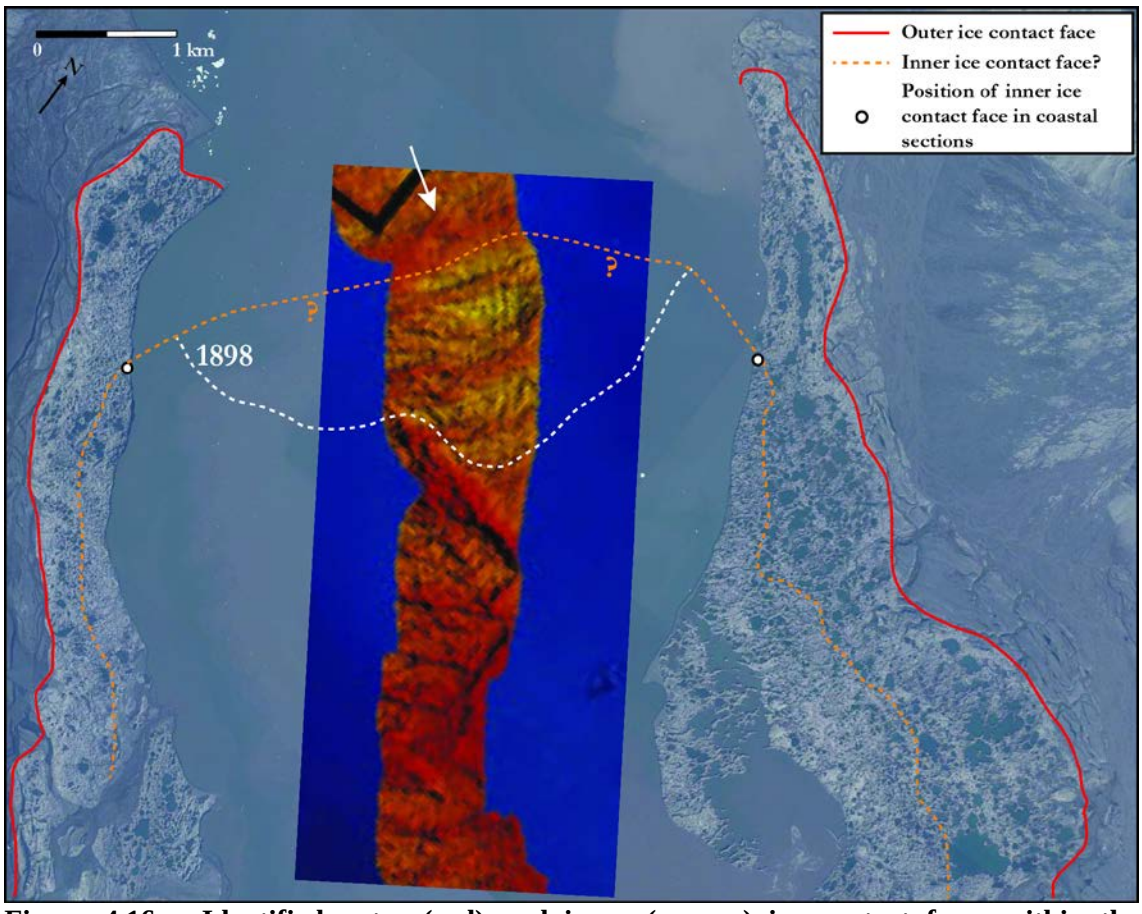

Figure 4.16 – Identified outer (red) and inner (orange) ice contact faces within the Nathorstbreen moraine system. White arrow highlights submarine ridge which corresponds closely to the inner position. Swath bathymetry data is from Ottesen *et al.* (2008), red indicates topographic high. 1898 glacier position is from Hamberg (1905). Underlying image is a 2011 aerial photograph provided by NPI.

4.7.2.3. Geometrical ridge networks

Geometrical ridge networks have been described at the terrestrial margins of several tidewater surge-type glaciers in Svalbard and two main processes have been proposed for their formation: the squeezing of subglacial debris into basal crevasses, particularly when the glacier settles back down to its bed upon surge termination (Gripp, 1929; Boulton *et al.*, 1996; Woodward *et al.*, 2002, 2003; Rea and Evans, 2011); and the thrusting of slabs of subglacial debris into englacial positions (Bennett *et al.*, 1996; Glasser *et al.*, 1998b; Bennett *et al.*, 1999). The Nathorstbreen geometrical ridges are typically composed of either LFA 1 or 2, which are interpreted as debris of a subglacial origin, and are consistent with both of the above processes. Similar to Gripp (1929; van der Meer, 2004), a basal crevasse squeeze interpretation is favoured for the majority of the geometrical ridges at Nathorstbreen, based on the following key observations: (i) muddy debris, consistent with a subglacial origin, was observed within near-vertical crevasses at the active glacier margin (Fig. 4.6d); (ii) the sharp-crested ridges and free-standing pinnacles, which are predominantly located close to the glacier margin, must be derived from englacial structures that were near-vertical, as lower-angle structures would distribute debris over a wider area when they melted-out (Bennett *et al.*, 1999; Kirkbride and Deline, 2013). This favours debris incorporated into near-vertical crevasses. It has also been suggested that debris pinnacles could form at the intersection of two debris-bearing thrusts (Bennett *et al.*, 1999); however, debris squeezed into vertical crevasses presents a simpler and more-logical interpretation, particularly as it is observed at the active margin (Fig. 4.6d); (iii) glaciomarine subglacial debris is likely to be soft and have a very low shear strength, which would appear to be more conducive to squeezing into basal crevasses than the tectonic elevation of cohesive slabs of debris via thrusts.

Investigations at Tunabreen, another tidewater surge-type glacier, are presented in *Chapter 5;* these demonstrate that debris can be incorporated into englacial positions during surges via several different processes, often in combination, and it is clear that englacial thrusting and faulting is one of these. However, as outlined above, the most important factor for forming such sharp-crested ridges and pinnacles as observed at Nathorstbreen is for the initial englacial debris inclusion to be near-vertical within the ice; this strongly favours injections of subglacial material into basal crevasses, followed by widespread ice stagnation.

The sharpest-crested, tallest and densest groups of crevasse squeeze ridges are located close to the active margin on both the Nordre and Søre Nathorstmorenen, within the zone where LFA 2 is the dominant lithofacies association (Fig. 4.15). The ridges become more rounded and degraded towards the distal parts of the moraine complexes (Fig. 4.15) and as a result are often difficult to identify as individual landforms within the general hummocky topography of the moraine. This notable change in ridge morphology provides a further indication that the moraine complex records at least two separate advances, with the freshest, sharpest ridges associated with the most-recent advance and the rounded ridges with a more-extensive, earlier advance. This is supported by the observations of sharp-crested ridges by Gripp (1929; van der

Meer, 2004) at the same locations as in this study, which indicates that they have not undergone significant degradation in the intervening ~80 years; therefore, it is unlikely that the more-rounded ridges in the distal parts of the moraine complex were formed contemporaneously, as they are significantly more-degraded and so are unlikely to have melted-out at approximately the same time.

4.7.2.4. Composite ridge systems

The composite ridge systems at the margins of Nordre Nathorstmorenen are interpreted as a terrestrial push moraine belt formed through proglacial glaciotectonic deformation of shallow marine sediments at the margins of the outermost advance. The push moraine belt can be broadly divided into sand-rich ridges, composed of LFA 3, and mud-rich ridges (Fig. 4.5). Parts of the sandy ridges are characterised by highly folded sands and flame structures (NNM02; Fig. 4.10b), indicating soft sediment deformation and associated liquefaction processes. Several observations support this interpretation: (i) the sediment composition is consistent with material sourced from a shallow marine environment and/or, in the case of the shell-rich and mud-rich part of the moraine belt, fjord-floor sediments. No diamict was observed within the push moraine belt and there is a sharp transition from diamict-rich hummocky moraine to diamict-free push moraine, supporting a proglacial origin for the latter; (ii) The majority of the multiple ridge crests, particularly within the sand-rich part of the push moraine, are oriented parallel to the contact with the hummocky moraine and, therefore, the inferred ice contact face (Fig. 4.5). This is consistent with ridge crests formed perpendicular to the direction of ice push (Hart and Watts, 1997; Boulton *et al.*, 1999; Bennett, 2001) as the glacier splays laterally towards the margins, as can be in Fig. 4.1; (iii) the strike of fold axes within NNM02 (Fig. 4.10b) and exposed on the moraine surface (Fig. 4.9i) are aligned parallel to ridge crests and perpendicular to the inferred ice contact face, suggesting that the principle direction of deformation was towards the lateral margins; this is consistent with proglacial glaciotectonics at a splayed ice margin.

The mud-rich part of the push moraine belt consists of clayey-silt with a similar grain size distribution to the active mud apron (Fig. 4.8) and is shell-rich (Fig. 4.9k). Based on this, it is interpreted as a mud apron formed by the proglacial bulldozing of fjord floor sediments into a terrestrial position, as suggested by Kristensen *et al.* (2009a) for the formation of the distal parts of the Damesmorenen, Geikemorenen and Torrelmorenen in inner Van Mijenfjorden (Fig. 3.2). This represents a terrestrial, palaeo example of the active mud apron at the margin of the current surge of Nathorstbreen. There is obviously a significant difference in the topography of the active mud apron, which is extremely flat in the areas where it has started to advance into terrestrial positions (Fig. 4.6f), and the mud-rich push moraine which is typically ~8-10 m high. As suggested by Kristensen *et al.* (2009a), this may reflect the highly-saturated and, therefore, significantly lower shear strength due to higher porewater pressure of the active mud apron (Fig.

4.6h). In a terrestrial position, the water would be able to drain away, decreasing the porewater pressure and increasing shear strength; this would be more conducive to the formation of steeper and higher ridges due to glaciotectonic deformation (Bennett, 2001), as would the presence of frozen sediments (Etzelmüller *et al.*, 1996; Etzelmüller and Hagen, 2005).

It is notable that push moraines are absent from the margins of Søre Nathorstmorenen. Two main reasons may explain this: firstly, Van Keulenfjorden is aligned north-south in the innermost areas, which favours ice expansion towards the Nordre Nathorstmorenen during glacier advances; this is demonstrated by the terminus splaying much more to the north and northeast during the current surge (Figs 4.1 and 4.3). This would clearly favour the proglacial bulldozing of shallow marine and fjord floor sediments towards the distal margins of the Nordre Nathorstmorenen. In contrast, there is little or no evidence of splaying towards the margins of the Søre Nathorstmorenen during the current surge, with the glacier flow largely focused along the central axis of the fjord in these locations (Figs 4.1 and 4.3). Secondly, the formation of push moraines is dependent on the availability of deformable sediment, and this may be more restricted in the southern parts of the fjord.

4.7.3. Surge history revisited

The sedimentological evidence for two separate advances within the Nathorstbreen moraine complexes does not fit into the existing chronology of surges suggested by Ottesen *et al.* (2008) and Kempf (2011). Based on the 1898 map by Hamberg (1905), Ottesen *et al.* (2008) suggested that the Nordre and Søre Nathorstmorenen and the large submarine ridge immediately downfjord of their distal margins (Fig. 4.3e) were formed by a surge in the 1870s or 1880s. This is a logical interpretation if the entire moraine complex relates to one advance; however, the sedimentological evidence presented in this study demonstrates that at least two former ice contact faces are present within the moraines. If the outermost part of the moraines was formed in the late 1800s, it is logical that the inner, stratigraphically younger advance would have occurred sometime between then and the current surge. This is not supported by the changes in terminus position recorded over this period, which show stepped retreat of the tidewater front back towards the inner parts of the fjord (Carlsen, 2004; Ottesen *et al.*, 2008).

Instead, it is suggested that the inner advance corresponds to the 1898 position. Fig. 4.16 shows the 1898 tidewater limit plotted with the position of the inner ice contact face, as exposed in coastal sections, and shows that they are in fairly good agreement. The shape of the 1898 margin is interpreted as a large calving bay, similar to Ottesen *et al.* (2008), implying that the glacier was in the early stages of retreat. The downfjord mismatch of ~0.5-1 km between the lateral margins of the 1898 front and the ice contact position could be explained by the presence of ‘horns’ at these locations, which typically develop within tidewater glacier fronts because calving rates are often greater in the centre of the fjord than at the margins. If this interpretation is valid, the surge maximum in this location should also be recorded in the submarine

geomorphology in the form of a cross-fjord ridge, as observed both in a position downfjord of the moraine complexes in Van Keulenfjorden (Fig. 4.2) and at other tidewater surge-type glacier margins in Svalbard (Plassen *et al.*, 2004; Ottesen and Dowdeswell, 2006; Ottesen *et al.*, 2008; Kristensen *et al.*, 2009a; Flink, 2013). Fig. 4.16 shows that there is a ~500 m-wide topographic high located immediately downfjord from the 1898 limit and inner ice contact position, but upfjord from the larger transverse ridge associated with the outer advance. This could therefore represent the surge maximum of the inner advance which occurred prior to 1898, suggesting that the ice margin was similar to the position shown in Fig. 4.16.

Based on this, the outer advance which reached the Nordre and Søre Leirodden and deposited the large transverse submarine ridge mapped by Ottesen *et al.* (2008) must be older than 1898. This is supported by the radiocarbon ages from *H. arctica* bivalve pairs on the mud-rich push moraine, which recorded well-clustered ages of between 854-1297 cal. a^{-1} BP (Table 4.1). This push moraine is located at the ice contact face of the outer advance, and is interpreted to have formed through proglacial glaciotectonic deformation. The bivalve pairs were all in life position on the moraine surface (Fig. 4.9k), which provides a strong indication that their ages can be correlated to the bulldozing of fjord floor sediments and emplacement of the push moraine in a terrestrial position. These older ages are in agreement with Kempf (2011), who suggested that the large transverse submarine ridge associated with the outer advance was considerably older than 1898. However, Kempf (2011) reported ages of 2,710±40 and 2,650±60 cal. a^{-1} BP for the debris flow associated with this ridge, indicating that this may record an older advance again. Based on this, there is evidence for glacier advances in Van Keulenfjorden in ~2,700 cal. a^{-1} BP, ~854-1297 cal. a^{-1} BP, ~1898 AD and 2008 to present; the current observations and landform-sediment assemblages associated with the older advances are consistent with these relating glacier to surges.

4.8. Summary

Nathorstbreen and its tributaries began surging in 2008 and by August 2013 had advanced ~18 km along Van Keulenfjorden at an average speed of 10 m d^{-1} (Sund *et al.*, 2013), making it one of the largest surges ever observed on Svalbard. A large mud apron was observed within the fjord at the glacier margin in July 2012, and this is interpreted as a continuously failing mobile push moraine formed as the glacier has advanced and bulldozed fjord floor sediments. The fjord is flanked by the lateral moraine complexes of the Nordre and Søre Nathorstmorenen, which record evidence for at least two more-extensive advances of Nathorstbreen. The outer advance reached the Nordre and Søre Leirodden and deposited a large transverse submarine ridge, mapped by Ottesen *et al.* (2008). This advance also bulldozed a push moraine belt composed of shallow marine fjord floor sediments at the distal margins of the Nordre Nathorstmorenen; the shell-rich and mud-rich part of the push moraine is interpreted as a palaeo terrestrial version of

the active mud apron at the glacier margin. Four bivalve pairs of *H. arctica* returned ages of between 854-1297 cal. a^{-1} BP, providing a maximum age for the outer advance.

A second, less extensive advance can be identified within the moraine complexes based on lithofacies associations exposed in coastal sections. These demonstrate that there are two diamicts (LFA1 and 2), interpreted as subglacial debris of a glaciomarine origin, which occur in geographically distinct locations. LFA 2 is found in the inner parts of the fjord, close to the active margin, and is closely associated with sharp-crested crevasse squeeze ridges. This diamict grades into LFA 3 and LFA 4, interpreted as highly deformed and undeformed shallow marine sediments, respectively, at a position ~2 km upfjord from the Nordre and Søre Leirodden, and is not found down fjord of this position; this is inferred to represent the former ice contact face of the inner advance. The distal margins of the moraine complex are composed of LFA 1, which is stratigraphically the lowermost of the two diamicts and is far more shell-rich. Based on this, it is interpreted that LFA 1 was deposited by the outer advance at ~854-1297 cal. a^{-1} BP, and LFA 2 was deposited by the inner advance. The inner ice contact positions correspond closely to the glacier margin mapped in 1898 by Hamberg (1905) and a sizable submarine ridge identified on the swath bathymetry data presented by Ottesen *et al.* (2008); it is suggested that this marks the surge maximum of the inner advance, which probably occurred slightly before 1898.

Chapter Five
Tunabreen

78º 32.0' N, 17º 30.0' E

After its location between Ultunafjella and Langtunafjella, named after the Swedish College of Agriculture, Ultuna, south of Uppsala, where Swedish geologist, chemist and botanist H. A. von Post, student of the Quaternary period, worked for several years.

The place names of Svalbard, Norsk Polarinstitutt

5. Tunabreen

5.1. Introduction

This chapter presents and interprets the results from two ice-marginal environments located at the front of Tunabreen, a tidewater glacier in the east of central Spitsbergen (Fig. 3.2). Fieldwork was conducted in both spring and summer seasons between 2011 and 2013. The spring work focused on the first ice-marginal setting: exposures of debris-rich basal ice and structures within the glacier terminus (*5.4.*). Sedimentological analysis, stable isotope analysis and structural descriptions and measurements were applied to two sections within the tidewater ice cliff, named the NW and SE (split into A and B) sections. Summer fieldwork investigated the second ice-marginal environment: the proglacial areas of Tunabreen and an adjacent glacier, Von Postbreen (*5.5.*). This work involved sedimentological analysis and geomorphological mapping from aerial photographs and swath bathymetry data. The first part of this chapter will describe the geographical and glaciological setting of the study area (*5.2.*) and provide a context for the later work by reconstructing the surge history of Tunabreen and neighbouring glaciers from published sources and remote sensing data (*5.3.*; see Table A1 for details on data sources used).

5.2. Study area

Tunabreen drains the Lomonosovfonna and Filchnerfonna ice caps (Hagen *et al.*, 1993; Nuth *et al.*, 2010) and terminates at the head of Tempelfjorden, a ~15 km-long and up to 5 km-wide fjord at the eastern end of Isfjorden in central Svalbard (Fig. 5.1). Bedrock geology in the area is composed of conglomerates, sandstones and shales of the Billefjorden Group overlain by sandstones, carbonates, shales and cherts of the Dickson Land Subgroup (Cutbill and Challinor, 1965; Dallmann *et al.*, 2002; Fleming *et al.*, 2013). The glacier is ~33 km long, has an area of ~174 km^2 (Nuth *et al.*, 2010) and is ~3 km wide for much of its length including at its tidewater margin, where it terminates as a ~40 m-high ice cliff grounded in water of approximately the same depth (Flink, 2013; Flink *et al.*, submitted). Hagen *et al.* (1993) reported a mean ice thickness of ~202 m for the whole glacier, and Hodgkins and Dowdeswell (1994) suggested that a deep trough below sea level is unlikely to extend far upglacier. Existing radio echo-sounding records indicate that the glacier is polythermal (Bamber, 1987). The neighbouring glaciers in the study area include Von Postbreen, Bogebreen, Brucebreen and Philippbreen (Fig. 5.1), all of which are currently land-terminating. Tunabreen, Von Postbreen, Bogebreen and Philippbreen are all confluent and separated by medial moraines.

5.3. Surge history

Of the glaciers that terminate at the head of Tempelfjorden, Tunabreen, Von Postbreen and Bogebreen are classified as surge-type glaciers (Hagen *et al.*, 1993). Tunabreen is unique in terms of Svalbard surging glaciers as it has been observed to surge three times (Forwick *et al.*,

2010; Mansell *et al.*, 2012) and this record of multiple advances, in conjunction with that of Von Postbreen, is the main focus of this section. Bogebreen underwent a surge that began prior to 1980 (Dowdeswell *et al.*, 1984) and Brucebreen and Philippbreen have no reported surges. However, a photograph of Brucebreen taken in 1910 and published in Lamplugh (1911) shows a heavily-crevassed glacier extending down to the fjord, indicating that it may have been surging at that time.

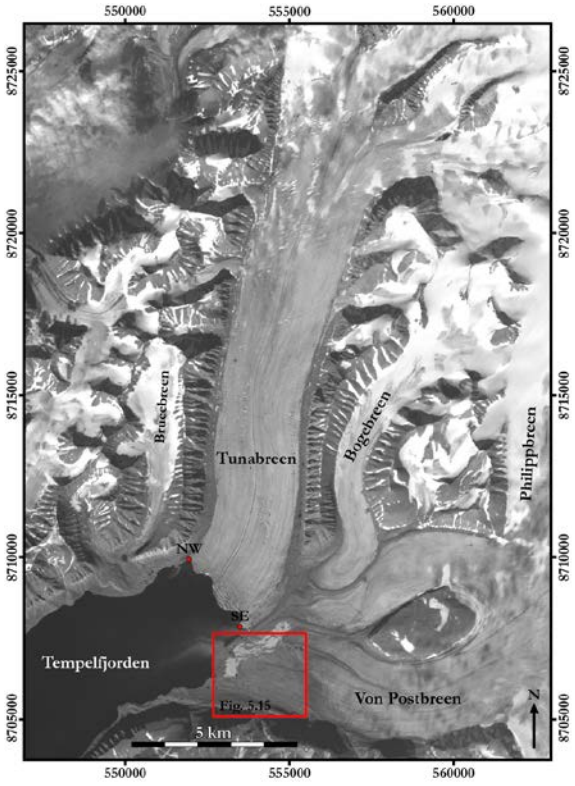

Figure 5.1 – Locations of Tunabreen, Von Postbreen and neighbouring glaciers at the head of Tempelfjorden shown on 2010 ASTER image. Location of NW and SE sections are shown. Red rectangle delimits area mapped in Fig. 5.15. See Fig. 3.2 for location in Svalbard

5.3.1. Tunabreen and Von Postbreen: 1870-2002

Figure 5.2 summarises the glacier terminus fluctuations of Tunabreen and Von Postbreen from 1870 up to 2012. The distances in Fig. 5.2b have been averaged along the entire length of the margin and are calculated from the position of the ice divide given by Hagen *et al.* (1993), apart from years 1924 and 1970 which are positioned relative to mapped limits based on published observations. The most-extensive position shown is that of Von Postbreen in 1870, as mapped by de Geer (1910) and reproduced in Plassen *et al*. (2004), when the glacier terminated ~4.5 km downfjord from the 2012 Tunabreen margin. This position is thought to be the result of a surge and represents the maximum glacier extent in Tempelfjorden during the Holocene, and the culmination of Little Ice Age (LIA) glacier regrowth following an extended period of stepwise retreat post-dating the last glacial (Forwick *et al.*, 2010). The mapped 1870 position coincides with a 70 m-high submarine moraine with a large debris flow lobe at its distal margin, and the downglacier limit of a subaerial lateral moraine located on the southern side of Tempelfjorden (Plassen *et al.*, 2004; Flink, 2013). The position of the Von Postbreen terminus was also mapped

in 1882, 1896 and 1908 by de Geer (1910), indicating a retreat of ~2 km in ca. 40 years (Fig. 5.2).

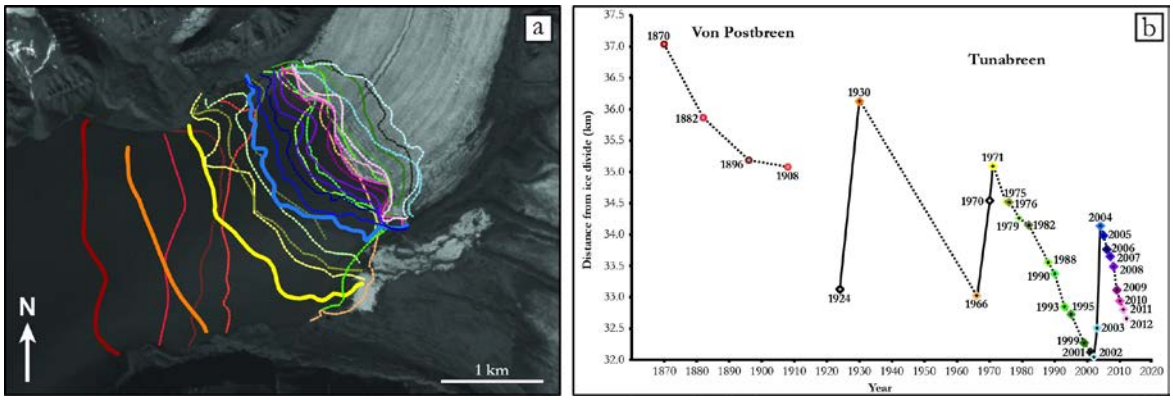

Figure 5.2 - Terminus fluctuations of Tunabreen and Von Postbreen 1870-2012. (a) Terminus positions overlain on 2010 ASTER image. Solid lines represent surge limits, dashed lines represent retreat positions. Graph of terminus position change. Colours in (a) correspond to dated points in (b).

There is no mapped record for the 1924 margin, so the position in Fig. 5.2b has been estimated relative to the mapped 1930 position (Liestøl, 1969). The switch of the dominant flow unit from Von Postbreen to Tunabreen during this advance is clear in oblique photographs published in Liestøl (1969), which show a small, pinched-out Tunabreen comprising <25% of the coalescent terminus and a deflected medial moraine in 1924. This contrasts with the situation in 1932, where Tunabreen makes up over a third of the advanced coalescent terminus and a straightened medial moraine is evident. The 1930s position marks the extent of a surge of Tunabreen, and coincides with a submarine moraine imaged on swath bathymetry data in Flink (2013). This position is ~1 km upfjord from the 1870 Von Postbreen surge limit.

Following the 1930s surge, the next available mapped position is 1966, recording a retreat of ~3 km in the intervening ca. 36 years (Fig. 5.2). Between 1966 and 1970, the glacier began to surge again and had advanced ~2 km by 1971 (Hodgkins and Dowdeswell, 1994). The 1971 surge limit was a further ~1 km upfjord from the 1930s surge limit (Fig. 5.2), and similarly coincides with a large submarine ridge mapped from swath bathymetry data by Flink (2013). The retreat of the margin following the 1970s surge is well documented, primarily due to the increased availability of satellite images at this time, and shows a stepped retreat of ~3 km in 31 years up to 2002.

5.3.2. Tunabreen: 2003-2012

Between June 2002 and August 2003 the Tunabreen margin began to advance, marking the onset of the most-recent surge (Fig. 5.2). The heavily-splayed 2004 margin delimits the surge maximum, as by 2005 the front had retreated by a few hundred metres, indicating that the surge terminated sometime between August 2004 and June 2005. At the 2004 maximum, the SE

margin splayed laterally into an embayment cut into the medial moraine which is visible on pre-surge imagery (indicated by black arrows in Fig. 5.3). During the surge the margin advanced by >2 km to a position ~1 km upfjord from the 1971 surge maximum. The broad-scale change in the crevasse pattern during this period is shown in Figure 5.3. This highlights an upglacier propagation of crevassing from 2002, when only the tidewater terminus exhibited large transverse crevasses, up to 2004 and 2005, when open crevasses existed along the entire length of the lower tongue.

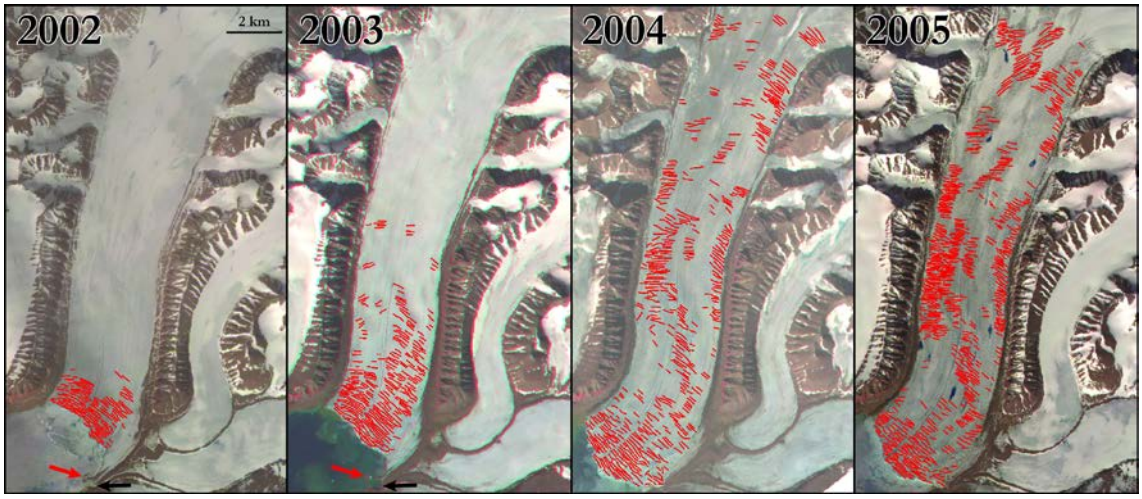

Figure 5.3 – Tunabreen crevasse pattern change 2002-2005 mapped from ASTER images. On the 2002 (pre-surge) and 2003 (early active phase) images, black arrows indicate embayment cut into medial moraine and red arrows indicate delta-shaped feature in the fjord.

Since 2004, the Tunabreen terminus has undergone stepped retreat of ~1.5 km to its 2012 position, which approximately corresponds with the glacier front in 1995 (Fig. 5.2). During this period two large calving bays have developed in the front, as well as a notable 'peninsula' at the SE margin (Fig. 5.4a), within which sections SE-A and SE-B are located (see *5.4.*). This 'peninsula' coincides with an isolated delta-shaped area of topography in the fjord, appearing to extend from supraglacial debris cover, which is visible on pre-surge imagery (indicated by red arrows in Fig. 5.3). A number of the post-2004 margin positions have been correlated to regularly-spaced, small (2-4 m high) crossfjord submarine ridges by Flink (2013) and Flink *et al.* (submitted), which were interpreted as annual moraines.

5.3.3. Observations summary

The surge histories of Tunabreen and Von Postbreen from 1870-2012 display some interesting patterns when plotted together (Fig. 5.2). The first notable observation is the consistent surge return period of Tunabreen of approximately 40 years over three surges, as previously reported by a number of studies (Dowdeswell *et al.*, 1991; Hagen *et al.*, 1993; Murray *et al.*, 2003b; Mansell *et al.*, 2012). This is the shortest surge cycle observed in Svalbard, with the next

shortest (based on two surges) being Blomstrandbreen (~47 years; Mansell *et al.*, 2012) and Hambergbreen (70 years; Dowdeswell *et al.*, 1991). It is also interesting that the maximum surge position of Tunabreen has been successively less-extensive by ~1 km each time, a pattern that is maintained if the 1870 Von Postbreen limit is also included (Fig. 5.2). Finally, the changing crevasse pattern during the most-recent surge (Fig. 5.3) suggests that an extensional stress regime propagated upglacier from the terminus. This may indicate that a surge front did not propagate downglacier during the surge, as observed at some surge-type glaciers in Svalbard (Murray *et al.*, 1997, 1998), but instead the surge initiated at the tidewater front (Rolstad *et al.*, 1997; Murray *et al.*, 2003a,b). These observations will be discussed in a wider context in *Chapter 9*.

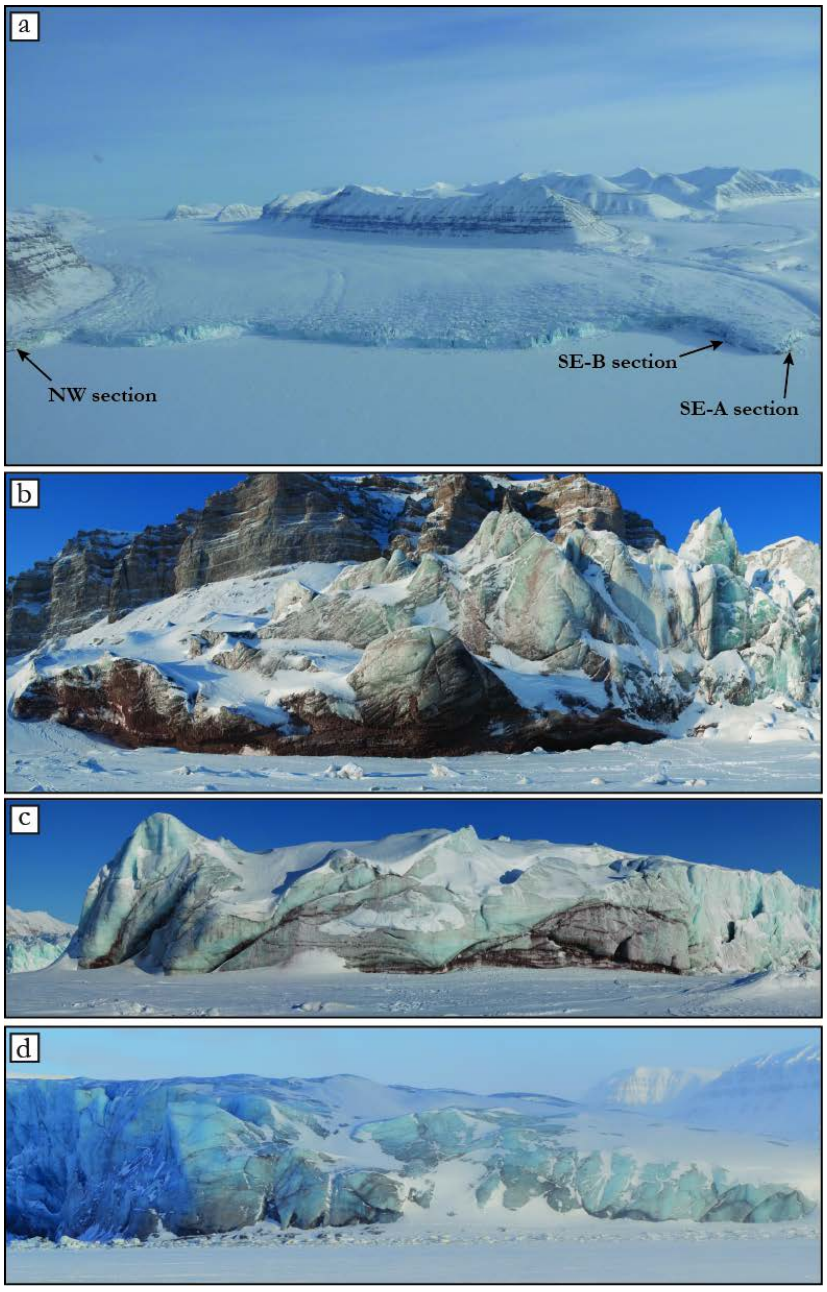

Figure 5.4 – Overview of Tunabreen section locations. (a) Tunabreen ice front in April 2011 with sections labelled (photo by Doug Benn). (b) NW section, March 2011. (c) SE-A section, March 2011. (d) SE-B section, April 2012.

5.4. Englacial debris-rich exposures

Calving and retreat of the Tunabreen terminus following surge termination in 2004 (Fig. 5.2) has exposed large areas of debris-rich ice and englacial structures in the ice cliff at two main sites, located at the northwest and southeast lateral margins of the glacier front (Figs 5.1 and 5.4). These sites were investigated in three successive spring field seasons (2011-2013), when the tidewater front could be accessed by snow scooter on the sea ice, and also in August 2011 by boat.

The site at the northwest margin, hereafter referred to as the NW section, is a ~100 m-long exposure of up to 15 m-thick debris-rich basal ice interspersed with clean ice layers (Fig. 5.4b and 5.5a). The section is located at the boundary between glacier ice and the ice-cored lateral moraine extending along the northern shore of Tempelfjorden, and is ~1 km upglacier from the 2004 surge maximum. The general orientation of the NW section is northeast-southwest, and the ice cliff above the northeastern end rises up to ~40 m. Data was only collected from this section in spring 2011, as by subsequent visits it had suffered large collapses and was too poorly exposed.

The exposures at the southeastern margin are located on either side of a grounded 'peninsula' between a large calving bay to the north and an embayment cut into the medial moraine to the south (Figs 5.1 and 5.4a). The 'peninsula' is coincident with a delta-shaped area of topography which is, along with the embayment, visible at the glacier margin on pre-surge imagery (Fig. 5.3). The SE-A section (Figs 5.4c and 5.5b) is located on the southern side and is ~180 m long, and the SE-B section (Figs 5.4d and 5.5c) on the northern side is ~160 m long. Both sections are within ~30 m high ice cliffs and contain discrete debris-rich structures or bands surrounded by predominantly clean ice. Areas of debris-rich basal ice interspersed with clean ice layers are also present, but these are not as continuous or as thick as at the NW section. The SE-A section is aligned broadly east-west and the SE-B section is aligned northeast-southwest. Fieldwork was conducted at the SE-A section in spring 2011 and 2012 and summer 2011, and at the SE-B section in spring 2012 and 2013.

In *5.4.1.*, the physical character of the clean and debris-rich ice facies at both sites is described, including thickness, sedimentological characteristics (including structure, clast shape, grain size distribution and debris content) and bubble content and type. Results from stable isotope analysis of the different ice facies are presented in *5.4.2.* The overall structure of the sections, including ice facies distribution and the character of debris-rich bands, is addressed in *5.4.3.*

Figure 5.5 – Tunabreen section logs. (a) NW section. (b) SE-A section. (c) SE-B section. Clast fabric data in (a) and debris-rich band structural data in (c) plotted onto lower hemisphere, equal-area stereographic projections. Red arrows on stereographs show centre-line ice flow direction at the terminus.

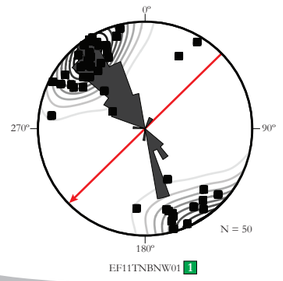

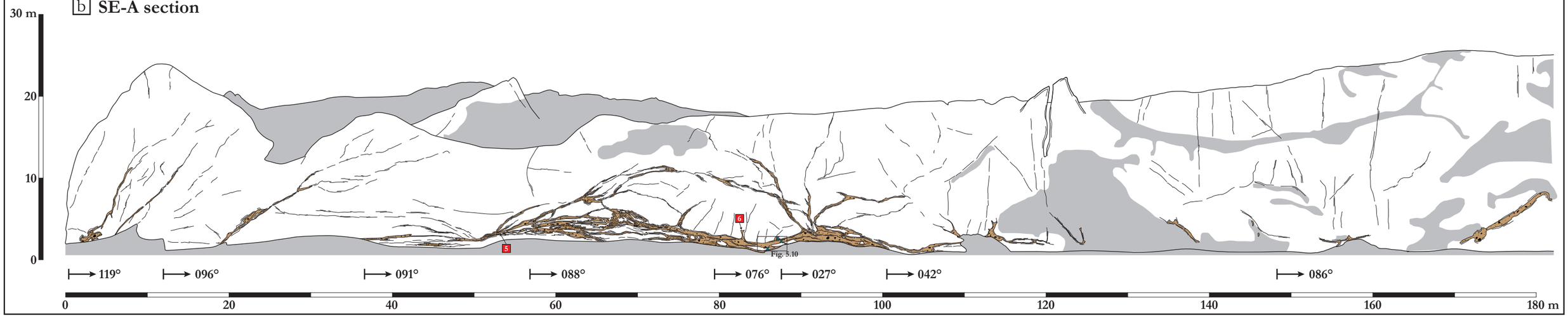

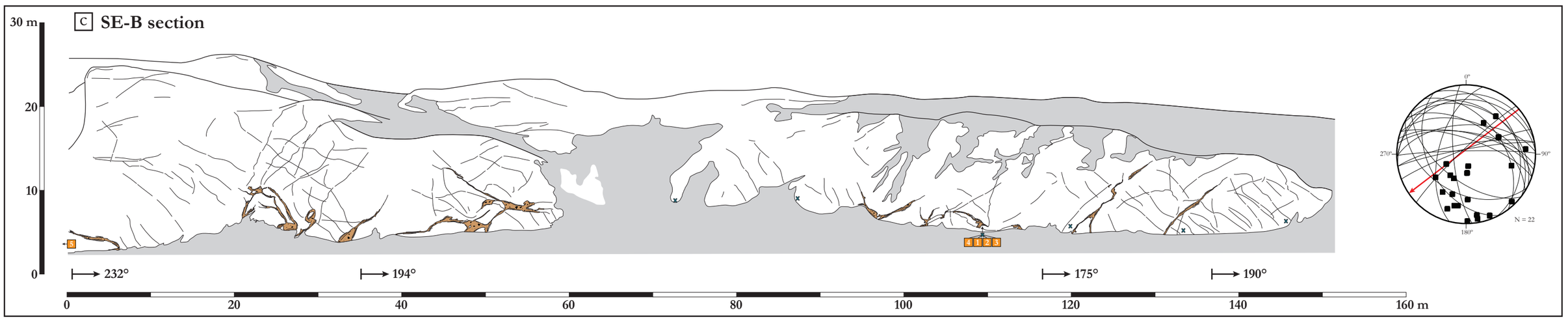

5.4.1. Ice facies physical character

The debris-rich basal ice exposed at Tunabreen is identified as stratified facies ice, which has been subdivided into three subfacies: solid stratified, banded and solid, following the Hubbard *et al.* (2009) scheme. In places, specifically at the SE sections, the differentiation between the solid stratified and banded subfacies is indistinct and they appear to exist on a continuum. This is particularly apparent where the solid stratified subfacies contains numerous ice lenses and the banded subfacies has a high debris content. The distinction between the two is clearest at the NW section, and this is reflected in the log (Fig. 5.5a), whereas at the SE sections it is overly complex and so only stratified facies ice is represented (Figs 5.5b and 5.5c). The areas of clean ice (defined as ice with a visually-estimated typical debris content of <1%) are predominantly composed of englacial facies ice, but also contains some geographically-restricted zones of a dispersed facies. The scale of the full section logs (Fig. 5.5) means that the complex distribution of the dispersed facies cannot be accurately represented.

5.4.1.1. Stratified facies

Solid stratified subfacies

This subfacies is composed of frozen diamict with interstitial ice in pores and small lenses of clean ice with no or very few bubbles (Figs 5.6a-e). The reddish-brown diamict is matrix-supported and has a polymodal grain size distribution, with identifiable peaks in the silt and sand size ranges (Fig. 5.7), and includes occasional boulders up to 0.5 m in diameter. At the SE-A section, thin layers of sorted sand were observed in some places (Fig. 5.6d). Clasts within the subfacies are typically sub-angular to sub-rounded (Fig. 5.8), with the majority displaying striations, gouges, grooves or faceting. Bullet-shaped clasts are common (typically 10-20%) and a variety of lithologies are present (including limestone and red and white sandstones). The subfacies is in general crudely stratified, highlighted by the presence of numerous thin clean ice lenses (Figs 5.6a and 5.6e), but can also appear structureless and largely devoid of ice lenses in some areas, particularly at the base of debris-rich bands at the SE sections (Fig. 5.6b). The clean ice lenses are typically between 0.2 and 3 cm thick and can be up to 15 cm long. Occasional larger clean ice lenses are present, and these have a core of bubble-rich ice surrounded by a 2-3 cm thick border of ice containing no bubbles (Fig. 5.6c).

The debris content of the stratified facies appears variable based on observations, and ranges from measured values of 9.6-52.0% (by volume) at one site in the SE-B section. The upper measured values of 50.0% and 52.0% are thought to be representative of the lower debris content end of the solid stratified subfacies, and visual estimations (relative to measured values) indicate typical contents of ~75%. The thickness of this subfacies ranges from 0.1-2.5 m across all sections, and is continuous throughout the NW section (Fig. 5.5.a).

Banded subfacies

The banded subfacies is characterised by laterally discontinuous, broadly parallel to sub-parallel debris-rich laminae separated by layers of clean ice containing no or very few bubbles (Figs 5.6f-l). The thickness of the debris-rich laminae ranges from <1-5 mm, with an observed maximum width of ~10 mm. The spacing between the laminae, or the thickness of the clean ice layers, ranges from ~1-40 mm across all sections. The debris-rich laminae are typically undulating and aligned sub-horizontally to the section base, and can be continuous for up to a metre but generally attenuate or merge beyond this (Figs 5.6f and 5.6l). The debris ranges from small fine-grained clots of silt and sand within the thinner laminae (Fig. 5.6g) up to diamict with a typical maximum grain size of 20-30 mm clasts for the thickest laminae (Fig. 5.6f). The diamict is identical in character to that of the solid stratified subfacies, which is reflected in the grain size distribution (Fig. 5.7) and clast shape (Fig. 5.8) datasets, although there are also some (unmeasured) areas of more angular material (Fig. 5.6h). The debris within the laminae can be both frozen and unfrozen, predominantly as a result of surface sublimation (Figs 5.6g and 5.6j) in the latter case. This subfacies is in general less debris-rich than the solid stratified subfacies, and the measured lower debris contents of 9.6% and 31% (by volume) for stratified facies ice are suggested to reflect the two end members of relatively debris-poor (Figs 5.6g and 5.6i) and debris-rich (Figs 5.6f and 5.6k) ice within this subfacies, based on visual estimations at all sections. The overall thickness of the banded subfacies varies; at the SE sections it is generally between 0.1-1 m thick, whilst at the NW section it but ranges from 0.1-15 m (Fig. 5.5).

Solid subfacies

This subfacies is a frozen, structureless diamict with interstitial ice and very few small, clean ice lenses (Fig. 5.6m), and is only observed in one place at the NW section (Fig. 5.5a). The matrix-supported diamict is grey in colour and contains predominantly angular clasts (Fig. 5.8), distinguishing it from the solid stratified subfacies. The clasts are almost entirely limestone and there are some small areas which are clast-supported with only interstitial ice, including a 0.2 m thick lens surrounded by the solid stratified subfacies (Fig. 5.6n). The unit ranges in thickness from 0.2-1 m.

5.4.1.2. Dispersed facies

This facies is composed primarily of clean ice with a typically very low debris content, visually-estimated at <1%, and is largely devoid of internal stratification. The debris within this facies predominantly takes the form of isolated small clots (Fig. 5.9i) and very thin (<5 mm) laminae of fine debris (Fig. 5.9j) with a unimodal grain size distribution exhibiting a peak in the silt size range, although some laminae also contained coarser sand particles (Fig. 5.7). The bubble content of this facies ranges from no or very few bubbles up to a medium bubble content, and often grades indistinguishably into overlying englacial ice. The main distinction between this

facies and englacial ice are the areas of very clear ice which are largely devoid of bubbles. The clarity of this ice allows bubbles and debris tens of centimetres inside the glacier to be observed, allowing 3D structures to be seen in extraordinary detail (Fig. 5.9a). This clear ice is almost

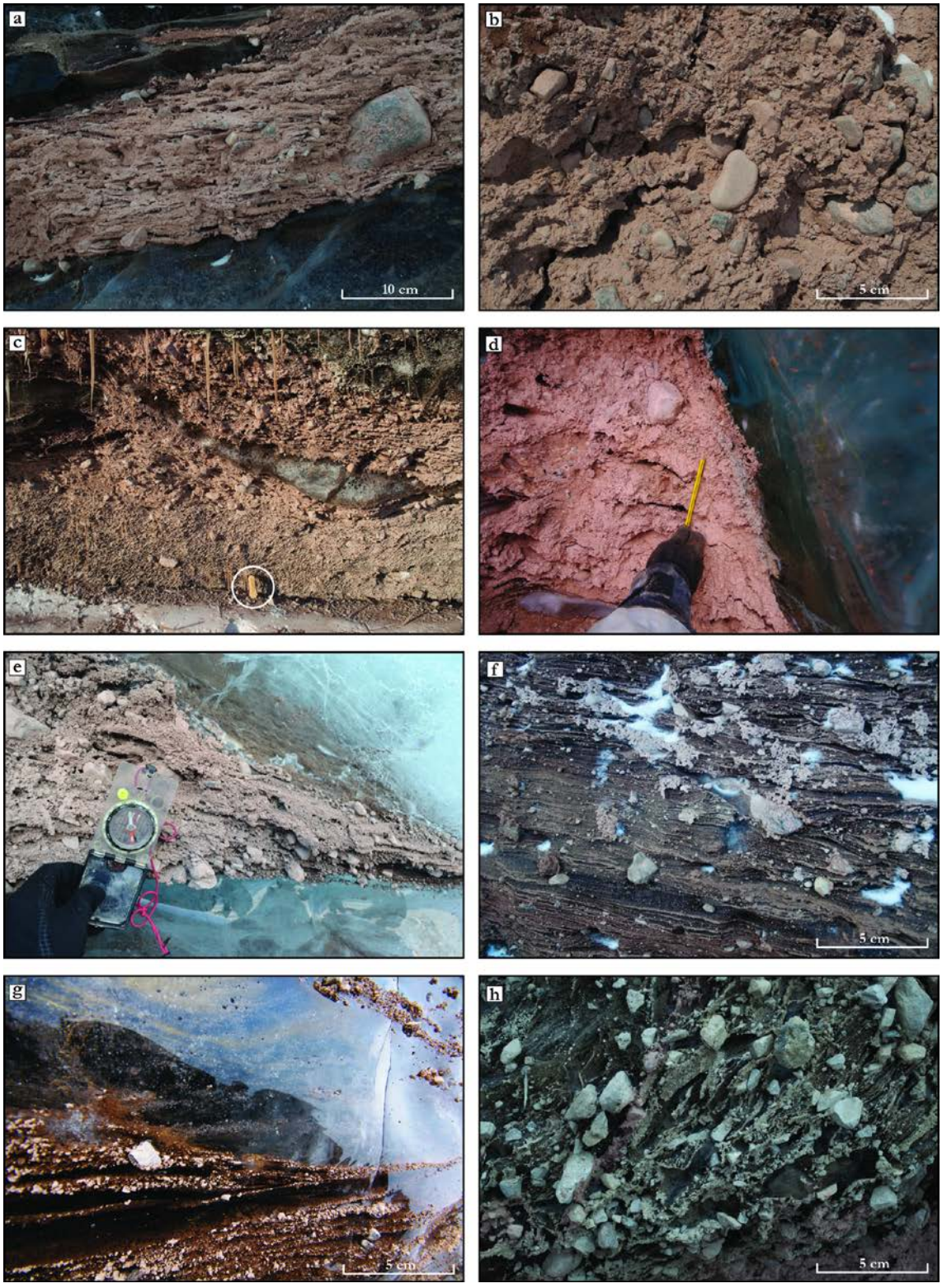

Figure 5.6

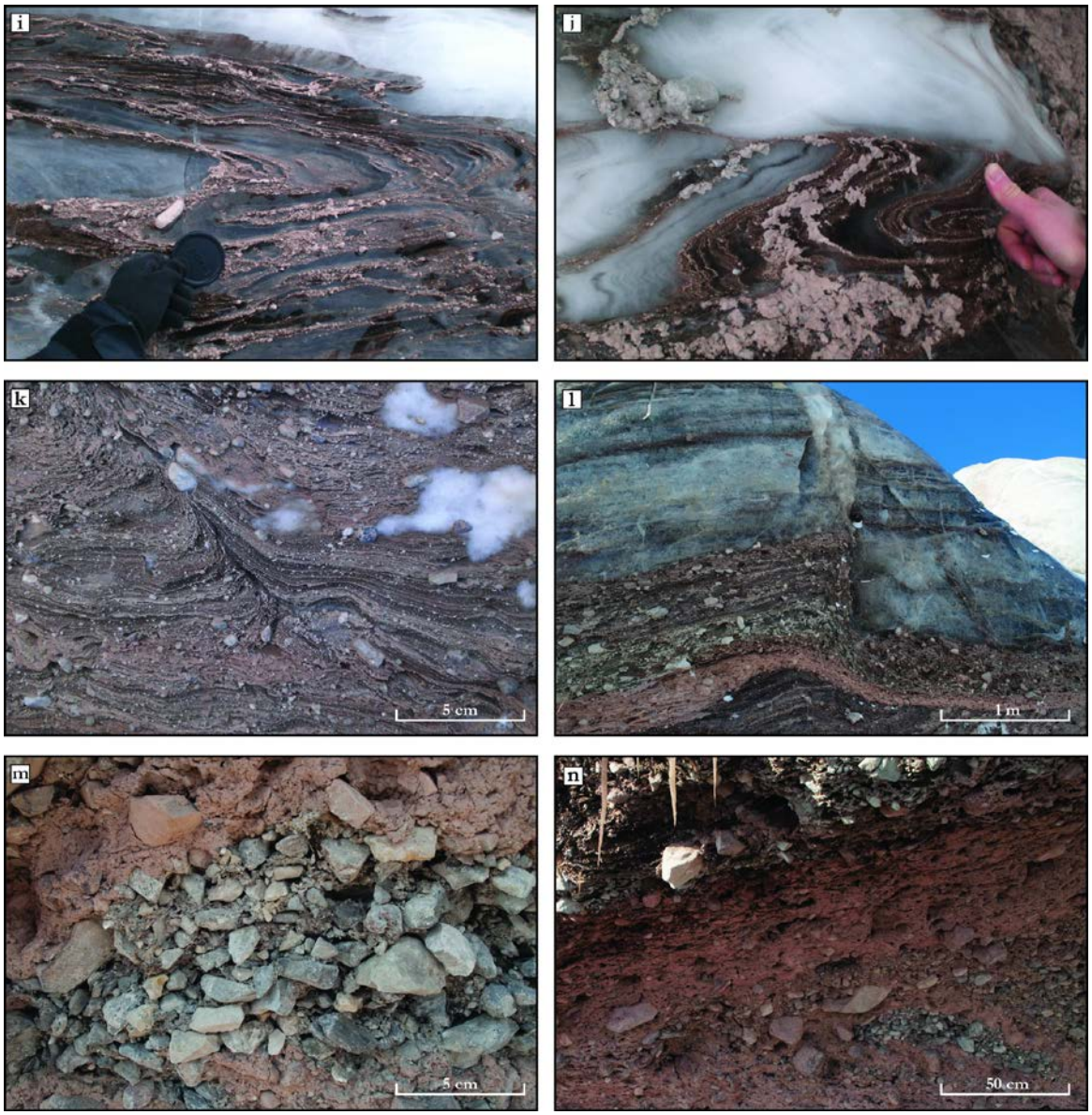

Figure 5.6 (this and preceding page) – Examples of debris-rich stratified basal ice facies. (a) Solid stratified subfacies, NW section. Note stratification picked-out by thin ice lenses. (b) Composition of solid stratified facies, SE-A section. (c) Clean ice lens within solid stratified subfacies, NW section. Note bubble-free border of dispersed facies. 20 cm brush circled for scale. (d) Solid stratified subfacies within debris-rich band, SE-A section. Note thin (~2 cm) layer of sorted sand and border of dispersed facies ice. (e) Stratified facies ice surrounded by dispersed facies ice, SE-B section. (f) Banded subfacies ice, NW section. (g) Banded subfacies ice, SE-A section. (h) Banded subfacies ice, NW section. Note angularity of clasts. (i) Isoclinal Z-shaped fold verging to right within banded subfacies ice, SE-A section (photo by Ed Fleming). (j) Isoclinal recumbent fold in banded subfacies ice truncated by englacial facies ice, SE-A section. (k) Overthrust nappe fold in banded subfacies ice, NW section. (l) Asymmetric open fold in solid stratified subfacies below a close, inclined z-shaped fold in banded subfacies, NW section. Both are overlain by englacial facies ice which has been normally faulted. (m) Pod of solid subfacies ice. Note angularity of clasts and colour contrast with solid stratified subfacies ice. (n) Pod of solid subfacies ice within solid stratified subfacies ice.

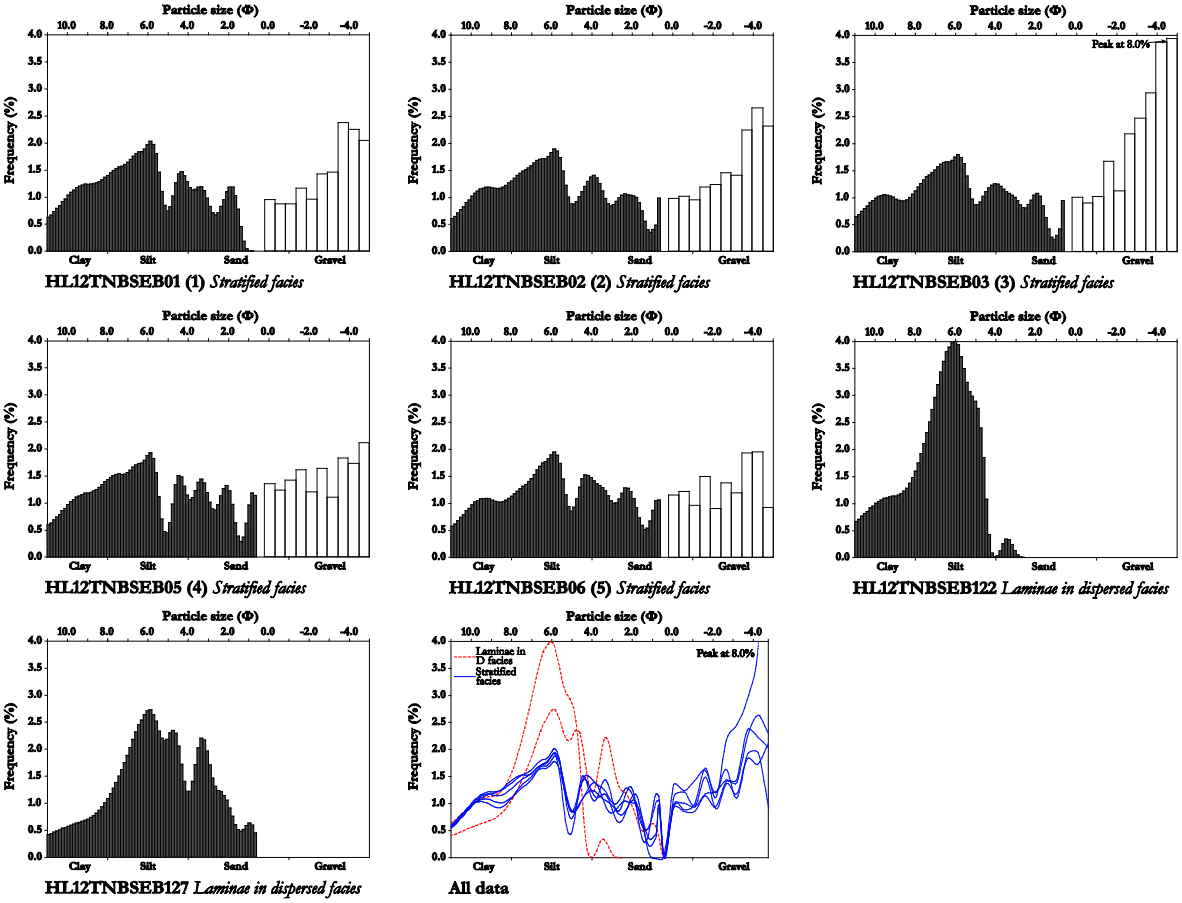

Figure 5.7 – Grain size distributions. Grey bars derived from laser sizing and white bars by dry sieving. Numbers in brackets after sample name refer to numbered sample locations on Fig. 5.5.

always in contact with debris-rich ice (Figs 5.6d, 5.9b and 5.9i) and in places contains discrete linear worm-like structures of very fine bubbles (<1 mm; Figs 5.9c and 5.9d). The individual strands of these structures are only one bubble thick and typically extend away from debris-rich ice. At the SE-B section, some of the bubble structures contained fine-grained debris (Fig. 5.9e). In places, a gradation can be seen from worm-like structures into wider (~1-10 mm) linear bubble structures with a planar form (Fig. 5.9f). These ribbon-like structures are typically several bubbles wide and can contain some larger bubbles (~1-5 mm diameter), although their general appearance as white ribbons means they are often difficult to determine individually. Both of these aforementioned structures appear to follow the boundaries of large (centimetre diameter) ice crystals. In some places, these structures grade into dense clouds of 1-5 mm diameter bubbles, often forming opaque ice with a medium bubble content (Fig. 5.9g), in places indistinguishable from englacial ice. The distribution of the dispersed facies is far more restricted than the englacial facies and displays a range of thicknesses from 0.1-1.5 m.

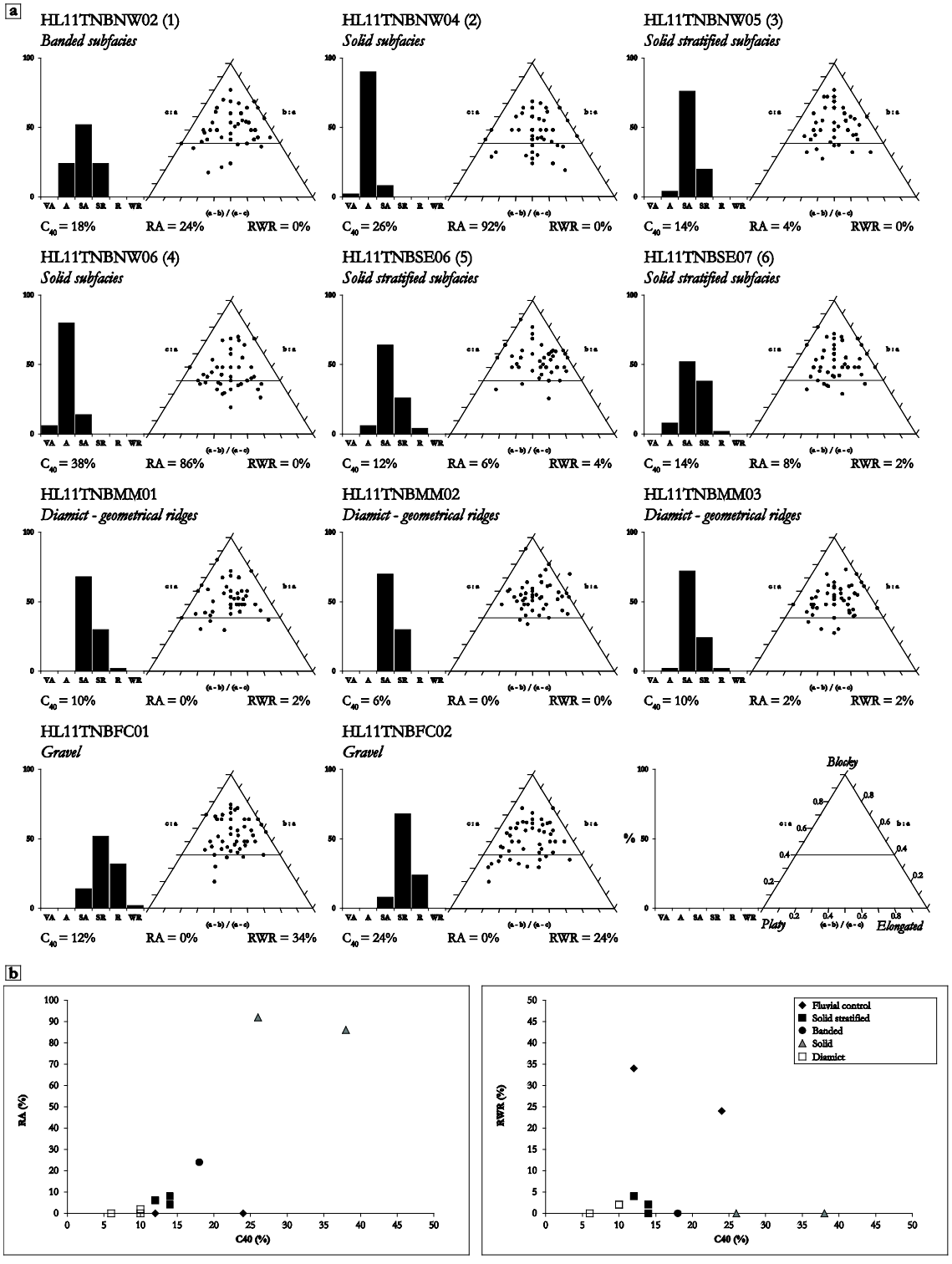

Figure 5.8 – (a) Clast shape data plotted on histograms (roundness) and ternary diagrams (shape). Each sample is of 50 limestone clasts. (b) RA-C_{40} (left) and RWR-C_{40} (right) diagrams.

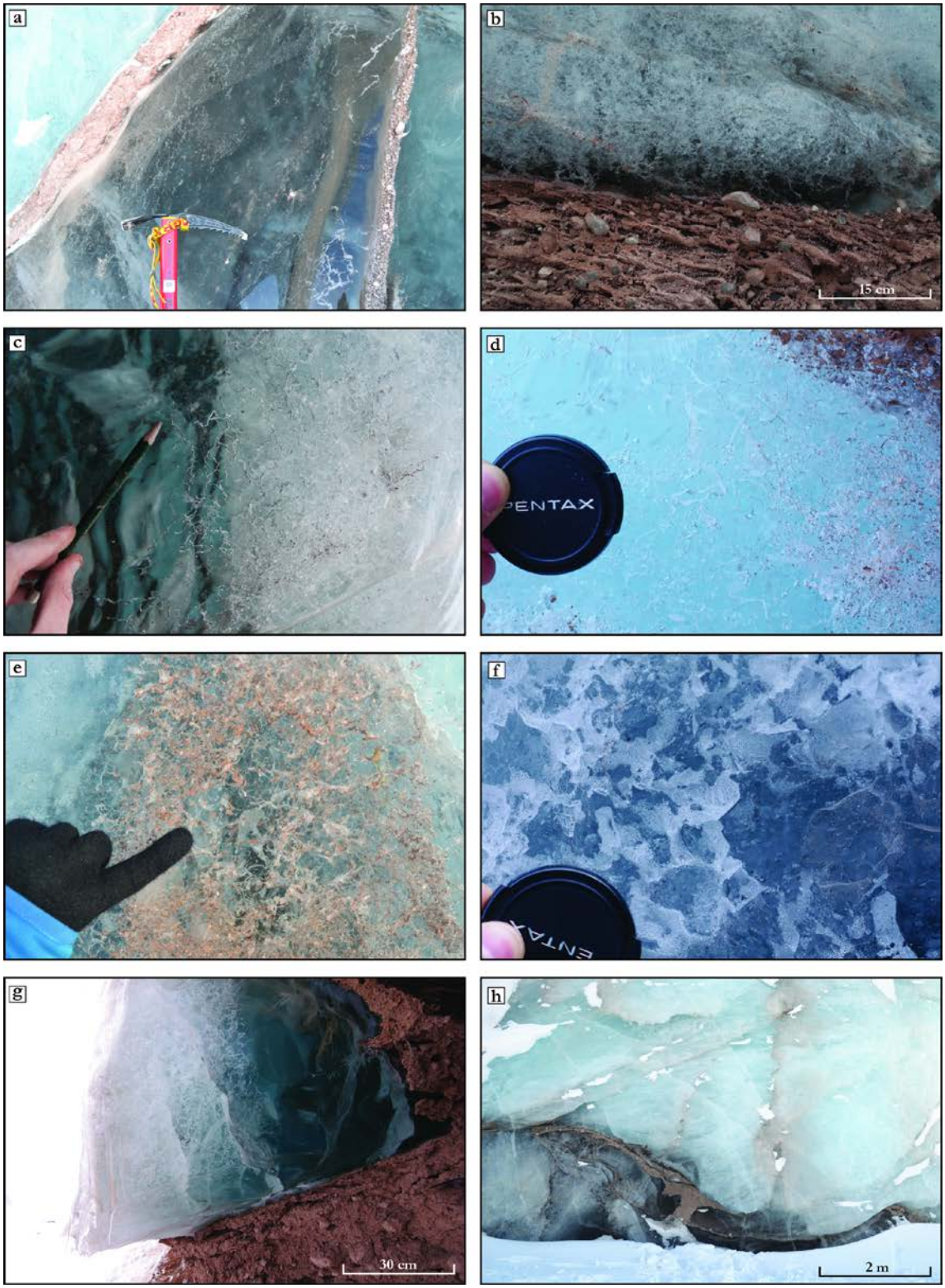

Figure 5.9 (this and next page) – Examples of dispersed and englacial ice facies. (a) Dispersed facies ice, SE-B section. (b) Thin border of dispersed facies ice overlying solid stratified subfacies ice, NW section. (c) Thin worm-like bubble structures within dispersed facies ice, SE-A section. (d) Thin worm-like bubble structures and debris clots within dispersed facies ice, SE-A section (photo by Riccardo Scotti). (e) Thin worm-like bubble structures and included fine debris within dispersed facies ice, SE-B section. (f) Planar ribbon bubble structures within dispersed facies ice, SE-A section (photo by Riccardo Scotti). (g) Dispersed facies ice bordering debris-rich band, SE-A section. (h) Englacial facies ice surrounding debris-rich band, SE-B section. (i) Dispersed facies ice, SE-A section. Note small debris grains and clots within clear ice. (j) Debris laminae within dispersed facies ice, SE-A section.

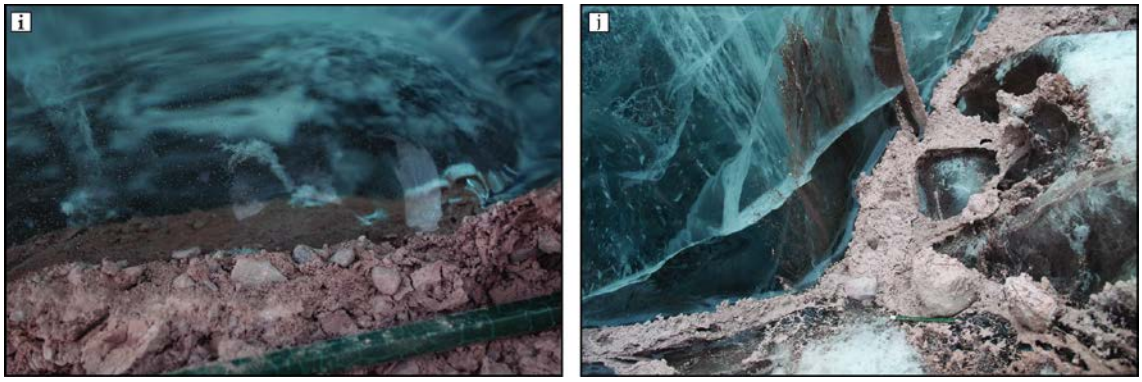

Figure 5.9 continued

5.4.1.3. Englacial facies

This facies consists of clean ice with a medium to high bubble content, giving it an opaque, bluish-white appearance (Fig. 5.9h). In places this facies is stratified at centimetre to decimetre scales in the form of intercalated largely horizontal layers of bubble-rich and bubble-poor ice (Fig. 5.9h), although this is not always visible and the ice often appears white and massive. Away from the debris-rich bands, the ice is generally free of debris other than occasional scattered grains and small clots of fine material. Apart from some 0.5-2 m thick layers and isolated lenses within the stratified facies (Fig. 5.5a), englacial facies ice typically overlies the debris-rich basal ice and comprises the vast majority of the ice cliff.

5.4.2. Stable isotope analysis

Samples for stable isotope analysis were taken from the stratified basal ice facies, dispersed facies and englacial facies at the SE-A and SE-B sections (Figs 5.5b, 5.5c and 5.10), and the results from these are summarised in Table 5.1. Analysis of 32 samples produced mean values of -14.36‰ and -102.75‰ and standard deviations of 0.98‰ and 6.78‰ for $\delta^{18}O$ and δD, respectively. These samples have been subdivided by ice facies to aid comparison of isotopic composition (Table 5.1. and Fig. 5.11). The englacial facies (n = 6) yielded mean compositions of -15.34‰ and -100.83‰ for $\delta^{18}O$ and δD, respectively (ranges of -14.62‰ to -16.13‰ for $\delta^{18}O$ and -86.51‰ to -105.40‰ for δD); the dispersed facies (n = 20) returned mean values of -14.20‰ ($\delta^{18}O$) and -103.12‰ (δD; ranges of -12.99‰ to -16.50‰ for $\delta^{18}O$ and -94.40‰ to -118.22‰ for δD); and the respective mean values for the stratified facies (n = 6) are -13.94‰ ($\delta^{18}O$) and -103.41‰ (δD; ranges of -13.57‰ to -14.31‰ for $\delta^{18}O$ and -94.40‰ to -110.45‰ for δD). These results show that the stratified facies $\delta^{18}O$ mean value is statistically distinct from the englacial facies mean value at the 95% confidence level (i.e. ±2 standard deviations). The mean δD value for the stratified facies is slightly higher than the mean for englacial ice but is not statistically distinguishable at the 95% confidence level (Table 5.1). Most of the dispersed facies samples have slightly higher $\delta^{18}O$ values than the englacial facies, but it also contains the

isotopically $\delta^{18}O$ lightest value of all samples of -118.22‰. The mean $\delta^{18}O$ values for the dispersed and stratified facies are similar, but the dispersed facies is not statistically distinguishable from the englacial facies mean at the 95% confidence level (Table 5.1). For δD, the results from all samples show very little variation and neither the dispersed nor stratified facies are statistically distinguishable from the englacial facies at the 95% confidence level (Fig. 5.11). In a co-isotopic plot of the stable isotope data (Fig. 5.12), none of the facies produced significant regression lines, either aligned with the local meteoric water line (LMWL) (Divine *et al.*, 2008) or on 'reliable' freezing slopes (Sugden *et al.*, 1987; Knight, 1989).

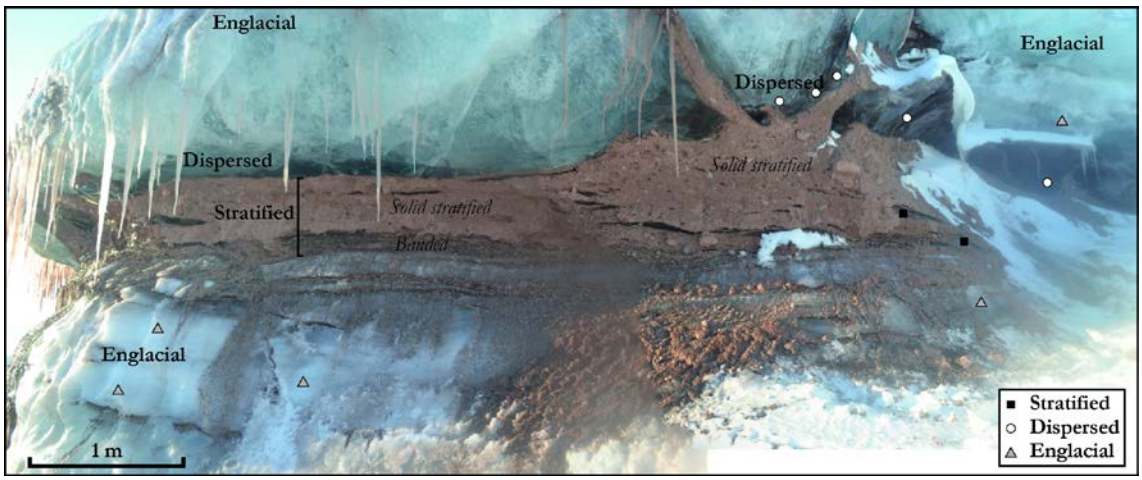

Figure 5.10 – Example of stable isotope sampling from different ice facies at SE-A section. Approximate location of photograph outlined in Fig. 5.5b.

Table 5.1 – Summary of stable isotope data.

Ice facies	*n*	Section	$\delta^{18}O$ mean (‰), standard deviation and range	Enriched	δD mean (‰), standard deviation and range	Enriched
All facies	32	SE-A and B	-14.36±0.98 (-12.99 to -16.50)	-	-102.75±6.78 (-86.51 to -118.22)	-
Englacial facies	6	SE-A	-15.34±0.68 (-14.62 to -16.13)	-	-100.83±7.16 (-86.51 to -105.40)	-
Dispersed facies	20	SE-A and B	-14.20±1.02 (-12.99 to -16.50)	No	-103.12±7.18 (-94.40 to -118.22)	No
Stratified facies	6	SE-A and B	-13.94±0.25 (-13.57 to -14.31)	Yes	-103.41±5.69 (-94.40 to -110.45)	No

5.4.3. Structure and distribution of ice facies and debris-rich bands

5.4.3.1. NW section

This section is characterised by thick (up to 15 m) sequences of stratified facies ice intercalated with thinner (up to 2 m) layers of clean ice (Fig. 5.5a). The majority of the section is comprised of banded subfacies ice, which is typically aligned parallel to sub-parallel to the base of the section, as exhibited by the wavy lamination (Figs 5.5a and 5.6f). This lamination is clearest in the lowermost 1-2 m and towards the right-hand (NE) end of the section; towards the left-hand (SW) end, where the subfacies is thickest, the stratification is much less distinct and, where lamination is evident, has often been folded. There are several clear examples of folds within

the banded subfacies throughout the section, including a small-scale overthrust nappe fold at ~30 m (Fig. 5.6k) and a close, inclined, asymmetric z-shaped fold at ~70 m (Fig. 5.6l). The latter example is closely associated with both a large-scale slightly-inclined open fold of the underlying solid stratified layer and a normal fault (vertical displacement ~70 cm) within the englacial ice above, the hanging-wall of which is also displaced laterally in a rotational manner (Fig. 5.6l).

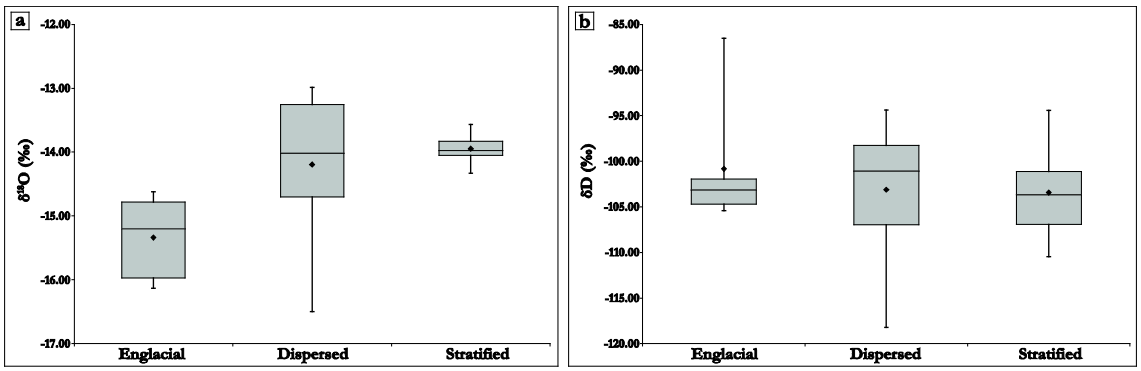

Figure 5.11 – Box plots of stable isotope analysis of Tunabreen ice facies showing maximum, upper quartile, median, mean (black diamond), lower quartile and minimum values. (a) $\delta^{18}O$ composition; (b) δD composition.

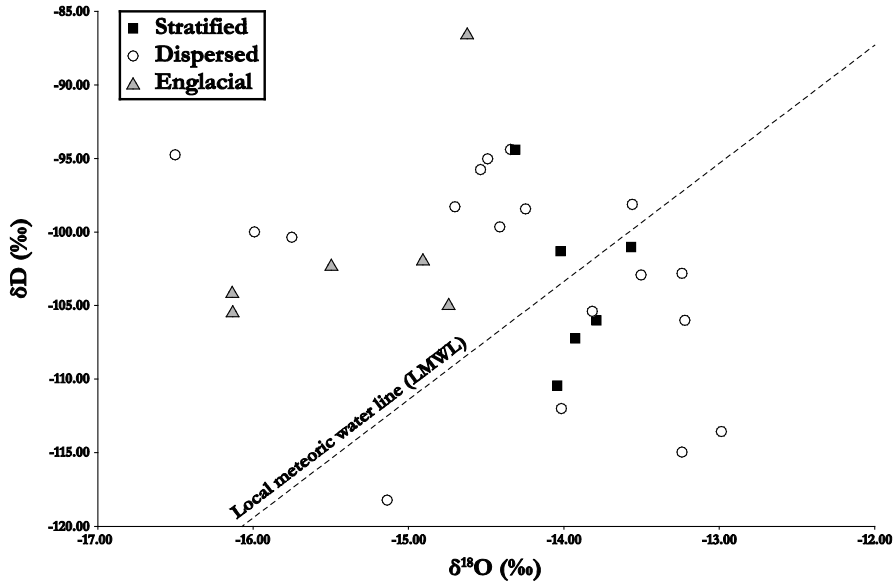

Figure 5.12 – Co-isotopic plot of Tunabreen ice facies. Local meteoric water line (LMWL; slope = 7.8) is from Divine *et al.* (2008).

The solid stratified subfacies forms a near-continuous layer at the NW section, typically 0.5 m thick and up to a maximum thickness of 2.5 m at ~11 m (Figs 5.5a and 5.13a). This layer overlies banded subfacies ice throughout and in some places there is evidence that the contact between the two is unconformable, such as between 70-80 m where the banded subfacies laminae are truncated by the solid stratified subfacies (Figs 5.5a and 5.13b). The solid stratified subfacies is typically overlain by a further layer of banded subfacies ice. The stratification

within this uppermost layer of banded subfacies ice is not as clear and it also contains a larger number of clasts, many of which are visually more angular than those within the lower layers (Figs 5.6h and 5.13b). Throughout the section, the lower banded subfacies layers (underlying the solid stratified subfacies) are generally bisected by discontinuous layers of englacial facies ice (Figs 5.5a, 5.13a, 5.13b and 5.13f). These englacial facies layers and lenses usually contain a thin (5-10 cm) upper and lower border of dispersed facies ice (Fig. 5.6c). The lower banded subfacies layer is truncated by englacial facies ice in at least two places at the right-hand (NE) end of the section, at ~70 m (5.13a) and 75 m (5.13g), where a 30 cm thick dyke-like feature extends from the englacial layer above. There is also a thin (~50 cm) layer of stratified facies ice within the overlying englacial ice at this location. Between 78-81 m an apparent isoclinal recumbent fold can be identified in the two-dimensional ice face, with thin layers of solid stratified ice forming the limbs around a central core of banded facies ice (Fig. 5.13h).

Both the solid stratified and banded subfacies also form sub-vertical and occasionally overturned intrusions into the overlying englacial ice, typically in the order of 1-2 m in length (Fig. 5.5a). The thickness of these structures ranges from <0.1 m to ~1 m and they can often be traced for up to 10 m as either thin, discontinuous debris-rich bands, fractures, or a combination of the two. The prominent intrusive structure at ~60 m (Fig. 5.13c) is comprised of both solid stratified and banded subfacies. In the latter subfacies, very faint stratification can be identified in a similar sub-vertical alignment as the overall intrusion structure.

In general, the typical vertical stratigraphy of the right-hand (NE) end of the NW section can therefore be summarised (from bottom to top) as follows: a 1.5 m-thick banded subfacies layer, a discontinuous 0.5-1 m-thick englacial facies layer with a ~0.1 m dispersed facies border, a 1.5-2 m-thick banded subfacies layer, a 0.5-1 m-thick solid stratified layer, a 1-1.5 m-thick banded subfacies layer, and an overlying metres-thick englacial facies layer (Fig. 5.5a). At the left-hand (SW) end of the section this order is slightly varied: a 1.5 m-thick banded subfacies layer, a 0.25-0.5 m solid stratified layer, a discontinuous 0.5-1 m-thick englacial facies layer with a ~0.1 m dispersed facies border, a 1.5-5 m-thick banded subfacies layer, and overlying englacial ice (Fig. 5.5a).

The one main area that does not conform to these two general stratigraphies is between approximately 30-45 m (Fig. 5.5a). Here, the lower banded subfacies layer is truncated by a ~1 m-thick combined layer of solid stratified and solid subfacies ice extending from the base of the section which dips at 39º (Fig. 5.13d). These subfacies thicken upwards and coalesce with the continuous solid stratified subfacies layer, forming a 2 m-thick unit between upper and lower banded subfacies layers. The solid subfacies, which is clast-rich and predominantly composed of angular material (Figs 5.6m and 5.6n) has a restricted extent and is entirely subsumed by the solid stratified subfacies within ~6-7 m. It is structureless apart from occasional thin (<10 cm) layers of solid stratified debris within, clearly identifiable due to the colour contrast between the subfacies (Fig. 5.13d). Close to the left-hand extent of the main area, there is a 20 cm-thick, 80

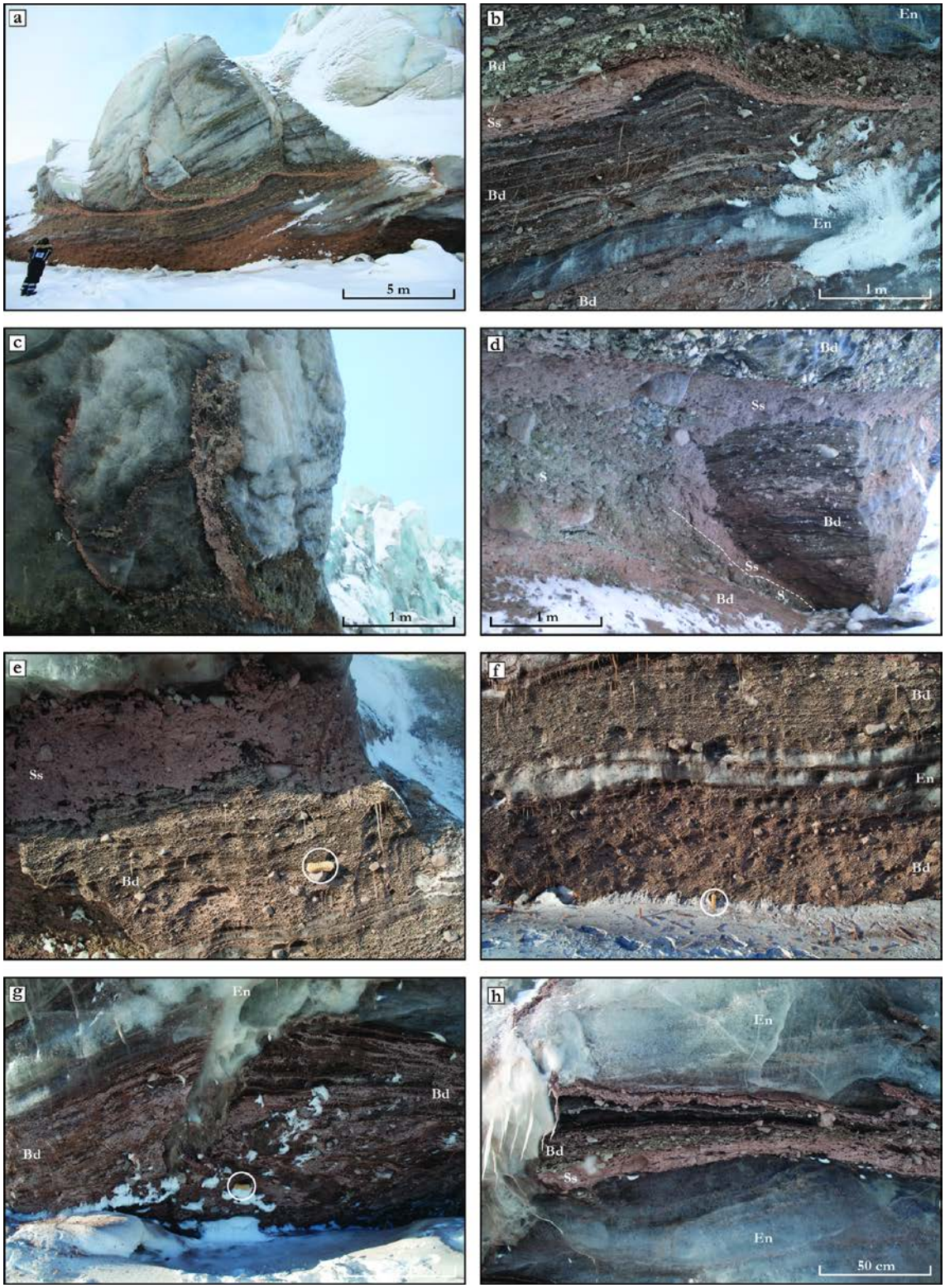

Figure 5.13 – Detail of NW section. (a) Overview of right-hand end of section (photo by Kathrin Naegeli). (b) Lamination within banded subfacies ice truncated by solid stratified subfacies ice. (c) Examples of vertical intrusions of solid stratified and banded subfacies into overlying englacial ice. (d) Truncation of banded subfacies ice by solid stratified and solid subfacies ice. White-dashed line divides the two latter subfacies. (e) Banded subfacies ice overlain by solid subfacies ice. 20 cm brush circled for scale. (f) Banded subfacies ice bisected by a layer of englacial facies ice. 20 cm brush circled for scale. (g) Banded subfacies ice truncated by englacial facies ice. 20 cm brush circled for scale. (h) Isoclinal recumbent fold of solid stratified and banded subfacies ice within englacial ice. Ss = solid stratified; S = solid; Bd = banded; En = englacial.

cm-long pod of clast-supported solid subfacies ice surrounded by solid stratified subfacies ice (5.6n). This is the only area where the solid subfacies was identified at Tunabreen.

5.4.3.2. SE sections

The SE sections are far less debris-rich than the NW section and are typified by stratified facies layers and bands within predominantly englacial facies ice (Figs 5.5b and 5.5c). The distribution and character of these debris-rich features can be broadly subdivided into two main types: generally thin (<50 cm), discrete bands comprised largely of solid stratified ice extending into the overlying englacial ice, ranging from sub-horizontal to vertical in alignment and often associated with large areas of debris at their base (Figs 5.5b, 5.5c and 5.14a-f), and intercalated layers of stratified facies ice (~1-50 cm thick) and clean ice exhibiting clear evidence for deformation in the form of folds and the stacking of units (Figs 5.9i-j and 5.14i-o).

The discrete debris-rich bands display a variety of morphologies and alignments across the SE sections. A large number of these features are <30 cm thick and attenuate towards their upper limits, which is typically at a height of 10-15 m (Figs 5.5b, 5.5c and 5.14a-c). In many cases the debris-rich bands extend from areas of solid stratified facies ice at their base (Figs 5.10 and 5.14a-d), which can be up to 2 m thick and 10 m wide (Fig. 5.14b). Thin debris laminae of mainly fine debris clots are also observed to emanate from the main band in several examples, often into bordering dispersed facies ice (Fig. 5.9j), and many of these are aligned sub-horizontally with the surface of the bands (Fleming *et al.*, 2013). The debris within the bands is predominantly solid stratified facies ice and often contains small clean ice lenses. In several places, small areas of sorted sands and gravels were observed within the bands (e.g. Fig. 5.6d; see also Figs 9.27c and 9.27d in Benn and Evans, 2010), which on rare occasions preserve crossbedding (e.g. base of debris-rich band in Fig. 5.14a).

The debris-rich bands exhibit a variety of orientations, dips and dip directions, and this is reflected in the small population of structural data recorded at the SE-B section (Fig. 5.5c). In general, the debris-rich bands at the SE sections are inclined (Figs 5.14a-e), but there are also examples of near-vertical structures both here (e.g. Fig. 5.14f) and within the ice cliff near the NW section (Fig. 5.14g). The debris-rich bands are typically bordered by dispersed facies ice, which is often bubble-free immediately adjacent to the band but grades into increasingly bubble-rich ice over a distance of tens of centimetres via thin worms, ribbons and clouds of bubbles (Figs 5.6d, 5.9g and 5.14f; see also *5.4.1.2.*). In places, debris-rich bands truncate bubble layering within the clean ice (5.14j).

When parts of the SE sections were visited in summer, small (<1 m high) proglacial ridges were observed to be emanating from the base of inclined debris-rich bands (Fig. 5.14h) across a narrow beach. These ridges consisted of poorly-sorted matrix-supported diamict, visually indistinguishable from the debris within the stratified facies ice.

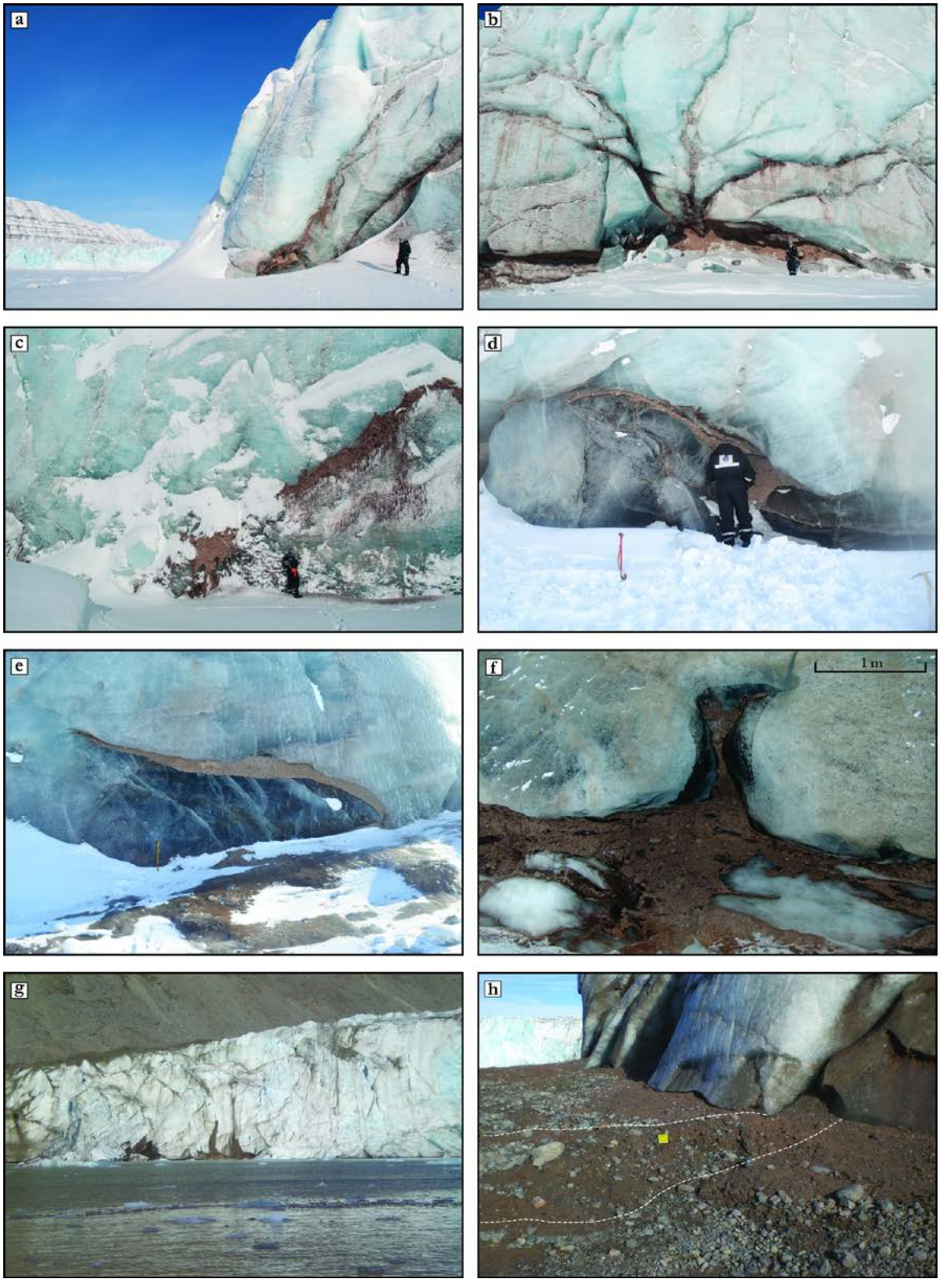

Figure 5.14

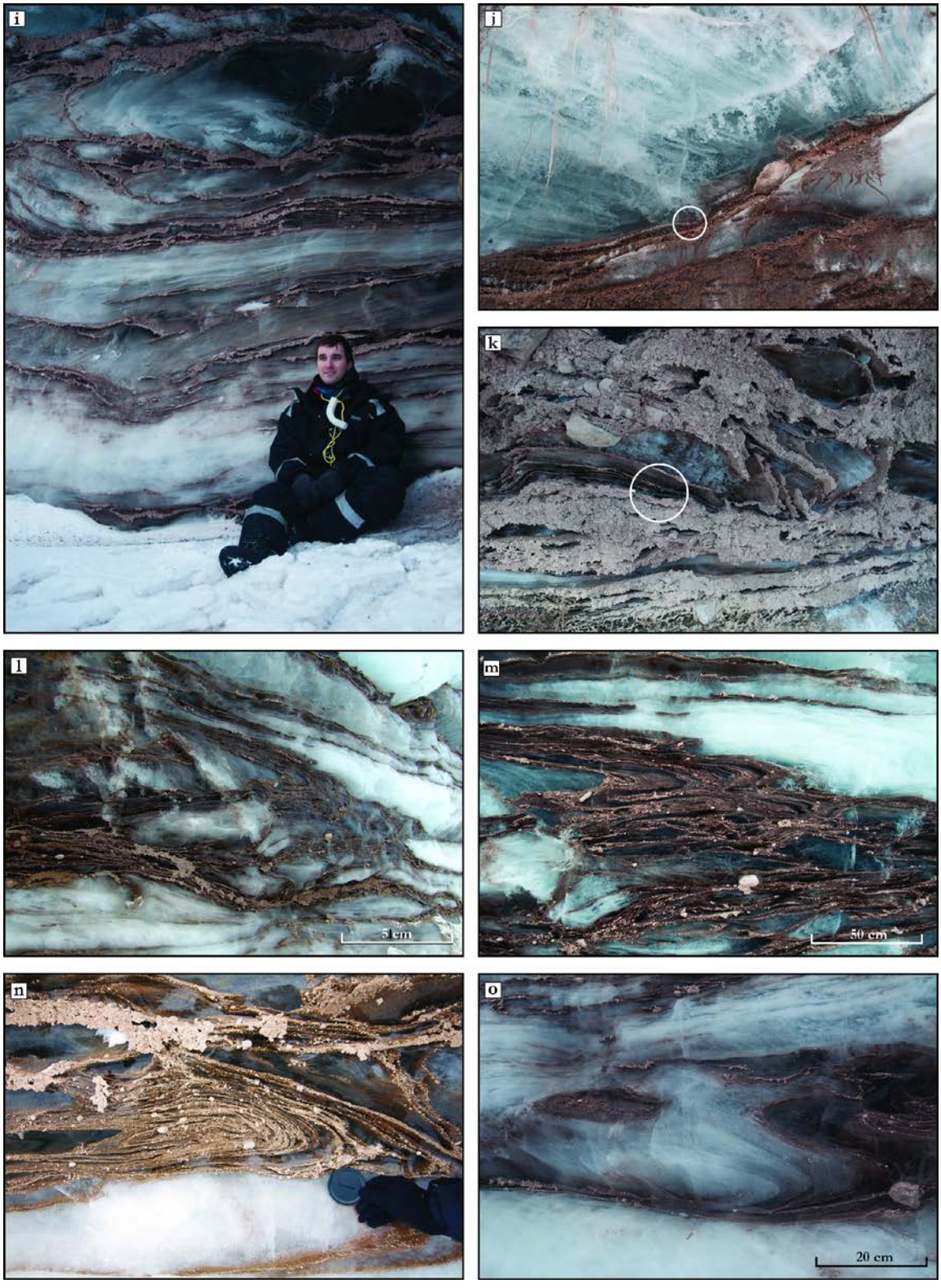

Figure 5.14

Figure 5.14 (preceding two pages) – Detail of SE sections. (a) Thin debris-rich bands at left-hand end of SE-A section (photo by Ed Fleming). Thin debris-rich bands extending from area of solid stratified facies ice, SE-A section (photo by Ed Fleming). (c) Debris-rich band at right-hand end of SE-A section (photo by Ed Fleming). (d) Debris-rich band at SE-B section where debris concentration, particle size analysis and stratified facies stable isotope samples were taken. (e) Debris-rich band at left-hand end of SE-B section. (f) Vertical diapiric-like debris structure at SE-A with clear dispersed ice border (photo by Roberto Colucci). (g) Vertical debris structures in ice cliff close to NW section. Ice cliff is ~30 m high. (h) Small ridge emerging from thin debris-rich band at SE-A section. (i) Intercalated layers of stratified facies and englacial facies ice, SE-A section. Brendan O'Neill for scale. (j) Debris-rich band truncating bubble stratification in clean ice, SE-A section. Pencil circled for scale. (k) Intercalated layers of stratified and englacial facies ice, SE-A section. Note inclined isoclinal fold. Pencil circled for scale. (l) Recumbent fold within banded subfacies ice, SE-A section (photo by Roberto Colucci). (m) Isoclinal recumbent folds verging to the right within banded subfacies ice, SE-A section (photo by Ed Fleming). Isoclinal recumbent fold within banded subfacies ice, SE-A section (photo by Roberto Colucci). (o) Augen-like shaped fold with concentric rings and double-vergence within banded subfacies ice, SE-A section (Photo by Ed Fleming).

Debris-rich ice at the SE sections also takes the form of areas of intercalated layers of stratified facies ice and clean ice (Figs 5.9i-j and 5.14i-o). The best exposure of this is at the SE-A section between ~35-90 m (Fig. 5.5b). The thicknesses of individual layers of both debris-rich and clean ice vary from <5 cm to 100 cm and the overall maximum thickness of this area is ~5-6 m. The order and structure of the intercalations is variable, ranging from thin (<5 cm) bands of solid stratified and banded subfacies ice within metres-thick englacial ice (5.14i) to tens of centimetres-thick solid stratified ice interspersed with englacial ice layers of <10 cm (5.14k). The layers of bubbly englacial ice often contain a thin (<10 cm) border of clear, bubble-free dispersed facies ice.

This area displays strong evidence of ductile deformation, best displayed by highly folded banded subfacies ice (Figs 5.6i-j and 5.14k-o) but also evident within the solid stratified subfacies and englacial facies ice. The translucent nature of the clean ice layers within the banded facies is advantageous as it often allows the folds to be observed in three dimensions (Fleming *et al.*, 2013). A variety of types of folding are evident, ranging from steeply inclined (e.g. Fig. 5.14k) to recumbent (Figs 5.6i and 5.14n), with tight to isoclinal interlimb angles and typically asymmetrical limbs. Boudinage is also common with the banded subfacies, forming augen-like rings of debris within the englacial ice (Fig. 5.14o). The vergence direction of the folds is variable and in some cases appears to be in two opposite directions when viewed in the two-dimensional ice face (Fig. 5.14l; Fleming *et al.*, 2013). In general, the debris within the highly folded areas is fine-grained and forms clots, although occasional larger clasts are also evident (Figs 5.6i, 5.14m and 5.14o).

5.5. Tunabreen-Von Postbreen glacier forelands and geometrical ridges

The area mapped in Figure 5.15 consists of part of the terrestrial forelands of Tunabreen and Von Postbreen. The majority of the geomorphology is associated with the former bed of the

Figure 5.15 – Geomorphological map of Tunabreen-Von Postbreen glacier foreland. See Fig. 5.1 for location of mapped area on southeastern shore of Tempelfjorden. Mapped from 2004 aerial photograph acquired from NERC Earth Observation Data Centre. A digital version of this map is included on the CD inside the back cover.

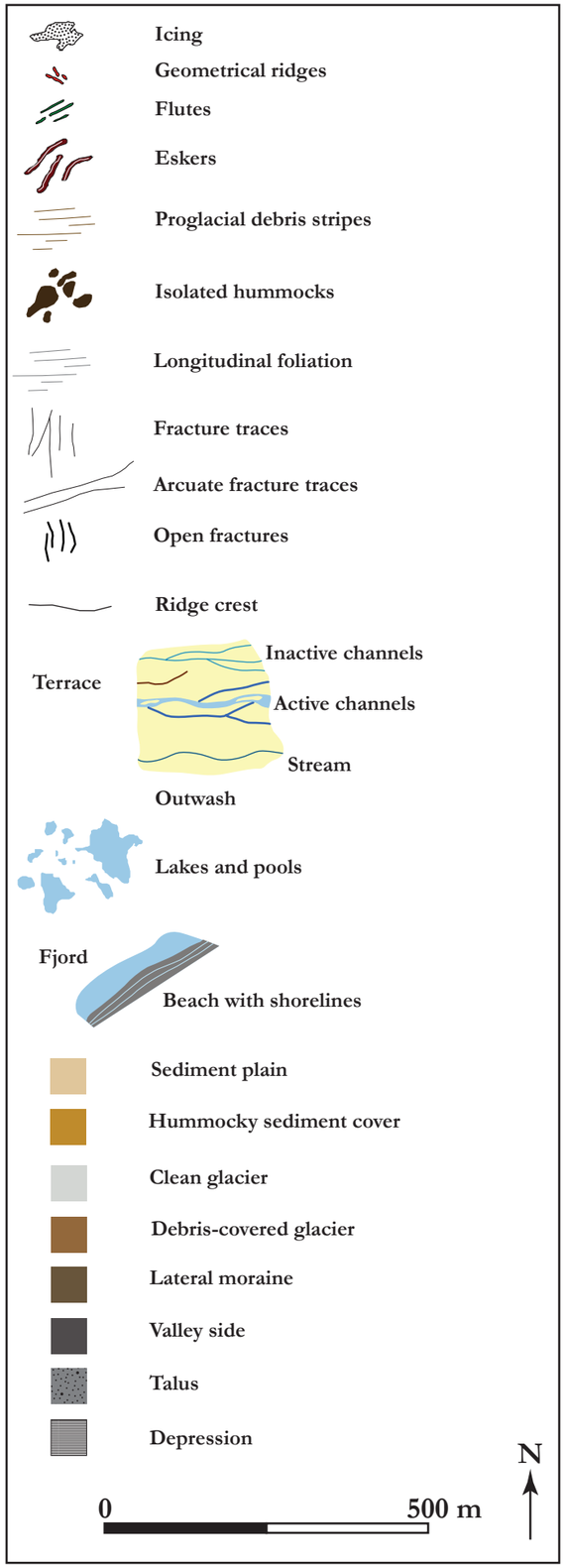

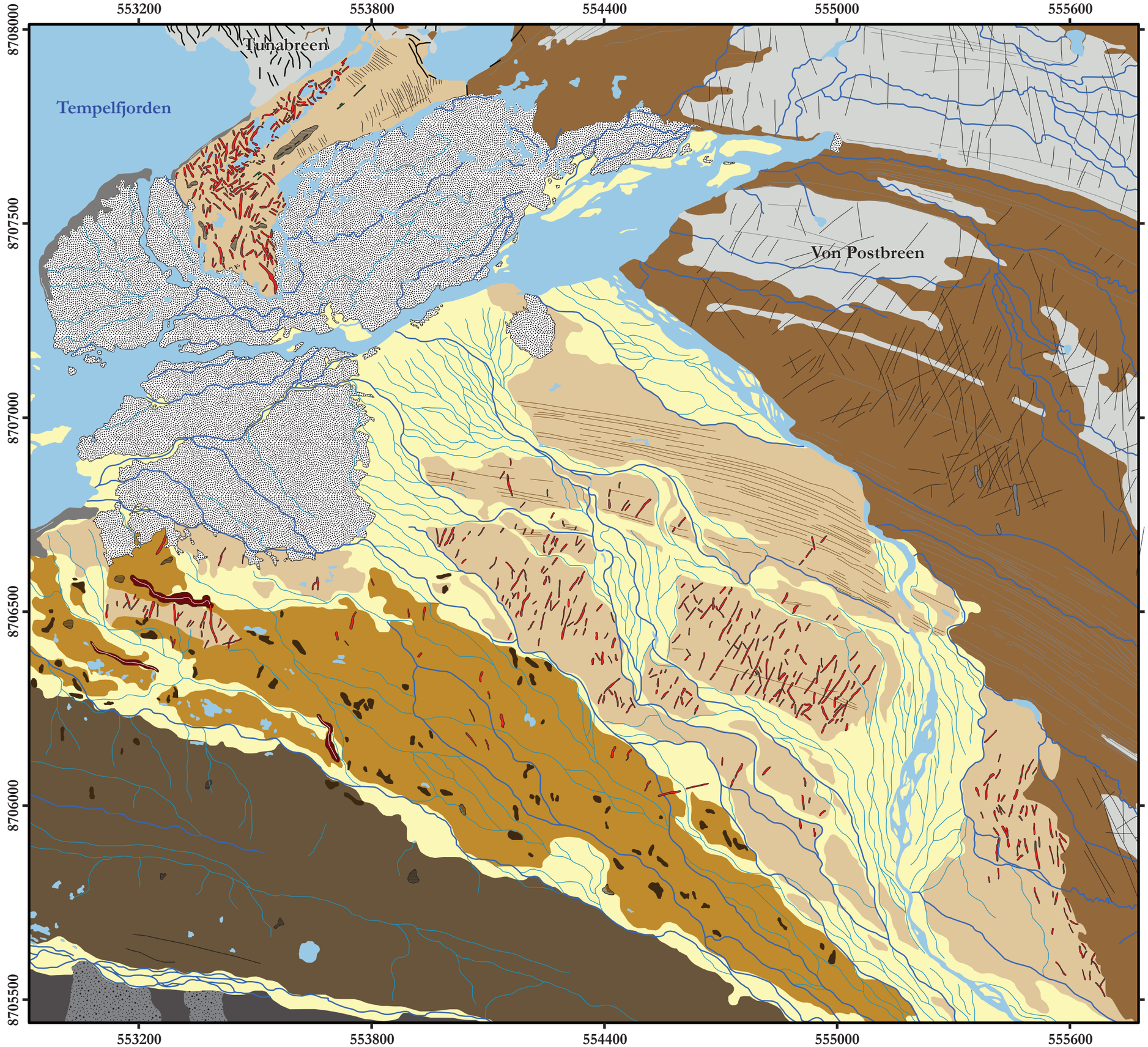

larger, currently terrestrially-terminating Von Postbreen, except a thin strip along the southeastern shore of Tempelfjorden aligned with the medial moraine between the two glaciers and located approximately 500 m across a small embayment from the Tunabreen SE sections (Figs 5.5b and 5.5c). A brief description of the geomorphology will be given in *5.5.1.*, followed by a more detailed focus in *5.5.2.* on one particular landform, geometrical ridges, in both terrestrial and submarine settings.

5.5.1. Glacial geomorphology overview

The glacier foreland between Von Postbreen and Tunabreen is a largely flat area (Fig. 5.16a) dominated by glaciofluvial activity, a perennial proglacial icing, and ridges and hummocks of varying morphologies (Fig. 5.15). The topography rises up to a ~50 m-high hummocky lateral moraine in the south of the mapped area, which extends along the southeastern shore of Tempelfjorden to a point broadly coincident with the 1870 Von Postbreen limit (Figs 5.2, 5.16c and 5.16e). The centre of the mapped area consists of a flat sediment plain superimposed by proglacial debris stripes, which can be traced as continuous features from longitudinal foliation on the ice surface, and a large network of geometrical ridges (Fig. 5.17a). These latter features will be described in detail in *5.5.2.* The sediment plain is highly-dissected by glaciofluvial outwash and active and inactive meltwater channels, including the main lateral channel of Von Postbreen which cuts between the debris-covered glacier front and the foreland before joining the main meltwater outlet (Fig. 5.15). This outlet exits from a portal in the centre of Von Postbreen (Figs 5.16f and 5.16g) and flows into Tempelfjorden.

The northwest of the mapped area contains large perennial proglacial icings which change position and size over time (e.g. compare 2004 mapping in Fig. 5.15 with 2011 field photographs in Figs 5.16b and 5.16c). The icings were typically 1-2 m thick in August 2011 (Fig. 5.16d), are closely associated with both outwash sediment and meltwater channels (Fig. 5.15) and are both meltwater and groundwater fed (Personal communication from A. Hodson, 2013). Between the icings and Tempelfjorden there is a 750 m-long, 250 m-wide strip of sediment cover consisting predominantly of reddish-brown poorly-sorted diamict (Fig. 5.18a). This area is aligned with the medial moraine between Tunabreen and Von Postbreen but they are separated by a small embayment (Fig. 5.3). A second dense network of geometrical ridges is located in this area (Figs 5.15, 5.17a and 5.18a).

In addition to the geometrical ridge networks, two other types of ridge features are apparent on the glacier foreland from aerial photographs. These are elongate, flow-parallel features that have been mapped as flutes, and sinuous ridges aligned sub-parallel to inferred ice flow that have been mapped as esker-like ridges (Fig. 5.15), neither of which could be field-checked.

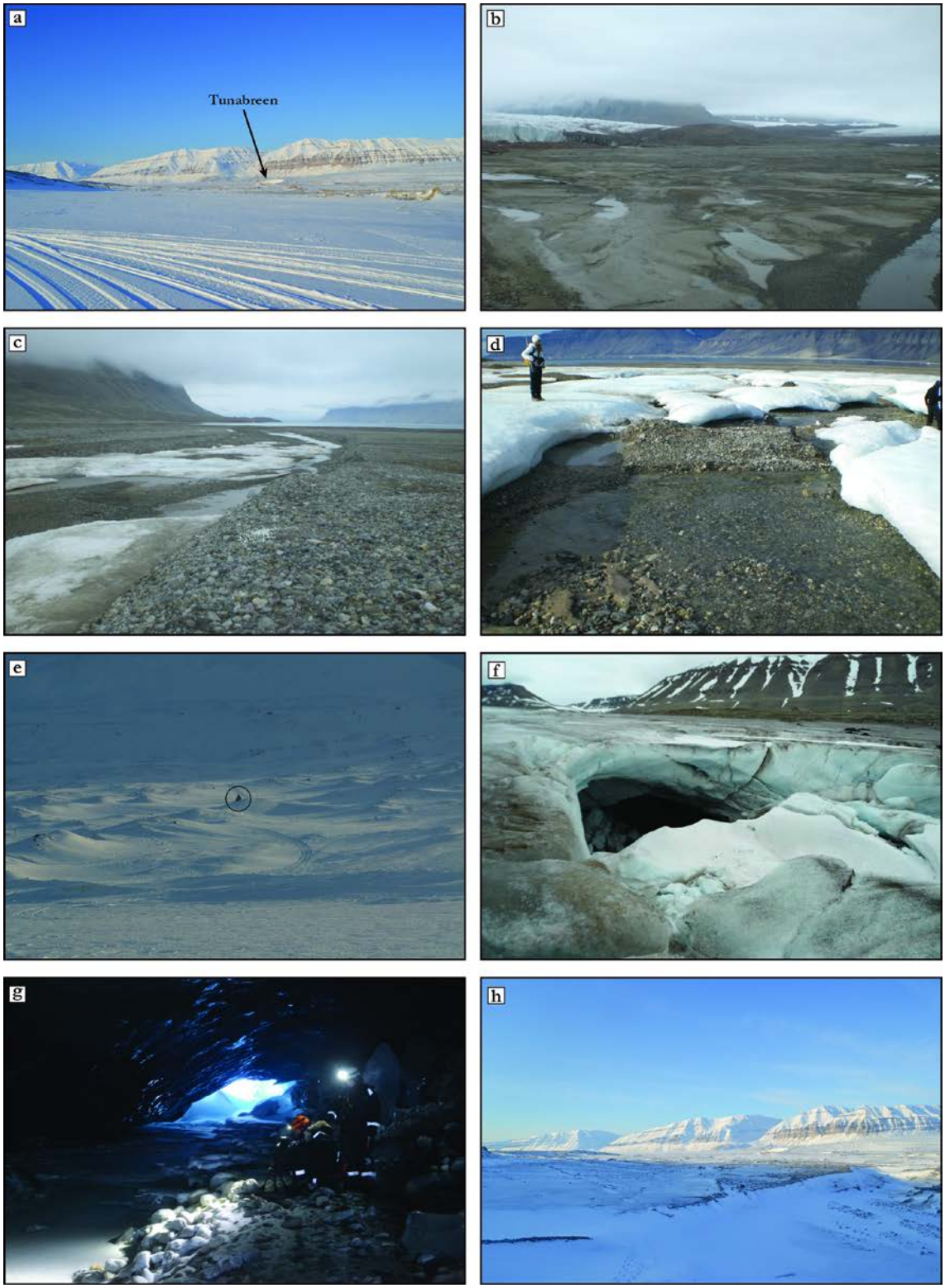

Figure 5.16 – Examples of features on glacier foreland. (a) View across foreland from Von Postbreen towards Tunabreen. Note lateral moraine to left. (b) View across outwash plain towards medial moraine between Tunabreen (to left) and Von Postbreen (to right). (c) View across outwash plain and proglacial icing towards mouth of Tempelfjorden. Note lateral moraine protruding into fjord. (d) Proglacial icing on outwash plain. (e) View from Tempelfjorden sea ice towards hummocky lateral moraine of Von Postbreen. Snowscooter circled for scale. (f) Von Postbreen main meltwater portal. Note lateral moraine in background. Photo by Thomas Shaw. (g) Inside Von Postbreen main meltwater portal. (h) View from Von Postbreen main meltwater portal across foreland towards Tunabreen and Tempelfjorden. Photo (e) taken in March 2011; photos (b), (c) and (d) taken in August 2011; photos (a), (g) and (h) taken in April 2012; photo (f) taken in July 2012.

5.5.2. Geometrical ridges

The glacier foreland contains two distinct populations of geometrical ridges separated by the main Von Postbreen meltwater outlet (Figs 5.15 and 5.17a) which share many characteristics with geometrical ridges described in *Chapter 4* at Nathorstbreen. These ridges range from 10-100 m in length and are typically <5 m wide. Maximum ridge heights are in general between 1-6 m across the foreland (Figs 5.18a and 5.18f), although those associated with Von Postbreen (in green in Fig. 5.17a) are typically <2 m in height (Fig. 5.18k). The majority are sharp-crested, asymmetric ridges and some form pinnacles (Figs 5.18c, 5.18e and 5.18k). In planform the ridges are predominantly linear or, occasionally, very slightly curvilinear features, and often form an interconnected network (Figs 5.15 and 5.17a). Ridge orientations within the Von Postbreen population are transverse to centre-line ice flow direction (Fig. 5.17b) and they form a rectilinear (Bennett *et al.*, 1996) or rhombohedral (Ottesen and Dowdeswell, 2006) network. The Tunabreen ridges (in red in Fig. 5.17a) display more variable orientations, ranging from sub-parallel to transverse to centre-line ice flow direction (Fig. 5.17b). These ridges are more densely spaced than the Von Postbreen ridges and do not form a clear rectilinear or rhombohedral network. The Tunabreen ridges are also closely associated with a number of small pools and lakes (Fig. 5.18h), which are largely absent within the Von Postbreen group.

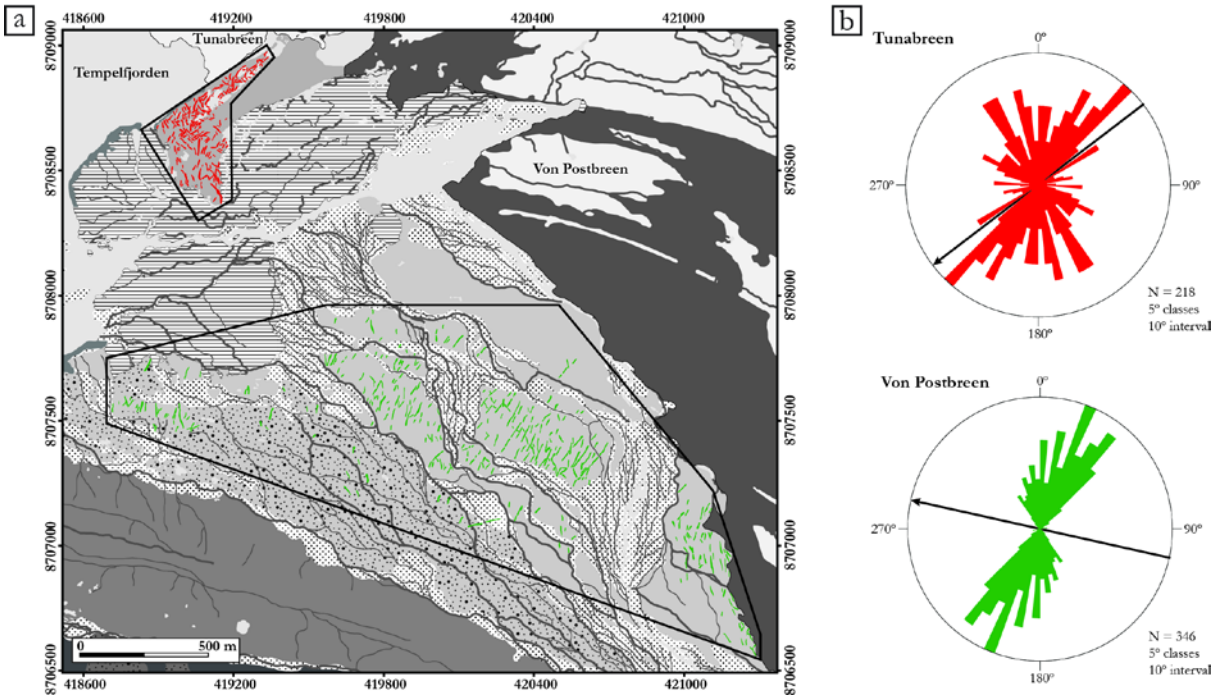

Figure 5.17 – Geometrical ridge networks. (a) Distinction between ridges associated with Tunabreen (in red) and Von Postbreen (in green). See Fig. 5.15 for detail on other geomorphology. (b) Rose diagrams of ridge orientations. Black arrows on stereographs show centre-line ice flow directions at the terminus.

The Tunabreen ridges are composed of a well-consolidated poorly-sorted diamict containing predominantly sub-angular to sub-rounded clasts (Figs 5.8 and 5.18i), with the

majority displaying evidence for striations, grooves, gouges or faceting, and some (~20% of sampled clasts) bullet-shaped morphologies. Large striated boulders (up to 1 m diameter) are common (Figs 5.18g and 5.18j), both on individual ridges and in inter-ridge areas. The diamict appears massive and structureless apart from occasional thin (<2 cm) and discontinuous lenses of coarse sand observed in some ridges. The composition of the Von Postbreen ridges is a well-consolidated poorly-sorted diamict containing striated clasts ranging from pebble to boulder sizes (Figs 5.18k and 5.18l), visually very similar to the diamict within the Tunabreen ridges. The main difference between the two is the colour of the diamict matrix: the Tunabreen sediment is reddish-brown whereas the Von Postbreen sediment is a lighter brown (Figs 5.18i-l).

A third population of geometrical ridges has been mapped on the Tempelfjorden seafloor from swath bathymetry data (Fig. 5.19). These positive-relief features are identified as thin (<10 m) linear to curvilinear ridges which form interconnected networks with a rectilinear or rhombohedral arrangement (Figs 5.19b, 5.19d and 5.19e). Ridge lengths range from 30-220 m and ridge heights from 0.5-4 m, with typical values of <2 m. The ridges are predominantly orientated at a 45° offset from the centre-line ice flow direction of Tunabreen (Fig. 5.19c). The submarine geometrical ridges can be subdivided into three populations based on their location relative to surge limits: the largest group (219 ridges) is located inside the 2004 surge limit, 78 ridges are located within the 1971 limit but outside the 2004 limit, and 17 ridges are located inside the 1930 limit but outside the 1971 limit (Fig. 5.19b). No geometrical ridges could be identified between the 1870 and 1930 limits. Flink (2013) did not map any geometrical ridges or similar features, but did map larger, continuous cross-fjord ridges and was able to correlate them to the 1870, 1930, 1971 and 2004 surge limits, and post-2004 retreat positions. See Flink (2013) for an extended geomorphological map of the Tempelfjorden seafloor including moraines, glacial lineations and debris flow lobes.

5.6. Interpretation

5.6.1. Ice facies

5.6.1.1. Stratified facies

Several processes have been demonstrated to be responsible for the formation of stratified debris-rich basal ice facies in different settings, including freeze-on of saturated subglacial sediments due to conductive cooling (Weertman, 1961); vertical regelation into subglacial sediments (Iverson, 1993, 2000); regelation around bedrock obstacles, hereafter referred to as regelation (Kamb and LaChapelle, 1964; Hubbard and Sharp, 1993); and glaciohydraulic supercooling associated with subglacial overdeepenings (Alley *et al.*, 1998, 2003; Cook *et al.*, 2010). This illustrates the possibility that basal ice facies with similar appearances may have a number of different origins (Waller *et al.*, 2000), and this will be addressed here in the context of the Tunabreen stratified facies and its subfacies.

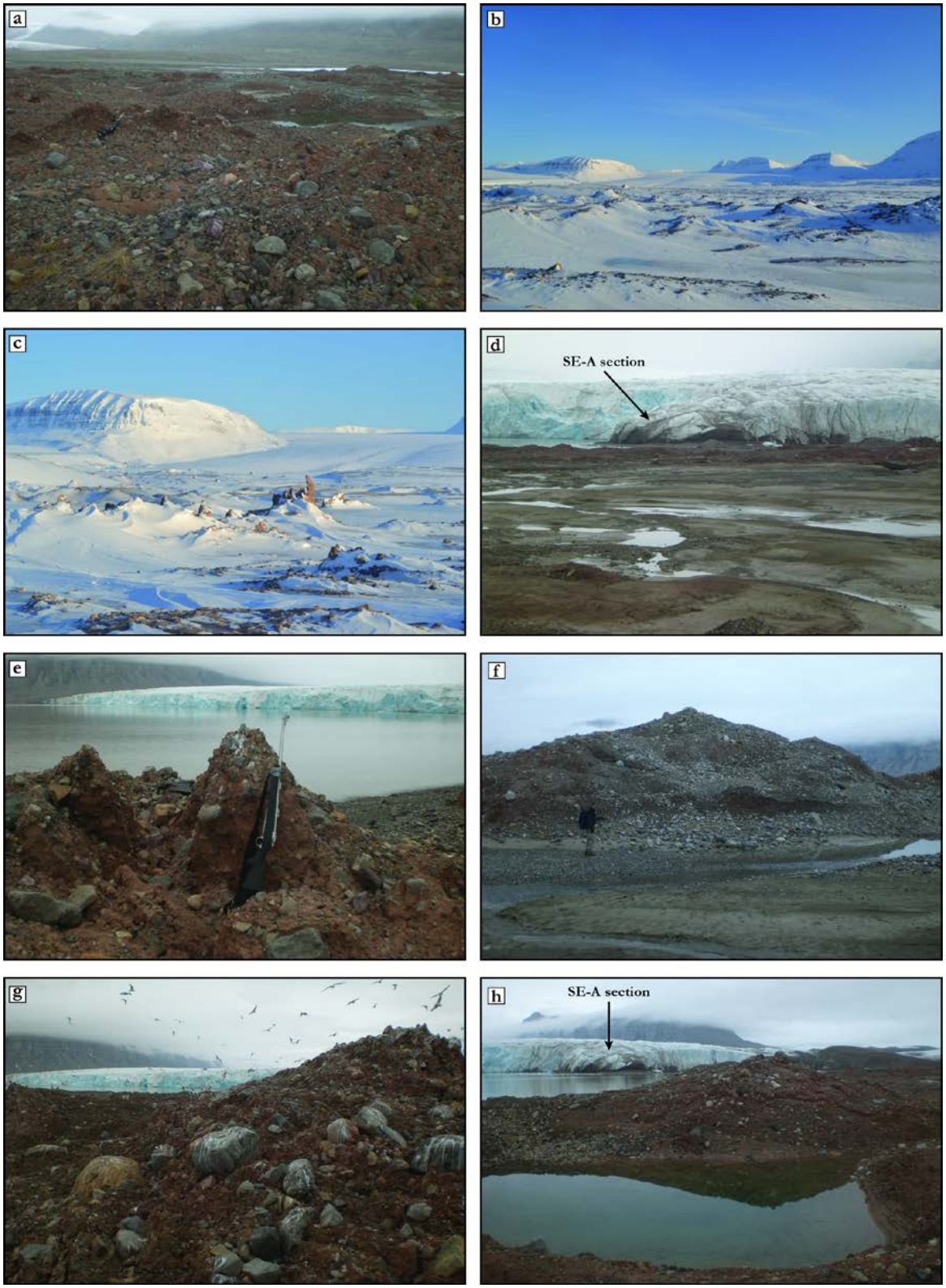

Figure 5.18

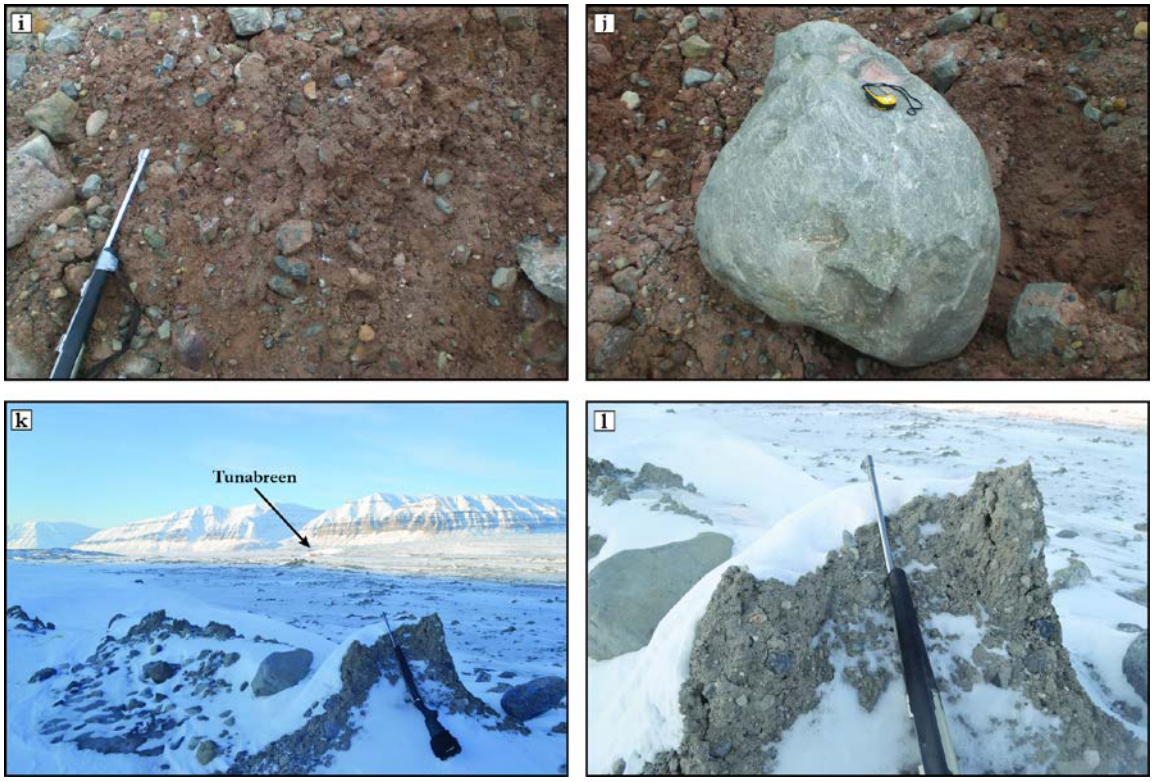

Figure 5.18 (this and preceding page) – Examples of geometrical ridges. (a) View across Tunabreen ridges towards Von Postbreen (top left) from close to Tempelfjorden shore. Flat white area in top right is the proglacial icing (see Fig. 5.15). (b) View across Tunabreen ridges towards Von Postbreen. (c) View across Tunabreen ridges towards Von Postbreen. Note sharp-crested ridges and distinct pinnacle. (d) View across Von Postbreen outwash plain towards Tunabreen ridges, with Tunabreen and SE-A section in the background. (e) Sharp-crested ridge close to Tempelfjorden shore with Tunabreen in the background. (f) Large ridge associated with Tunabreen close to Von Postbreen outwash and proglacial icing. (g) Ridge associated with Tunabreen. Note large, edge-rounded boulders and Tunabreen in the background. (h) Ridge close to Tempelfjorden shore. Note shallow pool in foreground and SE-A section in background. (i) Detail of poorly-sorted diamict within Tunabreen ridges. (j) Large edge-rounded and striated boulder within area of Tunabreen ridges. (k) Von Postbreen ridges with Tunabreen and Tempelfjorden in the background. Note sharp-crested morphology and large, edge-rounded boulders. (l) Detail of poorly-sorted diamict within Von Postbreen ridges. All photos taken in August 2011 apart from (b), (c), (k) and (l) taken in April 2012.

The textural characteristics of the solid stratified and banded subfacies, which predominantly consist of diamict with a polymodal grain size distribution (Fig. 5.7) and sub-angular to sub-rounded clasts (Fig. 5.8), are consistent with unconsolidated frozen debris of subglacial origin (Sugden *et al.*, 1987a; Sharp *et al.*, 1994; Spedding and Evans, 2002). These characteristics have been suggested to be indicative of *en masse* rather than particle-by particle debris accretion (Lawson, 1979), indicating that entrainment onto the glacier base occurred where the bed consisted of unconsolidated debris (Sharp *et al.*, 1994). This is likely to be the case below large parts of Tunabreen, as the surrounding geology comprises easily-erodible, fine-grained sedimentary lithologies (Dallmann *et al.*, 2002).

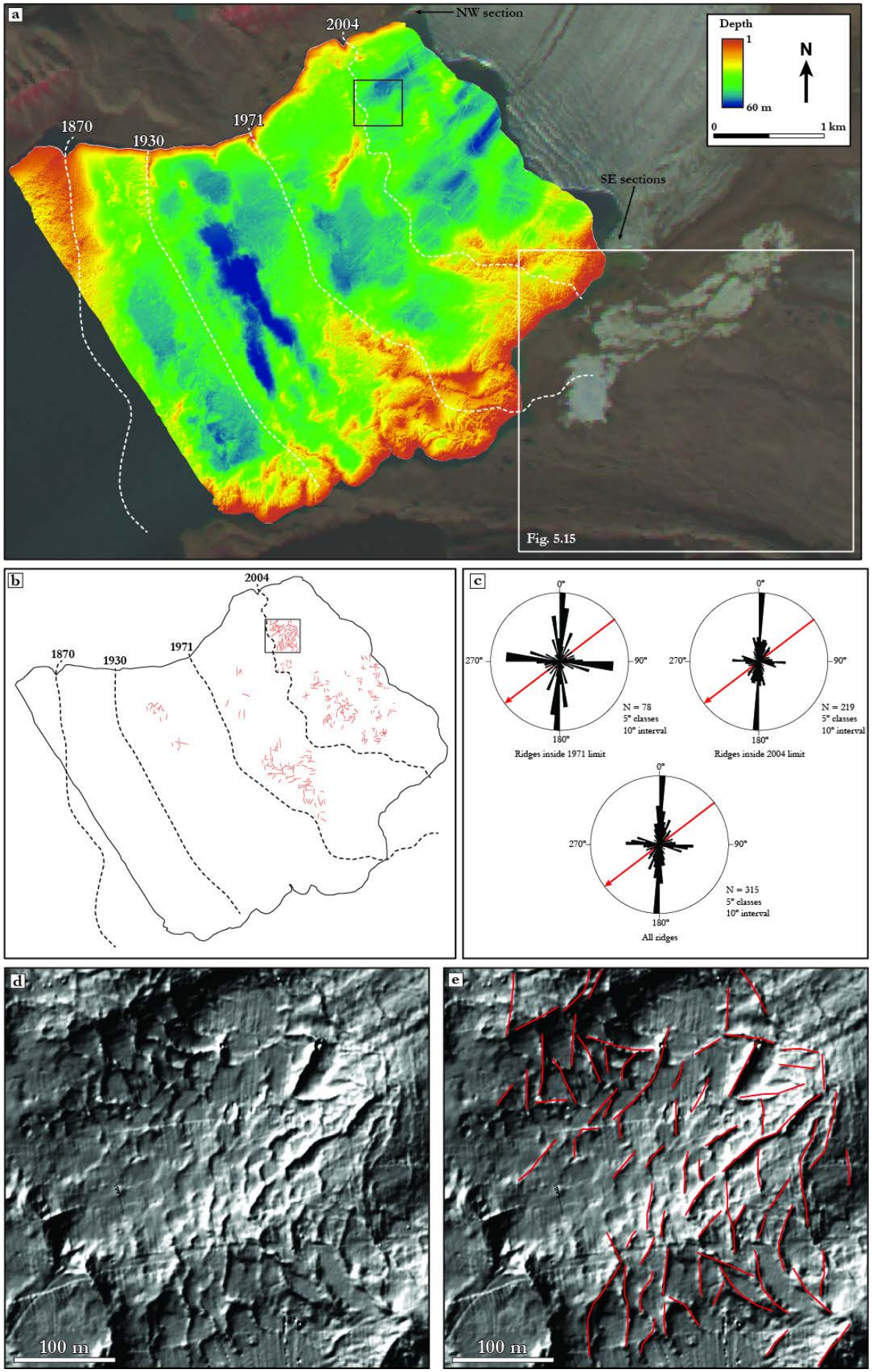
a
NW section
2004
1870
1930
1971
Depth
1
60 m
N
0
1 km
SE sections
Fig. 5.15
b
2004
1870
1930
1971
c
0°
270°
90°
180°
N = 78
5° classes
10° interval
Ridges inside 1971 limit
N = 219
5° classes
10° interval
Ridges inside 2004 limit
N = 315
5° classes
10° interval
All ridges
d
100 m
e
100 m

Figure 5.19

Figure 5.19 (preceding page) – (a) Swath bathymetry of inner Tempelfjorden with 2010 ASTER image as background. 1870, 1930, 1971 and 2004 surge limits are shown (see Fig. 5.2). Black rectangle delimits area shown in detail in (d) and (e); white rectangle shows area mapped in Fig. 5.15. (b) Mapped submarine geometrical ridges. 1870, 1930, 1971 and 2004 surge limits are shown (see Fig. 5.2). Black rectangle delimits area shown in detail in (d) and (e). (c) Rose diagrams of submarine geometrical ridge orientations. Red arrows show centre-line ice flow direction at the margin of Tunabreen. (d) Shaded relief image of area delimited by the black rectangles in (a) and (b). Note thin ridges displaying a variety of alignments. (e) Area shown in (d) with individual ridge crests highlighted in red. See Flink (2013) for a detailed map of other submarine landforms. Swath bathymetry data acquired by the Norwegian Hydrographic Service and UNIS.

Solid stratified

The thickness of the solid stratified facies (typically >0.5 m and up to 2.5 m) suggests it is unlikely to have formed by relegation, as this rarely produces layers in excess of 0.1 m thick (Nye, 1970; Hubbard and Sharp, 1993), but is consistent with freeze-on, vertical regelation and glaciohydraulic supercooling processes (Hubbard and Sharp, 1995; Alley *et al.*, 1998; Spedding and Evans, 2002). Ice formed by regelation has also been observed to have typically low debris concentrations (Kamb and LaChapelle, 1964; Hubbard, 1991), which contrasts with the high debris concentrations of the solid stratified subfacies. Based on these characteristics, regelation is unlikely to have been responsible for the formation of the solid stratified subfacies.

Vertical regel5.19ation into the bed was suggested by Alley *et al.* (1997) to be most effective at incorporating coarse-grained, clast-supported debris, with clasts already in the ice pushed further up by newly entrained clasts. The grain size distribution of the stratified facies, which has a silt-rich matrix (Fig. 5.7), indicates that such a process is unlikely to have been dominant in its formation, similar to the interpretations of Larsen *et al.* (2010). In addition, Alley *et al.* (1997) suggested that this mechanism required pore-water pressure within the subglacial sediments to be lower than ice pressure, a situation which is highly unlikely beneath a surge-type glacier in its active phase (Clarke *et al.*, 1984; Fowler *et al.*, 2001), although this could be the case soon after surge termination.

The solid stratified subfacies shares some physical similarities with the descriptions of debris-rich ice attributed to glaciohydraulic supercooling in other studies, including polymodal grain size distribution, medium to high debris concentrations, interstitial ice, small areas of sorted sediment (Fig. 5.6d), and overall facies thicknesses of >0.5 m (Lawson *et al.*, 1998; Cook *et al.*, 2007, 2010). These examples were also associated with additional features thought to be diagnostic of supercooling (e.g. upwelling vents, anchor ice terraces, fractures filled with platy ice; Evenson *et al.*, 1999), none of which were observed at Tunabreen, and an overdeepening with an adverse slope. There is no evidence for an overdeepening in the swath bathymetry of the fjord bed, which includes the area covered during the 2004 surge maximum position (Flink, 2013). Thus, although a supercooling origin for the solid stratified subfacies cannot be

discounted, the absence of key elements associated with the process suggests it is not the most obvious interpretation.

Based on the physical characteristics of the solid stratified subfacies, the favoured interpretation is that it has predominantly formed by a form of net freeze-on through conductive cooling at the ice margin (Weertman, 1961; Alley *et al.*, 1997). This process describes the situation where the 0°C isotherm migrates downwards into saturated subglacial material, either through cooling at the surface or the downward advection of colder ice, forcing a switch from net basal melting to net basal freezing (Alley *et al.*, 1997). In the case of a polythermal surge-type glacier, rapid freeze-on could occur (i) at the thermal transition between warm, surging ice and cold, inactive ice at the margin; (ii) on surge termination as a cold wave propagates downwards through a thinned and heavily-crevassed terminus; or (iii) as cold ice is advected downglacier during the final stages of the active phase (cf. Alley *et al.*, 1997; Larsen *et al.*, 2010). Freeze-on due to (ii) and (iii) would be uniquely associated with the end of surge activity, whereas (i) could occur throughout the surge as warm ice continuously meets cold marginal ice. The decreased basal movement associated with surge termination will also reduce frictional heating, enhancing excess upward heat flux as the temperature field adjusts slowly (Alley *et al.*, 1997). This in turn facilitates rapid net freeze-on of saturated sediment, creating frozen debris containing ice lenses. The observed areas with very low ice content within the solid stratified subfacies (i.e. frozen diamict) also support a freeze-on mechanism as they are indicative of *en masse* freezing of debris (Larson *et al.*, 2010). A freeze-on interpretation is favoured because it not only explains the formation of solid stratified subfacies ice in the basal zone, but also the *in-situ* freezing of saturated sediment within debris-rich bands and structures (Fig. 5.5) as the cold wave propagates through the thinned glacier. In these latter cases, a propagating cold-wave may not be necessary to induce freezing. Instead, elevated thin debris-rich structures surrounded by colder ice are likely to freeze simply due to the temperature gradient. In addition, in the context of multiple surges of the same glacier, some debris-rich bands could have been inherited from a previous surge cycle (see *5.6.2.2.*) and may remain frozen throughout the subsequent active phase.

The stable isotope data show that the stratified facies is enhanced in heavy ^{18}O isotopes relative to englacial facies ice (Table 5.1; Fig. 5.11). This is consistent with both a supercooling origin (Lawson *et al.*, 1998; Swift *et al.*, 2006; Cook *et al.*, 2010) and with ice formation through partial refreezing of water in close association with a debris-rich bed (Lawson, 1979; Knight, 1989; Hubbard and Sharp, 1993; Iverson and Souchez, 1996), such as freeze-on (Souchez *et al.*, 1988). In the latter case, ice formation by refreezing of a localised water source should plot on a freezing slope with a gradient lower than englacial ice (Jouzel and Souchez, 1982; Souchez and Jouzel, 1984); this cannot be observed on the co-isotopic plot for Tunabreen (Fig. 5.12). Similarly, according to Cook *et al.* (2010) ice formed by glaciohydraulic supercooling should plot along the local meteoric water line (LMWL); this is also not the case

with the stratified facies (Fig. 5.12). A further possibility is that ^{18}O enrichment is not a signature of refreezing, but may be the result of isotope exchange between water and hydroxyl-bearing minerals that have been subjected to subglacial abrasion (Souchez *et al.*, 1990). This is suggested to be particularly effective for fine-grained material, such as comprises the matrix of the frozen diamict at Tunabreen.

This indicates that the isotope composition is complex and may reflect a combination of processes and a range of different parent waters with variable isotopic compositions (Boulton and Spring, 1986; Hubbard and Sharp, 1993; Sharp *et al.*, 1994; Knight, 1997; Swift *et al.*, 2006). A possible explanation is that there was a continuous influx of different parent waters to the freezing environment (Sharp *et al.*, 1994), a situation which is consistent with net basal melting due to frictional heating at the base, resulting in subglacial sediment saturated by water from a variety of sources. This is indicative of open-system freezing, where the freezing front is in contact with a dynamic water body of variable isotopic composition, which is also consistent with isotopic enrichment (Boulton and Spring, 1986; Souchez *et al.*, 2000; Cook *et al.*, 2010). This demonstrates that, although the stable isotope data cannot conclusively distinguish the origin of the solid stratified subfacies, and may indicate that a range of processes was active, it is consistent with an interpretation of freeze-on of saturated subglacial debris containing waters from various sources.

The mean $\delta^{18}O$ value for the stratified facies (-13.95‰) is similar to values reported from Variegated Glacier by Sharp *et al.* (1994) for the basal stratified laminated (-14.24‰) and basal stratified solid (-14.06‰) facies, but is also significantly lighter than measured $\delta^{18}O$ values for descriptively-similar facies at other Svalbard glaciers (-10.85‰ to -12.80‰ at Kongsevengen, Midtre Lovénbreen and Austre Brøggerbreen; Hubbard *et al.*, 2004) and some Icelandic glaciers (-8.30‰ at Svínafellsjökull, -10.40‰ at Skaftafellsjökull, -8.30‰ to -11.70‰ at Kvíárjökull; Swift *et al.*, 2005; Cook *et al.*, 2010), and significantly heavier than $\delta^{18}O$ values recorded for stratified ice at Kuannersuit Glacier, West Greenland (-18.00‰; Larsen *et al.*, 2010). For δD, the Tunabreen solid stratified facies mean value (-103.41‰; Table 5.1) is heavier than values from Variegated Glacier (-107.25; Sharp *et al.*, 1994) and Kuannersuit Glacier (-129.70‰; Larsen *et al.*, 2010), and is lighter than mean values from Svínafellsjökull (-56.70‰) and Skaftafellsjökull (-70.90‰; Cook *et al.*, 2010). This highlights the large range in isotopic values that are possible for similar facies at different locations, which may reflect different isotopic compositions of the source water controlled by a range of processes, including the number of melting-refreezing events experienced by the parent water prior to ice formation and the time of year that the initial precipitation occurred (Cook *et al.*, 2010).

Banded subfacies

The grain size distribution of the stratified facies (Fig. 5.7) suggests that its subfacies are unlikely to have formed thorough vertical regelation into the bed, as this process will

theoretically produce clast-supported ice facies (Alley *et al.*, 1997). A glaciohydraulic supercooling origin has been suggested for visually similar facies (Larson *et al.*, 2010) and, although this cannot be discounted, it is not supported by wider evidence for supercooling in the form of fluvial sedimentary structures and occurrences of upwelling vents, anchor ice terraces and fractures filled with platy ice (Evenson *et al.*, 1999; Swift *et al.*, 2006). Alternatively, the characteristics of the banded subfacies are consistent with refreezing at the glacier base producing thin, discontinuous layers of alternating debris-rich and clean ice (Sugden *et al.*, 1987a; Sharp *et al.*, 1994; Hubbard and Sharp, 1995; Waller *et al.*, 2000; Larsen *et al.*, 2010), indicating a freeze-on (Weertman, 1961) and/or regelation (Hubbard and Sharp, 1993) origin. However, although theoretically capable of producing the thickness of banded facies typical at the SE sections (10-20 cm; Figs 5.6g and 5.10; Nye, 1970; Lliboutry, 1993; Alley *et al.*, 1997), regelation alone is unlikely to form the metres-thick units at the NW section (Fig. 5.5a). This has been explained in a number of other studies by a process of post-formational tectonic thickening due to longitudinal compression, through the folding and stacking of originally thin debris-rich ice layers (Sugden *et al.*, 1987a; Sharp *et al.*, 1994; Hubbard and Sharp, 1995; Waller *et al.*, 2000; Spedding and Evans, 2002; Swift *et al.*, 2006). The presence of folds (Figs 5.6i-l and 5.14k-o) and the intercalation of englacial and debris-rich ice (Figs 5.5a, 5.13f and 5.14i) indicate that significant tectonic thickening has occurred within the banded subfacies at all sections, providing an explanation for the overall facies thickness at the NW section. This tectonic deformation will be discussed in more detail in *5.6.2.*

Regelation is also associated with typical debris concentrations of only 5-10% (Kamb and LaChapelle, 1964; Alley *et al.*, 1997), which is consistent with the lowest measured concentration for the stratified facies (9.6%). Debris concentrations at the NW section are typically observed to be higher relative to this (Fig. 5.6f and 5.6 h), probably closer to the 31% measured at the SE-B section. This higher debris concentration, and the textural characteristics of this debris (e.g. polymodal grain size distribution, edge-rounded clasts; Figs. 5.7 and 5.8) indicates that net basal freeze-on, an important entrainment mechanism at the base of polythermal glaciers (Waller *et al.*, 2000), may also have been active at Tunabreen. Therefore, a combination of freeze-on and regelation is favoured for the formation of the banded subfacies, similar to the interpretations of Larsen *et al.* (2010), in conjunction with post-formational tectonic thickening through the folding and stacking of debris-rich and clean ice layers.

Ice formed by regelation is expected to be enriched in heavy isotopes relative to the parent water (Souchez *et al.*, 1988; Hubbard and Sharp, 1993, 1995), which is consistent with the ^{18}O composition of the stratified facies (Table 5.1; Fig. 5.11). However, ice formed through localised refreezing should also lie on a distinguishable freezing slope on a co-isotopic plot (Jouzel and Souchez, 1982; Souchez and Jouzel, 1984; Hubbard and Sharp, 1995), which is not the case at Tunabreen (Fig. 5.12). This indicates that a range of processes may have influenced the formation of the stratified facies, including the presence of a dynamic water body with

variable initial isotopic compositions (Sharp *et al.*, 1994), and isotopic enrichment through exchange with fine-grained hydroxyl-bearing minerals (Souchez *et al.*, 1990). Therefore, no one single mechanism can be invoked for the stratified facies based on the isotope data, but it is consistent with formation by a combination of freeze-on and regelation as indicated by the physical characteristics of the banded subfacies.

Solid subfacies

The structureless character of the solid subfacies ice and its composition of almost entirely angular to sub-angular clasts of a single (limestone) lithology are indicative of *en masse* entrainment by net freeze-on processes (Lawson, 1979; Lawson *et al.*, 1998). The clast-supported nature of this subfacies (Fig. 5.6m) is also consistent with a mechanism of regelation into the bed (Iverson and Souchez, 1996; Alley *et al.*, 1997). However, the close association of the solid and solid stratified subfacies suggests that they are likely to have formed by similar processes, with the main difference in physical character reflecting different debris sources. The restricted distribution and predominance of angular material within the solid facies is consistent with a localised source of material that is derived from rockfall and/or has undergone very little transport at the glacier bed.

5.6.1.2. Dispersed facies

The dispersed facies is characteristically similar to many aspects of ice previously described as *clear facies/subfacies* ice (Sharp *et al.*, 1994; Hubbard and Sharp, 1995; Hubbard *et al.*, 2000), specifically the bubble-poor nature, very low debris content, and typical proximity to subglacial debris (Fig. 5.9a-c). Similar to these studies, the dispersed facies at Tunabreen is interpreted as englacial facies ice that has undergone strain-induced metamorphism in close proximity to the glacier bed and/or debris-rich basal ice. The very clear, bubble-poor nature of much of this facies is consistent with the expulsion of gas during enhanced ice deformation (Hubbard and Sharp, 1995). This deformation has been suggested to involve melting and refreezing at grain boundaries (Kamb and LaChapelle, 1964) and the removal of gas in solution along triple-grain veins (Hubbard *et al.*, 2000). Strain heating is likely to be an important energy source for intergranular melting. The bubble structures observed within the dispersed subfacies are consistent with this process of gas expulsion. Figures 5.9c-e show that the fine worm-like bubble structures often trace the outline of ice crystals, demonstrating the routing of gas around grain boundaries. This pattern continues as the bubble structures grade into wider, more-planar ribbons, although the crystal boundaries appear far more diffuse (Fig. 5.9f). Occasional larger bubbles and parts of the more dispersed bubble clouds (Fig. 5.9g) may represent remnants from the englacial facies where gas expulsion was incomplete (Hubbard and Sharp, 1995).

The fine-grained sediment within the dispersed facies is consistent with re-distribution by water flowing within a vein network between ice crystals, as first suggested by Lliboutry

(1993). The larger clots of debris could be the result of sediment accumulation in voids, as demonstrated by Knight and Knight (1994) in laboratory experiments. The proximity of the dispersed facies to debris-rich stratified facies ice in almost all occurrences suggests that this debris is likely to be primarily sourced directly from the fine-grained material that comprises the bulk of the diamict matrix (Fig. 5.7). The sediment inclusions are thus largely inferred to be the result of water migration, either close to the basal zone (Knight and Knight, 1994) or debris-rich bands (Larsen *et al.*, 2010), mobilising available fine-grained sediment. The inferred routing of this muddy water through the vein network around individual grain boundaries is best illustrated in Fig. 5.9e. Although this process is suggested to be responsible for the vast majority of the debris within the dispersed facies, the occasional coarser grains (Fig. 5.7) are unlikely to have been distributed along the vein network. Hubbard and Sharp (1995) suggested that the coarser material within their characteristically similar *clear facies* was probably the result of the redistribution of initially thin debris layers by tectonic processes, and a similar mechanism is invoked for the dispersed facies. Tectonic deformation is evident within the thin debris laminae in the dispersed facies, which often display a strong linear component within the sediment (Fig. 5.9j), described as mineral stretching lineations in Fleming *et al.* (2013), and are indicative of shear. Therefore, similar to the interpretations of Hubbard and Sharp (1995), a combination of sediment distribution through water flow within intergranular vein networks and tectonic deformation is thought to have been active within the dispersed facies.

The stable isotope composition of dispersed facies ice is consistent with a metamorphosed origin, and specifically melting and refreezing at grain boundaries (Kamb and LaChapelle, 1964). Although the mean $\delta^{18}O$ value for the dispersed facies (-14.36‰) is slightly heavier than that for englacial facies (-15.34‰), this is insufficient to reflect isotope enrichment (Table 5.1; Swift *et al.*, 2006; Larsen *et al.*, 2010). In addition, the dispersed facies data do not produce a freezing slope on a co-isotopic plot, as may be expected if the ice is formed from a single initial water source of limited extent and with a specific isotopic composition (Souchez *et al.*, 1988). This may indicate that the melting and refreezing at grain boundaries is not confined to one cycle sourced only from the englacial facies, but may be the result of multiple melting and partial refreezing events with numerous water sources in an open-system (Sharp *et al.*, 1994; Cook *et al.*, 2010). It was suggested by Souchez *et al.* (1988) that multiple melting-refreezing events of basal ice at Jakobshavn Isbræ were possibly reflected in the high ranges in measured $\delta^{18}O$ and δD values (4.5‰ and 28‰, respectively), which are of the same order as the ranges within the dispersed subfacies at Tunabreen (3.51‰ and 23.82‰, respectively). This was inferred by (Souchez *et al.*, 1988) to be the result of no fractionation occurring upon melting of the ice formed (and partially enriched) in a previous freezing event, producing isotopically-heavier meltwater which becomes the initial liquid for the next freezing event, and therefore creating a higher range in values.

The mean $\delta^{18}O$ value for the dispersed facies (-14.20‰; Table 5.1) is similar to values for the descriptively-similar basal stratified clear facies reported at Variegated Glacier by Sharp *et al.* (-14.46‰), but is significantly lighter than the mean value for dispersed facies recorded by Cook *et al.* (2011) at Svínafellsjökull, Iceland (-10.90‰), and heavier than the mean of dispersed ice at Kuannersuit Glacier (-18.80‰; Larsen *et al.*, 2010). Mean δD values for the dispersed facies at Tunabreen (-103.12‰; Table 5.1) are similar to values reported from Variegated Glacier (-108.94‰; Sharp *et al.*, 1994), but are significantly lighter than those recorded at Svínafellsjökull (-71.90‰; Cook *et al.*, 2011) and heavier than values from Kuannersuit Glacier (-138.80‰; Larsen *et al.*, 2010). The similarity between the mean values for both $\delta^{18}O$ and δD at Tunabreen and Variegated Glacier, and the high range in values recorded at both (-12.99 to -16.50 at Tunabreen and -13.20 to -16.00 at Variegated Glacier for $\delta^{18}O$), is consistent with both forming through similar processes (e.g. strain-induced metamorphism of englacial ice). However, it is also clear that a large variation in isotopic values between different locations is possible for facies that are both descriptively similar and interpreted to form through similar mechanisms (e.g. dispersed ice at Svínafellsjökull and Kuannersuit Glacier; Larsen *et al.*, 2010; Cook *et al.*, 2011).

5.6.1.3. Englacial facies

This facies comprises the bulk of the glacier and the upper parts of the NW and SE sections, and is interpreted as meteoric ice formed by the firnification of snow in the accumulation area (Hambrey, 1975). The alternating layers of bubble-poor and bubble-rich ice reflect seasonal variations in firnification processes which produce stratification within the ice (Hambrey and Dowdeswell, 1997). These pre-existing layers may be realigned through transposition and folding as ice converges from a wide accumulation area into a narrow valley, forming longitudinal foliation (Hooke and Hudleston, 1978) (Fig. 5.15). The mean $\delta^{18}O$ composition of the englacial facies (-15.34‰; Table 5.1) is similar to 11-year running mean values for meteoric ice from the Lomonosovfonna ice core record (typically between -15 and -16‰) as reported by Divine *et al.* (2008), although the δD mean (-100.83‰) is significantly lower than the ice core equivalent (typically between -115 and -120‰). The mean $\delta^{18}O$ value for the englacial facies at Tunabreen is similar to that recorded at Variegated Glacier (-16.34‰; Sharp *et al.*, 1994), but is much lighter than mean values from Svínafellsjökull (-12.40‰; Cook *et al.*, 2011) and heavier than those reported from Kuannersuit Glacier (-19.80‰; Larsen *et al.*, 2010). The mean δD value for the Tunabreen englacial facies (-100.83‰; Table 5.1) is lighter than that recorded at Svínafellsjökull (-73.60‰; Cook *et al.*, 2011) and heavier than measured mean values at Variegated Glacier (-122.12‰; Sharp *et al.*, 1994) and Kuannersuit Glacier (-144.00‰; Larsen *et al.*, 2010), highlighting the range in meteoric ice isotopic compositions that are possible across different regions. The isolated grains and small clots of fine debris within this facies

probably originated as wind-blown dust (Lawson, 1979; Sharp *et al.*, 1994; Hubbard and Sharp, 1995; Larsen *et al.*, 2010).

5.6.2. Debris-rich structures and tectonic deformation

5.6.2.1. NW section

The overall structure and distribution of ice facies at the NW section is strongly indicative of tectonic thickening through the folding and stacking of debris-rich and clean ice layers at the lateral glacier margin. It is inferred that the section is close to the glacier bed in this area, although this was not directly observed, based on: the thick sequence of debris-rich ice comprised of sediment of subglacial origin; the location of the section at the lateral margin with subaerial ice-cored moraine; observations during summer 2011 that the section had a well-defined beach in front of it and was not actively calving; and swath bathymetry data which shows a water depth of <5 m approximately 100 m downfjord from the section (Fig. 5.19a).

The section stratigraphy (Fig. 5.5a) demonstrates that the ice layers have experienced significant reorganisation compared to basal sequences described at other sites (Lawson, 1979; Sugden *et al.*, 1987a; Waller *et al.*, 2000; Hubbard *et al.*, 2004), which from the bed upwards are typically similar to the following: a lowermost layer of stratified debris-rich ice consisting of solid subfacies ice or frozen diamict overlain by banded subfacies ice; a layer of debris-poor dispersed facies ice; and an uppermost layer of clean englacial facies ice. At the NW section, clean englacial ice layers are sandwiched between ~2 m-thick banded ice layers and the solid stratified ice layer is not the lowermost unit but overlies the intercalated banded and englacial layers, and in turn is overlain by a further layer of banded ice (Fig. 5.5a). This in effect represents a complex elevated repetition, with some evidence of a reversal in inferred original layering, of the basal ice sequence. This tectonic thickening is interpreted to be the result of a combination of large-scale folding and faulting within the ice. The complex stratigraphy can be explained by both: (i) a zone of imbricate thrust slices (e.g. Figs 5.20a and 5.20b); and (ii) intense ductile deformation (Figs 5.20c and 5.20d), or some combination of the two.

(i) The complex stacked stratigraphy, with repeated layers of banded subfacies ice sandwiching englacial ice and elevated solid stratified layers (Fig. 5.5a), shares similarities with imbricate thrust zones described from both glaciotectonic (Croot, 1987; Burke *et al.*, 2009) and hard rock geological (Tavarnelli *et al.*, 2004) settings (Figs 5.20a and 5.20b). In this interpretation, the solid stratified and banded ice would have to act as both a combined unit of stratified facies ice, such as the uppermost layers of debris-rich ice at ~45-75 m which are in inferred original stratigraphic order, and also as independent layers with a décollement between the two, such as where banded ice overlies englacial ice but with no solid stratified layer between (e.g. ~45-70 m, lower part of the section). Thrust faulting is also inferred to be responsible for the low angle stacking of solid stratified and banded ice on top of englacial ice and truncating the underlying banded ice layer at the far right-hand (NE) end of the section

(~70-90 m; Fig. 5.20d; cf. Fleming *et al.*, 2013). Without knowing exactly how close the section is to the glacier bed, it is difficult to assess the total amount of displacement experienced; however, the difference in height between the upper limits of the repeated banded ice layers at the right-hand end of the section is indicative of a displacement on the order of 2-3 m, similar to that described by Sharp *et al.* (1988) at Variegated Glacier. The significance of thrust faulting within glaciers is a subject of great debate (see Sharp *et al.*, 1994; Bennett *et al.*, 1996; Glasser *et al.*, 1998b; Bennett *et al.*, 1999; Woodward *et al.*, 2002; Evans and Rea, 2005; Moore *et al.*, 2010; Rea and Evans, 2011) and the Tunabreen observations and interpretations will be discussed in this wider context in *Chapter 9*.

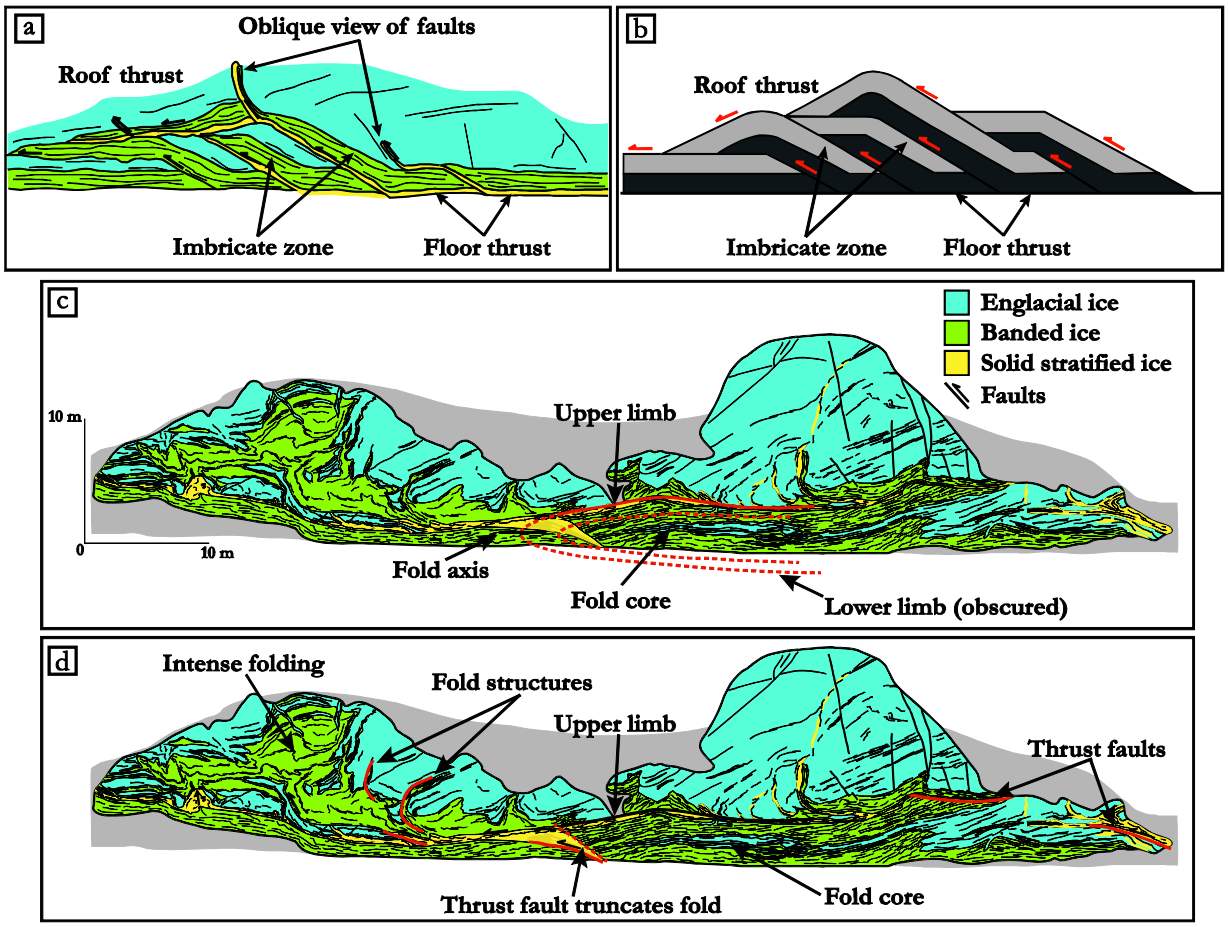

Figure 5.20 – NW section annotated to show possible development of tectonic structure. False colouring is to aid visual interpretation. (a) Interpretation of NW section formation as a series of imbricate thrust slices. Steepened appearance of faults may relate to their oblique intersection with the section face. (b) Schematic diagram of duplex-imbricate thrust slices (modified from Benn and Evans, 2010). (c) and (d) Alternative interpretation of section formation through the development of a recumbent fold (c) followed by thrust faults truncating fold structure and stacking solid stratified and banded ice over englacial ice (d).

(ii) The stacked layers of banded ice surrounding englacial ice and overlain by solid stratified ice at the right-hand (NE) end of the section could also be explained as a tight to isoclinal recumbent fold of the basal sequence around a core of englacial ice, in which the lowermost limb of solid stratified ice is just below the base of the section and so obscured (Fig.

5.20a). This style of folding, which may have developed through progressive attenuation of a drag fold which then became detached (see Fig. 5.10c, p. 121 in Twiss and Moores, 2007), could produce the apparent reversal of inferred original stratification within the basal sequence. The fold hinge appears to have been truncated by the layer of solid stratified and pod of solid subfacies ice (dipping at 39º) that emerges from the base of the section at ~45 m and overtops banded ice to the left, which is interpreted as a thrust fault (Fig. 5.20b). This truncation provides an explanation for the lack of clear evidence for the large-scale fold within the banded ice lamination, i.e. convergence of stratification within the upper and lower banded ice layers.

In several places, stratified facies ice intrudes into the overlying englacial ice (Figs 5.5a and 5.13c). This example contains both solid stratified and banded subfacies ice, and the stratification within the latter has been reoriented sub-vertically. Evidence for similarly aligned debris-poor structures can also be seen in the surrounding englacial ice. Similar structures comprised of only solid stratified ice could be indicative of a form of injection or squeezing of saturated basal sediments up into fractures or voids within the englacial ice (see *5.6.2.2.* and Fig. 5.21); however, such mechanisms are difficult to reconcile with the presence of banded subfacies ice and the preservation and reorientation of the stratification within. The steep, and in some cases overturned, appearance of the structures would perhaps suggest that a thrust fault origin is unlikely, as this typically produces structures with a dip of <45° (Twiss and Moores, 2007); however, this is based on a two-dimensional face and so the apparent steepness of the structures may be exaggerated, and what is seen is in fact oblique slices through the section.

An alternative interpretation is that the intruding structures are related to ductile deformation (Fig. 5.20d). This may indicate a velocity gradient within the section, whereby the highest rate of shear (and lowest resistance to deformation) is accommodated in the lower part of the section, and this resistance increases upwards. Lower velocities and higher resistance in the upper part of the section could result in the folding up and part rotation of layers when compressive forces are applied from an upglacier direction, leading to steepening and eventual overturning (Fig. 5.20d). Such a process is consistent with the preservation and reorientation of original stratification within the stratified facies ice. Further evidence for ductile deformation can be found within the banded ice throughout the section, particularly at the left-hand (SW) end where the thickest area of banded subfacies ice has been intensely folded and it is very difficult to identify any original horizontal stratification (Fig. 5.5a). These thick sequences may also include basal ice facies which formed during previous surges and has been subsequently redeformed during the most-recent active phase.

Clast fabric data from the banded subfacies at the NW section (Fig. 5.5a) display a-axis orientations (trending NW-SE) that are broadly similar to anisotropic magnetic susceptibility K1 orientations from the same facies measured by Fleming *et al.* (2013). AMS has been demonstrated to be a very useful technique for determining fabric data within debris-rich basal ice (Fleming *et al.*, 2013) and Pleistocene sediments (Fleming *et al.*, 2012). The orientations

deviate away from both centre-line and local ice flow directions at the margin. These may be the result of re-orientation due to lateral frictional drag in a marginal shear zone, such as that observed following the 1982-83 Variegated Glacier surge (Lawson *et al.*, 1994), and is indicative of non-coaxial deformation at the glacier margin (Fleming *et al.*, 2013).

The evidence within the NW section for both ductile and brittle deformation, in conjunction with quite different relationships between facies over short distances, indicates that different processes have been active at different times, or even at the same time. For example, at ~45 m the solid stratified facies truncates banded facies ice, yet within ten metres the two appear horizontally bedded (Fig. 5.5a). An explanation for this is that different deformational sub-environments are active at the same time over short distances, i.e. areas of the section may have been subjected to intense folding and thickening whilst within tens of metres the stacking of layers through thrust faulting was occurring. Support for such sub-environments over short distances can be seen on the time-lapse imagery taken during a surge of Paulabreen in 2005-06 (Kristensen and Benn, 2012; included on CD inside the back cover). In this, it is possible to see blocks of debris-rich ice being continuously stacked on top of and overriding each other in some places and, within a short distance and at the same time, debris-rich layers are clearly being folded and overturned. These processes may explain such a varied structure over short distances as observed at the NW section.

5.6.2.2. SE sections

The debris-rich bands and structures within the SE sections and observed elsewhere in the Tunabreen ice front display a variety of morphologies, orientations, dip angles and compositions (Figs 5.5b, 5.5c and 5.14a-g), making it unlikely they all formed through exactly the same process at the same time. The formation of englacial debris-rich bands observed within other tidewater surging glaciers, in particular Kongsvegen in NW Svalbard, has been interpreted by different studies to be either the result of englacial thrusting (e.g. Bennett *et al.*, 1996, 1999; Glasser *et al.*, 1998b) or the squeezing of basal debris into crevasses and subsequent re-orientation (Evans and Rea, 1999; Woodward *et al.*, 2002; 2003a), both strongly linked to surge activity. By contrast, the Tunabreen debris-rich bands are interpreted to be the result of at least three main mechanisms, often in combination and linked to the availability of saturated basal sediments.

The first mechanism is the squeezing of saturated subglacial debris into a heavily fractured glacier base, hereafter referred to as crevasse squeezes (Fig. 5.21a). This process is suggested to be responsible for vertical or near vertical debris-rich structures in the ice cliff, such as those shown in Fig. 5.14g. Aerial photographs and ASTER images show that Tunabreen was heavily crevassed at its surge maximum (Fig. 5.3), and it has been demonstrated that in such scenarios both full-depth and extensive basal crevassing are highly likely to occur (cf. Rea and Evans, 2011). Saturated basal material is squeezed into these crevasses/cavities as the

glacier settles back onto its bed post-surge. Crevasse squeezes have been widely invoked as a mechanism for forming englacial debris-rich structures and proglacial geometrical ridge networks at the margins of surging glaciers in both terrestrial and marine settings (e.g. Gripp, 1929; Sharp, 1985a; Solheim and Pfirman, 1985; Boulton *et al.*, 1996; Woodward *et al.*, 2002; Christoffersen *et al.*, 2005; Evans and Rea, 2005; Ottesen and Dowdeswell, 2006; Ottesen *et al.*, 2008).

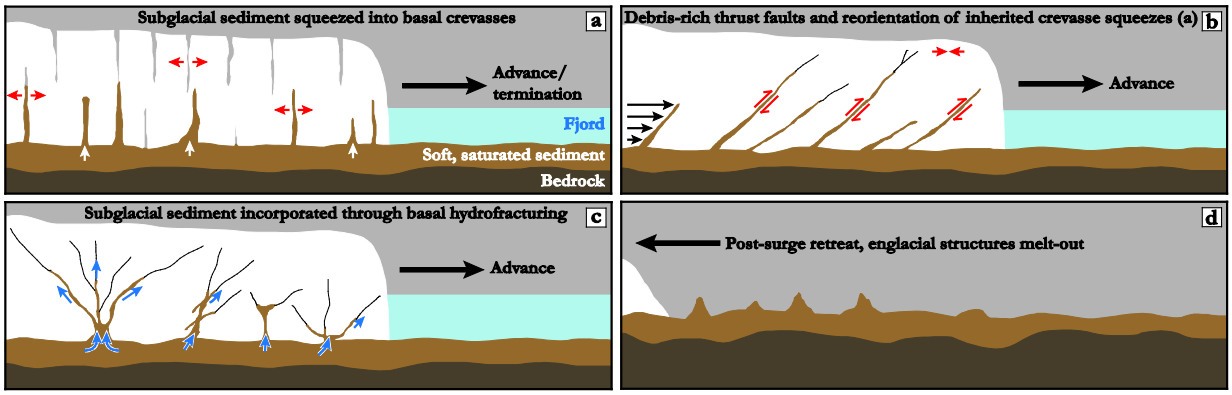

Figure 5.21 – Schematic diagram of types of englacial debris-rich structure formation. (a) Crevasse squeezes. (b) Thrust faults and reoriented crevasse squeezes which have subsequently undergone thrust style displacement (TSD) or strike-slip movement along the reoriented plane. (c) Hydrofracture squeezes. (d) Development of geometrical ridge network as englacial debris-rich structures melt-out during quiescence.

The second mechanism involves a combination of faulting and the reorientation and deformation of crevasse squeezes. Compressive stresses towards the margins of a surging glacier are likely to facilitate brittle fracture and the stacking of ice blocks on top of each other; it has been suggested that such processes can also elevate debris from the bed into englacial positions (Glasser *et al.*, 1998b). This interpretation has been criticised by a number of studies, which have focused on the excessive amount of total displacement required to elevate debris from basal positions through thrust faulting alone (Rea and Evans, 2011), and the common lack of evidence for such displacement in the form of a hanging wall extending an equal height above the debris-rich band. However, the time-lapse imagery of the Paulabreen surge in 2005 (Kristensen and Benn, 2012) clearly shows the stacking of ice blocks on top of each other and the subsequent collapse of the hanging wall section, suggesting that this may also have occurred at Tunabreen. It is also likely that initially vertical or sub-vertical crevasse squeezes incorporated during the active phase of a surge (Fig. 5.21a) may be tilted and reoriented during the subsequent return to quiescent phase flow conditions (Fig. 5.21b), producing inclined debris-rich bands (Fig. 5.14c). The reoriented crevasse squeeze would also provide a suitably oriented slip plane to facilitate further deformation during a return to the active phase of a surge (cf. Rea and Evans, 2011). A compressional stress regime, such as propagates downglacier at the surge front (cf. Murray *et al.*, 2003b), could result in thrust style displacement (TSD) along the favourable slip plane created by structure reorientation (Moore *et al.* 2010; Rea and Evans,

2011), attenuating the debris-rich band. In some places, thin debris laminae emanating from debris-rich bands were observed to be aligned sub-horizontally to the band surface (Fig. 5.9j), indicating possible oblique or transverse slip along the plane (cf. Fleming *et al.*, 2013). Structural measurements of similar englacial debris-rich bands at the lateral margin of Paulabreen, a tidewater surging glacier located 75 km south of Tunabreen, demonstrated that strike-slip motion was the dominant deformation style along the planar structures (Fleming and Lovell, in prep.). This raises the possibility that similar deformation was active at the SE sections, which are situated in an equivalent marginal position and experienced localised lateral ice flow during the 2003-2005 surge as surging ice splayed into a small embayment (cf. Fleming *et al.*, 2013). This combination of processes is suggested to be most likely for the formation of long and thin attenuated debris-rich bands at the SE sections (e.g. Figs 5.14a and 5.14d). Deformation along the reoriented planes, whether in the form of TSD or strike-slip, would represent a shear zone characterised by increased strain rates within the debris-rich structure and the surrounding englacial ice. It is likely this would result in strain-induced metamorphism within the englacial ice, expelling gas along ice crystal boundaries and forming dispersed facies ice (Hubbard and Sharp, 1995). This is inferred from the borders of clear dispersed facies ice and associated gradation of bubble structures observed surrounding many of the debris-rich bands (Figs 5.9c-g and 5.14f).

A third mechanism is necessary to explain debris-rich structures which cannot be satisfactorily explained as crevasse squeezes or reoriented and deformed crevasse squeezes, such as complex structures consisting of multiple thin and attenuated branches, often aligned in different directions, cutting across layering within the englacial ice, and emanating from a large area of debris at its base (e.g. Fig. 5.14b). This mechanism is suggested to be the injection of heavily saturated subglacial sediment into the ice through a process of basal hydrofracturing (Fig. 5.21c). During the active phase of a surge, high and sustained basal water pressures in combination with transitions between highly compressive and extensional stress regimes are ideal conditions for hydrofracturing of the glacier bed, particularly as basal water pressures approach overburden (cf. Rea and Evans, 2011). It is possible that the highly-pressurised saturated sediment exploits pre-existing weaknesses in the ice, such as the abundant healed and reoriented fractures within Tunabreen which are likely to have developed over multiple surge cycles. It is unclear whether this process could have acted almost instantaneously, or in an incremental manner as continuous injection of saturated sediments under high-pressure progressively forces pre-existing weaknesses apart in a wedge-like manner. Sediment-infilled hydrofracturing of glacier beds has also been described by Roberts *et al.* (2009) from Kuannersuit Glacier, a surge-type glacier in West Greenland. The main difference to examples provided by Roberts *et al*. (2009) is that they were composed primarily of water-sorted sediments such as sands and gravels, whereas the Tunabreen hydrofractures consist of solid stratified ice containing only occasional evidence for thin layers of sands and gravels (e.g. Fig.

5.6d; see also Fig. 9.27c and d in Benn and Evans, 2010). In addition, evidence for supercooling (e.g. crescentic layering, rosettes of ice crystals and vertical splinter ice; Roberts *et al.*, 2002) were also described by Roberts *et al.* (2009), but were not observed within the Tunabreen structures.

The SE sections, and in particular SE-A, contain evidence for intense post-formational folding and boudinage of the banded subfacies ice (e.g. Figs 5.6i, 5.6j and 5.14k-o). The dominant style of folding, recognised in the two-dimensional face as augen-like folds with concentric rings and double-vergence (e.g. Fig. 5.14o), is indicative of a form of non-cylindrical folding known as sheath folding (Alsop *et al.*, 2007; Fleming *et al.*, 2013). Sheath folds develop under non-coaxial stretching and simple shear in an extensional stress regime, as described in Fleming *et al.* (2013; Fig. 9). Similar to the NW section, there is clear evidence that folding has resulted in thickening of the banded subfacies layer, in this case forming repeated layers of intercalated banded and englacial ice (e.g. Figs 5.14i and 5.14l-o). Finally, debris laminae within both the banded and dispersed ice display a strong linear component as individual fine grains and clots have been smeared out and aligned (e.g. Fig. 5.9j). The orientations of these lineations as measured by Fleming *et al.* (2013) are parallel with sheath fold axes and AMS K1 measurements from the SE-A section, indicating that they are formed in the direction of extensional stretching and shear experienced by the ice at the lateral glacier margin. The evidence for compressive and extensional deformation observed at both NW and SE sections, in association with possible strike-slip and lateral movement at the glacier margin, is consistent with a transpressional glaciotectonic regime (cf. Fleming *et al.*, 2013). This will be discussed in further detail in *Chapter 9*.

5.6.3. Proglacial geometrical ridge networks

The similar scale, morphologies and spatial arrangement of the three populations of geometrical ridges (two terrestrial, one submarine; Figs 5.17a and 5.19b) suggests that they formed by a similar process or combination of processes. The link between geometrical ridge networks and basal debris incorporated into the ice during a surge has been made by a number of authors (Sharp, 1985a; Solheim and Pfirman, 1985; Bennett *et al.*, 1996; Boulton *et al.*, 1996; Glasser *et al.*, 1998b; Bennett *et al.*, 1999; Woodward *et al.*, 2002; Christoffersen *et al.*, 2005; Evans and Rea, 2005; Ottesen and Dowdeswell, 2006; Ottesen *et al.*, 2008). Similar to these studies, it is suggested that the Tunabreen-Von Postbreen ridges are melted-out englacial debris-rich bands and structures which are inferred to have formed by a number of mechanisms (outlined in *5.6.2.* and Fig. 5.21) during surges of Tunabreen and Von Postbreen. Support for this is provided by the following linkages between the englacial structures and geometrical ridges observed at the Tunabreen margin: firstly, the diamict within the Tunabreen terrestrial geometrical ridges is almost indistinguishable in character from the debris that comprises the majority of the stratified facies ice at the NW and SE sections (Figs 5.6b, 5.8 and 5.18i) and is therefore interpreted to be

the product of it melting out. The only difference between the two is the stratification within the ice facies compared to the massive diamict; however, since the ice facies stratification is controlled primarily by ice lenses, it is plausible that the melting of the lenses would produce a structureless diamict. In addition, the stratification in the solid stratified subfacies is not ubiquitous, particularly within debris-rich structures at the SE sections where the ice facies often appears massive (Fig. 5.6b).

Secondly, a number of thin, low ridges composed of diamict were observed to be actively melting out from debris-rich bands within the SE-A section in August 2011 (e.g. Fig. 5.14h). Although on a smaller scale than many of the mapped geometrical ridges, this demonstrates that the englacial debris-rich bands do melt out to form similar features. The difference in scales is likely to be controlled by the character of the individual debris-rich bands: the structure in Fig. 5.14h is a thin (<20 cm), gently-dipping attenuated band of debris, interpreted to the result of deformation along a reoriented debris squeeze structure (Woodward *et al.*, 2002; Rea and Evans, 2011), which would distribute sediment over a wide area when the ice is removed (Bennett *et al.*, 1999; Kirkbride and Deline, 2013) and so would be unlikely to form a significant ridge (e.g. Fig. 5.14h). By contrast, vertical or near-vertical englacial debris-rich structures, such as the features interpreted as crevasse squeezes shown in Fig. 5.14g, could produce ridges of greater height because the melted-out debris would only be distributed over a much smaller area once the lateral support of the ice was removed. This situation is also likely to be responsible for the formation of the distinct pinnacles on some ridges (Fig. 5.18c). In addition, some of the Von Postbreen ridges appear to emerge directly from the debris-covered glacier front (Fig. 5.15), providing a further indication that the geometric ridges are likely to be derived from englacial debris-rich bands.

The Tunabreen terrestrial ridges are located in an area which was not reached by the 2004 surge but are within the 1971 limit (Fig. 5.19a), indicating that they were exposed during the quiescent period between the two surges. The three groups of submarine ridges are suggested to have formed following the surges of 1930, 1971 and 2004 based on their respective locations within these limits (Fig. 5.19b). The Von Postbreen ridges are likely to have formed during the 1870 surge and have been exposed as the glacier retreated into a terrestrial position following this advance. This demonstrates that geometrical ridge networks can be associated with each of the four recorded tidewater surges in Tempelfjorden.

5.7. Summary

Tunabreen has undergone three surges since the 1930s, producing a remarkably consistent return period length of ~40 years. Calving retreat following the most recent surge of 2003-2005 has revealed exposures of debris-rich and clean ice at the NW and SE lateral margins of the tidewater front. These were identified as solid stratified; banded; solid; dispersed; and englacial facies/subfacies ice, and based on physical characteristics and stable isotope analysis data have

been interpreted as the result of freeze-on; regelation and freeze-on; freeze-on; strain-induced metamorphism; and meteoric processes, respectively. The SE sections are characterised by englacial debris-bands composed of subglacial sediment, which are interpreted to have formed as crevasse squeezes; reoriented and deformed squeeze structures inherited from previous surges; and hydrofracture squeezes. All sections display strong evidence for both ductile and brittle deformation in a lateral marginal position. The terrestrial and submarine glacier forelands of both Tunabreen and Von Postbreen contain geometrical ridge networks, which are inferred to be melted out englacial debris-rich bands and structures. Geometrical ridge networks can be associated with each of the three Tunabreen surges and with the 1870 surge of Von Postbreen. These observations and interpretations will be discussed in a wider context in *Chapter 9*.

Chapter Six
Finsterwalderbreen

77º 29.0' N, 15º 16.0' E

After Professor Sebastian Finsterwalder, b. 1862, German glaciologist.

The place names of Svalbard, Norsk Polarinstitutt

6. Finsterwalderbreen

6.1. Introduction

Push moraine complexes or composite ridge systems are found at the margins of a number of known surge-type glaciers in Svalbard and, as a result, have been suggested to be strongly linked to surging (cf. Croot, 1988). However, they are also found in association with glaciers where surges have not been observed and it has been argued that the formation of such push moraine complexes can be due to internal compression at the boundary between cold and warm ice in a polythermal glacier (Hambrey and Huddart, 1995; Huddart and Hambrey, 1996). The identification of multiple ridge-building events within individual composite ridge systems would provide support for their association with surges, as that would imply multiple glacier advances and cyclical behaviour, and could also provide important information on surge magnitude and frequency beyond the observational record. This hypothesis was investigated during fieldwork in summer 2012 at Finsterwalderbreen, a known surge-type glacier located on the southern shore of Van Keulenfjorden in the south of Spitsbergen (Fig. 3.2). This chapter begins by outlining the study area and surge history of Finsterwalderbreen (*6.2.*), before presenting geomorphological mapping of the proglacial area; this is subdivided into mapping of the push moraine complex (*6.3.1.*) and the inner glacier foreland (*6.3.2.*). Suggested interpretations of the landform assemblage are reported in *6.4.*

6.2. Study area and surge history

Finsterwalderbreen is ~11 km long and together with its main tributary, Revtannbreen, covers an area of ~35 km^2. The width of the main glacier trunk gradually decreases from ~4 km in the accumulation area to ~1 km at the lower tongue, which currently terminates as a gentle ramp ~3 km inland from the southern shore of Van Keulenfjorden (Fig. 6.1). Two smaller tributaries, Heimbreen and Leinbreen, are separated from Finsterwalderbreen by its eastern lateral moraine (Fig. 6.1). Radar data and borehole temperature measurements have demonstrated that the glacier is polythermal, with the majority of the bed at the pressure-melting point apart from the lower tongue where the ice thins to ~30 m (Ødegård *et al.*, 1996). Of the neighbouring glaciers, Hessbreen and Nathorstbreen (including its tributaries Dobrowolskibreen, Polakbreen and Zawadskibreen) are also known to have surged (Hambrey and Dowdeswell, 1997; Sund and Eiken, 2004; Ottesen *et al.*, 2008; Sund and Eiken, 2010; see *Chapter 4*), and Penckbreen has been suggested to be of surge-type based on its push moraine complex (Croot, 1988; Hart and Watts, 1997). The geology of the area immediately surrounding Finsterwalderbreen is diverse: the upper catchment and headwalls comprise Precambrian quartzites and schists of the Ariekammen and Gåshamna Formations, along with Permian-age carbonates and evaporitic and clastic sedimentary rocks of the Gipsdalen and Tempelfjorden Groups; the rest of the catchment is composed of Triassic to Cretaceous siltstones, sandstones and shales of the Sassendalen and Kapp Toscana Groups and Janusfjellet Subgroup (Dallmann *et al.*, 2002).

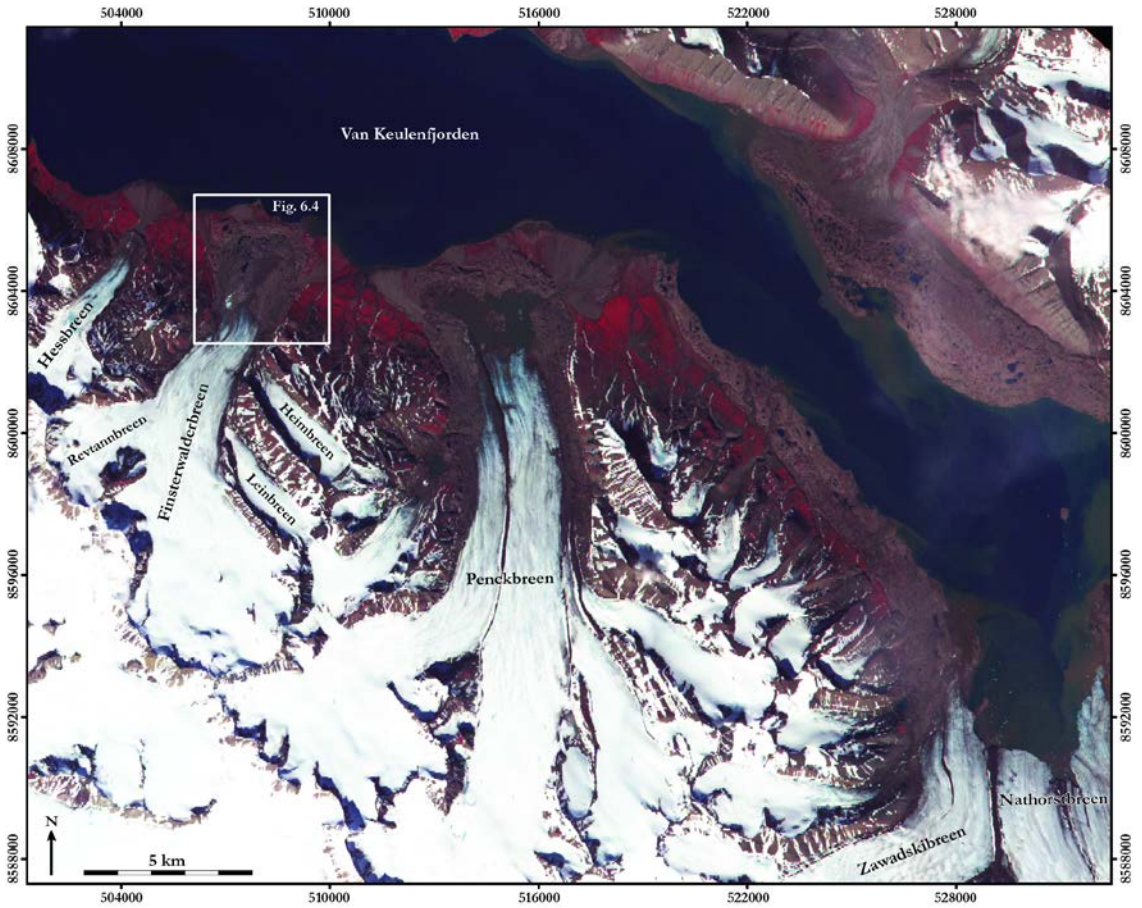

Figure 6.1 – Locations of Finsterwalderbreen and neighbouring glaciers on the southern shore of Van Keulenfjorden shown on 2005 ASTER image. White rectangle delimits area mapped in Fig. 6.3. See Fig. 3.2 for location in Svalbard.

The Finsterwalderbreen glacier foreland comprises an outer zone consisting of a large composite ridge system with multiple ridge crests and an inner zone of hummocky topography, outwash and numerous pools and channels; these zones will be described in detail in *6.3.* The map of Van Keulenfjorden in 1898 produced using photogrammetric techniques by Hamberg (1905) clearly shows Finsterwalderbreen terminating approximately 700 m upglacier from this composite ridge system (Fig. 6.2a). Further photogrammetric mapping conducted in 1920 showed that the glacier had advanced to a position immediately adjacent to the outer ridge system as a thicker and, in places, near-vertical ice front (Liestøl, 1969; Fig. 6.2b). From this, it was concluded that Finsterwalderbreen had surged sometime between 1898 and 1920. The timing of the surge was estimated to be ~1910-15 by Nuttall and Hodgkins (2005) based on the absence of open crevasses in the upper glacier on the 1920 photograph and crevasse healing rates reported from other Svalbard surging glaciers (Dowdeswell *et al.*, 1991). Fig. 6.2c shows the glacier front in 1936 when it was still adjacent to the composite ridge system. Further indication for the surge is provided by the impressive looped moraines at the terminus and the displaced flowlines further upglacier (Nuttall and Hodgkins, 2005); these displaced flowlines have since been transferred downglacier during quiescence and are currently melting out at the

snout (Fig. 6.2d). The current quiescent period has been characterised by strong thinning and retreat of the front to a position ~1.5 km further upglacier from the 1898 pre-surge position, and a gradual build-up of mass in the accumulation area (Liestøl, 1969; Nuttall *et al.*, 1997; Nuttall and Hodgkins, 2005). Like many Svalbard glaciers, Finsterwalderbreen has experienced consistently negative mass balance during this period, which may result in a lengthening of the quiescent phase (Nuttall *et al.*, 1997; Nuttall and Hodgkins, 2005). The glacier has also maintained an active and variable subglacial drainage system and a polythermal temperature regime, indicating that future surging is possible (Wadham *et al.*, 2001; Nuttall and Hodgkins, 2005; Hodgkins *et al.*, 2007).

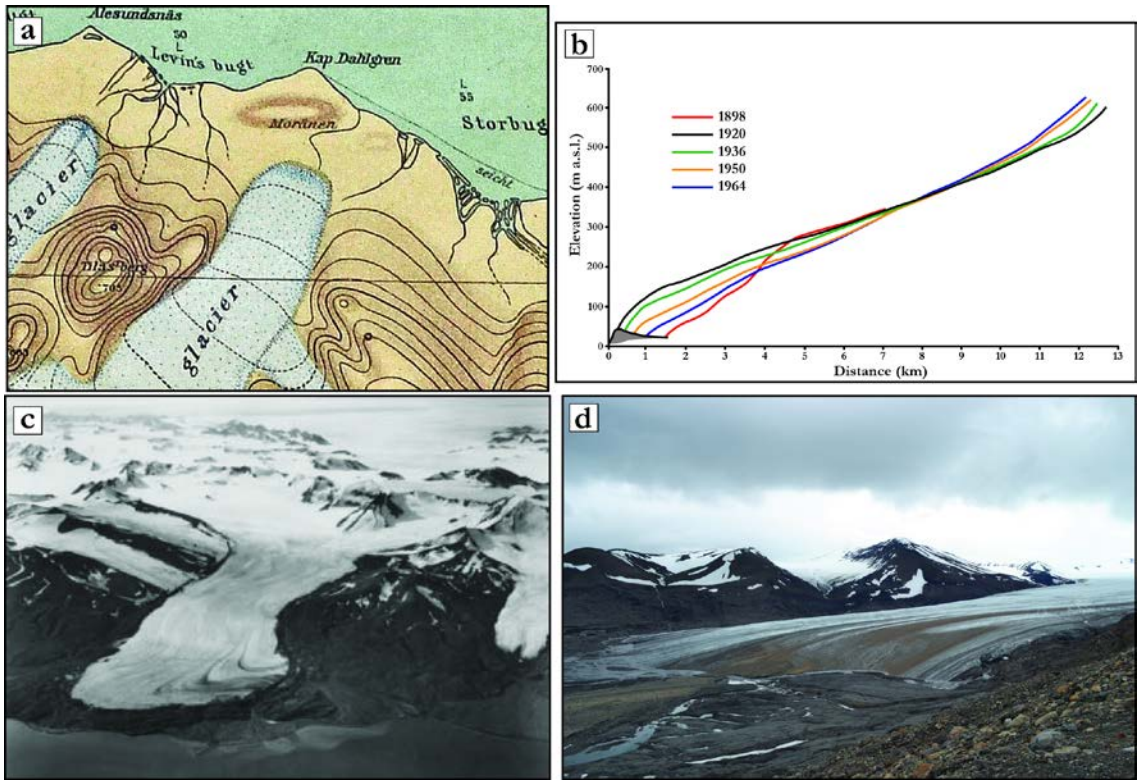

Figure 6.2 – (a) Map of Finsterwalderbreen terminus in 1898 (from Hamberg, 1905). Note clear separation between glacier front and moraine. (b) Finsterwalderbreen profile 1898 to 1964 (from Liestøl, 1969). (c) Photograph of Finsterwalderbreen in 1936 (© Norsk Polarinstitutt, photograph S36 3201; reproduced from Nuttall and Hodgkins, 2005). (d) Photograph of terminus in 2012. Note displaced flowlines/medial moraine melting out at front.

Based on lichenometry data and observed differences in individual ridge land surface consolidation and vegetation cover, it has been suggested that the Finsterwalderbreen composite ridge system records evidence for multiple glacier advances (Hart and Watts, 1997). Two zones were identified within the composite ridges: an inner zone exhibiting a very unconsolidated land surface and no lichen growth, attributed to the ~1910-15 surge, and an outer zone of multiple ridges displaying different lichen sizes and a well consolidated land surface. The internal composition of the ridges was reported to be predominantly coarse gravels with some thin silt beds. A detailed assessment was made of lichen sizes on the eastern side of the ridge system,

which showed that average lichen sizes decrease along an ice distal to proximal transect. This allowed Hart and Watts (1997) to divide the outer zone into three sub-zones, taken to represent push ridges formed by separate glacier advances, and in conjunction with the inner zone this was suggested to provide evidence for four surges recorded within the composite ridge system. Based on a curve generated from the lichen data (Werner, 1990) and the approximate age of the most-recent advance, Hart and Watts (1997) suggested a loose chronology for the older surges of (AD) 1800, 1696 and 1564, indicating an approximate return period of 115 years. However, a number of problems are apparent with this method, as acknowledged by Hart and Watts (1997): (1) each individual ridge-building advance may redeform and erode previously formed ridges, complicating the record. (2) Potential measurement errors associated with lichenometry are high and as a result the dataset may lack the sufficient resolution to differentiate between individual ridge-building advances. (3) The ridges were inferred to have formed thorough the deformation of pre-existing outwash surfaces, and therefore lichens may have developed on the outwash rather than following ridge formation. (4) There may also have been inputs of anomalously old material from supra- or extraglacial sources. Therefore, although Hart and Watts (1997) provide an indication that the Finsterwalderbreen composite ridge system may record multiple surges, further support from additional lines of evidence is required, particularly with respect to the exact number of ridge-building events. This chapter presents a geomorphological approach based on relationships between the composite ridge system and meltwater drainage routes.

6.3. Geomorphology

The glacier foreland can be divided into two zones: an outer zone consisting of the composite ridge system, and an inner zone of hummocky topography, outwash deposits and numerous pools (Figs 6.3 and 6.4). Several outwash fans also extend beyond the distal margins of the composite ridge system, documenting both contemporary and relict drainage into Van Keulenfjorden. The outer zone/composite ridge system is described in *6.3.1.* and the inner zone is described in *6.3.2.*

6.3.1. Composite ridge system (outer zone)

The outer zone is characterised by a latero-frontal composite ridge system covering an area of ~1.5 km^2 (Figs 6.3 and 6.4). The ridge system reaches heights of up to 50 m above the fjord and contains multiple individual ridge crests separated by linear depressions, typically ranging from ~1-10 m in depth (e.g. lower break-of-slope to ridge crest). These depressions are occasionally occupied by small pools, as seen in the northwest part of the system (Fig. 6.3d). The width of the outer zone in this area is ~700 m, but is typically 250-300 m across the entire ridge system. The number of individual ridge crests identifiable across the width of the outer zone ranges from 4-17 (Fig. 6.4). In several places, relict meltwater channels cut down through parts of the ridge system and feed outwash fans which extend to the fjord. These outwash fans separate the

composite ridge system from the fjord, apart from one ~500 m long section immediately to the west of the active meltwater channel where the ridge complex terminates at the beach (Fig. 6.4). Towards the glacier front, the composite ridge system grades into steep-sided lateral moraines which extend upglacier.

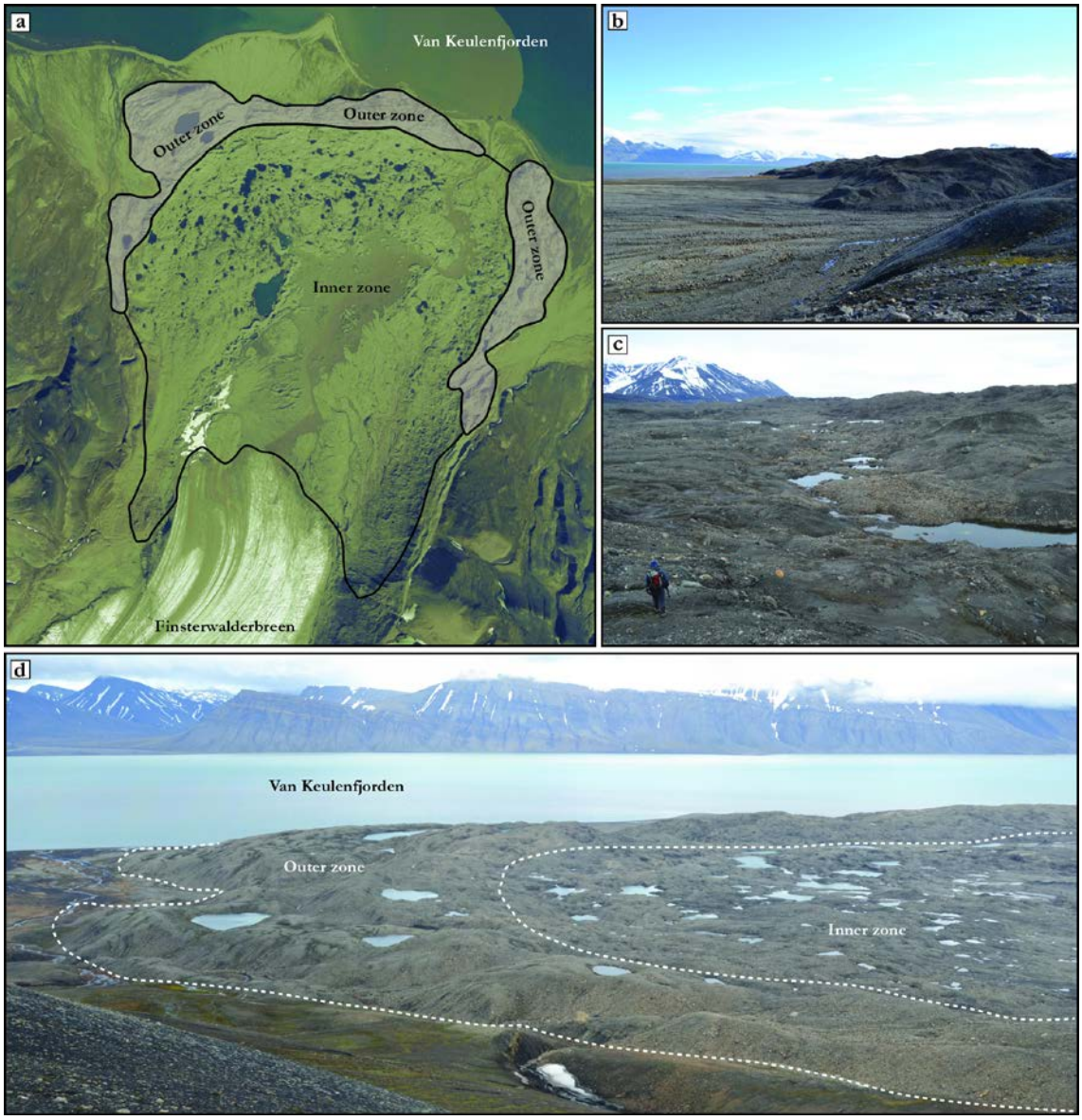

Figure 6.3 – Geomorphology of the Finsterwalderbreen foreland. (a) Aerial photograph of foreland in 2004 with outer (composite ridge system) and inner zones highlighted. Photograph provided by NEODC. (b) View of the northern part of the composite ridge system and outwash fans. (c) View of inner zone looking towards composite ridge system. Note hummocky topography and pools. (d) View across the northwestern part of the glacier foreland with boundary between outer (composite ridge system) and inner zones highlighted.

The morphology and surface sediment composition of the ridges varies across the width of the system. This will be described in greater detail below in *6.3.1.2.*, with a very brief overview included here. The outermost parts of the ridge system are typically gently sloping and rounded in morphology, with a predominant surface cover of sorted gravels and occasional large boulders. Moving towards the inner zone, the ridges become less rounded and areas of diamict

Figure 6.4 – Geomorphological map of Finsterwalderbreen foreland. See Fig. 6.1 for location of mapped area. Mapped from 2004 aerial photograph acquired from NEODC. A digital version of this map is included on the CD inside the back cover.

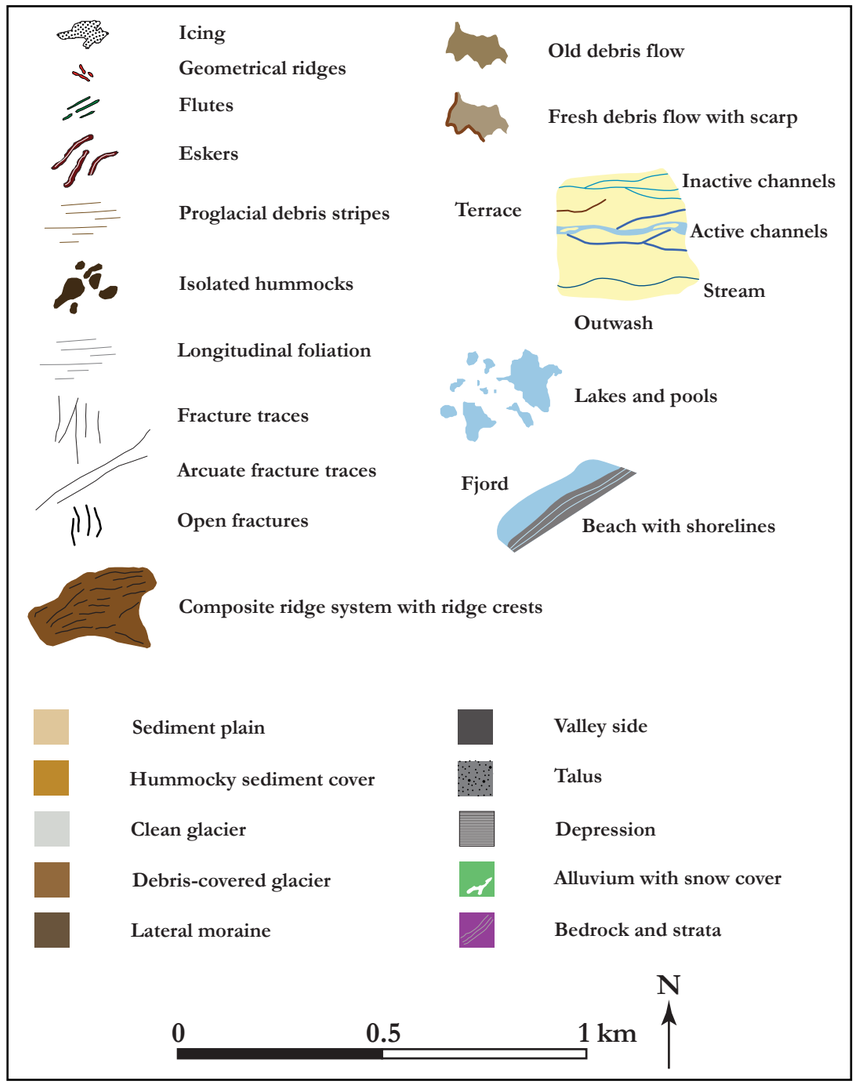

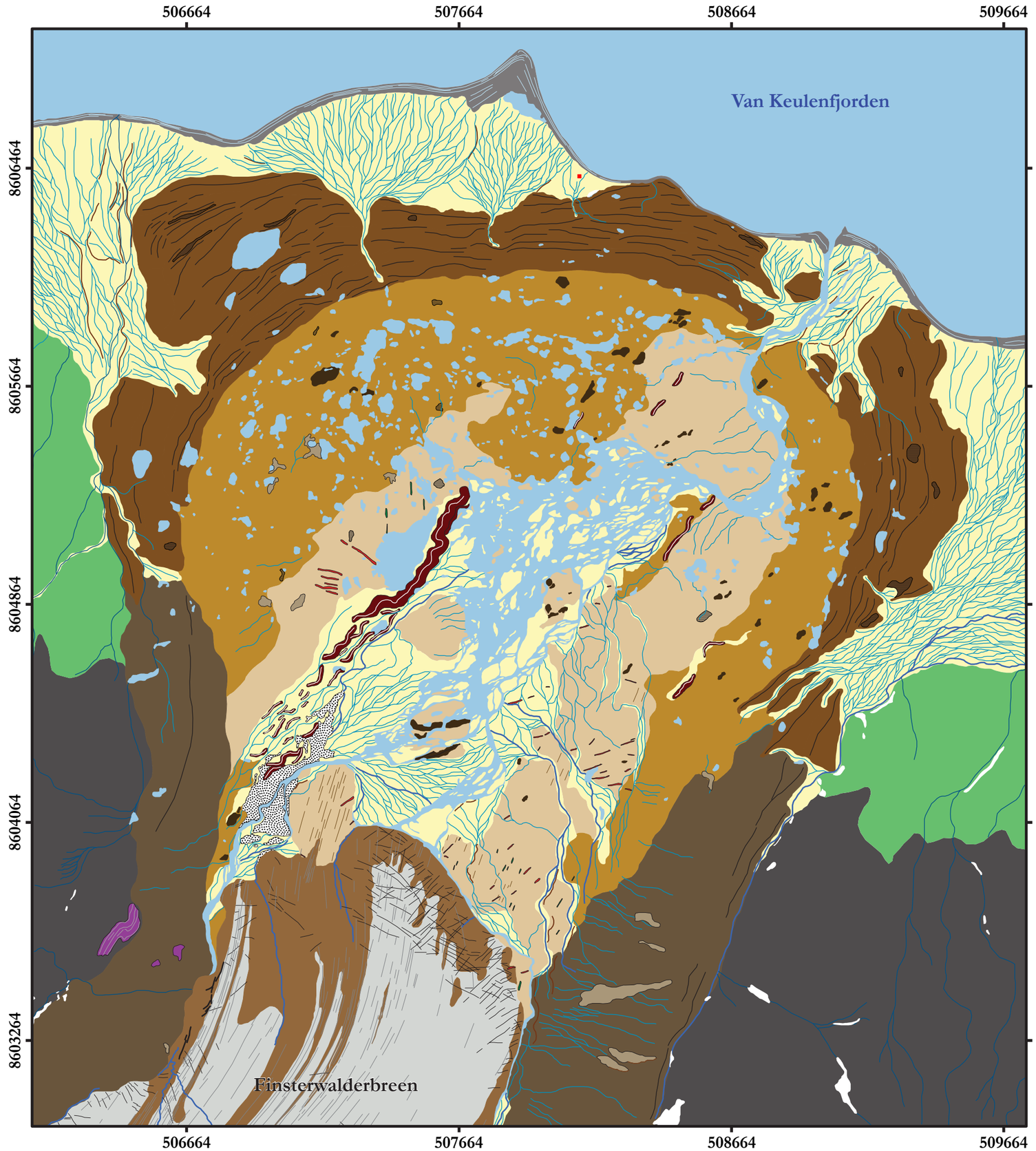

are more prevalent amongst the gravels and large boulders. The innermost part of the composite ridge system contains sharp-crested ridges composed of gravel, diamict, sand and mud, with frequent active debris flows and pools of various sizes. This area is characteristically similar to the inner zone of the glacier foreland described in detail in *6.3.2*.

6.3.1.1. Composite ridge system-meltwater drainage route relationships

At several places within the composite ridge system, a distinctive relationship between ridges and meltwater channels/outwash fans can be identified, providing an opportunity to determine the number of ridge-building events recorded within the system. This is based on the relatively simple observation that relict channels and associated outwash fans which breach outer parts of the ridge system have been blocked off by an inner ridge or ridges, demonstrating that the ridges within the composite ridge system cannot all have formed at the same time. In the context of push moraine formation, this geomorphic relationship can therefore be inferred to record separate ridge-building events and, thus, glacier advances. In addition to simply identifying more than one ridge-building event within the system, detailed assessment of this relationship may also provide an indication of the exact number of separate ridges, and thus a proxy for the number of glacier advances; this hypothesis is expanded upon below.

A number of relict outwash fans and inactive meltwater channels are evident both on aerial photographs and in the field (Figs 6.3b, 6.4 and 6.5). The inactive meltwater channels form narrow gorges through the ridge system and contain concentrations of coarse gravel and edge-rounded boulders, with no present day meltwater drainage routed along them (Fig. 6.5b). The channels feed several large relict outwash fans which extend beyond the distal margin of the composite ridge system (Figs 6.4 and 6.5); these fans are characterised by low gradient surfaces of coarse gravel and display varying degrees of vegetation cover (Figs 6.5e and 6.5f), suggesting a possible variation in length of inactivity. In almost all cases, the ice proximal extents of the inactive meltwater channels/outwash fans terminate within the composite ridge system, rather than continuing through to the inner zone of the foreland (Fig. 6.4). The only place where this is not the case is alongside the active meltwater drainage through the northeastern section of the ridge system. Within the ridge system, the fans/channels all terminate against a continuous ridge in an ice proximal position (Figs 6.5a-d), with the inner ridges effectively ‘blocking’ the meltwater routes. Clear examples of this are shown in Figures 6.5a and 6.5d, where the ice proximal edges or apexes of the relict outwash fans terminate abruptly against a large ridge. This is also typically associated with evidence for material avalanching off the front of the blocking ridge, burying or infilling the fan/channel apexes (Fig. 6.5c). This distinct geomorphic relationship, termed buried fan apexes (BFA), can be identified in ten separate locations across the composite ridge system (Fig. 6.6).


a
Breached ridge
Blocking ridge/ridges
Outwash fan
b
Outwash fan
Breached ridges
Breached ridges
Blocking ridge
Meltwater channel
c
Breached ridge i
Breached ridge ii
Avalanching
Meltwater channel
Blocking ridge
Breached ridge ii
d
Blocking ridge
Breached ridge
Breached ridge
Outwash fan
e
f

Figure 6.5

Figure 6.5 (preceding page) – Details of composite ridge system-meltwater drainage route relationships (termed buried fan apexes; BFA). Solid lines delimit front of blocking ridges, dashed lines delimit meltwater channel/outwash fans, dotted lines show direction of drainage. (a) Outwash fan blocked by an inner ridge on western side of composite ridge system (BFA 1 on Fig. 6.6). Lovell and Lukas circled for scale. Photo by Doug Benn. (b) Meltwater channel breaches outer ridges but is blocked by innermost ridge on northern side of ridge system (BFA 3 on Fig. 6.6). (c) Meltwater channel breaching two outer ridges but blocked by an inner ridge on northern side of ridge system (BFA 4 on Fig. 6.6). (d) Outwash fan breaching an outer ridge but blocked by an inner ridge on eastern side of ridge system (BFA 7 on Fig. 6.6). (e) Relict outwash fan emanating from BFA 3 on northern side of ridge system. (f) Relict outwash fan emanating from BFA 4 on northern side of ridge system. Note difference in vegetation cover between (e) and (f).

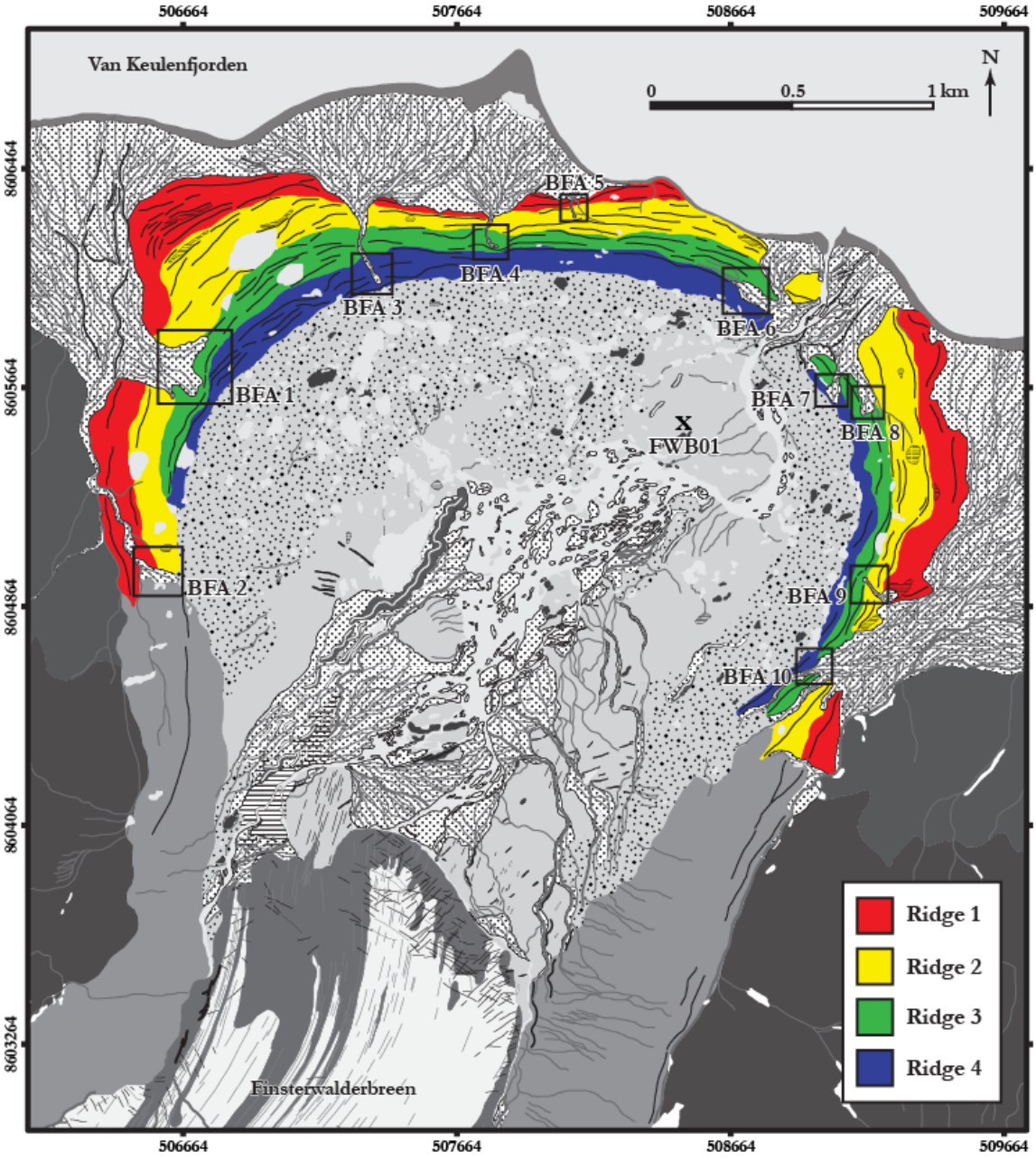

Figure 6.6 – Buried fan apex (BFA) locations and four identified separate ridges within the composite ridge system.

In all cases, outwash fans/meltwater channels with BFA breach outer parts of the ridge system but are blocked by an inner ridge. However, BFA are not all blocked by the same individual ridge or part of the ridge system; this provides an important way to assess the number of separate ridges within the ridge system and, therefore, the number of ridge-building events recorded within the complex. The explanation for this is as follows: across the outer zone, outwash fans/meltwater channels extend into the ridge system varying distances (Fig. 6.4). In all cases, the fans/channels breach parts of the ridges, cutting through ridge crests, and are blocked by an inner ridge, where the ridge crests are complete or continuous immediately adjacent to the BFA (Fig. 6.6). If the ridge crests associated with individual BFA are traced laterally across the ridge system, however, it becomes clear that the same ridge or set of ridges responsible for a BFA in one location have been breached by a fan/channel in another part of the ridge system. This demonstrates that the ridges cannot all be associated with the same ridge-building event. For example, if the semi-continuous ridge crests which block BFA 1 (Fig. 6.6) are traced in a north-easterly direction, they are clearly breached by the meltwater channel emanating from BFA 3; therefore, the ridge that blocks BFA 1 is not the same ridge that blocks BFA 3, indicating at least two separate ridge-building events. If this logic is applied across the composite ridge system by tracing the relationships between the ten BFA and ridge crests, four separate zones can be identified, equating to four separate ridge-building events (Fig. 6.6 and Table 6.1). These zones are termed ridges 1-4 and each can contain multiple ridge crests.

Table 6.1 – Buried fan apex (BFA)/composite ridge system relationships. See Fig. 6.6 for locations of BFA.

Buried fan apex	Breaches	Blocked by
BFA 1	Ridges 1 and 2	Ridge 3
BFA 2	Ridge 1	Ridge 2
BFA 3	Ridges 1 , 2 and 3	Ridge 4
BFA 4	Ridges 1 and 2	Ridge 3
BFA 5	Ridge 1	Ridge 2
BFA 6	Ridges 1 and 2	Ridge 3
BFA 7	Ridges 1, 2 and 3	Ridge 4
BFA 8	Ridges 1 and 2	Ridge 3
BFA 9	Ridges 1 and 2	Ridge 3
BFA 10	Ridges 1, 2 and 3	Ridge 4

6.3.1.2. Ridge character and relative age indicators

Changes in ridge characteristics were assessed qualitatively across the entire ridge system in order to identify if there were significant differences between the four zones classified using the ridge-meltwater drainage approach outlined above. This assessment was conducted according to

observations of the following, outlined in Table 6.2: (i) ridge morphology, focusing on ridge shape, relative height (e.g. lower break-of-slope to ridge crest), evidence for slope failure and presence of pools; (ii) characteristics of the sediments exposed on the surface of ridges; (iii) extent and type of vegetation and soil cover, including abundant plant species; and (iv) the range of lithologies that have been subject to frost-shattering, as different lithologies respond very differently to the same conditions depending on properties such as joint spacing (Jade and Sitharam, 2003), hardness (Augustinus, 1991) and anisotropy (Hall, 1987). These characteristics provide an indication of the relative age of the ridges based on the following basic principles: stable ridges with rounded morphologies, well-developed vegetation cover and evidence for a large range of frost-shattered lithologies are assumed to be older and to have formed earlier than sharp-crested, unstable ridges with little or no vegetation cover and only a very limited range of frost-shattered lithologies (e.g. easily-erodible shales). The lichenometry data collected by Hart and Watts (1997) are included, which also suggested four different ages for the ridges within the Finsterwalderbreen complex. These authors measured short axis lengths of *rhizocarpon* lichens across the eastern part of the ridge system; the mean values for each ridge are reported here.

Table 6.2 – Composite ridge system relative age indicators. [1]From Hart and Watts (1997). Lichenometry data is for *rhizocarpon*.

Ridge	Morphology	Sediment characteristics	Vegetation cover and lichenometry data[1]	Frost-shattered lithologies
Ridge 1	Rounded ridge crests; 3-8 m relative height; small solifluction lobes on surface; isolated small drained or infilled former pools between ridge crests.	Sorted rounded gravels; occas-sional large (>0.5 m diameter) boulders; small-scale polygons and stripes on surface (periglacial sorting).	Large areas of complete cover; isolated plants; patchy humic and mineral soils (~2 cm-thick) focused in depressions; *Silene acaulis, Dryas Octopetala, Oxyria digyna.* Mean lichen short axis = 49 mm[1].	Shale, sandstone, limestone, quartzite, schist.
Ridge 2	Rounded ridge crests; 5-10 m relative height; small solifluction lobes on surface; some slope failure evidence (de-icing scars); large pools between ridges.	Sorted rounded gravels and some diamict; frequent large (>50 cm diameter) boulders; accumulations of larger (20-30 cm) clasts; some small-scale periglacial sorting phenomena.	Patchy cover; patchy, thin (~0.5 cm-thick) soils; *Silene acaulis, Dryas Octopetala.* Mean lichen short axis = 31 mm[1].	Shale, sandstone, limestone, quartzite.
Ridge 3	Sharp-crested ridges; frequent evidence for slope failure (de-icing scars); large pools between ridges.	Coarse gravels, sand and diamict; frequent large boulders; weak periglacial sorting phenomena.	No complete areas; few isolated plants; patchy, thin (~0.5 cm-thick) soils; *Silene acaulis, Oxyria digyna.* Mean lichen short axis = 25 mm[1].	Shale, sandstone, limestone.
Ridge 4	Sharp-crested ridges; up to 15 m relative height; slope failure and debris flows abundant (de-icing scars); buried ice observed; frequent and abundant pools of all sizes.	Poorly-sorted gravels, sand, mud and diamict; frequent large boulders.	Very rare isolated plants; no soils. No lichens[1].	Shale, occasional sandstone.

Ridge 1

The outermost parts of the composite ridge system are characterised by rounded, gently-sloping ridges (Fig. 6.7a) with individual ridge heights ranging between 3-8 m. The ridge surfaces are

composed of sorted rounded gravels (Fig. 6.7b) with only very occasional larger boulders (Fig 6.7c). Small solifluction lobes and some small-scale surface sorting patterns in the form of polygons and stripes are observed in places. Large parts of ridge 1 are vegetated, particularly in hollows or depressions between ridges, with *Silene acaulis* (moss campian) and *Dryas octpetala* (mountain avens) most abundant. Patchy humic and mineral soils are observed, with a maximum thickness of ~2 cm. The hollows also show evidence for former pools (Fig. 6.7a), which generally appeared to have either drained along the linear depressions between ridges or been infilled. Frost-shattered shale, sandstone, limestone, quartzite and schist clasts are apparent. On the eastern part of the ridge system, Hart and Watts (1997) recorded a mean (short axis) lichen size of 49 mm from the area corresponding to ridge 1 in this study.

Ridge 2

This zone of the ridge system shares many characteristics with ridge 1, but with a few important differences. The ridges are rounded and gently sloping (Figs 6.7c and 6.7d) and there is patchy vegetation and soil cover, particularly in flat-topped areas and within hollows (Fig. 6.7d). One important distinction from ridge 1 is the surface sediment composition: there is an abundance of larger, less rounded clasts and large (>0.5 m diameter) boulders are frequently observed, demonstrating that the material is more poorly-sorted (Fig. 6.7c). Small solifluction lobes and small-scale sorting phenomena are also present within ridge 2. Large pools can be seen within this zone of the ridge system (Fig. 6.7d) and in places there is also evidence for slope instabilities in the form of small tension cracks. Apart from schist, the same lithologies as on ridge 1 had experienced frost-shattering. Mean lichen sizes of 31 mm were recorded by Hart and Watts (1997) from this area of the ridge system.

Ridge 3

Sharp-crested ridges with steep slopes are abundant in the areas associated with ridge 3, often displaying evidence for slope failures and tension cracks (Figs 6.7 e and 6.7f). The surface sediment composition includes coarse gravels, sands and poorly-sorted diamict with a fine-grained matrix, all of which are also exposed within ridges where slope failures have occurred (Fig. 6.7f). Sediment sorting patterns are infrequent and very weakly defined. Vegetation is characterised by a few isolated plants and small patches of *Silene acaulis* and *Oxyria digyna* (mountain sorrel); there are no areas of complete cover. Soil cover is patchy and, where observed, limited in thickness to ~0.5 cm. Only shale, sandstone and limestone clasts were observed to be frost-shattered; schist and quartzite clasts were intact. A mean lichen size of 25 mm was reported by Hart and Watts (1997).

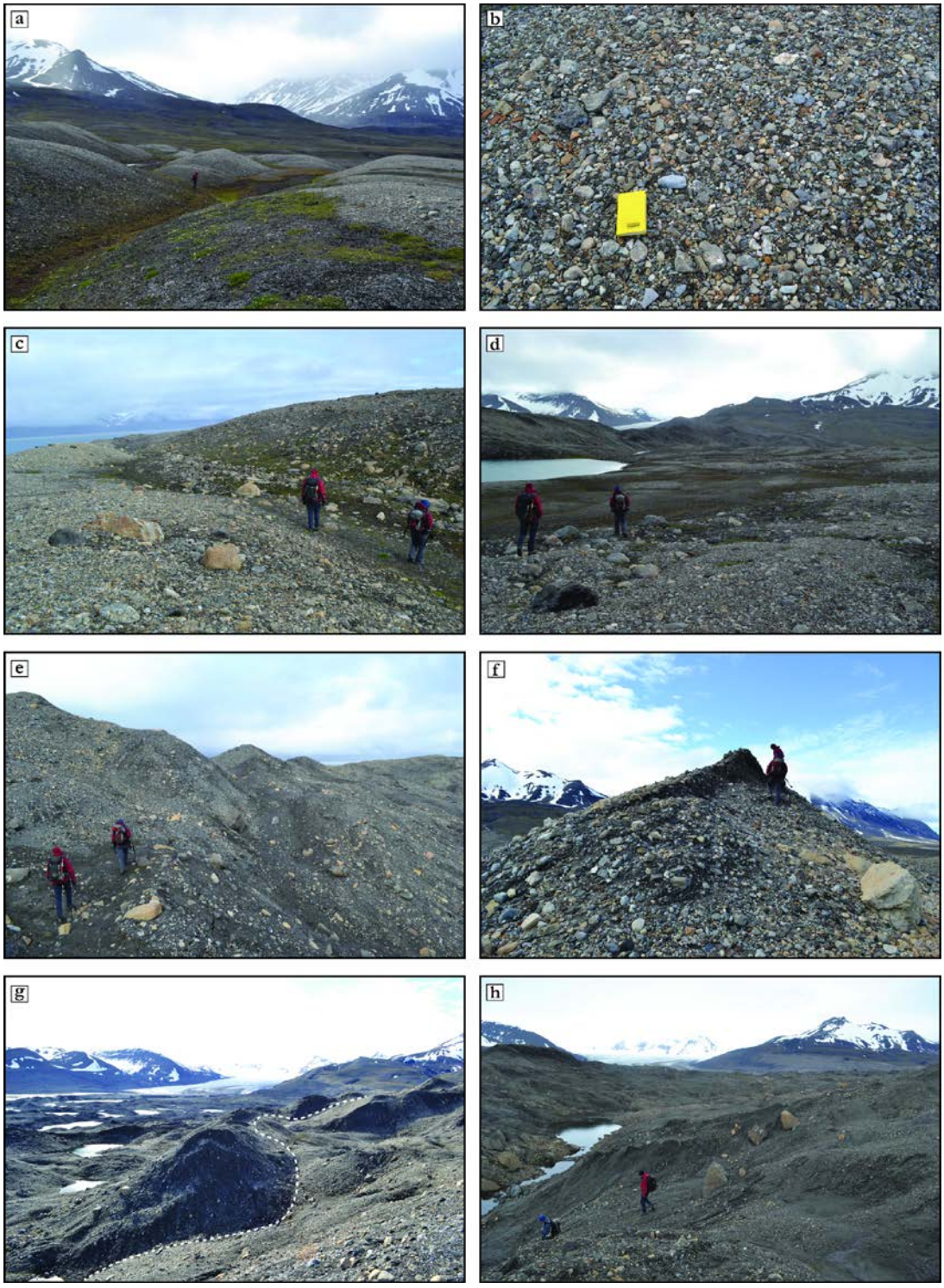

Figure 6.7 – Characteristics of the composite ridge system. (a) Ridge 1 on northwestern side of system. Note rounded morphology, sorted gravels, vegetation cover and infilled pool between ridges. (b) Sorted gravels on surface of ridge 1. (c) Boundary between ridge 1 (left) and ridge 2 (right) on northwestern side of system. Note abundance of larger clasts on ridge 2 and vegetation cover in hollow between ridges. (d) View from ridge 2 towards ridge 3 (ridge beyond large pool) on northwestern side of system. (e) Ice proximal slope of ridge 3. Note sharper ridge crests, tension cracks and poorly-sorted material. (f) Sharp-crested ridge 3. Note slope failure on ice distal (right-hand) side. (g) Boundary between ridge 4 (right) and ridge 3 (left) delimited by dashed line. Note sharp-crested unstable ridges and abundant pools associated with ridge 4 and the inner zone beyond. (h) Ice proximal slope of ridge 4 and inner zone of the glacier foreland. Note slope failures, debris flows and poorly-sorted material.

Ridge 4

This innermost part of the ridge system consists of sharp-crested, steep-sided and very poorly-consolidated ridges with an abundance of slope failures, tension cracks and debris flows evident (Figs 6.7g and 6.7h). These ridges are emplaced upon the ice proximal side of ridge 3 (Fig. 6.7g) and typically display a gradual transition to the inner zone of the glacier foreland (Fig. 6.7h), which is characteristically very similar. The ridges are predominantly composed of a mix of poorly-sorted fine-grained diamict, sand and gravel, with frequent large boulders. Small pools are abundant within this area and across the inner zone (Figs 6.4 and 6.7g) and shell fragments were also observed. Vegetation is restricted to rare, isolated plants and no soil development was observed. Shale and occasional sandstone clasts are the only lithologies observed to be frost-shattered; where seen, limestone, schist and quartzite clasts were intact. No lichens associated with ridge 4 were recorded by Hart and Watts (1997).

6.3.2. Glacier foreland (inner zone)

The inner zone of the glacier foreland describes the area between the glacier front and the composite ridge system (outer zone) and covers approximately 4.5 km^2 (Figs 6.3a and 6.4). As noted above, this zone shares many characteristics with ridge 4, which effectively forms the distal margin. The centre is dominated by a lagoon-like area which is fed by meltwater from all parts of the inner zone (Cooper *et al.*, 2011) and by the two main channels which follow the lateral margins of Finsterwalderbreen (Figs 6.8a and 6.8b). Here, the meltwater coalesces into a single channel and drains through the northeastern part of the composite ridge system to Van Keulenfjorden (Fig. 6.4). Outwash deposits are closely associated with the meltwater and form two large fans close to the glacier front. Proglacial icings are located on the western side of this outwash, adjacent to the meltwater channel in this area (Figs 6.4 and 6.8a). From this location, an esker system comprised of approximately 20 individual sinuous ridges extends in a northeastwards direction for ~1 km (Figs 6.4 and 6.8a). The largest of the individual eskers is ~0.5 km long and is ice-cored (Fig. 6.8c).

Large parts of the inner zone are characterised by hummocky topography and abundant small pools, particularly in the areas adjacent to the composite ridge system (Figs 6.3c, 6.3d, 6.4 and 6.8d). Small debris flows and tension cracks are common. The sediment composition of these areas, and the flatter areas mapped as sediment plains (Fig. 6.4), was observed to be a mixture of poorly-sorted diamict with large boulders, gravels and sand. Figure 6.9 shows an example of this from a small exposure within a hummock in a flat-topped part of the foreland. Here, an area of predominantly fine sand is overlain by poorly-sorted diamict (Fig. 6.8e). The fine sand is cross-cut by several thin layers of clay forming an interconnected network (Fig. 6.8f), giving the sand a breccia-like appearance. The diamict also extends down into the underlying sand in a dyke-like form. At other sites in this area, such as in the side of the pool shown in Figure 6.8d, diamict caps massive, undeformed sand, and there are several small

ridges of sand and gravel which have been mapped as esker fragments (Fig. 6.4). In addition to eskers, several small flutes and geometrical ridges are located on the foreland. The geometrical ridges are short (<50 m) and thin (<2 m) linear features which are aligned perpendicular or sub-perpendicular to ice flow direction; flutes are similar in size and morphology but are aligned in the direction of ice flow.

6.4. Interpretation

6.4.1. Push moraines and the breach-block process

The morphology and sediment composition of the composite ridge system is consistent with a push moraine complex formed by rapid glacier advance into proglacial sediments during surges, as previously interpreted by Croot (1988) and Hart and Watts (1997), and the relationships between ridges and meltwater drainage routes outlined in *6.3.1.1.* demonstrates that four separate advances/surges were responsible for its formation. This latter relationship is termed the 'breach-block process' and is outlined below and summarised conceptually in Figure 6.10.

The outermost part of the push moraine system is inferred to have formed by rapid glacier advance into proglacial sediments (Fig. 6.10a); this ridge corresponds to ridge 1 at Finsterwalderbreen. The predominance of sorted gravels within ridge 1 suggests that the glacier surged into mainly outwash deposits which had built-up at the margin pre-advance (Hart and Watts, 1997). Glacier advance into proglacial sediments can form ridges through the bulldozing of material at the margin and/or the folding, thrusting and stacking of material as glaciotectonic stresses are transmitted in front of the advancing margin (Boulton *et al.*, 1999; Bennett, 2001). The latter can form multi-crested ridge systems during just one advance through the development of folds (ranging from open and concentric to tight and recumbent) and imbricate thrust nappes (Hart and Watts, 1997; Boulton *et al.*, 1999). Furthermore, it has been argued that composite ridge systems can also form through the englacial thrusting/stacking of slabs of basal sediment, and therefore do not necessarily require a glacier advance into proglacial sediments for their formation (Hambrey and Huddart, 1995; Huddart and Hambrey, 1996). The internal structure of composite ridges can provide important information that can help to assess which of these formation mechanisms is valid, but suitable exposures were not found during this investigation. However, the limited evidence available suggests that a combination of bulldozing and folding, thrusting and stacking of sediments in front of an advancing margin was most likely responsible. This is based on sediment exposures recorded by Hart and Watts (1997) within the eastern part of the system, which consisted of gravel and lacked large-scale deformation structures but was suggested to have been subjected to some folding and faulting. In addition, in some parts of the moraine system possible thrust slabs are apparent (Fig. 6.7f). There is also clear evidence that Finsterwalderbreen advanced during the early part of the 20th century (Liestøl, 1969; Nuttall and Hodgkins, 2005). All of this is consistent with a proglacial glaciotectonic origin for the composite ridge system, although further sedimentological

investigation is necessary to elucidate the exact combination of mechanisms that were responsible.

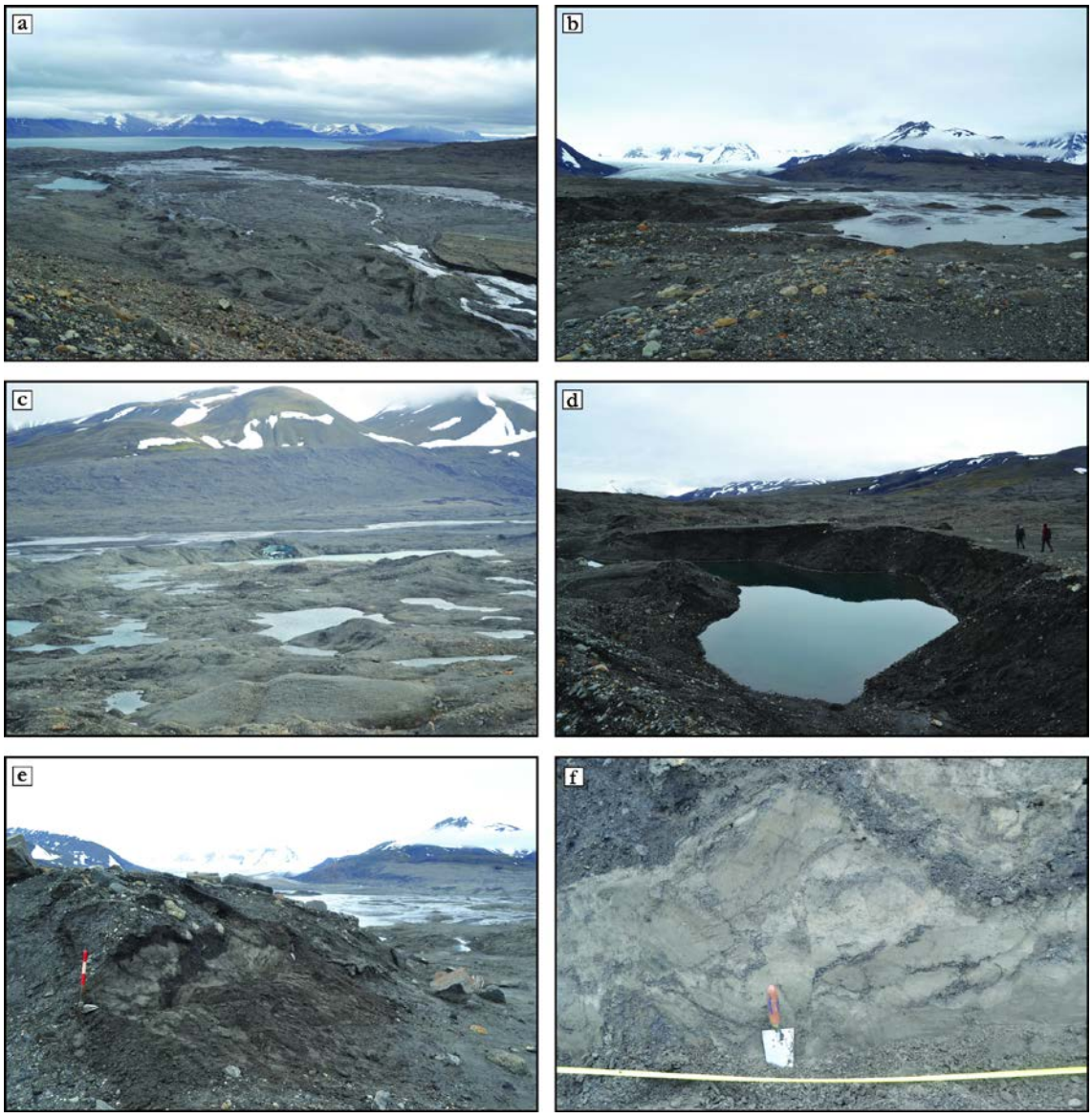

Figure 6.8 – Details of glacier foreland (inner zone). (a) View northeastwards across inner zone from western lateral moraine. Note esker system, proglacial icing and meltwater lagoon. (b) Meltwater lagoon looking towards glacier. (c) View of inner zone from northwestern part of the composite ridge system. Note ice core exposed in centre of esker, hummocky topography and abundant pools. (d) Meltwater pool in inner zone. (e) Section FWB01 (see Fig. 6.9) within inner zone, looking towards the glacier. See Fig. 6.6 for location. (f) Detail of section FWB01. Note thin layers of clay within area of fine sand and overlying diamict (top-left of image).

Once the outer push ridge had formed, meltwater from the glacier kept a breach open within it, which continued to be occupied as the glacier retreated from its previous maximum position during quiescence (Fig. 6.10b). A subsequent surge to almost the same maximum position formed a second push ridge on the proximal side of the first by similar bulldozing of the foreland (Fig. 6.10c). This ridge formed a barrier across the meltwater breach through the outer ridge, blocking the drainage route and making it inactive, and the meltwater from the

glacier was forced to find an alternative route through another part of the moraine system. It is possible that multiple meltwater breaches through different parts of the system occurred at the same time but this is simplified for the purposes of Figure 6.10. The sediment composition of ridge 2 includes larger, less rounded clasts, a number of boulders and was not as well-sorted as ridge 1; this is consistent with the glacier re-advancing into a mixture of proglacial sediments, which could include outwash deposits, lake deposits and glacially-transported material left behind by the glacier as it retreated from its ridge 1 position (Fig. 6.10b). During quiescence following the second surge, the glacier retreated and meltwater continued to occupy the new breach (Fig. 6.10d). Outwash, lake and glacial deposits accumulated on the foreland and provided the deformable proglacial sediments for a push ridge formed during a third surge; this ridge also formed a barrier to the meltwater drainage, forcing it to find a new route through the moraine system and making the second breach inactive. At Finsterwalderbreen, this process was repeated a further time to form a total of four separate zones within the push moraine. The inner ridges (3 and 4) are comprised of poorly-sorted material, with much higher diamict content than the outer ridges. This is consistent with the later surges deforming predominantly glacially-transported material deposited during previous quiescent periods. The present-day configuration of the Finsterwalderbreen foreland mapped in Figure 6.4 records a situation similar to that in Figure 6.10b, e.g. during the quiescent period following a ridge-building surge. If a subsequent surge to a similar position were to occur, the sediments in the inner zone would provide the material for a fifth push ridge.

Similar relationships between outwash channels and moraine systems have been described at glaciers in southeast Iceland (e.g. Evans and Twigg, 2002; Marren, 2004; Marren and Toomath, 2014). These studies of the forelands of Breiðamerkurjökull (Evans and Twigg, 2002) and Skaftafellsjökull (Marren and Toomath, 2014) identified that proglacial outwash can be topographically constrained between moraine belts, or between moraines and the ice margin, creating channels which flow parallel to the glacier front. As at Finsterwalderbreen, once these channels break through the moraine belt, they switch from narrow, confined corridors to unconfined fans (Fig. 6.10). The key observation from Finsterwalderbreen is that the confined parts of the system are often blocked or truncated by an inner moraine ridge, making the channel inactive and providing evidence for multiple ridge-building events, as described above. Similar examples of this are apparent at Breiðamerkurjökull, where in several places moraine belts truncate the ice-proximal parts of inactive outwash corridors, indicating that the formation of push moraines during small surges or periods of ice-margin stability during active retreat has blocked drainage routes (Evans and Twigg, 2002). The main difference between the Finsterwalderbreen and Breiðamerkurjökull examples, however, is that at Finsterwalderbreen this relationship provides a way to identify multiple advances within the composite ridge system, which could also have formed during one event (e.g. Boulton *et al.*, 1999). At Breiðamerkurjökull, the moraine systems are typically discrete belts separated by fluted terrain

(Evans and Twigg, 2002), and therefore the fact that they were formed by separate events is not in question. Finally, the temperate thermal regime of Breiðamerkurjökull means that the moraine belts can form on a far more regular basis (e.g. annually) than at Finsterwalderbreen, where the formation of significant push ridges can only be explained by periodic advances into the foreland, such as during surges.

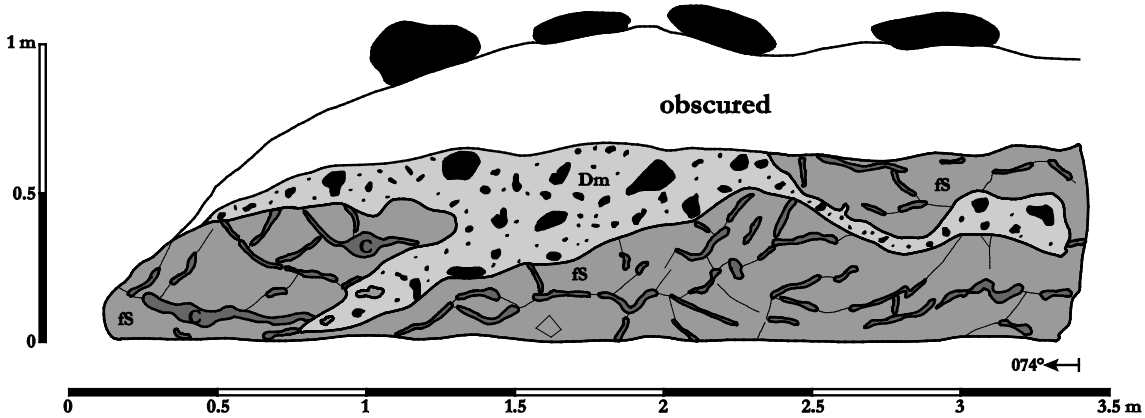

Figure 6.9 – Log of section FWB01. Dm = diamict; fS = fine sand; C = clay. See Fig. 6.6 for location, and Figs 6.8e and 6.8f for photographs.

6.4.2. Ice stagnation terrain

The inner zone predominantly represents the de-icing foreland associated with margin retreat and stagnation during the quiescent phase following the most-recent surge of Finsterwalderbreen. The hummocky terrain is inferred to be the result of differential melting of buried ice and debris reworking due to continuous topographic reversal, producing irregularly shaped hummocks and mounds (Evans *et al.*, 2014). The numerous isolated small pools within this area (Fig. 6.8d) represent kettle lakes and provide a clear sign of active de-icing. Reworked material takes the form of debris flows, indicative of the saturation and mobilisation of sediments as buried ice melts; a number of these are also found within the steep ice-cored lateral moraines that flank the glacier (Fig. 6.4).

In addition to ice stagnation, evidence for inferred glacier overriding of frozen proglacial sediments is also observed within the inner zone. An example of this is section FWB01 (Fig. 6.9), where an area of fine sand is capped by diamict. The fine sand is interpreted as sediment originally deposited within a pool which has been overridden whilst frozen, causing brittle fractures and forming the breccia-like arrangement. The inferred frozen nature of the sediment suggests the fractures are likely to be related to either (i) sub-marginal brittle deformation beneath cold ice at the glacier front (Waller *et al.*, 2012); and/or (ii) overriding of frozen sediments in winter or spring. The thin clay layers which delimit the margins of individual blocks within the breccia are suggested to be related to injections of pressurised muddy water originating either from meltwater at the glacier bed or possibly from a groundwater source (Waller *et al.*, 2012); this may reflect the passage from cold-based marginal

ice to warm-based surging ice as the glacier advances over the deformed area, or could perhaps result from progressive strain-induced warming and thawing of the ground as the glacier advances over it (Etzelmüller and Hagen, 2005). In either case, initial overriding is likely to have occurred in winter/spring. Similar evidence for inferred brittle deformation of frozen proglacial sediments by overriding ice has been described by Astakhov *et al.* (1996), Bennett *et al*. (2003) and Murton *et al.* (2005).

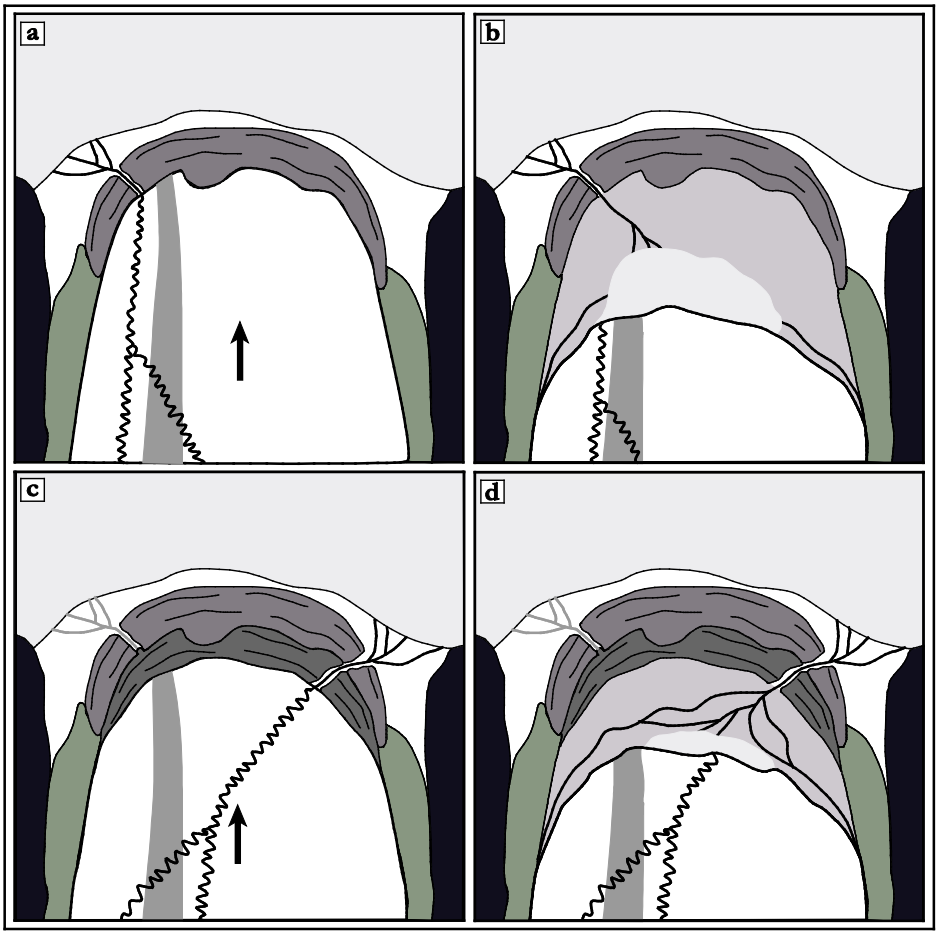

Figure 6.10 – Conceptual diagram of the breach-block process and the identification of multiple ridge-building events within push moraine complexes. See text for a full description.

The central part of the inner zone contains several different types of ridges, typically superimposed on the flatter areas of the foreland, including eskers, flutes and geometrical ridges (Fig. 6.4). The esker system extends for approximately one kilometre and is consistent with the deposition of glaciofluvial sediments within subglacial conduits. The exposure of ice within the esker (Fig. 6.8c) demonstrates that the sediment cover preserves an ice core in places, although it is not clear how extensive this is. Smaller ridges of sands and gravels with no observed ice core which are located close to section FWB01 (Fig. 6.6) are suggested to be fragments of the same esker system, as they follow a similar alignment. The geometrical ridges were not assessed in the field but are suggested to be crevasse squeeze ridges based on their similar planform morphologies and orientations to features interpreted as such at other sites within this

study (e.g. *Chapters 4 and 5)* and in previous work (Sharp, 1985a; Evans and Rea, 1999; Bennett *et al.*, 2003; Christoffersen *et al.*, 2005; Evans and Rea, 2005). Flutes are similar in size and planform morphology to crevasse squeeze ridges but are differentiated based on their alignment in the direction of ice flow; these features were also not assessed in the field and thus their sediment composition is unknown. These landforms are assumed to be related to the most-recent surge of Finsterwalderbreen.

6.4.3. Chronological controls

The innermost ridge of the push moraine complex, ridge 4, was formed by the most-recent surge in ~1910-15, as demonstrated by: (i) the sharp-crested, unvegetated, unstable and chaotic nature of the ridge and the inner zone; and (b) the coincidence between the ridge and the glacier front in 1936 (Fig. 6.2c), shortly after the end of the surge. The timings of the other three surges are unknown, but based on the lichenometric data a loose chronology was suggested by Hart and Watts (1997) of AD 1564 for the surge which formed ridge 1, AD 1696 for ridge 2 and AD 1800 for ridge 3. This indicates a surge return period of ~115 years, which is consistent with known surge cycle lengths for Svalbard glaciers (Dowdeswell *et al.*, 1991; Murray *et al.*, 2003b); however, this chronology effectively only provides an estimate for the age of the ridge-building events and would need to be corroborated by absolute dating techniques.

6.5. Other examples of the breach-block process in Svalbard

The breach-block process of differentiating between separate advances within moraine systems is also applicable to at least two further Svalbard glaciers, Grønfjordbreen and Hessbreen, and these examples are briefly outlined here. In both cases, this geomorphic relationship can be used to identify two individual ridge-building events.

6.5.1. Grønfjordbreen

Grønfjordbreen is located at the head of Grønfjorden in western Nordenskiöld Land (Fig. 3.2) and consists of two flow units, Vestre and Austre Grønfjordbreen, separated by a medial moraine. The glacier currently terminates partly in a large lagoon, Bretjørna, which is dammed by a large composite ridge system (Fig. 6.11a). Although no surges have been directly observed, it has been suggested that Vestre Grønfjordbreen may have previously surged based on the lobate nature of the medial moraine separating it from Austre Grønfjordbreen (Croot, 1988). Observations by Gripp (1929) showed that Grønfjordbreen terminated against the composite ridge system in the 1920s and was in a similar position on an NPI oblique aerial photograph in 1936, possibly reflecting a LIA advance (Watts, 2010). The glacier has retreated ~2 km since its 1936 position, allowing Bretjørna to re-form and expand to its current size (Watts, 2010).

Several inactive meltwater channels form gorges through the outer part of the composite ridge system, which contains multiple ridge crests (Fig. 6.11a), and feed outwash fans on the

fjord edge. These channels are typically blocked by an inner ridge at their ice proximal apexes (Figs 6.11a and 6.11c), indicating that a second ridge-building event has occurred. The sediment composition of the two ridges is notably different (Fig. 6.11b), with the outer ridge containing sorted rounded gravels and deformed sands (Watts, 2010) whilst the inner ridge has a much larger proportion of coarse clasts and large boulders; this forms a sharp boundary where the inner ridge has been emplaced on the proximal side of the outer part of the ridge system (Fig. 6.11b). The inner ridge grades into a narrow zone of poorly-consolidated hummocky topography, small pools and poorly-sorted sediments which separates the composite ridge system from Bretjørna (Fig. 6.11a). This zone and the inner ridge which blocks the channels are associated with the advanced position of the glacier in the 1920-30s, interpreted by Watts (2010) as a surge during the LIA. The outer part of the composite ridge system was formed during an older advance, and an optically stimulated luminescence (OSL) date taken from an area of deformed sands suggests a maximum age of 1.9±0.1 ka BP for the original deposition of the sand (D. Swift, personal communication, March 2013), indicating that the ridge-building event occurred after that.

6.5.2. Hessbreen

Hessbreen is a small valley glacier located ~4 km to the west of Finsterwalderbreen (Fig. 6.1) which has a large ridge system at its margin (Fig. 6.11d). The glacier surged in 1969-77 to a position just inside the outermost part of the ridge system, forming a small push ridge of poorly-sorted sediments (Fig. 6.11e). Hessbreen has retreated ~1 km since the surge, exposing an area of poorly-consolidated hummocky topography containing numerous small pools; this area and its associated push ridge contrast sharply with the morphology and stability of the outer part of the ridge system (Fig. 6.11d), which has been associated with an advanced position of the glacier mapped in 1898 (Hamberg, 1905; Sund and Eiken, 2004).

A variation of the breach-block process is evident in one small area of the foreland, providing further support for it being a good indicator of multiple ridge-building events. The 1969-77 ridge encroaches on an inactive outwash fan at the southwestern margin of the moraine system, which has cut into the side of the outer ridge (Figs 6.11d-f). This demonstrates that the outwash has eroded the outer part of the ridge system but formed prior to the 1969-77 surge, suggesting it developed between the two ridge-building events, and therefore providing additional evidence for two separate advances. Tens of centimetres high ridges can be seen on the surface of the outwash (Fig. 6.11f), and these are interpreted as minor push ridges formed as the most-recent surge advanced onto the fan.

6.6. Summary

The geomorphic relationship between ridges and meltwater drainage routes within the push moraine complex at the margin of Finsterwalderbreen allows the number of different ridge-

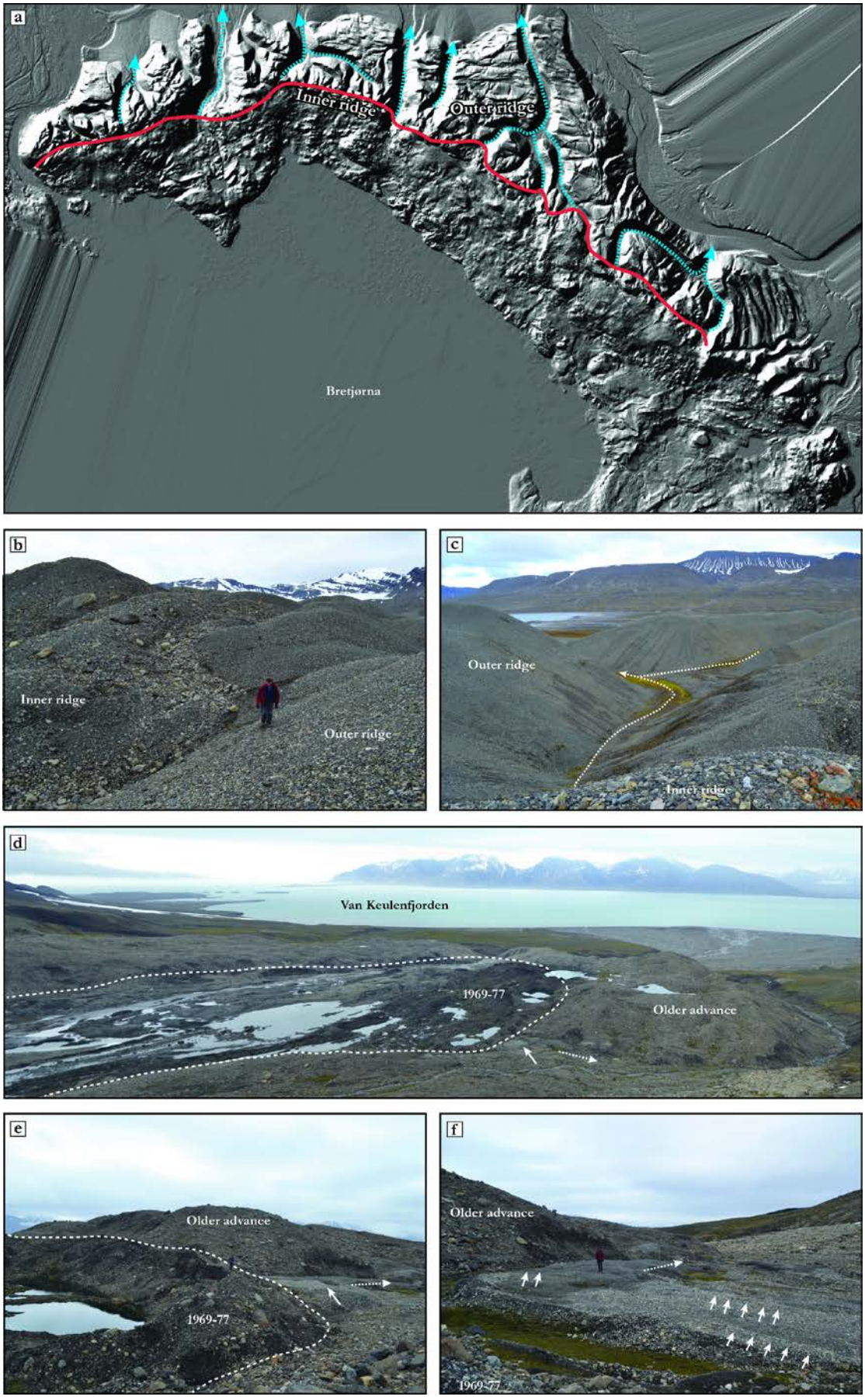
a
Inner ridge
Outer ridge
Bretjørna
b
Inner ridge
Outer ridge
c
Outer ridge
Inner ridge
d
Van Keulenfjorden
1969-77
Older advance
e
Older advance
1969-77
f
Older advance
1969-77

Figure 6.11

Figure 6.11 (preceding page) – Examples of the breach-block process at Grønfjordbreen and Hessbreen. (a) Hillshaded DEM of Grønfjordbreen composite ridge system. Blue dotted arrows are blocked meltwater channels; solid red line delimits boundary between the outer and inner (blocking) ridges. LiDAR data acquired from NEODC. (b) Boundary between inner ridge (left) and outer ridge (right). Note difference in sediment compositions. (c) Blocked channel (dotted arrow) through outer ridge viewed from inner (blocking) ridge. (d) Hessbreen moraine system. Dashed line delimits boundary between area associated with the 1969-77 surge and ridges of an older advance; solid arrow indicates blocked outwash fan shown in (e) and (f); dotted arrow shows drainage direction. (e) Ridge associated with 1969-77 surge blocking outwash fan (solid arrow). Dotted arrow shows drainage direction. (f) Outwash fan viewed from blocking ridge. Solid arrows highlight small push ridges in outwash; dotted arrow shows drainage direction.

building events to be assessed, and therefore the identification of multiple surges. This is based on the observation that inactive channels and outwash fans which cut through outer parts of the ridge system are blocked off by ridges in an inner position, indicating that the entire push moraine complex cannot have formed at the same time; this is termed the breach-block process. Ten examples of this are evident within the ridge system and, importantly, these demonstrate that not all drainage routes are blocked by the same ridge. This provides a way to assess not only if the ridge system was formed by multiple events, but also how many events are recorded. Four separate ridges are identified based on this, corresponding to four ridge-building advances or surges. These separate zones within the ridge system were also assessed based on their morphological characteristics, sediment composition, vegetation cover and range of frost-shattered lithologies observed, as this provides an indication of relative age. Based on these multiple lines of evidence, it is possible to distinguish between the four identified ridges, providing support for the number of ridge-building events identified through the breach-block process. Hart and Watts (1997) also suggested there were four separate zones within the ridge system based on lichenometry data from a small part of the push moraine complex. Apart from the innermost ridge, which was formed by the most-recent surge in ~1910-15, the timings of the different surges are unclear.

This work demonstrates a fairly simple method to assess the number of separate advances recorded within push moraine systems based on geomorphic relationships, and two further examples of its application to Svalbard push moraine complexes are presented (Grønfjordbreen and Hessbreen). This process is likely to have a wider application across Svalbard and in some formerly glaciated regions.

Chapter Seven
Scott Turnerbreen

78º 05.0' N, 15º 40.0' E

After Scott Turner, b. 1880, American geologist, general manager of Arctic Coal Co., Arctic Steamship Co. and Ayer & Longyear, 1911-16.

The place names of Svalbard, Norsk Polarinstitutt

7. Scott Turnerbreen

7.1. Introduction

This chapter presents a structural glaciological and geomorphological assessment of Scott Turnerbreen, a small valley glacier in Nordenskiöld Land, central Spitsbergen (Fig. 3.2), and aims to characterise the ice-sediment-landform assemblages associated with a surge-like advance in the 1930s (Hagen *et al.*, 1993). The previous three chapters have investigated associations produced by large tidewater (*Chapters 4 and 5*) and land-terminating (*Chapter 6*) surge-type glaciers in Svalbard. Based on previous studies, these examples are likely to be broadly representative of a significant proportion of the known surge-type glaciers in Svalbard which fit into these two categories, i.e. large tidewater glacier surges (e.g. Solheim, 1985; Solheim and Pfirman, 1985; Boulton *et al.*, 1996; Glasser *et al.*, 1998a; Jiskoot *et al.*, 2000; Dowdeswell and Benham, 2003; Murray *et al.*, 2003b; Ottesen and Dowdeswell, 2006; Ottesen *et al.*, 2008; Kristensen *et al.*, 2009a,b; Sund and Eiken, 2010; Kristensen and Benn, 2012; Mansell *et al.*, 2012) and land-terminating glacier surges which often contain large push/thrust moraine sequences at their margins (e.g. Croot, 1988; Hagen, 1988; Etzelmüller *et al.*, 1996; Huddart and Hambrey, 1996; Hart and Watts, 1997; Boulton *et al.*, 1999; Christoffersen *et al.*, 2005); there are also overlaps between, and variations within, these two categories (e.g. Huddart and Hambrey, 1996; Kristensen *et al.*, 2009b).

However, the examples in *Chapters 4-6* and those cited above do not satisfactorily characterise a further category of Svalbard surge-type glaciers, namely small valley glaciers. The latter are broadly defined here as land-terminating glaciers which are typically <5 km long, ~1 km wide, have well-defined accumulation areas (i.e. are not fed by a larger ice cap), are confined within a valley for much of their length and are largely independent ice bodies (i.e. not confluent with other glaciers, but can be contiguous). A small number of glaciers that fit these criteria have been suggested to have surged during the Little Ice Age (LIA) or at some point since (Table 7.1), largely based on the interpretation of single aerial photographs (Liestøl, 1988; Hagen *et al.*, 1993; Sund *et al.*, 2009).

The examples in Table 7.1 demonstrate that small valley glaciers in Svalbard can surge, yet very few have been observed do so to in the past century. In fact, almost all other small valley glaciers are thought to have either receded continuously and/or stagnanted since their LIA maximum positions at ~1900 AD (Hagen and Liestøl, 1990; Dowdeswell *et al.*, 1995; Hambrey *et al.*, 2005), typically marked by an ice-cored latero-frontal moraine belt (Boulton *et al.*, 1982; Werner, 1993), due to consistently negative mass balance during this period (Dowdeswell *et al.*, 1995; Hodgkins *et al.*, 1999) driven by an abrupt increase in mean annual air temperature (Hansson-Bauer *et al.*, 1990; Hanssen-Bauer and Førland, 1998). This has led to the suggestion that some glaciers may have surged during the LIA but are no longer able to build up sufficient mass for a subsequent surge due to a sustained period of climate-induced negative mass balance, and have therefore effectively been removed from the surge cycle

(Dowdeswell *et al.*, 1995; Hodgkins *et al.*, 1999; Hansen, 2003). Furthermore, this raises the possibility that additional small valley glaciers in Svalbard have experienced a similar change in dynamics from surge-type to non-surge-type since the LIA and, therefore, these present an important opportunity to investigate potential climatic controls on surge behaviour.

Table 7.1 – Small valley glaciers (<5 km in length) on Svalbard that have been suggested to be of surge-type. Glaciers which are tributaries of larger systems have been excluded.

Glacier	Location	Length (km)	Area (km²)	Year of surge	Evidence	Source
Austre Lovénbreen	78°52.4'N 12°08.6'E	4	5	~1900? ~1936?	Surface bulge	Midgley *et al.* (2013)
Brodtkorbfjellet	77°49.8'N 17°10.7'E	2.5	1.6	1990*	Crevassing	Sund *et al.* (2009)
Hessbreen	77°30.6'N 15°06.7'E	4.5	5	1969-77	Crevassing; terminus advance	Hambrey & Dowdeswell (1997); Sund and Eiken (2004)
Midtre Lovénbreen	78°52.8'N 12°02.4'E	4	5	~1890	Steep front; zig-zag eskers	Hagen *et al.* (1993); Hansen (2003)
Scott Turnerbreen	78°06.1'N 15°55.5'E	4.5	3.3	~1930	Steep, advanced terminus	Hagen *et al.* (1993)
Tinkarpbreen	77°59.1'N 17°11.7E	2.3	2	2000*	Crevassing	Sund *et al.* (2009)

*Year surge first observed

A major problem, however, is identifying possible surges or surge-like behaviour of small valley glaciers at the LIA, as direct observations or aerial photographs are typically absent. This reduces the possibility of inferring surges based on widespread crevassing or steep ice fronts, as is the case for several of the glaciers listed in Table 7.1. In the absence of such observations, the glaciological structure and geomorphology associated with small valley glaciers provides a way to assess their former flow dynamics and, of particular interest to this study, their evolution since the LIA (Etzelmüller *et al.*, 1996, 2000; Hambrey *et al.*, 2005; Lukas *et al.*, 2005; Midgley *et al.*, 2013). This approach is applied in both this chapter and *Chapter 8* as a way to assess possible surge-like behaviour of small Svalbard glaciers: firstly, by investigating the glaciological structure and geomorphology associated with a small glacier which has undergone a surge-like advance in the 20th century (Scott Turnerbreen, this chapter); and secondly, by examining similar evidence within a small glacier with no known surge history (Tellbreen, *Chapter 8*).

This chapter begins by outlining the geographical setting and surge history of Scott Turnerbreen in *7.2*, followed by a description of structural glaciological, sedimentological and geomorphological results from both the glacier surface and the glacier foreland in *7.3*. An interpretation of these results, and any similarities or discrepancies with previous work, is presented in *7.4.* In *7.5.*, the observed glaciological structure and geomorphology is assessed in the context of surge activity.

7.2. Study area and surge history

7.2.1. Geographical setting

Scott Turnerbreen is 4.5 km long, 0.5 km wide and covers an area of 3.3 km^2. It is located at the head of Bolterdalen, a 6 km long north-south aligned valley which feeds into Adventdalen (Fig. 7.1). The glacier covers an altitude range of between 230 and 680 m a.s.l. (Sletten *et al.*, 2001) and is fed by two north-facing accumulation basins, from which two distinct flow units extend downglacier. The flow units coalesce at ~500 m a.s.l. (Sletten *et al.*, 2001) and are separated by medial moraines. The western flow unit comprises almost the entire lower tongue in 2012 and pinches out the smaller eastern unit into the debris-covered lateral margin. Aerial photographs from 1961 and 1990 demonstrate that the eastern unit, although it still only comprised a third of the entire glacier width, was far better defined when the glacier front was in a more advanced position (Sletten *et al.*, 2001). The debris-covered glacier front currently terminates in a ~0.7 km^2 proglacial area of latero-frontal ridges, outwash and hummocky topography; this is described in more detail in *7.3.2.* The outermost frontal ridge has been interpreted to represent the LIA maximum (Sletten *et al.*, 2001) and is termed the 'LIA ridge' in this chapter (Fig. 7.1b). A proglacial icing develops on the glacier foreland in winter, which in the past has remained intact throughout summer (Hodgkins *et al.*, 2004), but was not observed in August of 2009, 2011 and 2012. The bedrock in the area is composed of easily-erodible sandstones, siltstones and shales of the Van Mijenfjorden and Adventdalen Groups (Dallmann *et al.*, 2002).

7.2.2. Surge history

An oblique aerial photograph from 1936 shows Scott Turnerbreen was significantly larger, thicker and terminated at a position ~0.75 km downvalley from the present-day debris-covered front (Figs 7.2a and 7.2b). Based on this, Hagen *et al.* (1993) inferred that Scott Turnerbreen was either surging at this time or had recently surged; there is no indication of the duration of the surge or the pre-surge geometry of the glacier. In the 1936 photograph (Fig. 7.2a), the glacier terminates adjacent to a prominent latero-frontal ridge, which Sletten *et al.* (2001) suggested was formed by the surge (Fig. 7.1b); this ridge is termed the 'surge ridge' in this chapter. From 1936-1990, Scott Turnerbreen underwent terminus retreat of ~0.25 km and thinned by at least 50-75 m in the ablation area (Fig. 7.2b), equating to a mass balance of -0.58 m a^{-1} w.e. (water equivalent) for this period (Hodgkins *et al.*, 1999). Since 1990 the glacier front has retreated a further 0.5 km and thinned significantly, driven by a second abrupt increase in summer air temperatures (James *et al.*, 2012). An average surface velocity of 0.09 m a^{-1} was measured by Hodgkins (1994), demonstrating that current flow rates are very low. Based on borehole thermistor and ground-penetrating radar data, the glacier has been shown to be cold-based and frozen to its bed throughout, including at its deepest point of 76 m (Hodgkins *et al.*, 1998, 1999). In addition to the lack of any evidence for mass building up in the accumulation

basins, Hodgkins *et al.* (1999) concluded that there was no prospect of a future surge, indicating that Scott Turnerbreen has transitioned from surge-type to non-surge-type since 1936.

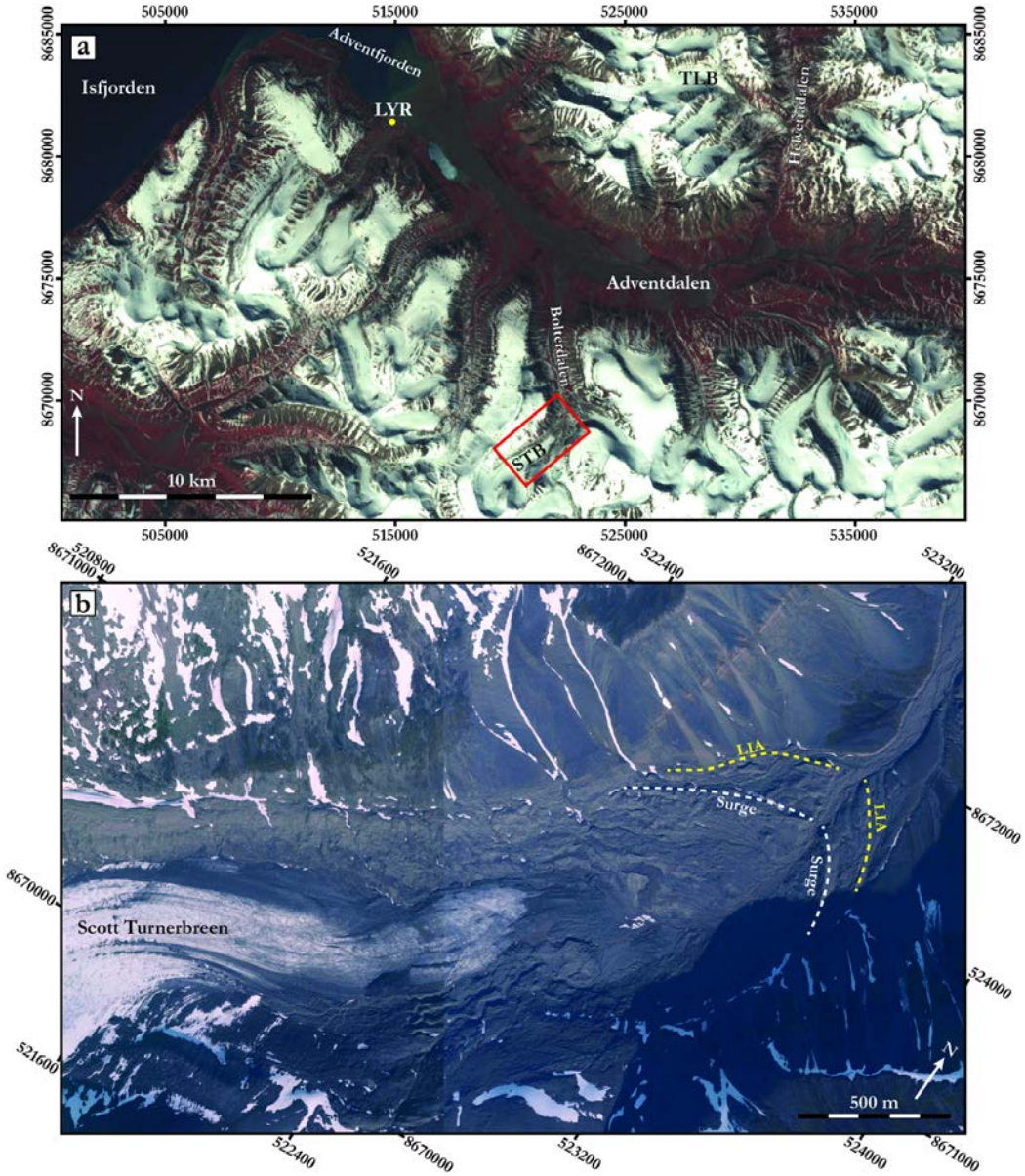

Figure 7.1 - Location map of Scott Turnerbreen in central Spitsbergen. (a) 2001 Landsat ETM+ image showing location of Scott Turnerbreen (STB) relative to Longyearbyen (LYR) and Tellbreen (TLB; see Chapter 8). Red rectangle delimits area shown in (b) and mapped in Fig. 7.3. See Fig. 3.2 for location in Svalbard. (b) 2009 NPI aerial photograph mosaic of Scott Turnerbreen lower tongue and foreland (©Norsk Polarinstitutt). Dashed lines show Little Ice Age (LIA; yellow) and 1930s surge (white) positions. See Fig. 7.3 for the geomorphological map of this area.

7.2.3. Previous geomorphological work

Scott Turnerbreen is the focus of a study by Sletten *et al.* (2001) into the formation and disintegration of its moraine system; however, this work did not specifically aim to characterise the ice-sediment-landform associations related to the surge and, therefore, a full reassessment has been made using a combined structural glaciological, geomorphological and

sedimentological approach. Consequently, there are some areas of overlap between the two studies and their interpretations, which both agree and differ in places; these will be highlighted throughout the chapter.

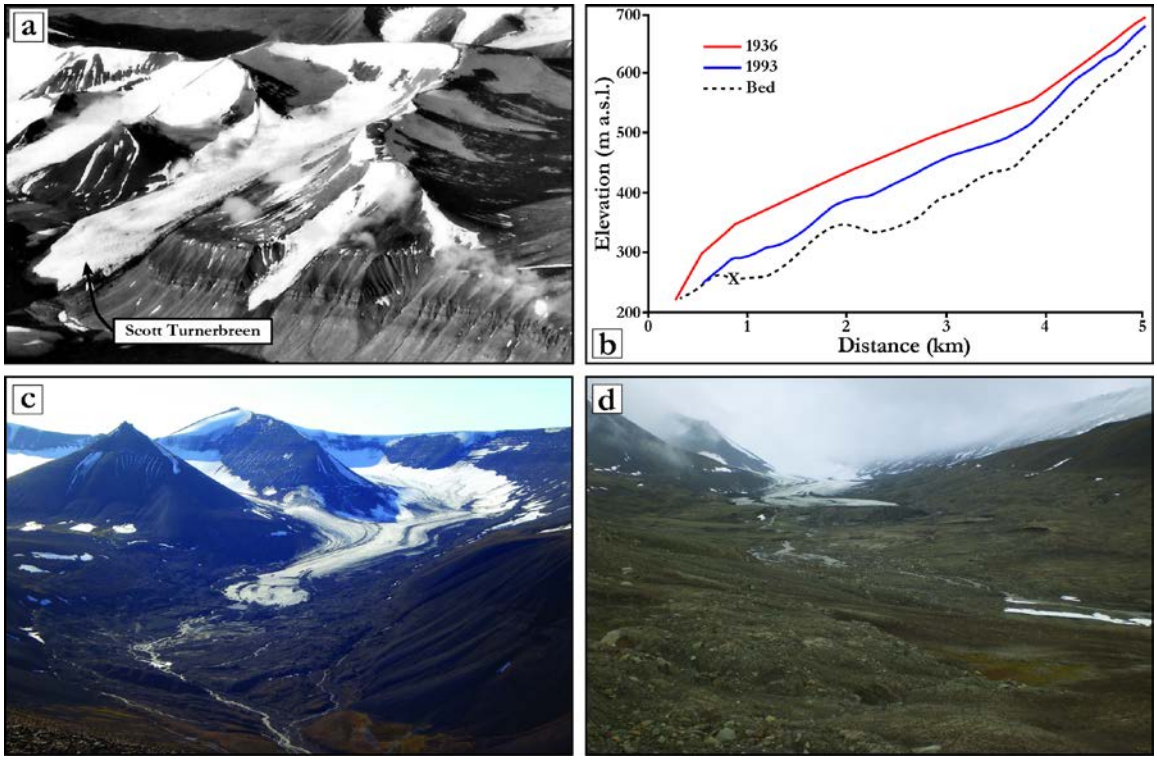

Figure 7.2 – (a) Photograph of Scott Turnerbreen in 1936 (©Norsk Polarinstitutt, photograph S36 2300; reproduced from Sletten *et al.*, 2001). (b) Surface profiles of Scott Turnerbreen in 1936 (from map sheet E9, Adventdalen; 50 m contour interval) and 1993 (field survey; 10 m contour interval). Location of bed determined by radio-echo profiling. X marks approximate position of debris-covered glacier front in 2009. Adapted from Hodgkins *et al.* (1999). (c) Photograph of Scott Turnerbreen in August 2011. (d) View across foreland towards Scott Turnerbreen in August 2011.

7.3. Results

7.3.1. Lower glacier tongue

Three aspects of the lower glacier tongue were investigated: glaciological structures and their relationship to each other (*7.3.1.1.*); the morphology and sediment composition of four types of supraglacial ridges (*7.3.1.2.*); and the character and distribution of widespread debris cover, particularly at the terminus (*7.3.1.3.*).

7.3.1.1. Structural glaciology

Five types of planar structure are identified within the lower tongue of Scott Turnerbreen from aerial photographs and field observations (Table 7.2, Figs 7.3 and 7.4) and these are termed S_0-S_4 in order of inferred formation following structural geological conventions and numerous structural glaciological studies (e.g. Lawson *et al.*, 1994; Hambrey and Dowdeswell, 1997; Glasser *et al.*, 1998b; Hambrey and Glasser, 2003; Hambrey *et al.*, 2005; Roberson and

Figure 7.3 – Map of Scott Turnerbreen glacial geomorphology and lower tongue supraglacial debris and structural glaciology. See Fig. 7.1 for location of mapped area. Mapped from 2009 aerial photographs acquired from NPI (©Norsk Polarinstitutt). A digital version of this map is included on the CD inside the back cover.

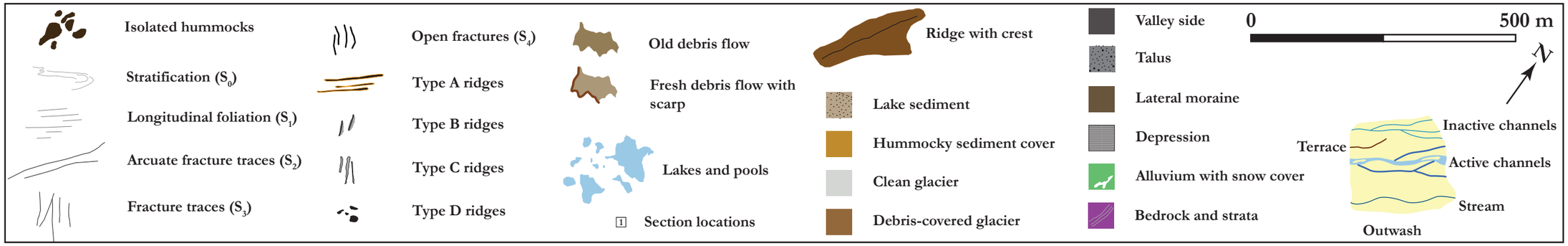

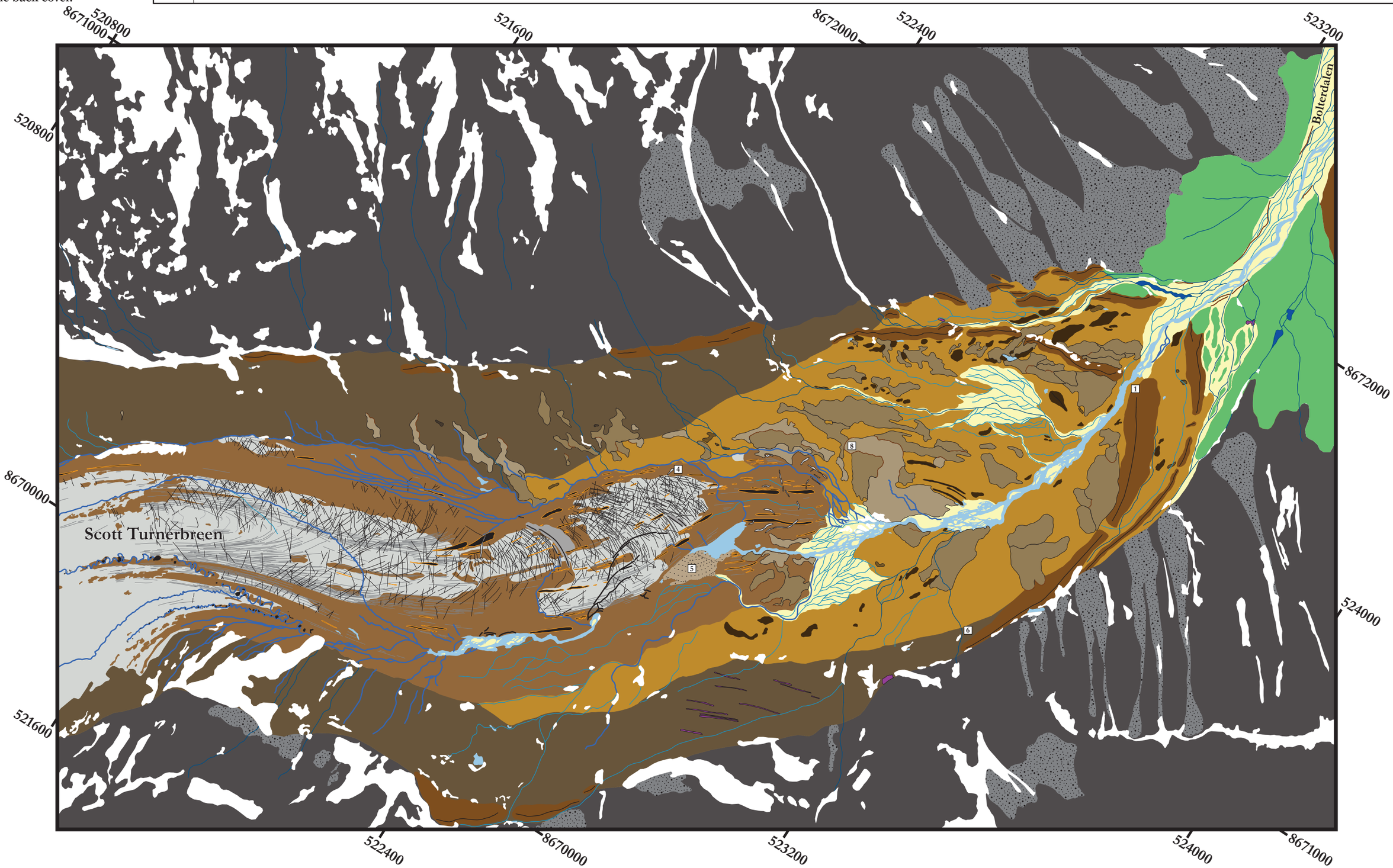

Hubbard, 2010; Midgley *et al.*, 2013). Of these, all were mapped from aerial photographs (Fig. 7.3) but only a small population of S_3 structures were measured in the field (strike/dip). This was to provide an indication of the range of orientations for these structures, which from the mapping were observed to be quite variable, rather than being part of a comprehensive structural investigation of all features S_0-S_4 (as presented for Tellbreen in *Chapter 8*).

S_0 – Stratification

This structure is defined by layering appearing as slight colour changes on the glacier surface which can be traced as irregular linear features in the uppermost part of the lower tongue, typically aligned perpendicular to ice flow (Fig. 7.3). Stratification is cross-cut by S_2 and S_3 structures (Fig. 7.3).

Table 7.2 – Summary of principal glaciological structures in Scott Turnerbreen. *S_0 and S_1 represent end-members of a structural continuum. $^{\Delta}$Field structural measurements only recorded for S_3 structures.

Planar glaciological structures	Description	Where observed
S_0*	Stratification	Surface
S_1*	Longitudinal foliation	Surface
S_2	Arcuate fracture traces	Surface
S_3^{Δ}	Fracture traces	Surface
S_4	Open fractures	Surface

S_1 – Longitudinal foliation

Linear surface stripes which are generally aligned parallel to ice flow are identified as longitudinal foliation (Figs 7.3 and 7.4a) based on their similarity to features mapped as such in previous studies (Hambrey and Dowdeswell, 1997; Glasser *et al.*, 1998b; Hambrey and Glasser, 2003; Hambrey *et al.*, 2005; Fleming *et al.*, 2013; Midgley *et al.*, 2013). Three main zones of longitudinal foliation are present in the central, eastern and western parts of the lower tongue, but these are harder to identify close to the debris-covered front. No structural measurements were taken from Scott Turnerbreen, but similar examples within other Svalbard valley glaciers have been steeply dipping and aligned parallel or sub-parallel to ice flow (Hambrey and Dowdeswell, 1997; Glasser *et al.*, 1998b; Roberson and Hubbard, 2010). Longitudinal foliation is closely associated with type A supraglacial ridges (*7.3.1.2.*).

S_2 – Arcuate fracture traces

Linear stripes aligned perpendicular and sub-perpendicular to ice flow and S_1 structures, which they cut across, are identified as arcuate fracture traces (S_2) and fracture traces (S_3). These represent trace evidence for brittle deformation within the glacier. Arcuate fracture traces appear as gently curving linear stripes which can be traced for tens to hundreds of metres across the glacier surface and are particularly densely spaced on the lowermost part of the tongue (Figs 7.3, 7.4a and 7.4b). S_2 structures rarely cross-cut each other but do occasionally intersect. These structures are similar to features mapped as transverse foliation (Lawson *et al.*, 1994), thrusts (Hambrey and Dowdeswell, 1997), arcuate fractures (Roberson and Hubbard, 2010) and arcuate crevasse traces (Midgley *et al.*, 2013) in previous studies.

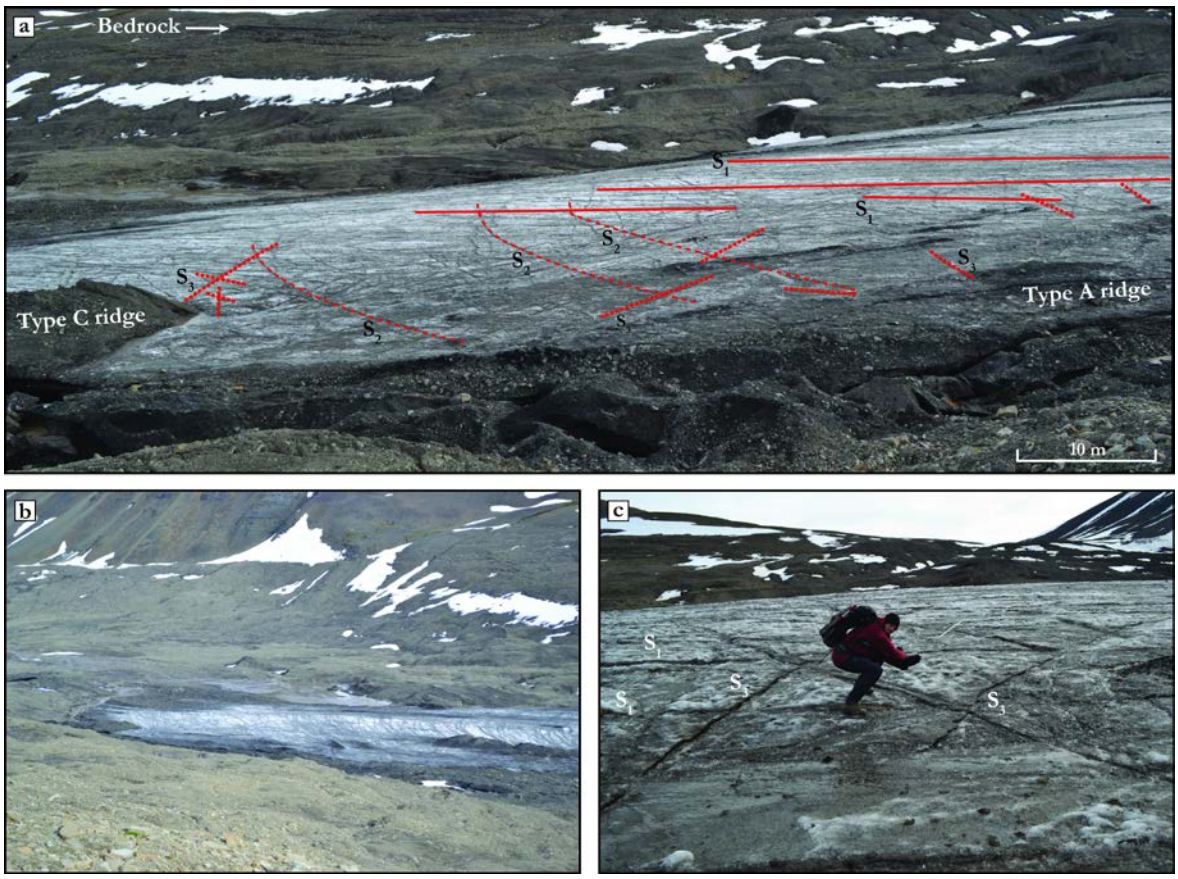

Figure 7.4 – Details of glaciological structures. (a) S_1, S_2 and S_3 structures highlighted on the lower tongue. (b) Densely spaced structures on lower tongue. (c) S_3 fracture traces cutting across S_1 longitudinal foliation.

S_3 – Fracture traces

A second group of fracture traces (S_3) are in general shorter, straighter and display a wide range of orientations, which is apparent both from the mapping (Fig. 7.3) and the structural data (Fig. 7.5a). These cross-cut S_0, S_1, S_2 and other S_3 structures (Figs 7.3, 7.4a and 7.4c). Fracture traces are located throughout the lower tongue but are particularly densely spaced close to the debris-covered front (Figs 7.3 and 7.4b). Similar structures have been mapped as crevasse traces in a

number of previous studies (Hambrey and Dowdeswell, 1997; Glasser *et al.*, 1998b; Hambrey *et al.*, 2005; Roberson and Hubbard, 2010; Midgley *et al.*, 2013).

S_4 – Open fractures

Several large open fractures are visible on the eastern side of the glacier surface, in some cases extending for ~300 m (Fig. 7.3). Shorter open fractures are closely associated with the eastern lateral channel and along the backwall in the uppermost part of the accumulation basins.

7.3.1.2. Supraglacial ridges

Four types of supraglacial ridge are identified within the lower tongue of Scott Turnerbreen based on morphology, sediment composition and orientation (Table 7.3). These are termed type A-D ridges and some can be roughly correlated to the three types of supraglacial ridges (A-C) recognised by Sletten *et al*. (2001), as highlighted below. The majority of the supraglacial ridges are also identified within the lower tongue of Tellbreen (*Chapter 8*).

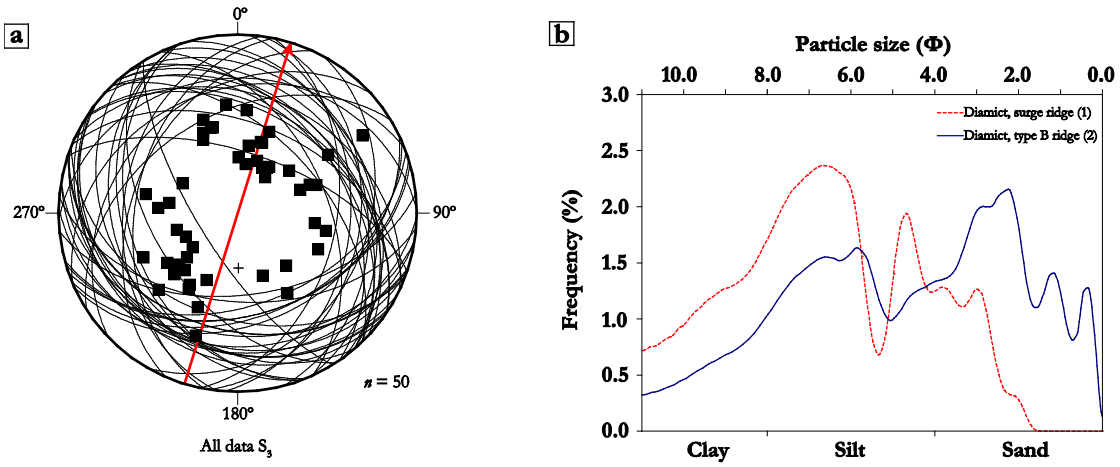

Figure 7.5 – (a) Lower hemisphere equal-area stereographic projection of S_3 fracture trace structural data. (b) Grain size distributions of diamict within western surge ridge and type B supraglacial ridge derived from laser sizing.

Type A ridges

These are linear ridges aligned parallel to ice flow and are the most common of the supraglacial ridges within the lower tongue (Table 7.2, Figs 7.3, 7.6a and 7.6b). Their length ranges from ~1-200 m, they are typically ~1-3 m wide, range in height from 0.1-3 m above the ice surface, and in planform often have a tapered upglacier end (Figs 7.6a and 7.6b). The surface morphology of type A ridges varies from flat-topped to sharp-crested and uneven, and in all cases the sediment cover is <10 cm thick over an ice core. The sediment is composed of poorly-consolidated angular and very angular sandstone and shale material ranging in size from coarse sand to large boulders (~1 m diameter) and is very similar to the general widespread debris cover across the

lower glacier tongue, upon which type A ridges are often superimposed (Figs 7.3 and 7.9a; *7.3.1.3.*).

Table 7.3 – Summary and interpretation of types of supraglacial ridges on Scott Turnerbreen.

Ridge	Dimensions (m)	Morphology	Sediment characteristics	Interpretation
Type A	1-200 (l) 0.5-10 (w) 0.1-3 (h)	Examples of both sharp-crested and rounded, flatter ridges; width typically tapers significantly at the upglacier end; linear ridges aligned parallel to ice flow and S_1 longitudinal foliation; ice-cored.	Typically angular to very angular clasts; range of grain sizes from coarse sand to boulders (~1 m diameter), individual ridges can also be sorted; poorly-consolidated; range of lithologies, predominantly shales and sandstones; maximum sediment thickness of ~0.1 m over ice core.	Rockfall debris buried within the original stratification which has then been tightly folded and melts out at the glacier surface as flow-parallel ridges (see also S_1 formation, *section 7.4.1.*).
Type B	5-100 (l) ~1 (w)* <1 (h)	Poorly-defined crestline; typically flat-topped; linear to curvilinear ridges aligned perpendicular to ice flow and type A ridges; slurry emanating from ridge core is more extensive on downglacier side; no ice core.	Highly-saturated, poorly-sorted diamict; predominantly sub-angular clasts (Fig. 7.8), many with evidence for striations and bullet-shaped morphologies; range of grain sizes from silt to boulders (~1 m diameter); very poorly-consolidated.	Subglacial debris incorporated into the glacier via crevasses and arcuate shear planes extending to the bed.
Type C	5-80 (l) 1-2 (w) 0.5-4 (h)	Examples of both sharp-crested and rounded, flatter ridges; can be straight or sinuous; aligned both perpendicular and sub-parallel to ice flow; ice-cored in some cases.	Stratified sands and gravels (Fig. 7.7a); predominantly edge-rounded clasts; grain sizes range from fine sand to cobbles; well-sorted layers/lenses of fine and coarse gravel.	Englacial meltwater channel infills which have melted out onto the glacier surface. In some cases may reflect meltwater occupying a crevasse system (e.g. *Ch. 8).*
Type D	1-10 (l) 0.5-5 (w) <2 (h)	Rounded cones or piles; located adjacent to supraglacial channels; various alignments.	Not assessed.	Meander infills abandoned during the evolution of cut and closure channels.

*not including slurry

Many of the larger clasts and boulders display evidence of surface oxidised weathering and there is a predominance of black shale across all grain sizes, giving the ridges a dark appearance (Fig. 7.6a). Most type A ridges are composed of this poorly-sorted range of grain sizes; the exceptions are several typically smaller ridges (<5 m long, 1 m wide and 0.1 m high) which contain almost entirely sorted black shale fine gravel. The ridges are closely related to the larger-scale and more-continuous medial moraines in terms of orientation and sediment composition and display the same orientations as S_1 longitudinal foliation (Fig. 7.3).

Type A ridges are characteristically similar to the type A ridges described by Sletten *et al.* (2001). The main observed differences between the two are (i) type A ridges in Sletten *et al.* (2001) are described as being concentrically-shaped and aligned parallel to the glacier front, forming arcs around the eastern flow unit, rather than aligned parallel to ice flow; and (ii) Sletten *et al.* (2001) identified that type A ridges were fed by englacial debris bands exposed in cross-section where the main channel cuts down through the debris-covered glacier front (e.g. Fig. 7.9c), displaying evidence for local folding and upglacier dips of 40-65º; no englacial components of type A ridges were observed in this study, despite investigation in a similar area, as the ice was very debris-rich and obscured by sediment cover (Fig. 7.9c).

Type B ridges

Type B ridges are typically oriented transverse or, in the case of two ridges at the eastern lateral margin, sub-parallel to ice flow, type A ridges and S_1 longitudinal foliation. They range in length from ~5-100 m (Table 7.3, Fig 7.6b) and have a limited distribution (n = 10) on the lowermost tongue only (Fig. 7.3). The ridge core is <1 m wide, 1 m high and highly-saturated slurry emanates from this in both an up- and downglacier direction; this slurry area is typically far more extensive on the downglacier side of the ridge and is similar to deposits described by Boulton (1968). The ridges were not ice-cored and in several places they were observed to cut through type A ridges (Fig. 7.6b). The debris within type B ridges is a very poorly-sorted and poorly-consolidated diamict ranging in grain-size from silt to boulders; the polymodal grain size distribution of the fraction <1 mm is shown in Figure 7.5b. The clasts within the diamict are predominantly sub-angular and ~30% are bullet-shaped and striated (sample HL11STB15, Fig. 7.8a). In at least one type B ridge, there is a sharp transition from diamict to sorted sands and gravel within the same ridge. Type B ridges are similar in planform morphology and orientations to both S_2 arcuate fracture traces and S_3 fracture traces (Fig. 7.3). Sletten *et al.* (2001) did not report any supraglacial ridges which are directly comparable to type B ridges in this study; their type B ridges appear broadly similar in orientation but were all reportedly ice-cored and composed of well-rounded pebbles and cobbles in a sandy matrix, with no observations of highly-saturated diamict.

Type C ridges

These are linear thin (<2 m) ridges composed of stratified sands and gravels which range in length from ~5-80 m and can reach heights of ~4 m above the glacier surface (Figs 7.3, 7.6e, 7.6f and 7.7b). Their orientations are variable, ranging from sub-parallel to transverse to ice flow, and they are primarily found on the lowermost debris-covered part of the glacier (Fig. 7.3). These ridges display two main planform morphologies: short and straight ridges, typically oriented transverse to ice flow, and longer sinuous ridges, typically oriented sub-parallel to ice flow (Fig. 7.3). Type C ridges are ice-cored, sharp-crested and covered by sediment which ranges in thickness from 0.5-2.5 m (Fig. 7.7b). In several places, type C ridges are clearly draped on top of type A ridges (Figs 7.3 and 7.6d). Section STB04 (Fig. 7.7b) shows an example of the sediment composition of a type C ridge, characterised by a matrix of coarse sand and fine gravel of approximately equal proportions, layers of sorted fine (2-4 mm) and coarse gravel (>4 mm) and scattered edge-rounded cobble-sized clasts (Fig. 7.6f). Well-sorted laminated fine sand was also found in some other type C ridges. A clast shape sample from the surface of section STB05 contained predominantly sub-angular, sub-rounded and rounded clasts, with 12% rounded or well-rounded (RWR %; Fig. 7.8). The dip of individual layers varies between the ridges and ranges from near-horizontal bedding to ~30º (Fig. 7.6f).

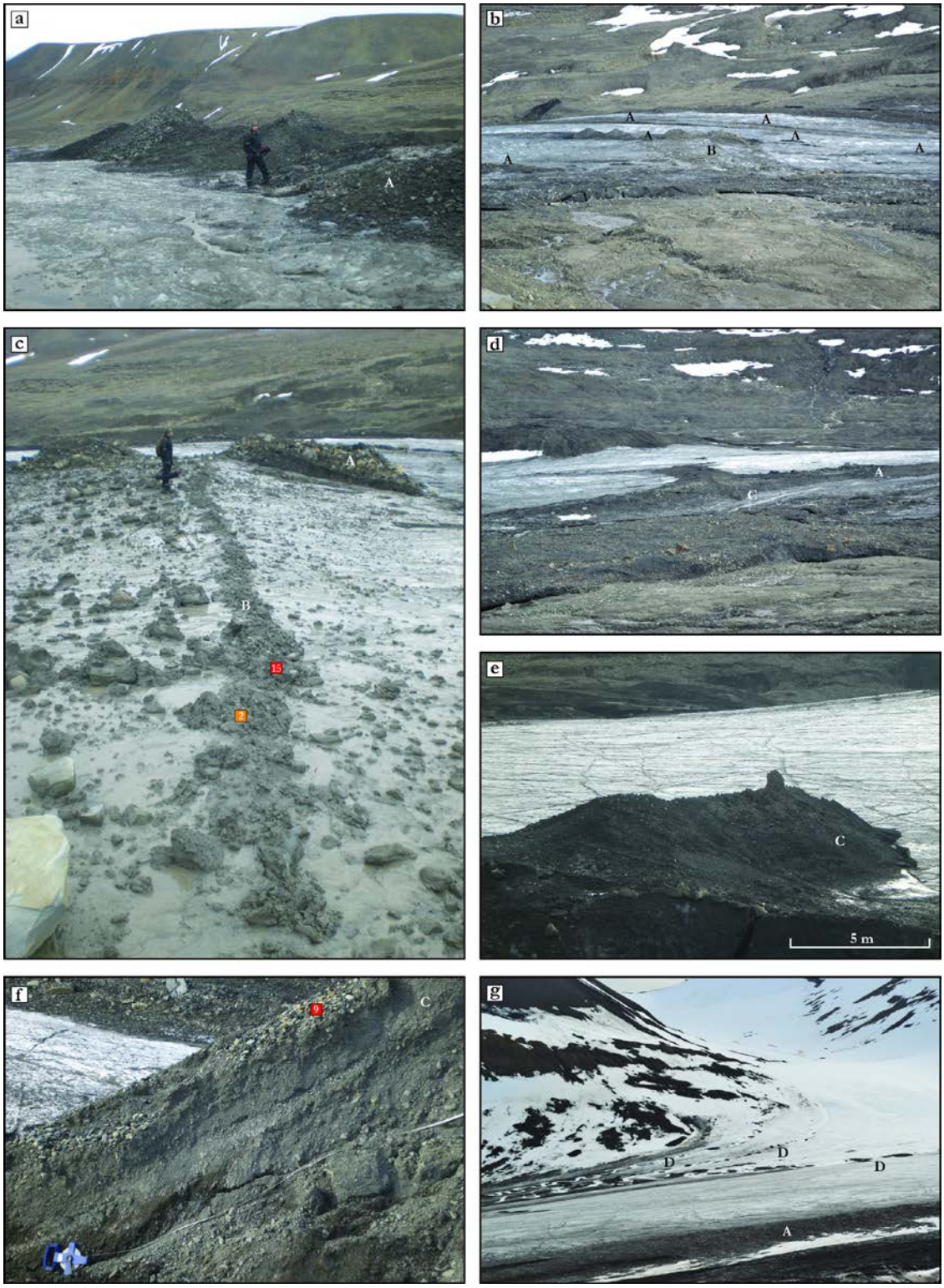

Figure 7.6 – Examples of supraglacial ridges. Numbered locations refer to grain size distribution (orange) and clast shape (red) samples in Figs 7.5a and 7.8a. (a) Type A ridge. Note angular material and predominance of black shale. (b) Type A ridges aligned in the direction of ice flow and a type B ridge aligned perpendicular to ice flow. Note large area of slurry associated with type B ridge. (c) Type B ridge. Note thin ridge core, edge rounded clasts, poorly-sorted debris and large area of slurry both up- and downglacier. (d) Type C ridge draped across type A ridge. (e) Sharp-crested type C ridge at western margin of lower tongue. See Fig. 7.7b for sediment log. (f) Detail of type C ridge shown in (e) and logged in Fig.7.7b. Note layers of sand and gravel and edge-rounded clasts on surface. (g) Type D ridges adjacent to supraglacial channels.

This characterises the sediment compositions of all type C ridges, regardless of planform morphology and orientation. These ridges are characteristically similar to those also classified as type C ridges by Sletten *et al.* (2001), with the main differences being (i) type C ridges in this study display far more variable orientations than those mapped by Sletten *et al.* (2001), which were predominantly sub-parallel to ice flow; (ii) no observations of type C ridges draped over type A ridges were reported by Sletten *et al.* (2001); (iii) no sinuous type C ridges were observed in their study; and (iv) in Sletten *et al.* (2001), type C ridges were linked to lens-shaped englacial debris bands exposed in cross-section where the main meltwater channel cuts through the debris-covered glacier front; this study did not identify such a relationship due to the debris-rich nature of the ice and sediment cover.

Type D ridges

Small piles of dark sediment adjacent to supraglacial channels in the upper part of the lower glacier tongue are mapped as type D ridges. These are typically 2-3 m long, 1-2 m wide and <2 m high and are predominantly located on the glacier surface on the inner side of meander bends. The sediment composition of type D ridges was not assessed at Scott Turnerbreen, but identical ridges identified at Tellbreen (*Chapter 8*) are characterised by tens-of-centimetre-thick piles of sand and fine gravel derived from black shale, typically with a small ice core (Fig. 8.12d). Nothing similar to type D ridges was mapped or described by Sletten *et al.* (2001), probably because their study focused only on the very lowermost part of the glacier tongue where they are absent.

7.3.1.3. Debris cover

Other than the discrete supraglacial ridges described in *7.3.1.2.*, surface debris cover on the lower tongue is focused within medial moraines and at the lateral margins and foremost ~300 m of the glacier, which is entirely debris-covered (Figs 7.1b, 7.3 and 7.9a). The debris cover thickness ranges from ~1-50 cm across the glacier and is typically <10 cm. The majority of this debris cover is composed of poorly-sorted sediment ranging from coarse sand to large boulders (~1 m diameter), with a large proportion of angular to very angular clasts (Fig. 7.9b). A large range of lithologies are evident, including sandstones, siltstones and shales; the sandy matrix is predominantly derived from black shale, giving a dark colouring to the debris cover (Figs 7.9a-c). Many of the larger clasts also display evidence for oxidised weathering on at least one face in the form of browny-orange surface layers. This material is very poorly-consolidated and forms an irregular surface, and the general debris cover is superimposed by several of the types of supraglacial ridge described in *7.3.1.2.* (Fig. 7.3). This is particularly apparent at the debris-covered front, which slopes gently in a downglacier direction for much of its length, before steepening at the distal margin down to the glacier foreland (Fig. 7.9a).

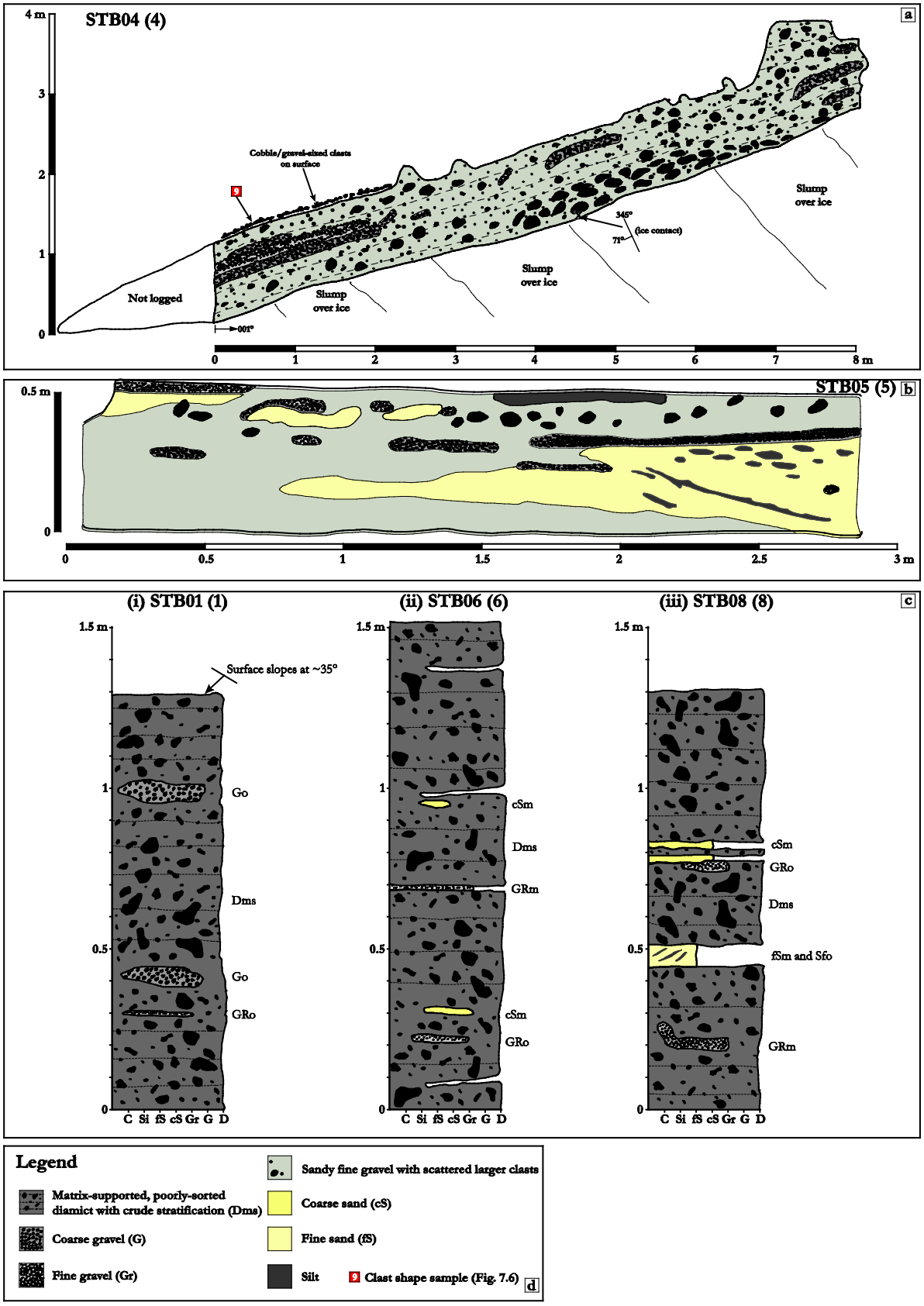
a
STB04 (4)
4 m
3
2
1
0
Cobble/gravel-sized clasts on surface
Slump over ice
345°
71°
(ice contact)
Slump over ice
Slump over ice
Not logged
001°
0 1 2 3 4 5 6 7 8 m
b
STB05 (5)
0.5 m
0
0 0.5 1 1.5 2 2.5 3 m
c
(i) STB01 (1)
(ii) STB06 (6)
(iii) STB08 (8)
1.5 m
Surface slopes at ~35°
Go
Dms
Go
GRo
cSm
Dms
GRm
cSm
GRo
cSm
GRo
Dms
fSm and Sfo
GRm
1
0.5
0
C Si fS cS Gr G D
Legend
Matrix-supported, poorly-sorted diamict with crude stratification (Dms)
Coarse gravel (G)
Fine gravel (Gr)
Sandy fine gravel with scattered larger clasts
Coarse sand (cS)
Fine sand (fS)
Silt
Clast shape sample (Fig. 7.6)
d

Figure 7.7

Figure 7.7 (preceding page) – Two-dimensional sediment logs. (a) Section STB04: exposure in a type C ridge located at the western margin of the debris-covered glacier front. See Figs 7.6e and 7.6f for photographs. (b) Section STB05: exposure of sand and gravel located close to the lake on eastern side of debris-covered glacier front. See Fig. 7.9g for photograph. (c) Vertical logs. (i) Section STB01: exposure in eastern side of 1930s surge ridge close to main channel breach. See Fig. 7.10e for photograph. (ii) Section STB06: sediments above ice core exposed in eastern lateral moraine. See Fig. 7.10g for photograph. (iii) Section STB08: exposure within headwall scarp of active debris flow on western side of glacier foreland. See Figs 7.11g and 7.11h for photographs. Numbers in brackets after section names refer to numbered locations on Fig. 7.3.

These debris flows are characterised by smooth, often saturated low-angle surfaces which have lobate margins and typically emanate from headwall scarps. Similar features are also found within the glacier foreland (*7.3.2.2.*).

The thin cover of predominantly angular material described above characterises the general debris cover across most of the glacier, including at the front, the lateral margins and within medial moraines; this material is also very similar to that within type A supraglacial ridges described below in *7.3.1.2.* One area that differs from this is at the eastern margin of the debris-covered front, adjacent to and immediately upglacier from a large supraglacial lake (Figs 7.3 and 7.9d), where the sediment cover is primarily composed of sorted sands and fine gravel (Figs 7.9e-g and 7.7a). Debris-covered ice slopes gently beneath the lake (Figs 7.9d and 7.9e), indicating it is supraglacial rather than ice-marginal, and it is fed by both the eastern (subglacial at point of entry) and a branch of the western (supraglacial at point of entry) lateral channels. The western branch cuts across the debris-covered front, indicating a change in drainage configuration since previous studies (Hodgkins *et al.*, 1998; Sletten *et al.*, 2001); the lake was also not present at these times. The lake level was observed to fluctuate ~0.5-1 m over multiple visits in August 2011 and it drains to the foreland via the main channel (Fig. 7.9c).

The area of sorted sands and fine gravel which borders the lake covers underlying ice to a depth of ~0.5 m and in section displays several types of lithofacies. The surface of this area is ~5 m above the lake level and is generally flat-topped, apart from where there are small gullys, and is steep-sided adjacent to the lake. At the lake margin, the sediments are poorly-consolidated and typically saturated, and there are several low-gradient fans that extend down to the water, often with a dark colouring indicating a high content of black shale (Fig. 6.4e). Approximately 3-4 m above the lake, there is an exposure of laminated fine and coarse sand with occasional fine gravel layers (Fig. 7.9f). This sediment is consolidated and the layers dip at ~19º; a maximum dip of 55º was recorded close to the example in Figure 7.9f. Nearby, at a position ~50 m upglacier from the lake, a narrow gully has exposed sediments within a flat-topped part of the area of sands and gravel, logged as section STB05 (Figs 7.9g and 7.7a). This section comprises a matrix of massive coarse sand and fine gravel of approximately equal proportions, within which there are small (~10 cm thick) lenses of fine sand, fine gravel (2-4 mm) and coarse gravel (>4 mm) and scattered cobble-sized edge-rounded clasts (Fig. 7.7a).

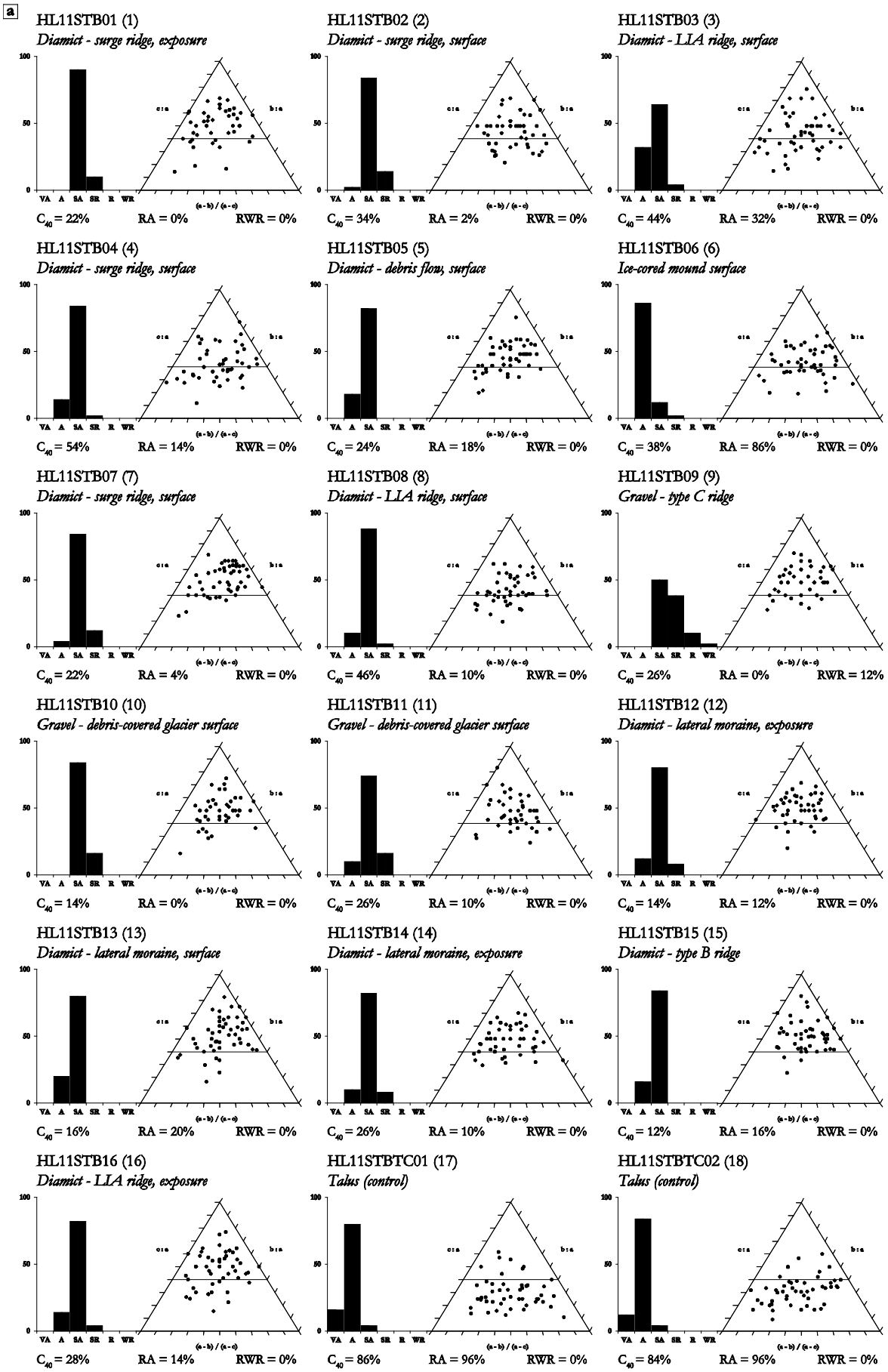
a
HL11STB01 (1)
Diamict - surge ridge, exposure
C40 = 22% RA = 0% RWR = 0%
HL11STB02 (2)
Diamict - surge ridge, surface
C40 = 34% RA = 2% RWR = 0%
HL11STB03 (3)
Diamict - LIA ridge, surface
C40 = 44% RA = 32% RWR = 0%
HL11STB04 (4)
Diamict - surge ridge, surface
C40 = 54% RA = 14% RWR = 0%
HL11STB05 (5)
Diamict - debris flow, surface
C40 = 24% RA = 18% RWR = 0%
HL11STB06 (6)
Ice-cored mound surface
C40 = 38% RA = 86% RWR = 0%
HL11STB07 (7)
Diamict - surge ridge, surface
C40 = 22% RA = 4% RWR = 0%
HL11STB08 (8)
Diamict - LIA ridge, surface
C40 = 46% RA = 10% RWR = 0%
HL11STB09 (9)
Gravel - type C ridge
C40 = 26% RA = 0% RWR = 12%
HL11STB10 (10)
Gravel - debris-covered glacier surface
C40 = 14% RA = 0% RWR = 0%
HL11STB11 (11)
Gravel - debris-covered glacier surface
C40 = 26% RA = 10% RWR = 0%
HL11STB12 (12)
Diamict - lateral moraine, exposure
C40 = 14% RA = 12% RWR = 0%
HL11STB13 (13)
Diamict - lateral moraine, surface
C40 = 16% RA = 20% RWR = 0%
HL11STB14 (14)
Diamict - lateral moraine, exposure
C40 = 26% RA = 10% RWR = 0%
HL11STB15 (15)
Diamict - type B ridge
C40 = 12% RA = 16% RWR = 0%
HL11STB16 (16)
Diamict - LIA ridge, exposure
C40 = 28% RA = 14% RWR = 0%
HL11STBTC01 (17)
Talus (control)
C40 = 86% RA = 96% RWR = 0%
HL11STBTC02 (18)
Talus (control)
C40 = 84% RA = 96% RWR = 0%

Figure 7.8

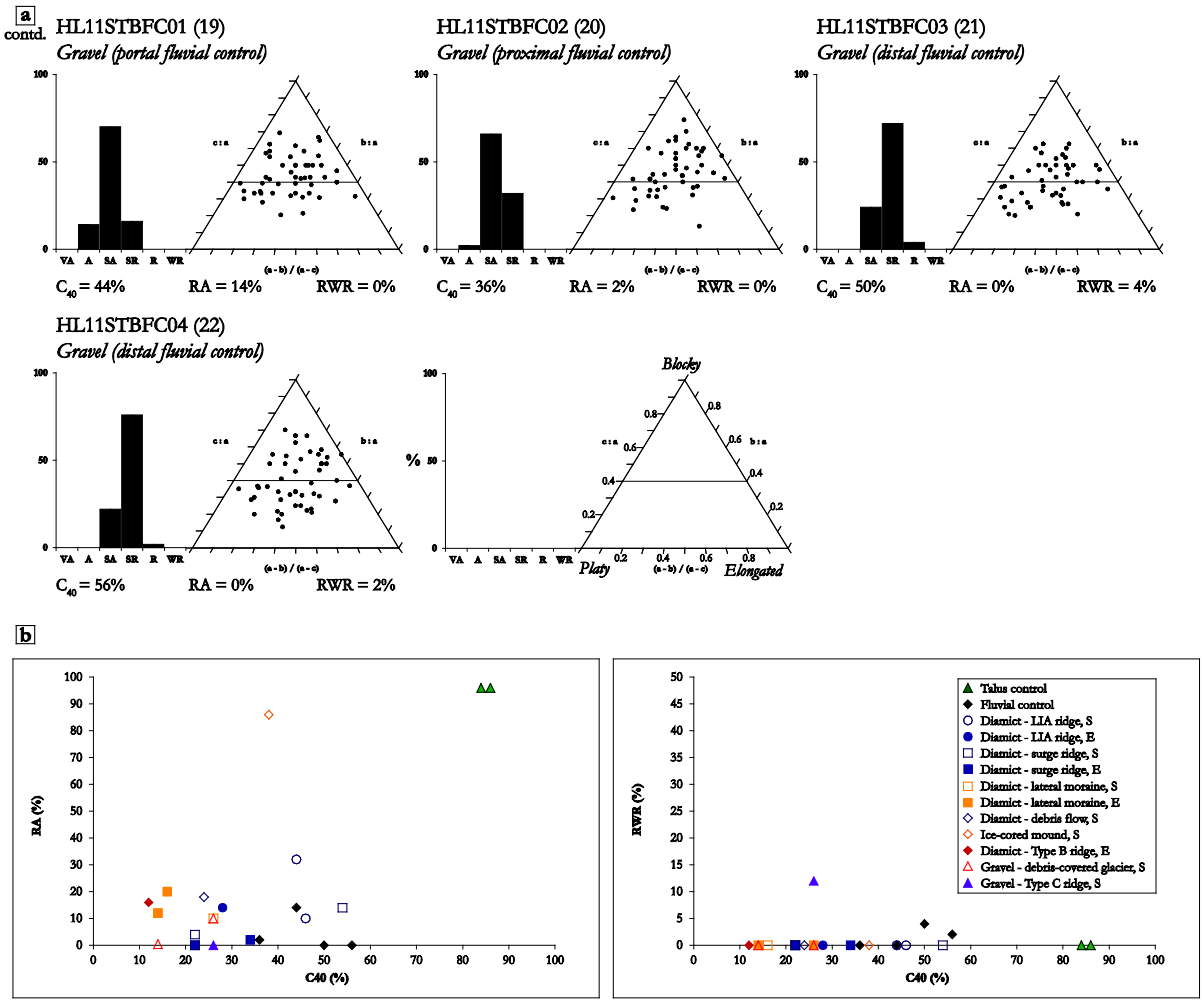

Figure 7.8 (this and preceding page) – (a) Clast shape data plotted on histograms (roundness) and ternary diagrams (shape). Each sample is of 50 sandstone clasts. Numbers in brackets refer to numbered locations on other figures. (b) RA-C_{40} (left) and RWR-C_{40} (right) diagrams.

Within the ~35 cm thick layer of massive fine sand towards the right-hand end of the section there are several thin (~10 cm) beds of coarse sand derived from black shale (Figs 7.9g and 7.7a). Several of these layers extend for tens of centimetres and dip at ~30º towards the right-hand end of the section (aligned with the long profile of the gully); these are identified as foresets. The surface of the exposure contains some small areas of silt amongst the general composition of sand and gravel (Fig. 7.7a), with a higher proportion of coarse gravel and cobble-sized clasts. Clast shape samples HL11STB10 and 11 were taken from the surface of this section and nearby (Fig. 7.8a).

7.3.2. Glacier foreland

The proglacial area can be broadly separated into latero-frontal ridges, typically of high-relief (~10-60 m), and low-relief areas of hummocky topography, outwash fans and numerous low-angle debris flows (Fig. 7.3). Two main latero-frontal ridges can be identified (Fig. 7.10a); the outermost of these represents the LIA maximum of Scott Turnerbreen, and the inner ridge was

formed by the 1930s surge (Sletten *et al.*, 2001). These merge upglacier and grade into high-relief lateral moraines which reach up to 60 m above the glacier surface and extend for ~3 km. The low-relief hummocky topography can be sub-divided into (i) a small zone between the two latero-frontal ridges; and (ii) a larger zone between the (inner) surge ridge, the debris-covered glacier front and the lateral moraines (Fig. 7.3). These zones contain several isolated hummocks or ridges; buried ice blocks; debris flows (see *7.3.2.2.* and Fig. 7.11); outwash deposits located both adjacent to the main meltwater channel and as individual fans, such as at the eastern side of the debris-covered front; and numerous smaller channels which are sourced from the lateral moraines and valley sides.

The isolated hummocks and ridges include a prominent mound located on the ice proximal side of the surge ridge, marked with an X in Figure 7.10h. This mound is steep-sided (~40^{o}), aligned perpendicular to the main channel and is composed of very poorly-consolidated angular and very angular material ranging from coarse sand to boulders of almost entirely green sandstone (Fig. 7.8a). Surface tension cracks are abundant and many of the clasts are covered by an oxidised weathering layer and evidence for frost-shattering. The angularity and dominant lithology of this material has a restricted distribution around the mound and contrasts with the general composition of the surrounding foreland. This feature was labelled 'ice-cored mound' in Sletten *et al*. (2001). In general, isolated hummocks and ridges display a variety of orientations across the foreland, with very little apparent linearity. One example where closely-spaced ridges do follow similar alignments is close to the western side of the main channel, on the distal side of the large active debris flow; here, four low-relief (<1 m) curvilinear ridges are nested inside each other (Figs 7.3 and 7.10h).

The main meltwater channel follows the centre of the foreland at its lowest point and breaches both the surge and LIA ridges before draining beyond the Rieperbreen ridges (Lyså and Lønne, 2001) and along Bolterdalen (Figs 7.1 and 7.3). The outwash corridor surrounding the channel expands to ~50 m wide immediately after the breach through the surge ridge. Beyond the LIA ridge, terraces ~1-1.5 m above the channel can be identified within the outwash, and these grade into the lateral channels which trace the distal side of the LIA ridge on both sides. These lateral channels are characterised by oversized outwash corridors containing small streams which, based on the clear water, are primarily sourced from the valley sides rather than a meltwater origin. Several similar oversized outwash corridors are evident within the inner part of the foreland, particularly at the debris-covered glacier front where a 10 m wide corridor containing frequent large edge-rounded boulders, but only a small stream, extends from the area of sands and gravels and feeds an inactive outwash fan (Fig. 7.3). In several places along the main channel, ice blocks overlain by stratified sands and gravels were observed. Extensive low-angle, well-vegetated surfaces are located immediately downvalley from the outermost LIA ridge on both sides at a height of ~5-10 m above the active channel (mapped as 'alluvium' in Fig. 7.3).

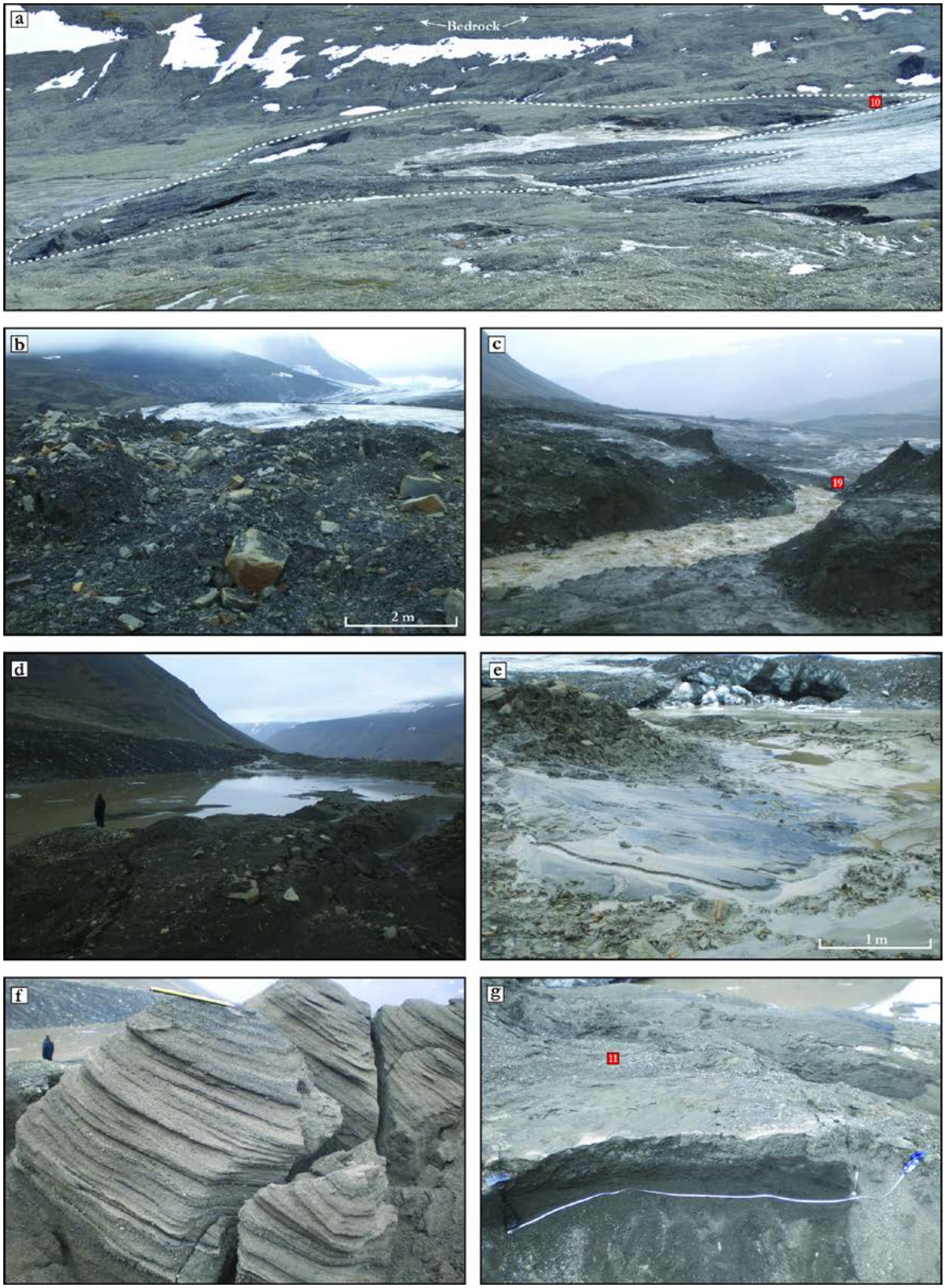

Figure 7.9 – Debris cover on the glacier surface. Numbered locations refer to clast shape samples in Fig. 7.8a. (a) Debris-covered glacier front in August 2012 delimited by dashed white line. Note meltwater-fed lake on surface. (b) Angular material within debris-covered glacier front. Note wide range of grain sizes. View is upglacier. (c) Main meltwater channel cutting down through debris-covered glacier front. Note active debris flows on both side of channel. (d) Detail of lake on debris-covered glacier surface shown in (a). (e) Deltaic sediments feeding into lake shown in (d). (f) Laminated sands and fine gravel close to lake. Individual layers dip at ~20º. (g) Exposure of sand and gravel close to lake logged as section STB05 (Fig. 7.7a).

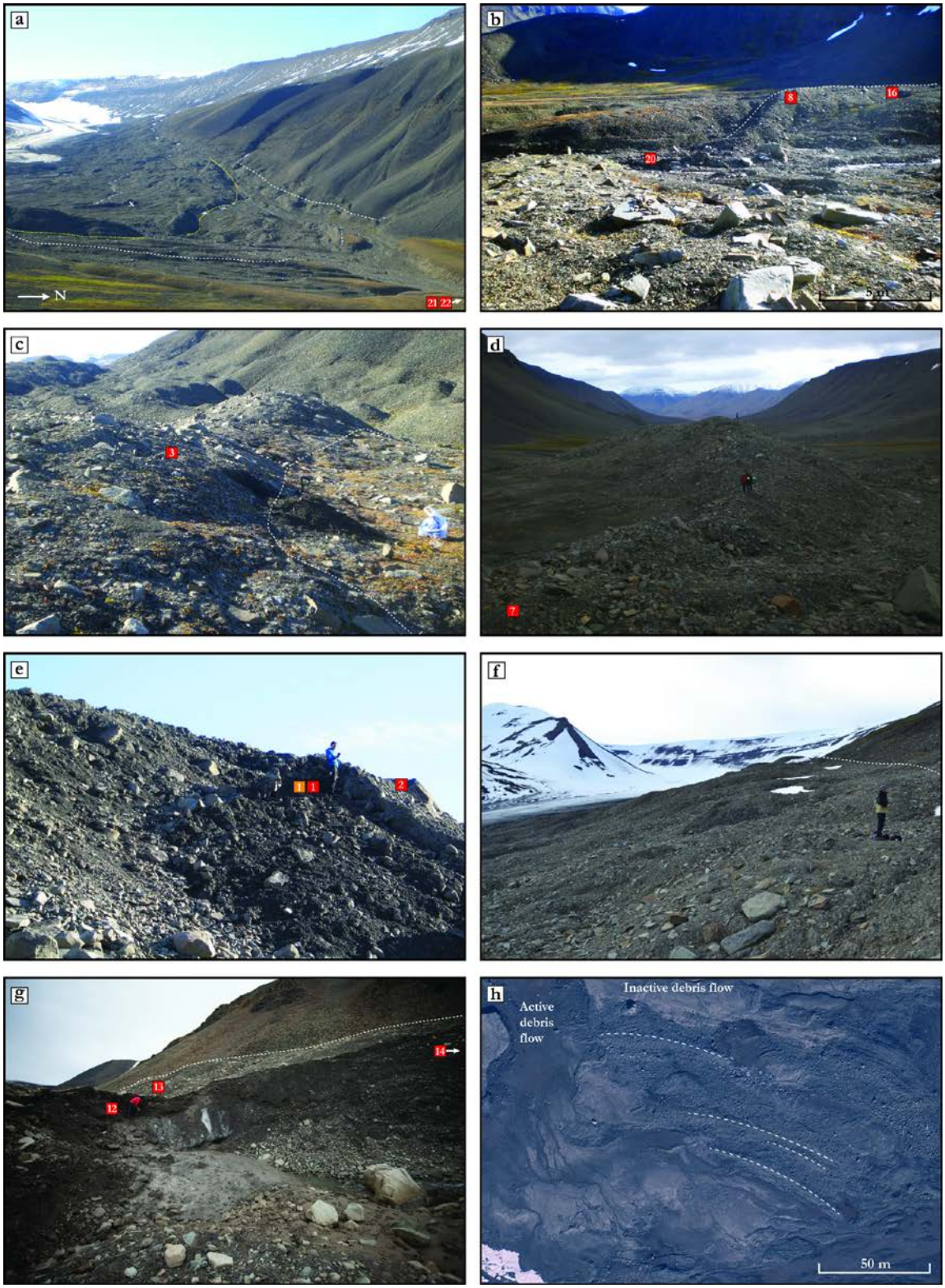
a
N
21 22
b
8
16
20
5 m
c
3
d
7
e
1 1
2
f
g
14
13
12
h
Inactive debris flow
Active
debris
flow
50 m

Figure 7.10

Figure 7.10 (preceding page) – Examples of ridges and other geomorphology on glacier foreland. Numbered positions refer to grain size distribution (orange) and clast shape (red) samples in Figs 7.5a and 7.8a. (a) Overview of latero-frontal ridges. LIA (white dashed line) and 1930s surge (yellow dotted line) ridges are highlighted. White X marks prominent mound. (b) LIA ridge on eastern side of channel. White dashed line delimits boundary between ridge and alluvial surface. (c) LIA ridge on western side of channel. Note how ridge (left) is draped on an alluvial surface (right); the boundary between the two is delimited by the white dashed line. (d) 1930s surge ridge on eastern side of foreland. Note smooth surface of a debris flow in an ice proximal position. (e) Exposure in 1930s surge ridge on eastern side, immediately above channel breach through the ridge. See Fig. 7.7ci for section log. (f) Lateral moraine on western side of glacier. (g) Exposure of ice core in lateral moraine on eastern side of foreland. White dashed line delimits boundary between ridge and talus slope. See Fig. 7.7cii for section log. (h) Nested low-relief curvilinear ridges on centre of glacier foreland. 2009 aerial photograph acquired from NPI (©Norsk Polarinstitutt).

Excavations within this surface revealed shattered shale bedrock, exposed in the channel sides, overlain by a silt-rich deposit containing scattered rounded and well-rounded clasts, and a surface covering of angular and very-angular clasts. Sletten *et al.* (2001: p. 276) described a "heavily disintegrated marginal moraine" on this surface, which was interpreted as a pre-LGM position of the glacier; however, detailed investigation in this study on both sides of the valley could find no evidence to support this.

7.3.2.1. Latero-frontal ridges and lateral moraines

LIA ridge

This is composed of several fragmentary ridges on both sides of the main channel which together create a slightly irregular lobate form (Fig. 7.3). The frontal ridges on the eastern and western sides are both draped on the ice proximal side of smooth, flat-topped surfaces which are well-vegetated and contain a number of angular to sub-angular boulders (Figs 7.10a-c). The contrast in morphology and vegetation cover between the LIA ridges and the vegetated surfaces is very distinct (Figs. 7.10a-c), indicating that this marks the LIA limit of Scott Turnerbreen. These surfaces are similar in character to the low-angle, vegetated valley side deposits located immediately downvalley, but are separated from these by lateral outwash corridors. On the eastern side of the main channel, the vegetated surface has been dissected by several channels (Fig. 7.3).

The LIA ridges are ~5-10 m in height above the main channel and are well-consolidated, with only occasional surface tension cracks visible. Slope angles on both the distal and proximal sides are typically ~30º. Exposures excavated into the ridges on both sides of the channel revealed crudely-stratified and poorly-sorted silt-rich diamict with grain sizes ranging up to large edge-rounded surface boulders (1 m diameter; 7.10c). Three clast shape samples taken from the surface (HL11STB03, HL11STB08) and an exposure (HL11STB16) show a predominance of sub-angular clasts (Fig. 7.8a) and C_{40} indices of 28-46% (Fig, 7.8b); 6% of clasts displayed bullet-shaped morphologies and a number were striated. A mix of lithologies

were observed, with green sandstone (selected for clast shape samples) comprising ~10% on the western side and ~20% on the eastern side. On the western side, the frontal LIA ridge is separated from lateral ridges by the eastern lateral outwash corridor (Fig. 7.3). The lateral ridges have a rounded morphology and mark the transition to the valley side and large talus fans, which have in places overtopped the ridges, creating a surface covering of angular material; this is also found on the eastern side of the valley. The lateral ridges appear to extend slightly further downvalley than the main frontal ridge on the western side, producing a slightly irregular margin (Figs 7.3 and 7.10a).

Surge ridge

This is a prominent high-relief latero-frontal ridge located ~200 m upglacier from the LIA ridge (Figs 7.3 and 7.10a). The area between the two is characterised by low-relief hummocky topography, isolated ridges aligned sub-perpendicular to the latero-frontal ridges and multi-tiered debris flows (*7.3.2.2.*), and is bisected by the main meltwater channel and associated outwash deposits. The surge ridges are up to 30 m high in a frontal position (Fig. 7.10d) and have typical slope angles of ~40º on both distal and proximal sides. The surge ridge is more-continuous than the LIA ridge and extends largely intact for ~1 km on both sides of the foreland, where it grades into the lateral moraine. Other than the main meltwater channel breach, there are two prominent gaps in the surge ridge: on the western side, where an inactive debris flow cuts through and extends to the zone between the latero-frontal ridges; and on the eastern side close to where the LIA and surge ridges merge at the valley side (Fig. 7.3).

Surface tension cracks are frequently observed, both in frontal and lateral positions, and there are several places where de-stabilised slopes have collapsed, exposing poorly-consolidated sediments; one example of this is section STB01 (Fig. 7.7ci) within the eastern ridge, above the main meltwater channel breach (Fig. 7.10e). The sediment composition is similar to that within the LIA ridge: poorly-sorted silt-rich diamict with grain sizes ranging up to edge-rounded boulders (Figs 7.7ci and 7.10e). The polymodal grain size distribution of the fraction <1 mm sampled from section STB01 is shown in Figure 7.5b. Within the diamict, which is very crudely stratified, there are thin (<10 cm) discontinuous layers of well-sorted fine and coarse openwork gravel which are devoid of fines apart from silt coatings in individual clasts (Fig. 7.7ci). These layers are aligned parallel to the surface of the ridge, which slopes at ~35º down to the main channel (Fig. 7.10e). Four clast shape samples taken from the surface of the surge ridge on both sides of the foreland (HL11STB02, HL11STB04, HL11STB07) and from within STB01 (HL11STB01) show a predominance of sub-angular clasts (Fig. 7.8a) and C_{40} indices between 22-54% (Fig, 7.8b). A mix of lithologies is apparent, with green sandstone visibly more abundant than on the LIA ridge and comprising ~25%. Twenty percent of clasts had bullet-shaped morphologies and a number were striated. Several inactive multi-tiered debris flows are

sourced from the distal and proximal slopes of the surge ridge on both sides of the main channel (Figs 7.3 and 7.11) and these are described in *7.3.2.2.*

Lateral moraines

The latero-frontal ridges grade into continuous high-relief ice-cored lateral moraines, the uppermost limits of which demarcate the boundary with the valley side (Fig. 7.10f). The lateral moraines have a hummocky morphology and in places individually-discernible ridges delimit the transition to the valley side, although often this is only marked by a single break-of-slope. Buried ice is observed in several places on the eastern lateral moraine, most notably where several channels have eroded the sediment cover (Fig. 7.10g). One such exposure (section STB06) is located ~5 m below the crest of the lateral moraine, where a small, highly-saturated active debris flow has exposed a block of opaque ice >4 m thick. This is covered by 1-2 m of poorly-sorted, crudely-stratified, matrix-supported diamict (Figs 7.7cii and 7.10g), interspersed with thin (~1-2 cm) horizontally-bedded silt-rich layers and discontinuous coarse sand and fine gravel layers (Figs 7.7cii). A small channel sourced from the valley side flows into the debris flow, where it forms a small pool before appearing to drain beneath the ice block (Fig. 7.10g). A number of similar active and inactive debris flows have also reworked material within the western lateral moraine, in places extending down to the debris-covered glacier surface (Fig. 7.3). Bedrock is exposed within the eastern lateral moraine in the form of sub-horizontal strata (Figs 7.3 and 7.9a).

Clast shape samples (Fig. 7.8a) were taken from within (HL11STB12) and the surface (HL11STB13) of section STB06, and from ~100 m upglacier within another exposure in the eastern lateral moraine (HL11STB14). These show a predominance of sub-angular clasts, with a slightly higher proportion of angular clasts within the surface sample (HL11STB13). Approximately ~20% of the clasts had bullet-shaped morphologies and many displayed striations. The uppermost parts of the lateral moraines on both sides typically contain a surface cover of angular to very angular large clasts and boulders (Fig. 7.10f).

7.3.2.2. Debris flows

Numerous debris flows are evident across the glacier foreland and lateral moraines and these can be classified as either stable and inactive or highly-saturated and active (Fig. 7.3). Inactive debris flows are distributed across this area, whereas active debris flows are concentrated on or immediately adjacent to the debris-covered glacier front and lateral moraines; a higher density of both are found on the western side of the foreland than the eastern side (Fig. 7.3). Individual debris flows range in length and width from ~2-3 m up to hundreds-of-metres. The inactive debris flows are characterised by smooth, low-angle (~1-15^{o}) lobate surfaces containing very few visible larger clasts (Figs 7.11a-f). The debris flows are often multi-tiered, with each step recording an elevation change of ~0.5-2 m (Figs 7.3 and 7.11d-f). The transition between steps

occurs as both near-vertical headwall scarps and low-angle lobes; headwall scarps are most common at the onset of active debris flows (e.g. Fig. 7.11g). Several inactive multi-tiered debris flows are sourced from the ice proximal slope of the surge ridge and descend inwards towards the main channel (Figs 7.3, 7.10d and 7.11e). There are also two examples on the distal side of the western surge ridge; a multi-tiered flow extending from the ridge down to the level of the main channel (Fig. 7.11d) and a debris flow sourced from the ice proximal hummocky topography which breaches the ridge (Fig. 7.3).

The inactive debris flows are typically composed of an upper ~5-10 cm silt-rich cap with occasional scattered clasts (Fig. 7.11h) which overlies poorly-sorted and crudely-stratified diamict, as exposed within the scarp headwall of a large active debris flow close to the debris-covered glacier front on the eastern side (section STB08; Figs 7.7ciii and 7.11g). Thin (~1-2 cm) horizontally-layered lenses and discontinuous layers of coarse sand and fine gravel and a thicker (~8 cm) layer of structureless fine sand are present within the diamict. Thin dipping structures of black shale within the fine sand may represent foresets. This is similar to descriptions of inactive debris flow headwall sediments in Sletten *et al.* (2001), although in this study no sedimentary structures (e.g. ripple cross lamination) could be determined from the sand and gravel layers and no evidence was found to suggest the diamict should be sub-divided into two separate units (e.g. units 1 and 3 in Sletten *et al.*, 2001). Some inactive debris flows also contained clay-rich areas associated with the former location of pools (Fig. 7.11f), such as those shown on the surface of a flow in Figure 7.11c. A clast shape sample (HL11STB05) taken from the surface of the multi-tiered flow on the proximal side of the western surge ridge (Figs 7.3 and 7.11e) contained predominantly sub-angular clasts (Fig. 7.8a), of which 16% were bullet-shaped and a number were striated.

Active debris flows typically emanate from sub-vertical headwall scarps (Fig. 7.11g) and are sourced from (i) the frontal slope of the debris-covered glacier, particularly where the main channel cuts through (Fig. 7.9c); (ii) steeply sloping lateral moraines (Figs 7.3 and 7.10g); and (iii) inactive debris flows (Figs 7.11g and 7.11h). The largest active debris flow is located immediately distal to the debris-covered front and emanates from a ~1.5 m high headwall scarp cut into a series of inactive flows (Figs 7.3 and 7.11g). This flow extends for ~200 m and terminates as a splayed lobe adjacent to the main meltwater channel. The debris within the flow is highly-saturated and similar in consistency to the slurry that emanates from type B supraglacial ridges (Fig. 7.6c); this probably corresponds to *type II flows* as classified by Lawson (1982). Levees of coarser material are visible at the edges of the active debris flows and small surface pools are common (Fig. 7.11g). Large grounded boulders within the flow indicate typical depths of ~0.5 m in the centre.

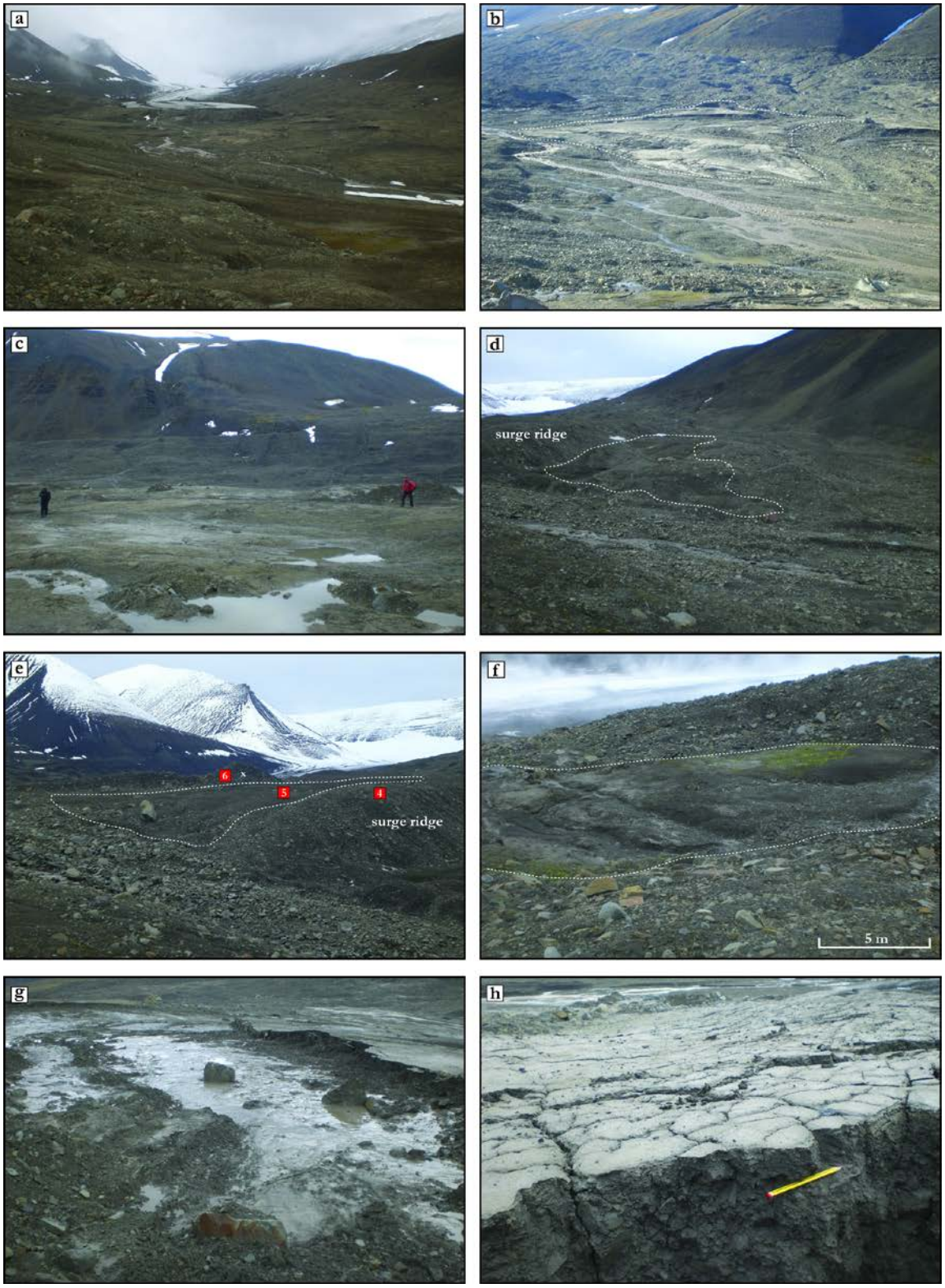

Figure. 7.11 – Examples of debris flows. Numbered positions refer to clast shape samples in Fig. 7.8a. (a) Overview of inner part of the foreland. Note smooth surfaces of several debris flows on both side of main channel. (b) Large multi-tiered debris flow on western side of foreland; flow is ~200 m wide. (c) Smooth surface of debris flow on western side of foreland. Note small pools in minor depressions. (d) Multi-tiered debris flow on distal side of 1930s surge ridge; flow is ~60 m wide. (e) Multi-tiered flow on proximal side of 1930s surge ridge. White X indicates prominent mound. (f) Smooth surface of debris flow on western side of foreland. (g) Active debris flow on western side of foreland. Note scarp cut into older debris flow surface. (h) Detail of active debris flow scarp shown in (g). See Fig. 7.7ciii for section log of headwall sediments at this location.

7.4. Interpretation

7.4.1. Structural formation of Scott Turnerbreen

Stratification (S_0) and longitudinal foliation (S_1)

S_0 and S_1 structures have been mapped as separate features, but it is suggested that these probably represent two end-members of the same structure rather than distinct features. Stratification (S_0) is formed through firnification processes in the accumulation area and represents the primary structure within the glacier. The alternating bubble-poor and bubble-rich layers, observed both within englacial ice and as colour changes on the surface, reflect seasonal variations in these processes (cf. Hambrey, 1975; Hambrey and Dowdeswell, 1997; Hambrey *et al.*, 2005). When it initially forms, this layering is likely to be broadly horizontal and display only slight undulations related to the formation of seasonal snow layers, but will become progressively deformed and folded as the result of flow from the accumulation area. Folds increase in tightness as the ice converges in the narrow confines of the lower glacier tongue and is subjected to lateral compression. Eventually the original layering (S_0) is folded to such an extent that the limbs become isoclinal and parallel to glacier flow. Where the hinge lines of the isoclinal folds intersect the glacier surface, they form linear stripes, mapped as longitudinal foliation or S_1 structures (e.g. Hambrey and Dowdeswell, 1997; Hambrey and Glasser, 2003; Roberson and Hubbard, 2010). S_1 are focused within the eastern and western flow units, which are easily-identifiable due to these concentrations and slight differences in their orientations (Fig. 7.3). Within the western flow unit, which comprises the majority of the lower glacier tongue, two main zones of S_1 are apparent and these converge towards each other in a central area (Fig. 7.3). This convergence represents a distortion of S_1, which are otherwise strongly aligned parallel to ice flow within the two flow units. Similarly-distorted flow lines are apparent on the 1961 aerial photograph (Sletten *et al.*, 2001), when Scott Turnerbreen was still close to the maximum position of the ~1930s surge; these are interpreted as an artefact of dynamic ice flow associated with the surge (Hambrey *et al.*, 2005).

Arcuate fracture traces (S_2)

These are interpreted as shear planes associated with longitudinal compression based on similarities with features observed at Tellbreen (*Chapter 8*) and in previous studies (Hambrey *et al.*, 2005; Roberson and Hubbard, 2010). The densest concentration of S_2 is on the lowermost part of the tongue (Fig. 7.4b), where the mapping shows they are typically aligned sub-parallel and occasionally intersect each other; this is consistent with their formation under conditions of flow compression near the front of the glacier. It seems very unlikely that shear planes are still active within Scott Turnerbreen given its current cold-based and near-stagnant flow conditions (Hodgkins *et al.*, 1999) and the high compressive stresses which are necessary to form them. The presence of S_2 therefore provides compelling evidence that the glacier has been much more dynamic and subjected to high strain rates in the past (cf. Hambrey *et al.*, 2005). The formation

of shear planes in polythermal glaciers is often suggested to occur at the thermal transition between active warm-based ice and inactive cold-based ice at the margin (King *et al.*, 2008), where compressive stresses might be expected to be highest. However, the validity of this was questioned by Moore *et al.* (2010, 2011), who found no evidence for a sharp slip/no-slip boundary at the thermal transition within Storglaciären, Sweden, and suggested that longitudinal compression at this boundary may be insufficient to generate compressive fractures. Moore *et al.* (2010) proposed that the required conditions for compressive fracturing are likely to be met only by thin (but actively flowing) glaciers subjected to high compressive stresses and with an abundance of pre-existing weaknesses, which characterises a surge-type glacier in its active phase. The necessary high compressive stresses would be generated at the transition between areas of extremely weak bed, facilitated by high subglacial water pressures, where ice is actively surging, and inactive, non-surging ice towards the glacier margin.

Fracture traces (S_3)

S_3 structures cut across all other structural elements and are interpreted as healed fractures or crevasses, commonly termed crevasse traces (Hambrey, 1976; Huddart and Hambrey, 1996; Hambrey and Dowdeswell, 1997; Glasser *et al.*, 1998b). Both mapped and measured fracture traces display a wide range of orientations (Figs 7.3 and 7.5a) with many aligned sub-perpendicular to or offset by ~45º from ice flow and S_1 longitudinal foliation, which is consistent with crevasses formed through longitudinal extension during a surge (Hodgkins and Dowdeswell, 1994; Lawson *et al.*, 1994). Similarly-oriented open crevasses can be identified in the upper basins and at the lateral margins of Scott Turnerbreen in the 1961 photograph (Sletten *et al.*, 2001), ~30 years after the surge, which suggests either (i) crevasse healing rates at Scott Turnerbreen took significantly longer than the ~5-10 years reported by Dowdeswell *et al.* (1991) from other Svalbard surging glaciers; or (ii) parts of the glacier were still experiencing dynamic flow in 1961. The dense population of crevasse traces on the lower tongue suggests that the glacier has been heavily crevassed, since when the crevasses have closed and been transported passively downglacier as crevasse traces (e.g. Hambrey *et al.*, 2005). S_3 crevasse traces appear to cut across S_2 shear planes in many places on the structural map (Fig. 7.3), suggesting that the ice underwent compressive flow followed by extension, which is consistent with the downglacier passage of a surge front or kinematic wave (cf. Lawson *et al.*, 1994).

Open fractures (S_4)

The open fractures visible on the eastern side of the lower tongue can be linked to the position of both former and active meltwater channels, rather than crevassing associated with current ice flow dynamics. The arcuate series of open fractures which extend towards the glacier centre follow a similar alignment to a supraglacial channel seen on both the 1961 and 1990 aerial photographs (Sletten *et al.*, 2001), suggesting that the present-day fractures may represent the

incomplete closure of the roof of a channel which has evolved through cut-and-closure processes (Gulley *et al.*, 2009a). This series of fractures contains three traceable strands, indicating that the channel has evolved laterally as well as vertically. The fracture closest to the debris cover on the eastern side originates where the active lateral channel disappears under the ice and can be traced towards the supraglacial lake, where the channel re-emerges; this suggests that this fracture may be the surface expression of the en-/subglacial component of the active channel.

7.4.2. Supraglacial ridge formation and sediment delivery

Type A ridges

These are inferred to originate as rockfall from extraglacial sources onto the glacier surface which becomes buried within stratification (S_0) in the accumulation basins (Hambrey and Glasser, 2003; Roberson and Hubbard, 2010). As stratification flows into the narrower channel of the lower tongue it experiences lateral compression and is tightly folded, including the layers of rockfall debris. Where the hinge line of a tightly folded debris-rich layer melts out on the glacier surface, it forms a flow-parallel supraglacial ridge. Several lines of evidence lend support to this interpretation: (i) type A ridges are composed of predominantly angular and very angular weathered debris with a limited range in lithologies (commonly black shale and green sandstone), which is consistent with rockfall derived from the headwalls in the accumulation area; (ii) the ridges have similar orientations as, and in places appear continuous with, longitudinal foliation (S_1), indicating a similar process of formation; and (iii) the distribution of ridges on the lowermost part of the tongue is consistent with buried debris being transported downglacier along flow lines and melting out as the ice front thins (Hodgkins *et al.*, 1999). This interpretation is broadly in agreement with that of Sletten *et al.* (2001) for the formation of type A ridges. The observed differences in ridge orientation are due to their study focusing on type A ridges that form the lobate fronts of the western and eastern flow units, which are therefore concentric in shape and aligned parallel to the ice front (Sletten *et al.*, 2001). Since their study, the terminus has retreated ~500 m and the individual ridges which form the frontal lobes of the flow units have melted out entirely; the nested curvilinear ridges on the foreland represent the proglacial remnants of these (Fig. 7.3). As these ridges are derived from structurally-controlled supraglacial debris, and still preserve the linearity inherited from the pattern of type A ridges, they are a clear example of controlled moraines (cf. Evans, 2009).

The similar sediment composition of type A ridges and the general debris cover at the front indicates that they play an important role in sediment delivery to the terminus. This is clearly demonstrated by the fact that the area where the western part of the debris-covered front is today is almost entirely debris free in the 1990 aerial photograph (Sletten *et al.*, 2001). The widespread cover is likely to result from re-distribution of the material that melts out on the

surface as type A ridges, which is subsequently mobilised through a combination of meltwater destabilisation and gravitational processes (Lukas *et al.*, 2005; Kirkbride and Deline, 2013).

Type B ridges

The sediment composition of type B ridges (poorly-sorted diamict, edge-rounded clasts, bullet-shaped morphologies, striae) is consistent with subglacially-transported material (Benn and Ballantyne, 1994; Benn and Evans, 1996; Evans *et al.*, 2006a), indicating that they represent the melting-out of debris which has been elevated from the glacier bed. Two main mechanisms have been invoked in previous studies to explain such a process: debris incorporated along shear planes or thrusts which extend to the bed (Hambrey and Huddart, 1995; Huddart and Hambrey, 1996; Glasser *et al.*, 1998b; Hambrey *et al.*, 2005; Evans, 2009); and debris squeezed into basal crevasses (Sharp, 1985a; Evans and Rea, 1999; Woodward *et al.*, 2002; Rea and Evans, 2011). The glaciological structure of Scott Turnerbreen demonstrates that arcuate shear planes (S_2) and crevasse traces (S_3) are abundant (Fig. 7.3; *7.4.1.*), providing evidence that the glacier has been subjected to longitudinal compressional and extensional stresses in the past. Type B ridges are closely related to both S_2 and S_3 structures in terms of orientations, morphology and lengths. For example, the large curvilinear type B ridge in Figure 7.6c is very similar in shape to S_2 structures, suggesting that the debris has been elevated to the surface within a shear plane; and at the eastern margin of the glacier there are two type B ridges which are oriented perpendicular to S_2 structures but parallel to nearby S_3 crevasse traces (Fig. 7.3), indicating that subglacial debris has been incorporated into basal crevasses.

This demonstrates that subglacial debris has most likely been incorporated into englacial positions within Scott Turnerbreen via both (i) shear planes extending from the bed formed due to longitudinal compression; and (ii) injections of sediment into basal crevasses which opened due to extensional stresses. It is important to note that it is unlikely the debris and/or structures extended to the surface when they first formed, presumably at a time when the glacier was thicker and more dynamic than at present (e.g. during the 1930s surge). This may explain why no type B ridges (as identified in this study) are apparent on the 1990 NPI photograph and why no supraglacial ridges composed of subglacial material were mapped by Sletten *et al.* (2001); the lowermost tongue of the glacier has only recently thinned sufficiently enough to expose them on the surface. Sletten *et al.* (2001) inferred that their type B ridges, composed of <20 cm thick sandy gravels and oriented transverse to ice flow, were possibly formed in thrusts. Thicker (~0.5-1 m) ridges but with similar sediment compositions and orientations have been mapped as type C ridges in this study (see below).

Type C ridges

These are interpreted as meltwater-derived stratified sands and gravels deposited within (i) englacial meltwater channels; and (ii) crevasse systems, which have subsequently melted-out on

the glacier surface. A number of type C ridges are sinuous in planform and aligned sub-parallel to ice flow, which is consistent with meltwater deposited in englacial channels. In several places these ridges are draped on top of type A ridges (Fig. 7.3), indicating that the channels probably developed through cut and closure processes whilst type A ridges were still in an englacial position. This interpretation is in agreement with that of Sletten *et al.* (2001) for the formation of their type C ridges. Within the debris-covered glacier front, several type C ridges are oriented perpendicular and sub-perpendicular to ice flow and present-day supraglacial channels, are typically shorter in length, do not have a sinuous planform, and in at least one example intersect with each other at an oblique angle (Fig. 7.3). These are consistent with pressurised meltwater occupying a crevasse system, as has been suggested by Ensminger *et al*. (2001) and Evans and Rea (1999), and are therefore crevasse infillings. This process has been suggested by Evans and Rea (1999) for the formation of concertina or zig-zag eskers associated with surge-type glaciers. The density of S_3 fracture traces provides a strong indication that Scott Turnerbreen was formerly heavily-crevassed, presumably associated with the ~1930s surge; in combination with a highly-pressurised subglacial drainage system this could lead to the occupation of crevasses by meltwater. Support for this is provided by section STB04 (Fig. 7.7b), which is within a ridge that is aligned in a similar direction to nearby crevasse traces. The dip of bedding within this ridge is probably related to differential melting of the ice core beneath the sediments. Type C ridges, therefore, represent the deposition of glaciofluvial sediments either within englacial channels, e.g. sinuous eskers, or within crevasse networks, e.g. concertina eskers.

A crevasse-occupation origin for some type C ridges is preferred to the Sletten *et al.* (2001) thrust-related interpretation for characteristically similar ridges on the basis that (i) no evidence was found for fractured clasts or displacement within the sediment, suggested by Sletten *et al.* (2001) to be indicative of shearing; (ii) a variety of orientations are displayed, not only perpendicular to ice flow, and the ridges are typically short and straight rather than longer and arcuate, which is more characteristic of S_3 crevasse traces than S_2 shear planes (Fig. 7.3); and (iii) in at least one example, both subglacial sediment and stratified sands and gravels are found within the same ridge, which is ~5 m long and aligned at 45º to ice flow and is consistent with basal debris and meltwater occupying the same crevasse; it is hard to envisage this situation occurring within a thrust.

Type D ridges

These are interpreted as abandoned channel fills associated with the cut-and-closure formation of meltwater channels (Gulley *et al.*, 2009a). As the channels incise into the ice, sands and gravels, typically deposited on the inside of meander bends, are left behind (Lukas *et al.*, 2005). These eventually melt-out on the glacier surface, usually immediately adjacent to the supraglacial channel (Fig. 7.3).

7.4.3. Supraglacial lake evolution and kame topography

The area of flat-topped debris cover composed of sands and gravels at the eastern margin of the debris-covered front (Figs 7.3 and 7.7a) are consistent with sediments deposited in a lake (e.g. Benardout, in review), recording the evolution of the existing lake and the development of supraglacial kame topography (Brodzikowski and Van Loon, 1991; Schomacker and Kjær, 2008; Livingstone *et al.*, 2010b). The lake is ice-walled, as demonstrated by the gently-sloping debris-covered ice at the margins (Fig. 7.9d), and is formed by the ponding of meltwater from both the western and eastern lateral channels in a topographic depression on the glacier surface. The area of sands and gravels which borders the lake, mapped as lake sediments in Figure 7.3, contains several indicators that it was deposited within such a lake: (i) the dipping coarse sand layers at the true right-hand end of section STB05 (Figs 7.9g and 7.7a) are interpreted as foreset structures deposited as part of a deltaic sequence where a channel or re-worked sediment drained into the lake, such as shown in Figure 7.9e; (ii) the laterally-continuous, laminated fine sand, coarse sand and fine gravel layers (Fig. 7.9f) are consistent with regular sedimentation in a lake (Schomacker and Kjær, 2008) and are very similar to those exposed by low water levels within the current lake. The variety in grain sizes may record periods of low energy (Jopling and Walker, 1968; Ashley *et al.*, 1982) and higher energy, low density turbidity currents (Smith and Ashley, 1985; Livingstone *et al.*, 2010b), and the observed dip of the layers is a result of differential melting of underlying ice; and (iii) the flat-topped nature of the this area is consistent with deposition within ice-walled or supraglacial lakes (Mager and Fitzsimons, 2007; Clayton *et al.*, 2008). The inactive outwash corridor which extends from the eastern margin of the lake sediments represents the main drainage route from the former lake and is analogous to the main meltwater channel draining the current lake (Fig. 7.9c).

The development of an elevated flat-topped area of lake sediments adjacent to a lake-filled depression is the result of topographic inversion (Livingstone *et al.*, 2010b) and supraglacial lake evolution. The initial formation of a lake at the eastern margin of the debris-covered glacier was possibly related to marginal collapse influenced by the subglacial portion of the eastern lateral channel in close proximity to this location. Following drainage, the ~0.5 m thick sediments deposited in this lake protect immediately-underlying ice from melting. Surrounding clean ice or that with a thinner debris cover downwastes, creating a depression on the ice surface where a new supraglacial lake forms as meltwater begins to pond. This topographic inversion creates steep sides to the area of lake sediments, encouraging marginal slope destabilisation and small debris flows (Fig. 7.9e). This would also be facilitated through differential melting of buried ice, which can produce reorientation of bedding (Fig. 7.9f) and deformation structures such as faults (Mager and Fitzsimons, 2007; Clayton *et al.*, 2008; Livingstone *et al.*, 2010b). Evidence for this is mainly restricted to the margin of the lake sediments, suggesting that the underlying ice is largely intact. When the current supraglacial

lake drains it is likely that this pattern of topographic inversion will be repeated, forming a tiered sequence of supraglacial lake sediments.

7.4.4. Development of glacial geomorphology

7.4.4.1. Ridge formation

Latero-frontal moraines formed during glacier surges at other locations in Svalbard typically display evidence for tectonic deformation and multiple ridges crests, as described in this study (Nathorstbreen, *Chapter 4*; Finsterwalderbreen and Grønfjordbreen, *Chapter 6*) and in previous work (Croot, 1988; Hagen, 1988; Kristensen *et al.*, 2009a,b). In contrast, the Scott Turnerbreen moraine system contains single ridges at both the surge and LIA limits and no tectonic deformation was observed within multiple exposures. The morphology and sediment composition of the Scott Turnerbreen latero-frontal ridges is, therefore, consistent with their development as ice-cored moraine in areas of continuous permafrost (Etzelmüller *et al.*, 1996, 2000; Sletten *et al.*, 2001; Lukas *et al.*, 2005; Evans, 2009) rather than ridges formed through proglacial tectonic deformation. This process of ridge formation, described by Etzelmüller *et al.* (1996) and in Figure 7.12, requires the preservation of an ice core beneath thick supraglacial debris cover at the glacier front. Following the termination of a rapid advance, the glacier experiences an extended period of vertical lowering across the lower tongue. The thicker debris cover at the very front of the glacier protects the underlying ice, resulting in differential melting and the development of an ice-cored ridge at the frontal position of the advance. Similar to Sletten *et al.* (2001), this process of formation is inferred to explain both the surge and LIA ridges.

Buried ice is observed within the lateral moraines in several locations, typically on the ice proximal slopes where channels have eroded the debris cover (Fig. 7.10g). In these examples, the overlying debris cover of diamict is ~1-2 m thick. No exposed buried ice was observed within the latero-frontal parts of the moraine system, but the ridges contain morphological indicators of instability which is consistent with the presence of an ice core: firstly, surface tension cracks are observed on both the surge and LIA ridges, not only on the steepest slopes, and are inferred to result from internal instabilities related to the degradation of buried ice. Tension cracks, although still observed, are less frequent on the lower LIA ridge, which may reflect greater stability of the ice core, a higher proportion of debris to ice (Midgley *et al.*, 2013) and/or a greater depth to the buried ice. Secondly, slope processes in the form of debris flows (Figs 7.10g and 7.11; *7.3.2.2.*) and collapse scars (Fig. 7.10e) are ubiquitous on the steeply-sloped (~40º) surge ridge and lateral moraines, providing further evidence for internal instability and sediment remobilisation (Lukas *et al.*, 2005). Such processes are also apparent within the internal structure of the surge ridge (STB01; Fig. 7.7ci), where crude stratification within the diamict and openwork gravel layers dip at ~35º, parallel to the slope surface; these

are interpreted as stacked debris flows, with the gravel layers having been winnowed of finer material (Lukas *et al.*, 2005).

Clast shape data from both within and on the surface of the latero-frontal ridges reveals a predominance of edge-rounded sub-angular clasts within the diamict, of which between 6-20% displayed bullet-shaped morphologies and many were striated (Fig. 7.8a). These characteristics are consistent with material of subglacial origin (Benn and Ballantyne, 1994; Benn and Evans, 1996; Evans *et al.*, 2006a), similar to that within type B supraglacial ridges (Fig. 7.8a). Angular clasts are also found, comprising a small proportion within all samples, which is higher within the LIA ridge and lateral moraines than the surge ridge (Fig. 7.8a). This suggests that the frontal debris cover associated with the formation of the latero-frontal ridges contained far more subglacial material than observed on the present-day debris-covered front, which is dominated by angular and very angular material (Fig. 7.9b). An explanation for this is that the elevation of subglacial debris via shear planes and crevasse injections to form type B ridges played a large role in sediment delivery to the margins (Boulton, 1968) when the glacier was at its LIA and surge extents, presumably related to higher extensional and compressional stresses associated with the advance of a thicker, warm-based glacier (Etzelmüller *et al.*, 2000; Lysså and Lønne, 2001; Sletten *et al.*, 2001; Lukas *et al.*, 2005). The presence of some angular clasts indicates (i) surface clasts have experienced frost-shattering; (ii) passively-transported rockfall material melting-out of type A ridges also contributed to the frontal debris cover, similar to the present-day situation; and (iii) ridges are draped in extraglacial talus material, particularly in a lateral position. The delivery of sediment to the glacier front via structurally-controlled type A and B ridges and the resultant formation of the ice-cored moraine ridges indicates that these are a form of controlled moraines (cf. Evans, 2009). The prominent mound composed of angular and very angular material located just inside the eastern surge ridge (Figs 7.8a and 7.11e) can be identified on the 1961 aerial photograph (Sletten *et al.*, 2001) as a transverse supraglacial debris accumulation; this is interpreted as a concentration of rockfall onto the glacier surface which has been passively transported downglacier. The poorly-consolidated nature of the sediment cover and frequent tension cracks suggest this mound is ice-cored, as also inferred by Sletten *et al.* (2001).

7.4.4.2. Destabilisation and disintegration processes within the foreland

Active and inactive debris flows are ubiquitous across the glacier foreland, the debris-covered glacier front and the latero-frontal moraine system (Fig. 7.3) and are a result of slope destabilisation and subsequent remobilisation of debris. Active debris flows are restricted to the glacier front, steep lateral moraines and ice-marginal parts of the foreland. In almost all cases these are closely associated with active channels, indicating that fluvial erosion plays an important role in triggering and sustaining debris flows (Etzelmüller *et al.*, 1996, 2000; Sletten *et al.*, 2001; Lukas *et al.*, 2005). Evidence for this can be seen within the eastern lateral moraine

(Fig. 7.10g), where a small channel has undercut sediments, creating a highly-saturated debris flow. This in turn has exposed buried ice, which may begin to melt during summer months, further destabilising the debris cover and initiating a self-sustaining cycle (Lukas *et al.*, 2005) governed by thermo-erosion processes (Etzelmüller *et al.*, 1996). Over time this may begin to affect a larger area, creating extensive debris flows (e.g. 7.11g).

The evolution of debris flows involves the retreat and incision of headwall scarps into the source material, initiating collapses of debris which are then liquefied by meltwater, creating the flow lobes observed across the foreland (Figs 7.3 and 7.11). Headwall scarp retreat rates of 3.5-7.8 cm d^{-1} were measured by Lukas *et al*. (2005) on nearby Larsbreen, providing an indication of the likely incision rates at Scott Turnerbreen. The active debris flows on the glacier foreland are commonly incised into older inactive debris flows (Fig. 7.3), reflecting several generations of re-activated flows; this is also indicated by the multi-tiered inactive flows which are common in the outer parts of the foreland and which have been described within ice-cored moraine systems elsewhere in Svalbard (Bennett *et al.*, 2000b; Lukas *et al.*, 2005). The sediment exposed within the inactive debris flow by headwall scarp retreat reveal crudely stratified diamict and thin layers of sand and gravel (Fig. 7.7ciii), similar to that exposed within the latero-frontal moraines and providing a further indication of earlier sediment remobilisation, perhaps relating to several generations of movement.

The exposure of some ice blocks and subsequent development of debris flows, largely governed by initial meltwater erosion, whilst other buried ice remains intact beneath debris cover (Lønne and Lauritsen, 1996), leads to topographic inversion on the glacier foreland. This is characterised by hummocky topography and depressions, which are sometimes occupied by small pools (Fig. 7.11c). Once they have drained, the fine sediment deposited within these pools provides a further source of material for debris flows. The stabilisation of debris flows and their transition from active to inactive is probably related to drying out (Lukas *et al.*, 2005) due to a reduction in meltwater input, perhaps due to the re-routing of channels or complete melting of an exposed ice block.

The processes of fluvial erosion, debris flow development and the exposure and subsequent decay of ice cores describe thermo-erosion within a deglaciating foreland (Etzelmüller *et al.*, 1996). This results in significant re-mobilisation of debris and is responsible for the destruction of almost all linearity inherited from the pattern of glaciological structures (Evans, 2009). This is clear within the Scott Turnerbreen foreland (and not including the latero-frontal ridges), where the only identifiable linearity is provided by the four low-relief curvilinear ridges which can be linked to type A ridges at the lobate margin of the eastern flow unit observed on the 1990 aerial photograph (Sletten *et al.*, 2001).

7.5. Surge evidence

The ~1930s surge of Scott Turnerbreen suggested by Hagen *et al.* (1993) was not observed at the time and appears to be largely based on the interpretation of a single oblique aerial photograph from 1936, which shows a much thicker glacier with a steep front terminating at a position adjacent to the large ice-cored latero-frontal moraine (Sletten *et al.*, 2001), termed 'surge ridge' in this study. This is consistent with Scott Turnerbreen experiencing a surge in or immediately prior to 1936, but lacks diagnostic evidence of surging such as widespread intense crevassing and the presence of looped moraines (Copland *et al.*, 2003; Grant *et al.*, 2009). With this in mind, it is worth briefly revisiting the data presented in this chapter which provide further support for Scott Turnerbreen having surged in the 1930s.

7.5.1. Glaciological indicators

Apart from that outlined above based on the 1936 oblique photograph, several surface indicators which suggest Scott Turnerbreen has previously surged can be identified. The 1961 aerial photograph shows a well-developed lobate front to the eastern flow unit, which has dislocated the medial moraines and flowlines between the two units, forming a looped moraine (also still visible on the 1990 aerial photograph). The western flow unit comprises the main bulk of the glacier and also appears thick and lobate in shape. This provides evidence that the two flow units acted semi-independently, which is consistent with glacier surges (Benn *et al.*, 2009). The eastern flow unit appears thicker than the rest of the glacier and multiple open crevasses can be identified in its upper basin in 1961; this suggests that ice within the eastern flow unit was active for longer than the rest of the glacier. In fact, a small bulge can be identified on the 1936 photograph at the confluence between the eastern basin and the main glacier trunk, and the distinct lobate front of the eastern flow unit is not obvious further downglacier at this time (Fig. 7.2a). Based on this, it is tentatively suggested that the eastern flow unit surged towards the end or following termination of the main glacier surge, which mainly involved the western flow unit, and was possibly still active in, or up to several years before, 1961.

The glaciological structure and character of supraglacial ridges provides further support for the 1930s position of Scott Turnerbreen being related to a surge. The densely-spaced crevasse traces (S_3) indicate that the glacier surface has previously been intensely crevassed (Hambrey and Dowdeswell, 1997; Hambrey *et al.*, 2005), which is consistent with increased ice velocities and extensional flow during a surge (Hodgkins and Dowdeswell, 1994; Lawson *et al.*, 1994; Sund *et al.*, 2009; Sund and Eiken, 2010). In addition, arcuate shear planes (S_2) are also abundant, recording longitudinal flow compression within the lower glacier tongue (Hambrey and Dowdeswell, 1997; Hambrey *et al.*, 2005). These do not offset the crevasse traces and so are inferred to have formed before. This pattern is consistent with the downglacier progression of a surge front as a kinematic wave and the transfer of ice through the system by plug flow, whereby flow compression occurs at and in front of the advancing surge front, forming shear

planes. Once the surge front has passed, the ice is subjected to extensional flow and crevasses develop (McMeeking and Johnson, 1986; Hodgkins and Dowdeswell, 1994; Lawson *et al.*, 1994; Hambrey and Dowdeswell, 1997). This means that ice affected by the passage of a surge front will first be subject to compression and the development of shear planes, followed by extension and the formation of crevasses (Hambrey and Dowdeswell, 1997); therefore, the passage of a surge front is consistent with the structural glaciological evidence.

Type B ridges demonstrate that subglacial material has been elevated from the bed within both shear planes and crevasses and this reflects a number of observations across Svalbard of debris elevation during surges (Hambrey and Dowdeswell, 1997; Murray *et al.*, 1997; Glasser *et al.*, 1998a,b; Woodward *et al.*, 2002); see also *Chapters 4 and 5* in this study. In addition, the interpretation that some type C ridges reflect meltwater occupation of the crevasse system provides an indication that highly-pressurised meltwater has exploited intersecting crevasses within the glacier (Ensminger *et al.*, 2001). This has been suggested as a possible method of formation for concertina or zig-zag eskers, which are strongly associated with high basal water pressures and extensional crevassing within surge-type glaciers (Evans and Rea, 1999).

7.5.2. Geomorphological indicators

It has been demonstrated in a number of studies that glacier surges produce distinctive landforms and landform-sediment assemblages in proglacial areas (e.g. Sharp, 1985a,b, 1988; Solheim, 1985; Croot, 1988; Boulton *et al.*, 1996, 1999; Bennett *et al.*, 1999; Evans and Rea, 1999, 2005; Christoffersen *et al.*, 2005; Ottesen and Dowdeswell, 2006; Ottesen *et al.*, 2008; Kristensen *et al.*, 2009a,b; Roberts *et al.*, 2009). At Scott Turnerbreen, the only identifiable geomorphological indicators are a large, ice-cored latero-frontal moraine which delimits the maximum position of the surge and areas of hummocky topography. The ice-cored moraine is inferred to form through the protection of underlying ice at the debris-covered front during post-surge stagnation and associated vertical lowering across the lower glacier tongue (Fig. 7.12). This type of moraine formation is therefore consistent with surges (Etzelmüller *et al.*, 1996; Brynjólfsson *et al.*, 2012) as it requires an advance; frontal debris cover due to the elevation of subglacial debris to the surface along shear planes and injected into crevasses, which is indicative of dynamic warm-based ice flow and possibly related to increased ice velocities; and widespread stagnation upon the cessation of dynamic flow. This widespread stagnation and associated processes of thermo-erosion produces the extensive supraglacial debris cover (Kirkbride and Deline, 2013) and the hummocky topography dominated by debris flows which characterises the majority of the proglacial area at Scott Turnerbreen. This demonstrates that the only identifiable geomorphological evidence which can be attributed to the surge are an ice-cored latero-frontal moraine and an extensive area of hummocky, ice-cored stagnation

topography. This also describes the vast majority of non-surge-type small valley glaciers on Svalbard (Boulton *et al.*, 1982; Werner, 1993; Lysså and Lønne, 2001; Lukas *et al.*, 2005).

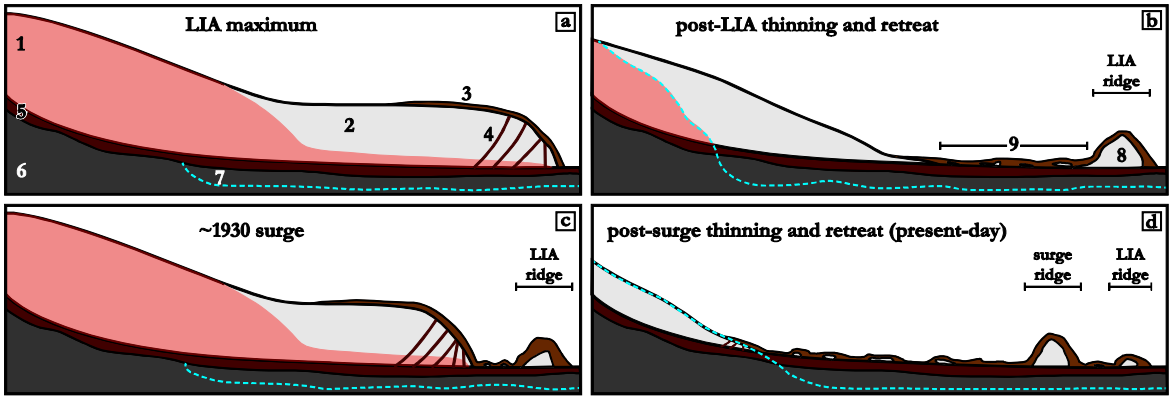

Figure 7.12 – Ice-cored ridge formation schematic. (a) LIA maximum; (b) post-LIA retreat and thinning; (c) surge in ~1930; (d) post-surge thinning and retreat to present-day. Key: 1. Temperate ice; 2. Cold ice; 3. Debris-covered glacier; 4. Subglacial debris elevated to surface along shear planes and injected into crevasses; 5. Glacier bed; 6. Bedrock; 7. Base of permafrost; 8. Ice-cored moraine; 9. Zone of thermo-erosion (buried ice blocks, debris flows).

The lack of diagnostic surge indicators on the foreland, such as proglacially-deformed push moraines, geometrical ridge networks, flutes and concertina/zig-zag eskers (Evans and Rea, 1999) is probably related to two main factors: (i) the glacier advanced over frictional, possibly frozen undeformable sediments. This would preclude the formation of push moraines, which require easily deformable proglacial sediments, typically of fluvial, lacustrine or marine origin (Croot, 1988; Boulton *et al.*, 1996; Hart and Watts, 1997; Boulton *et al.*, 1999; Kristensen *et al.*, 2009b). A predominantly coarse-grained bed and proglacial area would also reduce the likelihood of substantial crevasse squeezes and flutes forming, as these are also typically best defined in areas with a higher proportion of finer-grained sediment (Sharp, 1985b; Christoffersen *et al.*, 2005). (ii) The thermo-erosional processes which dominate across the glacier foreland are likely to negate the preservation of any small-scale or poorly-defined landforms produced by the surge due to widespread sediment remobilisation and meltwater action (Etzelmüller *et al.*, 1996; Evans, 2009). Type B and type C supraglacial ridges demonstrate that the processes which form geometrical ridge networks (crevasse injections and debris-rich shear planes) and concertina/zig-zag eskers were active during the surge, but clearly these have not been preserved on the foreland. This is unsurprising, as both types of ridges appeared to be related to thin englacial sediment inclusions, and type C ridges are ice-cored, suggesting that the de-iced landforms they produce are likely to be indistinct due to substantial reworking. Landforms of this type have been reported from small valley glaciers in Iceland which have surged, producing poorly-defined flutes and crevasse squeeze ridges (Brynjólfsson

et al., 2012); the main difference is that these are preserved on the foreland, whereas at Scott Turnerbreen, if formed, they have been destroyed by thermo-erosion processes.

7.5.3. LIA and surge ridge comparisons

The surge and LIA ridges are morphologically very similar and are inferred to have formed through the same fundamental process (Fig. 7.12). The LIA ridge is assumed to relate to the neoglacial maximum of Scott Turnerbreen, when the glacier was thicker, is likely to have been polythermal and had a positive mass-balance or was in equilibrium (Hodgkins *et al.*, 1999). The termination of the LIA in Svalbard, marked by an abrupt rise in mean annual air temperatures of ~5º (Hansson-Bauer *et al.*, 1990), and the associated switch to a negative mass-balance would result in glacier thinning, frontal retreat and a reduction in the proportion of temperate ice, eventually resulting in a transition from a polythermal to a cold-based thermal regime. This describes the situation experienced by all glaciers on Svalbard, excepting surge-type glaciers which have since surged, like Scott Turnerbreen, or are in the quiescent phase of the surge cycle (Hagen and Liestøl, 1990; Dowdeswell *et al.*, 1995). The LIA ridge is inferred to have formed through processes of ice core preservation beneath frontal debris cover as the lower glacier tongue experienced vertical lowering and terminus retreat following the LIA termination (Fig. 7.12b). The fact that Scott Turnerbreen subsequently surged in ~1930 indicates that the glacier remained polythermal and was still able to accumulate mass in the upper basins, but the retreat from the LIA maximum still reflects a change in flow dynamics and substantial frontal thinning. The conditions post-LIA are therefore comparable to the conditions post-surge, resulting in similar ridge formation processes.

The main differences between the surge and LIA ridges are the height, degree of vegetation and stability, as indicated by lower tension crack and debris flow abundance. The difference in size can be attributed to either a thinner initial debris cover, resulting in a smaller volume of debris within the ridge, substantial degradation of the ice core, or a combination of both (Etzelmüller and Hagen, 2005). If the LIA maximum was ~1900 (Hagen and Liestøl, 1990), the LIA ridge has had >30 years longer to de-ice than the surge ridge. Evidence for debris flows and topographic inversion is common within the zone between the LIA and surge ridges, and in several places poorly-sorted material from the LIA ridge forms a thin cover immediately distal to the ridge; this indicates that buried ice degradation and associated thermo-erosion processes have been active. The LIA ridge is also more fragmentary than the surge ridge, reflecting erosion by lateral meltwater channels associated with the surge. The channels have also eroded the non-glacial surfaces beyond the LIA limit, particularly on the eastern side, forming elongate ridges which are broadly parallel to the LIA and surge ridges (Fig. 7.3). At least one of these features has been interpreted as a pre-LIA glacier limit by Sletten *et al.* (2001); however, no evidence was found during this study to support this.

The Scott Turnerbreen moraine system records very similar morphologies and inferred formational processes for two separate ridges, one associated with the LIA and one with a later surge. This demonstrates that both climatically-controlled glacier expansion and surges, traditionally seen as aclimatically-controlled (Meier and Post, 1969), can produce morphologically, sedimentologically and genetically indistinguishable latero-frontal moraines in Svalbard.

7.6. Summary

Scott Turnerbreen is a small valley glacier which surged in the 1930s and has since become cold-based and frozen to its bed due to an extensive period of strongly negative mass balance driven by an abrupt increase in mean annual air temperatures in the twentieth century (Hansson-Bauer *et al.*, 1990; Hodgkins *et al.*, 1999). A consequence of this switch in thermal regime, accompanied by significant thinning and frontal retreat, is that Scott Turnerbreen has not re-entered the quiescent phase of the surge cycle and has effectively transitioned from a surge-type to non-surge-type glacier (Hodgkins *et al.*, 1999).

The proglacial geomorphology is characterised by two ice-cored latero-frontal ridges, attributed to the LIA maximum and ~1930 surge, which are inferred to have formed through differential melting and preservation of ice beneath a debris-covered glacier front. The glacier foreland is dominated by thermo-erosional processes driven by meltwater action and disintegration of buried ice, creating multiple debris flows and topographic inversion. No landforms which are diagnostic of surges (e.g. geometrical ridge networks, zig-zag eskers, flutes) were identified on the foreland and it is likely that these, if formed, have been destroyed by thermo-erosion (Evans, 2009). Therefore, the proglacial geomorphology associated with the surge consists of an ice-cored latero-frontal moraine and an extensive area of hummocky topography and debris flows, recording stagnation following the surge. This is indistinguishable from the LIA maximum moraine and zone between the two ridges and the proglacial areas of most similarly-sized valley glaciers in Svalbard which have thinned and retreated since the LIA and, therefore, is arguably not diagnostic of surging.

However, convincing evidence for former dynamic behaviour associated with the surge is recorded in the glaciological structure and supraglacial debris ridges exposed on the lower glacier tongue of Scott Turnerbreen. Abundant shear planes (S_2) and crevasse traces (S_3) reflect the passage of compressional and extensional stress regimes associated with the downglacier propagation of a surge front. In some cases these have elevated subglacial material to the surface, forming type B supraglacial ridges. A number of type C ridges, consisting of stratified sands and gravels, are interpreted as evidence for meltwater occupation of the crevasse system, reflecting high water pressures and extensional crevassing during the surge. In conjunction with a prominent looped moraine and distorted flowlines visible on the 1961 aerial photograph, this evidence demonstrates that the ~1930s surge left an identifiable record within the glacier. This

provides a template by which to assess additional possible former surges or surge-like advances of small valley glaciers on Svalbard, primarily through structural glaciological investigations.

Chapter Eight
Tellbreen

78º 10.0' N, 16º 00.0' E

After Wilhelm Tell, Swiss legendary hero, said to have died in 1354.

The place names of Svalbard, Norsk Polarinstitutt

8. Tellbreen

8.1. Introduction

This chapter describes ice facies and glaciological structures exposed in ice caves within Tellbreen, a small valley glacier in Nordenskiöld Land, central Spitsbergen (Fig. 3.2). Fieldwork was mainly conducted in spring 2012, with short visits also carried out in summer 2011 and spring 2013. The geographical and glaciological setting of Tunabreen will be outlined in *8.2.*, followed by a description of ice facies character and distribution, stable isotope results, structural glaciological measurements and glacial geomorphology in *8.3.* Interpretations of these results are made in *8.4.*

8.2. Study area and glaciological setting

Tellbreen is a 4 km-long, 0.5 km-wide land terminating valley glacier which flows into Helvetiadalen and is located approximately 12 km east of Longyearbyen, the capital of Svalbard (Fig. 8.1). The glacier is contiguous with Blekumbreen across a col in their accumulation areas, which flows westwards into Mälardalen, and the former is also fed by two high elevation accumulation basins (up to 950 m a.s.l.). The lower glacier tongue curves towards the southeast downglacier from the glacier midpoint and terminates at ~300 m a.s.l. in a ~0.5 m^2-area of ice-cored topography. The ice-cored area separates Tellbreen from an unnamed 2.5 km long glacier to the south, unofficially named Louis Careybreen in this study (Fig. 8.1). The bedrock in the area is comprised of readily erodible sandstones, siltstones and shales of the Van Mijenfjorden and Adventdalen Groups (Hjelle, 1993; Dallmann *et al.*, 2002).

Ground penetrating radar (GPR) data indicates that Tellbreen is currently almost entirely cold-based, with only a small isolated area of potentially warm ice near the thickest (~100 m) part of the glacier (Bælum and Benn, 2011). It has been suggested that more warm-based ice may have been present at the Little Ice Age (LIA) maximum extent of the glacier, but based on the minimal evidence for valley erosion, was unlikely to have been widespread or prolonged (Bælum and Benn, 2011). Since the LIA, Tellbreen has undergone significant terminus retreat of ~1 km (Fig. 8.1) and an estimated ~60-70% loss of ice volume and >50% reduction in glaciated area. A long-term mass balance (in metres water equivalent per year) figure of -0.6±0.2 m/yr has been calculated over this period (Bælum and Benn, 2011), similar to the average for all Svalbard glaciers of -0.55 m/yr (Dowdeswell *et al.*, 1997). Importantly in the context of this study, Bælum and Benn (2011) also concluded that there was no evidence to suggest Tellbreen was currently experiencing or had ever undergone surge behaviour, and no historical records of such activity exist.

Bælum and Benn (2011), Naegeli (2013) and Naegeli *et al.* (accepted) have demonstrated that Tellbreen has a dynamic and active drainage system characterised by a dendritic network of channels with supra-, en- and subglacial components. The en- and subglacial channels formed through the downcutting evolution of supraglacial channels by cut

and closure (Gulley *et al.*, 2009a,b), reflecting currently active processes. Naegeli (2013) and (Naegeli *et al.*, accepted) also described and investigated a ~40 m vertical moulin in the lower tongue area extending from the glacier surface to the bed, where it continued as a large Nye channel. One of the more interesting aspects of the Tellbreen drainage system is that running water is observed all year round, feeding a large proglacial icing during winter and spring months (Bælum and Benn, 2011). This has traditionally been interpreted as evidence for a polythermal regime (Hagen *et al.*, 2003), which is not supported by the GPR data at Tellbreen (Bælum and Benn, 2011), indicating that englacial water storage and subsequent release during winter also plays an important role in the drainage systems of cold-based glaciers (Hodgkins, 2001; Hodgkins *et al.*, 2004; Bælum and Benn, 2011; Irvine-Fynn *et al.*, 2011). For the purposes of this study, the presence of active and abandoned channels within the lower glacier tongue provides an accessible way to investigate ice facies and glaciological structures when they are frozen and (largely) free of water during spring (Fig. 8.2).

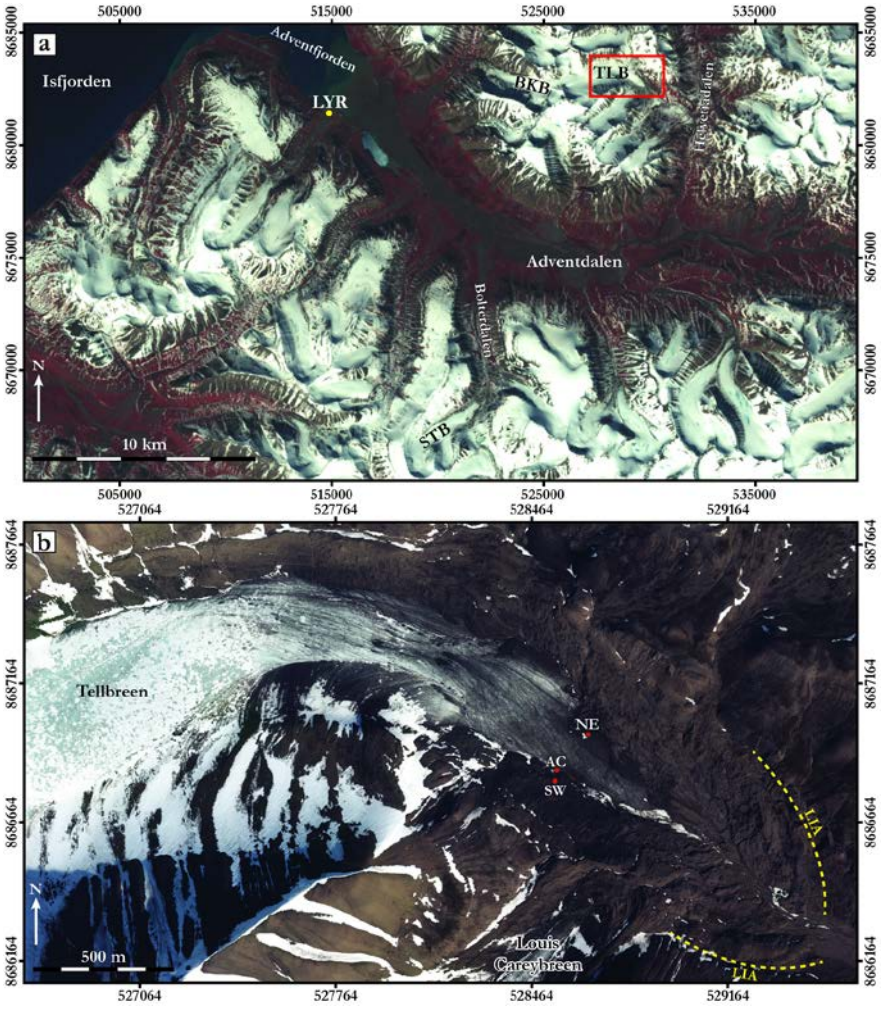

Figure 8.1 – Location map of Tellbreen in central Spitsbergen. (a) 2001 Landsat ETM+ image showing location of Tellbreen relative to Longyearbyen (LYR), Blekumbreen (BKB) and Scott Turnerbreen (STB; see Chapter 7). Red rectangle delimits area shown in (b) and mapped in Fig. 8.8. See Fig. 3.2 for location in Svalbard. (b) 2009 NPI aerial photograph of Tellbreen lower tongue. Red dots show location of SW, AC and NE cave entrances. Yellow dashed line shows Little Ice Age (LIA) maximum position based on Bælum and Benn (2011). See Fig. 8.8 for the geomorphological map of this area.

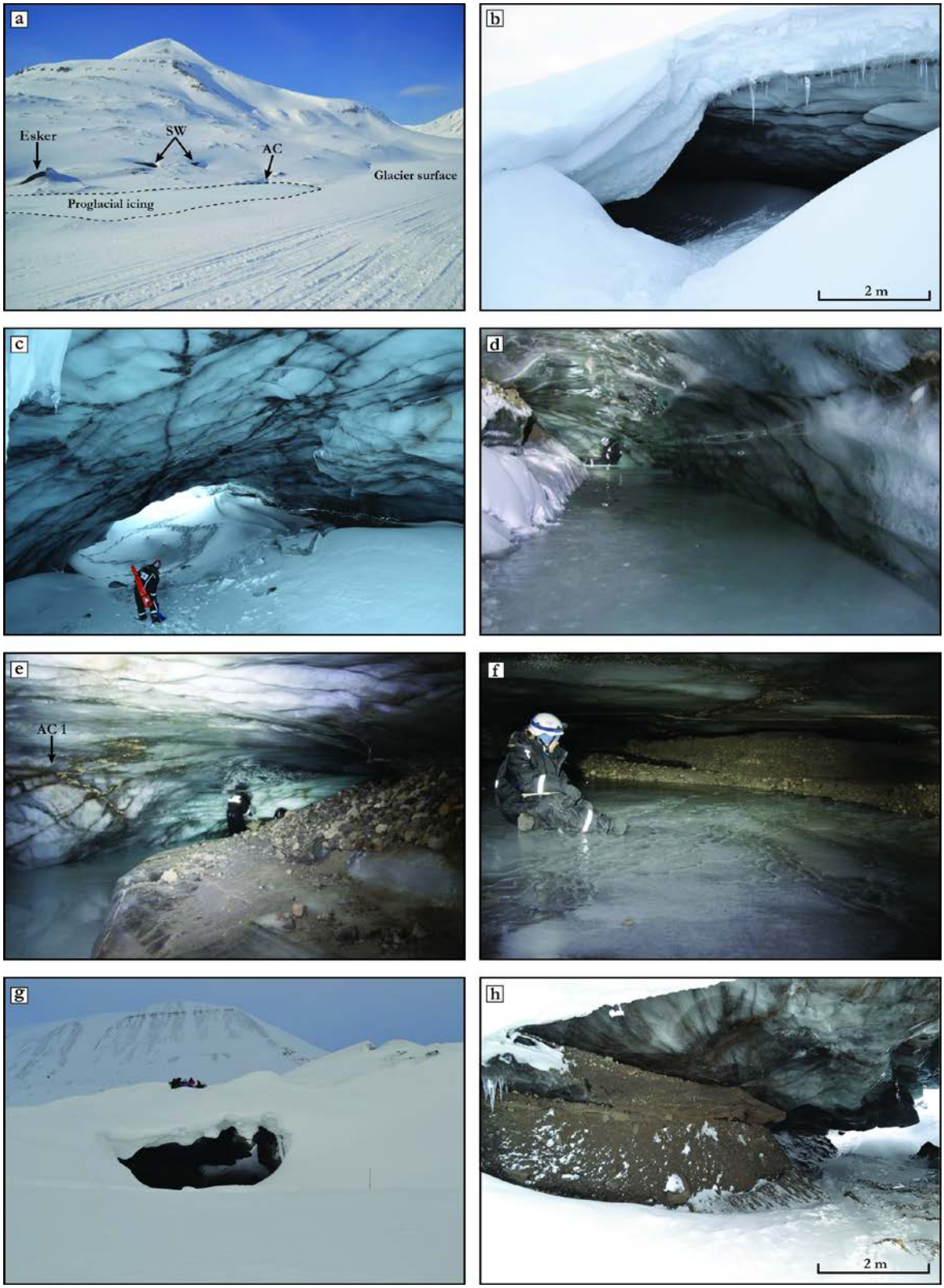

Figure 8.2 – Ice caves within Tellbreen lower glacier tongue. (a) Locations of SW and AC cave entrances. Note proglacial icing emerging from AC. (b) Upglacier entrance to SW cave. (c) Cross-cutting thin debris bands within SW cave. Note curved roof. View is towards downglacier entrance. (d) Interior of AC cave. Photo by Philipp Schuppli. (e) Cross-cutting thin debris bands within AC cave. Photo by Philipp Schuppli. (f) Ripple structures within floor of AC cave. Photo by Philipp Schuppli. (g) Downglacier entrance of NE cave. (h) Debris-rich ice and glaciofluvial sediments overlain by debris-poor ice within NE cave. Note thin debris laminae within debris-poor ice. All photos taken in April 2012 apart from (a) taken in April 2013.

8.3. Results

Ice facies and glaciological structures were investigated in three caves, named the southwest (SW), active channel (AC) and northeast (NE) caves (Fig. 8.1), in March and April 2012. The SW cave is an abandoned meltwater channel located close to the indistinct transition between ice-cored moraine and debris-covered glacier (Figs 8.2a and 8.2b). The cave is ~30 m long, ~5 m high, and has a curved roof and entrances at either end. The cave walls are characterised by cross-cutting thin debris bands within otherwise white, bubbly ice (Fig. 8.2c), which have been logged as sections SW1 and SW2 (Figs 8.3a and 8.3b). The AC cave is the lowermost englacial section of an active meltwater channel which emerges from the glacier front at the cave entrance (Fig. 8.2a). The cave is typically ~2-3 m high, ~5 m wide and sinuous in nature (Figs 8.2d). Section AC1 (Fig. 8.3c), the ~15 m long area of cross-cutting thin debris bands investigated in this study, is located approximately 40 m up-channel from the cave entrance (Fig. 8.2e). This cave was mapped as 'Crack cave' by Naegeli *et al.* (accepted). The NE cave is an open, cavern-like area formed by the northeast lateral meltwater channel (Fig. 8.2f). The main part of the cave is >10 m wide and extends in an upglacier direction for ~100 m, where there is a second entrance. The active channel enters the cavern area via a smaller, sinuous cave, which was mapped as 'Feather cave' by Naegeli *et al.* (accepted). The SW side of the main cave consists of an up to 5 m thick exposure of debris-rich ice and glaciofluvial sediments overlain by debris-poor ice (Fig. 8.2h), a ~40 m long stretch of which was logged as section NE1 (Fig. 8.3d).

The physical character and stable isotope analysis results from the ice facies exposed within the caves are described in *8.3.1.* and *8.3.2.*, respectively. The structural glaciology of Tellbreen, as determined from field measurements and aerial photograph mapping, is outlined in *8.3.3.*, and the geomorphology of the glacier foreland is described in *8.3.4.*

8.3.1. Physical character of ice facies

Four different ice facies are exposed within the caves at Tellbreen and based on their physical characteristics, following the Hubbard *et al.* (2009) scheme, are identified as debris-rich solid stratified facies; dispersed facies; clean facies; and englacial facies ice. The solid stratified and dispersed facies were not observed within the SW cave and the englacial facies was not observed in the NE cave.

8.3.1.1. Solid stratified facies

This facies consists of frozen poorly-sorted diamict with interstitial ice and small, largely bubble-free clean ice lenses (Figs 8.4a and 8.4b). The diamict is matrix-supported and contains clasts up to boulder size (0.5 m in diameter). The clasts within the diamict are predominantly sub-angular (Fig. 8.5) and ~20% of those sampled exhibited striations, gouges grooves or faceting, and/or had bullet-shaped morphologies. The grain size distribution of the facies is

Figure 8.3 – Two-dimensional section logs. (a) SW1 section. (b) SW2 section. (c) AC1 section. (d) NE1 section. A5 and A6 on (c) refer to cave measurement stations within Naegeli (2013) and Naegeli et al. (accepted), where it is named 'Crack cave'.

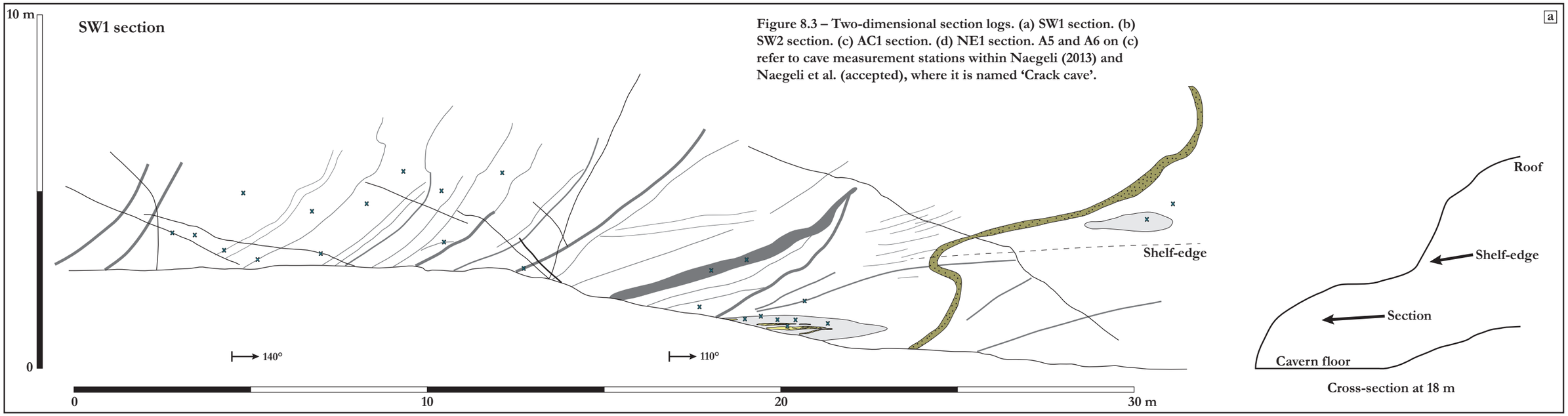

polymodal and displays distinct peaks within silt and sand (Fig. 8.6). At section NE1 (Fig. 8.3d), debris concentrations vary with height across the thickness of the facies, which ranges from 2-4 m. The debris concentrations grade over tens of centimetres from measured values of 52% close to the contact with overlying ice, in an area where numerous clean ice lenses are visible, to 80% at a depth of ~1 m (Fig. 8.4b). Intermediate debris concentrations of 65% and 70% were measured from the area between these two (Fig. 8.4b). The upper ice-rich area is observed to vary in thickness from ~0.1-1 m and displays crude stratification highlighted by the presence of ice lenses. This stratification becomes less distinct with depth and below ~1 m the facies appears structureless. The debris in this lowermost area contains only interstitial ice and is effectively frozen diamict. Two clast macrofabric samples recorded from either end of section NE1 (Fig. 8.3d) show mean lineation azimuths of 129º and 109º, respectively, and display moderate to weak clustering (S_1 values of 0.654 and 0.560; Table 8.1, Figs 8.9j and 8.9k). Occasional layers of sorted sediment are found within the facies, including an unfrozen area of deformed fine sand close to the downglacier entrance (left-hand end of section NE1) and a ~6 m-long, ~10 cm-thick clast-rich layer centred on approximately 30 m (Fig. 8.3d). This facies shares many characteristics with the solid stratified subfacies at Tunabreen (*Section 5.4.1.1.* in *Chapter 5*).

8.3.1.2. Dispersed facies

The dispersed facies is characterised by debris-poor ice with variable bubble content and character and typically overlies solid stratified facies ice (Figs 8.3d, 8.4c and 8.4d). The debris within the ice takes the form of suspended grains or clots, occasionally within thin laminae (<1 cm thick), of predominantly silt-sized fine sediment (Fig. 8.6). Suspensions of bright orange material, characteristically similar to precipitates of iron oxyhydroxide described within ice at other sites within Svalbard (Hodson *et al.*, 2008), were also observed. Debris concentrations of <1% (n = 4) were measured at section NE1. There is a strong linear component to the sediment within many laminae, identical to features at Tunabreen (*Chapter 5*) described as mineral stretching lineations in Fleming *et al.* (2013). The dispersed facies is also cross-cut by thicker bands (~5 cm thick) of sorted sands and gravels which are typically aligned sub-horizontally to the contact with underlying solid stratified ice (Figs 8.3d and 8.4c). Bubble content and character varies from clear areas of no or very few bubbles (Fig. 5.4b) to areas containing dense, white clouds of bubbles and intercalated bubble-rich and bubble-poor layers (Fig. 8.4c). The bubble-poor areas are typically located close to the contact with underlying solid stratified ice or glaciofluvial sediments (Figs 8.3d and 8.4b) and often contain worm like structures of very fine bubbles (Fig. 8.4d). In places, these structures grade into thicker, ribbon-like structures, several individual bubbles (~1-5 mm diameter) thick, and dense bubble clouds (Fig. 8.4c). In areas where they coincide, these bubble structures cut across intercalated layers of bubble-rich and bubble-poor ice within the dispersed facies. The observed thickness of the dispersed facies

ranges from <0.1 m (within the AC cave) to at least 2 m at NE1 (Fig. 8.3d). This facies is very similar in character to dispersed ice described at Tunabreen (*Section 5.4.1.2.* in *Chapter 5*).

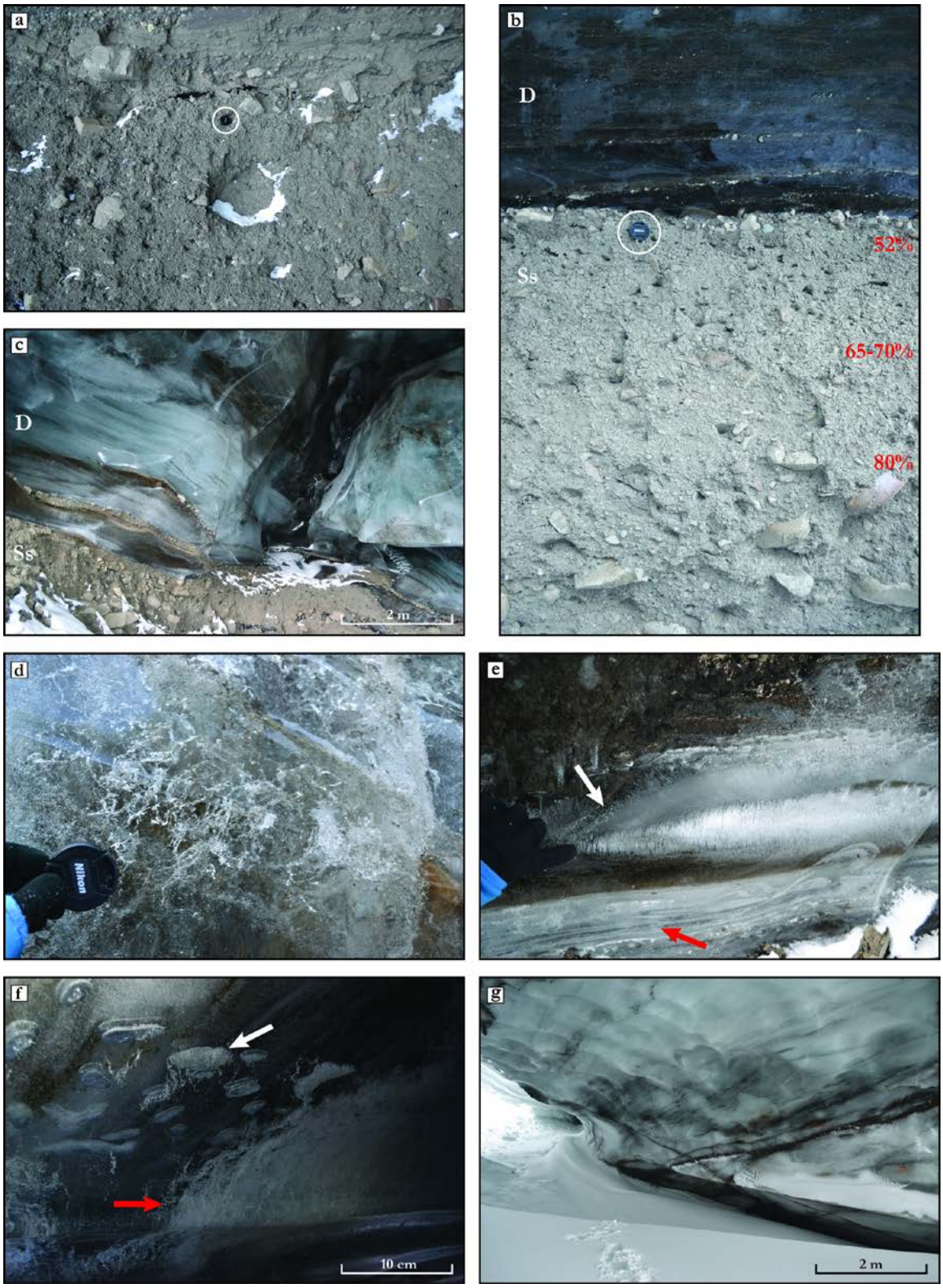

Figure 8.4

Figure 8.4 (preceding page) – Examples of ice facies. (a) Stratified solid facies at base of NE cave. Lens cap circled for scale. (b) Stratified solid facies overlain by dispersed facies in NE cave. Not clean ice lenses within solid stratified facies and thin layer of sands and gravels at contact with dispersed facies. Percentages in red are measured debris concentrations (by volume). Lens cap circled for scale. (c) Dispersed facies overlying solid stratified facies at base of NE cave. (d) Worm-like bubble structures within clear dispersed facies at NE cave. (e) Lens of clean facies within NE cave. White arrow shows area of fine needle ice. Red arrow shows layers of bubble-rich and bubble-free ice. Note solid stratified facies behind visible through the clear ice areas. (f) Clean ice within wall of AC cave. White arrow shows disk-like bubble feature. Red arrow shows vertically-aligned bubble wisps. Note debris laminae and bubble layers associated with dispersed facies behind visible through the clear ice areas. (g) Englacial ice within SW cave. Note white appearance and evidence for horizontally-aligned intercalated layers of bubble-rich and bubble-poor ice.

Table 8.1 – Fabric statistics of S_2 lineation and clast fabric data.

Sample no./section	Type/facies	n	Mean lineation azimuth (V_1)	S_1	S_2	S_3	S_3/S_1
SW1 and SW2	S_2 lineation	18	316.4	0.934	0.057	0.009	0.009
AC1	S_2 lineation	11	307.6	0.924	0.060	0.016	0.017
NE1	S_2 lineation	14	130.8	0.934	0.053	0.013	0.014
HL12TLBNE02	Solid stratified	50	129.3	0.654	0.284	0.061	0.093
HL12TLBNE03	Solid stratified	50	109.8	0.560	0.310	0.130	0.232
HL12TLBNE04	Gravel	50	13.87	0.574	0.261	0.165	0.287

8.3.1.3. Clean facies

This facies is almost entirely debris-free and is characterised by distinct bubble features within areas of bubble-free ice (Figs 8.4e and 8.4f). Three main types of bubble features are observed: Large (~0.1 m diameter) disk shaped bubbles suspended in clear ice (white arrow in Fig. 8.4f), vertically-aligned wispy clouds of bubble structures (red arrow in Fig. 8.4f), and horizontal layers of bubble-free and bubble-rich ice (red arrow in Fig. 8.4e). This latter feature is similar to layering within englacial ice (Fig. 8.4g), but is typically only centimetres thick and contains coarser bubbles. Dense areas of extremely fine vertically-aligned needle ice with a hair-like appearance (white arrow in Fig. 8.4e) are also seen within the ice. Frazil ice and ripple structures are also observed in places, such as within ice exposed in the floor of the AC cave (Fig. 8.2f). Clean facies ice ranges in vertical thickness from ~0.1-3 m but is typically <0.2 m deep, making it possible to see through the clear areas to other ice facies behind, including solid stratified (Fig. 8.4e) and dispersed (Fig. 8.4f) ice. This facies is found in the walls, floor and roof of the AC cave and as isolated lenses/blocks within the SW and NE caves, and is often closely associated with layers of horizontally bedded sorted sands and gravels (Fig. 8.3).

8.3.1.4. Englacial facies

The englacial facies comprises the majority of the glacier and is the dominant ice type within the SW and AC caves. It is bubble-rich and in general has a white, opaque appearance (Fig. 8.4h), with stratification visible at centimetre to decimetre scales in the form of intercalated layers of bubble-rich and bubble-poor ice (Fig. 8.4g) This layering is visible on the glacier surface as slight colour changes. Apart from the thin debris bands which cross-cut this facies at the SW and AC sections (Figs 8.2c, 8.2e and 8.3a-c), described below in *8.3.2.*, the ice contains only occasional suspended grains and small clots of fine sediment.

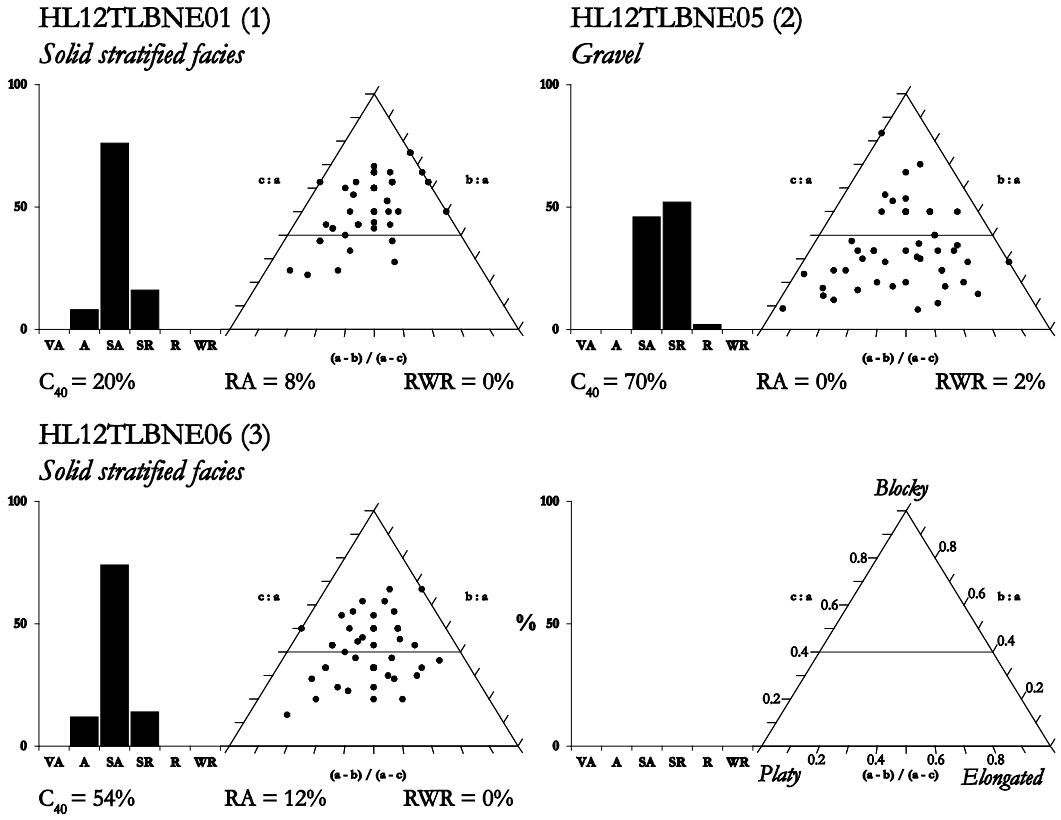

Figure 8.5 – Clast shape data for solid stratified facies ice and gravel at NE1 plotted on histograms (roundness) and ternary diagrams (shape). Each sample is of 50 sandstone clasts. Numbers in brackets after sample name refer to sample locations on Fig. 8.3.

8.3.2. Structural glaciology

Five types of planar structure are identified on and within the lower tongue of Tellbreen from field measurements, field observations and aerial photographs (Table 8.2, Figs 8.3, 8.7 and 8.8). These are termed S_0-S_4 (not to be confused with S_1-S_3 eigenvalues; Table 8.1) in order of inferred formation according to structural geological conventions and following numerous structural glaciological investigations (e.g. Lawson *et al.*, 1994; Hambrey and Dowdeswell, 1997; Glasser *et al.*, 1998b; Woodward *et al.*, 2002; Hambrey and Glasser, 2003; Hambrey *et al.*, 2005; Roberson and Hubbard, 2010).

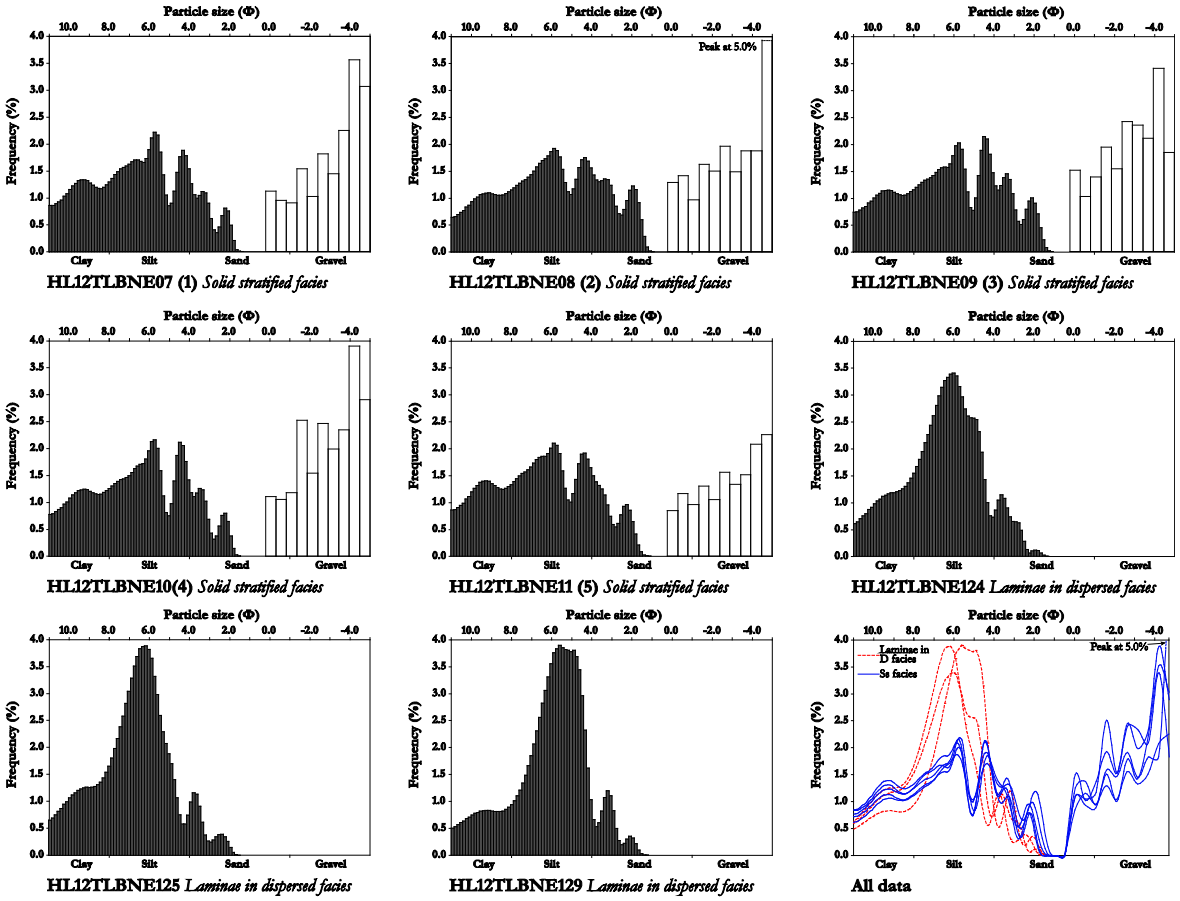

Figure 8.6 – Grain size distributions. Grey bars derived from laser sizing and white bars from dry sieving. Numbers in brackets after sample name refer to sample locations on Fig. 8.3. Troughs in the data are likely to be an artefact of combining the two techniques.

S_0 – Stratification

This structure is defined by the alternations of bubble-rich and bubble-poor ice within englacial ice (Figs 8.4g, 8.9a and 8.9d; see *8.3.1.4.*). This layering appears as slight colour changes on the glacier surface and in places can be traced as irregular linear features, although these are not identifiable in the lowermost part of the tongue (Fig. 8.8). Stratification is cross-cut by S_2 and S_3 structures (Figs 8.9a and 8.9d).

S_1 – Longitudinal foliation

Linear, flow-parallel stripes on the glacier surface are identified as longitudinal foliation based on their similarity with features mapped as such in other studies (Hambrey and Dowdeswell, 1997; Glasser *et al.*, 1998b; Hambrey *et al.*, 2005; Roberson and Hubbard, 2010; Fleming *et al.*, 2013; Midgley *et al.*, 2013). Longitudinal foliation is closely associated with flow-parallel supraglacial ridges composed of a thin (<5 cm) layer of angular material with an ice core, mapped as type A ridges (Figs 8.8 and 8.9b; see Table 7.2).

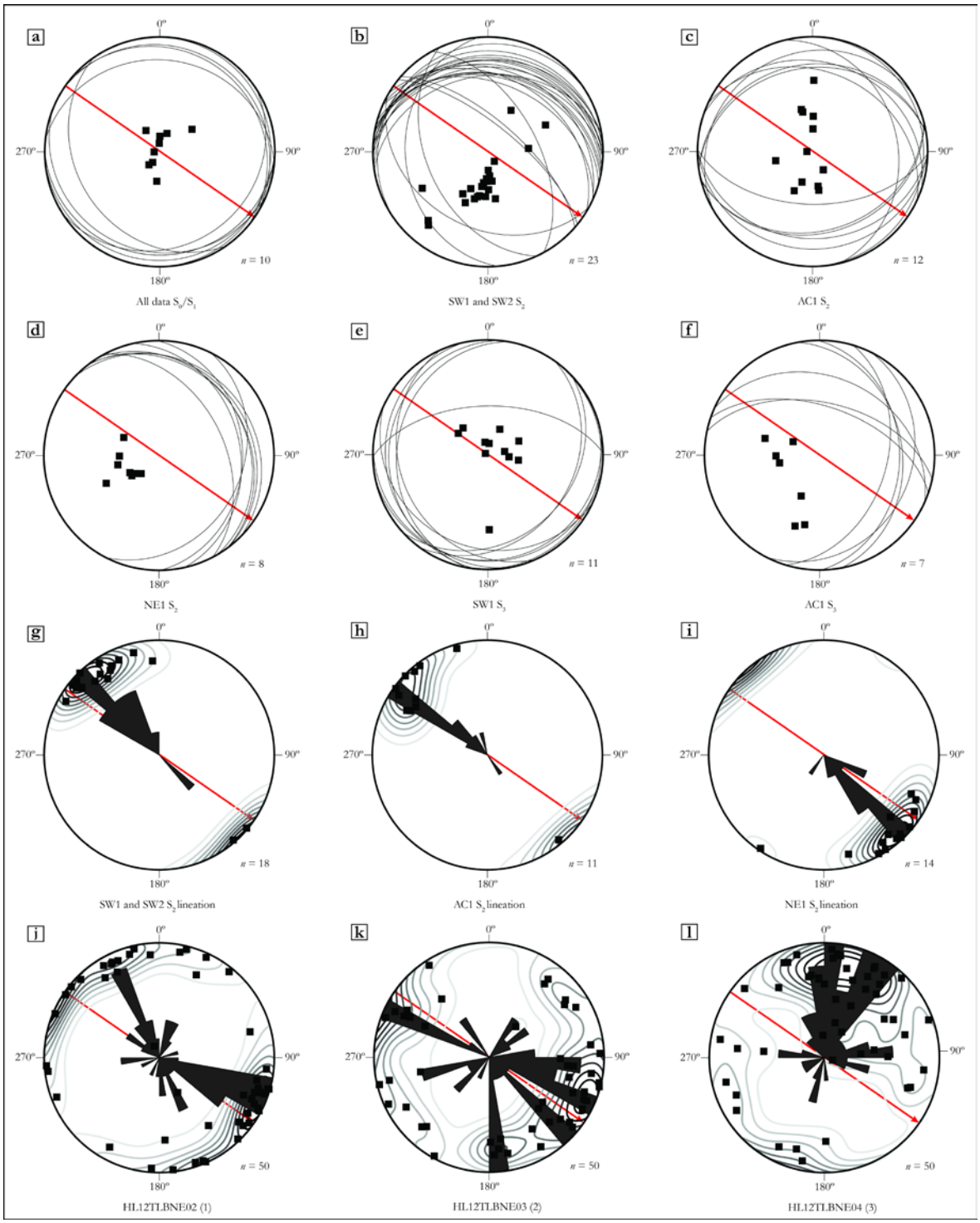

Figure 8.7 – Lower hemisphere equal-area stereographic projections and rose diagrams of structural and fabric data within Tellbreen. (a) S_0/S_1 in SW1, SW2 and AC1. (b) S_2 in SW1 and SW2. (c) S_2 in AC1. (d) S_2 in dispersed facies at NE1. (e) S_3 in SW1. (f) S_3 in AC1. (g) S_2 lineation in SW1 and SW2. (h) S_2 lineation in AC1. (i) S_2 lineation in NE1. (j) Clast fabric sample of solid stratified facies ice at NE1. (k) Clast fabric of gravel at NE1. (l) Clast fabric sample of solid stratified facies ice at NE1. Numbers in brackets after sample names in (j) to (l) refer to sample locations on Fig. 8.3. Red arrow shows centre-line ice flow direction at the terminus.

Figure 8.8 – Map of Tellbreen glacial geomorphology and lower tongue structural glaciology. See Fig. 8.1 for location of mapped area. Mapped from 2009 aerial photographs acquired from NPI. A digital version of this map is included on the CD inside the back cover.

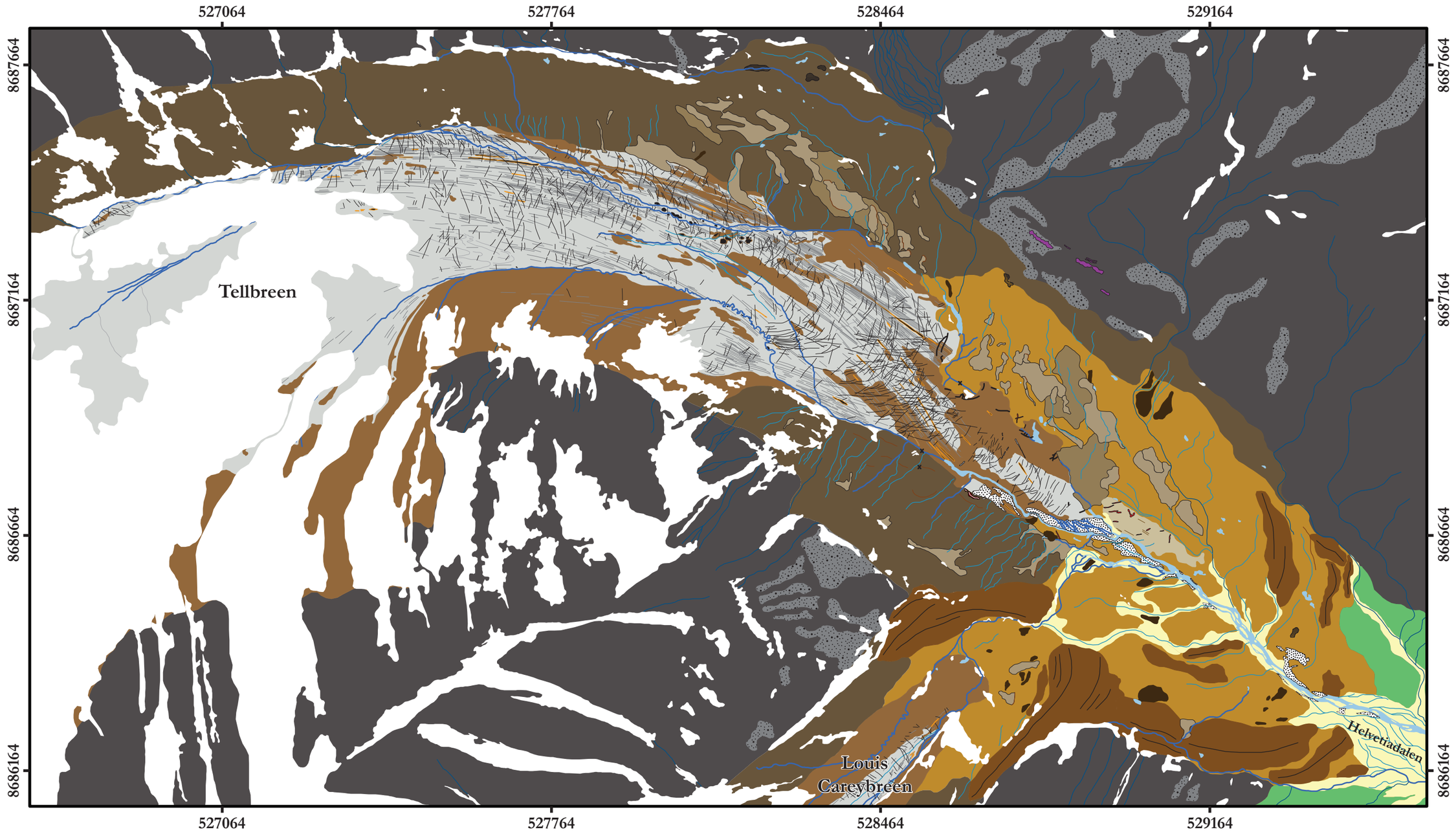

Table 8.2 – Summary of principal glaciological structures in Tellbreen. *S_0 and S_1 represent end-members of a structural continuum.

Planar glaciological structures	Description	Where observed
S_0*	Stratification	Surface and englacial
S_1*	Longitudinal foliation	Surface and englacial
S_2	Arcuate fracture traces	Surface and englacial
S_3	Fracture traces	Surface and englacial
S_4	Open fractures	Surface and englacial

S_2 – Arcuate fracture traces

The glacier surface contains a number of linear stripes orientated perpendicular and sub-perpendicular to S_1 structures and ice flow, identified as trace evidence of brittle deformation (Fig. 8.8). These are sub-divided into arcuate fracture traces (S_2) and fracture traces (S_3). Arcuate fracture traces appear on the glacier surface as gently curving linear stripes, often traceable for tens to hundreds of metres (Fig. 8.9b). Although no direct link was observed, based on their similar relationships to other structural elements, it is suggested that these features can be correlated to one set of the thin (<2 cm) debris bands exposed within the ice caves, also labelled S_2 (Figs 8.3 and 8.9), which cross-cut and occasionally offset S_0 layering. Structural measurements from the SW and AC caves show dominant orientations of ~350-010º; within the NE cave the orientations are typically ~040-060º (Figs 8.9b-d). Both on the glacier surface and in section, S_2 structures are rarely seen to cross-cut each other but do intersect on occasion (Figs 8.3 and 8.7). Fracture dip angles range from 04-71º and are predominantly between 20-50º. The sediments within S_2 structures are individual grains and small clots of fine material suspended within bubble-poor ice (Figs 8.9d, 8.9e and 8.9h) with a strong peak in the silt size range (Fig. 8.6). In almost all cases the sediments display a linear component (or mineral stretching lineations; Fleming *et al*., 2013) and macrofabric data from these show mean lineation azimuths of 316º (sections SW1 and SW2), 308º (AC1) and 131º (NE1), recording a northwest-southeast alignment (Table 8.1; Figs 8.11g-i). These data display strong clustering (S_1 values of 0.934, 0.924 and 0.534; Table 8.1) and indicate shear along the planar surface of the structure. S_2 structures are similar in planform to features mapped in previous work as transverse foliation (Lawson *et al.*, 1994), thrusts (Hambrey and Dowdeswell, 1997) and arcuate fractures (Hambrey *et al.*, 2005; Roberson, 2008; Roberson and Hubbard, 2010).

S_3 – Fracture traces

The second group of fracture traces (S_3) are in general shorter and display more variable orientations than S_2 structures when seen on the glacier surface (Fig. 8.9b), and are observed to

cross-cut S_0, S_1, S_2 and other S_3 structures (Fig. 8.8). These surface features are correlated to the second set of debris bands within the SW and AC caves, which clearly cross-cut both S_0 and S_2 structures (Figs 8.3, 8.9a, 8.9e and 8.9g) and in places can be directly traced to the surface (Fig. 8.9c). In addition to orientations (Figs 8.9e and 8.9f), the sediment composition and thicknesses of the S_3 structures are also more variable, ranging from <1 cm-thick bands of suspended grains and clots of well sorted silt-sized material (Figs 8.9e and 8.9g), to ~5-10 cm thick bands of poorly sorted sandy gravel with up to 2-3 cm diameter clasts (Fig. 8.9f). There is no evidence of mineral stretching lineations or shearing within S_3 structures. Similar features have been mapped as fracture or crevasse traces in a number of studies (Hambrey and Dowdeswell, 1997; Glasser *et al.*, 1998b; Hambrey *et al.*, 2005; Roberson and Hubbard, 2010; Midgley *et al.*, 2013).

S_4 – Open fractures

The final brittle structures visible on the glacier surface are open fractures, similar in length to S_3 fracture traces (Fig. 8.8). These have a very restricted distribution in the lower tongue and were typically only found in close association with the NE cave complex. Open fractures also occur in steep areas of the upper accumulation basins (Bælum and Benn, 2011).

8.3.3. Stable isotope analysis

Ice for stable isotope analysis was sampled from all facies across the three caves and from S_2 and S_3 structures within the SW cave (Fig. 8.3). These results are summarised in Table 8.3. Analysis of all samples (n = 74) produced means of -14.02‰ and -99.89‰ and standard deviations of 1.18 and 6.78 for $\delta^{18}O$ and δD, respectively. These results have been subdivided by ice facies and glaciological structures to allow comparison of their isotopic composition (Table 8.3 and Fig. 8.10). The englacial facies returned mean values of -14.89‰ ($\delta^{18}O$) and -101.26‰ (δD; ranges of -13.95 to -17.55 for $\delta^{18}O$ and -89.90 to -116.22 for δD), clean facies ice yielded mean compositions of -14.01‰ ($\delta^{18}O$) and -97.70‰ (δD; ranges of -12.16 to -17.34 for $\delta^{18}O$ and -88.67 to -116.94 for δD); the dispersed facies mean compositions were -13.92‰ ($\delta^{18}O$) and -102.13‰ (δD; ranges of -12.65 to -16.50 for $\delta^{18}O$ and -89.40 to -123.31 for δD); and the respective mean values for the solid stratified facies were -12.11‰ ($\delta^{18}O$) and -92.66‰ (δD; ranges of -11.72 to -12.57 for $\delta^{18}O$ and -86.64 to -104.00 for δD). The solid stratified facies $\delta^{18}O$ mean value is statistically distinct from the englacial facies mean value at the 95% confidence level (i.e. ±2 standard deviations). The mean δD value for the solid stratified facies is slightly higher than the mean for englacial ice but is not statistically distinguishable at the 95% confidence level (Table 5.1). Similarly, the clean facies typically returned heavier $\delta^{18}O$ values than englacial ice but is not statistically distinct at the 95% confidence level. The mean values and ranges of clean and dispersed facies ice are similar (Table 8.3 and Fig. 8.10a), indicating that the dispersed facies is also not statistically distinguishable from the englacial

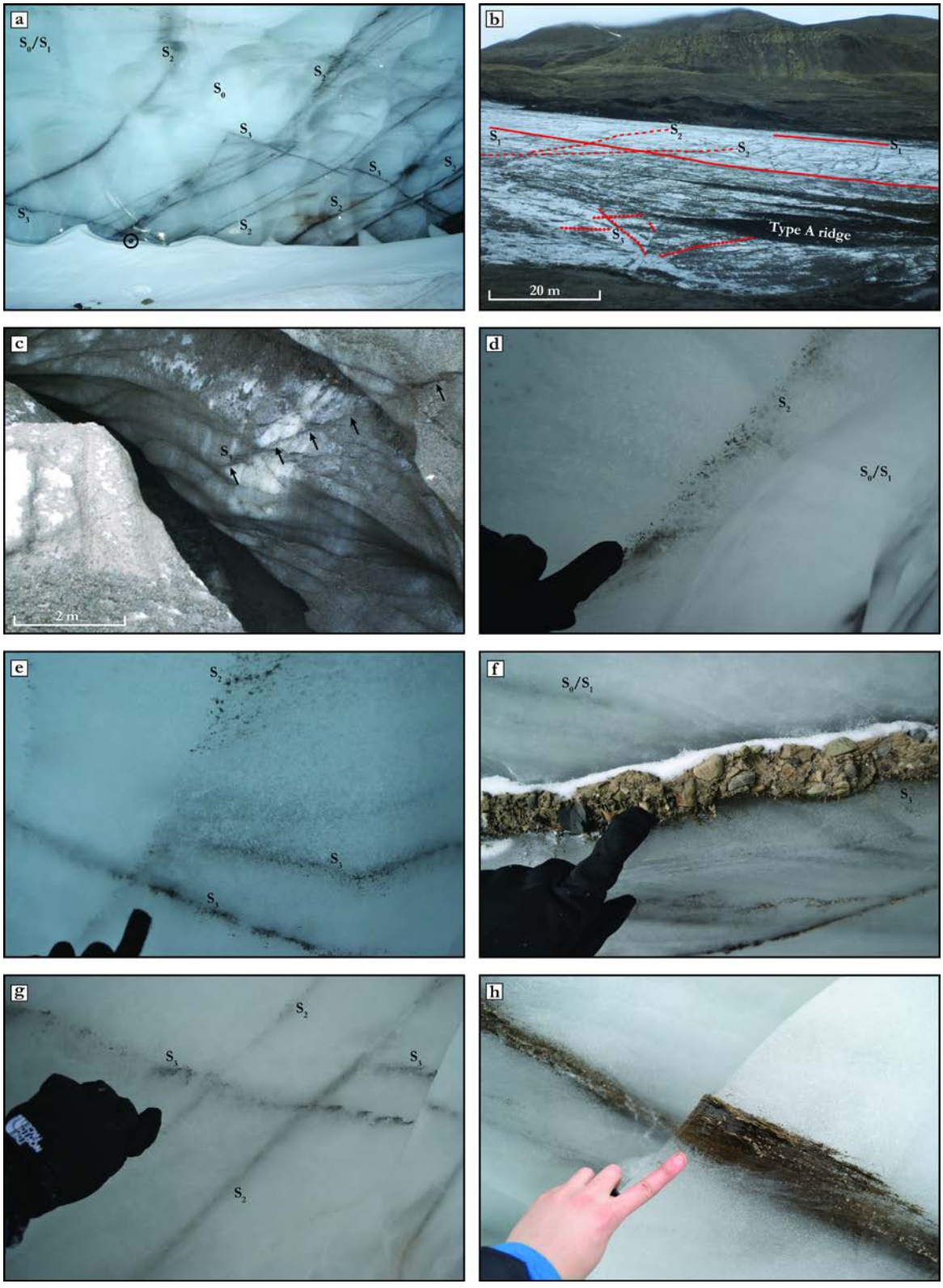

Figure 8.9

Figure 8.9 (preceding page) – Details of glaciological structures in Tellbreen. (a) S_0/S_1, S_2 and S_3 structures exposed in SW cave. Note how S_3 structures cut across S_2 structures. Lens cap circled for scale. (b) S_1 (solid lines), S_2 (dashed lines) and S_3 (dotted lines) structures exposed on the surface of Tellbreen. Note type A supraglacial ridges also. (c) S_3 structure exposed in side of a meltwater channel. It is observed to break the glacier surface just to the right of the photo, providing a link between the englacial and surface structures. (d) S_0/S_1 and S_2 structures within SW cave. Note linear smearing of sediment grains and clots within S_2 structures. (e) S_2 and S_3 structures within SW cave. Note linear smearing of sediment grains and clots within S_2 structures, which are cut across by S_3 structures. (f) Poorly sorted sandy gravel within S_3 structure in SW cave. (g) S_3 structures cutting across S_2 structures within SW cave. (h) Linearly smeared sediment within S_2 structures in SW cave. All photos taken in spring 2012 apart from (b) and (c) taken in summer 2011.

facies at the 95% confidence level. The mean $\delta^{18}O$ composition of ice within S_3 structures is slightly heavier than that within S_2 structures, although this is based on limited samples. Both S_2 and S_3 structures returned slightly heavier $\delta^{18}O$ compositions than englacial ice, but neither are statistically distinguishable at the 95% confidence level. In general, the δD results showed little significant variation across all samples (Fig. 8.10b). When plotted co-isotopically (Fig. 8.11), none of the ice facies produced regression lines either aligned with the LMWL (Divine *et al.*, 2008) or on 'reliable' freezing slopes (Sugden *et al.*, 1987a; Knight, 1989).

8.3.4. Distribution of ice facies, englacial and supraglacial debris

Solid stratified facies ice within the NE cave is overlain by dispersed facies ice along most of the length of the NE1 section (Fig. 8.3d). The dispersed ice is typically clear and almost bubble-free for thicknesses of ~10-100 cm close to the contact between the two (Figs 8.4b and 8.4c). This contact is often marked by a thin (<5 cm) layer of sandy gravel, particularly towards the right-hand (upglacier) end of the section (Figs 8.3d and 8.4b). Near the cave entrance at the left-hand (downglacier) end, the solid stratified ice is overlain by a ~1 m thick sequence of sands and gravels (Fig. 8.3d). This sequence includes well sorted fine sand lenses and layers with ripple-structures and cross-lamination, with evidence for small-scale folds and faults within the lamination (Fig. 8.12b). Similar but undeformed fine sand layers are also found in close association with clean ice facies in the lowermost parts of the SW1 and SW2 sections (Figs 8.3a and 8.3b). The fine sand layer within the NE1 section is overlain by interbedded gravels within a sandy-gravel matrix and underlain by a layer of imbricated gravel containing predominantly sub-angular and sub-rounded clasts (Fig. 8.5). Macrofabric data from this gravel have a moderate cluster (S_1 = 0.574) and a mean lineation azimuth of 14º (Table 8.1), recording up-channel dip relative to the active meltwater channel that occupies the NE cave (Fig. 8.7l).

Table 8.3 – Summary of stable isotope data.

Ice facies/ glaciological structures	*n*	Section	$\delta^{18}O$ mean (‰), standard deviation and range	Enriched	δD mean (‰), standard deviation and range	Enriched
All samples	74	All	-14.02±1.18 (-11.72 to -17.55)	-	-99.89±8.27 (-86.64 to -123.31)	-
Englacial	14	SW1, SW2	-14.89±0.88 (-13.95 to -17.55)	-	-101.26±7.30 (-89.90 to -116.22)	-
Clean	22	SW1, AC1, NE1	-14.01±1.48 (-12.16 to -17.34)	No	-97.70±6.86 (-88.67 to -116.94)	No
Dispersed	24	AC1, NE1	-13.92±0.82 (-12.65 to -16.50)	No	-102.13±10.17 (-89.40 to -123.31)	No
Solid stratified	4	NE1	-12.11±0.36 (-11.72 to -12.57)	Yes	-92.66±8.02 (-86.64 to -104.00)	No
S_1	8	SW1	-13.89±0.63 (-13.01 to -14.75)	No	-100.25±6.19 (-87.55 to 106.51)	No
S_2	2	SW1	-13.45±0.21 (-13.30 to -13.60)	No	-100.41±1.44 (-99.40 to -101.43)	No

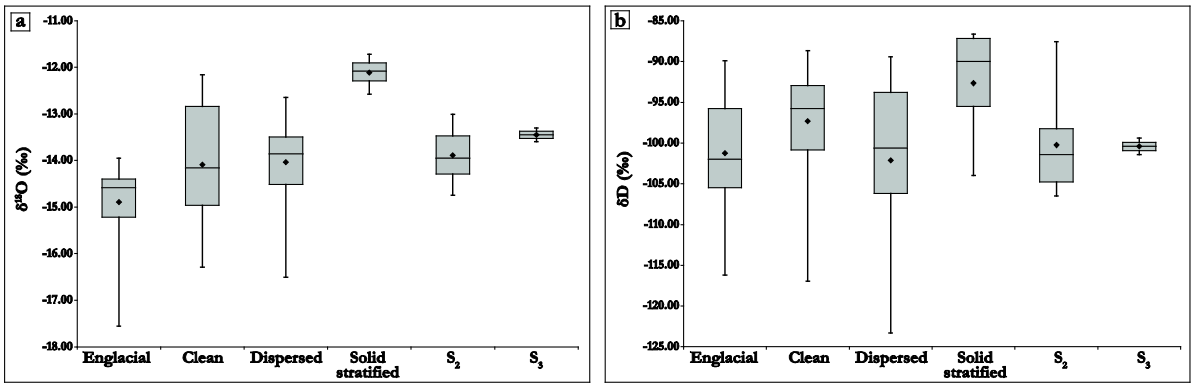

Figure 8.10 – Box plots of stable isotope analysis of Tellbreen ice facies and glaciological structures showing maximum, upper quartile, median, mean (black diamond), lower quartile and minimum values. (a) $\delta^{18}O$ composition; (b) δD composition.

Several examples of some of the four types of supraglacial ridge identified at Scott Turnerbreen (*Chapter 7*; Table 7.2) are also found at Tellbreen (Table 3.1 and Fig. 8.8). Type A ridges are up to 150 m long and consist of a thin (<5 cm) cover of angular material, typically black shale, overlying an ice core (Fig. 8.9b). These ridges are closely associated with and display similar alignments to longitudinal foliation (S_1), and are sometimes observed to emerge from S_1 structures, which are continuous on both the up- and downglacier sides of the ridge. No examples of type B ridges (Table 3.1) were observed in the field or from aerial photographs. Type C ridges are often aligned perpendicular and sub-perpendicular to ice flow direction and in the field take the form of sharp-crested ridges composed of layers of cross-bedded sand and gravels up to cobble size (Figs 8.7, 8.12e and 8.12f). The final example observed at Tellbreen are type D ridges, characterised by small piles of sand and fine gravel located on the glacier surface next to incised meltwater channels (Fig. 8.12d) and on shelves within the channel walls. These ridges follow the routes of channels and are mainly found on the upglacier part of the

lower glacier tongue (Fig. 8.8). The glacier surface is also covered in large areas of thin debris with no or very little topographic expression, shown as debris-covered glacier in Figure 8.8.

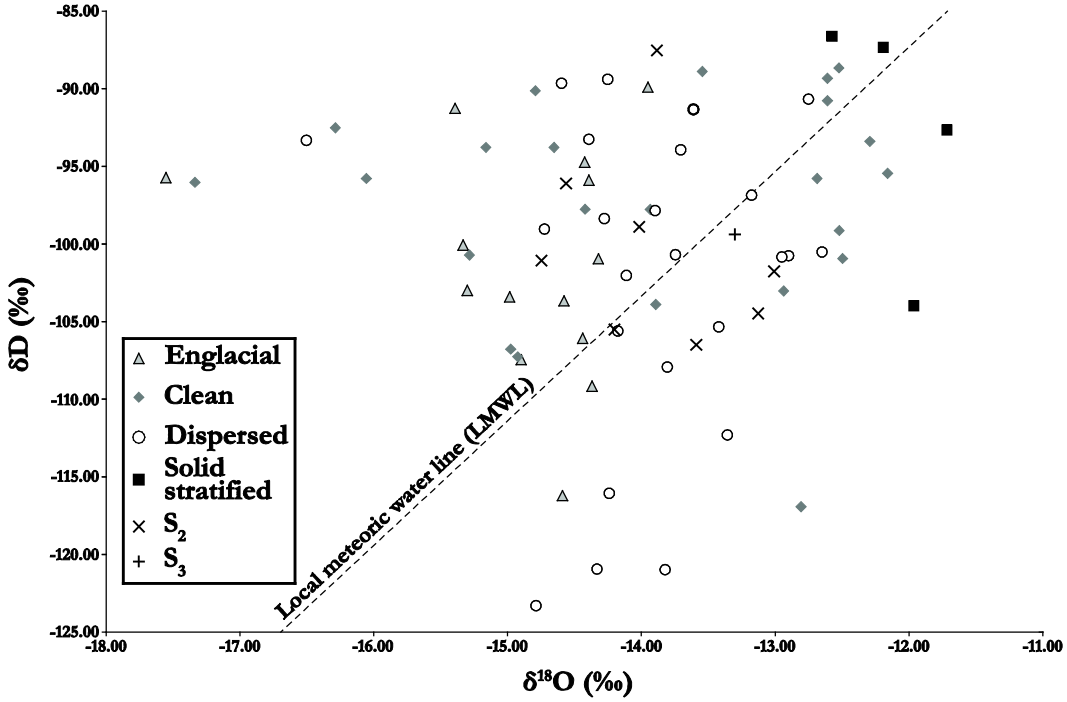

Figure 8.11 – Co-isotopic plot of Tellbreen ice facies and glaciological structures. Local meteoric water line (LMWL; slope = 7.8) is from Divine *et al.* (2008).

8.3.5. Glacial geomorphology and proglacial debris

Tellbreen is flanked by steep lateral moraines up to 50 m above the glacier surface which contain exposed ice, often associated with tiered debris flows and tension cracks in the surface. In places, such as from the northern lateral moraine, debris flows have advanced onto the glacier surface, further blurring the indistinct border between debris-covered glacier, lateral moraine and hummocky sediment cover (Fig. 8.8). The proglacial area is dominated by the main meltwater channel, the result of a confluence between the channels occupying the AC and NE caves, and its associated outwash corridor dissecting a wider area of hummocky sediment cover. The drainage system forms proglacial icings during winter and spring months, which are also visible on the aerial photographs taken in summer 2009 (Fig. 8.8) but were not seen in the field in August 2011. The hummocky sediment cover appears to be primarily composed of poorly-sorted debris displaying a wide range of grain sizes up to ~1 m diameter boulders (Fig. 8.12h) and was observed to be ice-cored. The northern side of the glacier tongue contains a number of tiered fresh (active) debris flows, sometimes reactivating older flow deposits (Fig. 8.8). A number of prominent ridges are identifiable within the general hummocky topography. The largest of these ridges are ~5-10 m high, extend for 100s of metres, and conform to the inferred shape of the former glacier margin. In conjunction with the lateral moraines, the furthest down valley of these ridges correspond to the LIA position of Tellbreen suggested by Bælum and

Benn (2011). The southern latero-frontal part of this ridge system appears to merge with frontal ridges associated with Louis Careybreen (Figs 8.7 and 8.12h).

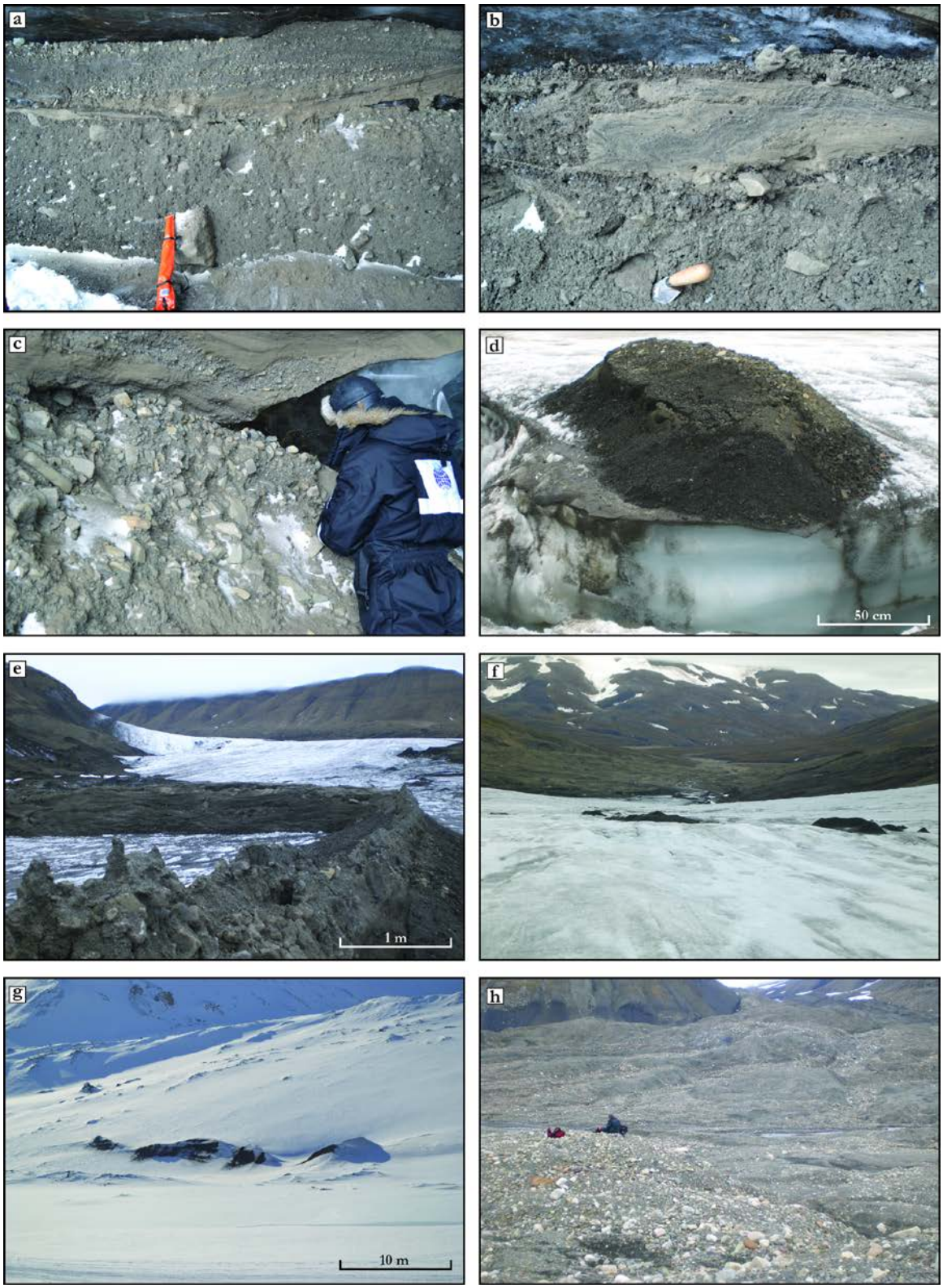

Figure 8.12

Figure 8.12 (preceding page) – Details of supra-, en- and proglacial sediments and landforms at Tellbreen. (a) Solid stratified facies (Ss) overlain by glaciofluvial sands and gravels (S + G) and dispersed facies ice (D), NE cave. (b) Close-up of deformed fine sand (fS) lens within NW cave. (c) Imbricated gravel layer (G) overlain by fine sand (fS) and interbedded sands and gravels (S + G), NW cave. (d) Type D ridge composed of sands and fine gravel on glacier surface adjacent to meltwater channel. (e) Sharp-crested type C ridge of sands and gravels close to terminus on lower glacier tongue. Note abrupt right-angle change in direction of ridge. (f) View towards Helvetiadalen across glacier foreland from lower tongue. (g) Esker-like ridge on glacier foreland. (h) View across Tellbreen glacier foreland and up towards Louis Careybreen (see Fig. 8.8 for locations). Note central meltwater channel and hummocky ridges composed of poorly-sorted sediments.

The Tellbreen ice-marginal area also contains some smaller ridges, including an sinuous ridge composed of stratified sands and gravels which extends for ~50 m on the southern side of the glacier tongue. The tongue terminates abruptly as a ~1.5 m high step down to outwash deposits, and in front of this there is a flat area of sediment cover superimposed by small ridges aligned at ~45º to ice flow, mapped as geometrical ridges (Fig. 8.8). These are oriented perpendicular to longitudinal debris stripes in the sediment, which are similar in character to longitudinal foliation on the glacier surface. The sediment composition of geometrical ridges was not assessed in the field.

8.4. Interpretation

8.4.1. Ice facies

8.4.1.1. Solid stratified facies

Stratified debris-rich ice is typically identified as the lowermost unit within basal ice sequences and has been suggested to form through different processes in different settings. These include regelation around bedrock obstacles (Kamb and LaChapelle, 1964; Hubbard and Sharp, 1993), hereafter referred to as regelation; vertical regelation into unlithified basal sediments (Iverson, 1993, 2000), hereafter vertical regelation; *en masse* basal freeze-on due to conductive cooling (Weertman, 1961), hereafter freeze-on; and glaciohydraulic supercooling (Alley *et al.*, 1998, 2003; Cook *et al.*, 2010). These possible formation processes can be assessed based on the physical properties and stable isotope analysis of the Tellbreen solid stratified ice (Figs 8.4a, 8.4b and 8.10). The textural characteristics of the solid stratified facies, which consists of poorly-sorted diamict with a wide range of grain sizes (Fig. 8.6) and predominantly sub-angular clasts displaying evidence of small-scale erosional features (Fig. 8.5), is indicative of entrained unconsolidated subglacial debris (Sugden *et al.*, 1987a; Sharp *et al.*, 1994; Spedding and Evans, 2002). The lowermost ~0.5-1 m of the facies at the NE cave was observed to be almost entirely frozen diamict with very little ice content (Fig. 5.4b), and in conjunction with the location of the cave close to the glacier terminus, it seems logical that the NE1 section is at the glacier bed.

The metres-thick sequence of solid stratified ice within the NE cave appears incompatible with regelation processes, as this should rarely form debris-rich layers thicker than ~0.1 m (Nye, 1970; Hubbard and Sharp, 1993). Thicker sequences can be produced through

tectonic deformation (Sharp *et al.*, 1994; Hubbard and Sharp, 1995; Waller *et al.*, 2000; Swift *et al.*, 2006), but the facies contains no obvious evidence of this (e.g. folds or faults). In addition, regelation generally forms ice facies with low debris contents (Kamb and LaChapelle, 1964; Hubbard, 1991), typified by banded layers or laminations of debris-rich and debris-poor ice (Larsen *et al.*, 2010), neither of which describes the Tellbreen solid stratified ice. A glaciohydraulic supercooling origin for the facies seems unlikely as there is no evidence for either an overdeepening beneath the lower tongue of Tellbreen (Bælum and Benn, 2011) or for additional features thought to be diagnostic of supercooling (e.g. upwelling vents, anchor ice terraces, fractures filled with platy ice, crescentic layering, rosettes of ice crystals; Evenson *et al.*, 1999; Roberts *et al.*, 2002).

The observed and measured evidence of a vertical gradation in debris concentrations within the solid stratified ice, which shows decreasing ice content with depth (Fig. 8.4b), is consistent with vertical regelation into the bed. This process describes ice regelating into pore spaces within underlying unconsolidated sediments with a lower pore-water pressure than ice pressure, thus incorporating material into the ice (Alley *et al.*, 1997). The rate of regelation decreases with increasing debris thickness, which could produce the gradation in ice content with depth seen within the solid stratified facies. This process is suggested to be effective beneath cold ice and when basal melt rates are low, which describes the current situation at Tellbreen (Bælum and Benn, 2011). However, Alley *et al.* (1997) also proposed that metres-thick debris layers entrained through vertical regelation should be predominantly clast-supported, with only thin (~0.1 m) layers of matrix-supported diamict produced; this suggestion is inconsistent with the Tellbreen solid stratified ice.

The favoured interpretation for the formation of the solid stratified facies is through *en masse* entrainment of unconsolidated subglacial debris due to net freeze-on at the glacier bed. This occurs where the 0ºC isotherm migrates into underlying saturated sediments through conductive cooling from the glacier surface or as cold ice is advected downwards, forcing a switch from net basal melting to net basal freezing (Weertman, 1961; Lawson, 1979; Alley *et al.*, 1997). Basal melting under warm-based conditions would allow meltwater to saturate the underlying permeable bed; the vertical gradation in ice/debris content within the facies may be an artefact of decreasing efficiency of meltwater percolation with depth, perhaps due to the hydraulic properties of the sediment (Christoffersen *et al.*, 2006) such as differences in consolidation and pore availability. The presence of a saturated and deformable bed is supported by sorted layers within the facies and at the contact with dispersed ice (inferred ice-bed interface; Fig. 8.3d), indicating water-transported sediment, and the clast fabric data from the solid stratified ice which shows a moderate to weak alignment in the direction of ice flow (Table 8.1, Figs 8.9j and 8.9k). The warm-based conditions this implies is in contrast to the current cold thermal regime of Tellbreen, but could be associated with a thicker and more extensive glacier at its LIA maximum (Bælum and Benn, 2011). Under these conditions, conductive

cooling and freeze-on could have been associated with the thermal transition from warm-based ice in the thicker parts of the glacier to cold-based ice towards the margins, a situation common in Svalbard polythermal glaciers (Ødegård *et al.*, 1996). Further evidence for former warm-based conditions within Tellbreen will be outlined below (*8.4.1.2.* and *8.4.2.*). Based on the physical characteristics of the facies, basal freeze-on of saturated sediment interpretation is preferred to vertical regelation as the dominant process because it better explains the formation of metres-thick debris-rich ice consisting of matrix-supported diamict (Sharp *et al.*, 1994; Larsen *et al.*, 2010). It has been suggested that these processes are not necessarily mutually exclusive, however, and possibly could have acted in combination as the subglacial water supply became increasingly restricted (Christoffersen *et al.*, 2006; Larsen *et al.*, 2010).

The results from stable isotope analysis demonstrate that the stratified solid facies is enhanced in heavy $\delta^{18}O$ isotopes relative to englacial facies ice (Table 8.3 and Fig. 8.10a), which is consistent with ice formation through refreezing of water in close association with a debris-rich bed (Lawson, 1979; Knight, 1989; Hubbard and Sharp, 1993; Iverson and Souchez, 1996), and therefore freeze-on of saturated sediments. It has been demonstrated that ice formed from refreezing of a localised parent water source, or closed system freezing (Knight, 1997; Cook *et al.*, 2010), should produce a freezing slope with a lower gradient than englacial ice when plotted on a co-isotopic graph (Jouzel and Souchez, 1982; Souchez and Jouzel, 1984). Figure 8.11 shows this is not the case for the solid stratified facies isotopic composition. An explanation for this is that the parent water was not from a single, localised source, but reflects a range of different sources with variable original isotopic compositions (Boulton and Spring, 1986; Hubbard and Sharp, 1993, 1995; Sharp *et al.*, 1994; Knight, 1997; Swift *et al.*, 2006). This is consistent with a freeze-on process of sediments saturated by water from various sources at a point when the basal freezing rate exceeds the water supply rate (Christoffersen *et al.*, 2006). The solid stratified samples plot at the heavier end of the isotopic spectrum (Fig. 8.11), which indicates that the facies, or at least the parts of the facies sampled, formed during the early stages of the freezing process (Sharp *et al.*, 1994; Knight, 1997).

The mean $\delta^{18}O$ value for the solid stratified facies (-12.11‰; Table 8.3) is similar to measured $\delta^{18}O$ values for descriptively-similar facies at Austre Brøggerbreen (-12.80‰; Hubbard *et al.*, 2004) but is lighter than mean $\delta^{18}O$ values reported from Kongsvengen (-10.85‰) and Midtre Lovénbreen (-11.05‰; Hubbard *et al.*, 2004) and some Icelandic glaciers (-8.30‰ at Svínafellsjökull, -10.40‰ at Skaftafellsjökull, -8.30‰ to -11.70‰ at Kvíárjökull; Swift *et al.*, 2005; Cook *et al.*, 2010), and is heavier than values reported from Variegated Glacier for the basal stratified laminated (-14.24‰) and basal stratified solid (-14.06‰) facies (Sharp *et al.*, 1994) and the mean value for stratified ice at Kuannersuit Glacier, West Greenland (-18.00‰; Larsen *et al.*, 2010). For δD, the Tellbreen solid stratified facies mean value (-92.66‰; Table 8.3) is heavier than values from Tunabreen (-103.41‰; *Chapter 5*), Variegated Glacier (-107.25; Sharp *et al.*, 1994) and Kuannersuit Glacier (-129.70‰; Larsen *et al.*, 2010),

and is significantly lighter than mean values from Svínafellsjökull (-56.70‰) and Skaftafellsjökull (-70.90‰; Cook *et al.*, 2010). This highlights the broad range of isotopic values that are possible for similar facies at different locations, which may reflect different isotopic compositions of the source water controlled by a range of processes, including the number of melting-refreezing events experienced by the parent water prior to ice formation and the time of year that the initial precipitation occurred (e.g. summer or autumn/winter; Cook *et al.*, 2010).

8.4.1.2. Dispersed facies

This facies shares many characteristics with ice described previously as *clear* (Hubbard and Sharp, 1995; Hubbard *et al.*, 2000), *clotted* (Knight, 1987), and *dispersed* (Lawson, 1979), in particular the bubble-poor nature, low debris content and typical proximity to subglacial debris (Figs 8.4b-d), and is similarly interpreted to be the product of strain-induced metamorphism of englacial ice close to the bed (Hubbard and Sharp, 1995; Knight, 1997; Hubbard *et al.*, 2000). The bubble-poor areas are consistent with gas expulsion in solution along triple-grain veins as a result of enhanced ice deformation causing melting and refreezing at grain boundaries (Kamb and LaChapelle, 1964; Hubbard and Sharp, 1995; Hubbard *et al.*, 2000). Strain heating could also provide an additional energy source for intergranular melting. This process provides an explanation for the bubble structures observed within the dispersed facies which are characterised by fine bubble strands tracing the outline of ice crystals (Fig. 8.4d), indicating a routing of gas around grain boundaries. Bubble-rich areas within the dispersed facies, in places displaying stratification not dissimilar to that within englacial ice (Fig. 8.4c), may represent preserved remnants of the latter facies where gas expulsion was incomplete (Hubbard and Sharp, 1995). The dispersed ice immediately overlying the solid stratified ice, and therefore at the inferred ice-bed interface, typically has the lowest bubble content (Fig. 8.4b), indicating that this is where metamorphism was most effective.

The fine-grained debris within dispersed ice, which takes the form of suspended grains and clots, is inferred to be due to the re-distribution of sediment by water within a vein network between ice crystals (Lliboutry, 1993; Knight and Knight, 1994). The thin debris laminae are inferred to be related to water flow within fractures (see *8.4.2.4.*). The presence of dispersed ice in close proximity to solid stratified ice suggests that the included debris is likely to be sourced from the fine-grained matrix of the latter (Fig. 8.6), indicating that they are related to the migration of muddy water in the basal zone (Knight and Knight, 1994). The presence of iron oxyhydroxide precipitates within the dispersed facies suggests that high levels of iron were in solution during the refreezing process, which is consistent with significant rock-water contact in a water-rich sedimentary environment (Hodson *et al.*, 2008). Stretching lineations on the planar surface of laminae at the NE cave display strong evidence of shear in a direction sub-parallel to ice flow (Table 8.1 and Fig. 8.7i), in agreement with clast fabric data from the underlying solid

stratified ice (Table 8.1, Figs 8.9j and 8.9k). This provides evidence for enhanced deformation within the dispersed facies, supporting the interpretation of formation by strain-induced metamorphism processes, and providing further possible evidence of a warm-based thermal regime at some point in the past.

Stable isotope results for dispersed ice are consistent with melting and refreezing at grain boundaries (Kamb and LaChapelle, 1964) and, therefore, a metamorphosed origin. The values for $\delta^{18}O$ are slightly heavier than those for englacial ice, but have not been enriched (Table 8.3). These data do not form a freezing slope on the co-isotopic plot (Fig. 8.11), indicating that the facies has not formed by the refreezing of parent water from a single source with specific isotopic composition (Souchez *et al.*, 1988). This may instead reflect multiple melting and partial refreezing events as part of the metamorphism process (Sharp *et al.*, 1994). Souchez *et al.* (1988) suggested that this may produce high ranges in $\delta^{18}O$ and δD values, such as the ranges of 3.85‰ and 33.91‰, respectively, measured for the dispersed facies (Table 8.3). The proposed reason for these high ranges is that no fractionation occurs upon melting of the ice formed (and partially enriched) during a previous freezing event, producing isotopically-heavier meltwater. This then becomes the initial liquid for the next freezing event, resulting in a higher overall range of values (Souchez *et al.*, 1988).

The mean $\delta^{18}O$ value for the dispersed facies (-13.92‰; Table 8.3) is similar to values for the dispersed facies at Tunabreen (-14.20‰; *Chapter 5*) and for the descriptively-similar basal stratified clear facies reported at Variegated Glacier by Sharp *et al.* (-14.46‰), but is lighter than the dispersed facies mean value recorded by Cook *et al.* (2011) at Svínafellsjökull, Iceland (-10.90‰), and heavier than the dispersed ice mean value at Kuannersuit Glacier (-18.80‰; Larsen *et al.*, 2010). Mean δD values for the dispersed facies at Tellbreen (-102.13‰; Table 8.3) are similar to values at Tunabreen (-103.12‰; *Chapter 5*) and reported from Variegated Glacier (-108.94‰; Sharp *et al.*, 1994), but are significantly lighter than those recorded at Svínafellsjökull (-71.90‰; Cook *et al.*, 2011) and heavier than values from Kuannersuit Glacier (-138.80‰; Larsen *et al.*, 2010). The similarity between the mean values for both $\delta^{18}O$ and δD at Tellbreen, Tunabreen and Variegated Glacier, and the high range in values recorded at all three (-12.65‰ to -16.50‰ at Tellbreen, -12.99‰ to -16.50‰ at Tunabreen and -13.20‰ to -16.00‰ at Variegated Glacier for $\delta^{18}O$), is consistent with the facies forming through similar processes (e.g. strain-induced metamorphism of englacial ice). However, it is also clear that a large variation in isotopic values between different locations is possible for facies that are both descriptively similar and interpreted to form through similar mechanisms (e.g. dispersed ice at Svínafellsjökull and Kuannersuit Glacier; Larsen *et al.*, 2010; Cook *et al.*, 2011).

8.4.1.3. Clean facies

The geographical distribution and types of bubble features observed within this facies (Figs 8.4e and 8.4f) are indicative of the freezing of meltwater within channels. The different types of structures reflect both different flow conditions and different stages in the freezing process. For example, the preservation of ripple structures (Fig. 8.2f) and cascades within the channel floors indicates the freezing of thin layers of moving water. Flowing water was heard during spring fieldwork, forming the large proglacial icing and areas of open water observed in front of the glacier (Bælum and Benn, 2011), suggesting that the formation of this facies may occur during this period as well as in the autumn. The disc-like bubbles, vertical bubble structures and stratification observed within the clean facies are indicative of gas occlusion as ice freezes downwards within stagnant or very low flow pools or lakes (Gow and Langston, 1977; Lorrain *et al.*, 2002; Boereboom *et al.*, 2012). Needle ice forms rapidly at the surface as a pool freezes, coalescing to form a thin top layer of ice (Perşoiu *et al.*, 2011). The remaining water then freezes slowly downwards, probably forming the stratified ice layers within the clean facies (Perşoiu *et al.*, 2011). The large, disk-shaped bubbles (Fig. 8.4f) could be related to sediment degassing (Boereboom *et al.*, 2012). The stable isotope results for clean ice show slightly heavier $\delta^{18}O$ and δD values than englacial ice but this is not statistically significant at the 95% confidence level (Table 8.3 and Fig. 8.10). Both $\delta^{18}O$ and δD display a wide range of values (5.18‰ and 28.27‰, respectively) which may reflect multiple parent waters with different isotopic compositions (Souchez *et al.*, 1988), a situation consistent with meltwater sourced from across the glacier (Souchez and de Groote, 1985).

8.4.1.4. Englacial facies

The physical character of this facies is consistent with meteoric ice formed by the firnification of snow in the accumulation area, with the alternating bubble-poor and bubble-rich layers (S_0 stratification) reflecting seasonal variations in firnification processes (Hambrey, 1975; Hambrey and Dowdeswell, 1997). Measurements of $\delta^{18}O$ of englacial ice (mean of -14.89‰; Table 8.3) are similar to values for recently formed meteoric ice within the Lomosovfonna ice core (Divine *et al.*, 2008). The mean $\delta^{18}O$ value for the englacial facies at Tellbreen is also similar to that recorded at Tunabreen (-15.34‰; *Chapter 5*), but is lighter than mean values from Svínafellsjökull (-12.40‰; Cook *et al.*, 2011) and heavier than those reported from Variegated Glacier (-16.34‰; Sharp *et al.*, 1994) and Kuannersuit Glacier (-19.80‰; Larsen *et al.*, 2010). The mean δD value for the Tellbreen englacial facies (-101.26‰; Table 8.3) is similar to the mean value for the same facies at Tunabreen (-100.83‰; *Chapter 5*), but lighter than that recorded at Svínafellsjökull (-73.60‰; Cook *et al.*, 2011) and heavier than measured mean values at Variegated Glacier (-122.12‰; Sharp *et al.*, 1994) and Kuannersuit Glacier (-144.00‰; Larsen *et al.*, 2010). This highlights the range in meteoric ice isotopic compositions that are possible across different regions. Aside from the thin debris bands (Fig. 8.3), the little

scattered debris there is within the ice probably originated as wind-blown dust (Lawson, 1979; Clarke *et al.*, 1984; Sharp *et al.*, 1994; Hubbard and Sharp, 1995; Larsen *et al.*, 2010).

8.4.2. Structural formation of Tellbreen

Figure 8.13 is a schematic diagram of the inferred structural development of Tellbreen and associated geomorphology, which is described in detail below and in *8.4.3*. The five different stages highlight the development of structures as a small body of ice progresses downglacier; Figure 8.13 should not strictly be viewed as a progression through time from (a) to (e), as the processes described may have been active at the same time but at different positions on the glacier. The active processes shown in (a) and (b) are relevant to both the current state of Tellbreen and a time when it was more dynamic, assumed to be at its LIA maximum (see below); those shown in (c) and (d) are related only to the inferred dynamic behaviour; and (e) reflects the current state of the glacier foreland and ice-marginal areas.

8.4.2.1. Stratification (S_0) and longitudinal foliation (S_1)

Although S_0 and S_1 structures have been mapped as separate features, in accordance with other structural glaciology studies (e.g. Hambrey and Dowdeswell, 1997; Hambrey and Glasser, 2003; Hambrey *et al.*, 2005; Roberson and Hubbard, 2010), it is suggested that these probably represent two end-members of the same structure rather than distinct features. Primary stratification (S_0) describes the layers of bubble-rich and bubble-poor ice formed through firnification processes in the accumulation area (cf. Hambrey, 1975; Hambrey and Dowdeswell, 1997) and is inferred to be the primary structure in the glacier (Table 8.2). When it initially forms, this layering is likely to be broadly horizontal and display only slight undulations related to the formation of seasonal snow layers, but will become progressively deformed and folded as the result of flow from the accumulation area. Folds increase in tightness as the ice converges in the narrow confines of the lower glacier tongue and is subjected to lateral compression. Eventually the original layering (S_0) is folded to such an extent that the limbs become isoclinal and parallel to glacier flow. Where the hinge lines of the isoclinal folds intersect the glacier surface, they form linear stripes, mapped as longitudinal foliation or S_1 structures (e.g. Hambrey and Dowdeswell, 1997; Hambrey and Glasser, 2003; Roberson and Hubbard, 2010). As with any continuum, some structural elements must exist between the two end-members; at Tellbreen, this is represented by the bubble stratification within the englacial ice facies (Fig. 8.4g), which was measured to dip gently in various directions within the SW and AC caves (Fig. 8.7a). As this has clearly been subjected to some degree of folding during transport from the accumulation area to the glacier front, this layering was recorded as S_1 structures, although in reality it is perhaps unnecessary to distinguish between the two as they represent the same structure.

Longitudinal supraglacial ridges, which are closely associated with longitudinal foliation, are interpreted to form through the same process. The debris was probably entrained as rockfall layers within stratification (Hambrey and Glasser, 2003; Roberson and Hubbard, 2010), which has then been tightly folded and melted out at the glacier surface as flow-parallel ridges (Figs 8.13a and 8.13b); this interpretation is supported by the predominantly angular debris within the longitudinal supraglacial ridges.

8.4.2.2. Arcuate fracture traces (S_2)

Similar to Roberson (2008) and Roberson and Hubbard (2010), S_2 arcuate fracture traces are interpreted as shear planes (Fig. 8.13c) based on the evidence that: (1) they cut across S_0 stratification at low angles and in places displace it vertically, and (2) the fine material within S_2 has a strong linear component (Fig. 8.9d), indicative of shear in the direction of ice flow (Table 8.1 and Figs 8.9g-i). The development of shear planes within polythermal valley glaciers is consistent with longitudinal compression at the margin leading to brittle failure and thrusting (Hambrey *et al.*, 2005; Roberson and Hubbard, 2010), and at Tellbreen this is supported by the vertical displacement of S_0/S_1 across S_2 planes, indicating high compressive stresses parallel to ice flow direction (Souchez, 1967; Rees and Arnold, 2007). However, the predominant orientation of S_2 structures measured at the SW sections show an approximate offset of 20º relative to ice flow direction, rather than the perpendicular relationship that might be expected in a purely compressional zone. The presence of sub-horizontal stretching lineations along these fractures (Fig. 8.9d) reveals that, rather than purely through dip-slip movement, strain along these fractures has been accommodated through a component of strike-slip (e.g. Fleming and others, 2013). Thus, the orientation of these structures suggests that the marginal areas of the glacier have experienced a transpressional stress regime (cf. Twiss and Moores, 2007; Fleming *et al.*, 2013). Transpression describes the situation where deformation along a fault deviates away from only simple shear, creating a simultaneous combination of strike-slip (simple shear) motion and co-axial strain. This results in strike-slip movement along the fault at the same time as shortening (or extension) is experienced perpendicular to the fault (Twiss and Moores, 2007). Evidence for this is found within the S_2 structures at Tellbreen, which display both a principle strike-slip (simple shear) movement along the fault (Figs 8.7b-d) in combination with an element of extension across the fault plane in the form of the mineral stretching lineations (Figs 8.7g-i and 8.9d). It has been suggested that the development of shear planes may also be facilitated by the presence of pre-existing planar structural weaknesses (Hambrey and Müller, 1978; Evans and Rea, 1999; Weiss and Schulson, 2000; Rea and Evans, 2011), such as healed crevasses (e.g. S_3 fracture traces, see *8.4.2.4.)*; the similar character and sedimentological compositions of S_2 and S_3 structures (Figs 8.10e and 8.10g) indicates that this may be the case at Tellbreen.

Stable isotope analysis of ice within the S_2 structures show slightly heavier values than englacial ice and lighter values than solid stratified ice for $\delta^{18}O$ (Table 8.3 and Fig. 8.10a), similar to the $\delta^{18}O$ composition of S_3 fracture traces (see *8.4.2.4.*). This isotopic relationship may reflect ice formation sourced from water in an open hydrological system which freezes *in situ* in a closed system (Ensminger *et al.*, 2001), and is discussed below in the context of inferred S_3 formation. The $\delta^{18}O$ values are also similar to the composition of dispersed ice, which is interpreted to result from strain-induced metamorphism of englacial ice and associated processes of recrystallisation, partial melting and removal of gases in solution (Kamb and LaChapelle, 1964; Sharp *et al.*, 1994; Hubbard and Sharp, 1995). Metamorphism of this type is likely to have occurred within S_2 structures, which contain largely bubble-free ice and display evidence of strong shear.

8.4.2.3. Fracture traces (S_3)

Fracture traces (S_3) are interpreted as healed fractures or crevasses which opened in response to extensional flow within the glacier (Hambrey, 1976; Hambrey *et al.*, 2005). Currently exposed S_3 fracture traces cross-cut S_2 shear plane structures both on the surface and in section, indicating that their formation postdates that of S_2 structures (Fig. 8.13d). Fracture traces display variable orientations with a predominant alignment perpendicular and sub-perpendicular to ice flow (Figs 8.7, 8.9e and 8.9f), which is consistent with extensional transverse crevassing, and dip at angles varying from 08-55º. In section, fracture traces contain debris ranging from well sorted individual grains and small clots of silt (Figs 8.9e and 8.9g) to poorly sorted sandy gravel containing edge-rounded clasts up to 2-3 cm diameter (Fig. 8.9f), with no evidence of shear. This debris is consistent with sediment that has been transported and partially sorted by water. These structures are explained as injections into basal crevasses of meltwater of varying turbidities and sediment loads under conditions of extensional flow and high basal water pressures, as has been actively observed at Matanuska Glacier, Alaska (Ensminger *et al.*, 2001) and described from Skeiðarárjökull, Iceland (Bennett *et al.*, 2000a). Similar to Ensminger *et al.* (2001), it appears that many of these crevasses could be better described as narrow cracks or fractures, which may not open much wider than millimetres, into which thin films or sheets of pressurised turbid water are injected. The preservation of the debris within the structures is indicative of *in situ* freezing, perhaps associated with conductive cooling from surrounding colder ice and/or fracture closure (Ensminger *et al.*, 2001). This situation describes the majority of the thin S_3 structures observed within the SW and AC caves (Figs 8.3a-c). The relatively low dip angles of these structures is inconsistent with the vertical crevasses/fractures traditionally associated with extensional flow (Rea and Evans, 2011), which may indicate they have been reoriented since formation (Evans and Rea, 1999; Woodward *et al.*, 2002; Rea and Evans, 2011; *Section 5.6.2.2.*; Figs 5.21b and 8.13d). The stable isotope analysis of ice within S_3 structures returned slightly heavier values of $\delta^{18}O$ compared to englacial ice and lighter values compared

to solid stratified ice (Table 8.3 and Fig. 8.10a), similar to the findings of Ensminger *et al.* (2001) for the debris bands at Matanuska Glacier. This may indicate formation of ice from an open hydrological system by *in situ* closed system freezing (Ensminger *et al.*, 2001), although caution is advisable as this is based on limited sampling (n = 2).

The thicker bands of sand and gravel in the SW cave are less common but are interpreted to be formed through the same process. No features similar to the coarser S_3 bands were described by Ensminger *et al.*, (2001), but they share sedimentary characteristics (poorly sorted sandy gravel) with features interpreted as upwardly injected hydrofracture structures at the bed of Kuannersuit Glacier, a surge-type glacier in West Greenland (Roberts *et al.*, 2009). The S_3 bands exposed in section demonstrate that even if the fractures reach the glacier surface, the debris within them may terminate below (Figs 8.3a-c). Not all S_3 fracture traces mapped in Figure 8.7 are likely to reach the bed or be full-depth; many may only represent surface crevassing (Rea and Evans, 2011). Type C supraglacial ridges, which are composed of sands and gravels and are mainly found on the lowest part of the glacier tongue (Figs 8.7 and 8.13d), are suggested to form from the melting-out of infilled fractures, although no direct link could be made between the two apart from similar sediment compositions and ridge orientations. The sharp-crested type C ridge displaying a prominent right-angle change of direction (Fig. 8.12e) is consistent with pressurised basal meltwater exploiting intersecting crevasses at a higher level in the glacier, as suggested by Evans and Rea (1999) for the formation of concertina or zig-zag eskers associated with surge-type glaciers. The evidence for a highly-crevassed glacier and pressurised, elevated water inferred from the S_3 fracture traces provides further support for Tellbreen having experienced extensional ice flow, high basal water pressure and a warm-based thermal regime at some point in the past.

8.4.2.4. Open fractures (S_4)

Open fractures (S_4) are extensional crevasses (Fig. 8.13d), which currently have a very restricted distribution on Tellbreen. The few examples on the lower glacier tongue (Fig. 8.8) are closely associated with the NE cave complex, where the ice margin has been gradually undercut by the northern lateral meltwater channel. The cave system has undergone significant collapse since March 2011 as observed during repeat visits, including the roof over the front part of the cave which was intact in April 2012 (Fig. 8.2g) but had collapsed by April 2013. The extensional crevasses observed in the 2009 aerial photograph in this area (Fig. 8.8) may be linked to the undercutting of the glacier margin by the meltwater channel, and as such are not directly related to the current flow regime of Tellbreen. Crevasses observed in the steepest parts of the upper basins represent bergschrund-type fracturing (Bælum and Benn, 2011).

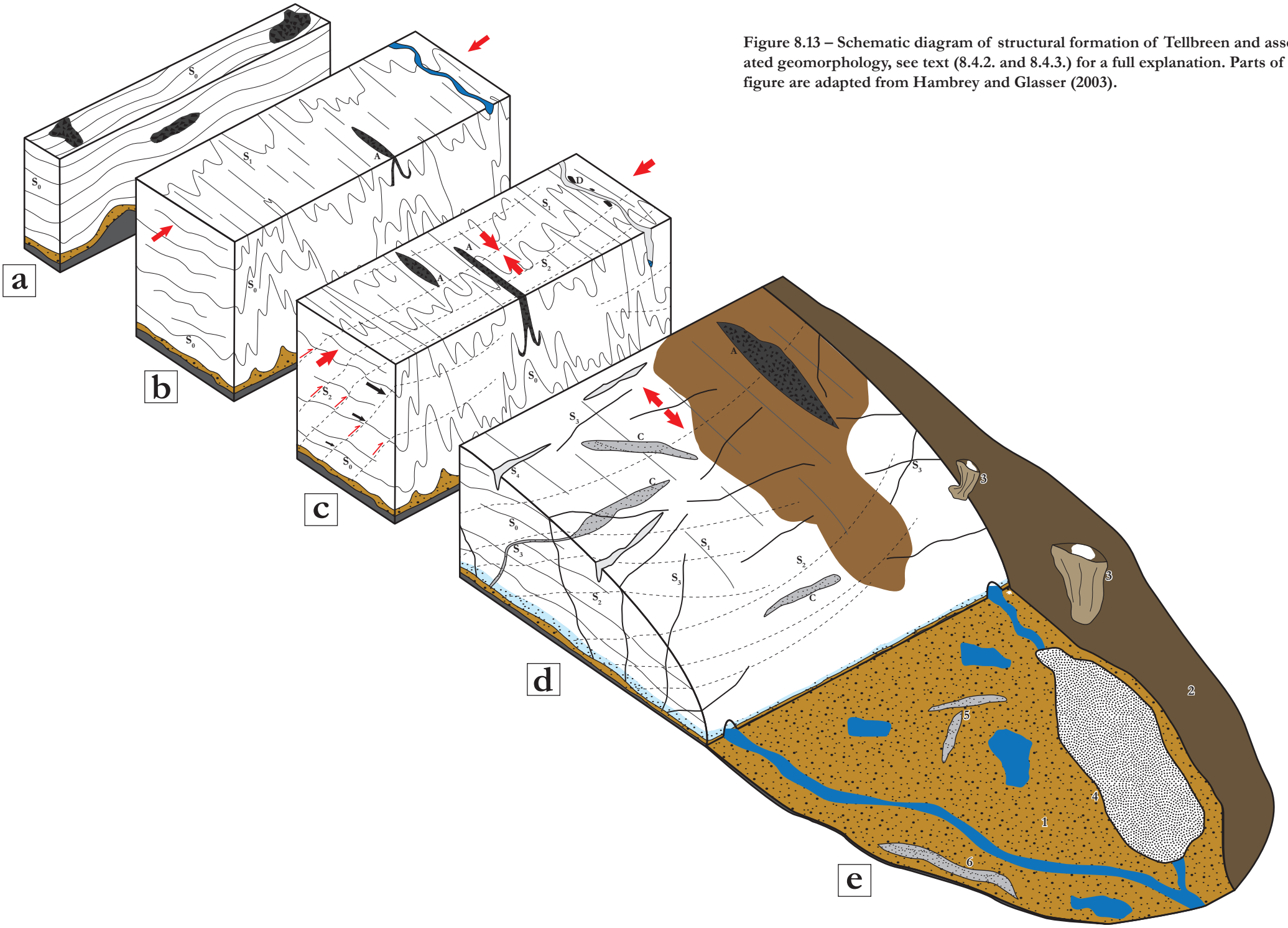

Figure 8.13 – Schematic diagram of structural formation of Tellbreen and associated geomorphology, see text (8.4.2. and 8.4.3.) for a full explanation. Parts of this figure are adapted from Hambrey and Glasser (2003).

8.4.3. Development of glacial geomorphology

The ice-marginal and proglacial geomorphology of Tellbreen is dominated by evidence for ice-cored topography and associated disintegration and sediment redistribution processes. This is apparent from the tension cracks and numerous active and relict debris flow deposits, formed by the melting and downwasting of ice cores followed by saturation and mobilisation of overlying sediment, as also described at Scott Turnerbreen (*Chapter 7*). These are often closely associated with small channels, which may have an important erosional role to play in the initiation of failure and exposure of ice cores (Sletten *et al.*, 2001). Debris flows are most common on the northern side of the glacier, in particular sourced from the lateral moraine, and sometimes extend on to the glacier surface (Figs 8.7 and 8.13e). The height of the lateral moraines (~50 m above the present glacier surface) and the downvalley extent of the latero-frontal moraine ridges provide a strong indication of the geometry of Tellbreen at its LIA maximum, demonstrating that it would have been much thicker and had a far greater ice volume (Bælum and Benn, 2011). Greater ice thicknesses and related ice flux increases are likely to have encouraged the development of warm ice at the bed (Bælum and Benn, 2011), which is consistent with the various lines of evidence within the basal ice (*8.4.1.*) and glaciological structure (*8.4.2.*) for a dynamic warm-based thermal regime of Tellbreen.

The glacier foreland is characterised by hummocky ice-cored topography (Figs 8.12h and 8.13e) indicative of *in situ* differential downwasting of a debris-covered glacier tongue. Isolated ice-cored mounds and kettle lakes on the general hummocky sediment cover exemplify this relief inversion. Active debris flows are rare within this outer zone, indicating that it is currently a fairly stable area. Based on their similar morphologies, the geometrical ridges on the Tellbreen foreland are possibly derived from type C supraglacial ridges, although their sedimentary composition was not investigated (Fig. 8.13e). It is also possible that the ridges are related to type B supraglacial ridges composed of subglacial material which, although not observed at Tellbreen, have been described in the similar valley glacier setting of Scott Turnerbreen (*Chapter 7*). In both cases, it is inferred that the geometrical ridges are related to sedimentary infilling of fractures or crevasses. The sinuous nature and alignment (sub-parallel to ice flow) of the esker-like ridge is consistent with its formation as an infilled englacial channel (Warren and Ashley, 1994), and based on its position is likely to represent a downglacier section of the same channel system that occupied the SW cave (Fig. 8.8). The sedimentary composition of the esker is very similar to the right-angled type C supraglacial ridge (Fig. 8.12e), indicating a similar glaciofluvial origin; the difference in planform morphologies is suggested to reflect deposition within a channel (esker) and within a crevasse system (type C ridge). The sands and gravels exposed within the NE cave (Figs 8.3d and 8.12a-d) are also inferred to have been deposited within the cut-and-closure channel and have effectively been superimposed on the basal ice sequence; the exceptions are the thin bands of sand and gravel found at the ice-bed interface which are inferred to represent water flow at this

contact. Type D supraglacial ridges (Figs 8.7 and 8.12d) are also glaciofluvial landforms and are interpreted as abandoned channel fills associated with the cut-and-closure formation of meltwater channels (Fig. 8.13c).

The proglacial meltwater system is dominated by large icings, which are particularly obvious during spring field seasons and often contain areas of open water (Figs 8.2a and 8.13e). These indicate that water is stored englacially all year round, as observed within the AC cave in spring, and is released periodically through the drainage system (Bælum and Benn, 2011; Naegeli, 2013; Naegeli *et al.*, accepted). In springs 2012 and 2013, observations were made of a slushy and raised AC cave floor relative to that seen the day before, indicating that this process can occur in concentrated pulses. These observations support the hypothesis of Bælum and Benn (2011), who, based on GPR data, suggested that water within Tellbreen was restricted to discrete conduits. The cold-based thermal regime of the glacier indicates that, in this case, subglacial water flow is not dependent on warm-based conditions and, therefore, cannot be directly linked to subglacial water production (Bælum and Benn, 2011; Naegeli *et al.*, accepted). The storage and release of water within a cold glacier to form icings during winter months has also been reported from nearby Scott Turnerbreen (*Chapter 7*), where the strict link between polythermal glaciers (e.g. warm-based ice) and proglacial icings was first questioned (Hodgkins *et al.*, 2004). In both cases, the origin of this water, and how it is able to be stored within cold glaciers and then be released in winter months, remains enigmatic.

8.5 Summary

Tellbreen is a currently cold-based valley glacier which has been retreating and downwasting since its LIA maximum, when it was significantly thicker and terminated ~1 km downvalley from its present position. It has been hypothesised that Tellbreen had a warm-based thermal regime at this time (Bælum and Benn, 2011) and this is supported by exposures of basal ice and glaciological structures in ice caves in the lower glacier tongue. The basal ice sequence is indicative of freeze-on of saturated and deformed subglacial debris at the ice-bed interface, forming solid stratified facies ice, overlain by dispersed facies ice which is inferred to have formed through processes of strain-induced metamorphism of englacial ice in close proximity to the bed. Both of these are strongly indicative of a warm-based thermal regime and an active basal meltwater system at some point in the past.

The glaciological structure of Tellbreen (Fig. 8.13) shares many similarities with similar valley glaciers investigated elsewhere in Svalbard (Hambrey and Dowdeswell, 1997; Glasser *et al.*, 1998b; Hambrey and Glasser, 2003; Hambrey *et al.*, 2005; Roberson and Hubbard, 2010; Midgley *et al.*, 2013), including stratification (S_0) derived from snowfall in the accumulation area; the development of longitudinal foliation (S_1) and flow-parallel supraglacial ridges through the intense folding of S_0 as ice flows into a narrow channel; and the presence of multiple fracture traces on the glacier surface. The fracture traces can be subdivided into two

populations and are linked to thin debris bands exposed in the ice caves. Arcuate fracture traces (S_2) are interpreted as shear planes displaying evidence for both vertical displacement and stretching in the direction of ice flow, and are suggested to form in zone of compression/marginal transpression; S_3 fracture traces are interpreted as healed crevasses, which cut across S_0-S_2 structures and indicate a widespread extensional stress regime at some point in the past. Silt, sands and gravels exposed within S_3 fractures are interpreted as injections of highly-pressurised and turbid basal meltwater which have frozen *in situ*, which may melt-out on the glacier surface to form type C ridges composed of glaciofluvial sediments. The glacier foreland is dominated by hummocky ice-cored topography, indicating downwasting and stagnation of a debris-covered glacier tongue.

The englacial exposures and proglacial geomorphology suggest that Tellbreen was formerly warm-based, had a dynamic and highly-pressurised subglacial meltwater system, experienced heavy crevassing and phases of compression-dominant and extension-dominant stress regimes, and has become cold-based and undergone significant terminus retreat and *in situ* downwasting since its LIA maximum; together, these factors are consistent with surge-type behaviour described from other Svalbard glaciers (Hambrey and Dowdeswell, 1997; Glasser *et al.*, 1998a; Woodward *et al.*, 2002; Sund, 2006).

Chapter Nine
Discussion

'While there is no scientific correlation between surging glaciers and the Little Ice Age climate, elders often merge discussions about extreme cold with those about troublesome behaviour of glaciers during the 19th century'

Cruickshank (2001; p.387)

9. Discussion

9.1. Introduction

This chapter draws together the main findings from *Chapters 4-8*, highlighting the common glaciological and geomorphological features which relate to surging and dynamic ice flow observed across several or all of the studied glaciers, before discussing these within a wider context. Dynamic ice flow is defined here as warm-based flow, typically associated with increased ice velocities and glacier advance. Five main interconnected themes are considered: the formation of basal ice facies (*9.2.*); the development of glaciological structures (*9.3.*); basal ice and structural glaciological signatures of surging (*9.4.*); landform-sediment assemblages produced by surging glaciers on Svalbard (*9.5.*); and the links between glacier surges on Svalbard and climate (*9.6.*).

9.2. Formation of basal ice facies

Only very few studies have investigated the formation of ice facies within Svalbard glaciers (e.g. Boulton and Spring, 1986; Jonsson and Hansson, 1990; Glasser and Hambrey, 2002; Hubbard *et al.*, 2004; Roberson *et al.*, 2011) and, of these, none have specifically looked at basal ice stratigraphies associated with glacier surges. It is suggested that the formation of the suite of facies exposed at Tunabreen can directly be linked to surge activity and, as such, this combination of ice facies represents a signature by which to identify evidence for surges or surge-like behaviour within glaciers with no record of surging (Fig. 9.1). The latter observation is based on similarities between the Tunabreen basal ice sequence and that at Tellbreen, a small, cold-based valley glacier with no known surge activity, but which was likely to have been more dynamic at its LIA maximum (*Chapter 8*). Due to the paucity of existing work on this topic in Svalbard, the interpretations of basal ice formation presented in this study have necessarily drawn on examples from other locations, predominantly of surge-type glaciers.

The formation of the stratified (comprised of solid stratified and banded subfacies; Table 9.1) and dispersed ice facies at Tunabreen and Tellbreen can be directly linked to processes active during periods of dynamic glacier flow; in the case of Tunabreen, this was during surges, and for Tellbreen during its LIA maximum position. This basal ice signature of surging/dynamic ice flow will be discussed in greater detail below.

9.2.1. Stratified facies

The solid stratified subfacies is interpreted as saturated subglacial debris which has been entrained by freeze-on, either at the glacier base or in an englacial position following processes including injections into basal crevasses, thrust faulting and hydrofracturing, or some combination of these (*section 5.6.2.2.*). The latter examples are discussed in further detail below (*9.3*) in the context of tectonic deformation and its links to dynamic flow, and so these processes will not be considered further here, other than the final freezing-on of the material once

incorporated into the ice. This subfacies is suggested to have originated as saturated subglacial material, demonstrated by the high ice content in the form of both interstitial ice and larger ice lenses. The presence of saturated subglacial debris is consistent with elevated basal water pressures associated with the active phase of a surge and/or warm-based conditions at the bed of a polythermal valley glacier. The stable isotope data from this facies at both Tunabreen and Tellbreen show that it has been enhanced in heavy ^{18}O isotopes relative to englacial facies ice (Tables 5.1 and 8.3; Figs 5.11 and 8.10a), which is interpreted as evidence that it formed by the refreezing of highly-saturated debris (Lawson, 1979; Knight, 1989; Hubbard and Sharp, 1993; Iverson and Souchez, 1996). The absence of freezing slopes when the data is plotted co-isotopically implies that the facies did not form by the refreezing of a parent water from a local source only; instead, this is interpreted as the isotope composition reflecting the continuous influx of a range of different parent waters with variable initial isotopic compositions (Sharp *et al.*, 1994), which then subsequently refreeze. This situation is consistent with the production of water through net basal melting across large parts of the bed which are at the pressure-melting point, saturating subglacial debris with water from various sources. The time-lapse imagery of the Paulabreen surge in 2005-06 (Kristensen and Benn, 2012; video included on CD inside back cover) demonstrates the large amount of deformation that occurs at the ice margin, with blocks of ice being rotated, folded, stacked on top of each other and collapsing as the ice advances downfjord. This has the potential for a large amount of mixing of different ice facies and/or ice sourced from different areas, which may have variable initial isotopic compositions (Souchez *et al.*, 1988). Melting of this ice at the bed would, therefore, lead to a mix of parent waters in any one localised area, saturating the subglacial debris. The debris is subsequently entrained on to the glacier via freeze-on processes: Firstly, at the transition between warm, active ice and cold, inactive marginal ice. This situation is likely during polythermal glacier surges, where inactive ice towards the margins remains cold (Murray *et al.*, 1997). The propagation of warm, active ice and associated saturated debris into these marginal areas creates a thermal transition, resulting in freeze-on of the solid stratified subfacies. This can happen throughout the active phase as warm ice propagates towards the cold margin. Secondly, freeze-on could occur during the final stages of the active phase or period of dynamic ice flow, when a cold wave or 'freezing front' propagates through a thin and heavily-crevassed glacier, or as cold ice is advected downglacier (Alley *et al.*, 1997; Larsen *et al.*, 2010).

This demonstrates that the formation of the solid stratified subfacies can be directly linked to processes active during surges or dynamic, warm-based ice flow, including: (i) the presence of saturated subglacial sediments; (ii) deformation and continuous reorganisation of the basal ice sequence resulting in the complex mixing of ice from various sources and with variable initial isotopic compositions. This mix of ice, when subjected to basal melting, provides the source for the parent waters which saturate the subglacial debris; (iii) the continuous propagation of warm, active ice into cold, inactive marginal areas, leading to freeze-

on of saturated debris at the thermal transition; (iv) the advection of cold ice downglacier during the final stages of the active phase and the propagation of a cold wave through a thin and heavily-crevassed glacier upon the termination of active flow, both of which would be associated with the progression of a freezing front into saturated subglacial debris.

The banded subfacies is interpreted to form through a combination of basal freeze-on and localised regelation processes, resulting in the entrainment of thin debris laminae of subglacial sediment separated by clean, bubble-poor ice. The thickness of the banded subfacies indicates that it has been subjected to significant tectonic thickening, largely through the folding and stacking of ice layers and blocks (Sugden *et al.*, 1987a; Evans, 1989; Sharp *et al.*, 1994). Evidence for such deformation is present at both the NW and SE sections at Tunabreen, largely in the form of folds and faults within the laminae and the complex stratigraphy of ice facies. This deformation can be observed in the time-lapse imagery of the Paulabreen surge presented by Kristensen and Benn (2012). It seems unlikely that the initial entrainment of the debris laminae within the banded subfacies, which are for the most part horizontally layered and continuous for tens of metres, could occur at the bed of a glacier which is being subjected to such variable and large-scale deformation as observed at Paulabreen. Instead, it is suggested that the banded subfacies predominantly formed prior to the active phase of the surge, i.e. during quiescence, and/or was inherited from a previous surge. This was then deformed and tectonically thickened during the subsequent active phase to produce the thick sequences and complex stratigraphy observed at the margin post-surge.

9.2.2. Dispersed facies

Dispersed facies ice, as identified at Tunabreen and Tellbreen, has been described from the basal ice sequences of a number of glaciers (Lawson, 1979; Larsen *et al.*, 2010; Cook *et al.*, 2011), and has also been referred to as ‘clotted facies’ (Knight, 1987; Sugden *et al.*, 1987b; Knight and Knight, 1994; Knight *et al.*, 1994) and ‘clear facies’ (Sharp *et al.*, 1994; Hubbard and Sharp, 1995; Hubbard *et al.*, 2000) ice. These facies are all descriptively similar (Cook *et al.*, 2011) but have been interpreted to have formed by a range of processes, including a combination of firnification and regelation (Lawson, 1979); regelation in the interior of ice sheets (Knight, 1987; Sugden *et al.*, 1987a); and metamorphism of englacial ice close to the glacier bed as a result of tectonic processes (Sharp *et al.*, 1994; Hubbard *et al.*, 2000; Cook *et al.*, 2011). This demonstrates that the origin of dispersed facies ice is, in general, still poorly understood (Cook *et al.*, 2011), with current interpretations favouring either a primarily sedimentary (Lawson, 1979; Knight, 1987; Sugden *et al.*, 1987b) or tectonic (Sharp *et al.*, 1994; Hubbard *et al.*, 2000; Cook *et al.*, 2011) origin. The characteristics of dispersed facies ice identified at Tunabreen and Tellbreen indicate that the latter interpretation is valid, and it is suggested that its formation can therefore be directly linked to processes active during surges or periods of dynamic ice flow (Table 9.1).

One of the main characteristics of dispersed facies ice is its largely bubble-poor nature, with some areas entirely devoid of bubbles. These areas are typically adjacent to the contact with stratified ice facies, which underlies dispersed facies ice in most cases (Fig. 9.1). This is interpreted as the result of strain-induced metamorphism of englacial ice close to the bed (Hubbard *et al.*, 2000) due to intense and variable shear, resulting in melting and refreezing at grain boundaries and the expulsion of gas in solution (Lliboutry, 1993) away from the shear zone. Evidence for the expulsion of gas takes the form of thin stringers or worms of bubbles routed along crystal boundaries which extend from the area of bubble-free dispersed ice (Fig. 9.1e). The second main characteristic of dispersed facies ice is the presence of individual grains or small clots of typically silt-sized material; this is inferred to be the result from thin films of muddy water sourced from adjacent saturated subglacial debris (which becomes solid stratified subfacies ice when it freezes-on) which have been squeezed along the intercrystalline vein network (Knight and Knight, 1994) in a manner similar to the expelled gases (Fig. 9.1e).

The formation of dispersed facies ice can be summarised as follows: pre-active phase, the ice sequence at the bed consists of stratified facies ice overlain by englacial facies ice, the latter characterised by intercalated layers of bubble-rich and bubble-poor ice (Fig. 9.1d). During the active phase, ice at the glacier bed is at the pressure-melting point and basal water pressures are high, facilitating increased ice velocities. A shear zone develops close to the bed where englacial ice overlies saturated subglacial debris. This shearing results in strain-induced metamorphism within the lowermost parts of the englacial facies ice, initiating multiple melting and refreezing events at grain boundaries and expelling gas and muddy water through the intercrystalline networks, the latter sourced from underlying saturated subglacial debris/stratified ice facies (Fig. 9.1e). The melting and refreezing and movement of muddy water and gases is envisaged to effectively occur in a wet ‘mush-like’ zone at the base of the englacial ice, where it has been warmed to the pressure-melting point. This demonstrates that the formation of dispersed facies ice is the result of tectonic activity at the glacier bed and, therefore, represents a diagnostic signature of dynamic ice flow, such as that experienced during surges.

9.2.3. Deformation sub-environments within basal ice sequences

The arrangement of ice facies at Tunabreen, particularly at the NW section, is indicative of different phases of deformation occurring over short distances. This is demonstrated by the different relationships between facies in close proximity, for example where banded facies ice is truncated by solid stratified ice in one area, but the two are horizontally-bedded within ~ten metres (Fig. 5.5a). This is suggested to provide evidence for different sub-environments of deformation occurring at the same time over short distances, as can be observed on the time-lapse imagery of the Paulabreen surge (Kristensen and Benn, 2012), and results in the complex stratigraphies of, and deformation evidence, within basal ice.

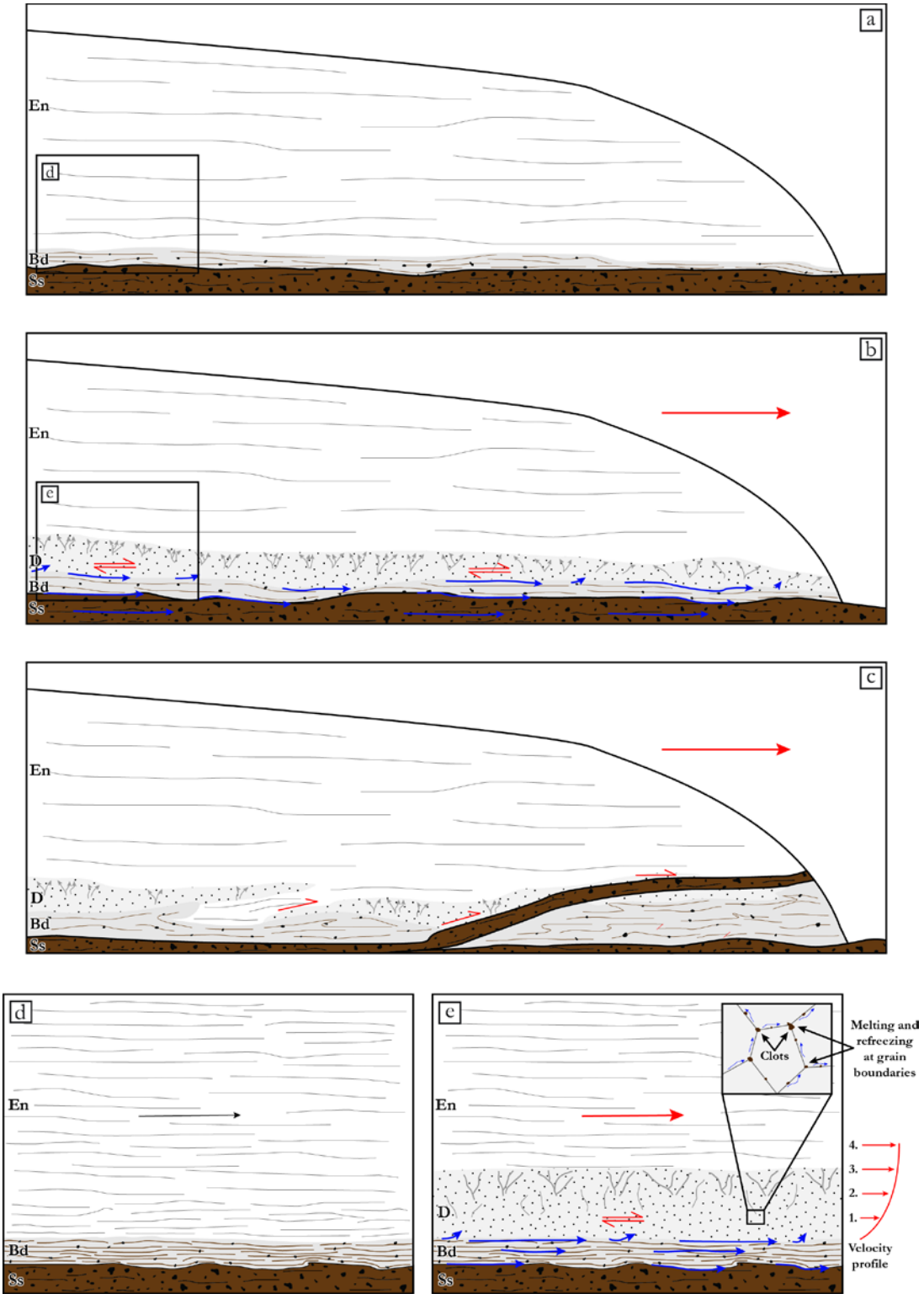

Figure 9.1 – Basal ice formation schematic. (a) Pre-surge stratigraphy shows stratified basal ice composed of solid stratified ice/subglacial debris overlain by banded ice and englacial ice. (b) The glacier surges, producing meltwater at the bed which saturates the subglacial debris and creating a zone of shearing and variable deformation at the base of the englacial ice, facilitating strain-induced metamorphism in the lowermost sections. (c) The basal ice sequence is tectonically deformed towards the ice margins, stacking ice facies on top of each other and thickening the banded subfacies through folding and faulting. The solid stratified subfacies forms through the freeze-on of saturated subglacial debris at thermal transition from warm, active ice to cold, inactive marginal ice, or upon surge termination. (d) and (e) Details on the formation of dispersed facies ice through strain-induced metamorphism of englacial ice. See (a) and (b) for location of insets.

Table 9.1 – Summary of basal ice facies formation and links to dynamic ice flow.

Basal ice facies	Sites	Inferred formation processes	Links to surge/ice flow dynamics
Solid stratified (Ss)	TNB, TLB	Freeze-on of subglacial debris	Marginal freeze-on of saturated subglacial debris, either at any point during the active/dynamic phase as warm active ice meets cold inactive ice; or close to surge termination as a cold wave propagates through a thin and heavily-crevassed terminus or as cold ice is advected downglacier.
Banded (Bd)	TNB	Freeze-on and regelation; tectonic thickening	Marginal/basal freeze-on and regelation processes associated with the thermal transition between warm and cold ice, followed by tectonic thickening through folding and stacking. Some of this facies may be inherited from a previous surge and subsequently redeformed.
Dispersed (D)	TNB, TLB	Strain-induced metamorphism of englacial facies ice (En)	Formed by intense shearing of warm and wet englacial ice during the active/dynamic flow phase, resulting in the expulsion of bubbles and the mobilisation of muddy water along the vein networks around grain boundaries.

9.3. The development of glaciological structure during surges

The mapping and evaluation of glaciological structures, typically exposed on the glacier surface, can provide important information about both current and former flow dynamics (Hambrey *et al.*, 2005), and a number of studies have undertaken structural investigations on surge-type glaciers on Svalbard and linked the development of different elements to changes in the stress regime which are unique to surges (e.g. Hodgkins and Dowdeswell, 1994; Hambrey *et al.*, 1996; Hambrey and Dowdeswell, 1997; Murray *et al.*, 1997, 2000; Glasser *et al.*, 1998b; Woodward *et al.*, 2002; Fleming *et al.*, 2013). These examples have advanced our understanding of ice flow dynamics during surges and the connections between glaciological structure and glacial geomorphology, which, as outlined below in *9.5.*, can be used to identify glacier surges where direct observations are lacking. However, particularly in the case of small valley glaciers, it is difficult to unequivocally link the geomorphology with surge activity, even when they have a known surge history (see *9.5.2.3.* below). Coupled with the fact that small valley glaciers have only rarely been observed during the active phase of a surge (Hambrey and Dowdeswell, 1997; Sund and Eiken, 2004; Roberts *et al.*, 2009; Larsen *et al.*, 2010), and a number are suggested to have surged during the LIA but show no signs of doing so again (Dowdeswell *et al.*, 1995; Hodgkins *et al.*, 1999; Hansen, 2003; Midgley *et al.*, 2013), it is possible that the total number of glaciers which are of surge-type or display evidence of having surged is underrepresented in Svalbard. Structural glaciological evidence linked to surge activity, ideally in conjunction with basal ice (*9.2.*) and glacial geomorphological (*9.5.*) investigations, provides an opportunity to assess former flow dynamics of glaciers and, therefore, can be an important way to identify surge-like behaviour of glaciers during the LIA. This section discusses the common structural elements (Table 9.2) identified on and within glaciers, both with a known and no surge history, and their links to flow dynamics which are diagnostic of surges or surge-like advances.

Table 9.2 – Summary of structural glaciological features and links to dynamic ice flow. *S_0 and S_1 represent end-members of a structural continuum.

Planar glaciological structures	Links to surge/ice flow dynamics
Stratification (S_0)*	Formed pre-surge/dynamic flow, may be folded during active flow phases.
Longitudinal foliation (S_1)*	Formed through compression and tight folding of S_0, may become deformed or dislocated during active flow phases.
Shear planes (S_2)	Formed during active flow phases due to both longitudinal compression and extensional shear parallel to ice flow towards the glacier margin, indicating a transpressional stress regime in lateral positions. Can elevate subglacial debris to en- and supraglacial positions.
Crevasse traces (S_3)	Formed during active flow phases due to extensional (transverse traces) or compressional (longitudinal traces) flow, followed by healing of crevasses upon active flow termination. Subglacial debris can be injected into crevasses during active flow, elevating it to en- and supraglacial positions.
Open crevasses (S_4)	Formed during active flow phases due to extensional (transverse traces) or compressional (longitudinal traces) flow. Subglacial debris can be injected into crevasses during active flow, elevating it to en- and supraglacial positions.

9.3.1. Primary stratification and longitudinal foliation

The development of horizontally-layered primary stratification occurs in the accumulation zone during the quiescent phase as mass accumulates and eventually becomes englacial ice due to firnification processes; this is common to all glaciers, surge-type or non-surge-type (Hambrey and Dowdeswell, 1997; Hambrey and Glasser, 2003). There is considerable evidence of the deformation of stratification, typically in the form of offset layers due to faulting associated with shear plane development (Fig. 8.13c; see *9.3.2.*), intense folding due to lateral compression (Fleming *et al.*, 2013) which is suggested to lead to the formation of longitudinal foliation (Hambrey and Glasser, 2003), and the erasing of layering due to intense shearing and strain-induced metamorphism of englacial ice close to the glacier bed, which causes the expulsion of gases along grain boundaries and forms dispersed facies ice (Fig. 9.1e).

Longitudinal foliation is thought to evolve from tightly folded primary stratification, which in effect are both on a continuum rather than separate structures, typically due to lateral compression as ice is funnelled from the accumulation zone into a narrow valley (Hambrey and Glasser, 2003). The development of longitudinal foliation occurs in all glaciers and, although indicative of intense internal deformation due to compressive stresses caused by a change in flow regime (e.g. from accumulation area to narrow trunk), does not require a surge or surge-like behaviour for its formation (Hambrey *et al.*, 2005). Evidence for dynamic flow associated with surging can be recorded in the configuration of longitudinal foliation, however. This typically takes the form of deformed or dislocated flow lines which are indicative of irregular flow within adjacent flow-units, such as observed at Finsterwalderbreen (e.g. Fig. 6.2c) and Scott Turnerbreen.

9.3.2. Shear planes

The arcuate fracture traces exposed on the surface towards the snout of many land-terminating glaciers on Svalbard (e.g. Hambrey and Dowdeswell, 1997; Hambrey and Glasser, 2003; Hambrey *et al.*, 2005; Roberson and Hubbard, 2010; Midgley *et al.*, 2013; Figs 7.3 and 8.9; this

study) and in other glacierised regions (e.g. Raymond *et al.*, 1987; Lawson *et al.*, 1994; Glasser *et al.*, 2003b; Goodsell *et al.*, 2005; Roberson, 2008; Appleby *et al.*, 2010) are typically interpreted as shear planes within the ice which develop in response to longitudinal compressive stresses. Similar interpretations have been made by this and other studies of surge-type glaciers on Svalbard for some inclined, often debris-laden, structures exposed in tidewater ice cliffs (Glasser *et al.*, 1998b; Fleming *et al.*, 2013) and identified from ground-penetrating radar data (Murray *et al.*, 1997; Murray and Booth, 2010). In all cases, these often contain subglacial debris and so clearly have the ability to elevate material from the bed to en- and supraglacial positions, which would require substantial (tens of metres) uplift and displacement along the shear planes; this has led a number of studies to suggest that the shear planes represent thrust faults within the glacier (Hambrey *et al.*, 1996, 2005; Murray *et al.*, 1997; Glasser *et al.*, 1998b; Murray and Booth, 2010). Directly observed evidence for such vertical displacement, however, is often lacking, or records only minimal movement (Hambrey *et al.*, 2005); a good example of this is at Tellbreen where displacement of stratification within englacial ice on either side of the shear planes is of the order of centimetres. This inconsistency has led to a number of criticisms of the widespread invoking of strictly thrust faulting as a method for elevating debris within glacial systems. (cf. Evans and Rea, 1999; Woodward *et al.*, 2002, 2003a; Moore *et al.*, 2010; Rea and Evans, 2011).

Based on the observations presented in this and other studies, it is suggested that: (i) the development of shear planes is common within Svalbard glaciers; (ii) shear planes develop due to longitudinal compression near the glacier snout, and so are consistent with dynamic flow within a polythermal glacier as active ice propagates into inactive ice, such as at a surge front (Murray *et al.*, 1997); (iii) several main formational mechanisms linked to dynamic ice flow are responsible for the development of shear planes, namely thrust faulting (Glasser *et al.*, 1998b; Hambrey *et al.*, 2005), thrust-style deformation along reoriented structural weaknesses (Evans and Rea, 1999; Woodward *et al.*, 2002; Rea and Evans, 2011), and strike-slip movement indicative of a transpressional glaciotectonic regime towards the lateral margins (Fleming *et al.*, 2013; Fig. 9.2); and (iv) shear planes are an important mechanism for incorporating and elevating subglacial debris within glaciers on Svalbard, particularly during surges. Some of these points will now be elaborated on.

The time-lapse video of the Paulabreen surge in 2005-06 (Kristensen and Benn, 2012) shows clear evidence for ice blocks at the margin being stacked on top of and overriding each other (e.g. between 00:20 and 00:40, towards the true right of the view) as the glacier advances. This demonstrates, perhaps unequivocally for the first time in Svalbard, that thrust faulting, in combination with folding and buckling, occurs within glacier ice during surges. The ice is clearly very debris-rich, including at the décollement between ice blocks, indicating the presence of sediment within shear planes. One of the main criticisms of a purely thrust fault origin for the elevation of subglacial material is the tens of metres of total displacement this

would require (Rea and Evans, 2011), evidence for which is typically lacking, such as a hanging-wall block of equal length extending beyond the top of the debris-rich structure. The time-lapse imagery from Paulabreen (Kristensen and Benn, 2012), however, suggests that the lack of a hanging-wall block is not surprising, as there is clear evidence for the continuous collapse of overriding ice blocks once they become too unstable due to the absence of underlying support (e.g. around 00:45). This evidence suggests that the elevation of subglacial material within classic thrust faults may be possible; however, the compressive nature of their development suggests that these would have very little space within them and would only form very thin (e.g. millimetre to centimetre scale) debris-rich structures, such as those shown in Figure 5.14a at Tunabreen. It is difficult to envisage how thicker bands (e.g. decimetre to metre scale) of debris could be incorporated through thrust faulting alone, particularly when the subglacial sediment is highly saturated, as is likely due to the high basal water pressures experienced during a surge, and therefore would be highly-deformable when subjected to compressive stresses. This suggests that the majority of thrust faults within glaciers are likely to be extremely debris-poor fractures, characterised by thin silt accumulations which indicate movement of thin films of water along the shear plane, such as observed within the lower tongue areas of Scott Turnerbreen (Fig. 7.3) and Tellbreen (Figs 8.9 and 8.10d). The evidence for water films within the shear plane also supports the suggestion that thrust fault development requires the structures to be in hydraulic communication with highly-pressurised water (Roberts *et al.*, 2009; Moore *et al.*, 2010).

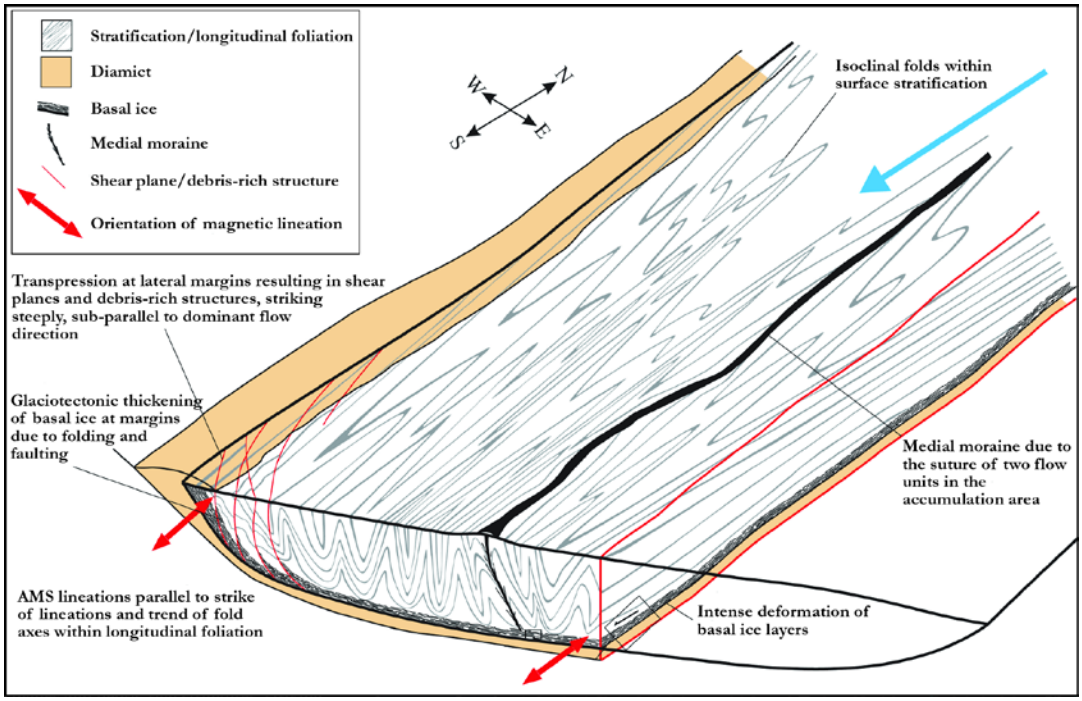

Figure 9.2 – Schematic diagram of Tunabreen glaciological structure and its relation to AMS lineation orientation, adapted from Fleming *et al.* (2013). Note zone dominated by transpressional glaciotectonic regime at lateral margin, resulting in steep shear planes with evidence for strike-slip movement along them.

Although thrust faulting alone may be able to elevate subglacial debris from the bed to englacial positions, this appears to be rare occurrence, and therefore the favoured explanation for the formation of many inclined debris-rich shear planes is through the deformation of reoriented pre-existing weaknesses. This mechanism was proposed by Evans and Rea (1999, 2005), Woodward *et al.* (2002) and Rea and Evans (2011) as a way to explain subglacial debris-rich shear planes within glaciers without the problems of accommodating the required tens-of-metres of displacement. It was suggested that near-vertical injections of subglacial debris into crevasses, as observed at the margins of both Nathorstbreen (Fig. 4.6d) and Tunabreen (Fig. 5.14g), associated with a previous surge, would be reoriented in the direction of ice flow during quiescence. This would then provide a favourable slip plane for thrust-style displacement (TSD) when subjected to compressive forces during a subsequent surge (Moore *et al.*, 2010; Rea and Evans, 2011). In this way, total displacements would be considerably smaller than required to elevate debris from the bed. In addition to TSD along reoriented slip planes, structural evidence from the lateral margins of Tunabreen (Fleming *et al.*, 2013), Tellbreen (this study) and Paulabreen (Fleming and Lovell, in prep.) demonstrate that shear along debris-rich structures can also be in a direction transverse to dominant ice flow, indicating strike-slip movement. This evidence takes the form of sheared debris lineations on the surface of the structures which record oblique or transverse slip (Fleming *et al.*, 2013), and is interpreted as evidence for a transpressional glaciotectonic regime towards the lateral margins, rather than purely a compressional regime aligned with the dominant ice flow direction. This is also envisaged to exploit reoriented pre-existing debris-rich structures, such as crevasse squeezes inherited from a previous surge.

The presence of shear planes of the types described above is suggested to be strongly indicative of surging or surge-like advances. This is particularly evident for the debris-rich faults interpreted as reoriented structures which have undergone subsequent deformation (TSD or strike-slip) along a favourable slip plane, as this requires the inheritance of pre-existing debris-rich structures. The simplest explanation for this is that they initially formed as near-vertical crevasse squeezes through the injection of highly-saturated subglacial material into basal crevasses during the active phase of a surge, and were then reoriented in the direction of ice flow during quiescent conditions, forming a favourably-inclined slip plane for TSD and strike-slip deformation during a subsequent surge (Evans and Rea, 1999, 2005; Moore *et al.*, 2010; Rea and Evans, 2011); these structures are therefore strongly diagnostic of surging. Arcuate shear planes are found towards the snout of most land-terminating glaciers on Svalbard, including both known surge-type and non-surge-type glaciers. This therefore implies that their formation does not necessarily require processes unique to surges, as they could also form at the transition between warm and cold ice within a polythermal glacier, and as a result it has been suggested that their presence does not provide diagnostic evidence of surging (Hambrey *et al.*, 2005). Shear planes do, however, provide evidence for dynamic, warm-based ice flow

(Hambrey *et al.*, 2005), which, when found within currently inactive or entirely cold-based glaciers (e.g. Scott Turnerbreen and Tellbreen), implies that a switch in thermal regime has occurred. In addition, the development of thrust faults within glacier ice was suggested by Moore *et al.* (2010) to possibly only occur under certain conditions, namely within thin ice subjected to longitudinal compression and where pre-existing weakness were exploited by highly-pressurised water; this describes conditions common during the active phase of surges. It is therefore suggested that the presence of shear planes within land-terminating glaciers is consistent with warm-based dynamic ice flow, such as experienced during the active phase of a surge (e.g. Scott Turnerbreen), or at a time when currently cold-based valley glaciers were thicker and more advanced, such as at their LIA maximum (e.g. Tellbreen).

One final observation is that arcuate shear planes of the type common within land-terminating glaciers are notably absent towards the front of large tidewater surge-type glaciers (e.g. Fig. 1 in Fleming *et al.*, 2013). This is suggested to reflect the dominance of extensional glaciotectonic regimes in the centre of tidewater glacier surges, reflected by the presence of widespread areas of transverse crevassing (e.g. Figs 4.4b and 5.3; Hodgkins and Dowdeswell, 1994). It has been noted that crevasse patterns often propagate upglacier from the terminus during tidewater surges (e.g. Fig. 5.3), leading to the suggestion that the glacier experiences an extensional regime throughout (Murray *et al.*, 2003b), rather than changes from compression-dominated to extension-dominated regimes associated with the passage of a surge front (Murray *et al.*, 1997). In these situations, compression is confined to the lateral margins, where warm surging ice meets cold inactive ice or topographic obstructions, and this is where debris-rich shear planes and faulting and folding of the basal ice is exposed (e.g. at Tunabreen). This variation in dominant stress regimes not only impacts the formation of debris-rich structures, but also the landform record left behind post-surge (see *9.5.1.5.*).

9.3.3. Open crevasses and crevasse traces

As highlighted above, the presence of large crevasses aligned transverse to flow is a key indicator of an extensional glaciotectonic regime and, when found throughout glaciers (e.g. not only at the very front of tidewater glaciers or close to headwalls in the accumulation zone), is generally diagnostic of increased ice velocities associated with surging (Meier and Post, 1969; Copland *et al.*, 2003). As a result, surges of many glaciers on Svalbard have been first identified based on the development of intense crevassing (Dowdeswell and Benham, 2003; Sund, 2006; Sund *et al.*, 2009). Towards the front of tidewater surge-type glaciers in their active phase, the crevassing can be so dense that it has a chaotic appearance, rather than only large transverse crevasses (e.g. Fig. 4.4). Crevasses can also form parallel or sub-parallel to ice flow, indicating zones of longitudinal compression (Hodgkins and Dowdeswell, 1994), and as conjugate pairs, often in shear zones at the lateral margins of surging ice (Rea and Evans, 2011); both of these were apparent within the crevasse patterns of Nathorstbreen and Tunabreen at the height of their

recent surges. Crevassing is also responsible for the formation of debris-rich structures within surge-type glaciers through the injection of highly-saturated subglacial debris into basal crevasses (e.g. Figs 4.6d and 5.14g), which either melt out during quiescence to form geometrical ridge networks on the glacier foreland (see *9.5.1.5.*; Sharp, 1985a) or are reoriented during quiescence and subjected to TSD (Evans and Rea, 1999, 2005; Rea and Evans, 2011) or strike-slip during a subsequent surge (see *9.3.2.*). A third mechanism for forming debris-rich structures proposed by this study is through hydrofracturing of ice by highly-saturated and pressurised subglacial sediment (Fig. 5.21c).

Widespread crevassing is a very clear indicator of actively surging glaciers on Svalbard. The identification of former extensional flow due to increased ice velocities during a surge (Hodgkins and Dowdeswell, 1994; Lawson *et al.*, 1994) within a glacier which no longer displays such obvious signs can be based on two main characteristics: the presence of geometrical ridge networks on the glacier foreland (see *9.5.1.5.*) and an abundance of crevasse traces on the glacier surface, which represent healed crevasses (Hambrey, 1976; Hambrey and Dowdeswell, 1997). Abundant crevasse traces are apparent on both glaciers which are known to have surged (Hambrey and Dowdeswell, 1997) and those which have no surge history (Hansen, 2003; Hambrey *et al.*, 2005; Midgley *et al.*, 2013). Similar to arcuate shear planes, the presence of crevasse traces is strongly indicative of former dynamic, warm-based ice flow, whether during known surges (e.g. Hessbreen, Scott Turnerbreen) or during LIA advances (e.g. Tellbreen, Midtre Lovénbreen, Austre Lovénbreen); both appear to produce an identical structural glaciological record.

9.4 Basal ice and structural glaciological signatures of surging

Glaciotectonic processes active during surges or periods of dynamic ice flow can be linked to the development and formation of basal ice sequences and glaciological structures with particular characteristics. This indicates that it may be possible to identify former dynamism based on similar evidence exposed in glaciers on Svalbard with an unknown flow history. Similar to when inferring former glacier dynamics based on geomorphological evidence using a landsystems approach (Evans, 2005; see *9.5.*), the presence of a combination of these elements provides the strongest case for such interpretations.

The unique signature of surging recorded in basal ice sequences is suggested to consist of: (i) layers or debris-rich structures of solid stratified ice, particularly in an englacial position, which indicate they have been elevated above the bed; (ii) thick sequences of banded ice with abundant evidence for glaciotectonic deformation; (iii) zones of dispersed facies ice at the interface between debris-rich basal ice and englacial ice; (iv) complex stratigraphies of all ice facies as a result of large-scale folding, faulting and stacking of layers; and (v) variability in relationships between facies over short spatial scales, reflecting different glaciotectonic sub-environments in action at the same time in close proximity.

A combination of glaciological structures are also suggested to record a unique signature of surging, including: (i) distorted or deformed longitudinal foliation; (ii) an abundance of shear planes exposed at the glacier margins, some of which are debris-rich, recording thrust faulting, TSD and strike-slip movement in compressional and transpressional glaciotectonic regimes; (iii) widespread and chaotic surface crevassing indicative of extension associated with increased ice velocities; (iv) vertical and sub-vertical debris-rich structures formed through the injection of highly-saturated subglacial debris into basal crevasses and hydrofracturing of the glacier base by pressurised, highly-saturated debris; and (v) an abundance of crevasse traces exposed on the glacier surface which record healed versions of (iii) and are indicative of a former extensional glaciotectonic regime.

These proposed signatures of surging recorded in basal ice sequences and by glaciological structures are based largely on evidence from the margins of Tunabreen and Scott Turnerbreen, but, in the case of the glaciological structures, are very consistent with observations from other surge-type glaciers on Svalbard (Hodgkins and Dowdeswell, 1994; Hambrey and Dowdeswell, 1997; Murray *et al.*, 1997; Glasser *et al.*, 1998b; Woodward *et al.*, 2002). No other studies have reported sufficiently on the basal ice sequences associated with surge-type glaciers on Svalbard, but the signature proposed here is consistent with observations made by the author at Paulabreen (Fleming and Lovell, in prep.), by Sharp *et al.* (1994) at Variegated Glacier in Alaska, and by Larsen *et al.* (2010) at Kuannersuit Glacier in West Greenland.

Strong evidence for both the basal ice and structural glaciological signatures are found within Tellbreen, which has no surge history and is currently almost entirely cold-based and inactive. This implies that Tellbreen has been far more dynamic in the past and experienced flow conditions consistent with those during the active phase of glacier surges. Such behaviour is likely to have occurred at the LIA maximum of the glacier, when it was significantly thicker, more advanced and was most probably warm-based (Bælum and Benn, 2011). The glaciological structure of Tellbreen is identical to that of Scott Turnerbreen, a known surge-type glacier of similar size and location, and a number of other glaciers which are suggested to have surged in the past (Hansen, 2003; Midgley *et al.*, 2013). It is therefore suggested that the signatures of surging are also consistent with dynamic, warm-based ice flow of small valley glaciers at the LIA which are now largely inactive, because such behaviour is similar to the active phase of a surge in the following ways: mass builds up in the glacier, leading to a switch in the thermal regime and warm-based conditions; the glacier experiences a period of dynamic ice flow and terminus advance, possibly with increased ice velocities; the advance terminates and the glacier stagnates, thins and retreats. This climatically-controlled surge-like behaviour is discussed in further detail in *9.6.3.*

9.5. Landform-sediment assemblages of surging glaciers on Svalbard

A number of studies have observed that certain landforms and suites of landforms are found at the margins of surge-type glaciers and that, much like the basal ice sequence and glaciological structures outlined in *9.2.* and *9.3.*, respectively, their formation can be linked to specific processes active during the surge cycle (e.g. Sharp, 1985b; Solheim, 1985; Croot, 1988; Sharp, 1988; Bennett *et al.*, 1996; Boulton *et al.*, 1996, 1999; Evans and Rea, 1999, 2005; Andrzejewski, 2002; Christoffersen *et al.*, 2005; Ottesen and Dowdeswell, 2006; Benediktsson *et al.*, 2008, 2009; Ottesen *et al.*, 2008; Brynjólfsson *et al.*, 2012). These observations have led to the conception of several idealised assemblages of landforms related to surge-type glaciers, known as landsystems (Evans, 2005), which provide a template for identifying possible surges based solely on geomorphological evidence (see *Chapter 2, section 2.6.*). The classic surge landsystem presented by Evans and Rea (1999, 2005) (Fig. 2.5a) summarises the main geomorphological elements formed by surges across various regions, with a strong focus on Icelandic examples. It has since been recognised that surge-type glaciers in different settings produce landsystems with subtly different characteristics to the Evans and Rea (1999, 2005) landsystem, demonstrating the breadth of surge environments. These include a submarine surge landsystem in Svalbard fjords (Ottesen and Dowdeswell, 2006; Ottesen *et al.*, 2008) (Fig. 2.5b); a polythermal surge valley landsystem based on Kuannersuit Glacier in West Greenland (Roberts *et al.*, 2009); and a small surge-type cirque glacier landsystem based on Icelandic examples (Brynjólfsson *et al.*, 2012). This study has focused on the terrestrial record produced by Svalbard surge-type glaciers and identified three distinct landsystem types which share some characteristics with the aforementioned examples, described in *9.5.2.* Firstly, in *9.5.1.* the landforms and landform assemblages identified across this study's sites will be summarised in the context of both their links to the surge cycle and similar landforms described in different surge environments.

9.5.1. Landforms and landform assemblages

9.5.1.1. Ice-cored latero-frontal moraines

An ice-cored latero-frontal moraine complex records the maximum position of the surge of Scott Turnerbreen and is formed due to the protection of an ice core beneath the debris-covered front as the glacier downwastes post-surge. Such moraines are common at the margins of almost all similar-sized valley glaciers throughout Svalbard, where they typically delimit the LIA maximum position (cf. Boulton *et al.*, 1982; Werner, 1993), and are, therefore, not necessarily unique to surge activity. However, in a context where they are related to the maximum position of a surge, such as at Scott Turnerbreen, it is possible to link their formation to processes active during the surge cycle; some of these are also consistent with the formation of ice-cored moraine belts at the LIA maxima of glaciers. Firstly, ice expansion and the associated advance of the terminus to the maximum position is required. Secondly, the formation of extensive

supraglacial debris cover at the terminus is necessary in order to protect an ice core; in the context of the surge of Scott Turnerbreen this was in part due to the elevation of subglacial debris along shear planes and injected into basal crevasses, indicating dynamic warm-based ice flow. This is also consistent with more-dynamic ice flow associated with the LIA maximum of many small valley glaciers, when they would have been thicker and polythermal in nature (Bælum and Benn, 2011). Finally, during the sustained period of ice stagnation following dynamic ice flow (either post-surge or post-LIA maximum), the debris-covered front protects the ice core as debris-free or debris-poor parts of the glacier undergo vertical thinning, resulting in topographic inversion and the preservation of an ice-cored latero-frontal moraine belt at the maximum position. This highlights the similarities between the formation of such moraine belts at the margins of small valley glaciers which have either surged (e.g. Scott Turnerbreen) or have an LIA maximum (e.g. most other examples in Svalbard), or, in the case of Scott Turnerbreen, both. This demonstrates that, although their formation can be linked to processes during the surge cycle, on their own ice-cored moraine belts are not a diagnostic criterion of surging.

9.5.1.2. Push moraine complexes

The link between proglacially-tectonised moraine belts and glacier surges in Svalbard was first made by Croot (1988), and a number of subsequent studies have supported this with detailed investigations of such complexes at the margins of a number of known surge-type glaciers (e.g. Hagen, 1988; Boulton *et al.*, 1996, 1999; Etzelmüller *et al.*, 1996; Hart and Watts, 1997; Ottesen and Dowdeswell, 2006; Ottesen *et al.*, 2008; Kristensen *et al.*, 2009b; Kristensen *et al.*, 2009b); large push moraines are also found at the margins of surge-type glaciers in other surge clusters, such as Iceland (e.g. Evans and Rea, 1999; Benediktsson *et al.*, 2008, 2009, 2010). Push moraines were found at the margins of several of the surge-type glaciers investigated in this study, typically in the form of multi-crested composite ridge systems (e.g. Nathorstbreen, Finsterwalderbreen, Grønfjordbreen), but also as a continuously-failing apron of marine muds (e.g. Nathorstbreen). These form due to the bulldozing of proglacial sediments at the glacier margin, typically in a frontal position but also at the lateral margins, and the composition and morphology is largely controlled by the nature and location of the proglacial sediments. For example, in submarine or shallow-marine settings within a fjord, the push moraines are typically composed of soft, deformable and highly-saturated marine muds which fail continuously as they are pushed by the ice margin (Kristensen *et al.*, 2009a) and typically have a low gradient debris flow lobe extending from their distal margin (Ottesen *et al.*, 2008). If the marine muds are pushed into a terrestrial position, such as at the lateral margins of the Nordre Nathorstmorenen (Fig. 4.5), the push moraine can take the form of a multi-crested ridge complex. This is inferred to be the result of de-watering and drying out of the muds once they are in a terrestrial position, reducing the pore-water pressure and increasing the cohesiveness of the sediment (Kristensen *et al.*, 2009a). When subjected to pushing at the ice margin, this can then form multi-crested ridges

reaching heights of ~10 m, rather than simply failing as a low-gradient debris flow when a critical angle of repose is reached.

Multi-crested push moraine complexes are also formed where the ice margin has advanced into coarser-grained sediments, such as the shallow marine sands and clays within the Nordre Leirodden composite ridges at Nathorstbreen (Figs 4.5 and 4.10b) and outwash gravels within the outer parts of the Finsterwalderbreen moraine complex (Figs 6.7b and 6.7c) (Hart and Watts, 1997). An exposure within the Nordre Leirodden ridges at Nathorstbreen revealed highly-folded sands with evidence for liquefaction (Fig. 4.10b), indicating significant soft sediment deformation. Multiple crests within the push moraine complexes can be formed in two main ways: Firstly, by multiple surge events to approximately the same maximum position, creating several ridges piggy-backed on each other. This has been identified at Finsterwalderbreen (Fig. 6.6) and Grønfjordbreen (Fig. 6.11a) based on the relationships between ridges and meltwater channels which demonstrate several ridge-building events, termed the breach-block mechanism (Fig. 6.10). An additional characteristic of such complexes is that the internal composition of ridges relating to different surges varies as a result of the sediment composition of the foreland that the glacier advances in to. For example, the outer ridges of both Finsterwalderbreen and Grønfjordbreen are almost entirely composed of outwash gravels, which are indicative of the first surges recorded in the moraine sequence having advanced into predominantly glaciofluvial sediments that had accumulated at the glacier margin. By contrast, ridges in an inner position are characterised by a range of sedimentary facies, including a much larger proportion of poorly-sorted glacially-transported material. This reflects the fact that subsequent surges have advanced into the deglaciated forelands relating to previous surges, and so have bulldozed a combination of outwash, lake and glaciogenic sediments. This is apparent at both Finsterwalderbreen and Grønfjordbreen, where the innermost ridges of the moraine complexes are largely composed of poorly-sorted glaciogenic sediments, in contrast to the well-sorted gravels of the outer ridges. Secondly, glaciotectonism at an advancing ice margin can transmit deformation horizontally through proglacial sediments for up to hundreds of metres, producing multi-crested ridges as the result of a single advance (Hart and Watts, 1997; Boulton *et al.*, 1999; Bennett, 2001). This is dependent on the nature and efficiency of the glacier-foreland coupling; the nature, the strength and deformability of the proglacial sediments; and the frictional characteristics of the décollement surface (van der Wateren, 1995; Bennett, 2001). Both (i) and (ii) can occur in combination, such as at Finsterwalderbreen and Grønfjordbreen where parts of the moraine complex relating to individual surges are also multi-crested (e.g. outermost ridge in Fig. 6.6).

9.5.1.3. Glacial lineations

Elongate features or areas of streamlined topography aligned in the direction of ice flow were identified in terrestrial positions at several of the studied glaciers (Nathorstbreen, Tunabreen,

Finsterwalderbreen). In almost all cases these were extremely low and subtle flutings that could not be identified in the field, but were apparent on aerial photographs. Larger, more prominent lineations have been imaged on the seafloor in front of both tidewater glaciers featured in this study, Nathorstbreen (Ottesen *et al.*, 2008) and Tunabreen (Flink, 2013). The formation of elongate glacial lineations has been linked to periods of rapid ice flow (Stokes and Clark, 2002; Clark *et al.*, 2003; King *et al.*, 2009; Lovell *et al.*, 2012), such as during the active phase of a surge, although the exact processes are still debated (Clark *et al.*, 2003; Clark, 2010; Fowler, 2010; Stokes *et al.*, 2013a,b). The formation of the subtle flutings common at the margins of terrestrial glacier surges are probably related to the infilling of sediments into cavities created by ice flowing around basal obstructions, such as boulders or patches of over consolidated sediment (Boulton, 1976; Benn, 1994; Christoffersen *et al.*, 2005; Roberson *et al.*, 2011), although as these were only identified on aerial photographs, this remains equivocal. In some places, the lineations could also be proglacial continuations of longitudinal foliations or type A ridges (e.g. Fig 5.15), which form through very different processes and are not diagnostic of rapid ice flow or surge activity; however these can typically be distinguished from flutes as they have only a very thin trace outline. The formation of the larger glacial lineations in submarine positions imaged within both Van Keulenfjorden (Ottesen *et al.*, 2008) and Tempelfjorden (Flink, 2013) is likely to be related to the ploughing of ice keels in an uneven bed over soft, saturated marine sediments (Clark *et al.*, 2003).

9.5.1.4. Eskers

Sinuous eskers were identified on the terrestrial forelands of almost all of the glaciers in this study, and have also been imaged in a submarine position within Van Keulenfjorden (Ottesen *et al.*, 2008). The sedimentary composition was not assessed for all examples, and so it remains unclear whether they are all composed of stratified glaciofluvial material, such as at Tellbreen (8.12g), or subglacial material which has been squeezed into an abandoned basal conduit system, as interpreted at Elisebreen in northwest Svalbard (Christoffersen *et al.*, 2005) and in front of the surge-type glacier Skeiðarárjökull in Iceland (Bennett *et al.*, 2000a). Sinuous eskers are also found in front of non-surge-type glaciers and do not require processes specific to surges for their formation, but, although alone they are not diagnostic of surging, they are a common element within surge landform assemblages. By contrast, concertina or zig-zag eskers have been suggested to be diagnostic of surge activity, and are interpreted to have formed due to the occupation of basal and englacial intersecting crevasse networks by highly-pressurised meltwater (Evans and Rea, 1999). Type C supraglacial ridges at Scott Turnerbreen and Tellbreen are interpreted as having formed in this manner and, therefore, are effectively concertina eskers, and are strongly indicative of surge or surge-like glacier behaviour; however, these were rarely found preserved on the glacier forelands.

9.5.1.5. Geometrical ridge networks

Interconnected networks of thin, linear ridges, typically aligned perpendicular or sub-perpendicular to ice flow, such as mapped at almost every glacier featured in this study, have been described at the margins of surge-type glaciers in several different regions, including elsewhere in Svalbard (e.g. Bennett *et al.*, 1996; Christoffersen *et al.*, 2005; Ottesen and Dowdeswell, 2006; Ottesen *et al.*, 2008), Iceland (e.g. Sharp, 1985a; Bennett *et al.*, 2000a; Evans *et al.*, 2009), the Yukon (e.g. Clarke *et al.*, 1984), Alaska (e.g. Ensminger *et al.*, 2001) and Novaya Zemlya (e.g. Grant *et al.*, 2009). These have largely been interpreted as crevasse squeeze ridges, formed by the injection of saturated subglacial material into basal crevasses which opened up during the surge, which then subsequently melt-out as the glacier stagnates *in situ* following surge termination (Sharp, 1985a; Christoffersen *et al.*, 2005; Rea and Evans, 2011). These are, therefore, arguably the most-diagnostic individual features of surge activity, as their formation relates to processes unique to surging: the opening of basal or full-depth crevasses in response to extensional stresses associated with increased ice velocities; the presence of highly-saturated subglacial sediments as a result of high basal water pressures; a relatively abrupt cessation to the period of increased ice velocities, resulting in the glacier settling down on to its bed and squeezing saturated subglacial sediment into the open crevasses; and an extended period of *in situ* stagnation of the glacier upon surge termination, allowing the crevasse squeezes to melt-out with minimal modification or re-working. This is interpreted to be the major formation process for the geometrical ridges mapped in this study, which is supported by observations of vertical or near-vertical debris-rich structures composed of subglacial material exposed at the margins of Nathorstbreen (Fig. 4.6d) and Tunabreen (Fig. 5.14g).

The englacial debris-rich structures exposed at Tunabreen display a variety of morphologies, and, as a result, some are also suggested to be thrust faults (Glasser *et al.*, 1998b), re-oriented and deformed crevasse squeezes inherited from a previous surge (Evans and Rea, 1999; Woodward *et al.*, 2002; Rea and Evans, 2011) and hydrofractures of highly-saturated subglacial debris (Fig. 5.21); these processes are also strongly linked to the active phase of a surge. These all potentially would form ridges upon melting-out (e.g. Fig. 5.14h), and so some of the geometrical ridges mapped in this study may have originated from these instead of purely crevasse squeezes. However, for two main reasons a crevasse-squeeze origin is favoured for the majority: firstly, many of the geometrical ridges mapped in this study, particularly at Nathorstbreen, are sharp-crested and ~2-10 m high, and some form vertical pinnacles; these are most-likely to have originated as vertical or near-vertical debris-rich structures (e.g. crevasse squeezes), as inclined bands (e.g. thrust faults and re-oriented crevasse squeezes) would distribute sediment over a wider areas when they melted-out, thus reducing the overall height of the ridge. An intersecting thrust origin has been suggested for similar pinnacles at the margins of Kronebreen in northwest Svalbard (Bennett *et al.*, 1999), but this overlooks the simplest interpretation of vertical crevasse squeezes which have melted-out, and is therefore

suggested to be less likely. Secondly, the orientations of ridges within the networks, particularly at the margins of Nathorstbreen (Fig. 4.5) and Von Postbreen (Fig. 5.17), are typically perpendicular or sub-perpendicular to ice flow, and form a pattern which is consistent with crevasses opened up due to longitudinal extension during a surge.

In contrast, the geometrical ridges at the margin of Tunabreen (Fig. 5.17) display far more variable orientations, including sub-parallel to ice flow. These are located at the lateral margin of the glacier, where a compressional and/or transpressional regime is likely to be more dominant as ice splays outwards towards the obstructions of non-surging ice and the terrestrial margins. This provides an explanation for the variety in englacial band morphologies at this margin (Figs 5.5b and 5.5c), many of which are inclined and thin, and are suggested to have formed as thrust faults, re-oriented crevasse squeezes and hydrofractures, or some combination of all three (Fig. 5.21). When these melt out, they are likely to form ridges with a wide variety of orientations and morphologies, such as the geometrical ridge network located close to the Tunabreen margin. This indicates that the morphology and orientation of geometrical ridges within networks possibly reflects their position in relation to the glacier centre, as the dominant processes that are in action vary according to this. For example, ridges located broadly in a central position relative to the glacier are typically oriented perpendicular or sub-perpendicular to flow, such as those in front of Von Postbreen (Fig. 5.17) or imaged in the centre of fjord floors (Ottesen and Dowdeswell, 2006; Ottesen *et al.*, 2008; Flink, 2013) (Fig. 5.19). These are suggested to largely originate as crevasse squeezes, as longitudinal extension is likely to dominate in these areas, as indicated by the predominance of transverse crevasses apparent in the centre of tidewater glacier fronts (e.g. Fig. 5.19a). In contrast, geometrical ridges located towards the margins, particularly in a terrestrial position, are likely to reflect a compressive and/or transpressive regime and may have undergone complex, possibly multi-phased deformation. This would produce a much more variably-oriented network of ridges upon de-icing.

Geometrical ridge networks reflect the incorporation of subglacial material into englacial positions during periods of dynamic flow related to increased ice velocities; this can be in both extension-dominated and compression-dominated parts of the glacier, the former of which has been most-commonly identified in previous studies (Sharp, 1985b; Ottesen and Dowdeswell, 2006; Ottesen *et al.*, 2008; Flink, 2013). These then melt out upon termination of the dynamic ice flow as the ice mass stagnates, preserving the network of ridges with minimal modification. Thus, geometrical ridge networks are strongly linked to surge activity, and can be described as a diagnostic geomorphological characteristic. Some recent studies have described similar features on the sea floor in relation to former ice streams (Klages *et al.*, 2013; Andreassen *et al*, 2014), where they are interpreted as evidence for dynamic rapid ice flow followed by stagnation; this is effectively the same processes that are active during glacier surges.

9.5.1.6. Ice-cored hummocky topography and debris flows

Large parts of the terrestrial forelands at all of the glaciers in this study consisted of ice-cored hummocky topography with numerous small pools and debris flows. These areas represent widespread subaerial stagnation of a deglaciating ice mass, characterised by differential melting of buried ice and associated thermo-erosion processes (Etzelmüller *et al.*, 1996). This results in topographic inversion of the glacier foreland and moraine area and the re-mobilisation of material in the form of debris flows, typically initiated by meltwater erosion. The formation of this topography requires there to be significant supraglacial debris cover, typically sourced from sub- (e.g. type B ridges) and extraglacial (e.g. type A ridges) sources but also including glaciofluvial (e.g. type C ridges) and glaciolacustrine sediments, the latter deposited within supraglacial pools or lakes (e.g. Fig. 7.9d). This sediment cover becomes re-mobilised during stagnation as parts of the margin downwaste at different rates due to the uneven distribution of debris, with some ice preserved beneath thicker debris cover whilst other areas undergo vertical thinning (Fig. 7.11). On some forelands, particularly those of the small valley glaciers Scott Turnerbreen and Tellbreen, thermo-erosion processes are responsible for destroying almost all geomorphological linearity inherited from the ice (Etzelmüller *et al.*, 1996; Evans, 2009), such as type A, B and C supraglacial ridges (Figs 7.3 and 8.9); this contrasts to areas of hummocky moraine at the margins of some surge-type glaciers in Iceland, for example, which are described as forming prominently-aligned belts (Evans and Rea, 1999).

Hummocky topography can be linked to the surge cycle as it records widespread *in situ* stagnation upon the cessation of dynamic flow, and effectively develops during the quiescent phase when ice velocities are extremely low and the glacier is thin and over-extended. However, such topography is common within the forelands of many land-terminating glaciers on Svalbard, most of which have been retreating and downwasting since their LIA maxima, and, therefore, alone it is not necessarily diagnostic of surging (Evans and Rea, 1999). The reasons for this is that the processes are very similar in both cases, recording a phase of ice expansion and warm-based, dynamic glacier flow, whether related to a surge or a climatically-controlled LIA maximum, followed by an extended period of stagnation. In the context of non-surge-type glaciers, this period of stagnation is controlled by warming since the LIA and strongly-negative mass balance experienced as a result (Hansson-Bauer *et al.*, 1990; Dowdeswell *et al.*, 1995).

9.5.2. Svalbard surge landsystems

The landform-sediment assemblage described in *9.5.1.* describes the main geomorphological features observed at the margins of the glaciers in this study and their links to surge/dynamic activity. However, not all features are present at all glaciers, and the characteristics of features also vary between glaciers. Based on this, and observations from other surge-type glaciers, it is suggested that three main surge landsystems exist on Svalbard. These are largely controlled by

the size of the glacier, the nature of the glacier terminus (e.g. tidewater or land-terminating) and the sediment composition at the margin. The three landsystems are: Type A - Tidewater glaciers (*9.5.2.1.*), Type B – Land-terminating glaciers (*9.5.2.2.*) and Type C – Small valley glaciers (*9.5.2.3.*), and are illustrated in Figure 9.3. These are described below in full, with common elements and the main differences between them highlighted. Table 9.3 lists examples of surge-type glaciers which are suggested to fit into each landsystem type.

9.5.2.1. Type A - Tidewater glaciers

Ottesen and Dowdeswell (2006) and Ottesen *et al.* (2008) proposed a landsystem for tidewater glacier surges on Svalbard based on submarine geomorphology, and this is built on here with the addition of the terrestrial landform assemblage found at the fjord margins (Fig. 9.3a). The submarine elements are described in detail in Ottesen and Dowdeswell (2006), Ottesen *et al.* (2008) and Flink (2013).

The terrestrial landform assemblage extends along the fjord shores to a position broadly level with the large submarine ridge which delimits the most-extensive surge position in the fjord. The margins of the moraine area can contain multi-crested push moraine complexes; at Nathorstbreen and Paulabreen (Rowan *et al.*, 1982; Kristensen *et al.*, 2009a,b) these consist of deformed shallow marine muds and sands which were bulldozed from the fjord and into a terrestrial position by the advancing ice margin. The push moraines are found both in frontal and lateral positions, and their presence or absence is likely to be controlled by the configuration of the fjord and glacier flow direction and the availability of deformable sediments at the margin. The submarine ridges which delimit the maximum position of surges are also inferred to have formed by the bulldozing of fjord floor sediments at the ice margin (Ottesen *et al.*, 2008; Flink, 2013), as observed at the active margin of Nathorstbreen in 2012.

Geometrical ridge networks are found both in terrestrial and submarine positions. The terrestrial examples of these are composed of subglacial material and can be up to 10 m high and sharp-crested, with some forming very thin pinnacles. These are predominantly interpreted as crevasse squeeze ridges, particularly when located in a central position relative to the axis of the fjord/glacier and where they are oriented perpendicular or sub-perpendicular to ice flow. Sinuous eskers and small flutes are found in a terrestrial position but are not as well defined as in the submarine record. The majority of the moraine area consists of ice-cored hummocky topography interspersed with small pools and lakes, recording subaerial stagnation of the ice mass and associated thermo-erosion processes. In a submarine position, annual retreat moraines are formed during quiescence by minor winter re-advances (Ottesen *et al.*, 2008; Flink, 2013), highlighting one major difference between the landform assemblages in submarine and terrestrial positions. In Tempelfjorden, these annual retreat moraines can be correlated with the position of the retreating tidewater front following the 2003-05 surge based on satellite imagery (Flink, 2013). The terrestrial moraine area is commonly dissected by outwash corridors or

meltwater channels, typically flowing from a lateral position towards the fjord; these represent channels initially guided by the ice margin as it retreated upfjord during quiescence and, where well developed (e.g. on Søre Nathorstmorenen) may indicate periods of relative stability during retreat.

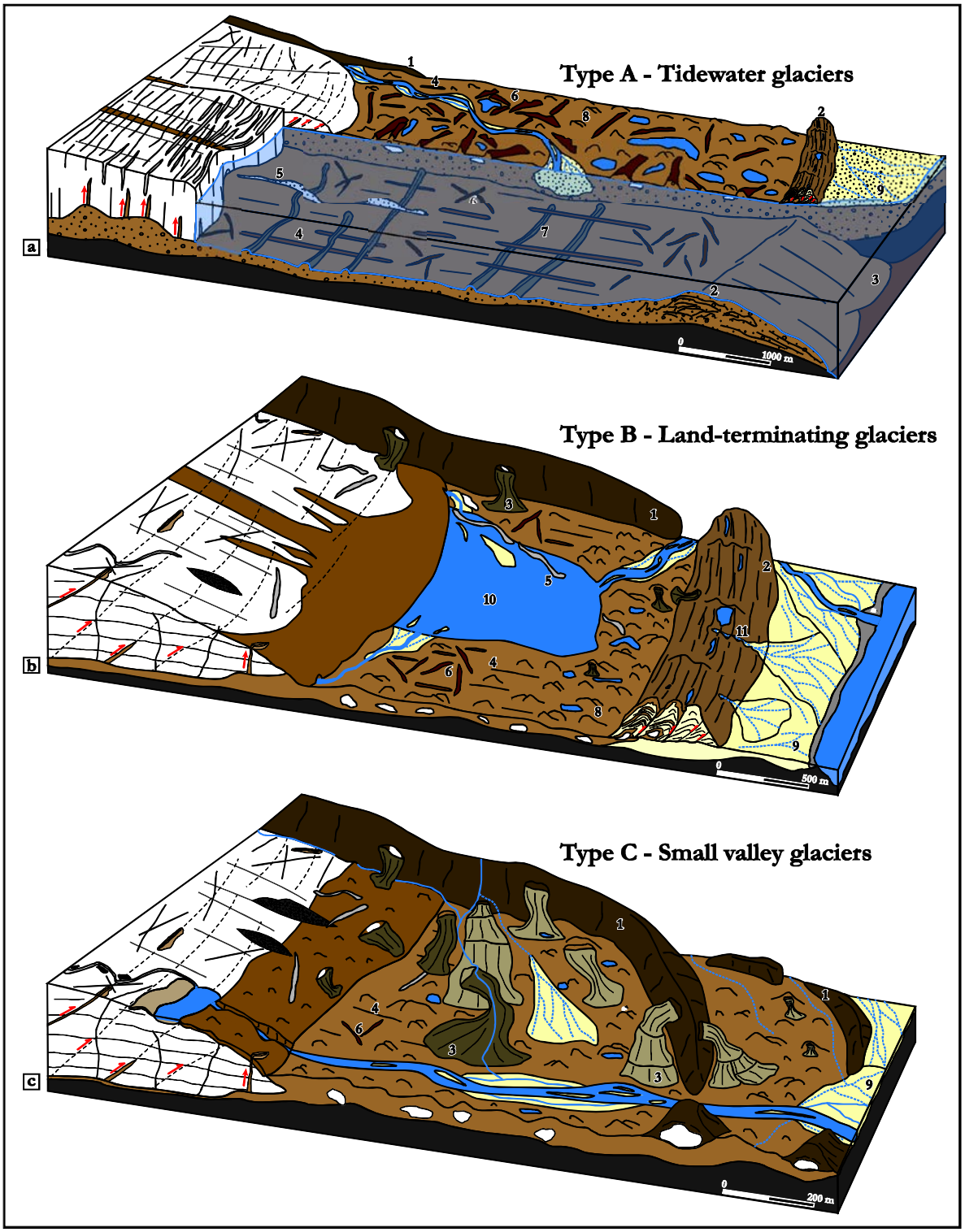

Figure 9.3 – Svalbard surge landsystems. (a) Type A – Tidewater glaciers. (b) Type B – Land-terminating glaciers. (c) Type C – Small valley glaciers. This figure is available in digital format on the CD inside the back cover.

9.5.2.2. Type B - Land-terminating glaciers

Large (>5 km long) land-terminating surge-type glaciers typically have glacier forelands which can be divided into an outer zone consisting of a composite ridge system and an inner zone of ice-cored hummocky topography, ponded meltwater, outwash fans, eskers, flutes and geometrical ridges (Fig. 9.3b). The composite ridge system typically takes the form of a multi-crested arcuate moraine belt which conforms to the shape of the glacier terminus (Fig. 9.3b). These are interpreted as push moraine systems formed by the proglacial bulldozing and deformation of sediments on the glacier foreland; these include outwash sands and gravels, glaciolacustrine sediments and glaciogenic sediments. In some cases (e.g. Finsterwalderbreen, Grønfjordbreen), the push moraine records multiple surges, with evidence for this provided by the geomorphological relationships between ridges and meltwater channels (e.g. Fig. 6.6); variations in ridge sediment composition, characterised by outer ridges typically composed of outwash or glaciolacustrine sediments, and inner ridges with a higher content of glaciogenic sediments which were deposited by a previous surge and subsequently re-worked into push moraine by a later advance; and relative age indicators, including morphology, vegetation cover, range of frost-shattered lithologies and lichenometric data. The identification of multiple ridge-building events within these moraine complexes provides compelling evidence that their formation is uniquely linked to repeated advances, and therefore their presence is a strong diagnostic geomorphological indicator of surge activity (Croot, 1988). Multi-crested push moraine sequences can also be formed by single surge advances, such as those at the lateral margins of Nathorstbreen (Fig. 4.5) and reported from surge-type glaciers elsewhere in Svalbard (Hagen, 1988; Hart and Watts, 1997; Boulton *et al.*, 1999), in Iceland (Benediktsson *et al.*, 2010) and in West Greenland (Roberts *et al.*, 2009).

It has been argued by Hambrey and Huddart (1995) and Huddart and Hambrey (1996) that surges or glacier advances are not necessary to form some multi-crested push moraines on Svalbard. Based on investigations at Comfortlessbreen and Uvêrsbreen in northwest Svalbard, it was suggested that englacial thrusting at the transition between warm and cold ice in a polythermal glacier could also form composite ridge systems, rather than only proglacial glaciotectonic deformation at an advancing ice margin (Hambrey and Huddart, 1995; Huddart and Hambrey, 1996). This led them to suggest that both Comfortlessbreen and Uvêrsbreen were not surge-type glaciers, contrary to the interpretations of Croot (1988); this conclusion was also reached independently by Jiskoot *et al.* (1998, 2000) based on multivariate statistical analysis. However, Comfortlessbreen has subsequently surged following these studies (Sund and Eiken, 2010) and Uvêrsbreen is showing signs that it is in the early stages of a surge (personal communication from H. Sevestre, January 2014), providing further support for Croot's (1988) observations, and those in this study, of the links between push moraine complexes and surge-type glaciers on Svalbard.

A second common feature on the forelands of land-terminating surge-type glaciers are large lagoons between the glacier front and the composite ridge system (e.g. Figs 6.4 and 6.11). At both Finsterwalderbreen and Grønfjordbreen these represent the ponding of meltwater behind the composite ridge system as the glacier front retreats during quiescence. Lagoons ponded behind composite ridges systems can also be identified at a number of other glacier margins in Svalbard (e.g. Battyebreen, Elisebreen, Holmströmbreen, Rabotbreen, Uvêrsbreen). Although ice-marginal lagoons are clearly not a diagnostic indicator of surging, when found in combination with composite ridge systems their occurrence is indicative of a ridge-building advance followed by a period of ice retreat and downwasting, consistent with surge activity. The development of ice-marginal lagoons also provides a source of soft, deformable glaciolacustrine sediments in a proglacial position for the formation of an additional push moraine during any subsequent surge advances (Watts, 2010).

In addition to ice-marginal lagoons, the glacier foreland contains large areas of ice-cored hummocky topography, composed largely of glaciogenic material, and associated small pools, typically located immediately adjacent to the composite ridge system; outwash fans and meltwater channels, which feed into the lagoon before draining out through a gap in the composite ridge system (e.g. Fig. 6.4); sinuous eskers; small flutes and proglacial debris stripes; and geometrical ridges. In some cases the flutes and geometrical ridges are well-defined and densely grouped, such as at Elisebreen in northwest Svalbard (Christoffersen *et al.*, 2005), whereas in other places (e.g. Finsterwalderbreen and Grønfjordbreen) the record is more fragmentary. The geometrical ridges are generally much smaller than those located at the terrestrial margins of tidewater surge-type glaciers, typically only reaching ~1 m high and <100 m long (Christoffersen *et al.*, 2005). Of these features, both flutes and geometrical ridges can be linked to dynamic warm-based flow during the active phase of a surge, with the latter being particularly diagnostic as they reflect the injections of subglacial material and/or meltwater into basal crevasses, or in some cases possibly thrust-faulting and deformation of reoriented crevasse squeezes, followed by melt-out during ice stagnation.

9.5.2.3. Type C - Small valley glaciers

The landform assemblage at the margins of small valley glaciers which have surged (e.g. Scott Turnerbreen), or are suspected to have surged (e.g. Midtre Lovénbreen, Austre Lovénbreen; Hansen, 2003; Midgley *et al.*, 2013), is characterised by an ice-cored latero-frontal moraine system and an inner zone of ice-cored hummocky topography, largely composed of glaciogenic sediments. Thermo-erosion processes dominate across the foreland, resulting in multi-tiered debris flows and topographic inversion due to the degradation of buried ice (Fig. 7.11). This assemblage is consistent with surges as it records ice expansion and the development of a debris-covered glacier front, fed by material from sub-and extraglacial sources, followed by widespread glacier stagnation and retreat; this results in the formation of the ice-cored latero-

frontal moraine as ice is preserved beneath thick debris cover at the margin whilst other areas undergo vertical thinning, and topographic inversion of the glacier foreland and associated sediment remobilisation due to thermo-erosion processes, leading to large areas of ice-cored hummocky topography. However, this describes the situation at most small valley glaciers on Svalbard which reached a maximum position during the LIA and have been retreating, stagnating and most-likely switching to an entirely cold-based thermal regime since. As a result, the main elements of this landsystem, although formed by, and consistent with, processes that are active during surges, are not diagnostic of surging.

Compelling evidence for dynamic, warm-based flow is recorded in the glaciological structure of Scott Turnerbreen, characterised by (i) the elevation of subglacial debris to en- and supraglacial positions through injections into basal crevasse and along shear planes (type B ridges); and (ii) meltwater occupation of crevasses (type C ridges). However, due to the dominance of thermo-erosion processes and associated sediment remobilisation as the glacier stagnates, these ridges, and other evidence for warm-based dynamic flow (e.g. flutes), appear to be very rarely preserved on the forelands of small valley glaciers; some fragmentary evidence for geometrical ridges and minor fluting was mapped at Tellbreen in this study, and Hansen (2003) mapped zig-zag eskers, which are comparable to type C ridges, at Midtre Lovénbreen. This indicates that it is very difficult to unequivocally identify surges of small valley glaciers based on the geomorphological record alone.

The type C landsystem shares a number of characteristics with that presented by Brynjólfsson *et al.* (2012) for the forelands of small surge-type cirque glaciers in northwest Iceland (Fig. 2.5d), which includes a latero-frontal moraine ridge delimiting the surge maximum, a large area of ice-cored hummocky topography, and some poorly-defined flutes and geometrical ridges. This reflects the similarity between the two types of glacier, including their size, typical configuration (i.e. single trunk with only one or two accumulation basins), and nature of the foreland into which the glacier advances (e.g. generally coarse, angular sediment). The better preservation of landforms on the Icelandic forelands probably represents the domination and efficiency of thermo-erosion processes and sediment remobilisation in Svalbard, resulting from the degradation of buried ice blocks (Etzelmüller *et al.*, 1996).

9.5.3. Landform preservation

The long-term preservation potential of the landform-sediment assemblages formed by surges is of importance when assessing evidence for possible historical and palaeo surges. This is likely to vary depending on the particular landform, the type of surge-type glacier that produced it (e.g. tidewater, land-terminating or small valley glacier) and whether the landforms are in a submarine or terrestrial position. In addition, a number of processes can be responsible for limiting the preservation potential of glacial landforms over a variety of timescales. In the simplest terms, the preservation of glacial landforms in a landscape is highly dependent on post-

formational erosional and/or depositional processes (Kirkbride and Brazier, 1998). Landforms can be removed or modified by erosion, such as by subsequent glacier advances ('obliterative overlap'; Gibbons *et al.*, 1984) and glaciofluvial activity, or can be buried beneath sediments from a variety of sources. Over multiple glacial cycles these processes can play a significant role in censoring the glacial record, and therefore can introduce complexities to the interpretation of glacial landscapes in relation to chronological control and climatic variations (Gibbons *et al.*, 1984; Kirkbride and Brazier, 1998; Barr and Lovell, accepted). Obliterative overlap is also likely to have a significant influence when the time period between glacier advances is much shorter, such as experienced by Svalbard surge-type glaciers (surge cycles of ~50-150 years). For instance, if a surge of a given glacier reaches a more-extensive position than that of the previous surge, it is probable that the landforms associated with the earlier advance would be erased. This could potentially skew interpretations of surge landsystems where at least some of the surges were unobserved, such as at Nathorstbreen (*Chapter 4*) and Finsterwalderbreen (*Chapter 6*), as evidence for less-extensive advances may have been removed. The result of this is that the apparent record of at least four successively less-extensive surges at both glaciers may not reflect the true frequency of surge activity. However, there are clearly also cases where the geomorphological record does reflect the sequence of surge activity, such as at Tunabreen where each surge since the LIA has reached a successively less-extensive downfjord position (*Chapter 5*).

Where glacial landforms have not been directly removed or buried by glacial and non-glacial (e.g. landslides) activity, their preservation over different timescales is still strongly controlled by a variety of factors and processes. The most relevant of these in the context of active terrestrial glacial environments is whether landforms have an ice core or not, as the degradation of these over time can significantly modify the resultant 'melted-out' landform (Lukas *et al.*, 2005; Schomacker, 2008). In dead-ice environments on glacial forelands, the melting of buried ice leads to resedimentation processes in the overlying debris cover. This remobilisation of sediment is largely controlled by gravity (mass movements) and the availability of water, which can erode and destabilise landforms, exposing ice cores to additional melting, whilst also reducing the shear strength of the overlying sediment due to liquefaction (Etzelmüller *et al.*, 1996; Lukas *et al.*, 2005; Schomacker and Kjær, 2008; Evans, 2009). Thus, de-icing of ice cores can clearly play a significant role in modifying glacial landforms, and can therefore affect their preservation potential. However, several elements need to be taken into account that can control both the effectiveness of (and time taken for), complete de-icing, and the character/morphology of the resultant melted-out landforms:

(i) The size of the ice core is clearly of importance, as landforms (for example, moraines) which are predominantly composed of ice and with only a thin debris cover would not preserve a sizable ridge (if any) upon complete de-icing. In addition, under similar climatic conditions and assuming the same thickness of debris cover, a moraine with a large ice core

may take longer to degrade than a moraine with smaller ice core. By contrast, a moraine which is largely composed of debris and has only a small ice core is more likely to preserve a significant ridge once de-icing is complete.

(ii) Following on from this last point, the thickness of sediment cover over an ice core is also of great importance. Thick debris cover may help to preserve an ice core for longer and delay degradation due to insulation effects. However, Lukas *et al.* (2005) observed that once melting is underway, areas of thick debris cover were just as vulnerable to remobilisation as those with only a thin cover.

(iii) As outlined in (i) and (ii), the relative ice and sediment volumes within initial landforms can clearly play an important role in their preservation potential. However, this oversimplifies reality in that it potentially ignores the effectiveness of remobilisation processes and the influence of gravity and meltwater action once an instability is created (Schomacker, 2008). Etzelmüller *et al.* (1996) and Lukas *et al.* (2005) noted that instabilities in ice-cored moraine areas are often initiated by meltwater erosion, which exposes the ice subaerially and facilitates additional melting, resulting in the development of debris flows as gravity and liquefaction processes take effect (termed 'thermo-erosion' by Etzelmüller *et al.*, 1996). This has the potential to rework large amounts of debris, reducing the size and morphology of the resultant de-iced landform. The type of ice-core degradation (e.g. backwasting of ice-cored slopes vs. downwasting of ice-cored ridges/mounds) also has an effect on the style of sediment remobilisation and the morphology of the eventual melted-out terrain, as backwasting tends to lead to multi-tiered debris flows and a general flattening of topography, whereas downwasting is more likely to resultant in topographic inversion and the development of hummocky topography (Kjær and Krüger, 2001; Schomacker, 2008; Schomacker and Kjær, 2008).

(iv) Climatic conditions can have an impact on rates of ice core degradation and backwasting/downwasting, although do not necessarily have a significant influence on the preservation potential of glacial landforms over long timescales (Schomaker, 2008). As perhaps might be expected, Schomacker (2008) found that backwasting rates in ice-cored moraine areas were lowest in the coldest climate (Dry Valleys, Antarctica) and highest in the warmest climate (Tasman Glacier, New Zealand). However, it was also found that the distribution of backwasting rates did not always follow different climatic conditions in a straightforward manner; for example, rates at Holmströmbreen in Svalbard (High-Arctic, permafrost conditions; Schomacker and Kjær, 2008) were as high as those recorded at Kötlujökull in Iceland (sub-polar, non-permafrost conditions; Kjær and Krüger, 2001). It is perhaps intuitive that permafrost conditions would help to slow down ice-core degradation, particularly if the debris cover is thicker than the active layer, but it may also encourage surface meltwater flow, and thus the potential for sediment remobilisation and associated feedback mechanisms in ice-cored areas (Schomacker and Kjær, 2008). Based on these observations, Schomacker (2008) suggested that topography and remobilisation processes, rather than climate, played a significant role in

controlling de-icing rates. In addition, as de-icing processes are similar regardless of climatic conditions (Schomacker, 2008), it is unlikely that climate will have a significant role to play in the eventual preservation of an ice-cored landform, but it may ultimately control how long it takes to become entirely de-iced.

(v) Time is the final factor which can have a control on de-icing rates, but is unlikely to be of great importance in the context of eventual landform preservation. For example, at Scott Turnerbreen (*Chapter 7*), the ice-cored moraine ridges that formed at the LIA maximum and during a surge ~40 years later are currently significantly different heights. It is possible that this difference is due to the LIA ridge de-icing for a longer period of time than the surge ridge, and if the ice-sediment ratio within both ridges was equal at the time of formation, when both eventually de-ice they would form moraine ridges of a similar size. It is of course also possible that the difference in ridge size is not due to their age difference alone, but is controlled by other factors such as differences in ice-sediment volume ratios. Despite not having a huge influence on landform preservation potential, at least on a timescale from initial formation to complete de-icing of a landform, time does have an impact on landform morphology and surface cover. For example, it is often noted that 'older' moraines are more-rounded, degraded and vegetated, whilst 'younger' moraines are sharper-crested and contain little vegetation cover (e.g. Kaplan *et al*., 2005), and these observations are often used as relative-age indicators where direct dating is absent. This of course makes a lot of assumptions, but in general terms seems to be applicable to observations in this study at Nathorstbreen (*Chapter 4*; different ages of geometrical ridges) and Finsterwalderbreen (*Chapter 6*; different ages of four ridges within the composite ridge system).

With these points in mind, perhaps the features with the best long-term preservation potential are push moraine complexes, as these are largely composed of sediment rather than buried ice bodies and would therefore undergo minimal degradation over time, assuming they are not overridden by subsequent advances (obliterative overlap). This is supported by the presence of several large push moraine belts in the terrestrial palaeo record across the globe (Aber, 1988; Kluiving, 1994; Evans *et al.*, 1999; Benn and Clapperton, 2000; Bennett, 2001; Evans *et al.*, 2008). Glacial lineations formed in terrestrial settings are typically small and poorly-defined flutes and are often located within the areas of ice-cored hummocky terrain which experience significant thermo-erosion processes due to the melting of buried ice. This leads to topographic inversion and sediment remobilisation, which may impact on the preservation of small landforms such as flutes. In contrast, glacial lineations formed on the fjord floor by tidewater glacier surges are much larger (Ottesen and Dowdeswell, 2006; Ottesen *et al.*, 2008; Flink, 2013) and the foreland is not subjected to the same subaerial degradation processes, resulting in minimal landform modification and erosion. This means that glacial lineations in submarine positions can be preserved for long time periods (Canals *et al.*, 2000; Graham *et al.*, 2009; Livingstone *et al.*, 2012; Andreassen *et al.*, 2014).

The preservation of geometrical ridge networks is also more likely in submarine settings, and several examples of their identification have been reported recently from the offshore record of Antarctica (Klages *et al.*, 2013) and within the Barents Sea (Andreassen *et al.*, 2014). At the terrestrial margins of tidewater surge-type glaciers, geometrical ridges can reach heights of ~6-8 m. Based on their interpretation as crevasse squeeze ridges, these are unlikely to contain ice, and therefore should not be subjected to significant thermo-erosion processes and modification. However, the two generations of geometrical ridge networks at Nathorstbreen demonstrate that the features associated with the ~1 ka advance are significantly more degraded and rounded than those formed in ~1870, suggesting that they may undergo a large degree of modification over longer time-scales. This may explain why geometrical ridge networks have only been identified in the palaeo record in a few studies (Patterson, 1997; Evans and Rea, 1999; Evans *et al.*, 1999). Smaller geometrical ridges and eskers in terrestrial positions are, similar to flutes, likely to have a low preservation potential due to the dominance of thermo-erosion processes on the glacier foreland.

Ice-cored hummocky topography will eventually de-ice completely to form areas of hummocky moraine and kame and kettle topography, reflecting the topographic inversion and presence of multiple pools resulting from de-icing processes and sediment remobilisation, highlighted in detail above. Areas of such terrain have been reported from the palaeo record at several locations (Clayton *et al.*, 1985; Patterson, 1997; Evans and Rea, 1999; Evans *et al.*, 1999; Benn and Clapperton, 2000; Darvill *et al.*, 2014), demonstrating that evidence for ice stagnation can be identified over long time periods. However, the development of this topography may also have resulted in the modification and erosion of additional landforms linked to surge activity, such as geometrical ridges, flutes and concertina eskers (Evans and Rea, 1999).

9.6. Glacier surges: an aclimatic phenomenon?

Based on initial observations that the occurrence of glacier surges did not appear to relate to climate variations, traditional definitions have tended to suggest that they are largely aclimatic phenomena, triggered by internal instabilities rather than external forcing (cf. Meier and Post, 1969; Post, 1969; Raymond *et al.*, 1987). Although internal mechanisms and changes at the glacier bed are still thought to control the onset of surging (cf. Kamb *et al.*, 1985; Kamb, 1987; Björnsson, 1998; Fowler *et al.*, 2001; Murray *et al.*, 2003b), it has been recognised that climate forcing can influence surge behaviour (cf. Dowdeswell *et al.*, 1995; Hodgkins *et al.*, 1999; Eisen *et al.*, 2001, 2005; Hansen, 2003; Frappé and Clarke, 2007; Hewitt, 2007; Flowers *et al.*, 2011; Striberger *et al.*, 2011). In Svalbard, Dowdeswell *et al.* (1995) noted that the number of surges occurring at one time had decreased significantly from 18 in 1936 to 5 in 1990, and a number of glaciers which had surged at the LIA were no longer appearing to build-up towards a subsequent surge. It was suggested that these observations can be linked to significant step-like

increases in annual mean air temperature both post-LIA (Hansson-Bauer *et al.*, 1990) and post-1990 (James *et al.*, 2012), and the strongly negative mass balance experienced by most glaciers as a result (Hagen and Liestøl, 1990; Dowdeswell *et al.*, 1995, 1997; Hodgkins *et al.*, 1999; James *et al.*, 2012). In addition to a decrease in the number of glaciers surging at one time, and the observations that some glaciers are no longer able to surge, it was also suggested that the changes in mass balance conditions were responsible for increasing the lengths of the quiescent phase between surges (Dowdeswell *et al.*, 1995). The influence of mass balance changes on surge periodicity was also noted by Eisen *et al.* (2001) at Variegated Glacier, which has surged seven times since ~1900 (Eisen *et al.*, 2005). Eisen *et al.* (2001) identified a strong relationship between mass balance and the occurrence of surges, which showed that the most recent three surges all began when the cumulative mass balance in the upper part of the glacier reached a consistent threshold of 43.5 m (ice equivalent). It was suggested that this 'surge level' controlled the periodicity of surges, with the length of the quiescent phase dependent on the average annual mass balance over this time; a higher mass balance leads to a shorter return period, and *vice versa* (Eisen *et al.*, 2001). This clearly demonstrates a strong link between mass balance changes, controlled by variations in air temperature and precipitation, and surge periodicity. Further evidence for this relationship was also presented for Eyjabakkajökull, Iceland, by Striberger *et al.* (2011). Analysis of a sediment core from a lake which is fed by discharge from Eyjabakkajökull allowed surge periodicity to be reconstructed for the past ~2000 years. At ~1700 cal a BP, the glacier began to surge at regular intervals of ~34-38 years. This periodicity approximately halved to ~21-23 years during the cold period of the LIA (~1600-1900 AD), before returning to ~35-40 years following the end of the LIA (Striberger *et al.*, 2011). These observations also demonstrate a clear link between climate variation and surge frequency, with the shortest surge return periods occurring during the coldest part (LIA) of the last ~2000 years, and a trend of increasing surge cycle length coinciding with post-LIA warming. Similar to the interpretations of Dowdeswell *et al.* (1995) and Eisen *et al.* (2001), it is thought to be the changes to mass balance due to climatic variations (air temperature and precipitation) that ultimately controls surge frequency at Eyjabakkajökull (Striberger *et al.*, 2011).

These observed changes to surge behaviour in direct response to climatically-controlled mass balance changes are discussed below in the context of the three broad categories of surge-type glacier outlined in *9.5.*: tidewater, land-terminating, and small valley glaciers (Table 9.3).

9.6.1. Tidewater surge-type glaciers

As highlighted above, Dowdeswell *et al.* (1995) hypothesised that surge-type glaciers might experience lengthening quiescent phases as a result of strongly negative mass balances due to warming during the 20th century. However, the long surge cycles experienced by Svalbard surge-type glaciers means that very few have been observed to surge more than once, and so

patterns related to surge frequency are hard to determine. Only Tunabreen has been observed to surge three times, and this has produced a remarkably consistent return period of ~40 years, rather than any sign of the quiescent phase lengthening in response to a long period of negative mass balance. Surge cycle lengths have also been calculated for Blomstrandbreen (~47 years), Hambergbreen (~70 years), Recherchebreen (~110 years), Fridtjovbreen (~133 years) and Nathorstbreen (~140 years; Dowdeswell *et al.*, 1991; Hagen *et al.*, 1993; Dowdeswell and Benham, 2003; Sund and Eiken, 2010; Mansell *et al.*, 2012; Sund *et al.*, 2013), but these are only based on two observed surges and so do not provide any further insight into possible changes to surge frequency.

An interesting observation from Tunabreen is that the maximum for each surge (1930s, 1970s and 2003-05) reached a position almost exactly 1 km less extensive than the previous surge (Fig. 5.2). This pattern continues if the ~1890 position of Von Postbreen, which was presumably confluent with Tunabreen, is included. This is a particularly interesting case, as previous studies on the influence of climate/mass balance changes on surge activity have all observed that it is surge periodicity that is affected (Dowdeswell *et al.*, 1995; Eisen *et al.*, 2001; Striberger *et al.*, 2001); at Tunabreen, the return period has remained constant (~40 years) but the maximum downfjord position reached by each surge has been decreasing at a consistent rate. This suggests that 20th century warming has not affected the length of the surge cycle, but has had an influence on either the length of the active phase, the amount of ice transferred during the surge, or some combination of both, resulting in successively less-extensive surge advances. Investigations at Nathorstbreen presented in this study suggest a similar pattern, with the currently ongoing surge reaching a position ~3 km upfjord from the ~1870 position, which in turn is located ~3 km upfjord from the maximum position reached in ~1 ka BP (Figs 4.2e, 4.2 and 4.16); however, as noted in section *9.5.3.*, it is possible (and perhaps even probable based on typical surge return periods on Svalbard) that additional surges occurred between ~1 ka BP and ~1870, but that evidence for these (presumably less-extensive) advances has been removed by obliterative overlap during the ~1870 (LIA maximum) surge.

The controlling mechanisms for the successively less-extensive surges experienced by Tunabreen, whilst maintaining a consistent return period of ~40 years, are likely to be linked to glacier mass balance and accumulation in the upper reservoir area, which in turn is linked to climate. The consistent return period suggests that there is some form of glaciological threshold which is reached in order for a surge to be initiated. However, this threshold appears to be of a different nature to that identified by Eisen *et al.* (2001) at Variegated Glacier, whereby a change in mass balance affects the time taken to reach the consistent threshold, and therefore quiescent phase lengths can both increase and decrease depending on mass balance conditions. In Svalbard, it is known that mass balance has generally been strongly negative across most glaciers since the LIA (Dowdeswell *et al.*, 1995), but it is unclear whether this has been reducing at a constant rate or whether regional differences have a significant influence on

individual glaciers (e.g. James *et al.*, 2012). However, the consistently less-extensive surges of Tunabreen do suggest that the amount of mass transferred during each surge has reduced at a consistent rate, which could in turn be linked to a consistent decrease in mass balance over this period. It is clear that much more work is necessary in order to investigate these links in full, but it is interesting to note the apparent impacts that climate and mass balance controls can have on surge cycles: either resulting in changes to surge periodicity (e.g. Dowdeswell *et* al, 1995; Eisen *et al.*, 2001; Striberger *et al.*, 2011) or, where surge cycle lengths remain constant, surge magnitude (e.g. Tunabreen).

In summary, this demonstrates that, although lengthening of the quiescent phase of some tidewater surge-type glaciers may be occurring in response to warming since the LIA, observations are still too scarce for this to be an equivocal link. However, there is some evidence that post-LIA warming may be having an effect on surge behaviour, reflected by the successively less-extensive maximum positions reached by Tunabreen during its three surges over this period.

9.6.2. Land-terminating surge-type glaciers

A brief review of recent literature reveals that almost all reported surges in Svalbard since ~1990 have been of tidewater glaciers, or glaciers with at least part of the terminus terminating in a fjord (Dowdeswell and Benham, 2003; Murray *et al.*, 2003a; Murray *et al.*, 2003b; Sund, 2006; Błaszczyk *et al.*, 2009; Sund *et al.*, 2009, 2013; Sund and Eiken, 2010; Mansell *et al.*, 2012). This contrasts to the period prior to this, particularly focused on the LIA, when both observations and geomorphological evidence indicate that significant numbers of land-terminating glaciers experienced surges (Croot, 1988; Hagen, 1988; Hagen *et al.*, 1993; Hambrey and Dowdeswell, 1997; Hart and Watts, 1997; Boulton *et al.*, 1999; Christoffersen *et al.*, 2005; Sund *et al.*, 2009). Dowdeswell *et al.* (1995) suggested that the trend of reducing numbers of active surges at one time could be related to lengthening of the surge cycle in response to post-LIA warming, and this has been supported by investigations at some land-terminating surge-type glaciers. Finsterwalderbreen has experienced at least four surges, based on the configuration of the push moraine complex (Fig. 6.6), the latest of which is thought to have occurred in ~1910-15 (Nuttall and Hodgkins, 2005). Since then, the glacier has experienced consistently negative mass balance, which led Nuttall *et al.* (1997) and Nuttall and Hodgkins (2005) to conclude that, although still demonstrating signs consistent with gradual mass build-up during the quiescent phase, the surge cycle may be lengthening in response to post-LIA warming. This may be more-widely applicable to similar glaciers across Svalbard which surged during the LIA but are yet to surge again (e.g. Grønfjordbreen, Holmströmbreen, Penckbreen).

Table 9.3 – Svalbard surge landsystem categories, examples of glaciers in each, and possible changes experienced as a result of post-LIA warming.

Surge landsystem	Examples across Svalbard	Possible changes in response to post-LIA warming
A - Tidewater glaciers	Tunabreen*	
	Nathorstbreen*	
	Borebreen	
	Sefströmbreen	
	Kongsvegen	
	Comfortlessbreen[B]	Successively less-extensive advances (this study)
	Paulabreen[B]	Lengthening surge cycle (Dowdeswell *et al.*, 1991)
	Fridtjovbreen	
	Hambergbreen	
	Blomstrandbreen	
	Recherchebreen	
B - Land-terminating glaciers	Finsterwalderbreen*	
	Grønfjordbreen*	
	Penckbreen	Lengthening surge cycle (Dowdeswell *et al.*, 1991)
	Usherbreen	Removal from surge cycle due to step in warming post-1990 (Malicki *et al.*, 2013)
	Holmströmbreen	
	Hørbyebreen	
	Elisebreen	
C - Small valley glaciers	Scott Turnerbreen*	
	Hessbreen*[B]	Removal from surge cycle due to step in warming post-LIA (Hodgkins *et al.*, 1999; Hansen, 2003; Midgley *et al.*, 2013)
	Tellbreen*	
	Midtre Lovénbreen	
	Austre Lovénbreen	

*Glaciers featured in this study; [B]Also shares characteristics with landsystem B.

In addition to possible lengthening of the quiescent phase, evidence from Hørbyebreen suggests that some land-terminating glaciers which surged in the past are no longer showing signs of possible future surge activity (Małecki *et al.*, 2013). The landform assemblage at the margin of Hørbyebreen is consistent with a surge (Evans *et al.*, 2012), suggested to have occurred early in the late 19th or early 20th century (Gibas *et al.*, 2005; Małecki *et al.*, 2013). Following the LIA, geometrical investigations from 1960-90 revealed that the glacier was thinning at the front and very slowly building-up mass in the upper accumulation zone, consistent with the quiescent phase of the surge cycle. However, since 1990 the mass balance has become increasingly more negative (from -0.40 m w. eq. a^{-1} in 1960-90 to -0.64 m w. eq. a^{-1} in 1990-09) and the upper accumulation zone thinned at -0.25 m a^{-1} rather than building-up mass (Małecki *et al.*, 2013). This change has coincided with the observed significant increase in summer mean air temperatures, suggested to be responsible for accelerated glacier thinning in Svalbard (James *et al.*, 2012). Based on this, it is suggested that some land-terminating glaciers which surged in the LIA, and were showing signs of mass build-up in the quiescent phase during the 20th century, may have been removed from the surge cycle by a step-like increase in warming post-1990. If strongly negative mass balance conditions persist, it is also conceivable that in time such glaciers will continue to thin and experience an eventual switch from a polythermal glacier with areas of warm ice to an entirely cold glacier, as has already occurred at some smaller valley glaciers on Svalbard (Hodgson *et al.*, 1999).

9.6.3. Small surge-type valley glaciers

It is fair to say that very few small valley glaciers on Svalbard have been observed throughout the active phase of a surge, with most suggested to be surge-type based on glaciological evidence on single aerial photographs, such as looped moraines, crevassing, and thick and advanced margins (Hagen *et al.*, 1993; Sund *et al.*, 2009; Midgley *et al.*, 2013), or occasional geomorphological evidence, such as concertina eskers (Hansen, 2003). Of these glaciers, most are known or assumed to have surged at some point during the LIA (Hodgkins *et al.*, 1999; Sletten *et al.*, 2001; Hansen, 2003; Midgley *et al.*, 2013), but are now either entirely cold-based (Hodgkins *et al.*, 1999) and/or are showing no signs of building-up mass towards a subsequent surge (Hansen, 2003; James *et al.*, 2012; Midgley *et al.*, 2013). This has led to the suggestion that post-LIA warming and associated negative mass balance has effectively removed some small valley glaciers from the surge cycle under current climatic conditions (Dowdeswell *et al.*, 1995; Hodgkins *et al.*, 1999; Hansen, 2003). Coupled with the observations presented in this study that the landform assemblage produced by such surges may not be diagnostic of surging (*9.5.2.3.*), this raises the possibility that many more small valley glaciers surged at the LIA but are no longer able to.

A possible example of this is Tellbreen, which displays strong glaciological evidence that the currently thin and cold-based glacier was much more dynamic in the past. Although direct dating evidence is unavailable, it is most likely that warm-based dynamic flow occurred at the Neoglacial maximum of the glacier, towards the end of the LIA, when Tellbreen was more extensive, contained ~60-70% more volume, and may have been up to 200 m thick (Bælum and Benn, 2011). The LIA represents the culmination of Neoglacial glacier expansion, which also typically records the most-extensive position reached by glaciers during the Holocene (Humlum *et al.*, 2005). Prior to this, conditions during the early and mid-Holocene are suggested to have been warmer than the present-day climate (Salvigsen *et al.*, 1992; Salvigsen, 2002), and most current valley glaciers on Svalbard are likely to have been considerably smaller (Svendsen and Mangerud, 1997; Mangerud and Landvik, 2007) or even non-existent (Ingólfsson, 2011) at this time. In the latter case, valley glacier build-up during the early part of the LIA would have been characterised by snow accumulation on permafrost initially leading to the development of cold-based ice; these conditions have persisted beneath some Svalbard glaciers throughout the LIA, as evidenced by the preservation of *in situ* plants in a subglacial position at Longyearbreen (Humlum *et al.*, 2005). Thickening and steepening associated with glacier growth would have insulated the ice-bed interface and encouraged strain heating of ice in the basal zone (Blatter and Hutter, 1991), creating areas at the pressure-melting-point, which in turn would lead to the generation of meltwater at the bed, facilitating related increases in dynamism in the form of sliding/subglacial deformation and higher ice velocities (Blatter and Hutter, 1991; Hambrey *et al.*, 2005; Bælum and Benn, 2011). This build-

up of mass and associated conditions at the bed is likely to have allowed Tellbreen to advance to its LIA maximum position, delimited by latero-frontal ice-cored moraines, and effectively records a switch from cold-based to warm-based conditions during the LIA. Following the LIA, the step-like increase in warming at the start of the 20th century (Hansson-Bauer *et al.*, 1990) initiated consistently negative mass balances, extensive thinning, and retreat of the lower tongue, instigating a thermal transition from a glacier with areas of warm-based ice back to one which is almost entirely frozen to its bed and in a state of low glacier activity. In simple terms, this represents a switch from a warm-based glacier in a cold period (e.g. LIA) to a cold-based glacier in a warmer period (e.g. today), and reflects a climatic influence on long-term glacier thermal regimes.

This suggested sequence of thermal switches experienced by Tellbreen since the beginning of the LIA to present day shares many similarities with the model proposed by Fowler *et al.* (2001) to explain surging of polythermal glaciers. According to this model, build-up of mass in the accumulation area of a largely cold-based glacier at the beginning of its surge cycle results in parts of the bed being raised to the pressure-melting point. This switch to warm-based conditions leads to the production of meltwater and increases subglacial water pressures and pore-water pressures in underlying sediments, resulting in a dramatic shift in glacier dynamics, associated positive feedbacks, and typically glacier advance during the active phase of the surge. Post-surge, the over-extended glacier thins rapidly and begins to freeze on to its bed, eventually switching back to largely cold-based conditions. The similarities in the thermal changes and associated flow dynamics experienced by polythermal surge-type glaciers and LIA advances of small valley glaciers on Svalbard has led to some discussion as to whether the latter describe surges or simply 'normal' polythermal glacier behaviour. An example of this is the case of Midtre Lovénbreen, which has been classified as both surge-type (Liestøl, 1988; Hansen, 2003) and non-surge-type (Hambrey *et al.*, 2005), and similar discussions have evolved in relation to Austre Lovénbreen (Jiskoot *et al.*, 2000; Midgley *et al.*, 2013) and Marthabreen (Hagen *et al.*, 1993; Glasser *et al.*, 1999). This difference of opinion, however, may be largely semantic. The key point is that a major change in glacier dynamics, controlled by changes to the thermal structure of the glacier, occurs during climate cycles in both cases. Some glaciers, such as Tellbreen, appear to have experienced a single dynamic cycle, characterised by glacier advance during the LIA, followed by a rapid rise in mean air temperatures resulting in strongly negative mass balance, widespread glacier thinning, terminus retreat, and a switch to a cold-based thermal regime, all of which would effectively remove glaciers from a surge cycle. Other (typically larger) glaciers have undergone several dynamic cycles, in the form of surges. This suggests an underlying dynamical similarity, expressed in different ways by different glaciers, and ultimately strongly linked to climatic controls on glacier mass balance and thermal regimes.

9.7. Summary

Observations of basal ice sequences, glaciological structures and glacial geomorphology associated with surge-type glaciers on Svalbard indicate that their formation can generally be linked directly to processes active during periods of dynamic, warm-based ice flow. In some cases, individual features are formed due to a range of processes which are thought to be unique to surging (e.g. geometrical ridge networks), and therefore the identification of these alone provides strong evidence for surge activity. However, when assessing glaciers with no known surge history, or the palaeo record, the most compelling evidence is presented at sites which exhibit a combination, or assemblage, of different features which together are consistent with surge activity.

Basal ice sequences associated with surge-type glaciers consist of debris-rich stratified ice and debris-poor dispersed ice facies. The formation of the stratified facies is linked to glaciotectonic deformation at glacier margins through the folding and stacking of pre-existing basal ice to form thick sequences of banded subfacies ice, and the freeze-on of saturated subglacial debris at the boundary between active surging ice and inactive marginal ice. Dispersed facies ice forms at the boundary between debris-rich stratified ice and overlying englacial ice due to strain-induced metamorphism of the latter in a shear zone, resulting in the expulsion of gases and routing of muddy films of water around grain boundaries. The basal ice sequence at glacier margins is subjected to considerable glaciotectonic deformation, resulting in intense folding, faulting and stacking of facies, and significant reorganisation of the original stratigraphy.

The development of glaciological structure during periods of dynamic, warm-based ice flow can also be linked to formational processes, allowing former flow histories to be reconstructed within currently inactive glaciers. Features which are diagnostic of former dynamic flow include dislocated or deformed longitudinal foliation, shear planes within the tongue, and dense groups of crevasse traces, interpreted as healed crevasses. The development of shear planes can in some cases relate to thrust faulting within the ice due to high longitudinal compressive forces and an active hydrological system; where shear planes are debris-rich it is suggested that they largely represent deformation along a favourable slip plane created by the reorientation of crevasse squeezes entrained during a previous surge.

The landform-sediment assemblage exposed at the margin of surge-type glaciers in Svalbard can also be linked to processes active during surges, and in particular the formation of debris-rich structures. The assemblage includes multi-crested push moraines, glacial lineations, geometrical ridge networks and areas of ice-cored hummocky topography, and shares common elements with surge landsystems presented from different settings and surge clusters. Distinct surge landsystems are identified for tidewater glaciers, land-terminating glaciers, and small valley glaciers, and it is suggested that, with some variability, most surge-type glaciers on Svalbard can be classified according to these. It is also recognised that the behaviour of the

different categories of surge-type glaciers may have been influenced by significant warming since the LIA.

This chapter highlights the strong links between the ice-sediment-landform associations produced during glacier surges and the processes active during such dynamic flow, and highlights how these observations can be used to assess possible evidence for surging.

Chapter Ten
Summary and Conclusions

'Annie Ned (b. 1890s) told about the near-surge of a glacier at the head of Kusawa Lake that occurred when a careless Southern Tutchone hunter used goat grease for cooking'

Cruickshank (2001; p.388)

10. Summary and Conclusions

This chapter summarises the main findings of this study and their wider implications within the fields of glaciology and glacial geomorphology. The aim of the study was to derive better understanding of the glaciological and geomorphological signatures produced during glacier surges on Svalbard, with a particular focus on how this is recorded in basal ice sequences, glaciological structure, and landform-sediment assemblages. To achieve this, glaciological, sedimentological and geomorphological evidence was presented from five glaciers, four of which are known to be of surge-type (Nathorstbreen, Tunabreen, Finsterwalderbreen and Scott Turnerbreen) and one which has no record of surging (Tellbreen). The main findings of these investigations are summarised below in the context of four main interconnected themes: the basal ice (*10.1.*), structural glaciological (*10.2.*), and geomorphological (*10.3.*) signatures of surging; and the influence of climate on surge behaviour (*10.4.*). Areas for further work which have arisen from this study are identified in *10.5.*

10.1. Basal ice signature of surging

Summary

Evidence for processes active during surges is recorded in the basal ice sequence exposed at the lateral margins of Tunabreen, a tidewater surge-type glacier which has surged three times since the 1930s. These processes can be linked to the formation of three basal ice facies, based on cryofacies descriptions, sedimentological analysis and stable isotope analysis: (i) solid stratified ice, which is formed by freeze-on of subglacial debris saturated by water from a wide variety of sources at a thermal transition between active surging ice and inactive marginal ice, or as a cold wave propagates through the glacier towards the end of the surge; (ii) banded ice, which is formed by a combination of freeze-on and localised regelation processes, and is subsequently thickened during the surge by intense folding, faulting and stacking; and (iii) dispersed ice, which is the result of strain-induced metamorphism of englacial ice in close proximity to the bed due to intense and variable deformation, and associated multiple melting-refreezing events, during the surge. The complex stratigraphy of the basal ice sequence records several phases of both ductile and brittle deformation, often in close proximity, indicating that different deformational sub-environments are active at the same time over small spatial scales. This basal ice sequence shares many similarities with that exposed at the margin of Tellbreen, a small, cold-based valley glacier with no record of surging.

Implications

The link between processes active during surges and the formation of basal ice sequences on Svalbard has not been previously made. It is suggested that these observations provide a framework which can be tested against additional known surge-type glaciers, and may allow previously unknown glaciers to be recognised as surge-type. An example of this is the observed

similarity between the Tunabreen and Tellbreen basal ice sequences, which provides strong evidence that Tellbreen has previously experienced more-dynamic flow conditions, perhaps relating to a surge-like advance at its LIA maximum. The identification of former surge-like behaviour based on their basal ice sequence is particularly important for glaciers which otherwise do not offer any indication of such activity (e.g. based on geomorphology at the margin).

10.2. Structural glaciological signature of surging

Summary

Elements of the glaciological structure of surge-type glaciers on Svalbard have been linked to processes active during surges, building on previous work on this theme (e.g. Hodgkins and Dowdeswell, 1994; Glasser *et al.*, 1998; Woodward *et al.*, 2002; Fleming *et al.*, 2013). Several key characteristics which are indicative of surging have been identified from the margins of Tunabreen, Finsterwalderbreen and Scott Turnerbreen: (i) deformed or dislocated longitudinal foliation; (ii) dense groups of shear planes, sometimes containing subglacial debris, which are interpreted as thrust faults and reoriented crevasse squeezes that have been subjected to thrust-style displacement and/or strike-slip movement within compressional and transpressional glaciotectonic regimes; (iii) dense groups of fractures which represent healed crevasses, providing evidence for a former extensional glaciotectonic regime related to increased ice velocities; and (iv) open crevasses, indicative of a predominantly extensional glaciotectonic regime, which in some cases have entrained subglacial debris via injections of saturated sediment into basal crevasses. Subglacial debris has also been elevated into englacial positions through hydrofracturing of the bed. Elements of this signature, and in particular (i), (ii) and (iii), are also evident within Tellbreen.

Implications

The signature of surging recorded within the glaciological structure of glaciers presented in this study presents an opportunity to reconstruct former flow dynamics of glaciers on Svalbard, particularly in relation to possible surges or surge-like advances. This is highlighted by the commonalities within the glaciological structures of Scott Turnerbreen (known surge) and Tellbreen (no recorded surge), providing further support for Tellbreen being more dynamic and experiencing a surge-like advance during the LIA. The structural glaciology signature presents a framework by which other possible surges or surge-like behaviour may be identified. Observations from the margin of Tunabreen indicate that a range of tectonic processes are responsible for the entrainment and elevation of subglacial debris during surges and, in accordance with previous observations, have demonstrated that the dominance of particular glaciotectonic regimes, and associated debris structure formation, varies across the margin. This

includes the recognition that, in addition to compression-dominated deformation, a transpressional glaciotectonic regime is active at the lateral margins (cf. Fleming *et al.*, 2013).

10.3. Geomorphological signature of surging

Summary

Observations of the landform-sediment assemblages exposed at the margins of surge-type glaciers in this study build-on and extend existing knowledge about the range of landsystems produced by surges. It has been demonstrated that three broad surge landsystems are produced by Svalbard surge-type glaciers: (i) type A – tidewater glaciers, which extends the existing submarine landsystem (cf. Ottesen and Dowdeswell, 2006; Ottesen *et al.*, 2008) with the addition of the landform-sediment assemblage exposed along the terrestrial margins; (ii) type B – land-terminating glaciers, characterised by large push moraine complexes and an inner zone of ice stagnation topography; and (iii) type C – small valley glaciers, which consists of ice-cored lateral-frontal moraine ridges and an extensive area of ice stagnation topography dominated by thermo-erosion processes. Of these, the type C landsystem, although consistent with surging, characterises the majority of forelands in Svalbard at glaciers which have been retreating since the LIA; this highlights the importance of additional glaciological evidence for dynamic, surge-like behaviour outlined in *10.2.* and *10.3.*

Implications

The landsystems presented in this study extend our understanding of the range of landform-sediment assemblages produced by surges and, for the first time, highlight the subtle, but distinct geomorphological differences between the surge imprints produced by different types of glaciers within a surge cluster. These observations can be used to identify previously unknown surges based on the geomorphology at their margins, allowing for a reassessment of the proportion of surge-type glaciers on Svalbard. There is also scope for the use of these surge landsystems as modern analogues for evidence of surging in the palaeo record.

10.4. Surge behaviour and climate

Summary

It has previously been recognised that climate has an influence on the behaviour of surge-type glaciers (Dowdeswell *et al.*, 1995; Eisen *et al.*, 2001, 2005) and this has been assessed in the context of the different types of Svalbard surge-type glaciers based on observations from this and other studies. It is possible that continuous negative mass balance since the LIA has resulted in the lengthening of quiescent phases for both tidewater and land-terminating glaciers (Dowdeswell *et al.*, 1995; Nuttall and Hodgkins, 2005). Evidence from Tunabreen indicates that, where surge cycles have remained consistent, the distance of glacier advance has become successively less-extensive since the LIA. There is an indication that some land-terminating

glaciers may have been removed from the surge cycle due to a step-like increase in warming since 1990 (James *et al.*, 2012; Małecki *et al.*, 2013). Finally, several studies have suggested that small valley glaciers may have surged during the LIA, but are no longer able to build-up sufficient mass for a subsequent surge due to an extended period of negative mass balance, and have therefore been removed from the surge cycle (Dowdeswell *et al.*, 1995; Hodgkins *et al.*, 1999; Hansen, 2003; Midgley *et al.*, 2013). This is supported by the glaciological evidence at both Scott Turnerbreen and Tellbreen, which are now entirely cold-based but have experienced more-dynamic surge or surge-like behaviour in the past.

Implications

There is an increasing realisation that climate has a strong influence on surge behaviour, moving away from the classic strict definition of surging as an aclimatic phenomenon (e.g. Meier and Post, 1969). The observations highlighted in this and other studies indicate that climate has had an impact on surge behaviour in Svalbard since the LIA, and this is an area that is worthy of further attention. Of particular importance is the realisation that many more glaciers on Svalbard may have experienced more-dynamic surge-like behaviour during the LIA than currently suggested.

10.5. Further research

Four main areas of further research attention are prompted by the findings of this study. These are:

(1) Further investigation into the basal ice and structural glaciological signatures of surging. This should focus on testing the applicability of the signatures presented in this study to a wider population of glaciers, both known surge-type glaciers and ones with no surge history. Additional observations from the basal ice sequences of surge-type glaciers would be beneficial to aid understanding of the links between glaciotectonic regimes at different stages during surges and the formation of ice facies.

(2) A reassessment of the population of surge-type glaciers on Svalbard based on the landsystems identified in this study and, where appropriate, the basal ice and structural glaciological signatures.

(3) Further investigation into the links between surge behaviour and climate on Svalbard, with a particular focus on identifying additional glaciers which may have surged during the LIA but are no longer able to.

(4) Looking for additional evidence for palaeo-surging at the margins of the former ice sheets based on the modern analogues presented in this and other studies.

References and Appendix

References and Appendix

References

Aber, J. (1988), Ice-shoved hills of Saskatchewan compared with Mississippi Delta mudlumps – implications for glaciotectonic models, *Glaciotectonic Forms and Processes*: 1-9.

Aizen, V., Kuzmichenok, V.A., Surazakov, A.B., and Aizen, E.M. (2007), Glacier changes in the Tien Shan as determined from topographic and remotely sensed data, *Global and Planetary Change*, **56**: 328-340.

Alley, R., Blankenship, D., Bentley, C., and Rooney, S. (1986), Deformation of till beneath ice stream B, West Antarctica, *Nature*, **322**: 57-59.

Alley, R., Cuffey, K.M., Evenson, E.B., Strasser, J.C., Lawson, D.E., and Larson, G.J. (1997), How glaciers entrain and transport basal sediment: physical constraints, *Quaternary Science Reviews*, **16**: 1017-1038.

Alley, R., Lawson, D.E., Evenson, E.B., Strasser, J.C., and Larson, G.J. (1998), Glaciohydraulic supercooling: a freeze-on mechanism to create stratified, debris-rich basal ice: II. Theory, *Journal of Glaciology*, **44**: 563-569.

Alley, R., Lawson, D.E., Evenson, E.B., and Larson, G.J. (2003), Sediment, glaciohydraulic supercooling, and fast glacier flow, *Annals of Glaciology*, **36** (1): 135-141.

Alsop, G., Holdsworth, R., and McCaffrey, K. (2007), Scale invariant sheath folds in salt, sediments and shear zones, *Journal of Structural Geology*, **29** (10): 1585-1604.

Andreassen, K., Winsborrow, M., Bjarnadóttir, L.R., and Rüther, D.C. (2014), Ice stream retreat dynamics inferred from an assemblage of landforms in the northern Barents Sea, *Quaternary Science Reviews*, **92**: 246-257.

Andrzejewski, L. (2002), The impact of surges on the ice-marginal landsystem of Tungnaárjökull, Iceland, *Sedimentary Geology*, **149**: 59-72.

Appleby, J.R., Brook, M.S., Vale, S.S., and Macdonald-Creevey, A. (2010), Structural glaciology of a temperate maritime glacier: lower Fox Glacier, New Zealand, *Geografiska Annaler: Series A, Physical Geography*, **92** (4): 451-467.

Arendt, A.A., Echelmeyer, K.A., Harrison, W.D., Lingle, C.S., and Valentine, V.B. (2002), Rapid wastage of Alaska glaciers and their contribution to rising sea level, *Science*, **297** (5580): 382-386.

Ashley, G.M., Southard, J.B., and Boothroyd, J.C. (1982), Deposition of climbing-ripple beds: a flume simulation, *Sedimentology*, **29** (1): 67-79.

Astakhov, V., Kaplyanskaya, F., and Tamogradsky, V. (1996), Pleistocene permafrost of West Siberia as a deformable glacier bed, *Permafrost and Periglacial Processes*, **7**: 165-191.

Augustinus, P.C. (1991), Rock resistance to erosion: some further considerations, *Earth Surface Processes and Landforms*, **16** (6): 563-569.

Bælum, K., and Benn, D.I. (2011), Thermal structure and drainage system of a small valley glacier (Tellbreen, Svalbard), investigated by ground penetrating radar, *The Cryosphere*, **5**: 139-149.

Bamber, J. (1987), Internal reflecting horizons in Spitsbergen glaciers, *Annals of Glaciology*, **9**: 6-10.

Barr, I.D., and Lovell, H. (accepted), A review of topographic controls on moraine distribution, *Geomorphology*.

Benardout, G. (in review), Ostracod-based palaeotemperature reconstructions for MIS 11 human occupation at West Stow, Suffolk, UK, *Journal of Archaeological Science*.

Benediktsson, Í.Ö., Möller, P., Ingólfsson, Ó., van der Meer, J.J.M., Kjær, K.H., and Krüger, J. (2008), Instantaneous end moraine and sediment wedge formation during the 1890 glacier surge of Brúarjökull, Iceland, *Quaternary Science Reviews*, **27**: 209-234.

Benediktsson, Í.Ö., Ingólfsson, Ó., Schomacker, A., and Kjær, K.H. (2009), Formation of submarginal and proglacial end moraines: implications of ice-flow mechanism during the 1963-64 surge of Brúarjökull, Iceland, *Boreas*, **38**: 440-457.

Benediktsson, Í.Ö., Schomacker, A., Lokrantz, H., and Ingólfsson, Ó. (2010), The 1890 surge end moraine at Eyjabakkajökull, Iceland: a re-assessment of a classic glaciotectonic locality, *Quaternary Science Reviews*, **29**: 484-506.

Benn, D.I. (1994), Fluted moraine formation and till genesis below a temperate valley glacier: Slettmarkbreen, Jotunheimen, southern Norway, *Sedimentology*, **41** (2): 279-292.

Benn, D.I. (1995), Fabric signature of subglacial till deformation, Breidamerkurjökull, Iceland, *Sedimentology*, **42** (5): 735-747.

Benn, D.I. (2004a), Clast morphology, **in:** *A practical guide to the study of glacial sediments*, Evans, D.J.A. and Benn, D.I. (Eds.), Hodder Education, London, pp. 78-92.

Benn, D.I. (2004b), Macrofabric, **in:** *A practical guide to the study of glacial sediments*, Evans, D.J.A. and Benn, D.I. (Eds.), Hodder Education, London, pp. 93-114.

Benn, D.I., and Ballantyne, C.K. (1993), The description and representation of clast shape, *Earth Surface Processes and Landforms*, **18**: 665-672.

Benn, D.I., and Ballantyne, C.K. (1994), Reconstructing the transport history of glacigenic sediments: a new approach based on the co-variance of clast form indices, *Sedimentary Geology*, **91**: 215-227.

Benn, D.I., and Evans, D.J.A. (1996), The interpretation and classification of subglacially-deformed materials, *Quaternary Science Reviews*, **15**: 23-52.

Benn, D.I., and Evans, D.J.A. (2010), *Glaciers and glaciation*, Hodder Education, London.

Benn, D.I., and Clapperton, C.M. (2000), Pleistocene glacitectonic landforms and sediments around central Magellan Strait, southernmost Chile: evidence for fast outlet glaciers with cold-based margins, *Quaternary Science Reviews*, **19** (6): 591-612.

Benn, D.I., Kristensen, L., and Gulley, J.D. (2009), Surge propagation constrained by a persistent subglacial conduit, Bakaninbreen-Paulabreen, Svalbard, *Annals of Glaciology*, **50** (52): 81-86.

Bennett, M. (2001), The morphology, structural evolution and significance of push moraines, *Earth-Science Reviews*, **53**: 197-236.

Bennett, M., Hambrey, M.J., Huddart, D., and Ghienne, J.F. (1996), The formation of a geometrical ridge network by the surge-type glacier Kongsvegen, Svalbard, *Journal of Quaternary Science*, **11** (6): 437-449.

Bennett, M., Hambrey, M.J., Huddart, D., Glasser, N.F., and Crawford, K. (1999), The landform and sediment assemblage produced by a tidewater glacier surge in Kongsfjorden, Svalbard, *Quaternary Science Reviews*, **18**: 1213-1246.

Bennett, M., Huddart, D., and Waller, R.I. (2000a), Glaciofluvial crevasse and conduit fills as indicators of supraglacial dewatering during a surge, Skeiðarárjökull, Iceland, *Journal of Glaciology*, **46** (152): 25-34.

Bennett, M.R., Huddart, D., Glasser, N.F., and Hambrey, M.J. (2000b), Resedimentation of debris on an ice-cored lateral moraine in the high-Arctic (Kongsvegen, Svalbard), *Geomorphology*, **35** (1): 21-40.

Bennett, M., Waller, R.I., Midgley, N.G., Huddart, D., Gonzalez, S., Cook, S.J., and Tomio, A. (2003), Subglacial deformation at sub-freezing temperatures? Evidence from Hagafellsjökull-Eystri, Iceland, *Quaternary Science Reviews*, **22** (8): 915-923.

Bennett, M.R., Huddart, D., Waller, R.I., Midgley, N.G., Gonzalez, S., and Tomio, A. (2004) Styles of ice-marginal deformation at Hagafellsjökull-Eystri, Iceland during the 1998/99 winter-spring surge', *Boreas*, **33**: 97-107.

Björnsson, H. (1998), Hydrological characteristics of the drainage system beneath a surging glacier, *Nature*, **395**: 771-774.

Björnsson, H., Pállson, F., Sigurđsson, O., and Flowers, G.E. (2003), Surges of glaciers in Iceland, *Annals of Glaciology*, **36**: 82-90.

Błaszczyk, M., Jania, J.A., and Hagen, J.O. (2009), Tidewater glaciers of Svalbard: Recent changes and estimates of calving fluxes, *Polish Polar Research*, **30** (2): 85-142.

Blatter, H., and Hutter, K. (1991), Polythermal conditions in Arctic glaciers, *Journal of Glaciology*, **37** (126): 261-269.

Blott, S.J., and Pye, K. (2001), GRADISTAT: a grain size distribution and statistics package for the analysis of unconsolidated sediments, *Earth Surface Processes and Landforms*, **26** (11): 1237-1248.

Boereboom, T., Depoorter, M., Coppens, S., and Tison, J.-L. (2012), Gas properties of winter lake ice in Northern Sweden: implication for carbon gas release, *Biogeosciences*, **9** (2): 827-838.

Boston, C.M. (2012), A glacial geomorphological map of the Monadhliath Mountains, Central Scottish Highlands, *Journal of Maps*, **8** (4): 437-444.

Bougamont, M., and Tulaczyk, S. (2003), Glacial erosion beneath ice streams and ice-stream tributaries: constraints on temporal and spatial distribution of erosion from numerical simulations of a West Antarctic ice stream, *Boreas*, **32** (1): 178-190.

Boulton, G. (1968), Flow tills and related deposits on some Vestspitsbergen glaciers, *Journal of Glaciology*, **7**: 391-412.

Boulton, G. (1976), The origin of glacially fluted surfaces - observations and theory, *Journal of Glaciology*, **17** (76).

Boulton, G. (1986), Push-moraines and glacier-contact fans in marine and terrestrial environments, *Sedimentology*, **33** (5): 677-698.

Boulton, G., and Spring, U. (1986), Isotopic fractionation at the base of polar and sub-polar glaciers, *Journal of Glaciology*, **32** (112): 475-485.

Boulton, G., Baldwin, C., Peacock, J., McCabe, A., Miller, G., Jarvis, J., Horsefield, B., Worsley, P., Eyles, N., and Chroston, P. (1982), A glacio-isostatic facies model and amino acid stratigraphy for late Quaternary events in Spitsbergen and the Arctic, *Nature*, **298**: 437-441.

Boulton, G., van der Meer, J.J.M., Hart, J.K., Beets, D.J., Ruegg, G.H.J., van der Wateren, F.M., and Jarvis, J. (1996), Till and moraine emplacement in a deforming bed surge - an example from a marine environment, *Quaternary Science Reviews*, **15**: 961-987.

Boulton, G., van der Meer, J.J.M., Beets, D.J., Hart, J.K., and Ruegg, G.H.J. (1999), The sedimentary and structural evolution of a recent push moraine complex: Holmstrømbreen, Spitsbergen, *Quaternary Science Reviews*, **18**: 339-371.

Brodzikowski, K., and Van Loon, A. (1991), *Glacigenic sediments*, Elsevier, Oxford.

Brook, M.S., and Lukas, S. (2012), A revised approach to discriminating sediment transport histories in glacigenic sediments in a temperate alpine environment: a case study from Fox Glacier, New Zealand, *Earth Surface Processes and Landforms*, **37** (8): 895-900.

Brynjólfsson, S., Ingólfsson, Ó., and Schomacker, A. (2012), Surge fingerprinting of cirque glaciers at the Tröllaskagi peninsula, North Iceland, *Jökull*, **62**: 151-166.

Burke, H., Phillips, E., Lee, J.R., and Wilkinson, I.P. (2009), Imbricate thrust stack model for the formation of glaciotectonic rafts: an example from the Middle Pleistocene of north Norfolk, UK, *Boreas*, **38** (3): 620-637.

Canals, M., Urgeles, R., and Calafat, A.M. (2000), Deep sea-floor evidence of past ice streams off the Antarctic Peninsula, *Geology*, **28** (1): 31-34.

Carlsen, M. (2004), Deglasiasjon av Van Keulenfjorden, Svalbard, de siste 130 år : Brefrontvariasjoner og glasiale prosesser, *MSc thesis*, University of Oslo.

Carr, J.R., Vieli, A., and Stokes, C. (2013), Influence of sea ice decline, atmospheric warming and glacier width on marine-terminating outlet glacier behavior in north-west Greenland at seasonal to interannual timescales, *Journal of Geophysical Research: Earth Surface*, **118** (3): 1210-1226.

Christoffersen, P., Piotrowski, J.A., and Larsen, N.K. (2005), Basal processes beneath an Arctic glacier and their geomorphic imprint after a surge, Elisebreen, Svalbard, *Quaternary Research*, **64**: 125-137.

Christoffersen, P., Tulaczyk, S., Carsey, F.D., and Behar, A.E. (2006), A quantitative framework for interpretation of basal ice facies formed by ice accretion over subglacial sediment, *Journal of Geophysical Research*, **111** (F1): F01017.

Clark, C.D. (2010), Emergent drumlins and their clones: from till dilatancy to flow instabilities, *Journal of Glaciology*, **56** (200): 1011-1025.

Clark, C.D., Tulaczyk, S.M., Stokes, C.R., and Canals, M. (2003), A groove-ploughing theory for the production of mega-scale glacial lineations, and implications for ice-stream mechanics, *Journal of Glaciology*, **49** (165): 240-256.

Clark, P., Mitrovica, J.X., Milne, G.A., and Tamisiea, M.E. (2002), Sea-level fingerprinting as a direct test for the source of global meltwater pulse 1A, *Science*, **295**: 2438-2441.

Clarke, G. (1987), Fast Glacier Flow: Ice Stream, Surging, and Tidewater Glaciers, *Journal of Geophysical Research*, **92** (B9): 8835-8841.

Clarke, G. (1991), Length, width and slope influences on glacier surging, *Journal of Glaciology*, **37** (126): 236-246.

Clarke, G. (2005), Subglacial processes, *Annual Review of Earth and Planetary Sciences*, **33**: 247-276.

Clarke, G., Collins, S.G., and Thompson, D.E. (1984), Flow, thermal structure, and subglacial conditions of a surge-type glacier, *Canadian Journal of Earth Sciences*, **21**: 232-240.

Clarke, G., Schmok, J.P., Ommanney, C.S.L., and Collins, S.G. (1986), Characteristics of surge-type glaciers, *Journal of Geophysical Research*, **91**: 7165-7180.

Clayton, L., Teller, J., and Attig, J. (1985), Surging of the southwestern part of the Laurentide Ice Sheet, *Boreas*, **14** (3): 235-241.

Clayton, L., Attig, J.W., Ham, N.R., Johnson, M.D., Jennings, C.E., and Syverson, K.M. (2008), Ice-walled-lake plains: Implications for the origin of hummocky glacial topography in middle North America, *Geomorphology*, **97** (1): 237-248.

Cook, S.J., Knight, P.G., Waller, R.I., Robinson, Z.P., and Adam, W.G. (2007), The geography of basal ice and its relationship to glaciohydraulic supercooling: Svínafellsjökull, southeast Iceland, *Quaternary Science Reviews*, **26** (19–21): 2309-2315.

Cook, S.J., Robinson, Z.P., Fairchild, I.J., Knight, P.G., Waller, R.I., and Boomer, I.A.N. (2010), Role of glaciohydraulic supercooling in the formation of stratified facies basal ice: Svínafellsjökull and Skaftafellsjökull, southeast Iceland, *Boreas*, **39** (1): 24-38.

Cook, S., Swift, D.A., Graham, D.J., and Midgley, N.G. (2011), Origin and significance of 'dispersed facies' basal ice: Svínfellsjökull, Iceland, *Journal of Glaciology*, **57** (204): 710-720.

Cooper, R., Hodgkins, R., Wadham, J., and Tranter, M. (2011), The hydrology of the proglacial zone of a high-Arctic glacier (Finsterwalderbreen, Svalbard): Sub-surface water fluxes and complete water budget, *Journal of Hydrology*, **406** (1): 88-96.

Copland, L., Sharp, M.J., and Dowdeswell, J.A. (2003), The distribution and flow characteristics of surge-type glaciers in the Canadian High Arctic, *Annals of Glaciology*, **36**: 73-81.

Croot, D.G. (1987), Glacio-tectonic structures: a mesoscale model of thin-skinned thrust sheets?, *Journal of Structural Geology*, **9** (7): 797-808.

Croot, D. (1988), Glaciotectonics and surging glaciers: a correlation based on Vestspitsbergen, Svalbard, Norway, **in:** *Glaciotectonics: forms and processes*, Croot, D.G. (Eds.), Balkema, Amsterdam, pp. 49-62.

Cruikshank, J. (2001), Glaciers and climate change: perspectives from oral tradition, *Arctic*, **54** (4): 377-393.

Cutbill, J., and Challinor, A. (1965), Revision of the Stratigraphical Scheme for the Carboniferous and Permian Rocks of Spitsbergen and Bjørnøya, *Geological Magazine*, **102** (05): 418-439.

Dallmann, W., Ohta, Y., Elvevold, S., and Blomeier, D. (Eds.) (2002), *Bedrock map of Svalbard and Jan Mayen*, Norsk Polarinstitutt Temakart No. 33.

Darvill, C.M., Stokes, C.R., Bentley, M.J., and Lovell, H. (2014), A glacial geomorphological map of the southernmost ice lobes of Patagonia: the Bahía Inútil - San Sebastián, Magellan, Otway, Skyring and Bella Vista lobes, *Journal of Maps*, **10** (3): 500-520.

de Geer, G. (1910), Guide de l'excursion au Spitsbergen. Excursion A1. (Guide to excursions on Spitsbergen A1.), *XI International Geological Congress*, Stockholm.

Divine, D.V., Isaksson, E., Pohjola, V., Meijer, H., van de Wal, R.S.W., Martma, T., Moore, J., Sjögren, B., and Godtliebsen, F. (2008), Deuterium excess record from a small Arctic ice cap, *Journal of Geophysical Research*, **113** (D19): D19104.

Dolgoushin, L., and Osipova, G.B. (1975), Glacier surges and the problem of their forecasting, *International Association of Hydrological Sciences Publication 104 (Symposium at Moscow 1971 - Snow and Ice)*: 292-304.

Domack, E., Duran, D., Leventer, A., Ishman, S., Doane, S., McCallum, S., Amblas, D., Ring, J., Gilbert, R., and Prentice, M. (2005), Stability of the Larsen B ice shelf on the Antarctic Peninsula during the Holocene epoch, *Nature*, **436**: 681-685.

Dowdeswell, J.A., and Collin, R.L. (1990), Fast-flowing outlet glaciers on Svalbard ice caps, *Geology*, **18**: 778-781.

Dowdeswell, J.A., and Williams, M. (1997), Surge-type glaciers in the Russian High Arctic identified from digital satellite imagery, *Journal of Glaciology*, **43**: 489-494.

Dowdeswell, J.A., and Benham, T.J. (2003), A surge of Perseibreen, Svalbard, examined using aerial photography and ASTER high resolution satellite imagery, *Polar Research*, **22** (2): 373-383.

Dowdeswell, J.A., Drewry, D.J., Liestøl, O., and Orheim, O. (1984), Airborne Radio Echo Sounding of Sub-Polar Glaciers in Spitsbergen, *Norsk Polarinstitutt Skrifter*, **182**: 1-41.

Dowdeswell, J.A., Hamilton, G.S., and Hagen, J.O. (1991), The duration of the active phase on surge-type glaciers: contrasts between Svalbard and other regions, *Journal of Glaciology*, **37** (127): 388-400.

Dowdeswell, J.A., Hodgkins, R., Nuttall, A.-M., Hagen, J.O., and Hamilton, G.S. (1995), Mass balance change as a control on the frequency and occurrence of glacier surges in Svalbard, Norwegian High Arctic, *Geophysical Research Letters*, **22** (21): 2909-2912.

Dowdeswell, J.A., Hagen, J.O., Björnsson, H., Glazovsky, A.F., Harrison, W.D., Holmlund, P., Jania, J., Koerner, R.M., Lefauconnier, B., and Ommanney, C.S.L. (1997), The mass balance of circum-Arctic glaciers and recent climate change, *Quaternary Research*, **48** (1): 1-14.

Dunér, N., and Nordenskiöld, A. (1865), Map of Spitsbergen, *Remarks on Geography of Spitsbergen. Kongl. Svenska Vetenskaps-Akademiens Handlingar*, **6** (5).

Echelmeyer, K.A., Butterfield, R., and Cuillard, D. (1987), Some observations on a recent surge of Peters Glacier, Alaska, U.S.A., *Journal of Glaciology*, **33** (115): 341-345.

Eisen, O., Harrison, W.D., and Raymond, C.F. (2001), The surges of Variegated Glacier, Alaska, U.S.A., and their connection to climate and mass balance, *Journal of Glaciology*, **47** (158): 351-358.

Eisen, O., Harrison, W.D., Raymond, C.F., Echelmeyer, K.A., Bender, G.A., and Gorda, J.L.D. (2005), Variegated Glacier, Alaska, USA: a century of surges, *Journal of Glaciology*, **51** (174): 399-406.

Engelhardt, H., and Kamb, B. (1998), Basal sliding of ice stream B, West Antarctica, *Journal of Glaciology*, **44** (147): 223-230.

Ensminger, S., Alley, R.B., Evenson, E.B., Lawson, D.E., and Larson, G.J. (2001), Basal-crevasse-fill origin of laminated debris bands at Matanuska Glacier, Alaska, U.S.A., *Journal of Glaciology*, **47** (158): 412-422.

Etzelmüller, B., and Hagen, J.O. (2005), Glacier-permafrost interaction in Arctic and alpine mountain environments with examples from southern Norway and Svalbard, *Geological Society, London, Special Publications*, **242** (1): 11-27.

Etzelmüller, B., Hagen, J., Vatne, G., Ødegård, R., and Sollid, J. (1996), Glacial debris accumulation and sediment deformation influenced by permafrost: examples from Svalbard, *Annals of Glaciology*, **22**: 53-62.

Etzelmüller, B., Ødegård, R.S., Vatne, G., Mysterud, R.S., Tonning, T., and Sollid, J.L. (2000), Glacier characteristics and sediment transfer system of Longyearbreen and Larsbreen, western Spitsbergen, *Norsk Geografisk Tidsskrift*, **54** (4): 157-168.

Evans, D.J.A. (1989), The nature of glacitectonic structures and sediments at sub-polar glacier margins, northwest Ellesmere Island, Canada, *Geografiska Annaler*, **71A** (3-4): 113-123.

Evans, D.J.A. (Ed.) (2005), *Glacial Landsystems*, Hodder Arnold, London.

Evans, D.J.A. (2009), Controlled moraines: origins, characteristics and palaeoglaciological implications, *Quaternary Science Reviews*, **28**: 183-208.

Evans, D.J.A., and Rea, B.R. (1999), Geomorphology and sedimentology of surging glaciers: a land-systems approach, *Annals of Glaciology*, **28**: 75-82.

Evans, D.J.A., and Twigg, D.R. (2002), The active temperate glacial landsystem: a model based on Breiðamerkurjökull and Fjallsjökull, Iceland, *Quaternary Science Reviews*, **21**: 2143-2177.

Evans, D.J.A., and Benn, D.I. (Eds.) (2004a), *A practical guide to the study of glacial sediments*, Hodder Education, London.

Evans, D.J.A., and Benn, D.I. (2004b), Facies description and the logging of sedimentary exposures, **in:** *A practical guide to the study of glacial sediments*, Evans, D.J.A. and Benn, D.I. (Eds.), Hodder Education, London, pp. 11-51.

Evans, D.J.A., and Rea, B.R. (2005), Surging glacier landsystem, **in:** *Glacial landsystems*, Evans, D.J.A. (Eds.), Edward Arnold, London

Evans, D.J.A., Lemmen, D.S., and Rea, B.R. (1999), Glacial landsystems of the southwest Laurentide Ice Sheet: modern Icelandic analogues, *Journal of Quaternary Science*, **14** (7): 673-691.

Evans, D.J.A., Phillips, E., Hiemstra, J., and Auton, C. (2006a), Subglacial till: formation, sedimentary characteristics and classification, *Earth-Science Reviews*, **78** (1): 115-176.

Evans, D.J., Twigg, D.R., and Shand, M. (2006b), Surficial geology and geomorphology of the þórisjökull plateau icefield, west-central Iceland, *Journal of Maps*, **2** (1): 17-29.

Evans, D.J.A., Twigg, D.R., Rea, B.R., and Shand, M. (2007), Surficial geology and geomorphology of the Brúarjökull surging glacier landsystem, *Journal of Maps*, **2007**: 349-367.

Evans, D.J.A., Clark, C.D., and Rea, B.R. (2008), Landform and sediment imprints of fast glacier flow in the southwest Laurentide Ice Sheet, *Journal of Quaternary Science*, **23** (3): 249-272.

Evans, D.J.A., Twigg, D.R., Rea, B.R., and Orton, C. (2009), Surging glacier landsystem of Tungnaárjökull, Iceland, *Journal of Maps*, **5** (1): 134-151.

Evans, D.J.A., Twigg, D.R., and Orton, C. (2010a), Satujökull glacial landsystem, Iceland, *Journal of Maps*, **6** (1): 639-650.

Evans, D.J.A., Shulmeister, J., and Hyatt, O. (2010b), Sedimentology of latero-frontal moraines and fans on the west coast of South Island, New Zealand, *Quaternary Science Reviews*, **29** (27): 3790-3811.

Evans, D.J.A., Strzelecki, M., Milledge, D.G., and Orton, C. (2012), Hørbyebreen polythermal glacial landsystem, Svalbard, *Journal of Maps*, **8** (2): 146-156.

Evenson, E.B., Lawson, D.E., Strasser, J.C., Larson, G.J., Alley, R.B., Ensminger, S.L., and Stevenson, W.E. (1999), Field evidence for the recognition of glaciohydrologic supercooling, *Geological Society of America Special Papers*, **337**: 23-35.

Eyles, N., Eyles, C.H., and Miall, A.D. (1983), Lithofacies types and vertical profile models; an alternative approach to the description and environmental interpretation of glacial diamict and diamictite sequences, *Sedimentology*, **30** (3): 393-410.

Fairchild, I.J., and Hambrey, M.J. (1984), The Vendian succession of northeastern Spitsbergen: Petrogenesis of a dolomite-tillite association, *Precambrian Research*, **26** (2): 111-167.

Fleming, E.J., Stevenson, C.T., and Petronis, M.S. (2012), New insights into the deformation of a Middle Pleistocene glaciotectonised sequence in Norfolk, England through magnetic and structural analysis, *Proceedings of the Geologists' Association*, **124**: 834-854.

Fleming, E.J., Lovell, H., Stevenson, C.T.E., Petronis, M.S., Benn, D.I., Hambrey, M.J., and Fairchild, I.J. (2013), Magnetic fabrics of basal ice in a surge-type glacier, *Journal of Geophysical Research*, **118** (4): 2263-2278.

Flink, A. (2013), Dynamics of surging tidewater glaciers in Tempelfjorden, Spitsbergen, *MSc thesis*, Stockholm University: 58 pp.

Flowers, G., Roux, N., Pimentel, S., and Schoof, C.G. (2011), Present dynamics and future prognosis of a slowly surging glacier, *The Cryosphere*, **5**: 299-313.

Førland, E., Hanssen-Bauer, I., and Nordli, P. (1997), Climate statistics and longterm series of temperature and precipitation at Svalbard and Jan Mayen, *Det Norske Meteorologiske Institutt Klima Report*, **21** (97): 1997.

Førland, E.J., Benestad, R., Hanssen-Bauer, I., Haugen, J.E., and Skaugen, T.E. (2012), Temperature and Precipitation Development at Svalbard 1900–2100, *Advances in Meteorology*, **2011**.

Forwick, M., Vorren, T.O., Hald, M., Korsun, S., Roh, Y., Vogt, C., and Yoo, K.-C. (2010), Spatial and temporal influence of glaciers and rivers on the sedimentary environment in Sassenfjorden and Tempelfjorden, Spitsbergen, **in:** *Fjord Systems and Archives*, Howe, J., Austin, W.E.N., Forwick, M. and Paetzel, M. (Eds.), Geological Society of London, London

Fowler, A. (2010), The formation of subglacial streams and mega-scale glacial lineations, *Proceedings of the Royal Society A: Mathematical, Physical and Engineering Science*, **466** (2123): 3181-3201.

Fowler, A., Murray, T., and Ng, F.S.L. (2001), Thermally controlled glacier surging, *Journal of Glaciology*, **47** (159): 527-538.

Frappé, T.-P., and Clarke, G.K.C. (2007), Slow surge of Trapridge Glacier, Yukon Territory, Canada, *Journal of Geophysical Research*, **112**: 1-17.

Gardner, J.S., and Hewitt, K. (1990), A surge of Bualtar Glacier, Karakoram Range, Pakistan: A possible landslide trigger, *Journal of Glaciology*, **36** (123): 159-162.

Gardner, A.S., Moholdt, G., Wouters, B., Wolken, G.J., Burgess, D.O., Sharp, M.J., Cogley, J.G., Braun, C., and Labine, C. (2011), Sharply increased mass loss from glaciers and ice caps in the Canadian Arctic Archipelago, *Nature*, **473** (7347): 357-360.

Gibas, J., Rachlewicz, G., and Szczucinski, W. (2005), Application of DC resistivity soundings and geomorphological surveys in studies of Arctic glacier marginal zones, Petuniabukta, Spitsbergen, *Polish Polar Research*, **26** (4): 239-258.

Gibbons, A.B., Megeath, J.D., and Pierce, K.L. (1984), Probability of moraine survival in a succession of glacial advances, *Geology*, **12**: 327-330.

Glasser, N.F., Huddart, D., and Bennett, M.R. (1998a), Ice-marginal characteristics of Fridtjovbreen (Svalbard) during its recent surge, *Polar Research*, **17** (1): 93-100.

Glasser, N.F., Hambrey, M.J., Crawford, K., Bennett, M.R., and Huddart, D. (1998b), The structural glaciology of Kongsvegen, Svalbard, and its role in landform genesis, *Journal of Glaciology*, **44** (146): 136-148.

Glasser, N.F., Bennett, M.R., and Huddart, D. (1999), Distribution of glaciofluvial sediment within and on the surface of a High Arctic valley glacier: Marthabreen, Svalbard, *Earth Surface Processes and Landforms*, **24**: 303-318.

Glasser, N.F., and Hambrey, M.J. (2002), δD-δ18O relationships on a polythermal valley glacier: Midtre Lovénbreen, Svalbard, *Polar Research*, **21** (1): 123-131.

Glasser, N.F., Hambrey, M.J., Bennett, M.R., and Huddart, D. (2003a), Comment: Formation and reorientation of structure in the surge-type glacier Kongsvegen, Svalbard, J. Woodward, T. Murray and A. McCaig (2002) Journal of Quaternary Science 17: 201–209, *Journal of Quaternary Science*, **18** (1): 95-97.

Glasser, N.F., Hambrey, M.J., Etienne, J.L., Jansson, P., and Pettersson, R. (2003b), The origin and significance of debris-charged ridges at the surface of Storglaciären, northern Sweden, *Geografiska Annaler: Series A, Physical Geography*, **85** (2): 127-147.

Glazovskiy, A., Macheret, Y.Y., Moskalevsky, M.Y., and Jania, J. (1991), Tidewater glaciers of Spitsbergen, **in:** *Glaciers-Ocean-Atmosphere: Interactions*, V.M., K., A., U. and A., G. (Eds.), IAHS Publication, pp. 229-239.

Goodsell, B., Hambrey, M., Glasser, N., Nienow, P., and Mair, D. (2005), The structural glaciology of a temperate valley glacier: Haut Glacier d'Arolla, Valais, Switzerland, *Arctic, Antarctic, and Alpine Research*, **37** (2): 218-232.

Gow, A.J., and Langston, D. (1977), Growth history of lake ice in relation to its stratigraphic, crystalline and mechanical structure, *CRREL Report*, Army Cold Regions Research and Engineering Laboratory, Hanover.

Graham, D.J., and Midgley, N.G. (2000), Technical Communication - Graphical Representation of Particle Shape using Triangular Diagrams: An Excel Spreadsheet Method, *Earth Surface Processes and Landforms*, **25** (13): 1473-1478.

Graham, A.G., Larter, R.D., Gohl, K., Hillenbrand, C.-D., Smith, J.A., and Kuhn, G. (2009), Bedform signature of a West Antarctic palaeo-ice stream reveals a multi-temporal record of flow and substrate control, *Quaternary Science Reviews*, **28** (25): 2774-2793.

Grant, K.L., Stokes, C.R., and Evans, I.S. (2009), Identification and characteristics of surge-type glaciers on Novaya Zemlya, Russian Arctic, *Journal of Glaciology*, **55** (194): 960-972.

Gripp, K. (1929), *Glaciologische und geologische Ergebnisse der Hamburgischen Spitzbergen-Expedition 1927*, Abhandlungen der naturwissenschaftlichen Verein Hamburg, Hamburg.

Gulley, J.D., Benn, D., Muller, D., and Luckman, A. (2009a), A cut-and-closure origin for englacial conduits in uncrevassed regions of polythermal glaciers, *Journal of Glaciology*, **55** (189): 66-80.

Gulley, J.D., Benn, D., Screaton, E., and Martin, J. (2009b), Mechanisms of englacial conduit formation and their implications for subglacial recharge, *Quaternary Science Reviews*, **28** (19): 1984-1999.

Hagen, J. (1988), Glacier surge in Svalbard with examples from Usherbreen, *Norsk Geografisk Tidsskrift*, **42**: 204-213.

Hagen, J., and Liestøl, O. (1990), Long-term glacier mass-balance investigations in Svalbard, 1950–88, *Annals of Glaciology*, **14** (102-106).

Hagen, J., Liestøl, O., Roland, E., and Jørgensen, T. (1993), Glacier atlas of Svalbard and Jan Mayen, *Norsk Polarinstitutt Meddelelser*, **129**: 1-141.

Hagen, J., Kohler, J., Melvold, K., and Winther, J.-G. (2003), Glaciers in Svalbard: mass balance, runoff and freshwater flux, *Polar Research*, **22** (2): 145-159.

Hall, K. (1987), The physical properties of quartz-micaschist and their application to freeze-thaw weathering studies in the maritime Antarctic, *Earth Surface Processes and Landforms*, **12** (2): 137-149.

Hamberg, A. (1905), Astronomische, photogrammetrische und erdmagnetische arbeiten der von AG Nathorst geleiteten Schwedischen Polarexpedition 1898, *K Sven. Videnskaps Akad. Handl*, **39** (6).

Hambrey, M. (1975), The origin of foliation in glaciers: evidence from some Norwegian examples, *Journal of Glaciology*, **14** (70): 181-185.

Hambrey, M. (1976), Structure of the glacier Charles Rabots Bre, Norway, *Geological Society of America Bulletin*, **87** (11): 1629-1637.

Hambrey, M., and Müller, F. (1978), Structures and ice deformation in the white glacier, Axel Heiberg Island, Northwest Territories, Canada, *Journal of Glaciology*, **20**: 41-66.

Hambrey, M., and Huddart, D. (1995), Englacial and proglacial glaciotectonic processes at the snout of a thermally complex glacier in Svalbard, *Journal of Quaternary Science*, **10** (4): 313-326.

Hambrey, M., and Dowdeswell, J.A. (1997), Structural evolution of a surge-type polythermal glacier: Hessbreen, Svalbard, *Annals of Glaciology*, **24**: 375-381.

Hambrey, M., and Glasser, N.F. (2003), The role of folding and foliation development in the genesis of medial moraines: Examples from Svalbard glaciers, *Journal of Geology*, **111**: 471-485.

Hambrey, M., Dowdeswell, J.A., Murray, T., and Porter, P.R. (1996), Thrusting and debris entrainment in a surging glacier: Bakaninbreen, Svalbard, *Annals of Glaciology*, **22**: 241-248.

Hambrey, M., Murray, T., Glasser, N.F., Hubbard, A., Hubbard, B., Stuart, G., Hansen, S., and Kohler, J. (2005), Structure and changing dynamics of a polythermal valley glacier on a centennial timescale: Midre Lovénbreen, Svalbard, *Journal of Geophysical Research: Earth Surface*, **110**: 1-19.

Hamilton, G.S., and Dowdeswell, J.A. (1996), Controls on glacier surging in Svalbard, *Journal of Glaciology*, **42** (140): 157-168.

Hansen, S. (2003), From surge-type to non-surge-type glacier behaviour: midre Lovénbreen, Svalbard, *Annals of Glaciology*, **36**: 97-102.

Hanssen-Bauer, I. (2002), Temperature and precipitation in Svalbard 1912-2050: measurements and scenarios, *Polar Record*, **38** (206): 225-232.

Hanssen-Bauer, I., and Førland, E. (1998), Long-term trends in precipitation and temperature in the Norwegian Arctic: can they be explained by changes in atmospheric circulation patterns?, *Climate Research*, **10** (2): 143-153.

Hansson-Bauer, I., Kristensen Solås, M., and Steffensen, E.L. (1990), The climate of Spitsbergen, *Det norske meteorologiske institutt, Report, 39/90*: 40.

Harrison, W.D., and Post, A.S. (2003), How much do we really know about glacier surging?, *Annals of Glaciology*, **36**: 1-6.

Harrison, W.D., Echelmeyer, K.A., Chacho, E.F., Raymond, C.F., and Benedict, R.J. (1994), The 1987-88 surge of West Fork Glacier, Susitna Basin, Alaska, U.S.A., *Journal of Glaciology*, **40** (135): 241-254.

Hart, J., and Watts, R.J. (1997), A comparison of the styles of deformation associated with two recent push moraines, south Van Keulenfjorden, Svalbard, *Earth Surface Processes and Landforms*, **22**: 1089-1107.

Heinrichs, T., Mayo, L.R., Echelmeyer, K.A., and Harrison, W.D. (1996), Quiescent-phase evolution of a surge-type glacier: Black Rapids Glacier, Alaska, U.S.A., *Journal of Glaciology*, **42** (140): 110-122.

Hewitt, K. (2007), Tributary glacier surges: an exceptional concentration at Panmah Glacier, Karakoram Himalaya, *Journal of Glaciology*, **53** (181): 181-188.

Hjelle, A. (1993), *Geology of Svalbard*, Norsk Polarinstitutt, Oslo.

Hodgkins, R. (1994), The seasonal evolution of meltwater discharge, quality and routing at a high-Arctic glacier, *PhD thesis*, University of Cambridge.

Hodgkins, R., and Dowdeswell, J.A. (1994), Tectonic processes in Svalbard tide-water glacier surges: evidence from structural glaciology, *Journal of Glaciology*, **40** (136): 553-560.

Hodgkins, R., Tranter, M., and Dowdeswell, J.A. (1998), The hydrochemistry of runoff from a 'cold-based' glacier in the High Arctic (Scott Turnerbreen, Svalbard), *Hydrological Processes*, **12** (1): 87-103.

Hodgkins, R., Hagen, J.O., and Hamran, S.-E. (1999), Twentieth-century mass balance and thermal regime change at an Arctic glacier, *Annals of Glaciology*, **28**: 216-220.

Hodgkins, R., Tranter, M., and Dowdeswell, J.A. (2004), The characteristics and formation of a high-arctic proglacial icing, *Geografiska Annaler*, **86A** (3): 265-275.

Hodgkins, R., Fox, A., and Nuttall, A.-M. (2007), Geometry change between 1990 and 2003 at Finsterwalderbreen, a Svalbard surge-type glacier, from GPS profiling, *Annals of Glaciology*, **46** (1): 131-135.

Hodson, A., Anesio, A.M., Tranter, M., Fountain, A., Osborn, M., Priscu, J., Laybourn-Parry, J., and Sattler, B. (2008), Glacial ecosystems, *Ecological Monographs*, **78** (1): 41-67.

Hoey, T. (2004), The size of sedimentary particles, **in:** *A practical guide to the study of glacial sediments*, Evans, D.J.A. and Benn, D. (Eds.), Hodder Education, London

Hoinkes, H.C. (1969), Surges of the Vernagtferner in the Ötztal Alps since 1599, *Canadian Journal of Earth Sciences*, **6**: 853-861.

Hooke, R.L., and Hudleston, P.J. (1978), Origin of foliation in glaciers, *Journal of Glaciology*, **20** (83): 285-299.

Hubbard, B. (1991), Freezing-rate effects on the physical characteristics of basal ice formed by net adfreezing, *Journal of Glaciology*, **37** (127).

Hubbard, B., and Sharp, M. (1993), Weertman regelation, multiple refreezing events and the isotopic evolution of the basal ice layer, *Journal of Glaciology*, **39** (132): 275-291.

Hubbard, B., and Sharp, M. (1995), Basal ice facies and their formation in the Western Alps, *Arctic and Alpine Research*, **27** (4): 301-310.

Hubbard, B., and Glasser, N.F. (2005), *Field techniques in glaciology and glacial geomorphology*, Wiley, Chichester.

Hubbard, B., Tison, J.L., Janssens, L., and Spiro, B. (2000), Ice-core evidence of the thickness and character of clear-facies basal ice: Glacier de Tsanfleuron, Switzerland, *Journal of Glaciology*, **46** (152): 140-150.

Hubbard, B., Glasser, N.F., Hambrey, M.J., and Etienne, J. (2004), A sedimentological and isotopic study of the origin of supraglacial debris bands: Kongsfjorden, Svalbard, *Journal of Glaciology*, **50** (169): 157-170.

Hubbard, B., Cook, S., and Coulson, H. (2009), Basal ice facies: a review and unifying approach, *Quaternary Science Reviews*, **28**: 1956-1969.

Huddart, D., and Hambrey, M.J. (1996), Sedimentary and tectonic development of a high-arctic, thrust-moraine complex: Comfortlessbreen, Svalbard, *Boreas*, **25**: 227-243.

Hulbe, C., and Fahnestock, M. (2007), Century-scale discharge stagnation and reactivation of the Ross ice streams, West Antarctica, *Journal of Geophysical Research: Earth Surface*, **112** (F3).

Humlum, O., Instanes, A., and Sollid, J.L. (2003), Permafrost in Svalbard: a review of research history, climatic background and engineering challenges, *Polar Research*, **22** (2): 191-215.

Humlum, O., Elberling, B., Hormes, A., Fjordheim, K., Hansen, O.H., and Heinemeier, J. (2005), Late-Holocene glacier growth in Svalbard, documented by subglacial relict vegetation and living soil microbes, *The Holocene*, **15**: 396-407.

Ingólfsson, Ó. (2011), Fingerprints of Quaternary glaciations on Svalbard, *Geological Society, London, Special Publications*, **354** (1): 15-31.

IPCC (2007), *Climate change 2007: the physical science basis. Working group 1 contribution to the fourth assessment report of the IPCC*, Cambridge University Press.

Irvine-Fynn, T.D., Hodson, A.J., Moorman, B.J., Vatne, G., and Hubbard, A.L. (2011), Polythermal glacier hydrology: a review, *Reviews of Geophysics*, **49** (4): RG4002.

Iverson, N.R. (1993), Regelation of ice through debris at glacier beds: Implications for sediment transport, *Geology*, **21**: 559-562.

Iverson, N.R. (2000), Sediment entrainment by a soft-bedded glacier: a model based on regelation into the bed, *Earth Surface Processes and Landforms*, **25**: 881-893.

Iverson, N.R., and Souchez, R. (1996), Isotopic signature of debris-rich ice formed by regelation into a subglacial sediment bed, *Geophysical Research Letters*, **23** (10): 1151-1154.

Jacob, T., Wahr, J., Pfeffer, W.T., and Swenson, S. (2012), Recent contributions of glaciers and ice caps to sea level rise, *Nature*, **482** (7386): 514-518.

Jade, S., and Sitharam, T. (2003), Characterization of strength and deformation of jointed rock mass based on statistical analysis, *International Journal of Geomechanics*, **3** (1): 43-54.

James, T., Murray, T., Barrand, N., Sykes, H., Fox, A., and King, M. (2012), Observations of enhanced thinning in the upper reaches of Svalbard glaciers, *The Cryosphere*, **6** (6): 1369-1381.

Jiskoot, H., Boyle, P., and Murray, T. (1998), The incidence of glacier surging in Svalbard: Evidence from multivariate statistics, *Computers & Geosciences*, **24** (4): 387-399.

Jiskoot, H., Murray, T., and Boyle, P. (2000), Controls on the distribution of surge-type glaciers in Svalbard, *Journal of Glaciology*, **46** (154): 412-422.

Jiskoot, H., Murray, T., and Luckman, A. (2003), Surge potential and drainage-basin characteristics in East Greenland, *Annals of Glaciology*, **36**: 142-148.

Jonsson, S., and Hansson, M. (1990), Identification of annual layers in superimposed ice from Storöyjökulen in northeastern Svalbard, *Geografiska Annaler. Series A. Physical Geography*: 41-54.

Jopling, A.V., and Walker, R.G. (1968), Morphology and origin of ripple-drift cross-lamination, with examples from the Pleistocene of Massachusetts, *Journal of Sedimentary Research*, **38** (4): 971-984.

Joughin, I., Tulaczyk, S., Fahnestock, M., and Kwok, R. (1996), A Mini-Surge on the Ryder Glacier, Greenland, Observed by Satellite Radar Interferometry, *Science*, **274**: 228-230.

Jouzel, J., and Souchez, R. (1982), Melting-refreezing at the glacier sole and the isotopic composition of the ice, *Journal of Glaciology*, **28** (98).

Kamb, B. (1987), Glacier Surge Mechanism Based on Linked Cavity Configuration of the Basal Water Conduit System, *Journal of Geophysical Research*, **92** (B9): 9083-9100.

Kamb, B., and LaChapelle, E. (1964), Direct observation of the mechanism of glacier sliding over bedrock, *Journal of Glaciology*, **5**: 159-172.

Kamb, B., Raymond, C.F., Harrison, W.D., Engelhardt, H., Echelmeyer, K.A., Humphrey, N., Brugman, M.M., and Pfeffer, T. (1985), Glacier Surge Mechanism: 1982-1983 Surge of Variegated Glacier, Alaska, *Science*, **227** (4686): 469-479.

Kaplan, M.R., Douglass, D.C., Singer, B.S., Ackert, R.P., and Caffee, M.W. (2005), Cosmogenic nuclide chronology of pre-last glacial maximum moraines at Lago Buenos Aires, 46°S, Argentina, *Quaternary Research*, **63**: 301-315.

Kempf, P. (2011), Sedimentary processes and palaeoenvironment in Van Keulenfjorden, Spitsbergen, *MSc thesis*, University of Tromsø.

Khatwa, A., Hart, J., and Payne, A. (1999), Grain textural analysis across a range of glacial facies, *Annals of Glaciology*, **28** (1): 111-117.

King, E.C., Smith, A.M., Murray, T., and Stuart, G.W. (2008), Glacier-bed characteristics of midtre Lovenbreen, Svalbard, from high-resolution seismic and radar surveying, *Journal of Glaciology*, **54** (184): 145-156.

King, E.C., Hindmarsh, R.C.A., and Stokes, C.R. (2009), Formation of mega-scale glacial lineations observed beneath a West Antarctic ice stream, *Nature Geoscience*, **2**: 585-588.

Kirkbride, M.P., and Brazier, V. (1998), A Critical Evaluation of the Use of Glacier Chronologies in Climatic Reconstruction, with Reference to New Zealand, **in:** *Mountain Glaciation*, Owen, L.A. (Ed.), Quaternary Proceedings No. 6, John Wiley & Sons Ltd., Chichester.

Kirkbride, M.P., and Deline, P. (2013), The formation of supraglacial debris covers by primary dispersal from transverse englacial debris bands, *Earth Surface Processes and Landforms*, **38** (15): 1779-1792.

Kjær, K.H., Korsgaard, N.J., and Schomacker, A. (2008), Impact of multiple glacier surges - a geomorphological map from Brúarjökull, East Iceland, *Journal of Maps*, **2008**: 5-20.

Klages, J.P., Kuhn, G., Hillenbrand, C.-D., Graham, A., Smith, J., Larter, R., and Gohl, K. (2013), First geomorphological record and glacial history of an inter-ice stream ridge on the West Antarctic continental shelf, *Quaternary Science Reviews*, **61**: 47-61.

Kluiving, S.J. (1994), Glaciotectonics of the Itterbeck-Uelsen push moraines, Germany, *Journal of Quaternary Science*, **9** (3): 235-244.

Knight, P.G. (1987), Observations at the edge of the Greenland ice sheet: boundary condition implications for modellers, *International Association of Hydrological Sciences Publication*, **170**: 359-366.

Knight, P.G. (1989), Stacking of basal debris layers without bulk freezing-on: isotopic evidence from West Greenland, *Journal of Glaciology*, **35** (120).

Knight, P.G. (1997), The basal ice layer of glaciers and ice sheets, *Quaternary Science Reviews*, **16**: 975-993.

Knight, P.G., and Knight, D.A. (1994), Glacier sliding, regelation water flow and development of basal ice, *Journal of Glaciology*, **40**: 600-601.

Knight, P.G., Sugden, D.E., and Minty, C.D. (1994), Ice flow around large obstacles as indicated by basal ice exposed at the margin of the Greenland ice sheet, *Journal of Glaciology*, **40** (135).

Knudsen, Ó. (1995), Concertina eskers, Brúarjökull, Iceland: An indicator of surge-type glacier behaviour, *Quaternary Science Reviews*, **14**: 487-493.

Koerner, R.M. (2005), Mass balance of glaciers in the Queen Elizabeth Islands, Nunavut, Canada, *Annals of Glaciology*, **42** (1): 417-423.

Kohler, J., James, T., Murray, T., Nuth, C., Brandt, O., Barrand, N., Aas, H., and Luckman, A. (2007), Acceleration in thinning rate on western Svalbard glaciers, *Geophysical Research Letters*, **34** (18).

Kotlyakov, V.M., Osipova, G.B., and Tsvetkov, D.G. (1997), Fluctuations of unstable mountain glaciers: scale and character, *Annals of Glaciology*, **24**: 228-343.

Krimmel, R.M., and Meier, M.F. (1975), Glacier applications of ERTS images, *Journal of Glaciology*, **15** (73): 391-402.

Kristensen, L., and Benn, D.I. (2012), A surge of the glaciers Skobreen-Paulabreen, Svalbard, observed by time-lapse photographs and remote sensing data, *Polar Research*, **31**.

Kristensen, L., Benn, D.I., Hormes, A., and Ottesen, D. (2009a), Mud aprons in front of Svalbard surge moraines: Evidence of subglacial deforming layers or proglacial glaciotectonics?, *Geomorphology*, **111**: 206-221.

Kristensen, L., Juliussen, H., Christiansen, H.H., and Humlum, O. (2009b), Structure and composition of a tidewater glacier push moraine, Svalbard, revealed by DC resistivity profiling, *Boreas*, **38**: 176-186.
Lamplugh, C.W. (1911), Of the shelly moraine of the Sefström Glacier and other Spitsbergen phenomena illustrative of British glacial conditions, *Proceedings of the Yorkshire Geological Society*, **17**: 216-241.
Larsen, N.K., Piotrowski, J.A., Christoffersen, P., and Menzies, J. (2006), Formation and deformation of basal till during a glacier surge; Elisebreen, Svalbard, *Geomorphology*, **81**: 217-234.
Larsen, N.K., Kronborg, C., Yde, J.C., and Knudsen, N.T. (2010), Debris entrainment by basal freeze-on and thrusting during the 1995–1998 surge of Kuannersuit Glacier on Disko Island, west Greenland, *Earth Surface Processes and Landforms*, **35** (5): 561-574.
Larson, G.J., Lawson, D.E., Evenson, E.B., Knudsen, Ó., Alley, R.B., and Phanikumar, M.S. (2010), Origin of stratified basal ice in outlet glaciers of Vatnajökull and Öræfajökull, Iceland, *Boreas*, **39** (3): 457-470.
Lawson, D.E. (1979), Sedimentological Analysis of the Western Terminus Region of the Matanuska Glacier, Alaska, *CRREL Report 79-9*, U.S. Army Cold Regions Research and Engineering Laboratory, Hanover.
Lawson, D.E. (1982), Mobilization, movement and deposition of active subaerial sediment flows, Matanuska Glacier, Alaska, *The Journal of Geology*, **90**: 279-300.
Lawson, D.E., Strasser, J.C., Evenson, E.B., Alley, R.B., Larson, G.J., and Arcone, S.A. (1998), Glaciohydraulic supercooling: a freeze-on mechanism to create stratified, debris-rich basal ice: I. Field evidence, *Journal of Glaciology*, **44** (148): 547-562.
Lawson, W.J., Sharp, M.J., and Hambrey, M.J. (1994), The structural geology of a surge-type glacier, *Journal of Structural Geology*, **16** (10): 1447-1462.
Lefauconnier, B., and Hagen, J.O. (1991), Surging and calving glaciers in eastern Svalbard, *Norsk Polarinstitutt Meddelelser*, **116**: 130.
Lefauconnier, B., Hagen, J.O., Ørbæk, J.B., Melvold, K., and Isaksson, E. (1999), Glacier balance trends in the Kongsfjorden area, western Spitsbergen, Svalbard, in relation to the climate, *Polar Research*, **18** (2): 307-313.
Liestøl, O. (1969), Glacier surges in West Spitsbergen, *Canadian Journal of Earth Sciences*, **6**: 895-897.
Liestøl, O. (1988), The glaciers in the Kongsfjorden area, Spitsbergen, *Norsk Geografisk Tidsskrift*, **42** (4): 231-238.
Liestøl, O. (1993), Glaciers of Svalbard, Norway, *U.S. Geological Survey Professional Paper*, **1386**: 127-151.
Lillesand, T., Kiefer, R., and Chipman, J. (2008), *Remote sensing and image interpretation*, John Wiley & Sons, Hoboken.
Lingle, C.S., and Fatland, D.R. (2003), Does englacial water storage drive temperate glacial surges?, *Annals of Glaciology*, **36**: 14-20.
Livingstone, S.J., Cofaigh, C.Ó., and Evans, D.J. (2010a), A major ice drainage pathway of the last British–Irish Ice Sheet: the Tyne Gap, northern England, *Journal of Quaternary Science*, **25** (3): 354-370.
Livingstone, S.J., Evans, D.J., Ó Cofaigh, C., and Hopkins, J. (2010b), The Brampton kame belt and Pennine escarpment meltwater channel system (Cumbria, UK): Morphology, sedimentology and formation, *Proceedings of the Geologists' Association*, **121** (4): 423-443.
Livingstone, S.J., Ó Cofaigh, C., Stokes, C.R., Hillenbrand, C.-D., Vieli, A., and Jamieson, S.S. (2012), Antarctic palaeo-ice streams, *Earth-Science Reviews*, **111** (1): 90-128.
Lliboutry, L. (1993), Internal melting and ice accretion at the bottom of temperate glaciers, *Journal of Glaciology*, **39** (131): 50-64.
Lønne, I., and Lauritsen, T. (1996), The Architecture of a Modern Push-moraine at Svalbard as Inferred from Ground-penetrating Radar Measurements, *Arctic and Alpine Research*, **28** (4): 488-495.
Lorrain, R., Sleewaegen, S., Fitzsimons, S., and Stievenard, M. (2002), Ice formation in an Antarctic glacier-dammed lake and implications for glacier-lake interactions, *Arctic, Antarctic, and Alpine Research*, **34** (2): 150-158.
Lovell, H., Stokes, C.R., Bentley, M.J., and Benn, D.I. (2012), Evidence for rapid ice flow and proglacial lake evolution around the central Strait of Magellan region, southernmost Patagonia, *Journal of Quaternary Science*, **27** (6): 625-638.
Lukas, S. (2005), A test of the englacial thrusting hypothesis of 'hummocky'moraine formation: case studies from the northwest Highlands, Scotland, *Boreas*, **34** (3): 287-307.
Lukas, S., Nicholson, L.I., and Ross, F.H. (2005), Formation, meltout processes and landscape alteration of High-Arctic ice-cored moraines - examples from Nordenskiöld Land, central Spitsbergen, *Polar Geography*, **29** (3): 157-187.
Lukas, S., Benn, D.I., Boston, C.M., Brook, M., Coray, S., Evans, D.J., Graf, A., Kellerer-Pirklbauer, A., Kirkbride, M.P., Krabbendam, M., Lovell, H., Machiedo, M., Mills, S.C., Nye, K., Reinardy, B.T.,

Ross, F.H., and Signer, M. (2013), Clast shape analysis and clast transport paths in glacial environments: A critical review of methods and the role of lithology, *Earth-Science Reviews*, **121**: 96-116.

Lyså, A., and Lønne, I. (2001), Moraine development at a small High-Arctic valley glacier: Rieperbreen, Svalbard, *Journal of Quaternary Science*, **16** (6): 519-529.

Mager, S., and Fitzsimons, S. (2007), Formation of glaciolacustrine Late Pleistocene end moraines in the Tasman Valley, New Zealand, *Quaternary Science Reviews*, **26** (5): 743-758.

Małecki, J., Faucherre, S., and Strzelecki, M.C. (2013), Post-surge geometry and thermal structure of Hørbyebreen, central Spitsbergen, *Polish Polar Research*, **34** (3): 305-321.

Mangerud, J. and Landvik, J.Y. (2007), Younger Dryas cirque glaciers in western Spitsbergen: smaller than during the Little Ice Age, *Boreas*, **36** (3): 278-285.

Mansell, D., Luckman, A., and Murray, T. (2012), Dynamics of tidewater surge-type glaciers in northwest Svalbard, *Journal of Glaciology*, **58** (207): 110-118.

Marren, P.M. (2004), Present-day sandurs are not representative of the geological record, *Sedimentary Geology*, **152**: 1-5.

Marren, P.M., and Toomath, S.C. (2014), Channel pattern of proglacial rivers: topographic forcing due to glacier retreat, *Earth Surface Processes and Landforms*, **39**: 943-951.

McMeeking, R.M., and Johnson, R.E. (1986), On the mechanics of surging glaciers, *Journal of Glaciology*, **32** (110): 120-132.

Meier, M.F. (1984), Contribution of small glaciers to global sea level, *Science*, **226** (4681): 1418-1421.

Meier, M.F., and Post, A. (1969), What are glacier surges?, *Canadian Journal of Earth Sciences*, **6** (4): 807-817.

Meier, M., and Post, A. (1987), Fast tidewater glaciers, *Journal of Geophysical Research*, **92** (B9): 9051-9058.

Meier, M.F., Dyurgerov, M.B., Rick, U.K., O'Neel, S., Pfeffer, W.T., Anderson, R.S., Anderson, S.P., and Glazovsky, A.F. (2007), Glaciers dominate eustatic sea-level rise in the 21st century, *Science*, **317** (5841): 1064-1067.

Melvold, K., and Hagen, J.O. (1998), Evolution of a surge-type glacier in its quiescent phase: Kongsvegen, Spitsbergen, 1964-95, *Journal of Glaciology*, **44** (147): 394-404.

Midgley, N.G., Cook, S.J., Graham, D.J., and Tonkin, T.N. (2013), Origin, evolution and dynamic context of a Neoglacial lateral-frontal moraine at Austre Lovénbreen, Svalbard, *Geomorphology*, **198**: 96-106.

Miles, B., Stokes, C., Vieli, A., and Cox, N. (2013), Rapid, climate-driven changes in outlet glaciers on the Pacific coast of East Antarctica, *Nature*, **500** (7464): 563-566.

Moore, P.L., Iverson, N.R., and Cohen, D. (2010), Conditions for thrust faulting in a glacier, *Journal of Geophysical Research*, **115** (F02005): 1-15.

Moore, P.L., Iverson, N.R., Brugger, K.A., Cohen, D., Hooyer, T.S., and Jansson, P. (2011), Effect of a cold margin on ice flow at the terminus of Storglaciären, Sweden: implications for sediment transport, *Journal of Glaciology*, **57** (201): 77-87.

Murray, T., and Booth, A.D. (2010), Imaging glacial sediment inclusions in 3-D using ground-penetrating radar at Kongsvegen, Svalbard, *Journal of Quaternary Science*, **25** (5): 754-761.

Murray, T., Gooch, D.L., and Stuart, G.W. (1997), Structures within the surge front at Bakaninbreen, Svalbard, using ground-penetrating radar, *Annals of Glaciology*, **24**: 122-129.

Murray, T., Dowdeswell, J.A., Drewry, D.J., and Frearson, I. (1998), Geometric evolution and ice dynamics during a surge of Bakaninbreen, Svalbard, *Journal of Glaciology*, **44** (147): 263-272.

Murray, T., Stuart, G.W., Miller, P.J., Woodward, J., Smith, A.M., Porter, P.R., and Jiskoot, H. (2000), Glacier surge propagation by thermal evolution at the bed, *Journal of Geophysical Research*, **105** (B6): 13491-13507.

Murray, T., Strozzi, T., Luckman, A., Pritchard, H., and Jiskoot, H. (2002), Ice dynamics during the surge of Sortebræ, East Greenland, *Annals of Glaciology*, **34**: 323-329.

Murray, T., Luckman, A., Strozzi, T., and Nuttall, A.-M. (2003a), The initiation of glacier surging at Fridtjovbreen, Svalbard, *Annals of Glaciology*, **36**: 110-116.

Murray, T., Strozzi, T., Luckman, A., Jiskoot, H., and Christakos, P. (2003b), Is there a single surge mechanism? Contrasts in dynamics between glacier surges in Svalbard and other regions, *Journal of Geophysical Research*, **108** (B5): 1-15.

Murton, J., Whiteman, C., Waller, R., Pollard, W., Clark, I., and Dallimore, S. (2005), Basal ice facies and supraglacial melt-out till of the Laurentide Ice Sheet, Tuktoyaktuk Coastlands, western Arctic Canada, *Quaternary Science Reviews*, **24** (5): 681-708.

Naegeli, K. (2013), Investigations of state and changes in drainage system, thermal structure and dynamics of Tellbreen, a High Arctic glacier on Svalbard, using glacio-speleology, *MSc thesis*, University of Zurich: 115 pp.

Naegeli, K., Lovell, H., Zemp, M., and Benn, D. (accepted), Formation of en- and subglacial drainage systems within cold glaciers by cut-and-closure processes, *Geografiska Annaler: Series A – Physical Geography*.

Nelson, A.E., Willis, I.C., and Cofaigh, C.O. (2005), Till genesis and glacier motion inferred from sedimentological evidence associated with the surge-type glacier, Bruarjokull, Iceland, *Annals of Glaciology*, **42** (1): 14-22.

Nielsen, N. (1937), A volcano under an ice-cap: Vatnajökull, Iceland. 1934-36, *The Geographical Journal*, **90** (1): 6-23.

Nielsen, L.E. (1969), The ice-dam, powder-flow theory of glacier surges, *Canadian Journal of Earth Sciences*, **6**: 955-961.

Nolan, M. (2003), The "Galloping Glacier" trots: decadal-scale speed oscillations within the quiescent phase, *Annals of Glaciology*, **36**: 7-13.

Nuth, C., Moholdt, G., Kohler, J., Hagen, J.O., and Kääb, A. (2010), Svalbard glacier elevation changes and contribution to sea level rise, *Journal of Geophysical Research*, **115**: 1-16.

Nuth, C., Kohler, J., König, M., von Deschwanden, A., Hagen, J., Kääb, A., Moholdt, G., and Pettersson, R. (2013), Decadal changes from a multi-temporal glacier inventory of Svalbard, *The Cryosphere*, **7** (5).

Nuttall, A.-M., and Hodgkins, R. (2005), Temporal variations in flow velocity at Finsterwalderbreen, a Svalbard surge-type glacier, *Annals of Glaciology*, **42**: 71-76.

Nuttall, A.-M., Hagen, J.O., and Dowdeswell, J.A. (1997), Quiescent-phase changes in velocity and geometry of Finsterwalderbreen, a surge-type glacier in Svalbard, *Annals of Glaciology*, **24**: 249-254.

Nye, J. (1970), Glacier sliding without cavitation in a linear viscous approximation, *Proceedings of the Royal Society of London. A. Mathematical and Physical Sciences*, **315** (1522): 381-403.

Ó Cofaigh, C., Stokes, C., Lian, O., Clark, C., and Tulacyzk, S. (2013), Formation of mega-scale glacial lineations on the Dubawnt Lake Ice Stream bed: 2. Sedimentology and stratigraphy, *Quaternary Science Reviews*, **77**: 210-227.

Ødegård, R., Hagen, J., and Hamran, S.-E. (1996), Comparison of radio-echo sounding (30-1000 MHz) and high-resolution borehole-temperature measurements at Finsterwalderbreen, southern Spitsbergen, Svalbard, *Annals of Glaciology*, **24**: 262-267.

Oerlemans, J. (1994), Quantifying global warming from the retreat of glaciers, *Science*, **264**: 243-245.

Oerlemans, J., and Fortuin, J. (1992), Sensitivity of Glaciers and Small Ice Caps to Greenhouse Warming, *Science*, **258** (5079): 115-117.

Osipova, G.B., and Tsvetkov, D.G. (1991), Kinematics of the surface of a surging glacier (comparison of the Medvezhiy and Variegated Glaciers), *Glaciers-Oceans-Atmosphere Interactions (Proceedings of the International Symposium)*, International Association of Hydrological Sciences Publication 208, St Petersburg.

Ottesen, D., and Dowdeswell, J.A. (2006), Assemblages of submarine landforms produced by tidewater glaciers in Svalbard, *Journal of Geophysical Research*, **111** (F01016): 1-16.

Ottesen, D., Dowdeswell, J., and Rise, L. (2005), Submarine landforms and the reconstruction of fast-flowing ice streams within a large Quaternary ice sheet: The 2500-km-long Norwegian-Svalbard margin (57–80 N), *Geological Society of America Bulletin*, **117** (7-8): 1033-1050.

Ottesen, D., Dowdeswell, J.A., Benn, D.I., Kristensen, L., Christiansen, H.H., Christensen, O., Hansen, L., Lebesbye, E., Forwick, M., and Vorren, T.O. (2008), Submarine landforms characteristic of glacier surges in two Spitsbergen fjords, *Quaternary Science Reviews*, **27**: 1583-1599.

Patterson, C.J. (1997), Southern Laurentide ice lobes were created by ice streams: Des Moines Lobe in Minnesota, USA, *Sedimentary Geology*, **111** (1): 249-261.

Perşoiu, A., Onac, B.P., Wynn, J.G., Bojar, A.-V., and Holmgren, K. (2011), Stable isotope behavior during cave ice formation by water freezing in Scărişoara Ice Cave, Romania, *Journal of Geophysical Research*, **116** (D2): 1-8.

Pfeffer, W.T., Harper, J., and O'Neel, S. (2008), Kinematic constraints on glacier contributions to 21st-century sea-level rise, *Science*, **321** (5894): 1340-1343.

Plassen, L., Vorren, T.O., and Forwick, M. (2004), Integrated acoustic and coring investigation of glacigenic deposits in Spitsbergen fjords, *Polar Research*, **23** (1): 89-110.

Post, A. (1969), Distribution of surging glaciers in western North America, *Journal of Glaciology*, **8** (53): 229-240.

Prior, D.B., Bornhold, B., and Johns, M. (1984), Depositional characteristics of a submarine debris flow, *The Journal of Geology*, **92**: 707-727.

Quincey, D.J., Braun, M., Glasser, N.F., Bishop, M.P., Hewitt, K., and Luckman, A. (2011), Karakoram glacier surge dynamics, *Geophysical Research Letters*, **38** (L18054): 1-6.

Radić, V., and Hock, R. (2011), Regionally differentiated contribution of mountain glaciers and ice caps to future sea-level rise, *Nature Geoscience*, **4** (2): 91-94.

Raper, S.C., and Braithwaite, R.J. (2006), Low sea level rise projections from mountain glaciers and icecaps under global warming, *Nature*, **439** (7074): 311-313.
Raymond, C.F., and Harrison, W.D. (1988), Evolution of Variegated Glacier, Alaska, U.S.A., prior to its surge, *Journal of Glaciology*, **34**: 154-169.
Raymond, C.F., Johannesson, T., Pfeffer, T., and Sharp, M.J. (1987), Propagation of a Glacier Surge Into Stagnant Ice, *Journal of Geophysical Research*, **92** (B9): 9037-9049.
Rea, B.R., and Evans, D.J.A. (2011), An assessment of surge-induced crevassing and the formation of crevasse squeeze ridges, *Journal of Geophysical Research*, **116** (F04005): 1-17.
Reimer, P.J., Bard, E., Bayliss, A., Beck, J.W., Blackwell, P.G., Ramsey, C.B., Grootes, P.M., Guilderson, T.P., Haflidason, H., and Hajdas, I. (2013), IntCal13 and Marine13 radiocarbon age calibration curves 0–50,000 years cal BP, *Radiocarbon*, **55** (4): 1869-1887.
Rignot, E., Rivera, A., and Casassa, G. (2003), Contribution of the Patagonia Icefields of South America to sea level rise, *Science*, **302** (5644): 434-437.
Rignot, E., Velicogna, I., Van den Broeke, M., Monaghan, A., and Lenaerts, J. (2011), Acceleration of the contribution of the Greenland and Antarctic ice sheets to sea level rise, *Geophysical Research Letters*, **38** (5).
Roberson, S. (2008), Structural composition and sediment transfer in a composite cirque glacier: Glacier de St. Sorlin, France, *Earth Surface Processes and Landforms*, **33** (13): 1931-1947.
Roberson, S., and Hubbard, B. (2010), Application of borehole optical televiewing to investigating the 3-D structure of glaciers: implications for the formation of longitudinal debris ridges, midre Lovénbreen, Svalbard, *Journal of Glaciology*, **56** (195): 143-156.
Roberson, S., Hubbard, B., Coulson, H.R., and Boomer, I. (2011), Physical Properties and Formation of Flutes at a Polythermal Valley Glacier: Midre Lovénbreen, Svalbard, *Geografiska Annaler: Series A, Physical Geography*, **93** (2): 71-88.
Roberts, D.H., Yde, J.C., Knudsen, N.T., Long, A.J., and Lloyd, J.M. (2009), Ice marginal dynamics during surge activity, Kuannersuit Glacier, Disko Island, West Greenland, *Quaternary Science Reviews*, **28**: 209-222.
Roberts, M.J., Tweed, F.S., Russell, A.J., Knudsen, Ó., Lawson, D.E., Larson, G.J., Evenson, E.B., and Björnsson, H. (2002), Glaciohydraulic supercooling in Iceland, *Geology*, **30** (5): 439-442.
Röller, K., and Trepmann, C.A. (2008), Stereo 32 - version 1.0.1., edited, Ruhr-Universität Bochum, Institut für Geologie, Mineralogie & Geophysik., Bochum.
Rolstad, C., Amlien, J., Hagen, J.O., and Lundén, B. (1997), Visible and near-infrared digital images for determination of ice velocities and surface elevation during a surge on Osbornebreen, a tidewater glacier in Svalbard, *Annals of Glaciology*, **24**: 255-261.
Roush, J.J., Lingle, C.S., Guritz, R.M., Fatland, D.R., and Voronina, V.A. (2003), Surge-front propagation and velocities during the early-1993-95 surge of Bering Glacier, Alaska, U.S.A., from sequential SAR imagery, *Annals of Glaciology*, **36**: 37-44.
Rowan, D.E., Péwé, T.L., Péwé, R.H., and Stuckenrath, R. (1982), Holocene glacial geology of the Svea lowland, Spitsbergen, Svalbard, *Geografiska Annaler. Series A. Physical Geography*, **64** (1/2): 35-51.
Salvigsen, O. (2002), Radiocarbon dated Mytulis edulis and Modiolus modiolus from northern Svalbard: climate implications, *Norwegian Journal of Geography*, **56**: 56-61.
Salvigsen, O., Forman, S., and Miller, G.H. (1992), Thermophilous molluscs on Svalbard during the Holocene and their palaeoclimatic implications, *Polar Research*, **11**: 1-10.
Schomacker, A. (2008), What controls dead-ice melting under different climate conditions? A discussion, *Earth-Science Reviews*, **90**: 103-113.
Schomacker, A., and Kjær, K.H. (2008), Quantification of dead-ice melting in ice-cored moraines at the high-Arctic glacier Holmströmbreen, Svalbard, *Boreas*, **37** (2): 211-225.
Schytt, V. (1969), Some comments on glacier surges in eastern Svalbard, *Canadian Journal of Earth Sciences*, **6**: 867-873.
Sharp, M. (1985a), "Crevasse-fill" ridges - a landform type characteristic of surging glaciers?, *Geografiska Annaler*, **67A** (3-4): 213-220.
Sharp, M. (1985b), Sedimentation and Stratigraphy at Eyjabakkajökull - An Icelandic Surging Glacier, *Quaternary Research*, **24**: 268-284.
Sharp, M. (1988), Surging glaciers: Geomorphic effects, *Progress in Physical Geography*, **12** (4): 533-559.
Sharp, M., Lawson, W., and Anderson, R.S. (1988), Tectonic processes in a surge-type glacier, *Journal of Structural Geology*, **10** (5): 499-515.
Sharp, M., Jouzel, J., Hubbard, B., and Lawson, W. (1994), The character, structure and origin of the basal ice layer of a surge-type glacier, *Journal of Glaciology*, **40** (135): 327-340.
Shepherd, A., and Wingham, D. (2007), Recent sea-level contributions of the Antarctic and Greenland ice sheets, *Science*, **315** (5818): 1529-1532.

Sletten, K., Lysså, A., and Lønne, I. (2001), Formation and disintegration of a high-arctic ice-cored moraine complex, Scott Turnerbreen, Svalbard, *Boreas*, **30**: 272-284.

Smith, N., and Ashley, G.M. (1985), Proglacial lacustrine environment, **in:** *Glacial Sedimentary Environments*, Ashley, G.M., Shaw, J. and Smith, N. (Eds.), Society of Economic Palaeontologists and Mineralogists

Smith, A.M., Murray, T., Davison, B.M., Clough, A.F., Woodward, J., and Jiskoot, H. (2002), Late surge glacial conditions on Bakaninbreen, Svalbard, and implications for surge termination, *Journal of Geophysical Research*, **107** (B8): 1-16.

Solheim, A. (1985), Submarine evidence of glacier surges, *Polar Research*, **4**: 91-95.

Solheim, A., and Pfirman, S.L. (1985), Sea-floor morphology outside a grounded, surging glacier; Bråsvellbreen, Svalbard, *Marine Geology*, **65**: 127-143.

Souchez, R., and Jouzel, J. (1984), On the isotopic composition in δD and $\delta^{18}O$ of water and ice during freezing, *Journal of Glaciology*, **30** (106).

Souchez, R., and de Groote, J. (1985), δD-$\delta^{18}O$ relationships in ice formed by subglacial freezing: palaeoclimatic implications, *Journal of Glaciology*, **31** (109).

Souchez, R.A., and Lorrain, R.D. (1991), *Ice Composition and Glacier Dynamics*, Springer, Berlin.

Souchez, R., Lorrain, R., and Tison, J.L. (1988), Co-isotopic signature of two mechanisms of basal-ice formation in Arctic outlet glaciers, *Annals of Glaciology*, **10**: 163-166.

Souchez, R., Lemmens, M., Lorrain, R., Tison, J.-L., Jouzel, J., and Sugden, D. (1990), Influence of hydroxyl-bearing minerals on the isotopic composition of ice from the basal zone of an ice sheet, *Nature*, **345** (6272): 244-246.

Souchez, R., Jouzel, J., Lorrain, R., Sleewaegen, S., Stiévenard, M., and Verbeke, V. (2000), A kinetic isotope effect during ice formation by water freezing, *Geophysical Research Letters*, **27** (13): 1923-1926.

Spedding, N., and Evans, D.J. (2002), Sediments and landforms at Kvíárjökull, southeast Iceland: a reappraisal of the glaciated valley landsystem, *Sedimentary Geology*, **149** (1): 21-42.

Stewart, T.G. (1991), Glacial marine sedimentation from tidewater glaciers in the Canadian High Arctic, *Geological Society of America Special Papers*, **261**: 95-105.

Stokes, C., and Clark, C.D. (2002), Are long subglacial bedforms indicative of fast ice flow?, *Boreas*, **31**: 239-249.

Stokes, C., Spagnolo, M., Clark, C., Ó Cofaigh, C., Lian, O., and Dunstone, R. (2013a), Formation of mega-scale glacial lineations on the Dubawnt Lake Ice Stream bed: 1. Size, shape and spacing from a large remote sensing dataset, *Quaternary Science Reviews*, **77**: 190-209.

Stokes, C.R., Fowler, A.C., Clark, C.D., Hindmarsh, R.C., and Spagnolo, M. (2013b), The instability theory of drumlin formation and its explanation of their varied composition and internal structure, *Quaternary Science Reviews*, **62**: 77-96.

Striberger, J., Björck, S., Benediktsson, Í.Ö., Snowball, I., Uvo, C.B., Ingólfsson, Ó., and Kjær, K.H. (2011), Climatic control of the surge periodicity of an Icelandic outlet glacier, *Journal of Quaternary Science*, **26** (6): 561-565.

Stuiver, M., and Reimer, P.J. (2006), Extended (super 14) C data base and revised CALIB 3.0 (super 14) C age calibration program, *Radiocarbon*, **35** (1): 215-230.

Sugden, D., Clapperton, C., Gemmell, J., and Knight, P. (1987a), Stable isotopes and debris in basal glacier ice, South Georgia, Southern Ocean, *Journal of Glaciology*, **33** (115).

Sugden, D., Knight, P., Livesey, N., Lorrain, R., Souchez, R., Tison, J.-L., and Jouzel, J. (1987b), Evidence for two zones of debris entrainment beneath the Greenland ice sheet, *Nature*, **328** (6127): 238-241.

Sund, M. (2006), A surge of Skobreen, Svalbard, *Polar Research*, **25** (2): 115-122.

Sund, M., and Eiken, T. (2004), Quiescent-phase dynamics and surge history of a polythermal glacier: Hessbreen, Svalbard, *Journal of Glaciology*, **50** (171): 547-555.

Sund, M., and Eiken, T. (2010), Correspondence: Recent surges on Blomstrandbreen, Comfortlessbreen and Nathorstbreen, Svalbard, *Journal of Glaciology*, **56** (195): 182-184.

Sund, M., Eiken, T., Hagen, J.O., and Kääb, A. (2009), Svalbard surge dynamics derived from geometric changes, *Annals of Glaciology*, **50** (52): 50-60.

Sund, M., Lauknes, T., and Eiken, T. (2013), Surge dynamics in the Nathorstbreen glacier system, Svalbard, *The Cryosphere Discussions*, **7** (5): 4937-4976.

Svendsen, J.I., and Mangerud, J. (1997), Holocene glacial and climatic variations on Spitsbergen, Svalbard, *The Holocene*, **7**: 45-57.

Swift, D.A., Evans, D.J.A., and Fallick, A.E. (2006), Transverse englacial debris-rich ice bands at Kvíárjökull, southeast Iceland, *Quaternary Science Reviews*, **25**: 1708-1718.

Tarr, R.S., and Martin, L. (1914), *Alaskan glacier studies of the National Geographic Society in the Yakutat Bay, Prince William Sound and lower Copper River regions*, National Geographic Society, Washington D. C.

Tavarnelli, E., Holdsworth, R.E., Clegg, P., Jones, R.R., and McCaffrey, K.J. (2004), The anatomy and evolution of a transpressional imbricate zone, Southern Uplands, Scotland, *Journal of Structural Geology*, **26** (8): 1341-1360.

Thomas, R., Rignot, E., Casassa, G., Kanagaratnam, P., Acuña, C., Akins, T., Brecher, H., Frederick, E., Gogineni, P., and Krabill, W. (2004), Accelerated sea-level rise from West Antarctica, *Science*, **306** (5694): 255-258.

Thorarinsson, S. (1969), Glacier surges in Iceland, with special reference to the surges of Brúarjökull, *Canadian Journal of Earth Sciences*, **6**: 875-882.

Twiss, R.J., and Moores, E.M. (2007), *Structural Geology*, Second ed., W. H. Freeman & Co Ltd., New York.

van der Meer, J.J. (2004), *Spitsbergen Push Moraines*, Elsevier, Amsterdam.

van der Wateren, D. (1995), Processes of Glaciotectonism, *Glacial environments Vol. 1. Modern glacial environments: Processes, dynamics and sediments*: 309-335.

Wadham, J.L., Hodgkins, R., Cooper, R.J., and Tranter, M. (2001), Evidence for seasonal subglacial outburst events at a polythermal glacier, Finsterwalderbreen, Svalbard, *Hydrological Processes*, **15**: 2259-2280.

Waller, R. (1997), The role of tectonism in the distribution, appearance and dynamic behaviour of debris-rich basal ice, *PhD thesis*, Keele University.

Waller, R., Hart, J., and Knight, P. (2000), The influence of tectonic deformation on facies variability in stratified debris-rich basal ice, *Quaternary Science Reviews*, **19**: 775-786.

Waller, R.I., Murton, J.B., and Kristensen, L. (2012), Glacier–permafrost interactions: processes, products and glaciological implications, *Sedimentary Geology*, **255**: 1-28.

Warren, W.P., and Ashley, G.M. (1994), Origins of the ice-contact stratified ridges (eskers) of Ireland, *Journal of Sedimentary Research*, **64** (3a): 433-449.

Watts, T.P. (2010), The origin and significance of the Grønfjordbreen moraine complex, *MSc thesis*, University of Sheffield: 32 pp.

Weertman, J. (1961), Mechanism for the formation of inner moraines found near the edge of cold ice caps and ice sheets, *Journal of Glaciology*, **3** (30): 965-978.

Weiss, J., and Schulson, E. (2000), Grain-boundary sliding and crack nucleation in ice, *Philosophical Magazine A*, **80** (2): 279-300.

Werner, A. (1990), Lichen growth rates for the northwest coast of Spitsbergen, Svalbard, *Arctic and Alpine Research*, **22** (2): 129-140.

Werner, A. (1993), Holocene moraine chronology, Spitsbergen, Svalbard: lichenometric evidence for multiple Neoglacial advances in the Arctic, *The Holocene*, **3** (2): 128-137.

Woodward, J.T., Murray, T., and McCaig, A. (2002), Formation and reorientation of structure in the surge-type glacier Kongsvegen, Svalbard, *Journal of Quaternary Science*, **17** (3): 201-209.

Woodward, J.T., Murray, T., Clark, R.A., and Stuart, G.W. (2003a), Glacier surge mechanisms inferred from ground-penetrating radar: Kongsvegen, Svalbard, *Journal of Glaciology*, **49** (167): 473-480.

Woodward, J.T., Murray, T., and McCaig, A. (2003b), Reply: Formation and reorientation of structure in the surge-type glacier Kongsvegen, Svalbard, *Journal of Quaternary Science*, **18** (1): 99-100.

Yde, J.C., and Knudsen, N.T. (2005), Observations of Debris-rich Naled Associated with a Major Glacier Surge Event, Disko Island, West Greenland, *Permafrost and Periglacial Processes*, **16**: 319-325.

Yde, J.C., Knudsen, N.T., Larsen, N.K., Kronberg, C., Nielsen, O.B., Heinemeier, J., and Olsen, J. (2005), The presence of thrust-block naled after a major surge event: Kuannersuit Glacier, West Greenland, *Annals of Glaciology*, **42**: 145-150.

Appendix

Table A1 - Remote sensing and published data sources used in this project, including type, details, data provided and source.

Type	Details	Data provided	Source
Published data			
Hamberg (1908)	Map of Van Keulenfjorden in 1898.	1898 terminus position of NHB	
Liestøl (1969)	Photogrammetric mapping of TNB in 1924 and 1932.	Description of TNB terminus change 1924-1932	
Hodgkins and Dowdeswell (1994) Plassen *et al.* (2004)	1970s surge mapped from vertical aerial photographs. Map of terminus change in Tempelfjorden, including positions based on de Geer (1910) and Liestøl (1969).	Description of TNB terminus change 1966-1971 1870, 1882, 1896, 1908, 1930, 1966 and 1971 terminus positions of TNB	
Ottesen *et al.*	Swath bathymetry data of	Submarine geomorphology	

(2008)	inner Van Keulenfjorden.	associated with NHB	
Norwegian Polar Institute (NPI) maps (1:100,000 scale)	B11 – Van Keulenfjorden C8 – Billefjorden C9 - Adventdalen C11 - Kvalvågen	1990 and 1993 terminus positions of TNB	
Satellite imagery Landsat MSS (80 m pixel resolution)	p232, r004 (09/04/75) p230, r004 (18/07/76) p245, r003 (24/07/79) p214, r004 (19/10/82)	1975 TNB terminus position 1976 TNB terminus position 1979 TNB terminus position 1982 TNB terminus position	USGS Earth Explorer (https://earthexplorer.usgs.gov)
Landsat TM (30 m pixel resolution)	p217, r003 (26/06/88) p212, r004 (27/07/2006)	1988 TNB terminus position 2006 TNB terminus position	Global Land Cover Facility (www.landcover.org)
Landsat ETM+ (30 m pixel resolution)	p211, r004 (09/07/99) p214, r004 (17/06/01) p212, r004 (18/08/11) p212, r004 (19/07/12)	1999 TNB terminus position 2001 TNB terminus position 2011 NHB terminus position 2012 NHB terminus position	USGS Earth Explorer (https://earthexplorer.usgs.gov)
ASTER (15 m pixel resolution)	(13/06/02) (12/07/03) (25/07/04) (16/06/05) (08/04/08) (01/08/10) (02/08/10)	2002 TNB terminus position and crevasse distribution 2003 TNB terminus position and crevasse distribution 2004 TNB terminus position and crevasse distribution 2005 TNB terminus position and crevasse distribution 2008 NHB terminus position 2010 TNB terminus position 2010 NHB terminus position	Land Processes Distributed Active Archive Center (http://LPDAAC.usgs.gov)
Aerial photographs	S95 1153 (20/08/95) *1:50,000 scale* S2009_13835 00024 and 00105 (27/07/09) S2009_13835 00426, 00427 and 00428 (27/02/09) S2011_25163 S2011_25163 *All 1:15,000 scale* NERC 4117, 4140, 4142 and 4144 (27/07/04) *1:15,000 scale*	1995 TNB terminus position STB geomorphological map TLB geomorphological map FWB geomorphological map NHB geomorphological map TNB/VPB geomorphological map	Norwegian Polar Institute (NPI) NERC Earth Observation Data Centre (http://www.neodc.rl.ac.uk/)
Swath bathymetry data	Inner Tempelfjorden *1 m grid*	Mapping of geometrical ridge networks in Tempelfjorden	Norwegian Hydrographic Service and UNIS